Department of Applied Geology

Quantification of an Archaean to Recent Earth Expansion Process Using Global Geological and Geophysical Data Sets

James Maxlow

This thesis is presented as part of the
requirement for the award of the
Doctor of Philosophy
of
Curtin University of Technology

June 2001

Abstract

Global geological and geophysical data, while routinely used in conventional plate tectonic studies, has not been applied to models of an expanding Earth. Crustal reconstructions on Archaean to Recent models of an expanding Earth presented here are the first time that reconstructions have been extended back to the Archaean, and the first time that continental and oceanic geology has been utilised to constrain plate assemblage and palaeoradius of the Earth. A set of twenty four spherical models have been constructed, twenty three covering the Archaean to Recent and one projected to five million years into the future. Construction of these spherical models relies on the fundamental premise that crustal lithosphere is cumulative with time, and historical markers preserved in the oceanic and continental geology accurately constrain both palaeoradius and plate reconstruction from the Archaean to Recent.

Post-Triassic reconstructions of oceanic lithosphere demonstrate a plate fit-together along each plate margin at better than 99% fit. During the Triassic, continents envelope the Earth as a complete continental shell at a reduced Earth radius, and marginal and epi-continental sedimentary basins merge to form a global network surrounding continental cratons and orogenic zones. Continental crust is reconstructed on Pre-Jurassic models using the primary crustal elements of cratons, orogens and basins, with expansion primarily manifested as crustal extension within an established network of epi-continental rifts, orogens and sedimentary basins. By removing all basin and pre-orogenic sediments a primordial proto-Earth at a palaeoradius of approximately 1700 kilometres is achieved during the Mesoproterozoic, comprising assembled cratons and Proterozoic basement rocks.

For all models, an intracratonic to intracontinental spatial integrity is maintained throughout Earth history during processes of Precambrian and Palaeozoic continental crustal extension, Late Palaeozoic crustal rupture, Permo-Triassic continental break-up, and Mesozoic and Cenozoic continental dispersal to the Recent. Palaeomagnetic pole data delineate diametrically opposed palaeomagnetic pole clusters for each era back to the Archaean, without the need to consider random crustal dispersion-amalgamation-dispersal cycles. The palaeopole data is further supported by palaeogeographic, palaeobiogeographic, and palaeoclimatic indicators, which define palaeoequators and palaeoclimatic zones consistent with palaeomagnetic determinations. The distribution of latitude dependent lithofacies

including glacigenic strata, carbonates, coal, and faunal and floral species is shown to coincide precisely with established palaeopoles and palaeoequators for all expanding Earth models.

For climatic and biotic indicators a distinct latitudinal zonation paralleling the established palaeoequator is evident and a distinct northward shift in climatic zonation suggests that an inclined Earth rotational axis, inclined to the pole of the ecliptic, was well established during the Palaeozoic and persists to the Recent. Coastal geography on expanding Earth models shows that large Panthallassa, Tethys and Iapetus Oceans are not required during reconstruction. Instead, epi-continental Panthallassa and Iapetus Seas represent precursors to the modern Pacific and Atlantic Oceans and the Tethys Sea represents a precursor of the present Eurasian continent. Emergent land surfaces during the Precambrian and Phanerozoic equate to the conventional Rodinia, Gondwana and Pangaea supercontinents and smaller sub-continents, and demonstrate a spatial intracratonic and intracontinental integrity throughout Earth history.

On each spherical model constructed proto-continental development is evolutionary and defined by a progressive extension of epi-continental sedimentary basins, pulsed orogenesis, eustatic and transgression-regression of epi-continental seas, and opening of modern oceans during the Mesozoic to Recent. Metallogenic modelling of Precambrian and Phanerozoic metal deposits shows a broad global Precambrian metallogenic provinciality coinciding with cratons and intracratonic settings, to regional provinces clustering as specific metal associations. The Phanerozoic metallogenic distribution highlights the abundance of porphyry and granite associated metals concentrated within Phanerozoic orogenic belts, and orogenic belts are shown to crosscut and displace pre-existing Palaeozoic and Precambrian metallogenic provinces.

A proposed causal model for Earth expansion has expansion due to an exponential increase in mass with time. Earth expansion then involves an increase in mass by condensation, or segregation of new matter from the Earth's core. This new matter accumulates at the core-mantle interface and the increase in volume results in a swelling of the mantle, which is then manifested in the outer crust as crustal extension. Matter generation within the Earth's core is seen as an endothermic reaction, which will ultimately result in a decay of the matter formation process and cessation of expansion with time.

Acknowledgements

The author is grateful for financial assistance received through the Australian Postgraduate Award Scheme and administrative assistance received through the Office of Research and Development, Graduate Studies and Scholarships Division, Curtin University of Technology.

I thank the staff of the School of Applied Geology, Curtin University of Technology and fellow research students for their encouragement and stimulating discussion, in particular:

Dr. Peter Collins, my supervisor;

Dr. Krish Sappal, my co-supervisor;

Dr. Peter Cawood, my chairperson;

and fellow Ph.D. student, Marcus Sweetapple.

Thanks go to Philippe Bouysse of the Commission de la Carte Geologique du Monda, Paris. Permission was granted to use and digitise the *Geological Map of the World at 1:25,000,000 M scale* (1990), published by the Commission for the Geological Map of the World and UNESCO ©.

Acknowledgements and thanks go to Simon Brown of Geoviz, Perth, Western Australia, for digitising the *Geological Map of the World* base map used in this thesis and ongoing computer support. Anita Maxlow of Terrella Graphics for assistance in graphical display, Paul Wilkes of the Curtin School of Exploration Geophysics for initial technical discussion, George Borzyskowski of the Curtin School of Design for advice on graphical software and Bruce Myles for the use of his digital camera.

Sincere thanks must also go to fellow expansionists Professor Sam Warren Carey for his ongoing advice and encouragement. Thanks also go to Klaus and Eva-Marie Vogel for their generous hospitality and stimulating discussion while in Germany, Jan Koziar and Leszek Jamozik of the Institute of Geological Sciences, Wroclaw University and Dr. Stefan Cwojdzinski, Polish Geological Institute, for their generous hospitality and encouragement while in Poland, and Malcolm McClure for his hospitality while in London. David Ford provided discussion and assistance with some figures and Professor Cliff Ollier, Australian National University gave assistance with editing and stimulating discussion on mountains.

May we all expand in unison.

CONTENTS Volume 1 of 2

LIST OF FIGURES

LIST OF TABLES

1. INTRODUCTION

Global tectonics is a concept that embraces and integrates all facets of the Earth sciences and includes theories as diverse as plate tectonics and Earth expansion. The rapid increase in global tectonic research during the past three decades, coupled with advances in computer technology, has resulted in the accumulation of a vast array of global geological and geophysical data. This data, while routinely used in conventional plate tectonic studies, has previously not been applied to an expanding Earth model.

In this thesis it is intended to use global geological and geophysical data, including examples from geology, space geodetics, palaeomagnetics, palaeogeography, palaeobiogeography, palaeoclimate and metallogeny to investigate a potential Archaean to Recent Earth expansion process. The primary geological and geophysical data, including spatial configuration of established crustal plates, is not contested in this thesis, only the global tectonic platform used to quantify the data.

The terms Earth expansion and expanding Earth model used in this thesis refer to crustal extension and lithospheric plate motion on an Earth whose surface area increases with time in sympathy with an increase in Earth radius. This increase in surface area is manifested primarily as extension within the oceanic mid-ocean-rift zones and as crustal extension within continental rift zones and sedimentary basins.

The investigation of Earth expansion dates back to the modelling studies of Hilgenberg (1933) and has since been extensively promoted by Carey (1958, 1976, 1988, 1996) and modelled by Vogel (1983, 1984, 1990). Past rejection of Earth expansion as a viable alternative tectonic concept dates back to the 1960s and 1970s, before the development of modern plate tectonics, and is based primarily on the inability of early researchers to quantify an expansion process and constrain expansion against time. Since the completion of modern global geological and geophysical data sets quantification of an Earth expansion process is now possible.

In contrast, conventional plate tectonic theory has been promoted to explain a diverse range of tectonic phenomena and is now widely accepted in science. The term conventional is used in this thesis to refer specifically to the plate tectonic model, characterised by lithospheric plate motion on an Earth of essentially fixed volume and surface area. In plate tectonic theory, palaeomagnetic determinations of

palaeoradius have been used to conclude that Earth's radius has remained approximately constant throughout geological history (eg. McElhinny & Brock, 1975). Based on this conclusion the outer lithospheric crust of the Earth is then portrayed as being segmented into a mosaic of rigid, shifting plates created at oceanic ridges, consumed at oceanic trenches and sliding past one another along transform faults (Chatterjee & Hotton, 1992). Chatterjee & Hotton (1992) consider that this dynamic model links all geologic phenomena, from the age and composition of sea floors to the rise of mountains and the past distribution of flora and fauna.

Intensive geological and geophysical research since the introduction of both Earth expansion and plate tectonic theories has now increased the global database available to thoroughly test all global tectonic theories. In particular, space geodetic, palaeomagnetic, palaeogeographic, palaeobiogeographic and palaeoclimatic studies have advanced to enable quantification of plate reconstruction of continents and their displacement histories throughout geological time. An important geophysical contribution to the quantification of modern global tectonics has been the completion of oceanic magnetic mapping and radiometric and palaeontologic age dating of crust beneath all Earth's major oceans. This oceanic mapping has placed finite time constraints on the plate motion history of all ocean basins back to the Early Jurassic, and is now available to quantify plate reconstruction and rate of crustal generation on both plate tectonic and expanding Earth models.

Previous research into post-Triassic Earth expansion (Maxlow, 1995) utilised the oceanic mapping of CGMW & UNESCO (1990) to constrain plate reconstructions on models of an expanding Earth extending from the Recent to Early Jurassic. By successively removing oceanic geology from along mid-ocean-ridge spreading axes shown in CGMW & UNESCO (1990), and reuniting the primary continental and oceanic plates at reduced Earth radii, Maxlow (1995) demonstrated that all crustal plates reunite with a better than 99% fit-together for each model constructed. It was concluded from this research that, oceanic magnetic mapping provides a definitive means to test and quantify a potential rate of Earth expansion and a means to constrain plate configuration with a precision not previously available to early researchers. The post-Triassic modelling studies by Maxlow (1995) then prompted the need to extend research to the Archaean by incorporating continental geology and applying the concept of Earth expansion to modern geological and geophysical data.

1.1 Research Objectives

The primary objective of this thesis is to investigate the concept of Earth expansion as an explanation for observed Archaean to Recent global geological and geophysical data. To achieve this objective a series of 24 spherical models of an expanding Earth have been constructed using 300 millimetre diameter polystyrene foam spheres. These spheres have then been digitally resized to the same scale to display and present global geological and geophysical data in an expanding Earth conceptual framework.

The constructed spherical models form the basis for secondary objectives, including:

1. The reconstruction of oceanic and continental geology on each expanding Earth model, ranging in age from the Archaean to Recent.
2. An application of mathematical constraints to the models to investigate the rate and variation of a potential Archaean to Recent Earth expansion process.
3. Speculation on a potential future expansion of the Earth by reconstructing oceanic and continental geology at 5 million years into the future.
4. The use of published palaeomagnetic data to locate palaeopoles and establish palaeoequators and palaeogeographical grids on each expanding Earth model.
5. An investigation into the distribution of global geological and geophysical data in relation to reconstructed geology and the established palaeogeographical grids.
6. An investigation into the geological history of Australia in relation to adjoining continents.
7. Speculation on a proposed model for the causal mechanisms of Earth expansion, from the pre-Archaean to the distant future.

It is acknowledged that if the concept of Earth expansion is wrong then the global geological and geophysical data will highlight any inconsistencies on the expanding Earth models. It is also acknowledged that specific studies in each of the geological and geophysical fields to be investigated, when taken out of conventional plate tectonic context, may lead to quite different interpretations to accepted plate tectonic practice. Provision is made to compare and contrast these interpretations and present Earth expansion as a viable alternative tectonic concept.

1.2 Research Methodology

On a celestial scale, the Earth can be considered a sphere and spherical models represent the best means to display geological and geophysical data. Traditional map projections cannot be used to model this data on an expanding Earth because of inherent unrealistic projection distortion and the difficulty in reconstructing accurate global plate configurations in a map format.

This research therefore represents the first time that modelling of the Earth's crust to the Archaean has been attempted and the first time that continental and oceanic geology has been utilised for plate reconstruction. To achieve the objectives of this research, research methodology will involve four interactive phases, with each phase dependant on the completion and quantification of the previous.

The four phases include:

1. **Empirical modelling**: Construction of a series of 24 spherical models of an expanding Earth, ranging from the Archaean to 5 million years into the future, by utilising published maps of Phanerozoic and Precambrian continental and oceanic geology to constrain palaeoradius and plate configuration. These empirical models are used to determine a mathematical expression for a potential rate of Earth expansion to enable palaeoradius to be constrained against time.
2. **Database Modelling**: Application of published global geological and geophysical data to the expanding Earth models to investigate the spatial and temporal distribution of the data within a conceptual expanding Earth tectonic framework. This information is to be used to establish the interdisciplinary relationships and to compare and contrast with conventional plate tectonic distributions.
3. **Detailed Study**: To use this conceptual framework to investigate the spatial and temporal tectonostratigraphic history of Australia, with emphasis on the metallogenic distribution with respect to adjoining intercontinental cratons.
4. **Speculation**: To speculate on a causal mechanism for a potential Earth expansion process from the pre-Archaean to the future, based on the results of the empirical expanding Earth models and the distribution of applied geological and geophysical data.

1.3 Thesis Presentation

Because of the difficulty in displaying the large amount of spherical modelling involved in this research coloured figures are used wherever possible, with video animations replacing selected figures in a CD-ROM disc (Appendix A6; back cover of Volume 2 of 2). The video animations listed in Appendix A6 are accessed via hyperlinks within the CD-ROM as required. It is advisable to read the text in conjunction with these video animations in order to gain a full four-dimensional visual appreciation of the expanding Earth concept.

Videos have been created from a series of 72 GIF images of each expanding Earth model taken at intervals of 5° longitude and centred on the established equator. These images are then assembled into video clips in Adobe Premiere version 5.0 at 640 x 480 pixel frame size, 24 fps frame rate and saved in MPG file format. The range of video clips (Appendix A6) include:

1. Video clips of each individual model at an as-constructed 300mm diameter model size.
2. Video clips of each individual model digitally re-sized to the same scale.
3. Video clips of both as-constructed and re-sized Archaean to Future models assembled into extended video strings.

1.4 Post-Triassic Expanding Earth Research

Research into post-Triassic Earth expansion was presented in Maxlow (1995). This research utilised the oceanic magnetic mapping of CGMW & UNESCO (1990) to recreate models of an expanding Earth previously constructed by Hilgenberg (1933), Barnett (1962) and Vogel (1983). Oceanic magnetic mapping was not available to these early model makers and its completion represents a means to accurately constrain post-Triassic reconstructions and a means to quantify palaeoradius against time.

It was concluded from the oceanic model studies presented in Maxlow (1995) that post-Triassic Earth expansion is a viable tectonic process, which justifies extending research back to the Archaean and speculating on expansion into the future. This thesis uses Maxlow (1995) as a basis to extend and elaborate on the concept of Earth expansion by additional modelling studies and extensive global data

investigation. The following is a brief summary of the geological implications addressed in Maxlow (1995).

Since the modelling studies of Hilgenberg (1933), Barnett (1962, 1969) and Vogel (1983, 1984, 1990) it has been demonstrated that if all of the Earth's continents were fitted together they would neatly envelope the Earth with continental crust at approximately 55 to 60 percent of the present Earth size. This led Hilgenberg (1933) to conclude that Earth expansion resulted in the break-up and gradual dispersal of continents as they moved radially outwards during geological time. Vogel (1983) suggested it was also theoretically possible for the continents, without shelves, to fit together at approximately 40 percent of the present Earth radius by considering that continental shelves were formed after the continental crust had fragmented. Vogel (1983) concluded from his modelling studies that the Earth has expanded with time, from an early Pangaean configuration to the Recent, with continental separation caused by a radial expansion of the Earth.

Carey (1958), in researching the concept of continental drift, demonstrated that if all the continents were reassembled into a Pangaean configuration on a model representing the Earth's modern dimensions, the fit was reasonably precise at the centre of the reassembly and along the common margins of north-west Africa and the United States east coast embayment, but became progressively imperfect away from these areas. Carey (1958) concluded from this research that the fit of the Pangaean reassembly could be made much more precise in these areas if the diameter of the Earth was smaller at the time of Pangaea. With the acceptance of plate tectonics, these basic observations and conclusions of Carey (1958) have since been ignored.

To quantify a variation in Earth's palaeoradius and constrain post-Triassic plate configuration with time using oceanic mapping, it was considered necessary to take into account the area and sea-floor pattern of post-Triassic oceanic lithosphere (Maxlow, 1995), portrayed in global geological maps such as Larson *et al.* (1985) and CGMW & UNESCO (1990). By using the method of least squares to calculate gradients of curves of best fit from digitised cumulative oceanic area data, the goodness of fit of the resultant curves was best described by an exponential increase in lithospheric area with time. Palaeoradius was then determined from this cumulative area data and an equation for a post-Triassic increase in palaeoradius of the Earth established.

To present Earth expansion as a viable global tectonic concept and test the derived mathematical expression for expansion a series of eleven spherical models were constructed in Maxlow (1995) utilising the global geologic data of CGMW & UNESCO (1990) (Figure 1.1). These models demonstrate that continents, when reconstructed on an expanding Earth, coincide fully with the sea floor spreading and geological fit-data and accord with the derived mathematical expression for palaeoradius. This coincidence applied not only to the passive margin oceans, where conventional reconstructions agree in principle, but also to the Pacific Ocean where the necessity for subduction of all or part of the oceanic lithosphere generated at spreading ridges was contested. Maxlow (1995) demonstrated that the mechanism of sea-floor spreading defined by oceanic mapping provides a definitive means to accurately quantify post-Triassic Earth expansion.

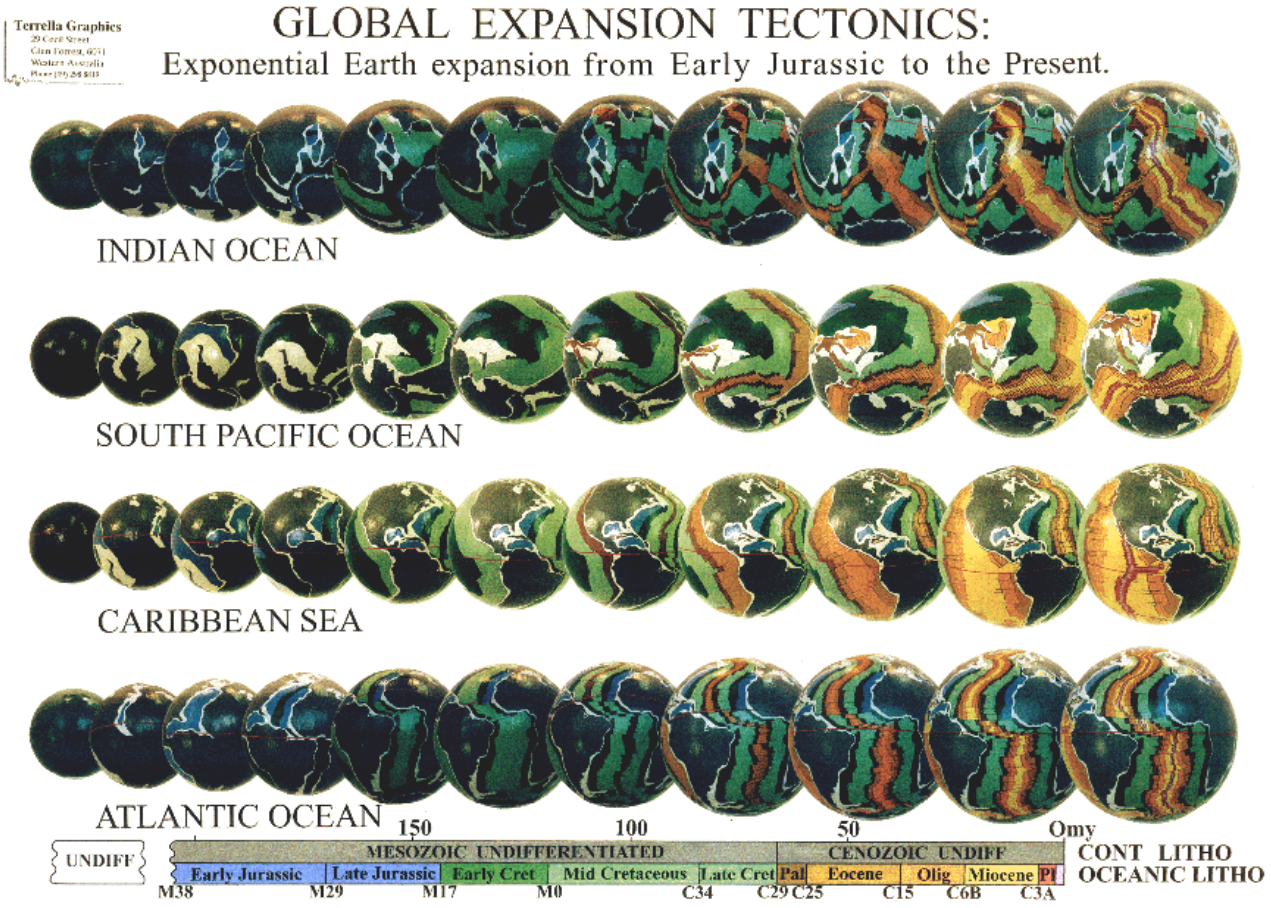

Figure 1.1 Spherical models of post-Triassic Earth expansion (after CGMW & UNESCO, 1990). Models demonstrate that continents reconstructed on an expanding Earth coincide fully with sea-floor spreading and geological data and accord with a derived mathematical expression for an exponential increase in palaeoradius (after Maxlow, 1995).

Models for relief of surface curvature and orogenesis during Earth expansion were considered at length by Rickard (1969), Carey (1975, 1976, 1983b, 1988) and Glikson (1979). Relief of surface curvature was an expression used by Maxlow (1995) defining a process of crustal adjustment by intracratonic motion and gravity induced collapse to relieve vertically induced crustal stresses during an increase in palaeoradius. Orogenesis on an expanding Earth was restricted to zones of intracratonic to intracontinental interaction, magmatism and syn-kinematic metamorphism, resulting from gravity induced collapse, isostatic adjustment and relative motion of proto-continents as they adjusted for changing surface curvature.

Post-Triassic orogenesis on an expanding Earth was considered to be intimately related to a process of asymmetric expansion (Maxlow, 1995). Asymmetric Earth expansion resulted in a northward shift of the continents during continental break-up, with a preferential development of oceanic crust and opening of oceans in the southern hemisphere. This asymmetric expansion initially resulted in establishment of large epi-continental sedimentary basins, prior to continental break-up and dispersal to the Recent. The post-Triassic expanding Earth models (Figure 1.1) empirically demonstrate the onset of Alpine-Himalayan orogenesis as continental crust fragmented, interacted and dispersed during an accelerating post-Triassic increase in surface area.

Rickard (1969) and Carey (1975, 1976, 1983b, 1988) put forward models for orogenesis and geosynclinal development under conditions of surface curvature adjustment and demonstrated that continental collision may not be required to promote orogenesis, as required by plate tectonics. The magnitude of both horizontal shortening and extension of crust, during isostatic adjustment of surface curvature, demonstrated the potential for both tangential and radially directed motion acting within a continental plate during expansion of the Earth. The radial and tangential vector components of this expansion process gave rise to a continuum of orogenic models.

During Earth expansion the whole column of atmosphere, hydrosphere, oceanic lithosphere and underlying mantle was considered to have been added at an accelerating rate through geological time (Maxlow, 1995). Carey (1983b) suggested that this column is accreted primarily at the mid-ocean-spreading ridges and rift zones with the generation of ocean water and atmosphere keeping pace with the growth of oceanic lithosphere.

The nature of mantle fluids and mantle metasomatism indicated (eg. Anderson, 1975; Wyllie, 1979; Jackson & Pollark, 1987; Menzies & Hawkesworth, 1987) that the volatile species in the system C-O-H-S can exist in the Earth's mantle in volatile bearing minerals, dissolved in silicate- or carbonate-rich melts, in a separate supercritical fluid or possibly in a dense silicate-volatile fluid. It was considered by Eggler (1987) that solution of volatiles in crystalline minerals represents a significant repository for volatiles. During Earth expansion, retention of these species within the mantle may be possible by potentially high P-T (pressure, temperature) and low g (surface gravity) conditions (Maxlow, 1995). Devolatilization of the C-O-H-S system to form the hydrosphere and atmosphere then becomes a progressive and possibly accelerating process of devolitilisation of the mantle with time, as a direct consequence of a variation in the prevailing P-T-g conditions.

Palaeomagnetics is traditionally considered the cornerstone of modern plate tectonics and was extensively interrogated in Maxlow (1995). Fundamental premises regarding the constancy of continental surface area, used to determine palaeoradius from palaeomagnetics, originate from the early 1960s prior to development of modern global tectonic concepts and completion of the oceanic crustal database. Mathematical equations developed by palaeomagneticians insist that continental surface areas have remained essentially constant (eg. van Hilten, 1968) and any variation in palaeoradius has been negligible with time (McElhinny & Brock, 1975). Since the establishment of palaeomagnetics, modern global tectonic concepts have demonstrated that the Earth's crust is not a passive adjunct of lithospheric plates but a dynamic, interactive layer of the Earth (Grant, 1992). The application of palaeomagnetics to determine a palaeoradius of the Earth was then considered by Maxlow (1995) to be misleading and in need revision.

The potential causes of Earth expansion were investigated by Maxlow (1995) and extensively reviewed by Egyed (1963), Wesson (1973) and Carey (1983a). Five main themes were considered, including:

1. **A pulsating Earth** where cyclic expansion of the Earth opened the oceans and contractions caused orogenesis (eg. Khain, 1974; Steiner, 1967, 1977; Milanovsky, 1980; Smirnoff, 1992; Wezel, 1992). This proposal failed to satisfy exponentially waxing expansion. Carey (1983a) considered the theme to have

arisen from a misconception that orogenesis implies crustal contraction and saw no compelling evidence for intermittent contractions.

2. **Meteoric and asteroidal accretion** (eg. Shields, 1983a, 1988; Dachille, 1977, 1983; Glikson, 1993). This was rejected by Carey (1983a) as the primary cause of Earth expansion since expansion should then decrease exponentially with time. It also does not explain ocean floor spreading.
3. **A constant Earth mass** with phase changes of an originally super-dense core: (eg. Lindemann, 1927; Egyed, 1956; Holmes, 1965; Kremp, 1983). Carey (1983a) rejected this because he considered the theme to imply too large a surface gravity throughout the Precambrian and Palaeozoic.
4. **A secular reduction of the universal gravitation constant, G** (eg. Ivanenko & Sagitov, 1961; Dicke, 1962; Jordan, 1969; Crossley & Stevens, 1976; Hora, 1983). Such a decline of G was considered to cause expansion through release of elastic compression energy throughout the Earth and phase changes to lower densities in all shells. Carey (1983a) again rejected this proposal as the main cause of expansion for three reasons: a) that surface gravity would have been unacceptably high; b) that the magnitude of expansion would probably be too small and; c) the arguments for a reduction in G were considered not to indicate an exponential rate of increase.
5. **A cosmological cause involving a secular increase in the mass** of the Earth (eg. Hilgenberg, 1933; Kirillov, 1958; Blinov, 1973, 1983; Wesson, 1973; Carey, 1976; Neiman, 1984, 1990; Ivankin, 1990).

Carey (1983a) considered that the first four proposals for cause of Earth expansion are soundly based and may have contributed in part to Earth expansion. Potential limitations on surface gravity in the past (eg. Stewart, 1977, 1978, 1983) suggested to Carey (1983a) that there may be no alternative but to consider an exponential increase of Earth mass with time as the main cause for expansion. Where the excess mass came from was considered at length by Carey (1983a, 1988, 1996) and he suggested that new mass added to the Earth must occur deep within the core. The ultimate cause of Earth expansion must however be sought in conjunction with an explanation for the cosmological expansion of the Universe (Carey, 1996).

It was concluded in Maxlow (1995) that post Triassic Earth expansion is a viable alternative global tectonic process which enables the dynamic principles behind all major geologic phenomena to be resolved and readily explained.

2. EMPIRICAL MODELLING OF GEOLOGICAL MAPPING

Empirical modelling and investigation into the potential for Earth expansion from the Archaean to Recent is based on the global geology shown in the *Bedrock Geology of the World* map (CGMW & UNESCO, 1990) (Figure 2.1) and accompanying legend (Figure 2.2). The geology in this map is time-based, with continental basement geology representing the major geological Eras and oceanic basement geology representing geological Periods from the Jurassic to Recent.

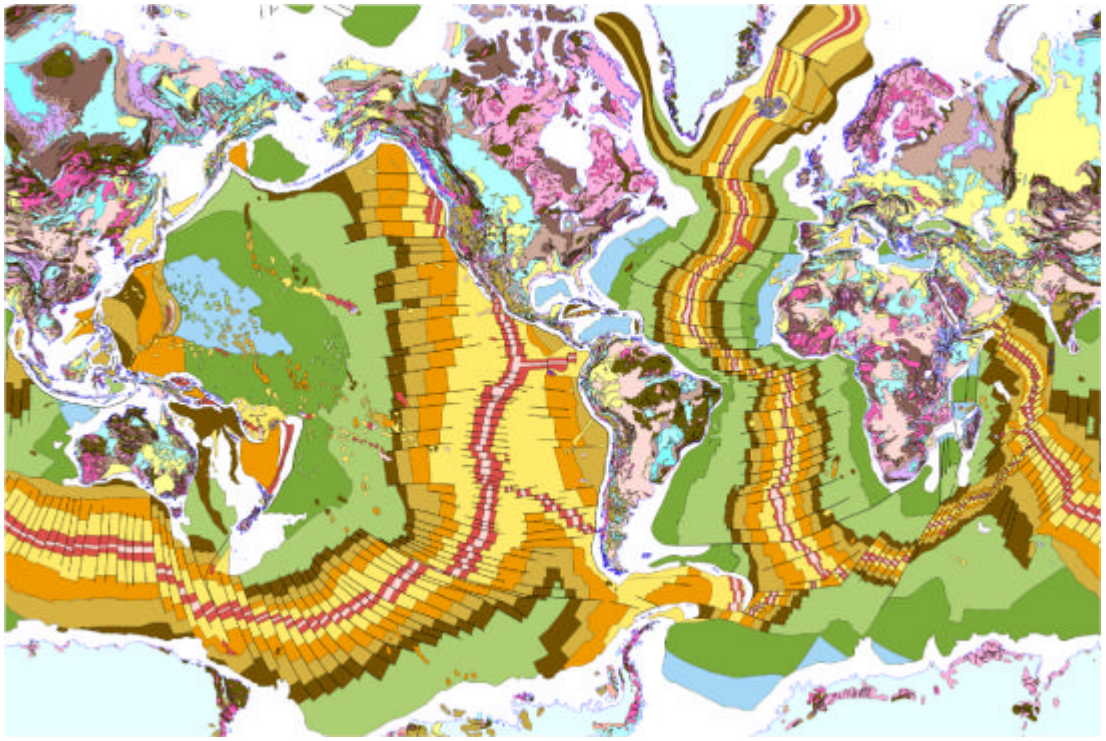

Figure 2.1 Digitised Geological Map of the World. Map is shown in conventional Mercator map projection extending to 80 degrees north and south latitude only. For legend see Figure 2.2. Continental bedrock geology represents major geological Eras and oceanic geology represents geological Periods from the Recent to Jurassic (digitised with permission after CGMW & UNESCO, 1990).

The oceanic basement geology (Figure 2.1) originates from magnetometer surveys, ocean drilling, and radiometric and palaeontologic age dating over the oceans and mid-oceanic-ridges (MOR) carried out since the 1960s. These surveys revealed total magnetic field anomalies that are symmetrical about and parallel to mid-ocean-ridge axes. Anomalies were interpreted by Vine & Mathews (1963) and Morley & Laurchelle (1964) as evidence for sea-floor spreading, where mantle-derived basaltic lava wells up along the length of the ridge axes as the central

spreading zones are continuously widened. As the erupted basaltic lava cools it retains a permanent magnetisation with a polarity identical to the ambient magnetic field of the time. The continuous injection of basalt at ridge axes, in the presence of an irregularly reversing magnetic field, then produces a characteristic pattern of alternating polarities on each side of the ridge axes.

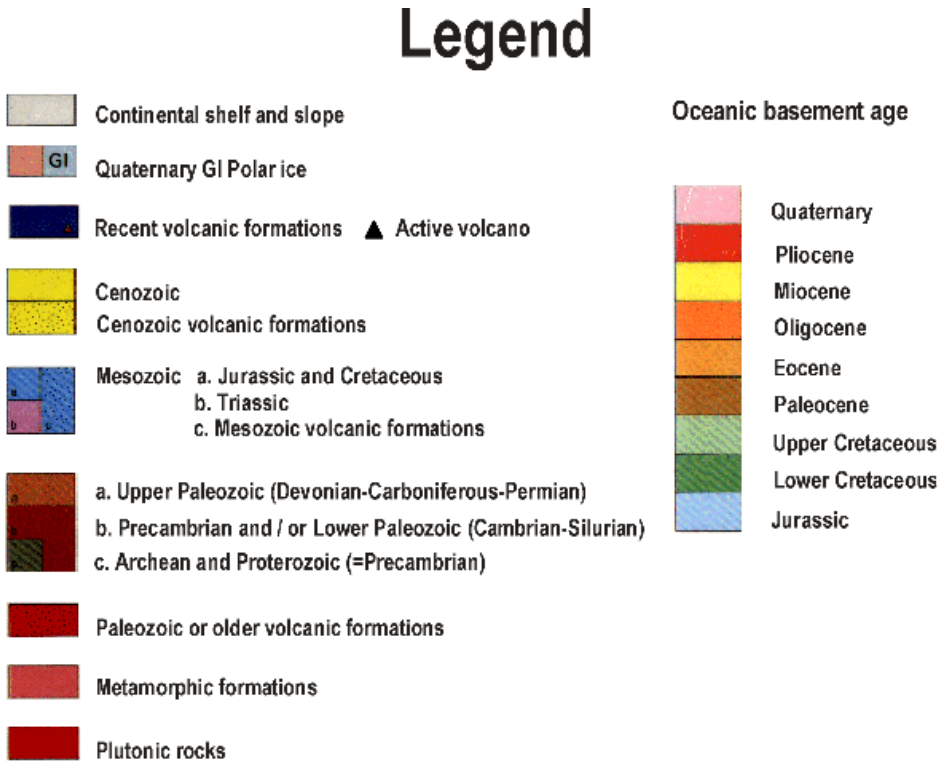

Figure 2.2 Legend for continental and oceanic geology. Some colour variation occurs between expanding Earth models and the legend colours are a guide only. (After CGMW & UNESCO, 1990).

The distribution of oceanic geology (Figure 2.1) demonstrates that all the oceans contain mid-oceanic-ridges, and distribution of geology symmetrically about and parallel to mid-ocean-ridge axes demonstrates that all the oceans are undergoing extension approximately normal to the ridge axes. This observation is substantiated by space geodetic determinations of plate motion where present geodetic rates compare with the post-Pliocene magnetic plate history (eg. DeMets *et al*., 1990).

In conventional plate tectonic theory it is presumed that the Earth's radius is static with time, hence lithosphere generated at spreading ridges displaces pre-existing lithosphere, which is then disposed of elsewhere by subduction. For an Earth undergoing expansion it is presumed that lithosphere generated at spreading axes is a reflection of an increase in Earth radius with time, ranging from partial expansion,

where some pre-existing lithosphere and some subduction is required, to full expansion where no pre-existing lithosphere and no subduction is required.

In both plate tectonic and Earth expansion theories it is inferred that, by moving backwards in time successive geological intervals parallel to each of the mid-ocean spreading ridges (Figure 2.1) must then be removed and adjacent plates must be reunited along their common mid-ocean-ridge axes.

2.1 Lithospheric Budget

The accountability of continental and oceanic crustal surface area was addressed in Maxlow (1995) and is summarized in Figure 2.3 for the Triassic to Recent. Earth's lithospheric budget was determined by computing the cumulative surface areas of oceanic magnetic mapping to the limit of the data shown (chron M38, approximately 205 Ma) (Table 2.1 of Maxlow, 1995), based on the oceanic magnetic mapping of Larson *et al.* (1985) and CGMW & UNESCO (1990).

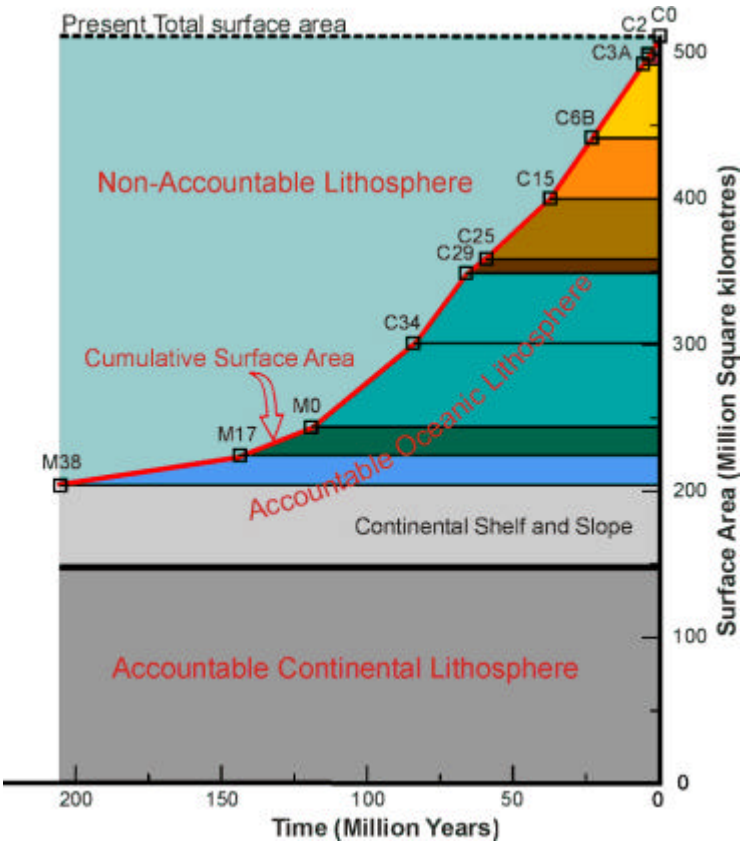

Figure 2.3 Accountability of present-day continental and oceanic crust. Red line represents cumulative surface areas of continental and oceanic crust at chron intervals shown and present total surface area is shown as dashed line at top. Accountable oceanic and continental lithosphere lies below the red line and non-accountable lithosphere is shown above. (After Maxlow, 1995; data after: Larson *et al*., 1985; CGMW & UNESCO, 1990).

The cumulative surface areas of Triassic to Recent oceanic lithosphere can be compared to the present total surface area (Figure 2.3). Areas of accountable oceanic and continental lithosphere are shown below the cumulative surface area curve and non-accountable, or presumed pre-existing lithosphere is shown between the cumulative surface area curve and the present total Earth surface area line (Figure 2.3). Non-accountable lithosphere represents the total surface area of continental and oceanic lithosphere, which must have existed prior to inferred subduction if a constant Earth surface area is to be maintained since the Triassic.

The accountability of both oceanic and continental lithosphere can be investigated by considering the premises of the three main global tectonic theses:

1. **Constant Earth radius (Plate tectonics)**: where excess lithosphere generated at spreading centres is continuously disposed of along subduction zones, displacing and recycling pre-existing lithosphere into the mantle. To maintain a constant surface area it must be presumed that non-accountable lithosphere existed prior to subduction. No record of this lithosphere exists and an explanation must be provided for the accelerating rate of increase in surface area shown.
2. **Partial increase in Earth radius**: where excess lithosphere is disposed of along subduction zones during limited Earth expansion (eg. Owen, 1976; Steiner, 1977). To maintain a partially cumulative surface area it must be presumed that some non-accountable lithosphere existed prior to partial subduction. The accelerating increase in surface area, since the Triassic, must again be explained.
3. **Increasing Earth radius (Earth expansion)**: where lithosphere generated at spreading centres is cumulative with time and the increase in surface area since the Triassic results from an increase in palaeoradius. On an expanding Earth, non-accountable lithosphere does not exist, subduction is not required and cumulative surface area is a measure of the rate of change in palaeoradius.

Both Earth expansion and plate tectonic theories represent end-points of a spectrum of global tectonic possibilities. Plate tectonics has been adequately tested elsewhere and partial expansion extensively tested by Owen (1976), while full Earth expansion has never been tested using modern oceanic and continental mapping.

For an expanding Earth the cumulative oceanic surface area data represents a means to quantify a potential rate of increase in palaeoradius, in keeping with the primary assumption that Earth's radius has increased with time. This thesis is primarily concerned with testing the extreme case of Earth expansion, where no subduction and no pre-existing, non-accountable lithosphere is required.

2.2 Rate of Earth Expansion

A rate of potential Earth expansion was determined in Maxlow (1995) by digitising the areas of post-Triassic oceanic mapping data (after Larson *et al*., 1985) and mathematically modelling the resultant cumulative lithospheric surface areas using formulae developed by Koziar (1980) and Blinov (1983). This rate was then confirmed by utilising the oceanic mapping of CGMW & UNESCO (1990). A linear regression analysis of cumulative surface area data demonstrated that the goodness of fit of the data was best described by an exponential increase in surface area with time. From this empirical cumulative surface area data a mathematical expression for post-Triassic exponential increase in Earth palaeoradius was derived and palaeoradius determined (Figure 2.4).

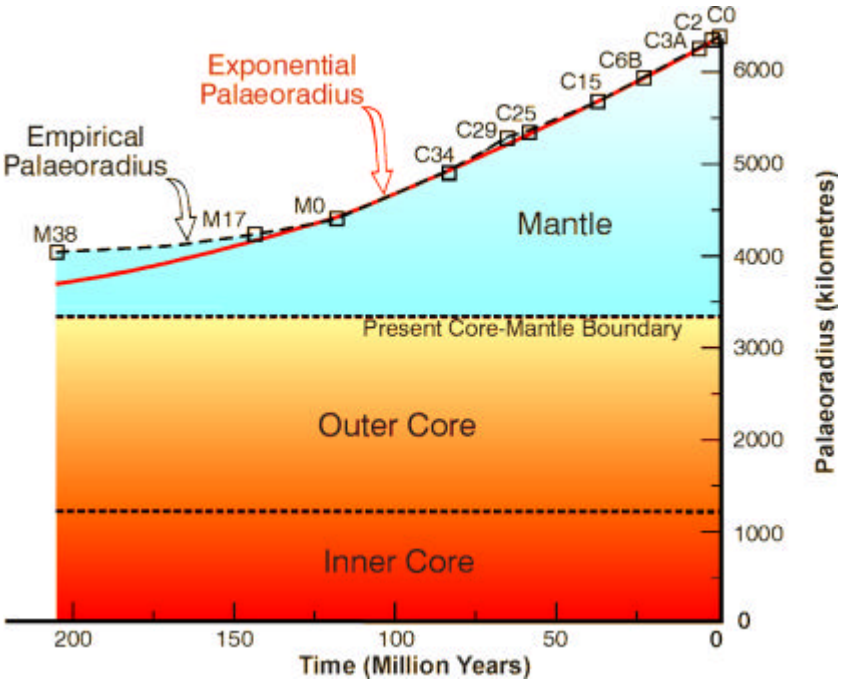

Figure 2.4 Palaeoradius of the Earth from the Triassic to Recent. Palaeoradius is calculated from digitised areas of post-Triassic oceanic mapping data, after Larson *et al*. (1985) and CGMW & UNESCO (1990). Shortfall in measured palaeoradius between M17 and M38 represents accumulation of marginal basin sediments along continental slopes and shelves. (After Maxlow, 1995).

In contrast to the finite constraint provided by post-Triassic oceanic mapping, determining a mathematical expression for rate of potential Earth expansion from the Archaean to Recent depends on establishing a Precambrian primordial Earth radius.

A number of possible scenarios are summarised in Figure 2.5, ranging from adoption of the present total continental surface area (Figure 2.5, Curve A), to an estimate of the total surface area of preserved Archaean crust (Figure 2.5, Curve D). Studies carried out by Blatt & Jones (1975) to determine the relationship between sedimentary rock age and amount of outcrop area on the present land surface, while speculative, demonstrate a lognormal increase in outcrop area with time. This data is plotted as a cumulative percentage of total continental surface area and, when converted to a radius curve (Figure 2.5, Curve C), provides a further potential constraint to palaeoradius during the Neoproterozoic and Phanerozoic.

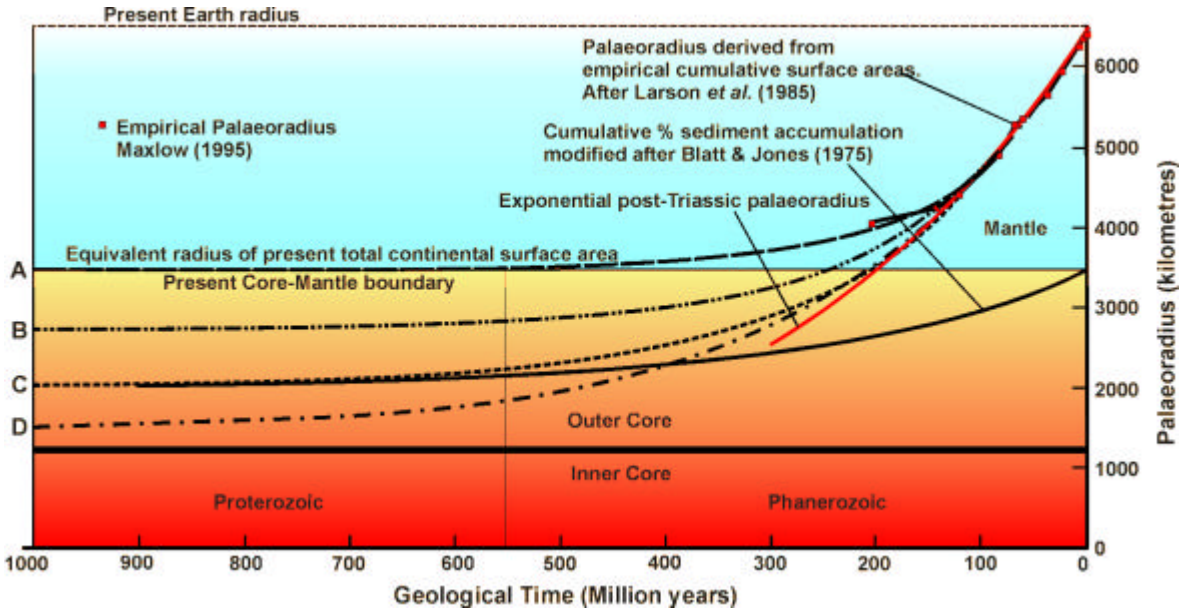

Figure 2.5 Constraints to determining a Precambrian primordial Earth radius. Data is shown as time-variant palaeoradii for all curves. Curves depict Earth expansion constrained by Curve A: the present total continental surface area; Curve B: present total continental surface area less marginal basins; Curve C: cumulative sediment areas (converted to equivalent palaeoradius after Blatt & Jones, 1975) and; Curve D: total estimated area of Archaean crust. (After Maxlow, 1995).

Because of the difficulty in quantifying a primordial Earth radius and estimating surface area of present-day Precambrian crust, the pre-Triassic modelling presented in this thesis is empirically constrained during model construction by reducing palaeoradius in incremental stages until Archaean cratonic complexes and Proterozoic basement rocks are assembled. This construction method involves progressive removal of all Phanerozoic and Late Proterozoic continental crust and

restoration of basins and rift zones to a pre-extension or pre-rift configuration (outlined in Section 2.5).

Unlike the modelling studies of Koziar (1980) and Vogel (1983), Proterozoic sedimentary basins are also partially removed during modelling to allow for formation of Proterozoic to Archaean extensional basin settings (eg. Etheridge *et al*., 1987, for ensialic extension within the Palaeoproterozoic basins of northern Australia). This results in an Archaean-Mesoproterozoic model, comprising Archaean and remnant Palaeoproterozoic basement rocks, with an indicated primordial Earth radius of approximately 1700 kilometres. This empirically derived primordial Earth radius represents a potential limiting palaeoradius for an Archaean to Early Proterozoic proto-Earth. The implications of a primordial Earth will be quantified in Chapter 3.0 by incorporating modern geological and geophysical data sets to the established expanding Earth framework.

A mathematical equation for an exponential rate of potential Earth expansion from the Archaean to Recent is then derived by considering the mathematical equation for linear regression:

$$y = Ax + B \qquad \text{Equation 2.1}$$

Where: y = the Y axis, x = the X axis, A = the gradient of a line, B = the y-intercept of the line.

For a linear increase in palaeoradius this equation is written as:

$$R = At + B \qquad \text{Equation 2.2}$$

Where: R = Earth radius, t = time before the present (negative).

To determine an exponential increase in palaeoradius Equation 2.2 can be written as:

$$\ln R_a/R_0 = At + B \qquad \text{Equation 2.3}$$

Where:ln = natural logarithm, R_0 = present Earth radius at time t_0, R_a = ancient Earth radius at time t_a.

Equation 2.3 simply expresses the exponential curve as a straight line, suitable for analysis using the linear regression Equation 2.1. Rearranging Equation 2.3 for palaeoradius:

$$R_a = R_0 e^{(At+B)} \qquad \text{Equation 2.4}$$

Where:e = base of natural logarithm.

Mathematical modelling of a rate of post Triassic Earth expansion in Maxlow (1995) demonstrated that the y-intercept B is negligible and can be disregarded. The

gradient of the line (A), representing palaeoradius, is a constant k. Equation 2.4 can then be written as:

$$R_a = R_0 e^{(kt)} \qquad \text{Equation 2.5}$$

The Archaean-Mesoproterozoic primordial Earth radius R_p, determined from empirical modelling (Section 2.4), is approximately 1700 kilometres. This represents the radius of an Archaean to Early Proterozoic proto-Earth at formation or crustal stabilisation. It is inferred that Earth expansion then increases exponentially from this primordial proto-Earth radius to the present radius. An equation for exponential increase in Earth radius from the Archaean to Recent is then expressed as:

$$\mathbf{R_a = (R_0 - R_p)e^{kt} + R_p} \qquad \text{Equation 2.6}$$

Where: $k = 4{\cdot}5366 \times 10^{-9}$/year.

The constant k is determined from Equation 2.3 by using post-Triassic palaeoradii derived from empirical oceanic data (Table 2.1 of Maxlow, 1995) and 1700 kilometres as the limiting primordial proto-Earth radius to solve for gradient A.

Exponential Earth expansion from the Archaean to Recent, calculated from Equation 2.6, is shown in Figure 2.6. The palaeoradius determined by Koziar (1980), based on a 2800 kilometre primordial Earth radius for the Late Neoproterozoic and by Vogel (1990), based on a 2850 kilometre primordial Earth radius for the late Neoproterozoic are also shown for comparison. Both Koziar (1980) and Vogel (1990) determined a primordial Earth radius by estimating the surface area of preserved Precambrian crust. The locations of expanding Earth models constructed in both Maxlow (1995) and in this thesis are also shown.

The exponential palaeoradius curve (Figure 2.6) suggests that during the early Archaean to late Mesoproterozoic Earth's palaeoradius remained relatively static, increasing by approximately 60 kilometres during 3 billion years of Earth history. Since the Mesoproterozoic the Earth has then undergone an accelerating expansion to the Recent. This accords with published literature (eg. Glikson, 1979) which suggests there is no evidence for Earth expansion prior to the Mesoproterozoic.

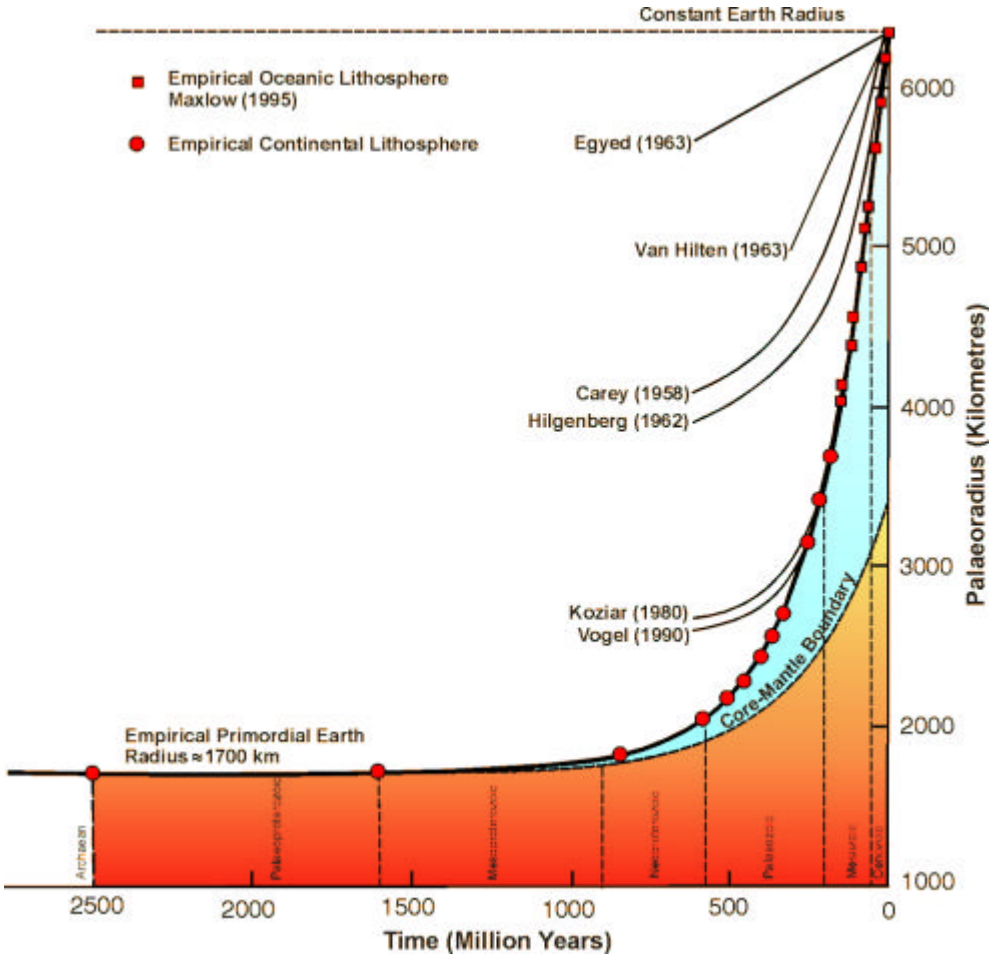

Figure 2.6 Exponential Earth expansion from the Archaean to Recent. Graph shows post-Triassic expansion derived from oceanic mapping and pre-Jurassic expansion derived from an Archaean primordial Earth radius of 1700 km. Palaeoradius determinations of Koziar (1980) and Vogel (1990), and early estimates of Egyed (1963), Van Hilton (1963), Carey (1958) and Hilgenberg (1962) are shown for comparison. Expanding Earth models constructed are shown as red coloured circles and squares. A suggested core-mantle boundary remains speculative. (After Maxlo w, 1995).

2.3 Kinematics of Earth Expansion

The potential incremental variations in the physical dimensions of an Earth undergoing expansion with time are qualified by considering radius, circumference, surface area and volume. Consideration is also given to mass, density and surface gravity under conditions of constant Earth mass and constant Earth density. The hypothetical variations in mass, density and derived surface gravity are included to qualify the postulated cause of Earth expansion proposed by Carey (1983a, 1988, 1996). Derivation of formulae used to determine these variables is included in Appendix A1.

The potential physical variation in radius, circumference, surface area and volume of an Earth undergoing expansion from the Archaean to Recent is shown in

Figure 2.7. Each graph shows a 3 billion year history of pre-Mesoproterozoic crustal stability, with palaeoradius increasing by approximately 60 kilometres, followed by a steady to rapidly accelerating period of expansion to the Recent.

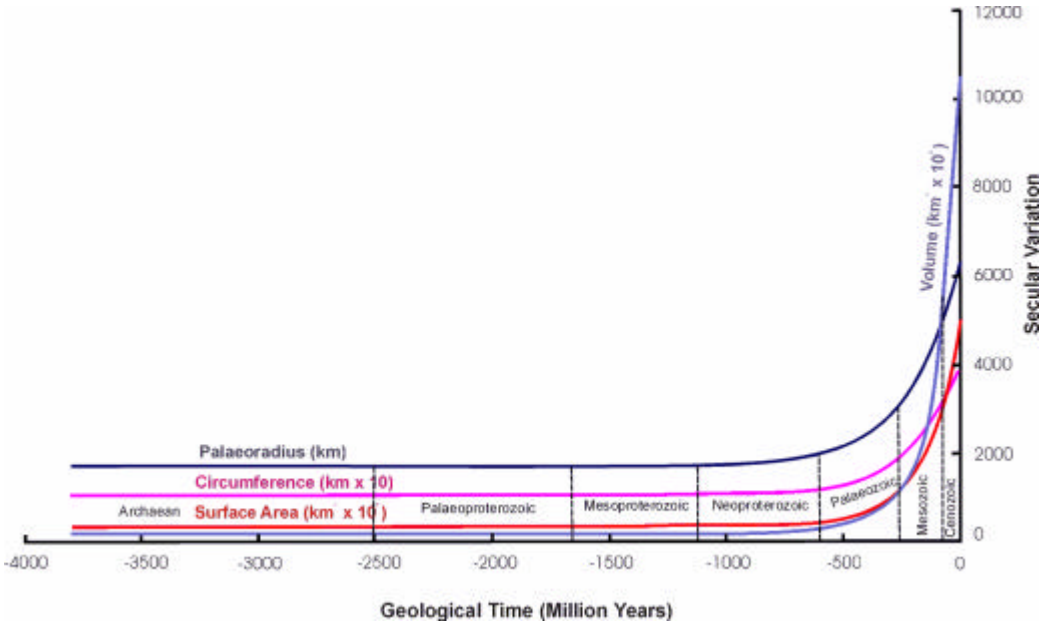

Figure 2.7 Physical variation of radius, circumference, surface area and volume. Graphs range from the Archaean to Recent and are derived from Equation 2.6. Each variable shows a 3 billion year history of pre-Mesoproterozoic stability, followed by a steady to rapid acceleration to the Recent.

Present annual variations in radius, circumference, surface area and volume are derived using Equation 2.6 (Appendix A1.3). The present annual incremental rates of potential Earth expansion are:

Radius	dR/dt_0 = 22 mm/year
Circumference	dC/dt_0 = 140 mm/year
Surface area	dS/dt_0 = 3·5 km^2/year
Volume	dV/dt_0 = 11,000 km^3/year

Present annual incremental rates of mass and surface gravity as a function of constant density are:

Mass	$dM/dt_0 = 60 \times 10^{12}$ tonnes/year
Surface gravity	$dg/dt_0 = 3{\cdot}4 \times 10^{-8}$ $msec^{-2}$/year

The incremental rates of Earth expansion determined here compare favourably with estimations derived from published data. For example, Steiner (1977) estimated a global rate of areal sea-floor spreading during the past 5 m.y. of

3·19 km^2/yr. This equates to a calculated rate of radial expansion of 20 mm/yr. Also, Garfunkel (1975) calculated an areal spreading rate of 3·15 km^2/yr and Parsons (1982) 3·45 km^2/yr, which equate to radial expansion rates of 20 and 23 mm/yr respectively. These figures are substantiated by early space geodetic measurements of intercontinental chord lengths, with a speculative rate of increase in Earth radius calculated by Parkinson (in Carey, 1988) of 24 ± 8 mm/yr and a global mean value calculated by Robaudo & Harrison (1993) of 18 mm/yr.

The rate of equatorial circumferential expansion of the Earth was calculated by Blinov (1983) to be 120 mm/yr by considering relative plate motions in the Pacific, Atlantic and Southern Oceans, giving a rate of radial expansion of 19·1 mm/yr. Using areas of oceanic magnetic data, Steiner (1977) calculated the average ocean-basin-wide sea-floor spreading rates for the past 5 m.y. to be approximately 96 mm/yr for the Pacific Ocean, 76 mm/yr for the Indian Ocean and 43 mm/yr for the Atlantic Ocean which, although not equatorially or meridionally aligned, approximate the present-day calculated rate of 140 mm/yr increase in equatorial circumference.

For a hypothetical Earth expanding as a function of a constant Earth mass, density (Figure 2.8, Curve B) decreases exponentially from a peak of approximately 290 grams/cm^3 during the Archaean and Palaeoproterozoic, to a present value of 5·52 grams/cm^3 and approaches zero at about 300 million years in the future. Assuming that the universal gravitation G is constant, or near constant throughout Earth's history, surface gravity (Figure 2.8, Curve C) decreases exponentially from a peak value of approximately 138 metre sec^{-2} during the Archaean and Palaeoproterozoic, to 95 metre sec^{-2} during the Cambrian, 9·8 metre sec^{-2} during the Recent and approaches zero at about 300 million years in the future.

For a hypothetical Earth expanding as a function of constant density, mass (Figure 2.8, Curve D) increases exponentially from approximately 1·1 x 10^{23} kilograms during the Archaean and Mesoproterozoic, to a present value of 5·97 x 10^{24} kilograms and 190 x 10^{24} kilograms at about 300 million years in the future. Assuming that G is constant, or near constant throughout Earth's history, surface gravity (Figure 2.8, Curve F) increases exponentially from approximately 2·6 metre sec^{-2} during the Archaean and Mesoproterozoic, to approximately 30 metre sec^{-2} at about 300 million years in the future.

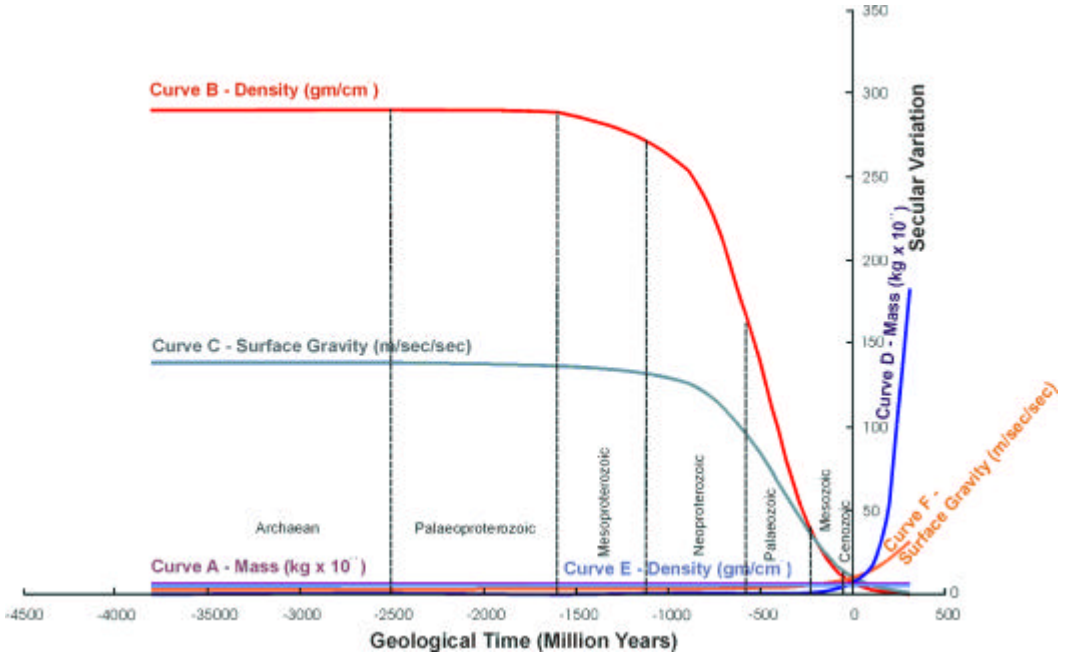

Figure 2.8 Kinematics of mass, density and surface gravity. Graphs are shown for conditions of constant mass (Curves A, B, C) and exponentially increasing mass (Curves D, E, F). The graphs suggest that an increasing mass scenario is more representative of the planets within the present Solar System and qualifies the conclusions of Carey (1983a).

The kinematics of mass, density and surface gravity shown in Figure 2.8 represent the end-points of possible causes of Earth expansion. Without additional cosmological constraints the exact kinematics, and hence cause of Earth expansion is indeterminate. At a constant mass, the Earth's density and surface gravity during the Precambrian is shown (Figure 2.8) to be excessively high when compared to the densities and surface gravity of the present Sun and outer planets of the Solar System (eg. Stacey, 1977). As Carey (1983a) concluded, because of the limitations of surface gravity (eg. Stewart, 1977, 1978, 1983) in the past, there may be no alternative but to consider an exponential increase in Earth mass with time as the primary cause of Earth expansion.

2.4 Spherical Earth Models

Spherical models are the best means of displaying and quantifying geological and geophysical data on an Earth undergoing expansion from the Archaean to Recent. Traditional map projections cannot be used to model this data because of inherent projection distortions and difficulty in reconstructing accurate plate configurations in

a two dimensional format. A set of eleven models were constructed by Maxlow (1995), ranging from the Early Jurassic to Recent, using oceanic magnetic mapping and continental outlines only (Figure 1.1). These models have been reconstructed during this research to include both oceanic and continental geology (Video A1.1a), and modelling is extended to the Archaean (Video A1.1b).

The primary base map used during construction (CGMW & UNESCO, 1990; Figure 2.1) provides a comprehensive global coverage of both continental and oceanic time-based geology. Although some cartographic discrepancies were noted in this map, for the purpose of this thesis the map is accepted in its entirety with minor cartographic modification as required.

A set of twenty four spherical models have been constructed, twenty three covering the Archaean to Recent and one projected to five million years into the future. This is the first time that both oceanic and continental geology has been modelled on an expanding Earth, and the first time that modelling has been extended to the Archaean and speculated into the future (Table 2.1) (Video A2.10).

Table 2.1. Expanding Earth models constructed for the Archaean to Future. Table shows sequential model number, geological Period or Era, approximate age and palaeoradius of each model constructed.

Model N^{o}	Geological Period/Era	Approx Age	Palaeoradius
1	Archaean to Mesoproterozoic	1·6 Ga	1703 km
2	Mid Neoproterozoic	850 Ma	1799 km
3	Late Neoproterozoic	700 Ma	1895 km
4	Late Neoproterozoic	600 Ma	2007 km
5	Cambrian	565 Ma	2060 km
6	Mid Ordovician	455 Ma	2293 km
7	Mid Silurian	420 Ma	2395 km
8	Early Devonian	380 Ma	2533 km
9	Late Devonian	360 Ma	2612 km
10	Early Carboniferous	320 Ma	2794 km
11	Early Permian	260 Ma	3136 km
12	Triassic	245 Ma	3237 km
13	chron M34 - Early Jurassic	205 Ma	3543 km
14	chron M29 - Late Jurassic	160 Ma	3960 km
15	chron M17 - Early Cretaceous	144 Ma	4130 km
16	chron M0 - Mid Cretaceous	118 Ma	4435 km
17	chron C34 - Late Cretaceous	84 Ma	4891 km
18	chron C29 - Paleocene	66 Ma	5162 km
19	chron C25 - Eocene	59 Ma	5274 km
20	chron C15 - Oligocene	37 Ma	5649 km
21	chron C6B - Miocene	23 Ma	5908 km
22	chron C3A - Pliocene	6 Ma	6245 km
23	chron C0 - Recent	0 Ma	6370.8 km
24	Future	+5 Ma	6478 km

2.5 Modelling Methodology

The method adopted during construction of each model required the *Geological Map of the World* (CGMW & UNESCO, 1990; Figure 2.1) to be digitised and coloured using MapInfo (version 4.50) GIS software. The existing Mercator projection was then converted, using a purpose built macro, into twenty-four (Figure 2.9), thirty-six and forty eight-gore sinusoidal projection maps. A sinusoidal projection format is adopted to enable undistorted, true-to-scale printed geological information from anywhere within the map area to be cut and pasted onto each of the spherical models.

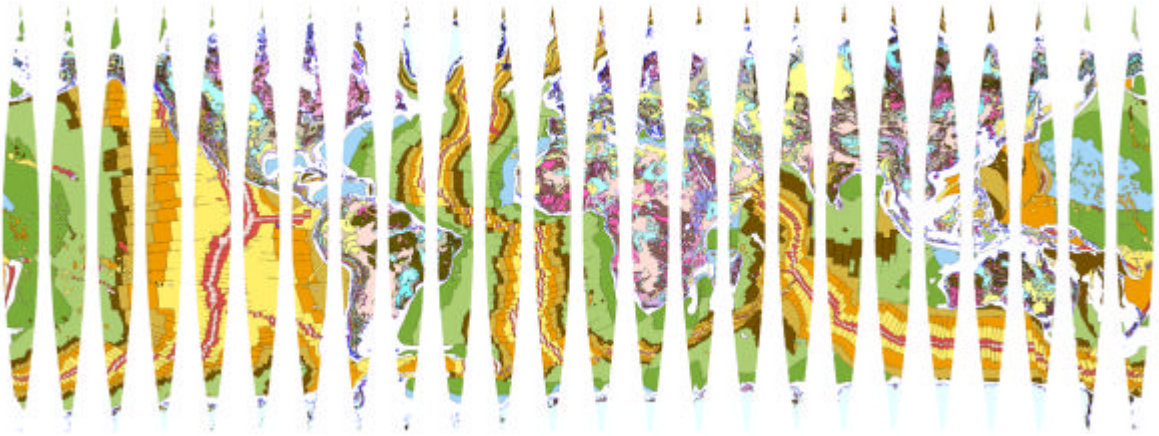

Figure 2.9. 24-gore sinusoidal map projection after CGMW & UNESCO (1990). This projection enables the geological map of the world to be displayed in distortion-free spherical format and forms the primary base-map for reconstructions within this thesis. Print output scale of the map is adjusted as required for model construction. See Figure 2.2 for legend.

In contrast to the post-Triassic models by Maxlow (1995; Figure 1.1), where models were constructed to the same scale and at increasing radii, all models within this thesis are constructed using 300 millimetre diameter polystyrene foam spheres. These spheres are used because they are commercially available and dimensionally stable. The varying palaeoradii of each model constructed is allowed for by varying the output scale of the printed sinusoidal base maps.

For each expanding Earth model (Figure 2.10; Video A2.10) plate reconstruction is established and maintained by manually cutting the continental and oceanic geological information from the sinusoidal base maps and pinning and pasting to the polystyrene foam spheres as required. Geological information used during cutting and pasting is, in general, confined to basement geological data older than the model under construction and younger information is progressively

eliminated backwards in time. Primary assumptions, crustal mechanisms and construction methods used are outlined in Section 2.5.1.

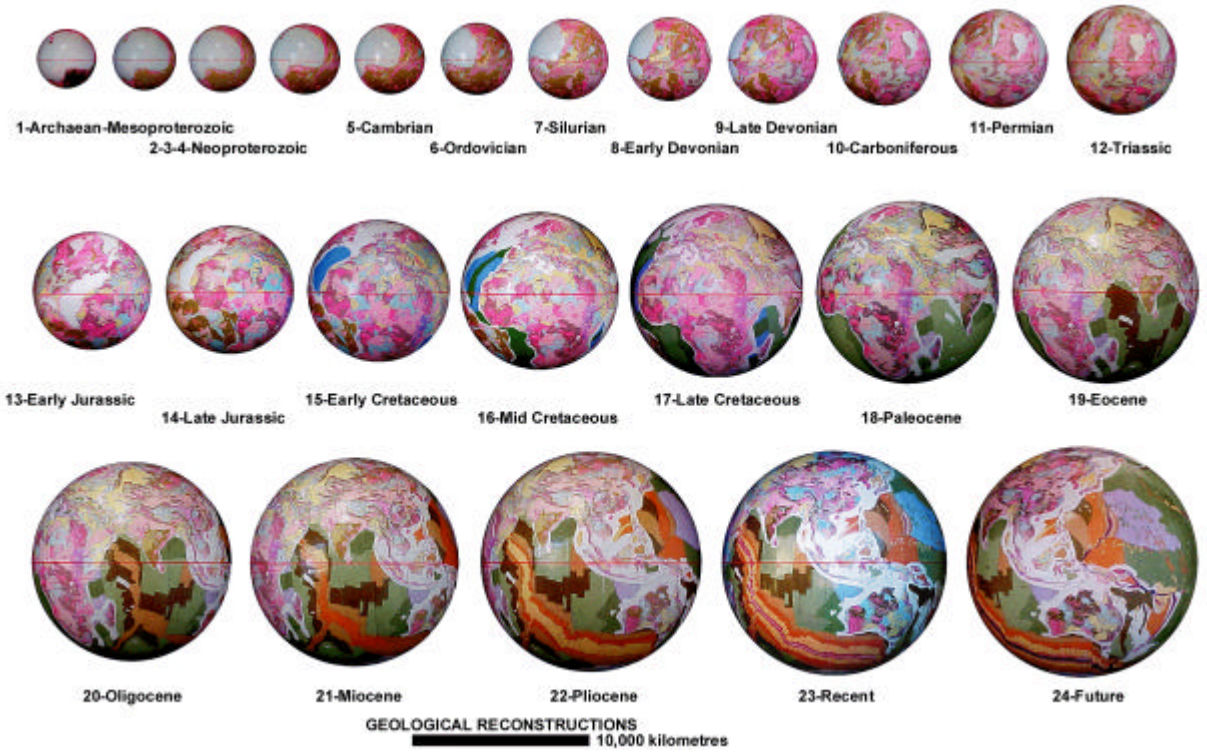

Figure 2.10 Spherical Archaean to future expanding Earth geological models. Models show relative increase in Earth radii, showing both continental and oceanic geology. Models range in age from the late-Archaean to Recent, plus one model projected 5 million years into the future. Relative sizes are listed in Table 2.1. See figure 2.2 for legend. (Geology after CGMW & UNESCO, 1990).

The models shown in selected figures within this thesis and video clips in the enclosed CD-ROM (Appendix A6) have been digitally re-sized to the same scale for presentation. Geographical grids are established for each model by using the published palaeomagnetic data set of McElhinny & Lock (1996) to locate magnetic poles and palaeoequators (Section 3.3). Longitude is established by adopting Greenwich as zero degrees longitude for each model and an equator established by scaling from each of the established palaeomagnetic poles.

2.5.1 Primary Assumptions Used During Reconstruction

The assumptions used to construct plate configurations on each model are summarised below and quantified in Chapter 3. For simplicity, the models constructed are distinguished as pre-Jurassic and post-Triassic to accord with current modelling and modelling by Maxlow (1995), respectively. For each post-Triassic

model in Maxlow (1995; Figure 1.1; Video A1.1a) and reconstructed post-Triassic models within this thesis (Figure 2.10), it is assumed that, for an Earth undergoing exponential expansion:

- The Earth's overall oceanic and continental lithospheric budget is cumulative with time.
- The surface area of oceanic lithosphere, as represented by the oceanic mapping data, is fully fixed in the rock record.
- Oceanic lithosphere is not removed by subduction.

For reconstruction of continental plate configurations for each of the pre-Jurassic models within this thesis (Figure 2.10; Video A1.1b) it is assumed that, for an Earth undergoing exponential expansion:

- Continental basin sedimentation and magmatism represent continental lithosphere accumulated primarily in extensional settings.
- Continental basin sedimentation and magmatism is not removed by subduction.

The only premise required during transferral of geologic data between successive models is that:

- Continental and oceanic lithosphere must undergo isostatic and surface area adjustment to allow for change in surface curvature of the Earth with time.

Each of the assumptions used during reconstruction are consistent with the primary assumption that, for an Earth undergoing expansion, the surface area of the Earth increases with time as a direct consequence of an increase in Earth radius.

The term subduction is restricted in this thesis to the plate tectonic usage, which implies hundreds to thousands of kilometres of intraplate convergent motion (eg. Larson & Pitman, 1972). It is acknowledged that intraplate interaction may occur at convergent plate boundaries on an expanding Earth, but only at a local observational scale.

2.5.2 Primary Mechanism for Crustal Extension

The response of lithosphere to an applied tectonic tensile force was investigated by Kusznir & Park (1987) and Lynch & Morgan (1987). Lithospheric strength has been shown (Kusznir & Park, 1987) to be primarily controlled by lithospheric rheology and is dependent on geothermal gradient and lithospheric composition. These observations are consistent with heat-flow data from currently active and inactive tectonic regions of the Earth and Lynch & Morgan (1987) conclude that rifts, or zones of extension, are common in the continents, in contrast to oceans, with some continental areas more susceptible to rifting than others. Lynch & Morgan (1987) also note that volcanism commonly precedes rifting by several million years, supporting the concept that lithosphere is heated and weakened prior to rifting This suggested to Lynch & Morgan (1987) that changes in the geotherm may also control the structural style of crustal extension.

Extension within both continents and oceans is considered the primary mechanism for increase in continental and oceanic surface area and formation of ocean basins during Earth expansion. Primary mechanisms considered to represent crustal extension during Earth expansion include (Figure 2.11):

- **Simple crustal stretching** accompanied by basement extension, thinning, basin formation and sedimentation (Figure 2.11a).
- **Crustal rifting** accompanied by basin sedimentation and volcanism, forming horst and graben-type rift structures with listric faulting along each margin. Sedimentary prisms young towards the centre of each basin (Figure 2.11b).
- **Simple brittle fragmentation** of cratonised crust, accompanied by basin sedimentation, and intrusive and extrusive volcanism within newly formed rifts (Figure 2.11c).

Zones of crustal thinning or crustal rifting (Figures 2.11) are inferred to be accompanied by elevated mantle derived heat flow and magmatism (eg. Kusznir & Park, 1987; Lynch & Morgan, 1987). This elevated heat flow represents a potential mechanism for metasomatism, metamorphism and granitization, accompanied by mantle-derived magma and associated volatiles. Fragments of cratons or orogenic

crust dislodged from crustal regions during extension or rifting may also represent a mechanism for formation of displaced or exotic terranes.

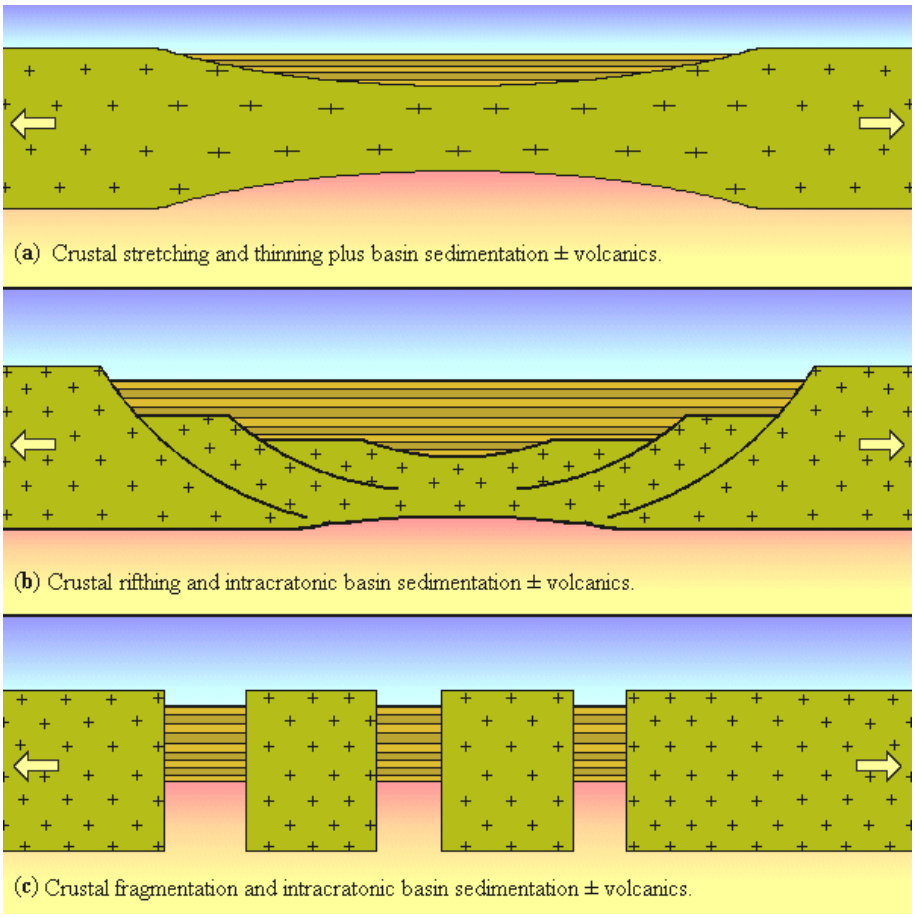

Figure 2.11 Primary mechanisms for crustal extension during Earth expansion. Figure a) Simple crustal stretching; b) crustal rifting; c) crustal fragmentation. In each figure continental crust is shown as green, mantle as pink shading, and intracratonic basin sedimentation shown as horizontal stripes.

2.5.3 Post-Triassic Model Reconstructions (Video A1.1a)

Unlike conventional palaeomagnetically constrained plate tectonic reconstructions, where constraint of palaeolongitude is limited (Li *et al.*, 1993) and multiple plate fit-options occur, palaeolatitude and palaeolongitude are accurately constrained on an expanding Earth using oceanic magnetic isochron mapping. This finite positional constraint enables each plate to be spatially reassembled with only one fit-option and removes the plate tectonic requirement for introduction of pre-existing crust along inferred subduction zones.

In reconstructing post-Triassic expanding Earth models (Figure 2.10) the continental and oceanic geology (Figure 2.1) is presumed to show the spatial and temporal distribution of oceanic and continental lithosphere within each ocean basin

and continent. During reconstruction, moving backwards in time from the Recent, successively older geological Periods paralleling the active mid-ocean spreading ridges are removed. Each plate is then restored to a pre-spreading or pre-extension configuration, at a reduced Earth radius, along a common mid-ocean spreading ridge or continental margin respectively.

By removing the oceanic geology for each Period in succession and reuniting the primary continental and oceanic plates along their common spreading axes at a reduced Earth radius, Maxlow (1995) demonstrated that all plates reunite with a better than 99% fit-together for each post-Triassic model constructed (Figure 1.1). This estimate of fit-together is made from observed plate interaction at plate margins and the accuracy is confirmed in reconstructed post-Triassic models (Figure 2.10). Interaction along plate margins results from a combination of map compilation errors, cartographic discrepancies and graphical limitations on restoration of post-fit extension along plate margins. Plate margin and within-plate extension is inferred to occur continuously during Earth expansion to compensate for the change in surface curvature of the Earth with time.

For the Mesozoic models constructed (Figure 2.10), as the palaeoradius of the Earth is reduced backwards in time, oceanic lithosphere is removed in succession and each continent is progressively re-united along their continental plate margins. The continental shelf and slope outlines of CGMW & UNESCO (1990; Figures 2.1 and 2.2) are used in this thesis to define continental margins. By the Triassic, all preserved oceanic magmatic lithosphere is removed and all continents are re-united along their shelf outlines at a reduced palaeoradius (Figure 2.10). The finite latitudinal and longitudinal positional constraint maintained by oceanic mapping during the Cenozoic is then of limited use.

As each continent is re-united during the Mesozoic, a network of continent-to-continent docking-points is established. These docking-points form plate positional constraining points, which compliment oceanic mapping, and are maintained throughout the Mesozoic and extended to pre-Jurassic constructions. The oceanic mapping and established docking-points are further constrained by consideration of sea-floor bathymetric data (eg. Gahagan *et al.*, 1988).

Examples of continental docking-points used on each of the pre- and post-Jurassic models (Figure 2.12) include: south-west Australia to Wilkes Land of East Antarctica; Tasmania to both south-east Australia and Victoria Land of East

Antarctica; South Africa to New Schwabenland of East Antarctica adjacent to the Weddell Sea; west Africa to South America; India to Queen Maud Land of East Antarctica; Siberia to Alaska; the Canadian Northwest Territories to Greenland; Greenland to Norway; Spain to Morocco; and Arabia to Africa.

Figure 2.12 Examples of continent-to-continent docking-points used to constrain Mesozoic and pre-Jurassic continental reconstructions. These include: Australia and Tasmania to Antarctica; Africa to South America; and India to Antarctica, Madagascar, and Africa. White dilation space on Early Cretaceous figure represents pre- Alpine-Himalayan orogenic basin extension.

A number of the docking-points established here conflict with conventional palaeomagnetic-based plate tectonic reconstructions, such as the positioning of Madagascar against east Africa (Scotese *et al*., 1979). Madagascar and the surrounding oceanic areas are associated with north-south orientated transform faults displaying sinistral movement within Jurassic and Cretaceous oceanic lithosphere (Figure 2.10). Docking of Madagascar adjacent to Mozambique on an expanding Earth is then dictated by a restoration of these transform faults, as distinct from a Kenyan position using palaeomagnetic arguments (Scotese *et al*., 1979). Similarly, India is positioned adjacent to Queen Maud Land in East Antarctica on an expanding Earth by using the oceanic mapping constraints (Figure 2.10), as distinct from a position adjacent to Enderby Land in East Antarctica using the palaeomagnetic based positioning of Powell *et al*. (1980, 1988). (See Section 3.2 for palaeomagnetics).

Post-Triassic modelling (Figures 1.1 and 2.10) confirms that, as oceanic crust is progressively removed from mid-ocean-ridge spreading axes each of the Earth's plates and continents can be progressively fitted together at reduced Earth palaeoradii. During the Triassic, all oceanic magmatic crust is removed and continental crust plus continental shelf sediments envelop the Earth at a much-reduced palaeoradius. Continental shelf sediments and epi-continental sedimentary basins during the Triassic then form a global network, surrounding continents, continental cratons and orogenic zones.

2.5.4 Pre-Jurassic Model Constructions (Video A1.1b)

Continental crust on pre-Jurassic models (Figure 2.10) is constructed within the context of the three primary crustal tectonic elements: cratons, orogens, and basins. Definition of these tectonic elements is summarised from Trendall (1990):

- **A craton** is defined as part of the Earth's crust that has attained stability, and has been little deformed for a prolonged period of time. Cratons must have attained stability by about 2.4 Ga and since then have undergone little deformation compared to adjacent parts of the crust.
- **An orogen** refers to a tectonic belt characterised by regional metamorphism and abundant plutonic intrusion. The rocks of an orogen can include deformed and reworked parts of older cratons, as well as new volcanic and weathering derived sedimentary rocks. An orogen is conceived to have been established by a distinct

tectonic pulse of relatively short duration. It is also possible for orogens to be reactivated during later tectonic episodes and they normally remain as permanent zones of weakness in the Earth's crust.

- **A basin** refers to areas underlain by a substantial thickness of sedimentary rocks which posses unifying characteristics of stratigraphy and structure. Sediments are deposited during a regionally restricted episode of crustal depression or a related sequence of such events. The term basin is synonymous with sedimentary basin.

Continental basement rocks shown in Figure 2.1 are time-based and coincide with the Cenozoic, Mesozoic, Upper Palaeozoic and Lower Palaeozoic Eras and Precambrian Aeons. Construction of pre-Jurassic models involves progressive removal of basin sediments and magmatism from each Era, depending on assemblage constraints imposed by restoration of cratons and orogens. Pre-Jurassic models have been constructed by progressive removal of younger basin sedimentation and magmatism and restoration of each basin to a pre-extension or pre-rift configuration. The models are constructed for the pre-Jurassic at regular time intervals coinciding with the Eras to maintain spatial continuity between models.

Construction of pre-Jurassic models is continued backwards in time until removal of Phanerozoic and Proterozoic basin sedimentation and magmatism is complete and Archaean cratons and Proterozoic basement rocks are assembled. Positional constraint is maintained by utilising the continental docking-points established for post-Triassic models (Figure 2.12) and recognition of additional intracratonic docking-points during removal of pre- and post-Jurassic basin sedimentation. For each craton, intracratonic docking points are established and maintained on each Palaeozoic model, such as the western and central Australian cratons to Antarctica, Canadian cratons to the Baltic cratons, and north Australian cratons and Precambrian orogens to Canadian and North American cratons. The spatial relationship of each docking point established is maintained across each basin and orogen until assemblage of cratons is complete during the Precambrian.

Moving backwards in time the spatial integrity of orogens (Trendall, 1990) is maintained during model construction until restoration to a pre-orogenic sedimentary basin or cratonic configuration is required. Pre-orogenic basin sediments are then subsequently removed and basins restored to a pre-extension configuration in conjunction with non-orogenic basins. During the Early Proterozoic, Precambrian

orogens form an intracratonic network (Figure 2.13) inferred to represent basement rocks surrounding Archaean cratons. The integrity of cratons (Trendall, 1990) is also maintained backwards in time in conjunction with the removal of non-orogenic basin sediments, pre-orogenic sediments and younger magmatic rocks.

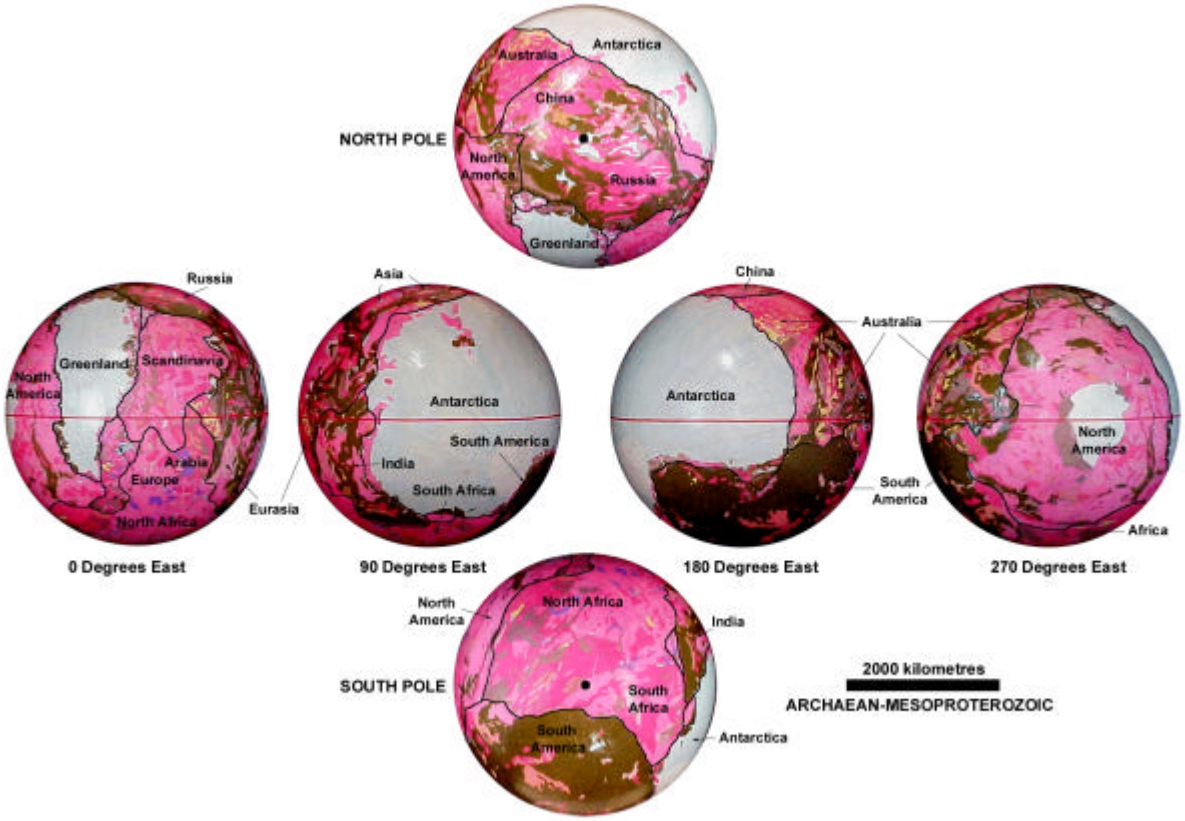

Figure 2.13 Archaean-Mesoproterozoic expanding Earth model. Model shows distribution of remnant cratons and zones of Precambrian continental crustal extension. Cratons are shown as pink and red, Proterozoic basement rocks are shown as khaki, present Antarctic and Greenland ice-caps are shown as pale blue. Palaeoequator is shown as horizontal red line and poles are shown as black dots. Primitive continents are outlined in black. Models are centred on longitude shown.

Precambrian models (Figure 2.10; Video A2.13) empirically demonstrate that basement extension, thinning and rifting of a proto-Archaean crust occurs within zones of crustal weakness surrounding cratons. The presence of magmatism within these zones, and proximity of Proterozoic orogens suggests a high heat flow accompanying extension and intracratonic mobility. These zones of crustal weakness coincide with Proterozoic sedimentary basins, forming the loci for initial seawater accumulation, orogenesis and regional metamorphism. Tensile fracturing during crustal extension is not shown on the models and is inferred to be accompanied by extensive dyke swarms. Rifting may also be accompanied by rift phase volcanics and

associated platform volcanic and banded iron formation rocks, and seawater accumulation within basin settings.

Palaeozoic modelling reveals that the distribution of epi-continental sedimentary basins, continental magmatism and orogenic zones is consistent with the established Precambrian intracratonic network and represents zones of primary continental crustal extension and weakness during Earth history. The Archaean-Mesoproterozoic intracratonic network (Figure 2.13) then forms the loci for continental crustal extension, basin sedimentation and intracratonic mobility during the Proterozoic and Palaeozoic (Figure 2.10, models 5 to 11), and represents the primary loci for continental break-up and opening of the modern oceans during the post-Permian (Figure 2.10, models 12 to 24). This process of progressive continental crustal extension during Earth expansion demonstrates a spatial integrity of all tectonic elements and continents throughout Earth history (Video A2.10).

2.6 Continental Development on an Expanding Earth

In this section a brief review of the tectonostratigraphic development of each of the continents on an expanding Earth is given, based on observations from expanding Earth models constructed (Figure 2.10). These observations are global scale and no attempt is made to incorporate lithostratigraphic or tectonic detail. Qualification of observations is given in Chapter 3 dealing specifically with space geodetics, palaeomagnetics, palaeogeography, palaeobiogeography, palaeoclimate and metallogeny. For each expanding Earth model geographical orientations relative to the palaeoequator are given in lower case (eg. Australia is orientated north-south during the Precambrian) and geographical descriptors relative to the present-day equator are given in upper case (eg. Eastern Australia).

Overall, expanding Earth models show a tectonic development of continents and oceans, which can be considered as four distinct phases of Earth history. These four phases are shown in Figure 2.14 (Video A2.14) and include:

- **Phase (1)**: a pre-Neoproterozoic phase of minimal expansion. Expansion during this phase is manifested as continental crustal extension, magmatism and basin development. Sedimentation is confined to a global network of intracratonic basins coinciding with epi-continental seas. Orogenesis is ensialic and confined

to linear intracratonic zones (Section 3.3.10) and continent to basin elevation contrast is considered low.

- **Phase (2)**: a Neoproterozoic to Carboniferous phase of steadily increasing expansion. Expansion is manifested as continental crustal extension and magmatism within continental sedimentary basins. Sedimentation is confined to intracratonic epi-continental basins, which increase in surficial area throughout the Palaeozoic. Intracratonic motion during relief of surface curvature during Earth expansion results in polyphase orogenesis and post-orogenic basin extension. Elevation contrast between basins and continents is considered to increase during periods of increasing orogenesis.
- **Phase (3)**: a Late Palaeozoic transitional phase where expansion is manifested as rifting, continental rupture, break-up and initial opening of the modern oceans. Sedimentation progressively shifts from a continental to an oceanic depocentre, preserved in marginal shelf and ocean plateau settings.
- **Phase (4)**: a post-Triassic phase where expansion is predominantly manifested as mid-ocean-rifting within modern oceans. During this phase mid-ocean-ridge magmatism exceeds oceanic sedimentation and magmatism is preserved as sea-floor lithosphere.

During the Precambrian and Early Palaeozoic Phases (1) and (2) the primary depocentres for epi-continental basin sedimentation are located within Eurasia, equating to the Tethys region in conventional plate tectonic reconstructions, and the Central America and Eastern Australian regions. Throughout the Palaeozoic these primary depocentres continue to extend during expansion to include basins in North America, Africa, Asia and Russia. During the Late Palaeozoic transitional Phase (3) continental extension and associated epi-continental sedimentary deposition is confined primarily to the Eurasian region, as continental break-up commences and modern oceans rapidly open during Phase (4).

Each phase is governed by the rate of Earth expansion (Figure 2.6). The pre-Neoproterozoic to Carboniferous phases represent prolonged periods of steady to steadily accelerating expansion, followed by Late Palaeozoic continental rupture and a transition to a post-Jurassic phase of rapidly accelerating expansion, continental break-up and dispersal, and modern ocean development to the Recent.

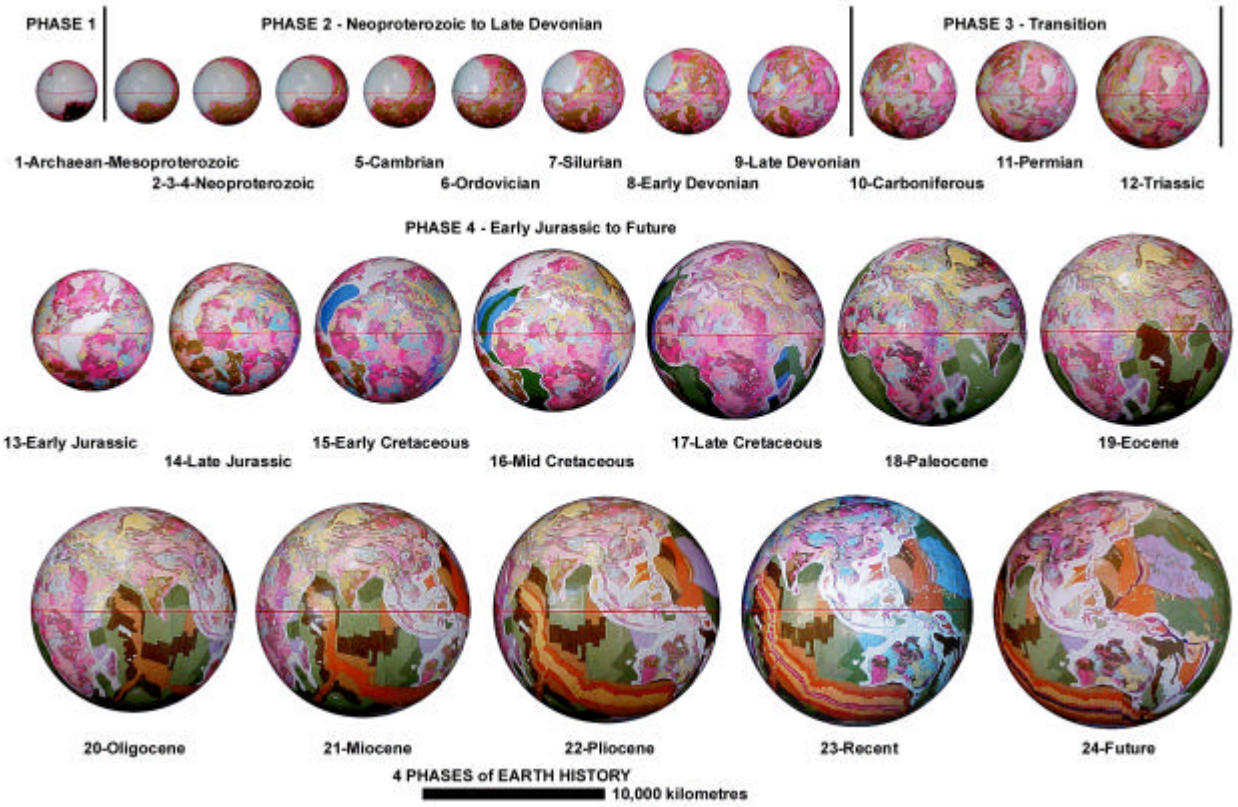

Figure 2.14 Four phases of expanding Earth developmental history. Phase 1):a pre-Neoproterozoic phase of minimal expansion; Phase 2): a Neoproterozoic to Carboniferous phase of steadily increasing expansion; Phase 3): a Late Palaeozoic transitional phase where oceanic magmatism exceeds continental crustal extension and oceanic sedimentation exceeds oceanic magmatism; Phase 4): a post-Triassic phase where expansion is predominantly manifested within the modern oceans.

2.6.1 Tectonostratigraphic Development of Australia

The tectonostratigraphic development of Australia (Figure 2.15) originates from an Archaean cratonic and Palaeoproterozoic basin assemblage comprising Central and Western Australian cratons and orogens. Throughout the Precambrian and Palaeozoic Australia is orientated north-south relative to the palaeoequator and rotates anticlockwise during the Mesozoic to a present east-west orientation as the Pacific Ocean opens. During the Precambrian and Palaeozoic, cratonic regions of China abut to the north, Canada and North America to the east, South America to the south, and East Antarctica to the west. The palaeoequator passes through Central Australia and Archaean cratons of Western Australia are located within mid to high northern latitudes.

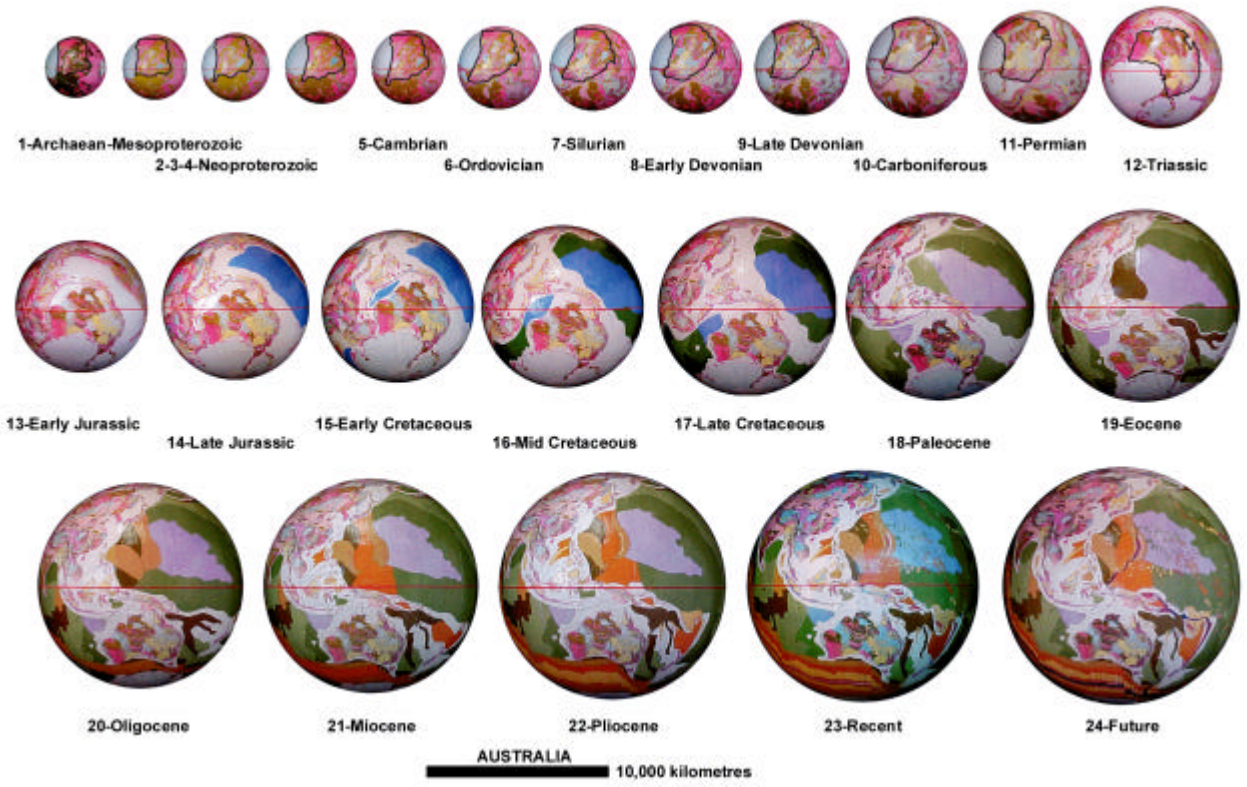

Figure 2.15 Tectonostratigraphic development of Australia. Pre-Jurassic Australia is outlined in black. During the Precambrian to Late Palaeozoic Australia is orientated north-south, prior to rotating anticlockwise to the present east-west orientation during opening of the Pacific Ocean. Horizontal red line represents the palaeoequator. (After CGMW & UNESCO, 1990).

The Proterozoic basins of Northern and Central Australia form part of an intracratonic network extending north into an assemblage of Proterozoic basins comprising Alaska, Canada, Northern Russia and Asia. To the east and south these basins are also linked to the Proterozoic basins of North America, Central America and South America. During the Proterozoic and Palaeozoic the spatial integrity of each basin is maintained as the basins extend and Palaeozoic sedimentary basins develop. Palaeozoic sedimentation primarily develops to the south (Eastern Australia), where they are intracratonic to South America, North America, and Antarctica.

Orogenesis is primarily focused within the Proterozoic and Palaeozoic basins of Central and Eastern Australia, associated with the Andean events of South America and the Appalachian and Grenville orogenic events of Eastern North America. Tectonic remnants of the Cordilleran orogenic event of Western North America and Canada occur within Northern Australia. Proterozoic orogenic events in

Central and Northern Australia in particular, reflect intracratonic motion between Australia and North America.

Post-orogenic intra-continental rupture, initiating continental break-up and development of the modern oceans, occurs to the northeast, adjacent to the Pilbara Craton and Kimberley Basin, and in the south, adjacent to Eastern Australia during the Early Permian. These sites represent initiation of the North Pacific Ocean and South Pacific Ocean respectively. The early North and South Pacific Oceans rapidly extend throughout the Permo-Triassic and then merge, separating Australia from North America and Australia from China during the Jurassic. Rifting between Australia and East Antarctica commenced during the Paleocene and has continued to the Recent. After rotating anticlockwise during the Permo-Triassic to its present east-west orientation Australia has remained geographically isolated since the Paleocene, and has migrated to a low to mid southern latitude.

2.6.2 Tectonostratigraphic Development of Africa-Arabia

A description of the tectonic development of Africa and Arabia is marred by the poor quality of African mapping presented in CGMW & UNESCO (1990) and reconstructions are speculative. Africa and Arabia originate from an Archaean cratonic configuration located adjacent to the Archaean and Proterozoic regions of South America, North America, Central Europe, Scandinavia, India, and East Antarctica (Figure 2.16). The North Pole is located within Central West Africa throughout the Precambrian and Palaeozoic, and migrates south, along the present West African coast, during the Mesozoic to the present location in Antarctica (Section 3.2). This continental configuration, relative to surrounding continents has remained spatially integral throughout Earth history.

Tectonic development of Africa and Arabia has involved intracratonic extension; Palaeozoic sedimentation and intracratonic motion between each of the South, East and West African cratons during the Precambrian and Palaeozoic. Throughout North Africa Phanerozoic basin extension and sedimentation occurred in conjunction with extension of the Mediterranean, Central Europe and Asian Tethys Sea regions (Section 3.3).

Precambrian and Palaeozoic orogenesis is located along the present East African coast, associated with events in Madagascar and India, and West African

coast, associated with Grenville, Appalachian and Hercynide events in Eastern North America and Europe. Remnants of tectonism associated with the Cenozoic Alpine-Himalayan orogenic event also occur within North Africa.

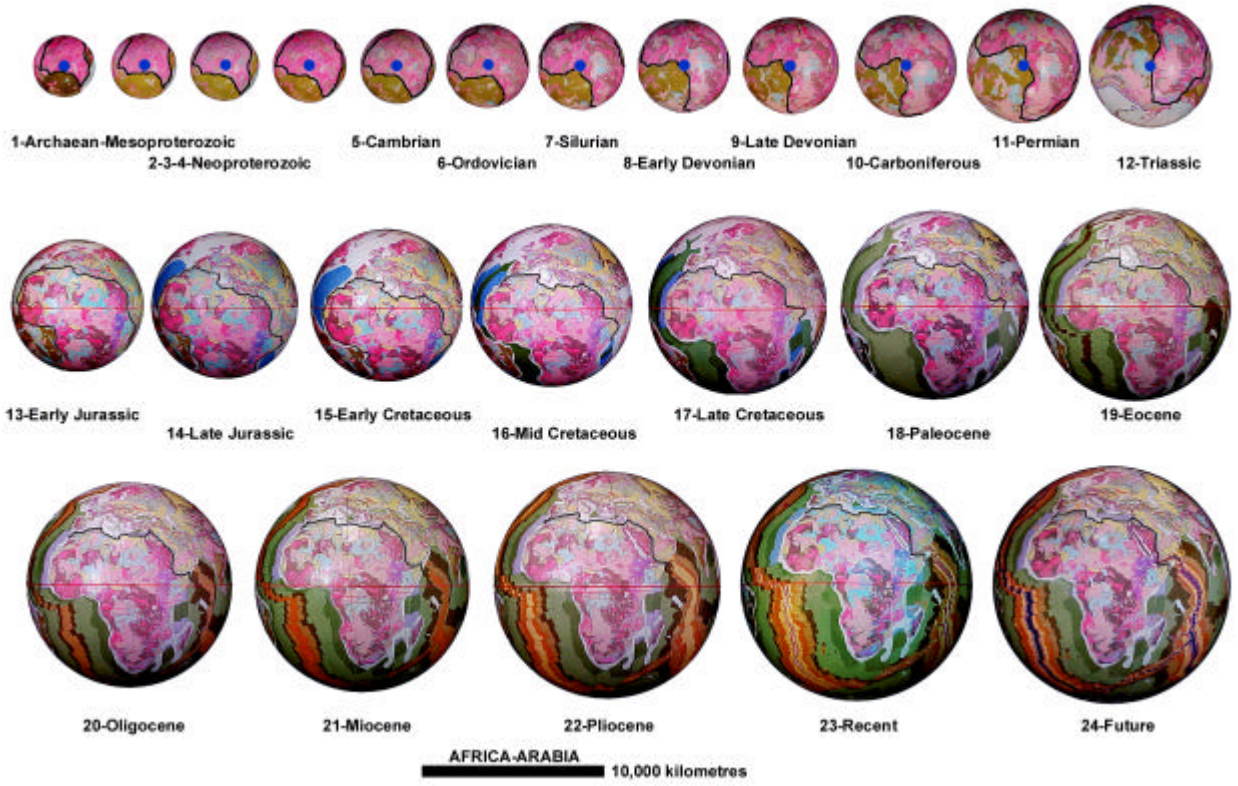

Figure 2.16 Tectonostratigraphic development of Africa and Arabia. In each of the Precambrian and Palaeozoic images North Africa is located south of the palaeoequator and the South Pole is located in west Central Africa. Triassic to Archaean models are centred on the south pole (red dots). Red line represents palaeoequator, blue lines represent palaeocoastlines (Section 3.3) and the black line represents the African continental outline. (After CGMW & UNESCO, 1990).

Post-orogenic continental break-up was initiated between West Africa and North America during the Permo-Triassic, forming the North Atlantic Ocean. Rifting between South America and Africa, and between Africa, Antarctica, Madagascar and India commenced during the Jurassic. Rifting between Africa and Arabia, and the Mediterranean and Asian regions commenced during the Cretaceous and has continued to the Recent. During the Mesozoic to Recent Africa migrated north, relative to the South Pole, into equatorial to high southern latitudes.

2.6.3 Tectonostratigraphic Development of Antarctica

The tectonic development of both East and West Antarctica is speculative because of the widespread present-day ice cover. Reconstructions indicate that an

East Antarctican continent comprises mainly Precambrian crust and has remained spatially intact throughout Earth history. During model construction younger crust within West Antarctica is progressively removed, backwards in time, to remnant Proterozoic crustal fragments only. East and remnant West Antarctica straddled the palaeoequator throughout the Precambrian and Early Palaeozoic and were situated adjacent to Australia, South America, South Africa, India, and Central and Southeast Asia (Figure 2.17).

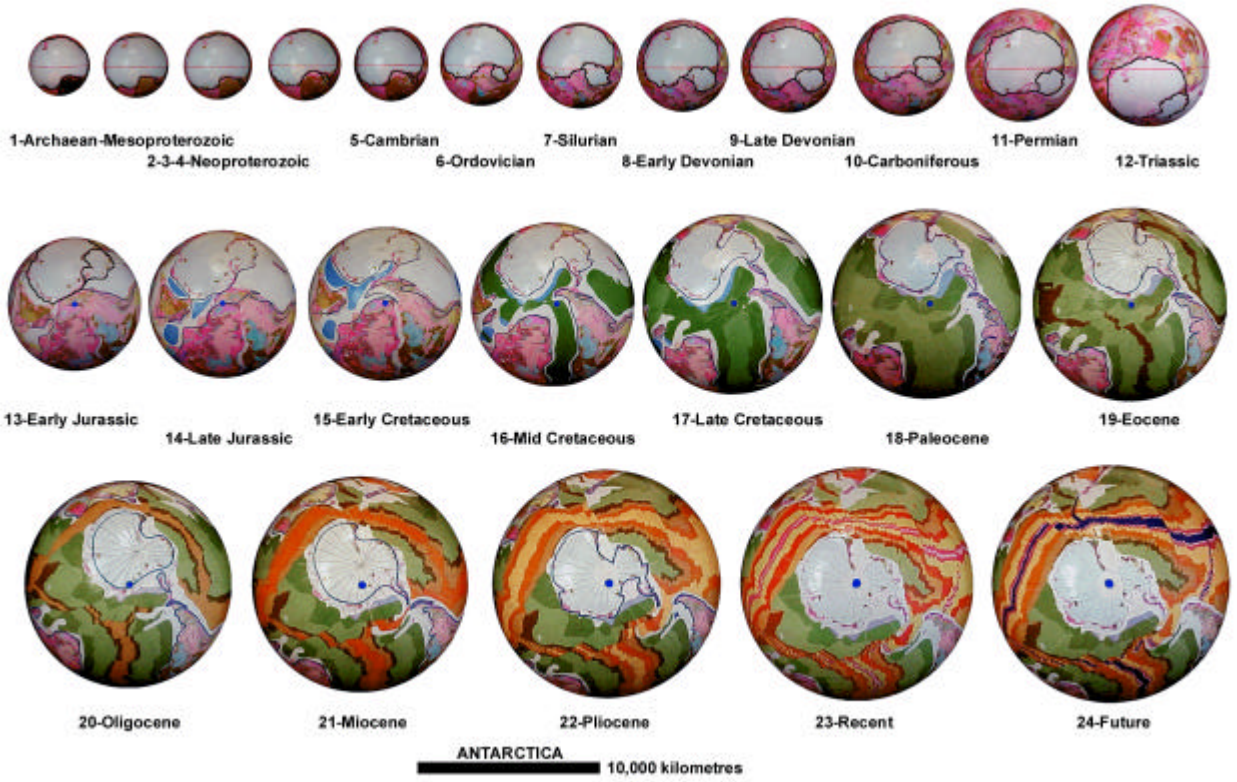

Figure 2.17 Tectonostratigraphic development of East and West Antarctica (pale blue). During the Archaean to Late Palaeozoic Antarctica straddles the palaeoequator prior to a rapid transit south, as the modern oceans open, to its present location at the South Pole. Red line represents palaeoequator and blue lines are palaeocoastlines (Section 3.3). Models 13 to 24 are centred on the south pole. (After CGMW & UNESCO, 1990).

Proterozoic and Palaeozoic orogens and sedimentary basins of India, Central and Southeast Asia, Australia, South America and West Antarctica are peripheral to East Antarctica, with basins possibly extending into the East Antarctican continent beneath the present ice-sheet. Orogenic regions in West and East Antarctica are associated with, and extensions of, orogenic events in Eastern Australia and Andean orogenic events in South America.

Break-up of the Antarctican continent commenced with opening of the South Pacific Ocean during the Early Permian. By the Late Jurassic, opening of the Indian and South Atlantic Oceans had commenced, and rifting between Australia and East Antarctica commenced during the Paleocene. Crustal extension and tectonic motion of West Antarctica relative to East Antarctica is intimately related to the rapid opening of the South Pacific Ocean during the post-Permian. By the Late Cretaceous, West Antarctica separated from East Antarctica and rotates clockwise, relative to East Antarctica, during opening of the South Pacific Ocean to the Recent. During opening of the South Pacific Ocean the West Antarctican Peninsular remains in contact with southern South America, until separation and rifting during the Miocene.

From a Precambrian and Palaeozoic equatorial location the Antarctican continent migrated south, relative to the South Pole, to a present south polar location during the Mesozoic to Recent. Oceanic mapping (Figure 2.1) demonstrates that all the continents are now migrating north, away from Antarctica, as new ocean crust is injected along the Southern Ocean mid-ocean-rift zone.

2.6.4 Tectonostratigraphic Development of Europe and Asia

The tectonic development of Europe and Asia is a complex mixture of Proterozoic to Cenozoic crustal extension and sedimentary basin development, orogenesis and magmatism. During the Archaean and Early Proterozoic the Eurasian continent is an elongate intracratonic basin comprising a network of Proterozoic sedimentary basins, small fragments of Archaean cratons and larger Mongolian and Chinese cratons. The Eurasian proto-continent represents the primary depocentre for sedimentation within an epi-continental Tethys Sea during the Precambrian to Mesozoic (Section 3.3).

The Asian region of the Eurasian proto-continent is centred on the North Pole throughout the Precambrian and Palaeozoic, extending to the palaeoequator within the European region. East Antarctica is located along the eastern margin, with Australia located to the north, Canada to the northwest, Greenland to the west, Scandinavia and Arabia to the southwest and India to the south. This north-south orientated basin extends to include the Proterozoic sedimentary basins of Central Australia and Proterozoic basins of India (Figure 2.18).

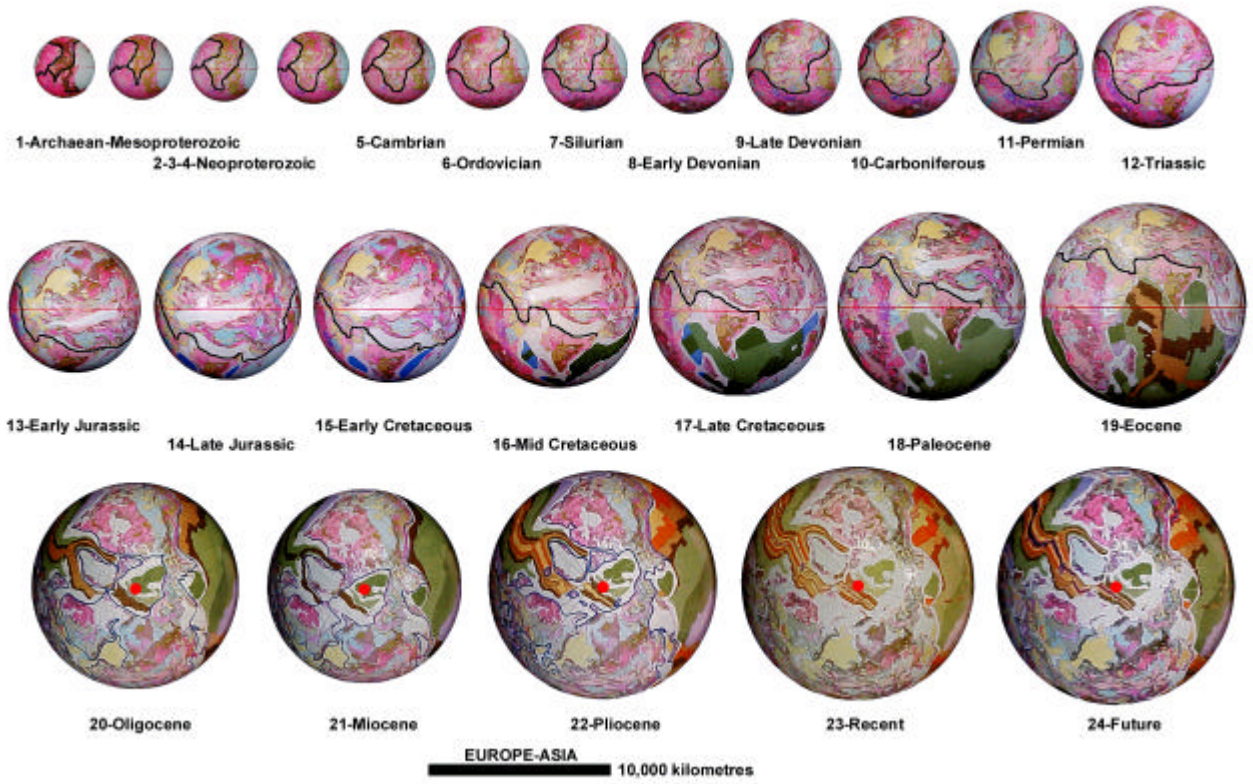

Figure 2.18 Tectonostratigraphic development of Europe and Asia. Models 20 to 24 are centred on the north pole (red dots). During the Precambrian and Palaeozoic Eurasia is a north-south orientated sedimentary basin, prior to complex polyphase extension and orogenesis to the Recent. White dilation space shown in central Asia during the Early Jurassic to Paleocene represents pre-orogenic extension prior to Cenozoic Alpine-Himalayan orogenesis. Red line represents palaeoequator, blue line represents palaeocoastlines and black line represents continental outline of Europe and Asia. (After CGMW & UNESCO, 1990).

Throughout Earth history orogenesis within Eurasia is a complex polyphase history of primary basin extension, intracratonic and intra-orogenic motion, and secondary basin extension within an overall clockwise extensional tectonic regime. The Eurasian region represents a zone of Proterozoic and Palaeozoic extension, basin development and sedimentary deposition, receiving sediments from each of the surrounding proto-continents. The crustal extension and sedimentary deposition progressively shifted to, and was replaced by extension within the modern North Pacific Ocean during the post-Permian continental break-up and dispersal phase. Epi-continental sedimentation continued within Eurasia during the Early Permian continental break-up and epi-continental seas regressed during the Cenozoic exposing Eurasia as an elevated continent.

2.6.5 Tectonostratigraphic Development of India

The tectonic development of India is portrayed in conventional plate tectonic reconstructions as migrating north during the Mesozoic to collide with Asia during the Cenozoic (eg. Chatterjee, 1992). India on an expanding Earth is located within mid-southern to equatorial latitudes throughout the Precambrian and Palaeozoic, prior to a brief period within high-southern latitudes during the Mesozoic and a return to low-northern latitudes during the Cenozoic to Recent. This apparent migration is related to its location relative to the rapidly extending Eurasian epi-continental Tethys basin, migration of continents away from the pre-Palaeozoic south pole, then located in central West Africa, and post-Jurassic opening of the Indian Ocean (Figure 2.19).

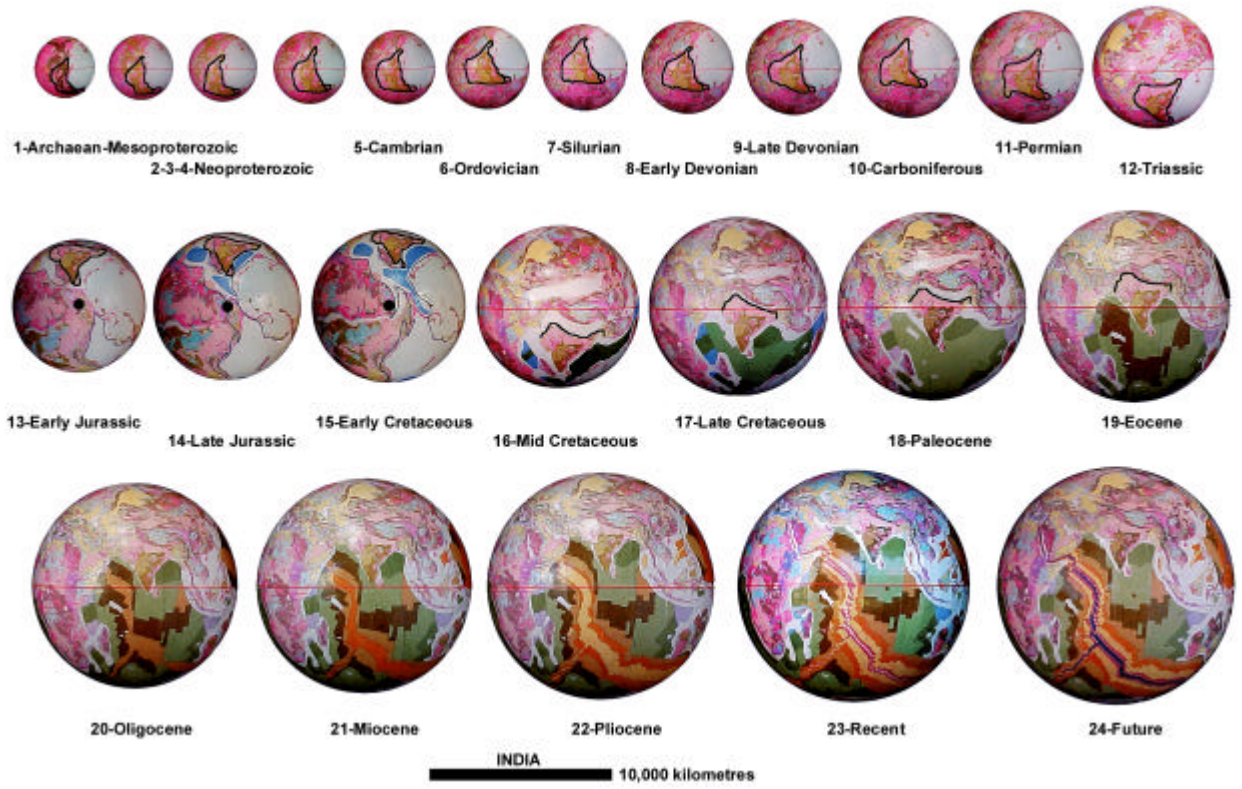

Figure 2.19 Tectonostratigraphic development of India. Throughout the Precambrian to Late Palaeozoic India straddles the palaeoequator, prior to migration to mid-southern latitudes during the Mesozoic and low northern latitudes during the Cenozoic to Recent. Early Jurassic to Early Cretaceous models are centred on the south pole (black dots). Red line represents palaeoequator, blue lines represent palaeocoastlines (Section 3.3) and black lines represent Indian continental outlines. (After CGMW & UNESCO, 1990).

The Indian continent formed as a southern extension of the Eurasian Proterozoic epi-continental Tethyan basin. During the Precambrian and Palaeozoic

India is located adjacent to East Antarctica to the northeast, Madagascar and South Africa to the southwest, and Arabia to the west. Crustal extension occurred between the north and south Indian cratonic regions during the Proterozoic, continuing to the Mesozoic. The tectonic developmental history of India then remained relatively stable to the Recent. Pre-Palaeozoic orogenesis is confined to crustal movement relative to both Antarctica and Madagascar-Africa, and polyphase Palaeozoic to Cenozoic orogenesis along the northern contact with Eurasia.

Continental separation and rifting between Antarctica and Africa commenced during the Jurassic with opening of the Indian Ocean. Madagascar and Sri Lanca began rifting away from India during the Early to Mid-Cretaceous, with Sri Lanca continuing to remain in close proximity with India to the Recent.

In contrast to conventional plate tectonic reconstructions, India on an expanding Earth remains attached to the Asian continent throughout Earth history. Extensive periods of polyphase extension-orogenesis-extension and epi-continental basin development within Eurasia to the north, geographically isolated continental India from the elevated Asian continent during much of Earth history. During the Mesozoic, geographic studies (Section 3.3) show that India existed as an island continent attached to the Asian continent until commencement of Alpine-Himalayan orogenesis during the Cenozoic. As the Eurasian epi-continental Tethys Sea regressed during the Cenozoic, India and Eurasia were then exposed as a contiguous continent.

2.6.6 Tectonostratigraphic Development of North America-Greenland-Scandinavia

The tectonic development of North America is intimately linked to the Canadian, Greenland and Scandinavian Archaean and Proterozoic cratons, and will be discussed together as a North American cratonic cluster. Each of these cratons straddle the palaeoequator throughout the Precambrian and Palaeozoic and range from mid-southern to mid to high-northern latitudes. The North American cratonic cluster abuts the Eurasian Tethyan basin to the north, Australian Proterozoic basins to the west, South America to the southwest and West Africa to the south and southeast. Precambrian European crustal fragments are clustered adjacent to, and southeast of Greenland and Scandinavia (Figure 2.20).

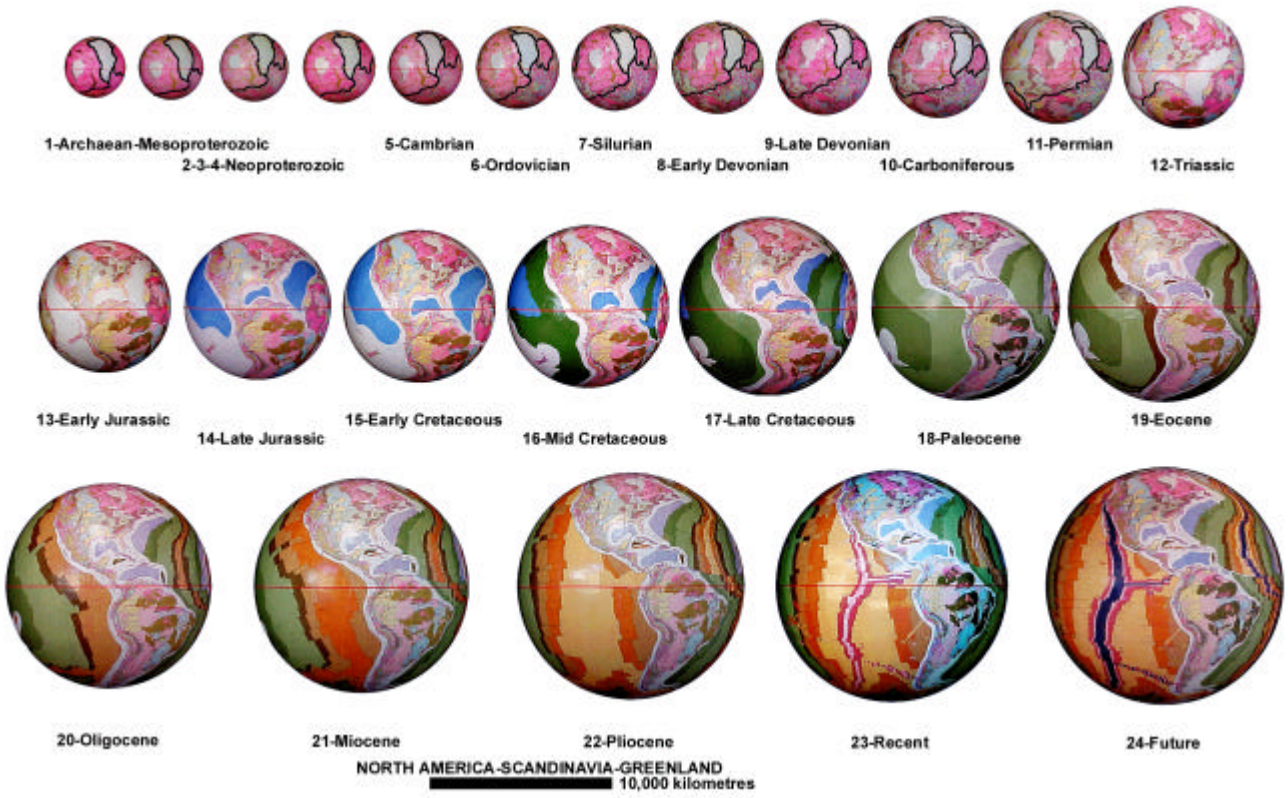

Figure 2.20 Tectonostratigraphic development of North America-Greenland-Scandinavia. During the Precambrian to Late Palaeozoic the North America-Greenland-Scandinavia cratons straddle the palaeoequator, prior to continental break-up and migration to mid- to high-northern latitudes during the Mesozoic to Recent. Red line represents palaeoequator and black lines represent North American, Greenland and Scandinavian continental outlines. (After CGMW & UNESCO, 1990).

The tectonic development of the North American cratonic cluster involves intracratonic extension and Proterozoic and Palaeozoic basin sedimentation within a peripheral network of epi-continental sedimentary basins. The North American cratonic cluster remained intact until post-Jurassic continental break-up and opening of the North Atlantic Ocean. Scandinavia then remained attached to Europe, as the North Atlantic and Arctic Oceans opened, and Greenland remained in close proximity to North America.

Precambrian and Palaeozoic orogenesis occurs as elongate orogenic belts located around the margins of the North American cratonic cluster. During post-Jurassic continental break-up the Grenville and Appalachian orogenic belts remained accreted to Eastern North America and the Cordilleran orogenic belt remained accreted to Western North America. The Hercynides remained accreted to Europe; the Caledonides to Scandinavia, Mauritanides to West Africa and the Russian

platform was separated from the northern margin of the cratonic cluster. The northern extension of the Cordilleran orogenic belt continued, via Alaska, into Asia and had a prolonged history of extension and terrane displacement until continental break-up between Siberia and North America during the Early Jurassic.

Continental break-up of the North American cratonic region commenced during the Early Permian with opening of the North Pacific Ocean and initial opening of the Arctic Ocean. During the Early Jurassic spreading rapidly developed in the Arctic and North Atlantic Oceans. Throughout the Late Jurassic to Miocene north and south extensions of the Cordilleran orogenic belt continued to maintain a continuous continental link from South America to North America and Siberia. The Siberian connection was severed during the Pliocene during opening of the Bering Strait. Fragmentation of the northern Canadian Islands began during the Jurassic and is intimately related to rifting between Canada and Greenland. Rifting in the Northern Canadian region is ongoing to the Recent.

From its original equatorial location the North American cratonic cluster has progressively rotated clockwise during Earth expansion, and each craton has migrated north to a present mid to high northern latitude relative to the North Pole.

2.6.7 Tectonostratigraphic Development of South America

The tectonic development of South America originates from a cluster of South American Precambrian cratonic and orogenic regions located within the Precambrian southern hemisphere. The proto-continent ranged from low equatorial to high south polar latitudes throughout the Palaeozoic and Precambrian. East Antarctica and Precambrian remnants of West Antarctica are located to the northwest; Australia is located to the north, North America to the northeast, and Africa to the east, south and west. During the Late Palaeozoic to Mid Cretaceous South America migrated north, in conjunction with Africa, relative to the South Pole. The south pole, from a Precambrian and Palaeozoic Central West African location, tracked south along the then rifting Atlantic Ocean during the Mesozoic, continuing south to its present location within Antarctica during the Cenozoic (Figure 2.21).

The tectonic history of South America involves a prolonged period of crustal extension and cratonic fragmentation since the Early Palaeozoic, in sympathy with events within South and West Africa. During the Palaeozoic intracratonic extension

and extensive basin sedimentation occurred between South America, Antarctica, Australia and North America. Palaeozoic orogenesis is located between Australia and South America giving rise to the Andean-Tasman orogenic zones, with orogenic remnants remaining accreted to South America, New Zealand and Australia.

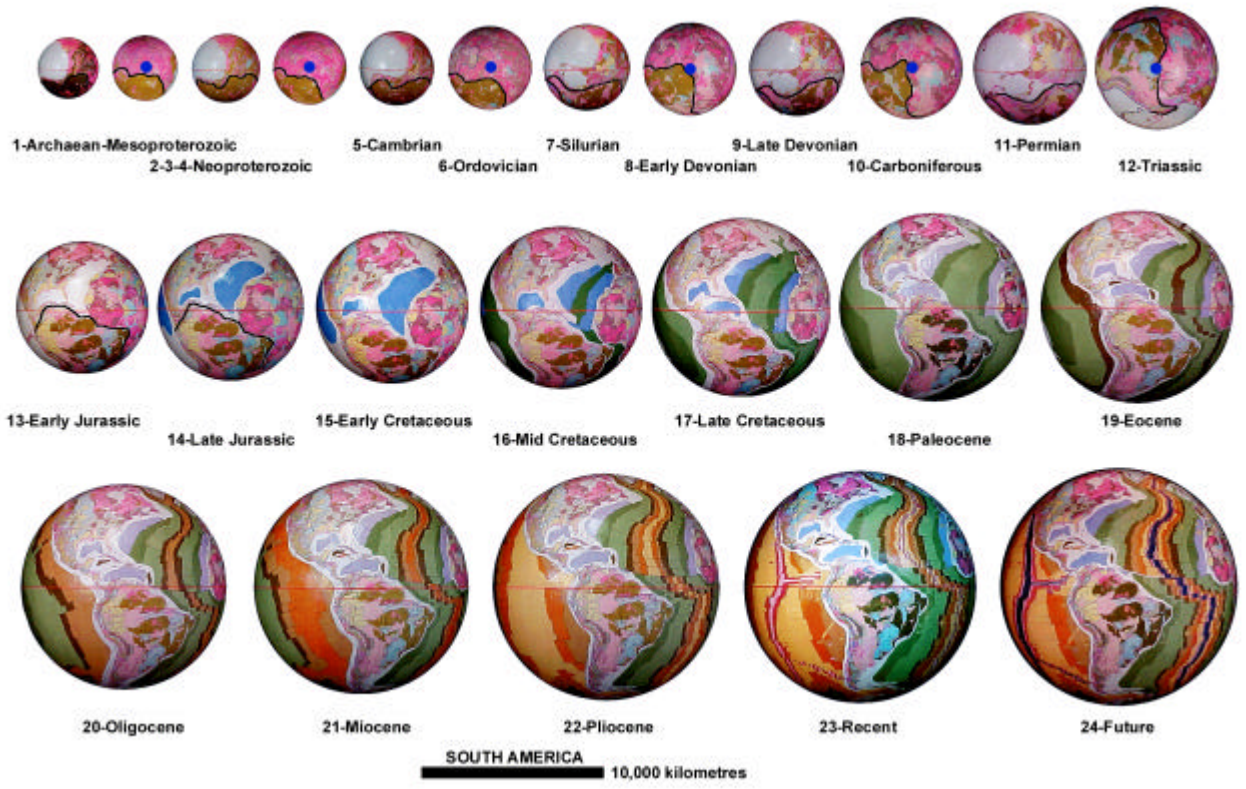

Figure 2.21 Tectonostratigraphic development of South America. For the Archaean to Triassic both polar and equatorial views are shown. During the Precambrian and Palaeozoic South America is located adjacent to the south pole, prior to migration into mid- to low-southern latitudes during the Mesozoic to Recent. Red line represents palaeoequator, blue dots represent south pole and black lines represent South American continental outline. (After CGMW & UNESCO, 1990).

Continental break-up between Australia, South America and Antarctica commenced during the Early Permian with opening of the South Pacific Ocean. During the Triassic the North Atlantic Ocean and Caribbean Sea commenced opening, and during the Late Jurassic rifting between South America and West Africa commenced, forming the South Atlantic Ocean. A land connection between the West Antarctica Peninsular and southern South America remained until separation during the Miocene and a land connection remains along the South America and Central American peninsulas.

2.7 Oceanic Development on an Expanding Earth

The tectonic development of post-Permian oceans and seas on an expanding Earth is based on observations from expanding Earth models (Figure 2.10) and summarised from Maxlow (1995) (Figure 1.1). The inclusion of detailed continental geology on reconstructed models (Figure 2.10) has provided a revised reconstruction of Southeast Asia, New Zealand, the Mediterranean, Caribbean and Bering regions, and has enabled ocean development to be extended back to the Permian.

Conventional reconstructions of Pangaea on a constant radius Earth (eg. Weijermars, 1989; Scotese *et al.*, 1988; Scotese, 1994) require the Pacific and Arctic Oceans and the Caribbean and Mediterranean Seas to contract in area during the Mesozoic and Cenozoic during opening of the Atlantic, Indian and Southern Oceans. During this time the area of early Mesozoic Panthallassa and Tethys Oceans decreased by the sum of the areas of the Atlantic, Southern and Indian Oceans. The conventional Mesozoic and Cenozoic oceanic history is then portrayed as an east-west and north-south contraction of the Panthallassa and Tethys Ocean areas to the size of the modern Pacific Ocean, subduction of all pre-Mesozoic oceanic crust and subduction of a substantial quantity of oceanic crust generated during the Mesozoic to Cenozoic. On an expanding Earth continental rupture, break-up and opening of the modern oceans commenced during the Early Permian as small extensional basins within the North and South Pacific and Arctic Ocean regions (Figure 2.22). Record of this early phase is preserved as marginal basin and ocean plateau sediments within each basin area (eg. Dickins *et al.*, 1992). Opening of the oceans continued throughout the Permian and Triassic and preservation of oceanic magmatism (eg. CGMW & UNESCO, 1990) commenced during the Early Jurassic. Opening of the Atlantic and Indian Oceans commenced during the Early to Late Jurassic and the Southern Ocean commenced opening during the Paleocene.

The opening of each of the oceans and seas shows two distinct phases corresponding to the Mesozoic and Cenozoic Eras. Throughout the Mesozoic the ocean basins continued to enlarge in what are interpreted to be passive basin settings. Mesozoic spreading ridges within each basin occur as: asymmetric spreading ridges along the perimeters of the North and South Pacific Oceans; as symmetric spreading ridges in the North and South Atlantic and; a combination of both asymmetric and symmetric-type spreading ridges in the Indian Ocean.

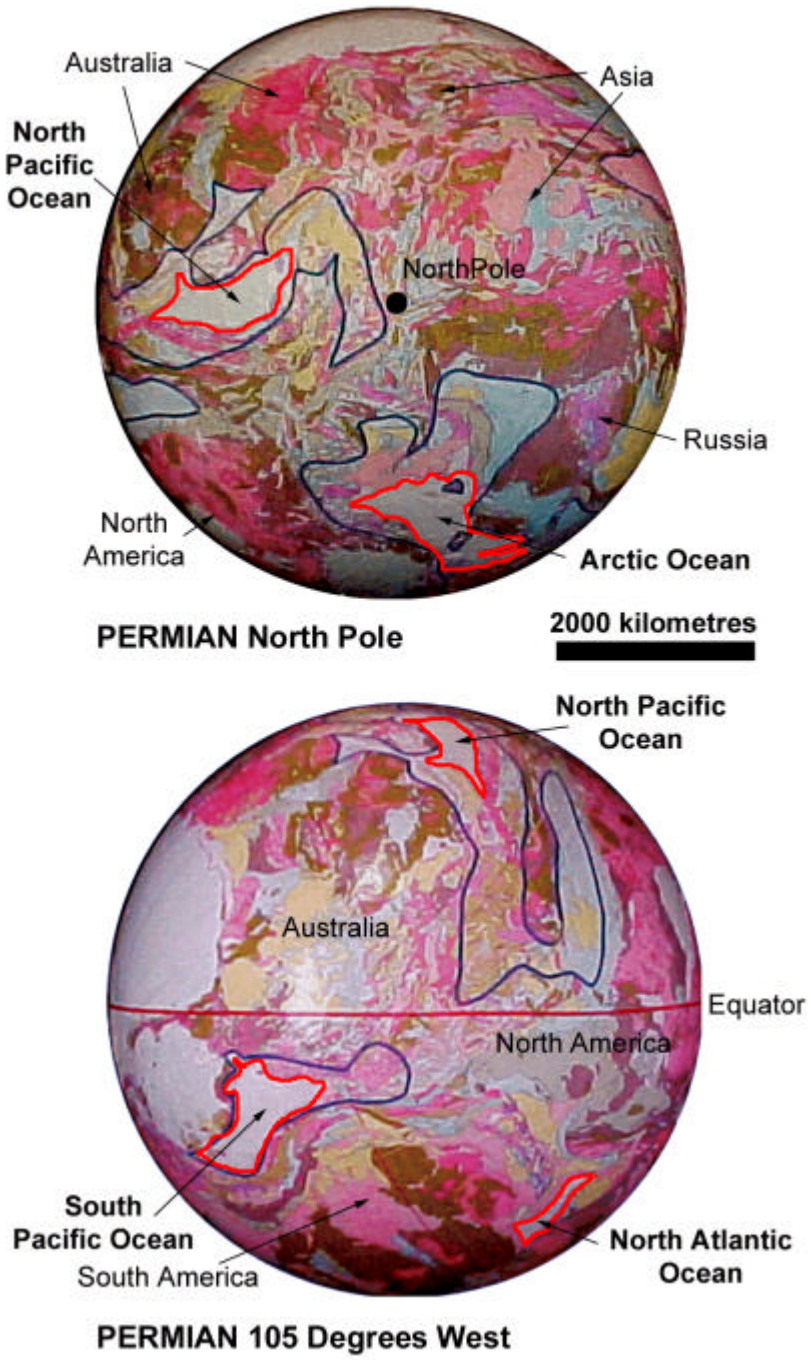

Figure 2.22 Location of continental rupture on a Permian expanding Earth. Rupture shown as red outlines. Subsequent continental break-up and dispersal leads to an enlargement of rupture sites and opening of the modern oceans during the Mesozoic to Recent. Blue lines represent Permian palaeocoastlines (after Scotese *et al*., 1979; Scotese, 1994).

During the Mesozoic to Cenozoic transition symmetric-type mid-ocean spreading ridges became established and the Cenozoic is then characterised by initiation and extension of symmetric-type spreading axes throughout all of the major ocean basins. This is accompanied by rifting and isolation of continental areas such

as Australia, Antarctica and Greenland, as well as breaching of land links between Antarctica and Australia, Antarctica and South America, North America and Europe, and Africa and Europe.

2.7.1 Development of the Arctic Ocean

The Arctic Ocean comprises two large basins, the Amerasia and Eurasia Basins, separated by the Lomonosov ridge. Detailed magnetic mapping in the Eurasian Basin (Figure 2.23) shows that the majority of oceanic lithosphere was generated during the Late Palaeozoic and Mesozoic, followed by Cenozoic to Recent spreading within the active Nansen-Gakkel mid-ocean-ridge. The Nansen-Gakkel spreading ridge forms a continuation of the mid-Atlantic ridge, offset by the Spitzbergen fracture zone. The development of the Amerasian Basin indicates that spreading ceased in this basin during the Late Cretaceous and there are no active spreading centres today.

Conventional reconstructions for the Arctic and North Atlantic Oceans (eg. Srivastava & Tapscott, 1986; Savostovin *et al.*, 1986; Scotese *et al.*, 1988) predict strain histories that are not compatible with the circum-Arctic geology, amounting to an excess of 790 kilometres across regions where no evidence of shortening exists (Rowley & Lottes, 1988). Rowley & Lottes (1988) conclude from a revision of reconstructions that the evolution of the circum-North Atlantic region is dominated by the relative motion history of North America, Eurasia and Greenland. Sea floor spreading between North America and Eurasia began approximately 110 m.y. ago and the geology of the circum-Arctic shelf is characterised by extension and strike-slip basins, with no evidence of Mid Mesozoic or younger structures associated with contractural deformation (Rowley & Lottes, 1988).

On an expanding Earth the Arctic Ocean (Figure 2.23) commenced opening during the Permian to Jurassic during intra-continental extension between North America and Eurasia, forming a small proto-Arctic Ocean. This proto-ocean progressively extended southeast during the Mesozoic, joining with a northern extension of the Atlantic Ocean during the Eocene. Throughout the Mesozoic to Pliocene the Alaskan and Siberian Peninsulas remained joined and the Arctic Ocean remained as a northern extension of the Atlantic Ocean. Throughout the Mesozoic and Cenozoic the North Pole was located within the Arctic Ocean region.

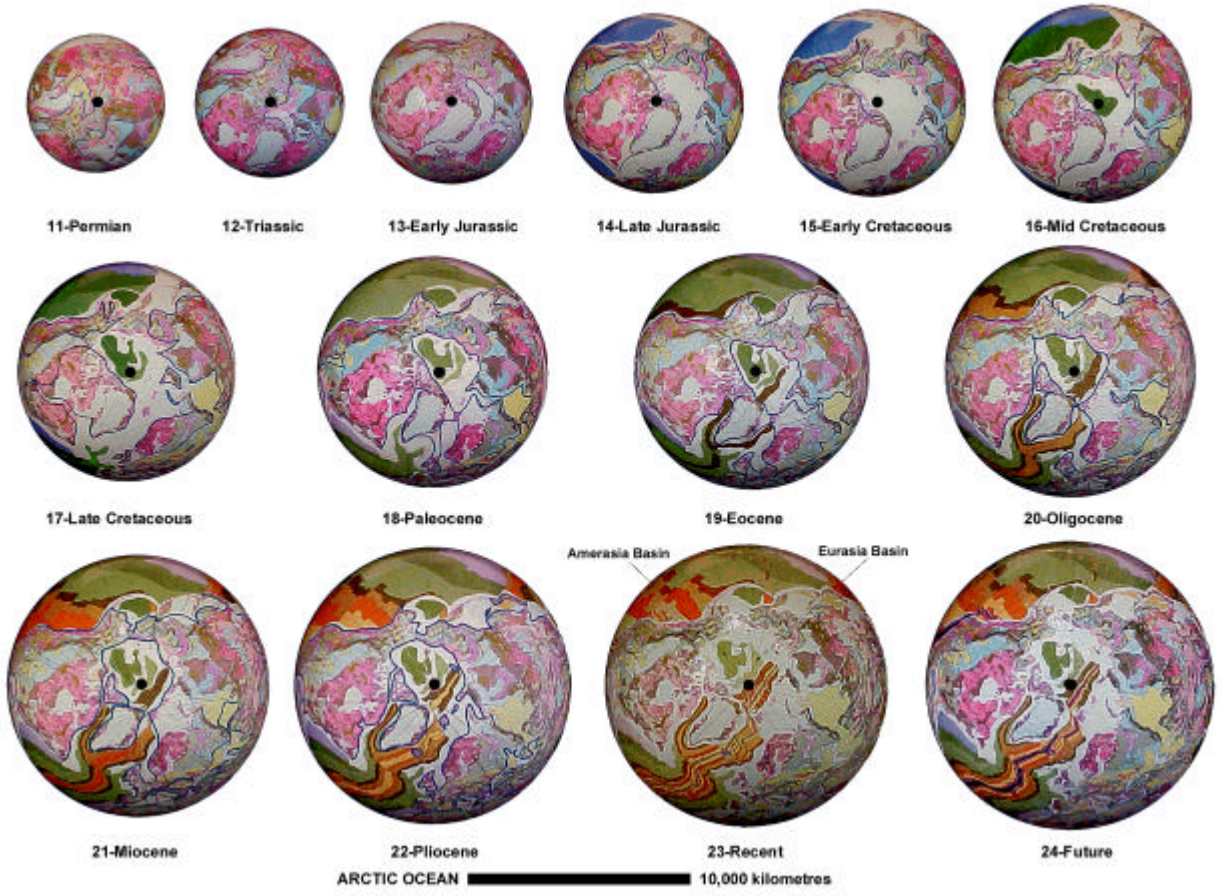

Figure 2.23 Tectonic development of the Arctic Ocean. The Arctic Ocean (white) commenced opening during the Early Permian as an extensional basin located between North America and Eurasia, and since the Eocene merged to form an extension of the North Atlantic Ocean. ● north pole, blue lines represent palaeocoastlines. (After CGMW & UNESCO, 1990).

Oceanic magmatism within the Amerasian and Eurasian Basins commenced during the Cretaceous in association with an early, rapid opening of the north Pacific Ocean. Opening of the Arctic Ocean basins was accompanied by extension and strike-slip dislocation along the Alaskan and Siberian Peninsulas, plus fragmentation and separation of the Canadian Arctic Islands, Greenland and Hudson Bay during the Paleocene.

From the Late Cretaceous to Recent a northward migration of the North Atlantic mid-oceanic-ridge extended into the Arctic Ocean region as the Nansen-Gakkel spreading ridge resulting in rifting between Greenland, Canada and Eurasia. During this phase sedimentation within the Arctic Ocean shifted from shallow basinal to marginal shelf settings bordering the deep ocean spreading ridge. The Cenozoic represents a continuing phase of oceanic and continental crustal extension, resulting in further separation of the Canadian Arctic Islands, opening of Hudson

Bay, rifting between Greenland and Canada and separation of the Alaskan and Siberian Peninsulas across the Bering Straight during the Pliocene.

2.7.2 Development of the Atlantic Ocean

The Atlantic Ocean can be subdivided into north and south Atlantic regions. Opening of the Atlantic Ocean on an expanding Earth (Figure 2.24) commenced during the Permian as a meridional orientated basin in the north Atlantic region, located between Africa and North America. Differential movement of North America, South America and Africa during the Mesozoic and Cenozoic resulted in extension of the North Atlantic Ocean into the South Atlantic Ocean region, and opening of the Gulf of Mexico and Caribbean regions.

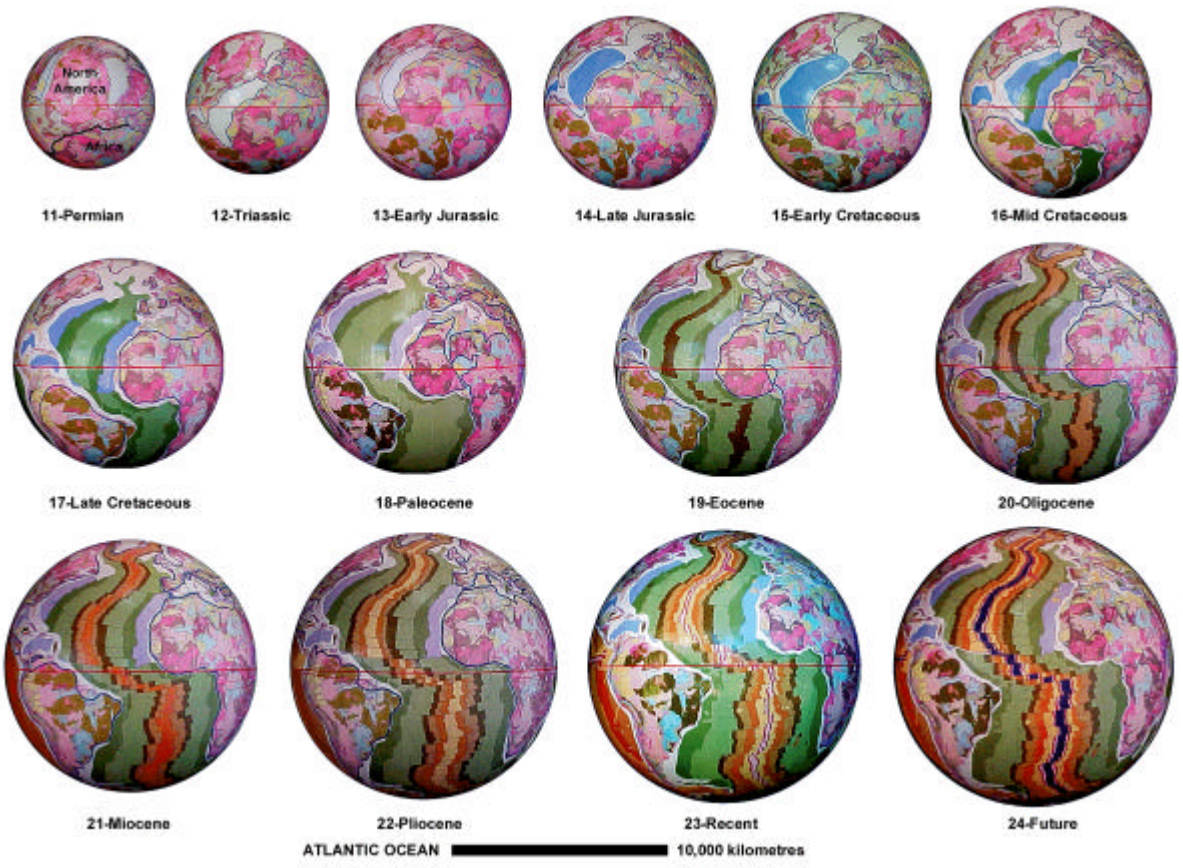

Figure 2.24 Tectonic development of the Atlantic Ocean. The Atlantic Ocean commenced opening during the Early Permian as a meridional orientated rift basin located between North America and Africa. The North and South Atlantic Oceans merged during the Late Cretaceous and have a symmetrical mid-ocean-ridge spreading axis. Blue lines represent palaeocoastlines (Section 3.3) and black lines represent continental outlines. (After CGMW & UNESCO, 1990).

Conventional reconstructions of South America and Africa (eg. Mascle *et al.*, 1988; Scotese *et al.*, 1988; Scotese, 1994) fit the corresponding margins of North

Brazil and Guinea according to the geological matches. This produces a narrow triangular void widening south between the continental margins of South America and Africa south of the Niger Delta region. To minimise this southern misfit the margin of South America may also be fitted against Africa, south of the Niger Delta region. This then produces a narrow triangular void between the Guinea and north Brazil margins widening westwards, producing a significantly greater area of misfit between Florida and Central America.

To address these misfit problems Sundvik & Larson (1988) and Unternehr *et al.* (1988) incorporated intraplate deformations within Africa and South America into reconstructions of the Atlantic Ocean. This produces a tighter fit of the continents in the south Atlantic region but then shifts the problem of misfit to the Mediterranean and Caribbean Sea regions.

On an expanding Earth (Figure 2.24) misfitting between the continental margins of North and South America, Eurasia and Africa in the North and South Atlantic Oceans is eliminated. The intraplate deformations addressed by Sundvik & Larson (1988) and Unternehr *et al.* (1988) are however, incorporated in reconstructions to allow for relief of surface curvature within the African and South American continents.

North Atlantic Ocean

Opening of the North Atlantic Ocean (Figure 2.24) during the Permian progressively extended north into the Arctic Ocean and south into the South Atlantic Ocean with time. From the Early Jurassic an anti-clockwise rotation of the assembled South American and African supercontinent, relative to North America, resulted in rifting and spreading between North America and Africa, extending west into the Caribbean Sea.

During the Early Cretaceous the North Atlantic Ocean spreading ridge extended north between the Grand Banks continental shelf of Canada and Iberia in response to progressive widening of the more southerly basin regions of the North Atlantic Ocean. During the Late Cretaceous the North Atlantic spreading axes extended further into the Arctic Ocean, branching north-west into the Labrador Sea rift zone between Canada and Greenland and north-east, resulting in rifting and rotation of Spain relative to France and England. From the Late Cretaceous to Recent the North Atlantic mid-ocean-ridge continued as a symmetrical spreading axis, in conjunction with the Nansen-Gakkel spreading ridge within the Arctic Ocean.

South Atlantic Ocean

The South Atlantic Ocean (Figure 2.24) commenced opening during the Late Jurassic as a continental rift basin located between Africa and South America and opening in the south coincided with opening and extension of the Indian Ocean. Basin separation commenced during the Late Jurassic along the now separated Agulhas and Falklands fracture zones in the southern South Atlantic Ocean. This separation progressively extended north, and merged with the North Atlantic spreading ridge during the Early Cretaceous along the Nigerian and Brazilian continental rift zone, forming a single Atlantic Ocean.

From the Late Cretaceous to Recent, spreading in both the North and South Atlantic Oceans occurs along a common mid-Atlantic spreading ridge, extending to the north and south. Subsequent spreading in both regions is then symmetrical, with a clockwise rotation of South America relative to Africa giving a greater spreading rate in the southern South Atlantic Ocean.

2.7.3 Development of the Caribbean Sea

The Caribbean Sea comprises the Mexico, Colombian and Venezuelan Basins separated by the Antilles Arc. The development of the Caribbean Sea and accompanying basins is intimately associated with the plate motion histories of South America and Africa relative to North America. Oceanic mapping shows that spreading was active within each basin during the Jurassic and was reactivated along the Antilles Arc from the Paleocene to Recent.

Conventional plate tectonic reconstructions of the Caribbean Sea (eg. Pindell *et al.*, 1988; Ross & Scotese, 1988; Scotese *et al.*, 1988; Scotese, 1994) fit the Brazil and Guinean coastlines together to minimise the central Atlantic misfit. Pindell *et al.* (1988) consider that the Caribbean basins resulted from a divergence of North and South America to approximately their present relative positions from the Late Triassic? to Late Cretaceous. The relative motions between the North and South American plates during the Late Cretaceous to Recent were considered to have had only minor effects on the structural development of the Caribbean region. During the Late Cretaceous to Mid-Eocene minor relative motion occurred, with South America diverging approximately 200 kilometres. Since the Mid-Eocene the region then underwent minor north-south convergence (Pindell *et al.*, 1988).

Ross & Scotese (1988) describe the Caribbean region as a buffer zone between the North American plate, the South American plate and subducting oceanic plates of the Pacific Ocean. This supported Pindell & Barnett's (1987) suggestion that the Caribbean plate is a preserved piece of the Pacific Ocean Farallon plate and was considered allochthonous with respect to North and South America. Pindell & Barnett (1987) supported their argument by referring to the origin and timing of formation of the Guatemala Santa Cruz Ophiolite and progressive emplacement of arc material onto the continental margin of northern South America.

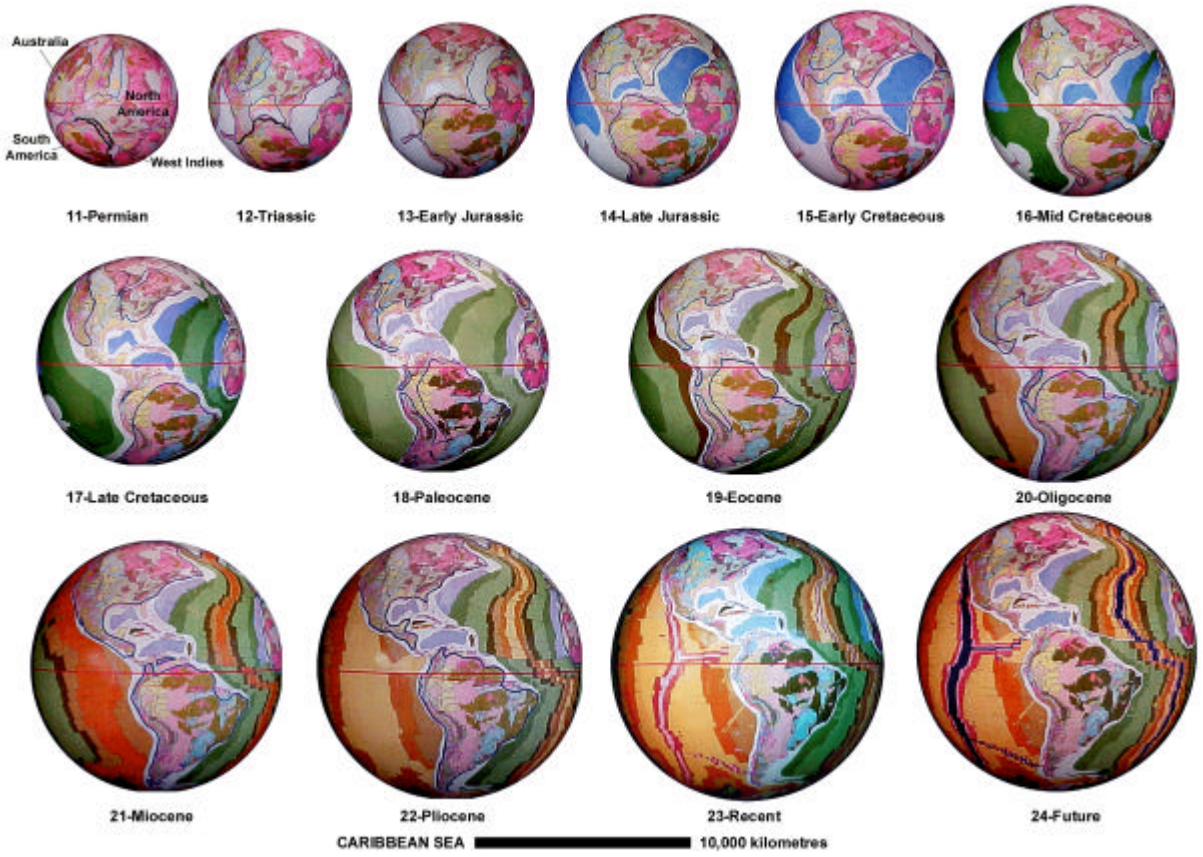

Figure 2.25 Tectonic development of the Caribbean Sea. The Caribbean Sea is intimately related to the tectonic development of the North Atlantic Ocean and divergent plate motion history of North and South America. Blue lines represent palaeocoastlines (Section 3.3) and black lines represent continental outlines. (After CGMW & UNESCO, 1990).

On an expanding Earth the Caribbean region (Figure 2.25) originates during the Triassic to Early Jurassic as intracontinental basin extension between the North and South American continents, accompanied by marine sedimentation within the Mexico basin. This early basin development is associated with opening of the North Atlantic Ocean and subsequent rifting of Africa. Development is related to a northwest migration of North America relative to the assembled South American and

African supercontinent. The Colombian and Venezuelan basins opened during the Cretaceous, separated by the Antilles Arc, however timing and opening of the basins may extend to the Jurassic with the Antilles Arc forming as an island arc.

This early extensional phase lasts until commencement of rifting and break-up of South America and Africa during the Early Cretaceous. During this phase the Nicaraguan and Panama Peninsula remain joined to South America and undergoes extension and strike-slip dislocation. After separation of South America and Africa, South America rotates clockwise relative to North America in response to spreading in the South Atlantic Ocean, resulting in extension and elongation of the Caribbean basins and isolation of the Antilles island arc.

From the Paleocene to Recent, South America continues to rotate clockwise relative to North America resulting in sinistral strike-slip motion along the Antilles Arc, extending to the western margin of Mexico and Gulf of California. Differential motion between the North and South American continents results in rotation of the Panama Isthmus and minor south to north compression.

On an expanding Earth an allochthonous origin for the Caribbean region is unnecessary. The timing and formation of the Gulf of Mexico and Caribbean Sea agrees with the conclusions of Pindell *et al.* (1988) and Tanner (1983), and emplacement of Santa Cruz Ophiolite and continental arc material reflects the ongoing extensional stress regime between the two continents.

2.7.4 Development of the Mediterranean Sea

The Mediterranean to Middle East region on a constant radius Earth forms the western apex of a triangular shaped Tethys Ocean (eg. Ciric, 1983), widening eastward towards a Panthallassa Ocean and separating Gondwana to the south from Laurasia in the north. During amalgamation and break-up of Pangaea smaller younger basins were considered to have formed within the Tethys Ocean as continental fragments were rifted away from the palaeo-Tethyan margins, later to be consumed in the progressive collision of Africa and Eurasia (Turnell, 1988).

Conventional reconstruction of the Mediterranean to Middle East region (eg. Gealey, 1988; Turnell, 1988; Scotese, 1994) depict the region as evolving from a number of microplates drifting between Africa and Eurasia during the Mesozoic closure of a Tethys Ocean. The subsequent history during the Mesozoic and

Cenozoic is then a progressive elimination of the Tethyan Ocean by subduction or thrusting of its pre-Late Triassic lithospheric crust (Owen, 1976).

The evolution of the Mediterranean to Middle East region on an expanding Earth (Figure 2.26) is related to intra-continental extension between the African and Eurasian proto-continents in association with development of an epi-continental Tethys Sea (Section 3.3). The Mediterranean Sea and tectonic development of the Middle East region commences during the Jurassic as a result of clockwise rotation of Europe, relative to Africa, in conjunction with opening of the Atlantic Ocean. The opening of the Caspean Sea during the Early Cretaceous, Black Sea during the Mid-Late Cretaceous and Aral Sea during the Mid-Paleocene represent regions of continental crustal dilation resulting from interaction between the Arabian plate and central Europe.

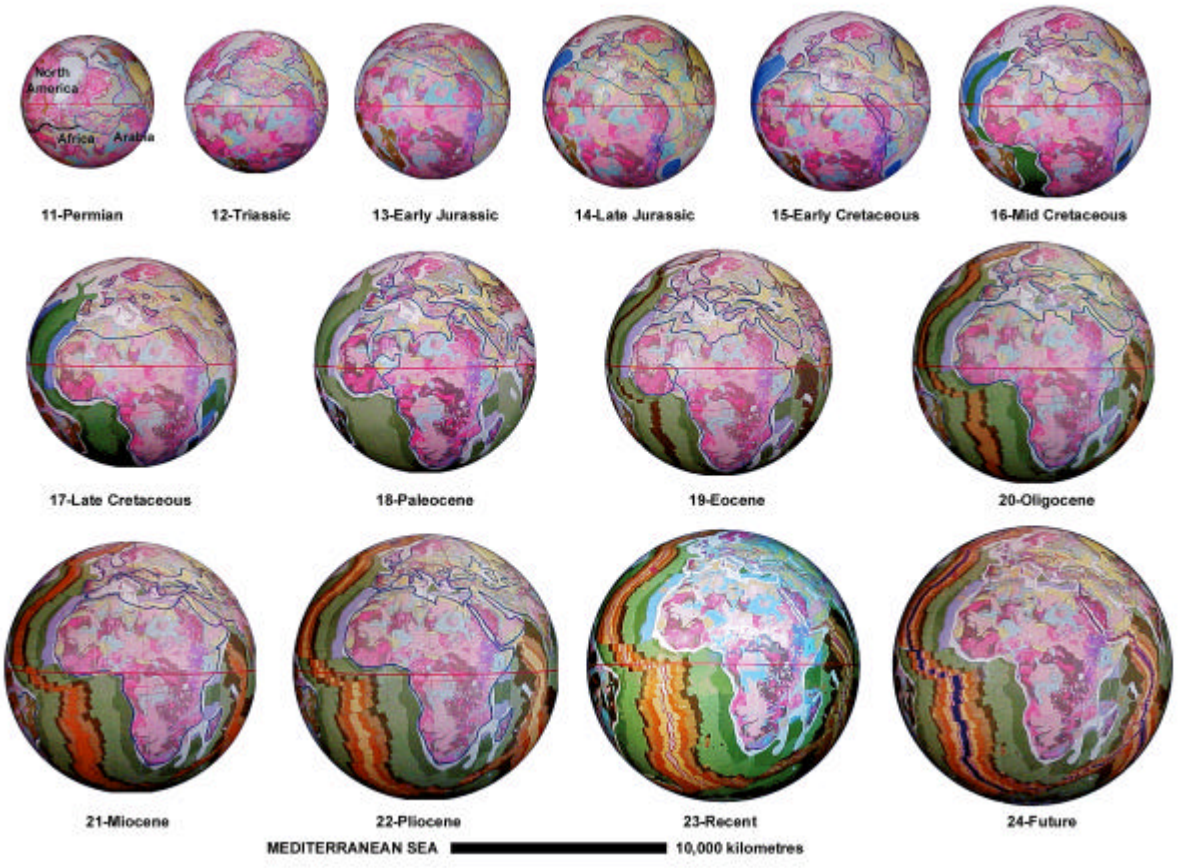

Figure 2.26 Tectonic development of the Mediterranean Sea. The Mediterranean Sea opened during the Jurassic in conjunction with opening of the Atlantic Ocean and clockwise rotation and divergence of Europe relative to Africa. Blue lines represent palaeocoastlines (Section 3.3) and black lines represent continental outlines. (After CGMW & UNESCO, 1990).

Oceanic mapping (Figures 2.1 and 2.26) shows that extension within the Mediterranean to Middle East region was active during the Jurassic and Early

Cretaceous. From the Mid-Cretaceous to Miocene complex poly-phase orogenic motion (Section 3.3.10) between Africa and Europe is marked by Alpine orogenesis, followed by continental extension and basin formation within eastern Europe. The Alpine orogenic event coincides with a northward extension of the North Atlantic Ocean spreading axis, marked by opening of the Bay of Biscay between Spain and France during the Late Cretaceous. Similarly, opening of the Persian Gulf and Red Sea commences during the Eocene, continuing to the Recent. Sea-floor spreading is re-activated in the western Mediterranean region during the Miocene accompanied by continental rifting between West Africa and Spain.

On an expanding Earth a large Tethyan Ocean separating Gondwana and Laurasia and a north-south closure of the Tethyan Ocean during the Mesozoic and Cenozoic is not required. Instead, opening of the Mediterranean to Middle East region is a result of clockwise rotation and extension of Eurasia relative to the adjoining African-Arabian continent. This continental motion, extending from the Iberian Peninsula to the Tibetan Plateau, results in a rotation of Italy and fragmentation of the Alpine mountain belts during the post-Mid Cretaceous to Recent.

Expanding Earth reconstructions (Figure 2.26) also suggest a straightforward development of the Black Sea region, the orogenic belts of the Balkens, Turkey and the Caucuses, the platform tectonics of the southern Russian platform north of the Black Sea and development of the Aegean Sea during the Late Cenozoic.

2.7.5 Development of the Indian Ocean

Reconstructions of the Indian Ocean (eg. Powell *et al.*, 1988; Royer *et al.*, 1988; Scotese *et al.*, 1988; Scotese, 1994) and assemblage of circum-Indian Ocean continents is crucial to an understanding of the break-up and dispersal of Gondwana relative to Laurasia. Conventional reconstructions place India within Gondwana adjacent to Africa, Madagascar and Antarctica, and the Indian Ocean formed during subsequent Pangaean continental break-up and dispersal.

On conventional Pangaean reconstructions a wide Tethyan Ocean is located between the southern Gondwana and northern Laurasia supercontinents (eg. Audley-Charles *et al.*, 1988; Scotese, 1994). India is inferred to have migrated north, as an island continent from an initial Gondwanan configuration adjacent to Africa,

Madagascar and Antarctica during the Jurassic, to collide with the Asian continent along an inferred Indus Suture Zone (Valdiya, 1984). This migration necessitated subduction of some 5000 kilometres of oceanic crust to close the Tethys Ocean during the Mesozoic to Early Cenozoic and collision with Asia resulted in formation of the Himalayan mountain belts during the Cenozoic (eg. Valdiya, 1984).

On an expanding Earth the Indian continent remains attached to the Asian continent throughout Earth history (Figure 2.27) and the Indian Ocean forms during post-Permian continental break-up and dispersal. Break-up and rifting between Africa, Madagascar, India and Antarctica commences during the Early Jurassic, forming the Somali Basin adjacent to East Africa and an inferred Indian-Antarctican basin located between India and Antarctica.

Figure 2.27 Tectonic development of the Indian Ocean. The Indian Ocean opens during the Jurassic and India remains part of Asia throughout Earth history. A triple junction forms during the Cenozoic, cross-cutting previous spreading axes. Blue lines represent palaeocoastlines (Section 3.3) and black lines represent continental outlines. Triassic to Mid Cretaceous models are centred on the south pole (black dot). (After CGMW & UNESCO, 1990).

This early extensional phase continues until the Mid-Cretaceous with the Somali Basin extending south, forming the Mozambique Channel between

Madagascar and Africa, to a triple junction located south of Madagascar. The southern limb of this triple junction extends to the South Atlantic Ocean, opening near the present Falkland Islands, and the east limb extends through the inferred Indian-Antarctican basin eastwards to join with the emerging Wharton Basin adjacent to west Australia. By the Mid Cretaceous, Madagascar, the Somali Basin and the Mozambique Channel are rifted from India and remain part of the African plate.

From the Mid-Cretaceous to Paleocene sea-floor spreading shifts to the Arabian Sea located between Madagascar and India. The Indian Ocean undergoes a north south widening between Australia, Antarctica, Africa and South East Asia with a rapid northward displacement of India and Asia relative to Antarctica. Extension and complex intra-continental motion between Australia and South East Asia results in formation of the South East Asian island arcs and initiation of the Java Trench. The Java Trench represents a complex zone of intraplate translational displacement between South East Asia and the Wharton Basin, relative to Australia.

During the Paleocene to Recent a central Indian Ocean triple junction is established, with extension of new spreading axes cross-cutting old established oceanic crust. In the southern Indian Ocean region a southwest-spreading axis splits across older spreading patterns and joins with the South Atlantic Ocean mid-ocean-ridge system. The Ninetyeast spreading axis, located within the eastern Indian Ocean, is abandoned during the Eocene and a new spreading axis extends southeast into the Eucla Basin of Australia, initiating separation and northward migration of Australia relative to Antarctica and opening of the Southern Ocean. The Gulf of Aden is formed during the Miocene during a northwest extension of the central Indian Ocean and Carlsberg spreading ridges, with a second triple junction forming at the western end of the Gulf of Aden. This triple junction is represented by the actively spreading Red Sea axis and East African Rift Valley system.

On an expanding Earth India remains in intimate contact with Asia throughout the Mesozoic and Cenozoic (eg. Davidson, 1983; Stocklin, 1983; Ahmad, 1988) without the need for a wide Tethyan Ocean. The differential crustal extension and clockwise motion of the Mediterranean and European continental regions relative to Asia is accompanied by an anticlockwise rotation of India relative to Asia during the Cenozoic. This results in complex plate motion along the Himalayan orogenic belt, extending east to the Java Trench and South East Asian island arcs. A

northward migration of India and Asia relative to Antarctica is accompanied by an anticlockwise rotation of India relative to Asia, resulting in 1400 kilometres of crustal shortening in the Himalayan region.

2.7.6 Development of the Pacific Ocean

The present Pacific Ocean occupies nearly half the surface area of the Earth and is arbitrarily subdivided into a North and South Pacific Ocean at the present equator, and reference is made to the central Pacific Ocean region. In all conventional Pangaean reconstructions (eg. Weijermars, 1989; Scotese *et al.*, 1988; Scotese, 1994) the pre-cursor to the Pacific Ocean was a large Panthallassa Ocean (Scotese, 1987). This early Mesozoic Panthallassa Ocean possessed an oceanic crust generated during the Triassic and Palaeozoic, and the Mesozoic and Cenozoic history was one of east-west and north-south contraction of the oceanic area to the size of the modern Pacific Ocean. All pre-Mesozoic crust is inferred to have been subducted around the circum-Pacific margins as well as subduction of a substantial quantity of oceanic crust generated within Pacific Ocean mid-ocean-rifts during the Mesozoic to Cenozoic.

On conventional plate tectonic reconstructions the eastern North Pacific Ocean region is inferred to have been progressively overridden by the North American continent as it is displaced westward during sea-floor spreading within the central Atlantic Ocean (Owen, 1976). The North Pacific Ocean spreading axis was then overridden and subsequently dislocated along the North American Pacific margin (eg. Scotese, 1987; Scotese *et al.*, 1988).

To dispose of the excess oceanic lithosphere generated in the Atlantic, Indian, Arctic, Southern and South Pacific Oceans the continental margins of the circum-Pacific Ocean in conventional reconstructions are inferred to consist of two main types (Owen, 1976; Scotese, 1987). The eastern and northern margins are marked by subduction zones along the Peru-Chile Trench adjacent to South America, zones adjacent to North America and along the Aleutian Trench subduction zone flanked by the Aleutian Island arc. Ocean floor within these subduction zones is inferred to be thrust down beneath the Cordilleran and Andean fold belts of North and South America. Marginal oceanic basins are characteristic of the western Pacific margin and separate the various west Pacific island arcs, such as the Japanese Islands, from

the Asian continent to the west. Here, the principal subduction zones are inferred to lie east of the island arcs and are marked by deep trenches such as the Marianas Trench.

Along the southern margin of the Pacific Ocean adjacent to Antarctica no active subduction zones are present, although Owen (1976) considers that subduction zones may have existed during the Mesozoic. The western boundary of the South Pacific Ocean has marginal oceanic basins, such as the Coral and Tasman Seas, which separate the Australian continental margin and the active Tongan and Kermadec Trench subduction zones. Subduction zones in this region are flanked by island arcs including New Zealand and New Caledonia.

On an expanding Earth an expansive pre-Mesozoic Panthallassan Ocean, and similarly a Tethyan Ocean, is not required and subduction of between 5,000 to 15,000 kilometres of Pacific oceanic lithosphere (eg. Larson & Pitman, 1972) is unnecessary. The Pacific Ocean originates during the Early Permian as two separate intra-continental extensional basins, a North Pacific basin (Figure 2.28) located between northwest Australia, Canada and China, and a South Pacific basin (Figure 2.29) located between east Australia, South America, New Zealand and Antarctica. These basins progressively extend south and north along the west coasts of North and South America respectively during the Triassic and merge to form a single Pacific Ocean during the Late Triassic.

Remnants of this early basin history are preserved as continental margin and marine plateau sediments within South East Asia and the Coral Sea regions (eg. Dickins *et al.*, 1992). The evolution of the North and South Pacific Oceans then involves rapid northeast to southwest extension relative to North and South America and Australia. Preservation of oceanic magmatism within the North Pacific Ocean commences during the Jurassic and by the Late Jurassic a deep ocean extends southeast and south along the west coasts of North and South America, initiating oceanic magmatic development in the South Pacific Ocean.

Throughout the Mesozoic the North Pacific Ocean rapidly enlarges and spreading axes extend southeast into the South Pacific region. Oceanic mapping indicates that ocean-floor spreading and magmatism is generally arcuate shaped, following the west coasts of North and South America, and extends west from South America, fragmenting the Coral Sea basin plateau sediments during the Cretaceous. During the Mid to Late Jurassic rifting between a New Zealand and New Caledonia

proto-continent, South America, Australia and Antarctica results in isolation of the Coral Sea plateau, Lord Howe Rise and New Zealand complex, leaving the New Zealand proto-continent as an island continent.

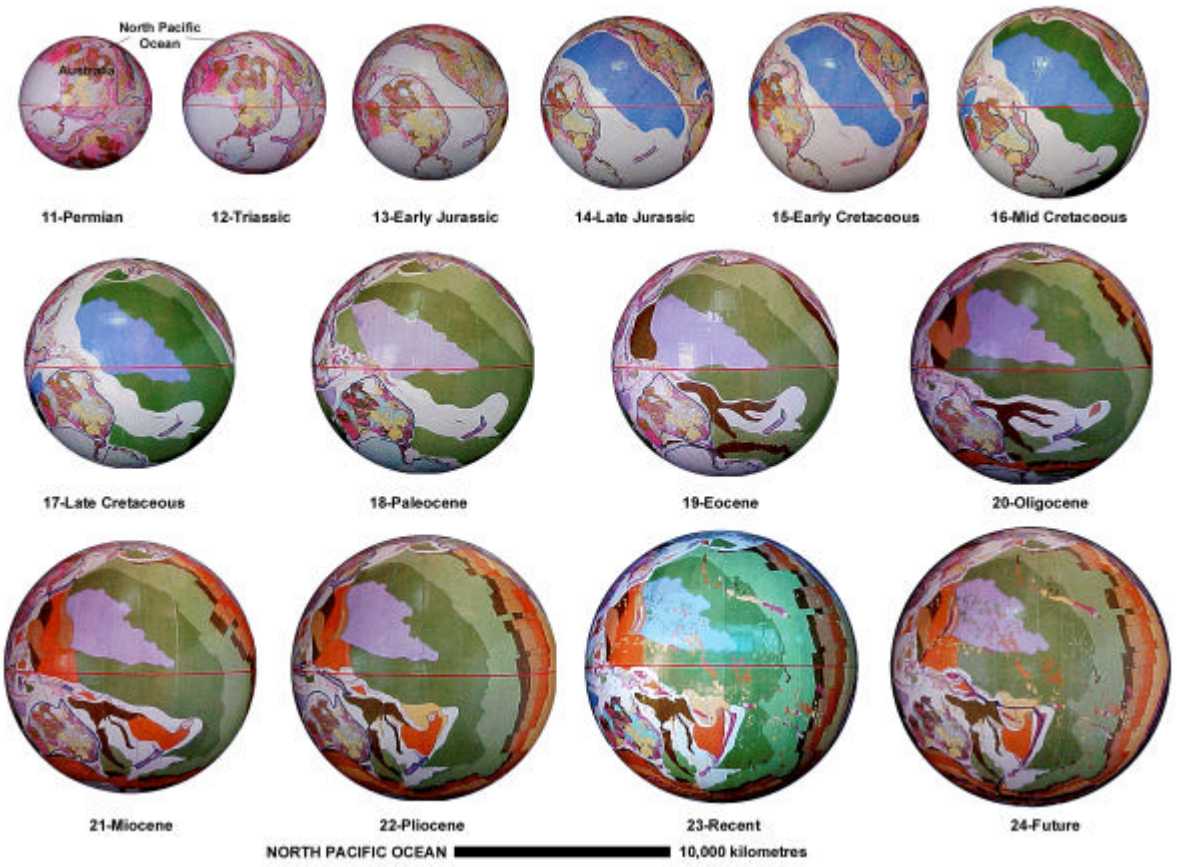

Figure 2.28 Tectonic development of the North Pacific Ocean. The Pacific Ocean commenced opening during the Early Permian as a small extensional basin prior to rapid opening and extension during the Mesozoic and Cenozoic. An asymmetric spreading axis is located along the North American west coast. Blue lines represent palaeocoastlines (Section 3.3). (After CGMW & UNESCO, 1990).

Oceanic development during the Cenozoic is characterised by initiation and extension of symmetric style ocean-floor spreading, commencing in the Tasman Sea during the Palaeocene and extending east towards South America during the Eocene. Elsewhere around the Pacific Rim, ocean-floor spreading continues to be asymmetric, extending into the Coral Sea adjacent to Eastern Australia and into the Philippine and China Sea regions. An extension of symmetric style ocean-floor spreading continues north, extending along the west coast of North America to the present location adjacent to California.

Translational crustal interaction between the North Pacific Ocean plate, Australia, South East Asia and China results in formation of the island arc systems characteristic of the western Pacific region. This region represents a complex interplay of transtension and transpressive plate motions in an otherwise tensional regime generated during adjustment of surface curvature of the North Pacific Ocean Jurassic ocean crust (Section 2.5). The Aleutian, Japanese, Philippine and Solomon Islands and similarly the Indonesian island arcs result from extension, accompanied by volcanism, related to this translational motion and intraplate interaction.

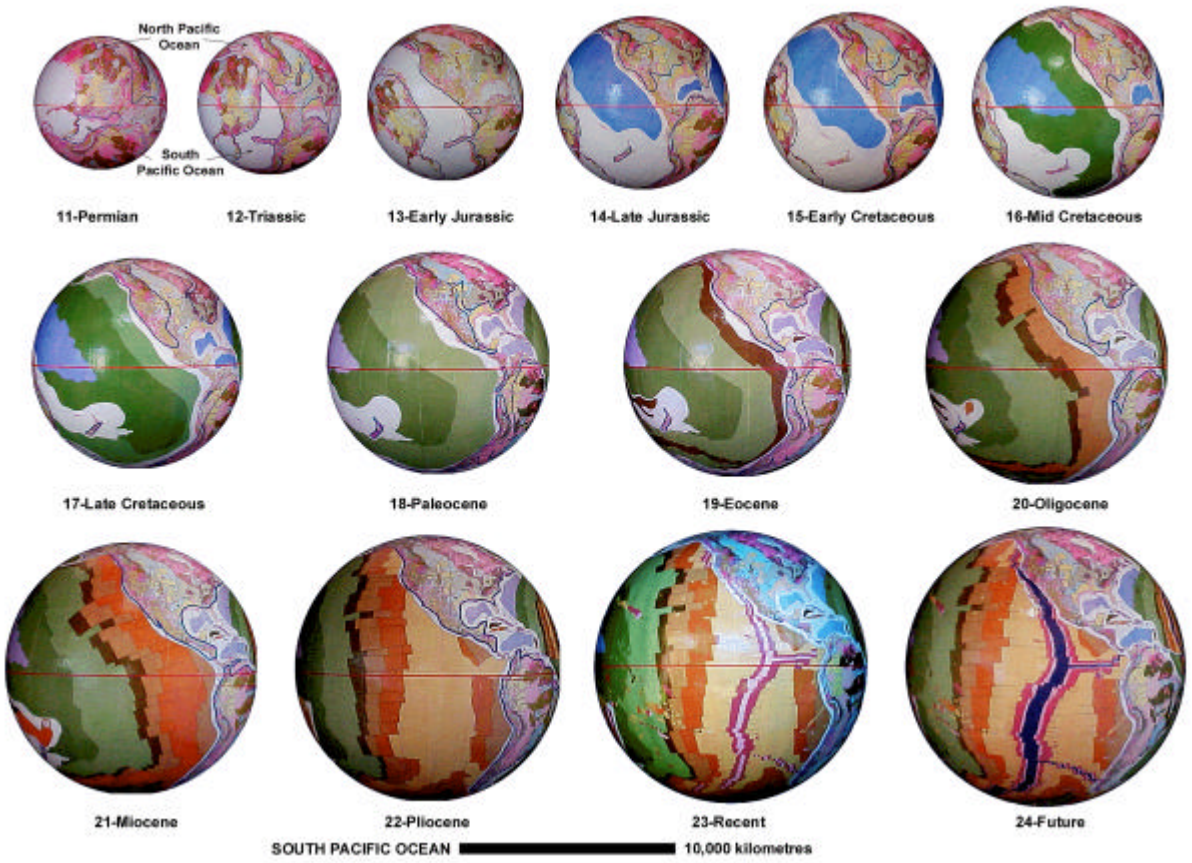

Figure 2.29 Tectonic development of the South Pacific Ocean. The South Pacific Ocean commenced opening during the Early Permian as a small extensional basin prior to extending north and merging with the North Pacific Ocean during the Triassic. Asymmetric spreading evolves to symmetric spreading during the Cenozoic. Blue lines represent palaeocoastlines (Section 3.3). (After CGMW & UNESCO, 1990).

The development of the Pacific Ocean on an expanding Earth cannot be reconciled with conventional reconstructions on a constant sized Earth because of the spatial and temporal restrictions imposed by an Early Mesozoic Panthallassan Ocean and circum-Pacific subduction of oceanic lithosphere. The oceanic magnetic spreading patterns (Figure 2.1), generated during opening and spreading within each

of the modern oceans, negate the need for subduction of pre-existing oceanic crust. The complex oceanic crustal patterns displayed are readily explained by asymmetric to symmetric evolution of the Pacific Ocean spreading axes and plate margin regions are explained by translational plate interaction during relief of surface curvature.

2.7.7 Development of the South East Asian Seas and South-West Pacific Ocean

The South East Asian region comprises the Philippine, South China, Celebes, Banda and Java Seas and is treated separately to the southwest Pacific Coral and Tasman Sea regions. Conventional reconstructions on a constant sized Earth (eg. Scotese *et al.*, 1988) interpret these areas as representing marginal or back-arc ocean basins, separated from the various island arcs by back-arc spreading along zones of crustal subduction and deep trenches (Owen, 1976; Seno & Maruyama, 1984; Gray & Norton, 1988).

South East Asian Seas

On an expanding Earth the South East Asian region is an area of passive basin extension and complex clockwise rotation, fragmentation and associated translational motion and island arc volcanism resulting from south-east to north-west intracontinental extension between Asia and Australia. This contrasts with a plate tectonic requirement for collision and complex subduction of the Australian and North Pacific plates against the Asian and Philippine plates.

The South East Asian region on an expanding Earth (Figure 2.30) represents the remnants of basin sediments deposited within a Permian North Pacific proto-ocean. This Permian basin is located between Australia, China and North America prior to rapid opening of the Pacific Ocean during the Triassic to Recent. Development of the region is complexed by the plate motion of Australia relative to Asia and opening of the Pacific and Indian Oceans. Progressive crustal extension during the Late Cretaceous to Pliocene results in opening of the South China, Celebes and Banda Seas and fragmentation of the South East Asian island arcs.

South-West Pacific Ocean

The southwest Pacific Ocean region is structurally complex. The region is related to opening and development of the South Pacific Ocean and is influenced by clockwise translational motion and intraplate interaction along the margin of the

Indo-Australian and Pacific plates. This contrasts strongly with plate tectonic reconstructions where the Australian plate is depicted as moving north and the Pacific Ocean plate is being subducted along the Tongan to Marianas trench arc system (eg. Gray & Norton, 1988, Scotese *et al*., 1988).

On an expanding Earth the south-west Pacific region represents the remnants of basin sediments deposited within a Permian South Pacific proto-ocean, prior to opening and merging with the North Pacific Ocean during the Triassic (Figure 2.30). During the Early Permian, West Antarctica and New Zealand are located adjacent to Australia and South America, and rifting between South America, New Zealand and West Antarctica forms the South Pacific proto-ocean. During the Triassic to Early Jurassic, New Zealand and New Caledonia rift away from Australia and remain attached to Ecuador until separation from South America during the Mid Jurassic.

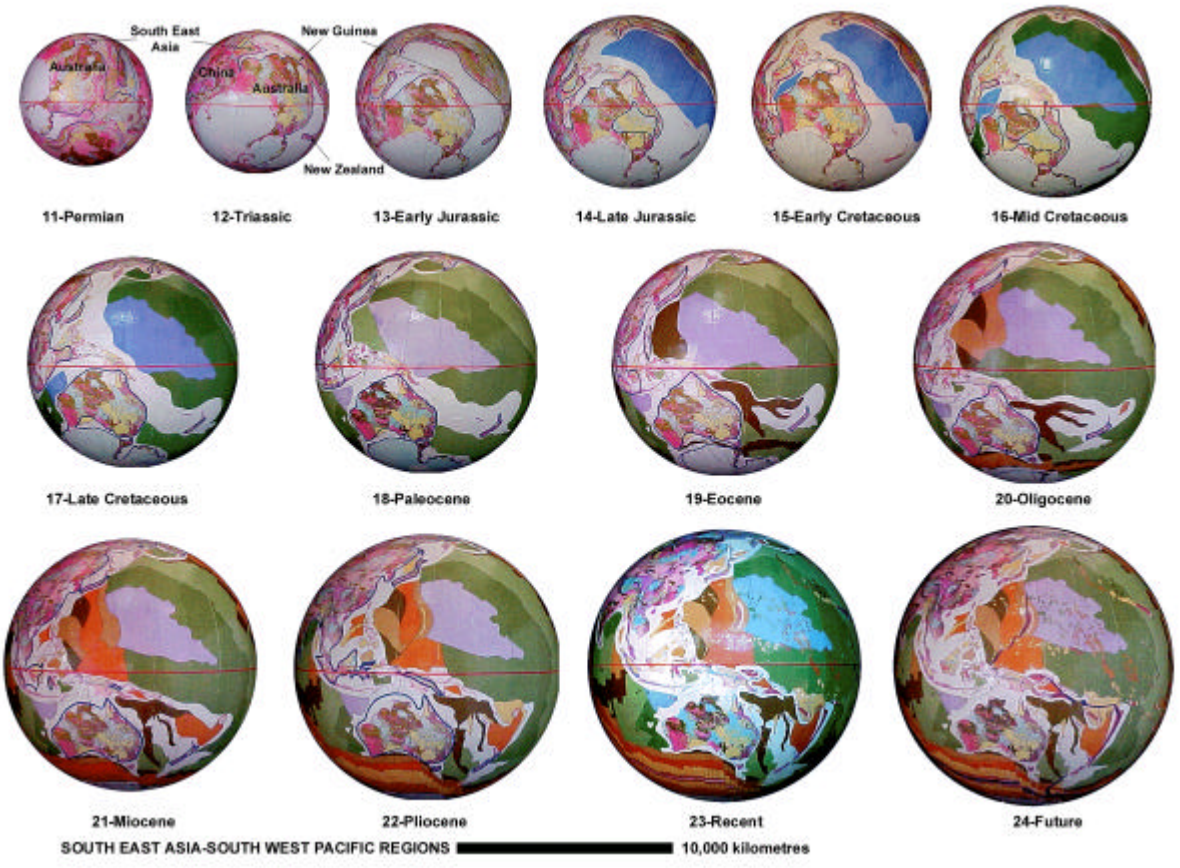

Figure 2.30 Tectonic development of the South East Asian Seas and Southwest Pacific Ocean. The development of both regions is related to opening of the Indian and Pacific Oceans and divergent continental plate motion between Asia, Australia, North and South America and Antarctica. Blue lines represent palaeocoastlines (Section 3.3). (After CGMW & UNESCO, 1990).

During the Mid to Late Jurassic a New Zealand and New Caledonia proto-continent comprising the Coral Sea plateau, Lord Howe Rise and New Zealand island arc complex is established, representing the present South-west Pacific region. Asymmetric ocean-floor spreading in the South Pacific Ocean extends west during the Cretaceous, opening the Tasman Sea and isolating the Lord Howe Rise and New Zealand from Antarctica and Australia. Rifting and opening of the Southern Ocean between Australia and Antarctica commences during the Paleocene with symmetric ocean-floor spreading extending from the Southern Ocean east to South America.

The Tongan to South Solomon and New Hebrides trench and island arc systems on an expanding Earth represent complex plate interaction between the New Zealand and New Caledonia proto-continental plate and the Pacific Ocean plate. This complex interaction during adjustment for changing surface curvature results in clockwise translational motion along the trench and arc systems and fragmentation of the New Zealand and New Caledonia plate during the Cenozoic. Rapid symmetric ocean-floor spreading in the South Pacific Ocean results in rotation of the south-west Pacific region away from Australia during the Cenozoic, and complex plate motion along the Kermadec and Tongan tench and arc system during the Early Miocene results in up to 1000 kilometres of translation along the Alpine fault system of New Zealand.

Both the South East Asian and southwest Pacific basin regions cannot be reconciled with conventional plate tectonic reconstructions. Both regions are interpreted from reconstructions of an expanding Earth as resulting from a progressive evolution of the North and South Pacific Oceans, intraplate interaction accompanied by translational displacement and island arc volcanism, and intracontinental extension between Australia, Asia, North and South America and Antarctica.

2.8 Expansion Extrapolated to the Future (Video A2.31)

An estimate of Earth radius at any time in the future is made by calculating palaeoradius using Equation 2.6 (Section 2.2). Extrapolation of Earth radius to the future indicates that the Earth will approach the radius of the planets Jupiter and Saturn by approximately 500 million years (Appendix A1, Table A1.2).

Plate reconstruction is made at five million years into the future (Figure 2.31). During this time Earth radius would increase by 107 kilometres to 102% of the present Earth radius. Plate reconstruction is based on maintaining the same spatial configuration of plates as the present Earth and adding oceanic lithosphere along each mid-ocean-ridge axis, at a similar rate to current lithospheric generation. The series of images (Figure 2.31) show that expansion to 5 million years in the future is consistent with a continued spreading and elongation of all present-day mid-ocean-ridge axes.

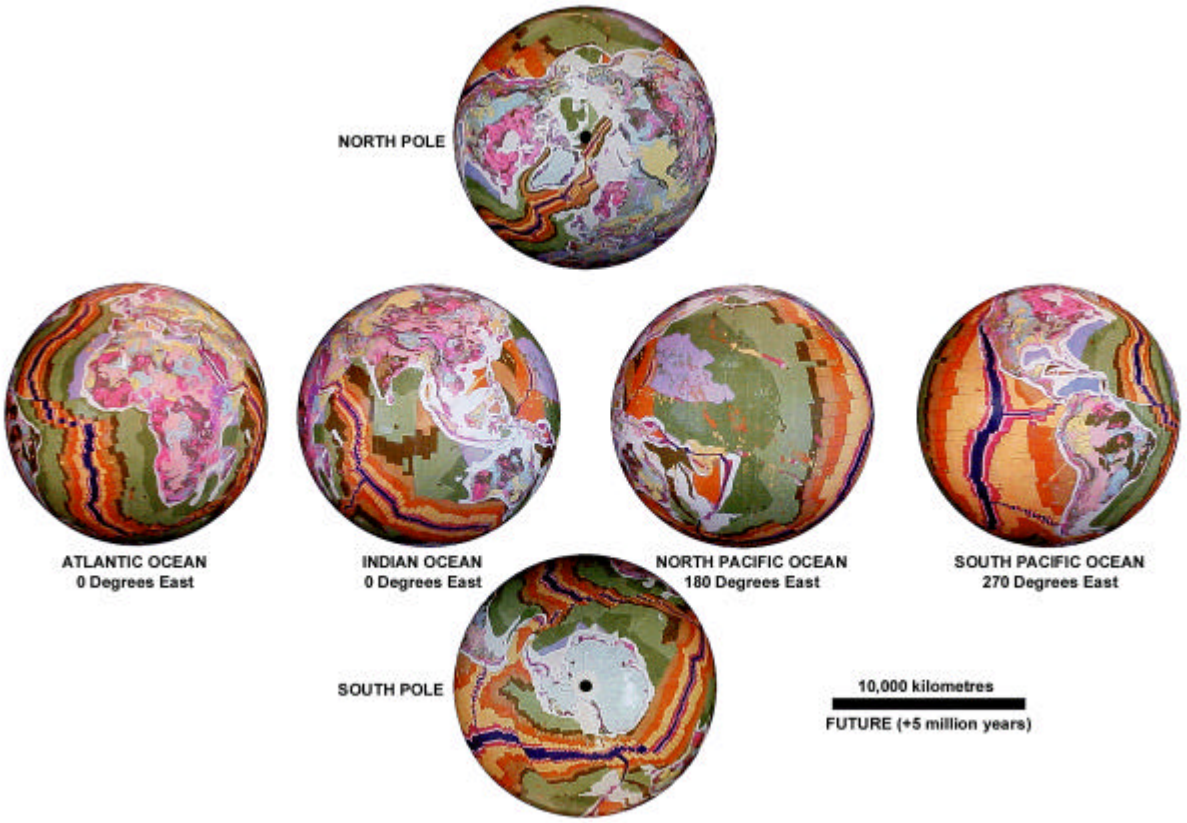

Figure 2.31 The expanding Earth projected to 5 million years into the future. Dark blue chron interval represents spreading at mid-ocean-ridges for the next 5 million years and shows an elongation of ridge axes into seismically active areas such as Turkey, Japan, California and New Zealand. (After CGMW & UNESCO, 1990).

Elongation, or lengthening of mid-ocean-ridge spreading axes during sea-floor spreading is consistent with an increase in Earth circumference with time. Elongation of mid-ocean-ridge spreading axes during Earth expansion is currently occurring within major earthquake prone areas of the world. These include a northward extension of the East Pacific spreading axis through the Gulf of California, rifting and isolating the Californian Peninsula from North America. A

northward extension of the Red Sea Rift through the Gulf of Aqaba and Dead Sea into Turkey, rifting and separating the Sinai Peninsula from Arabia. A northern extension of the Marianan spreading axis to Japan and a southern extension of the Tongan spreading axis through New Zealand.

On an expanding Earth each of these earthquake prone areas represent extensional regimes and earthquake activity results from tensile fracture of the crust, causing rifting and intraplate motion. This contrasts with the conventional plate tectonic requirement for plate convergence and subduction of oceanic crust within each of these areas. Figure 2.31 shows that elongation of mid-ocean-ridge spreading axes during Earth expansion represents a means where seismic activity progressively migrates with time, in conjunction with intracontinental or intraplate rifting.

2.9 Summary of Empirical Modelling (Video A2.14)

Oceanic magnetic mapping, age dating and correlation of all Earth's ocean basins have provided a means to accurately quantify plate reconstruction and a potential rate of expansion on an expanding Earth. The oceanic mapping (Figure 2.1) shows that all ocean basins contain mid-oceanic-ridges and all oceanic lithosphere increases in age away from mid-ocean-ridges towards the continents. The distribution of geology symmetrical about and parallel to mid-ocean-ridge axes (Figure 2.1) demonstrates that all oceanic lithosphere is undergoing extension approximately normal to the ridge axes as continents move apart.

The accountability and distribution of oceanic lithosphere on an expanding Earth (Figure 2.3) is based on the premise that lithosphere generated at mid-ocean-ridge spreading axes is cumulative with time and the increase in post-Triassic surface area is a result of an increase in palaeoradius. For an expanding Earth the cumulative surface areas of oceanic lithosphere represent a means to mathematically quantify a potential rate of increase in palaeoradius, in keeping with the primary assumption that the Earth's radius has increased with time.

By successively removing oceanic lithosphere and reuniting the primary continental and oceanic plates along their common plate margins at a reduced Earth radius, post-Triassic models show that all plates reunite with a better than 99% fit-together (Figures 1.1 & 2.10). During the Triassic, continental marginal basins and epi-continental sedimentary basins form a global network surrounding continental

cratons and orogenic zones, enveloping the Earth with a complete continental shell. This unique fit-together demonstrates that post-Triassic Earth expansion is a viable process and gives justification to extending modelling studies to the Archaean.

Pre-Jurassic modelling reveals that the distribution of epi-continental sedimentary basins, continental magmatism and orogenic zones form an intracratonic network surrounding Precambrian cratons and orogens. An Archaean-Mesoproterozoic intracratonic network (Figure 2.13) forms the loci for ongoing continental crustal extension, basin sedimentation and intracratonic mobility during the Proterozoic and Palaeozoic (Figure 2.10, models 5 to 11) and represents the primary loci for continental break-up and opening of the modern oceans during the post-Permian (Figure 2.10, models 12 to 24). This process of progressive continental crustal extension during Earth expansion shows a spatial integrity of all tectonic elements, continents and oceans throughout Earth history.

3. MODELLING OF GLOBAL GEOLOGICAL AND GEOPHYSICAL DATA ON AN EXPANDING EARTH

In the previous chapter models of an Archaean to Future expanding Earth have been constructed by assuming that the Earth's surface area has increased with time as a direct consequence of an increase in Earth radius. The expanding Earth models constructed empirically demonstrate that expansion from the Archaean to Recent is a viable process and that expansion is primarily manifested as continental and oceanic crustal extension. Each of the expanding Earth models show that, during Earth expansion, intracratonic, intracontinental and intraplate spatial integrity is maintained throughout Earth history as continental crust progressively extends prior to continental rupture, break-up and dispersal to the Recent.

In this chapter global geological and geophysical data sets have been plotted on the Archaean to Future expanding Earth models to investigate the spatial and temporal distribution of the data within a conceptual expanding Earth tectonic framework. The distribution of data is used to test the empirical geological observations made from expanding Earth models and to compare and contrast with similar distributions on conventional plate tectonic models.

It is acknowledged that palaeomagnetics is traditionally considered the cornerstone of conventional plate tectonic theory and, along with space geodetic determination of plate motion history, is used to negate Earth expansion (eg. McElhinny & McFadden, 2000). This contrasts with the views of biogeographers where biogeographic map reconstructions differ widely from conventional palaeomagnetic-based plate tectonic reconstructions (eg. Briggs, 1995; Meyerhoff *et al.*, 1996) and alternatives to conventional reconstructions are considered to better fit the field evidence (eg. Stevens, 1997a; Shields, 1998).

The primary function of palaeomagnetics, however, is to determine the palaeolatitude of a site sample and a direction to the palaeopole, from which a palaeopole location can be calculated. Palaeomagnetics is used within this context to determine the palaeopole and palaeoequator locations on each of the expanding Earth models to establish a geographical grid for each model. Both space geodetic and palaeomagnetic data sets are interrogated on the expanding Earth models to determine how these geophysical concepts relate to an expanding Earth. This

information then forms the geographical basis for a comprehensive investigation of palaeogeographic, palaeobiogeographic, palaeoclimatic and metallogenic data.

3.1 Space Geodetic Measurement Data

Space geodetics uses a network of radio telescopes, satellites and ground-based receiver and transmitter stations to routinely measure the dimensions and plate motion history of the Earth. Measuring techniques developed include Very Long Baseline Interferometry (VLBI) (eg. Rogers *et al*., 1993), Satellite Laser Ranging (SLR) (eg. Degnan, 1993), Lunar Laser Ranging (LLR), Global Positioning Systems (GPS) (eg. Blewitt, 1993) and Doppler Orbitography and Radiopositioning Integrated by Satellite (DORIS) (eg. Crétaux *et al.*, 1998).

The development and application of space geodetic measurement techniques to Earth dynamic studies is reviewed in Vyskocil *et al.* (1989), Montag & Reigber (1992), Smith & Turcotte (1993) and Beutler *et al.* (1995) and fundamental geodetic techniques are covered in standard texts such as Lambeck (1988) and Hooijberg (1997). Space geodetic solutions to the global geodetic network are routinely published on the Internet by the International Earth Rotation Service (IERS) Central Bureau (http://lareg.ensg.ign.fr/ITRF/) and by the Goddard Space Flight Centre (GSFC) (http://lupus.gsfc.nasa.gov/). The published global network solutions include observation-site geocentric co-ordinates and their time derivatives, plus time evolutions of baseline vector components between two or more observation sites.

The application of advanced space geodetic techniques to Earth dynamic studies has progressed to the point where precise estimation of present-day tectonic motion is now quoted to sub-centimetre accuracy (eg. Degnan, 1993; Ma & Ryan, 1998). This geodetic information is routinely used to compare present-day models of horizontal plate motion derived from geophysical evidence (eg. Minster & Jordan, 1978; DeMets *et al.*, 1990; Smith *et al.*, 1990; Robbins *et al.*, 1993; Smith D. E. *et al.*, 1994; Larson *et al.*, 1997; Crétaux *et al.*, 1998). These measurements have shown that current-day horizontal motion of the major plates is close to the million year average motion vectors determined from oceanic magnetic mapping.

Vertical crustal motion studies have been studied by Dunn & Torrence (1993), Argus (1996), Heki (1996), Larson *et al.* (1997) and Soudarin *et al.* (1999). Heki (1990) concludes that systematic and random errors in space geodetic

measurement are largest in the vertical component of a site co-ordinate to which VLBI is inherently insensitive. Similarly, for SLR, the greatest discrepancies between estimates of plate motion and established plate model values is in the vertical component (Bianco *et al.*, 1998) and the largest systematic error source for absolute height determination is the value of G·M [product of Universal Gravity G and Earth mass M] (Smith *et al.*, 1985). Larson *et al.* (1997) conclude that there is no persuasive evidence for significant vertical crustal motions and Soudarin *et al.* (1999) conclude that, with the exception of a few stations, vertical plate motion rates are generally less than 5mm/yr.

Sources of error in space geodetic measurements are attributed to the fundamental differences in measurement between VLBI, SLR, GPS, and DORIS. VLBI uses a celestial reference frame based on measurements to natural, extragalactic radio sources (Rogers *et al*., 1993). SLR uses Earth based laser stations that range to a number of orbiting target satellites equipped with laser retroreflectors (Degnan, 1993). GPS (Blewitt, 1993) and DORIS (Crétaux *et al.*, 1998) use electronic signals to a number of Earth orbiting satellites emitted to or from mobile ground receivers. The primary limiting factor to accuracy of measurements in all four methods is the systematic errors, which come from seasonal atmospheric interference (Herring & Pearlman, 1993; Heki, 1996; Hefty & Gontier, 1997). For SLR, GPS, and DORIS, additional factors include satellite tracking and force field modelling used for satellite altimetry control (Herring & Pearlman, 1993).

Hefty & Gontier (1997) discuss biases in currently adopted atmospheric modelling procedures, reference frames and Earth Orientation Parameter series (EOP) which cause observable discontinuities in the use of Universal Time (UTI) used during measurement (Ray, 1996). Recommendations for inclusion of additional global parameter corrections to existing atmospheric models were proposed by Hefty & Gontier (1997) to significantly increase the internal consistency of observation and computational matrices during statistical treatment of raw data and to remove a seasonal part of the discrepancies associated with observing schedules. This ongoing matrix refinement has served to improve the global correlation between both the terrestrial and celestial geodetic reference frames used by the various measurement techniques, which then form a basis for horizontal plate motion studies.

Force field premises used for satellite altimetry control are based on a constant universal gravity G, Earth mass M and in particular, the product G·M

(Herring & Pearlman, 1993). Satellite positioning and altimetry control is sensitive to both UTI and the value of G·M (Tapley *et al*, 1985). The origin of the ITRF coincides with the centre of mass of the Earth and has a positional uncertainty of 100 millimetres (Hooijberg, 1997). Any small difference between the force field values can result in an offset in the origin of the centre of Earth mass of between 20 to 50 mm in the XYZ international terrestrial reference frame axes (eg. Tapley *et al*, 1985).

A thorough interrogation of the mathematical and statistical methodology behind space geodetic measurement and global solution is beyond the scope of this thesis. Space geodetic solutions to present-day geodetic motion are based on selected sets of individual solutions from VLBI, SLR, GPS, DORIS and LLR observations submitted to the International Earth Rotation Service (IERS) Central Bureau (http://lareg.ensg.ign.fr/ITRF/). Individual solutions submitted to the IERS are incorporated into the global geodetic solution by a simultaneous combination of observation site positions and velocities using full variance and covariance matrices, and a rigorous weighting scheme based on the analysis and estimation of the variance components.

Attempts to use space geodetic data to quantify Earth expansion originate from Parkinson (in Carey, 1988). A radial increase in Earth radius value of 20·8 ± 8 mm/yr was determined by Parkinson using selected chord lengths between ground stations derived from available NASA VLBI results. While comparable with the value of 22 mm/yr, determined from oceanic mapping (Section 2.3), Parkinson used space geodetic data, which is now superseded by more recent observations and more recent mathematical methodology. Calculations of a potential increase in Earth radius based on published GSFC VLBI baseline vectors (Ma & Ryan, 1998) now indicate a mean global increase in radius of 4·1 ± 3 mm/yr.

In contrast, when Robaudo & Harrison (1993) combined SLR solution UT/LLA9101 (including all data from 1976 to the beginning of 1991) and VLBI solution GBL660 (containing data up to the end of 1990) data sets to derive observation station horizontal motions for plate motion studies, they allowed all stations to have three independent motion velocities. These calculations, based on a global observational network, gave "a Root Mean Squared (RMS) value of up-down [increase in Earth radius] motions of over 18 mm/yr" (Robaudo & Harrison, 1993, page 53). This value was considered by Robaudo & Harrison (1993) to be extremely

high when compared to expected deglaciation rates, estimated at less than 10 mm/yr (Argus, 1996).

It is significant to note that Robaudo & Harrison (1993) "expected that most VLBI stations will have up-down [radial] motions of only a few mm/yr" and recommended that the vertical motion be "restricted to zero, because this is closer to the true situation than an average motion of 18 mm/yr" (Robaudo & Harrison, 1993, page 54). This recommendation is now reflected in current solutions to the global VLBI network (eg. Ma & Ryan, 1998), where values for radial motion have a calculated global average value of 0·35 mm/yr over 144 stations (established from Geocentric Positions Velocities solution 1102g6, Ma & Ryan, 1998).

3.1.1 Modelling Space Geodetic Data

Space geodetic modelling of vertical motion on expanding Earth models is limited by the mathematical and statistical constraints to VLBI, SLR, GPS, DORIS, and LLR solutions, imposed by the IERS during calculation of global geodetic solutions. The application of complex variance and covariance matrices and weighting schemes for the measurement variance components by the IERS effectively minimises all aberrations in measurement techniques. By adopting these solutions to plate tectonic terrestrial models, observational data, which might otherwise indicate an expansion of the Earth, is potentially being forced into a static radius Earth model.

Modelling published space geodetic data on an expanding Earth will be two-fold. Firstly, an interrogation of published IERS solutions investigates vertical trends within the data sets to indicate potential expansion, or periodic adjustments to the data that may suggest constraint to a static radius Earth. Secondly, published horizontal plate motion studies will be plotted on a Recent Earth model and a descriptive overview of plate motion given.

3.1.2 Vertical Plate Motion Trends

Appendix A2 contains charted and tabulated information from 88 VLBI, SLR, GPS and LLR observation sites used by the IERS during the period 1992 to 1997 inclusive. The total number of observation sites now exceeds 560, but not all have extended periods of occupancy useful to this study. A selection of typical charts

showing actual Earth radius and derived variation in Earth radius for the period 1992 to 1999 inclusive is shown in Figures 3.1 to 3.4. There are large lateral variations in the complete set of charts illustrated in Appendix A2 and Figures 3.1 to 3.4 must be viewed in context.

Figures 3.1 to 3.4 and charts in Appendix A2 show plots of the variation of actual Earth radius of a particular observing site, derived from the published International Earth Rotation Service geodetic solutions for 1992, 1993, 1994, 1996 and 1997 (http://lareg.ensg.ign.fr/ITRF/). Site position geocentric co-ordinates and velocity vectors of VLBI, SLR, GPS and LLR (one observation) solutions are tabulated with each chart (Appendix A2 only). Graphs shown on all charts represent plots of Earth radius relative to the geocentric centre of the Earth for each year of publication, followed by radii derived from published velocity vectors, projected in yearly increments to 1999.

For each chart the 1992 (ITRF92) site solution is adopted as a starting point for plotting the predicted radial expansion of the Earth at 22 millimetres per year, derived from Equation 2.6 (Section 2.2). The actual variation in radius is shown for comparison, generated by joining the published solutions for each year shown. The plot of actual radius gives an indication of the variance in Earth radius relative to: a) Earth expansion; b) radii derived from published solutions and; c) published velocity vectors. For each VLBI site (Appendix A2.1), the GSFC geodetic solution for 1998 is also included for reference only. This VLBI geodetic solution is constrained by the IERS within the ITRF97 geodetic solution.

The complete set of charts (Appendix A2) show a wide variation in predicted and actual Earth radii, ranging from zero radial change consistent with a static Earth radius (Figure 3.1), to rapid radial change consistent with Earth expansion (Figure 3.2). In both Figure 3.1 and Figure 3.2 velocity vectors are consistent with the actual radial changes observed during 1992 to 1997. Between each of these extreme changes in radius, charts show evidence for large periodic adjustments to site parameters (Figure 3.3) to small regular adjustments (Figure 3.4). These large fluctuations and periodic adjustments are consistent with the rigorous weighting scheme used by the IERS to accommodate for the measurement variance components from each individual VLBI, SLR, GPS and DORIS geodetic solution.

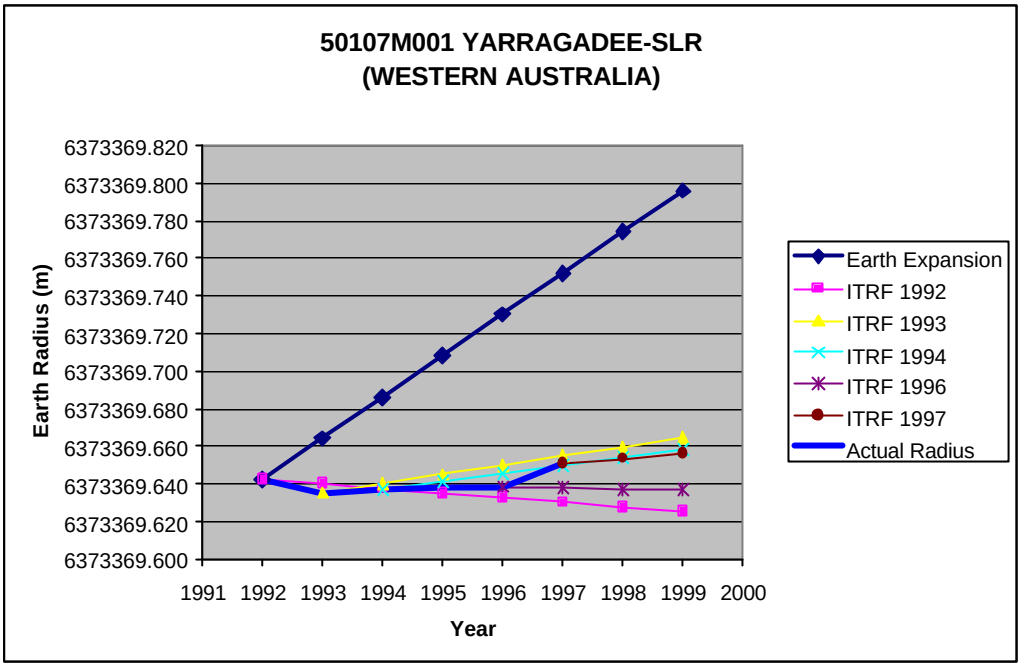

Figure 3.1 Time variance of Earth radius, Yarragadee SLR site, west Australia. Data derived from published IERS solutions for 1992 to 1997. Site shows prolonged stability of measurements with minor periodic adjustment to site parameters.

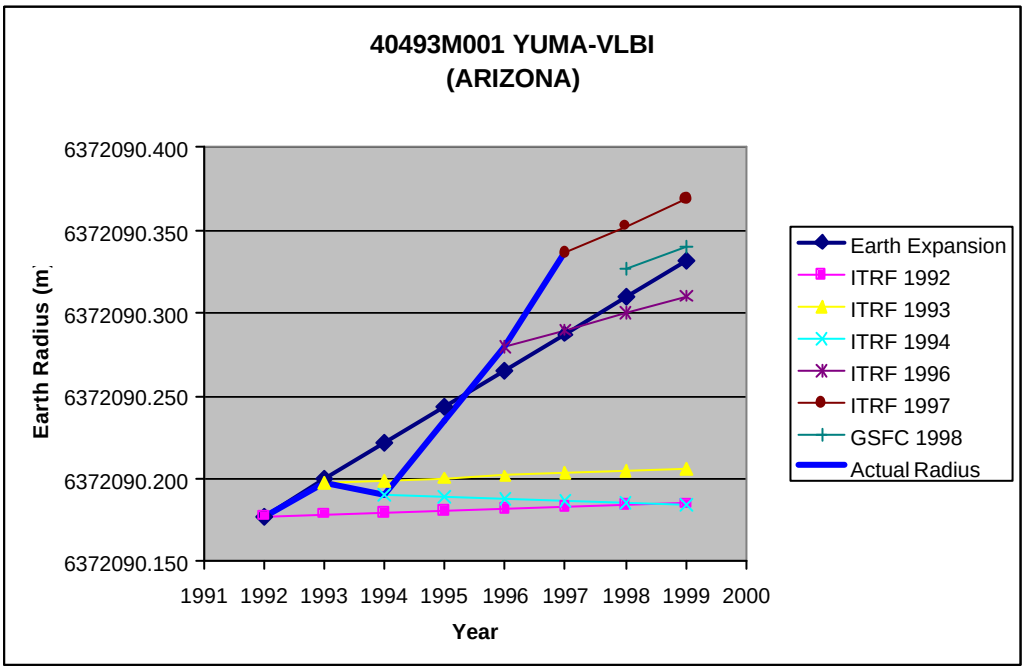

Figure 3.2 Time variance of Earth radius, Yuma VLBI site, Arizona, USA. Data derived from published IERS solutions for 1992 to 1997. Graphs show an actual increase in Earth radius consistent with Earth expansion.

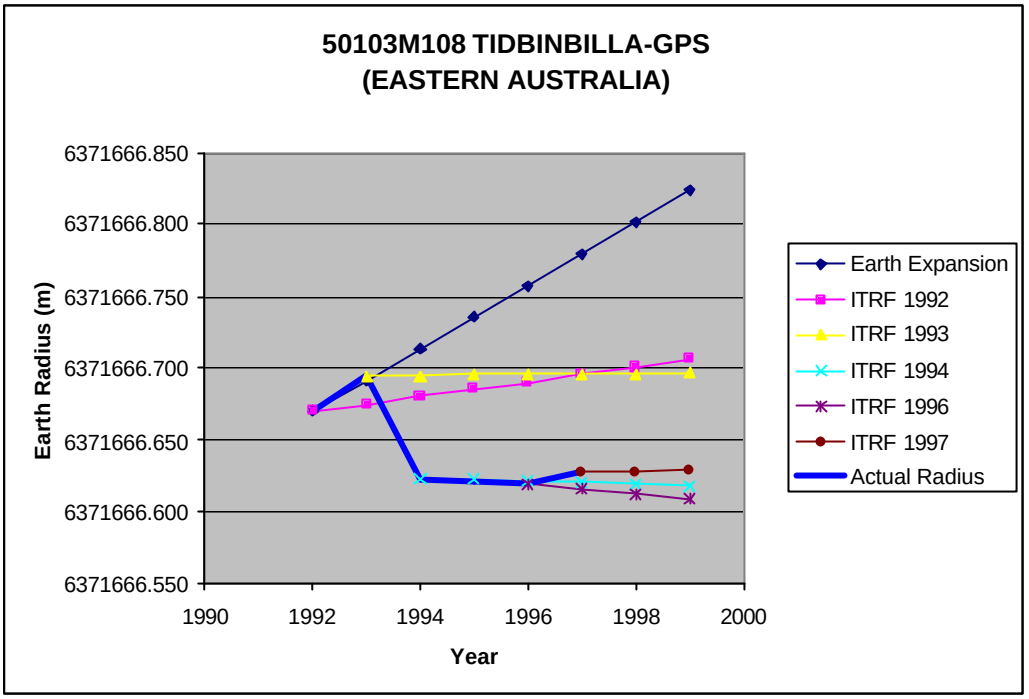

Figure 3.3 Time variance of Earth radius, Tidbinbilla GPS site, Canberra. Data derived from published IERS solutions for 1992 to 1997. Graphs show a large adjustment to actual Earth radius of 71 mm between 1993 and 1994.

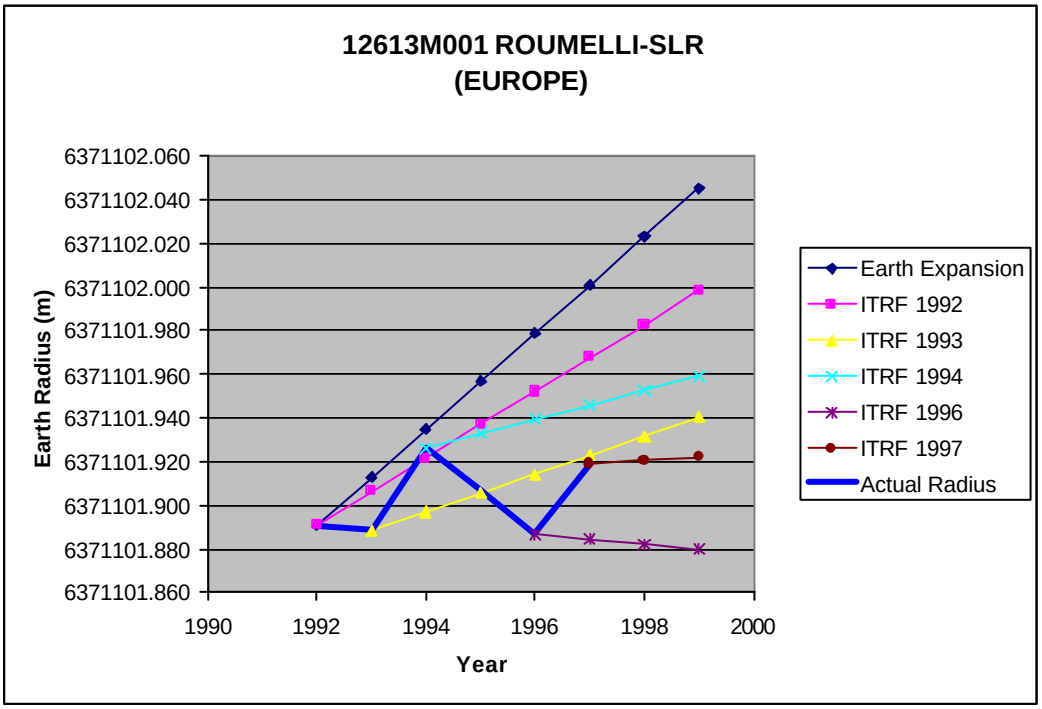

Figure 3.4 Time variance of Earth radius, Roumelli SLR site, Europe. Data derived from published IERS solutions for 1992 to 1997. Graphs show large fluctuations in Earth radius suggestive of periodic adjustments to site parameters.

The 1992-1997 period of site occupancy chosen for this study is a period when space geodetic measurement is routine and mathematical analysis well established. Precision within each individual space geodetic measurement technique is routinely quoted to sub-centimetre accuracy, yet the large fluctuations in Earth radii shown in Figures 3.1 to 3.4 and Appendix A2 confirm the conclusions of Dunn & Torrence (1993), Argus (1996), Heki (1996), Larson *et al.* (1997), and Soudarin *et al.* (1999) where geodetic solutions are not as sufficiently well constrained in the vertical as they are in the horizontal.

3.1.3 Horizontal Plate Motion (Video A3.5)

Figure 3.5 is a Recent Earth model showing the Cenozoic mid-ocean-ridge spreading data and modern plate boundaries only (after CGMW & UNESCO, 1990). Horizontal plate motion vectors plotted from the published VLBI, SLR, GPS and DORIS geodetic solutions of Heki (1996), Larson *et al.* (1997) and Ma & Ryan (1998) are shown as thin arrows. These vectors represent tangential site motion relative to the centre of the Earth. Large arrows represent modern spreading rates at mid-ocean-ridges plus continental plate motion vectors summarised from the detailed vector data. The tail of each arrow is scaled to represent the measured plate motion in millimetres per year. A scale bar of 140 mm/yr represents the amount of great-circle crustal extension required during expansion of the Earth per year.

Minster & Jordan (1978), DeMets *et al.* (1990), Smith *et al.* (1990), Robbins *et al.* (1993), Smith D. E. *et al.* (1994), Larson *et al.* (1997) and Crétaux *et al.* (1998) each conclude that current-day horizontal motion of the major plates is close to the million year average motion vectors determined from oceanic magnetic mapping. Figure 3.5 and expanding Earth models (Figure 2.10) confirm this observation and show that conventional space geodetic derived plate motion vectors and mid-ocean-ridge spreading vectors are in agreement with plate motion on an expanding Earth. For Earth expansion models the horizontal plate motion vectors also include a vertical vector component and hence represent 3-D plate motion. The significance of the vertical vector component on an expanding Earth is best observed as expansion between successive models (see enclosed CD-ROM; Appendix A6).

The video clip of post-Triassic Earth expansion (Appendix A6) for example, shows a northward migration and anticlockwise rotation of North and South

America, and in part Antarctica, in conjunction with a northward migration and clockwise rotation of Africa and Eurasia. This continental motion results from a rapid opening of the North Pacific, South Pacific and Southern Oceans during the Mesozoic and Cenozoic, and plate motion is consistent with present plate motion vectors determined by space geodetics (Figure 3.5). This plate motion has been prominent since ocean basin extension initiated during the Early Permian and has continued to the Recent. The large geodetic rates within the Pacific Ocean plate, and similarly lesser rates in the Atlantic and Indian Oceans, are consistent with a rapid post-Triassic opening of the modern oceans and are independently verified by the global oceanic magnetic mapping (CGMW & UNESCO, 1990).

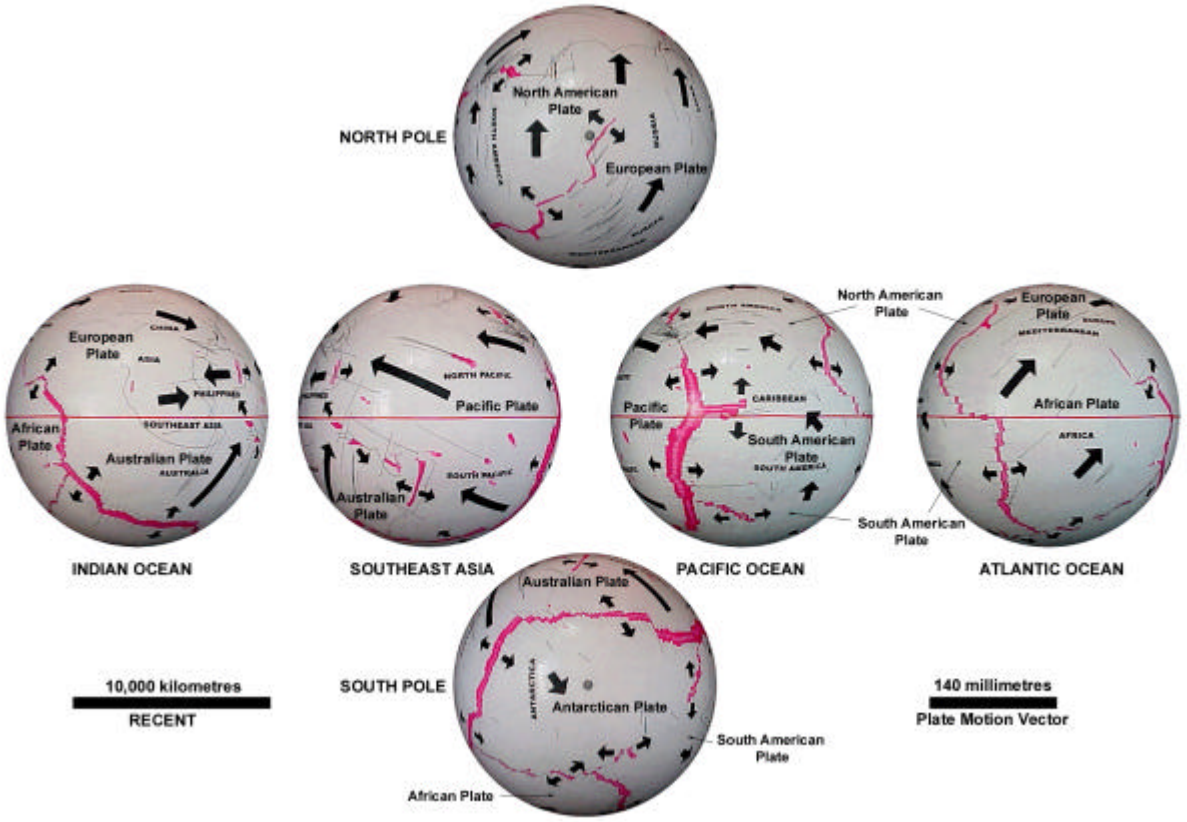

Figure 3.5 VLBI, SLR, GPS, and DORIS horizontal plate motion vector plots. Images show plate outlines and Pliocene to Recent mid-ocean-rifting (pink and red) on the Recent model. Large arrows (excluding arrowhead) represent plate vectors to scale shown at lower left, small arrows represent mid-ocean-rifting, fine-line arrows represent motion vectors plotted from published solutions. Plate motion vector scale bar at lower right represents required great circle Earth expansion per year. (VLBI, SLR, GPS and DORIS data after Heki, 1996, Larson *et al*., 1997, and Ma & Ryan, 1998).

On an expanding Earth the calculated equatorial or meridional great-circle increase in circumference is at present approximately 140 mm/yr. The horizontal plate motion vectors for the Pacific plate, relative to the circum-Pacific continents

(Figure 3.5), appear to show plate convergence from all directions consistent with plate tectonics. However, these motions are plate motions relative to the centre of the Earth and opposing vectors, such as the North Pacific and Eurasian plates, are readily absorbed within the net 140 mm/yr circumferential expansion, without the need to resort to consumption of oceanic crust by subduction. This net expansion and circumferential rate-balance also provides a valid explanation for the presence of extensional regimes, such as within the Philippine, Mauritius and Tongan arc regions, located within conventional back-arc compressive regimes.

3.1.4 Summary of Space Geodetic Results

At present excesses in global measurement due to atmospheric interference and time variance of G, M and UTI values are either constrained to zero, not considered or are indeterminate. As recommended by Robaudo & Harrison (1993) the excesses in vertical measurement are globally zeroed, resulting in a static Earth radius premise being imposed on space geodetic observational data. It is emphasised that this premise forces observational data into horizontal plate motion and severely limits measurement of vertical plate motion.

Precision of each individual space geodetic measurement technique for the 1992 to 1997 period of space geodetic occupancy is routinely quoted to sub-centimetre accuracy, yet large fluctuations in Earth radii shown in Figures 3.1 to 3.4 and Appendix A2 confirm the conclusions of Dunn & Torrence (1993), Argus (1996), Heki (1996), Larson *et al.* (1997), and Soudarin *et al*. (1999) where space geodetic solutions are not as sufficiently well constrained in the vertical as they are in the horizontal.

For horizontal plate motion Minster & Jordan (1978), DeMets *et al*. (1990), Smith *et al*. (1990), Robbins *et al*. (1993) Smith D. E. *et al*. (1994), Larson *et al*. (1997) and Crétaux *et al*. (1998) each conclude that current-day horizontal motion of the major plates is close to the million year average motion vectors determined from oceanic magnetic mapping. The current plate motion, plotted as space geodetic vector data (Figure 3.5), is consistent with expanding Earth modelling (Figure 2.10).

3.2 Geophysical Palaeomagnetic Data

The principles and techniques of palaeomagnetism are described in Irving (1964), Tarling (1983), Butler (1992) and McElhinny & McFadden (2000). The application of palaeomagnetism to an expanding Earth and derivation of palaeomagnetic formula, used to determine palaeopole locations on the present Earth surface, has been extensively reviewed in Maxlow (1995) and is summarised in Appendix A3.

Palaeomagnetism is the study of fossil remnant magnetism residing in rocks (Piper 1989). Rocks that contain small amounts of ferro- or paramagnetic materials aquire a weak but permanent magnetism with an orientation and polarity that is parallel to the Earth's magnetic field at the location and time of cooling or deposition (Lambeck, 1988). The application of palaeomagnetics to global tectonics was appreciated by Creer *et al.* (1954) who noted that remnant magnetism in a series of rocks from the same general area, but of increasing age, yielded a progressive change in the magnetic vector.

This change in magnetic vector suggested to Creer *et al*. (1954) that the apparent magnetic pole had moved because of changes in either the position of the pole or the position of the sample site. A distinction between these alternatives was made possible by comparing the apparent polar wander (APW) paths from different continents, and early tests by Runcorn (1956) and Irving (1956) showed that the continents had indeed moved relative to each other. This observation now forms the basis for plate tectonic theory and detailed analyses of palaeomagnetism residing in rocks of all ages is used to constrain conventional plate tectonic reconstructions on a static radius Earth model.

The collection and statistical treatment of palaeomagnetic site data has reached a high degree of precision (eg. Butler, 1992; McElhinny & McFadden 2000) and the fundamental premises of palaeomagnetism are not contradicted by Earth expansion. However, a number of limitations on conventional palaeomagnetics must be clarified prior to establishing a basis for palaeomagnetic modelling on an expanding Earth. These limitations are:

1. Measurement of remnant magnetism in rocks determines the palaeolatitude of a site sample and direction to the palaeopole only (Butler, 1992).
2. Palaeomagnetics cannot determine or constrain palaeolongitude of a site sample (Li *et al*., 1993).

3. Determining an Earth palaeoradius using palaeomagnetic data is based on the assumption that continents have maintained a constancy of surface area with time (van Hilten, 1968).
4. Palaeopole locations established from palaeomagnetic site data are derived quantities based on the assumption that Earth radius is constant (McElhinny & McFadden, 2000).

These present significant limitations to conventional plate tectonic reconstructions and plate motion studies on a static radius Earth because they generate multiple plate-fit-options. To constrain plate tectonic reconstructions, palaeomagnetic data from adjoining continents is then used to establish an apparent polar wander path for each continent and additional geological data, such as palaeogeography and palaeoclimate is used to limit fit-options (Li *et al*., 1993).

An interrogation of palaeomagnetic methods used to determine palaeoradius and palaeopoles based on the conventional magnetic dipole formula is given in Maxlow (1995) and summarised here. An investigation of palaeomagnetics on an expanding Earth is limited to its primary role of determining palaeolatitude of a site sample and determining palaeocolatitude to the palaeopole. This information is then used to establish a palaeogeographical grid for each expanding Earth model.

3.2.1 Palaeomagnetic Determination of Palaeoradius

Determining a palaeoradius of the Earth using conventional palaeomagnetics depends on a fundamental premise that the surface area of continents has remained constant and continents have acted as rigid plates with time (van Hilten, 1968). Determining a palaeoradius of the Earth is then carried out by three methods (summarised from van Andel & Hospers, 1968):

1. **Palaeomeridian method**: used for palaeoradius calculations based on palaeomagnetic data situated approximately on the same palaeomeridian.
2. **Triangulation method**: used for palaeoradius calculations based on palaeomagnetic data situated on substantially different palaeomeridians.
3. **Method of minimum scatter** of virtual magnetic poles calculated from site observations.

Published estimates of palaeoradii vary from fast expansion rates (eg. van Hilten, 1963; Ahmad, 1988) that are compatible with expansion rates derived from expanding Earth modelling, to slow or negligible expansion rates (eg. Cox & Doell, 1961; Ward, 1963; Hospers & van Andel, 1967; McElhinny & Brock, 1975). Palaeomagneticians conclude from these studies that the amount of potential Earth expansion is limited to less than 0.8% of the present Earth radius during the past 400 million years.

Since these calculation methods were first developed, modern global tectonic concepts have demonstrated that Earth's crust is not a passive adjunct of lithospheric plates but a dynamic, interactive layer of the Earth (Grant, 1992). For each of the palaeoradius calculation methods used intra-site distances between palaeomagnetic site data are typically in excess of 5000 kilometres and represent a significant proportion of an ancient Earth circumference (Figure 3.6).

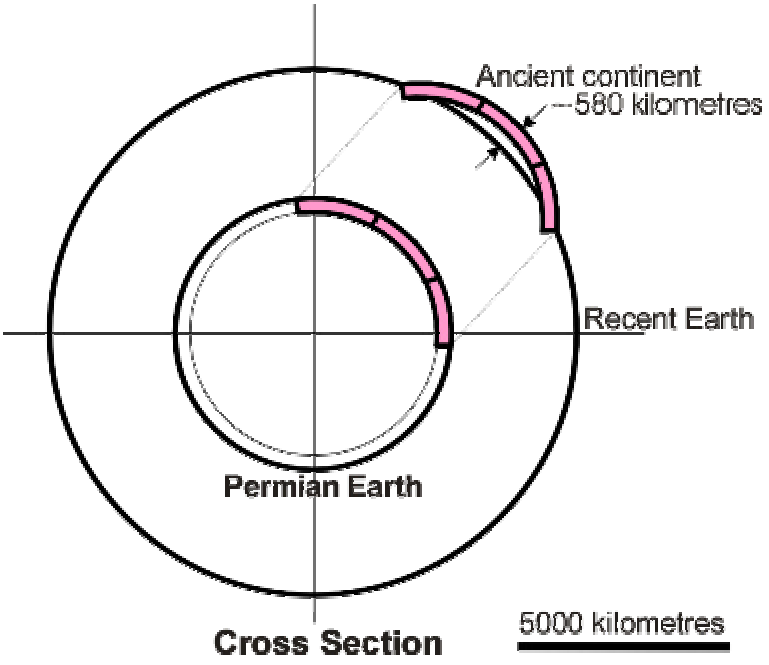

Figure 3.6 Schematic cross section of a Permian and Recent Earth. An ancient Permian crustal fragment is shown at both Earth radii to demonstrate the amount of radial crustal adjustment required for a 5000 kilometre long continent (arc length), typically used to determine palaeoradius using conventional palaeomagnetic methods. Vertical crustal adjustment of continent during changing surface curvature amounts to ~580 kilometres during post-Permian expansion to Recent.

Extensive crustal studies from each continent now show that, over these distances, continents have undergone varying degrees of intracratonic crustal extension and contraction, which is contrary to premises placed on the Eurasian

palaeomagnetic data of Egyed (1960), Cox & Doell (1961) and van Hilten (1963). Continental dispersal is well established and is demonstrated by both oceanic mapping and apparent-polar-wander studies, which is contrary to the premises imposed on the Eurasian and North American palaeomagnetic data of van Hilten (1963). Intracratonic rotation is also recognised within continents (eg. Sundvik & Larson, 1988; Unternehr *et al.*, 1988; Visser & Praekelt, 1998) which is contrary to premises imposed on the African palaeomagnetic data of McElhinny & Brock (1975).

Without the constraint of constancy of continental area, determining a palaeoradius of the Earth from conventional palaeomagnetic data using either of the three calculation methods becomes invalid. Palaeomagnetic conclusions based on these calculations must then be reconsidered and plate motion studies based on derived apparent-polar-wander palaeopole data must be re-evaluated.

3.2.2 Palaeomagnetic Dipole Formula

Conventional palaeomagnetic formulae (Appendix A3), used to determine palaeolatitude and palaeopole locations, are based on a geocentric axial dipole model of the Earth (Figure 3.7) and utilise measurements of natural remnant magnetism from site samples. These conventional palaeomagnetic formulae are based on the assumption that Earth's palaeoradius is equal to, or approximately equal to the present Earth radius (eg. Butler, 1992; van der Voo, 1993; McElhinny & McFadden, 2000). From the derived palaeopole locations, apparent-polar-wander of continents and the displacement history of tectonostratigraphic terranes is then determined and used to constrain continental positioning and limit fit-options during conventional plate tectonic reconstruction.

The geocentric axial dipole model (Butler, 1992) (Appendix A3.1) represents the basis for palaeomagnetic studies. In this model (Figure 3.7) a magnetic field is produced by a single magnetic dipole M, located at the centre of the Earth and aligned with the rotation axis. Derivation of a dipole equation to determine palaeolatitude, or palaeocolatitude from site data is given in Butler (1992) and defined as:

$$\tan I = 2 \tan \lambda = 2 \cot p \qquad \text{Equation 3.1}$$

Where:

- I is the mean inclination of the magnetic field, increasing from -90° at the geographic south pole to +90° at the geographic north pole;
- λ is the geographic latitude determined from I and represents the angular meridional distance from the equator to the site;
- p is the geographic colatitude determined from I and represents the angular meridional distance from the site to the pole.

Rearranging the dipole equation 3.1 gives colatitude p as:

$$\mathbf{p = \cot^{-1} (\tan I/2) = \tan^{-1} (2/\tan I)} \qquad \text{Equation 3.2}$$

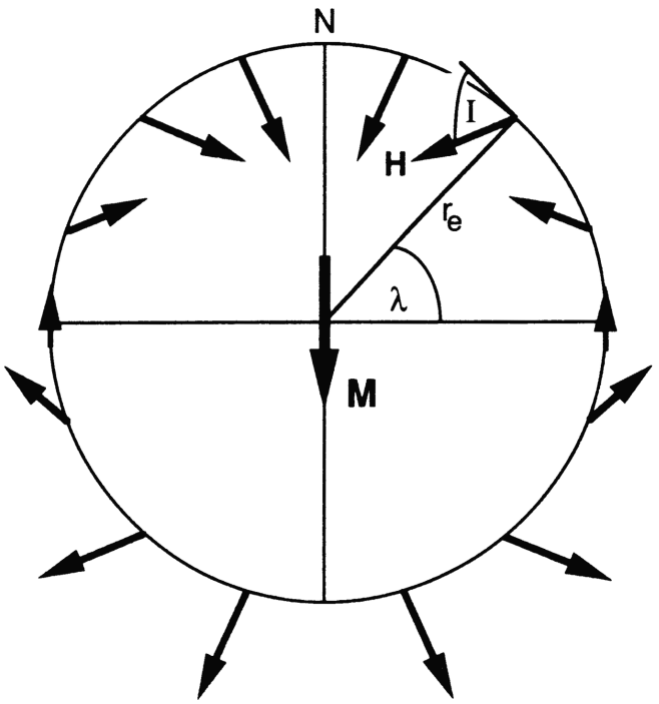

Figure 3.7 Conventional geocentric axial dipole model of the Earth. A magnetic dipole **M** is located at the centre of the Earth and aligned with the rotation axis. The geographic latitude is l, the mean Earth radius is $\mathbf{r_e}$. The magnetic field directions at the Earth's surface, produced by the geocentric axial dipole are schematically shown. Inclination **I** is shown for one location and **N** is the North geographic pole. (from Butler, 1992)

Site mean data determined from a set of site samples are assumed by palaeomagneticians to represent a time-averaged field, which compensates for any

secular variation caused by non-dipole components (Tarling, 1983). For a geocentric axial dipole field (Figure 3.7) the time-averaged and structurally corrected inclination I, determined from site data, establishes the palaeocolatitude (Equation 3.2) existing at the site when the site data were locked into the rock-record, and a time-averaged declination D determines the direction along a palaeomeridian to the palaeopole. To calculate the palaeomagnetic pole position on the present Earth surface spherical trigonometry is used, based on the conventional dipole Equation 3.2, to determine the angular distance between the observing locality and the pole position (Figure A3.4; Appendix A3.2).

By using the conventional palaeomagnetic formulae (Appendix A3.2) to determine palaeopole location it is assumed by palaeomagneticians that the angular dimension of the palaeogeographical co-ordinate system, indicated by the age of the site-data, equals the angular dimension of the geographical co-ordinate system represented by the Recent site location. To determine a palaeopole position the two geographical systems are then simply added, using spherical trigonometry, to give a palaeopole latitude and longitude that equates to the present geographical grid system.

The limitations of conventional palaeopole, and hence palaeoradius determination is shown in schematic cross sections of an ancient and Recent Earth (Figures 3.8). In Figure 3.8A an ancient Earth of palaeoradius R_a contains three palaeomagnetic sample sites labelled I_1, I_2, and I_3 located on an ancient continent with a common ancient palaeopole P_a. As the Earth expands the ancient continent fragments into three cratons with extensional intracratonic basins.

In Figure 3.8A the ancient Earth has undergone a simplistic radial expansion from R_a to a Recent radius R_0. At the Recent radius the intra-site distances between each sample have increased and the palaeopole locations determined from each sample site, using conventional palaeomagnetic formulae, remain coincident at $P_{1,2,3}$. Conventional palaeomagnetic interpretation would insist that each craton has remained spatially intact during this interval of time, with no apparent polar wander and no increase in palaeoradius. This situation is similar to palaeoradius determinations within Eurasia by Egyed (1960), Cox & Doell (1961) and van Hilten (1963). Actual palaeopole locations for each site, determined from modified expanding Earth palaeomagnetic equations (Appendix A3.2), are shown dispersed at

P_{a1}, P_{a2} and P_{a3}. On the ancient Earth these same actual palaeopoles cluster as coincident poles at P_a.

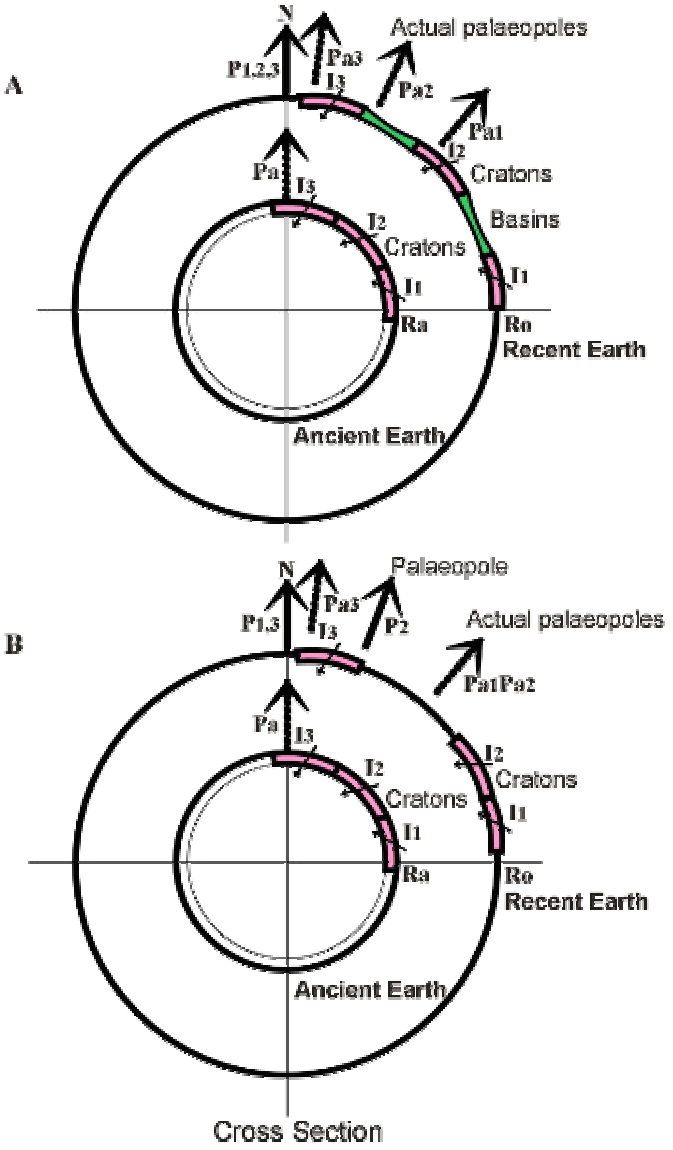

Figure 3.8 Schematic cross sections of an ancient and Recent Earth. **Figure 3.8A** An ancient continent at radius R_a expands to radius R_0. During expansion continent fragments and develop intracratonic basins Three palaeomagnetic sample sites have inclinations I_1, I_2 and I_3. An ancient palaeopole is located at P_a. Conventional palaeomagnetic poles are located on the Recent Earth at P_1, P_2 and P_3 and actual ancient palaeopoles are located at P_{a1}, P_{a2} and P_{a3}. **Figure 3.8B** The same ancient continent expands from R_a to R_0. During expansion continents break-up and disperse. Three palaeomagnetic sample sites have inclinations I_1, I_2 and I_3. An ancient palaeopole is located at P_a. Conventional palaeomagnetic poles on the Recent Earth are located at P_1, P_2 and P_3 and actual ancient palaeopoles are located at P_{a1}, P_{a2} and P_{a3}.

In Figure 3.8B the same ancient continent containing palaeomagnetic sample sites I_1, I_2 and I_3, breaks-up and undergoes radial expansion from an ancient radius R_a to a Recent radius R_0. In this example one craton disperses by mid-ocean-rifting and two cratons remain intact. Conventional palaeopoles determined from each sample

site on the present Earth are located at $P_{1,3}$ and P_2. Palaeopoles P_1 and P_3 are coincident and P_2 is isolated. The conventional palaeopole locations would infer that the two continents have undergone apparent polar wander relative to sample site I_2 or, have remained spatially intact relative to sites I_1 and I_3. This situation compares with palaeoradius determinations between Eurasia and North America by van Hilten (1963). Palaeopoles P_1 and P_2, originating from the same continent, suggests terrane displacement relative to each sample site and also suggests intra-continental apparent polar wander relative to site I_2. In contrast, actual palaeopoles P_{a1} and P_{a2} coincide requiring no terrane displacement and the isolation of P_{a3} demonstrates intracontinental rifting. All three palaeopoles again cluster as coincident poles at P_a on the ancient Earth.

Figure 3.8 illustrates the limitations imposed on palaeomagnetic interpretation when assuming continental stability to determine palaeoradius from palaeomagnetic site data. These limitations are compounded by choosing sample sites with excessive intra-site distances, sites that straddle both continental basin and oceanic rift zones and by not considering the potential for intracratonic rotation.

The global palaeomagnetic database is now extensive (eg. McElhinny & Lock, 1996) with conventional palaeomagnetic studies showing an increase in complexity of apparent-polar-wander between continents and tectonic displacement between lithostratigraphic terranes. This complex motion is not shown on an expanding Earth (Figure 2.10) and is not required for constraint of expanding Earth reconstructions.

3.2.3 Palaeomagnetics on an Expanding Earth

The mathematical application of palaeomagnetism to Earth expansion is detailed in Appendix A3.2 by reconsidering the conventional palaeomagnetic dipole Equation 3.2 in conjunction with an exponential increase in Earth radius (Equation 2.6; Section 2.2). Modified palaeomagnetic formulae (Equations A3.12 to A3.19; Appendix A3.2), used to determine actual pole locations on the present Earth, are then derived by incorporating palaeoradius Equation 2.6 into the conventional palaeomagnetic dipole based formulae of Butler (1992).

To determine an actual ancient palaeopole position P_a on the present Earth with palaeoradius varying exponentially with time consider Figure 39. At site S_0

located at the present Earth radius R_0 an inclination I, using the conventional palaeocolatitude equation (Equation 3.2), gives a colatitude p_0 that equals the ancient palaeocolatitude p_a locked into the rock record from site S_a at palaeoradius R_a. On the present Earth the ancient pole determined from p_0 is located at P_0, which is not equal to the actual pole position located at P_a determined from p_a. To determine the actual pole position on the present Earth consideration is given to the arc distance D_a defined by palaeocolatitude p_a and, for an expanding Earth, to the age of the site sample to determine palaeoradius R_a.

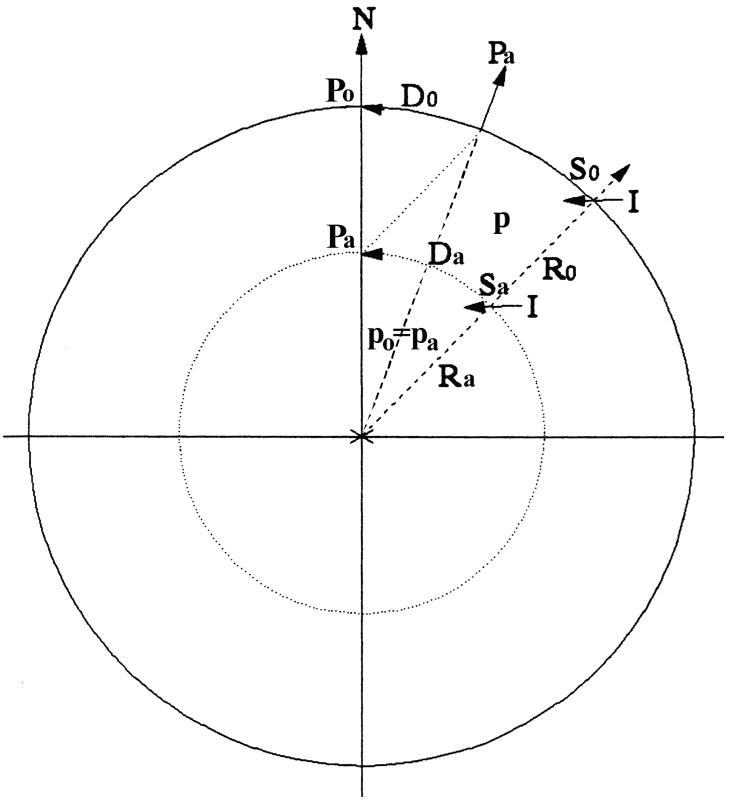

Figure 3.9 Determining an actual palaeopole located on the present Earth. For an inclination **I**, site $\mathbf{S_0}$, and present radius $\mathbf{R_0}$, the arcuate distance to palaeopole **P** is $\mathbf{D_0}$ and colatitude is $\mathbf{p_0}$. For site $\mathbf{S_a}$, palaeoradius $\mathbf{R_a}$ and arcuate distance $\mathbf{D_a}$, the colatitude $\mathbf{p_a}$ is the same for site $\mathbf{S_0}$ but the actual palaeopole position on the present Earth is located at position $\mathbf{P_a}$ determined from $\mathbf{D_a}$.

At site S_a the arc distance D_a is equal to:

$$D_a = R_a p_a \qquad \text{Equation 3.3}$$

Where p_a is in radians.

Rearranging, the ancient palaeocolatitude:

$$p_a = (D_a/R_a) \times 180/\pi \qquad \text{Equation 3.4}$$

Where p_a is in degrees.

To determine the location of the ancient palaeopole position P_a on the present radius Earth, the actual palaeocolatitude:

$$p = (D_a/R_0) \times 180/\pi \qquad \text{Equation 3.5}$$

Incorporating Equation 3.3 for D_a where p_a is in degrees:

$$p = (R_a p_a \times (\pi/180)/R_0) \times 180/\pi = R_a p_a /R_0 \qquad \text{Equation 3.6}$$

Where p is in degrees.

The mathematical relationship for an exponential increase in Earth's palaeoradius from the Archaean to Recent, derived from empirical measurements of oceanic and continental surface area data (Equation 2.6; Section 2.2), is:

$$R_a = (R_0 - R_p)e^{kt} + R_p \qquad \text{Equation 2.6}$$

Incorporating Equation 2.6 for R_a into Equation 3.6 gives:

$$p = ((R_0 - R_p)e^{kt} + R_p)p_a/R_0 \qquad \text{Equation 3.7}$$

and incorporating Equation 3.2 for p_a gives the actual palaeocolatitude:

$$\mathbf{p = ((R_0 - R_p)e^{kt} + R_p))\ (\tan^{-1}\ (2/\tan I))/R_0)} \qquad \text{Equation 3.8}$$

For any site sample constrained by the age of the rock sequence containing the site data Equation 3.8 is used to convert the palaeocolatitude indicated by the sample site to an actual palaeocolatitude of the ancient pole located on the present Earth. This modified dipole formula (Equation 3.8) results in an actual ancient palaeopole which is located closer to the sample site than for a palaeopole determined using the conventional dipole equation. Equation 3.8 however, is only used to locate the actual palaeopole on the present Earth and is not representative of the geographical palaeolatitude. Palaeolatitude is an angular measurement, which is independent of palaeoradius and is determined by using the conventional dipole Equation 3.2. Only when site location data is transferred to a sphere of palaeoradius representative of the age of the site data will geographical grid systems and pole locations coincide.

3.2.4 Palaeomagnetic Data Modelling

The global palaeomagnetic database of McElhinny & Lock (1996) has 8249 palaeomagnetic entries from rocks ranging in age from the Archaean to Recent. Of these, 1673 entries are listed as structurally corrected. Structural correction of site

samples is a means of restoring samples to their original orientation to enable accurate measurement of remnant magnetic properties. Details of the database are given in McElhinny & Lock (1996) and data published on the Internet is current to year 2000 (ftp://ftp.ngdc.noaa.gov/Solid_Earth/Paleomag/). Only the structurally corrected entries have been used here, with the exception of the Recent data where structural correction is minimal. The modified palaeomagnetic formulae A3.12 to A3.19 (Appendix A3.2) are used to determine the actual palaeocolatitude and ancient pole locations on the present radius Earth. Modified palaeomagnetic values are listed in Tables A4.1 to A4.22 (Appendix A4) and are used to locate palaeopoles on each expanding Earth model.

Recent magnetic north pole locations plotted using the published locations of McElhinny & Lock (1996) (Table A4.1; Appendix A4) are shown in Figure 3.10. Figure 3.10 illustrates 35 degrees of scatter, or secular variation of poles to be expected from the Recent north magnetic pole data. This scatter of poles is due to a combination of magnetic secular variation, and errors introduced during measurement and structural correction of site samples.

To determine a mean North Pole location this data is statistically treated to establish a mean, time-averaged geocentric magnetic pole (GP) coinciding with the north geographical pole. For magnetic poles other than the Recent, conventional magnetic pole data is statistically meaned to establish a virtual geocentric magnetic pole (VGP) for each continent or selected portions of a continent. These poles are then used in conventional plate tectonics to provide latitudinal constraint in determining an apparent polar wander between continents. Similarly, statistically treated poles from selected site locations within a continent are used to determine an inferred terrane displacement between the selected locations.

Conventional palaeomagnetic North Pole data, shown as point locations (Figure 3.10) are re-plotted (Figure 3.11) by manually drawing each pole as a small circle arc, with a radius equal to the site colatitude centred on the site location. The secular variation of poles (Figure 3.10) from each continent is summarised in Figure 3.11 as a swath of small circle arcs, typically between 20 to 30 degrees wide.

This small circle arc method demonstrates an alternative method of displaying the latitudinal variation in pole locations for each continent. Each continent is defined by its own swath, or multiple swaths and each continental swath straddles the present geocentric magnetic pole (Figure 3.11). The intersections of

each swath collectively determine the mean Recent geocentric magnetic north pole coincident with the geographical North Pole.

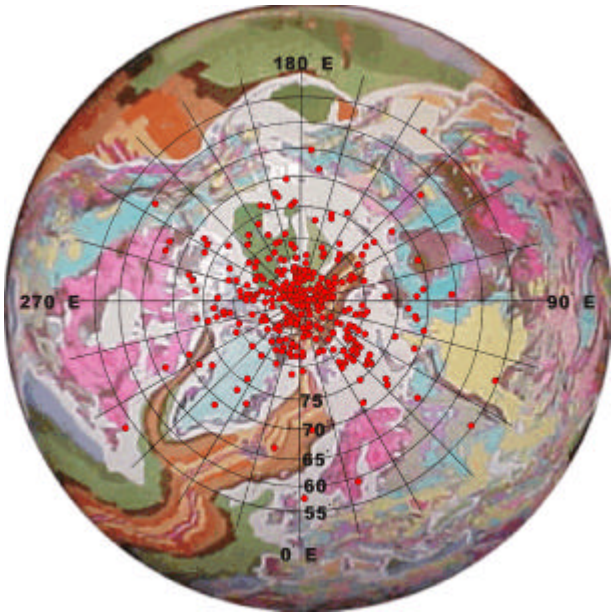

Figure 3.10 Recent north pole palaeomagnetic virtual geomagnetic poles. North pole locations shown as red dots are plotted from the published data of McElhinny & Lock (1996) and show a 35 degree radial scatter of pole data. These pole locations are statistically treated to give a mean, time-averaged geocentric magnetic north pole. Geographic grid shown in 5 degree intervals of latitude and 15 degrees longitude centred on the Recent north pole. (Recent geology after CGMW & UNESCO, 1990)

Figure 3.11 Recent north palaeomagnetic poles plotted as small circle arcs. Small circle arcs for each continent labelled form a continental swath, typically 20 to 30 degrees wide. Swaths shown from each continent straddle the mean geomagnetic pole position, shown as a red bulls-eye and collectively determine the mean pole location. (Data after McElhinny & Lock, 1996. Recent geology after CGMW & UNESCO, 1990)

3.2.5 Palaeopoles on an Expanding Earth (Videos A3.13 & A3.14)

The small circle arc method is used to determine mean geocentric palaeopole locations for each of the Archaean to Pliocene expanding Earth models (Figure 2.10). This method is adopted because declination values, used to determine the palaeopole location from each site sample, are angular measurements defined by the present geographical co-ordinate system (Butler, 1992). These angular declination measurements cannot be reproduced on expanding Earth models because the palaeogeographical co-ordinate systems do not equate to the present system.

To locate palaeopoles on expanding Earth models the site locations of McElhinny & Lock (1996) have been manually transferred from the Recent model to each expanding Earth model. The actual palaeocolatitude for each site mean sample (Tables A4.1 to A4.22; Appendix A4) is then manually drawn as a small circle arc, centred on the site location. For each expanding Earth model this results in a cluster of diametrically opposed small circle arcs coinciding with the north and south geocentric magnetic palaeopoles.

Approximately 95% of the small circle arcs plot within twenty-five degrees radius of each palaeopole for each expanding Earth model. This accords with the secular variation of poles for the Recent North Pole magnetic data shown in Figure 3.10. The remaining, less than five percent of small circle arcs are presumed to represent sporadic site related errors and are neglected. For each model, the magnetic pole positions are then established by visually averaging the cluster of small circle north and South Pole arcs. Each pole location is then transferred through 180 degrees to the opposite pole and both pole locations averaged to determine a mean north and south geocentric magnetic pole (Figure 3.12). An equator is then established by scaling through 90° of latitude from each mean pole position and longitude established by adopting Greenwich as zero degrees longitude. An example of north and South Pole small circle arcs and location of mean geocentric magnetic poles for the Archaean to Mesoproterozoic is shown in Figure 3.12.

North and south geocentric magnetic palaeopole positions established for each expanding Earth model are shown in Figures 3.13 and 3.14 respectively. The sequential images are centred on the north and south palaeopoles and show the movement of continents as they migrate, relative to the poles, during continental extension, break-up and dispersal to the present.

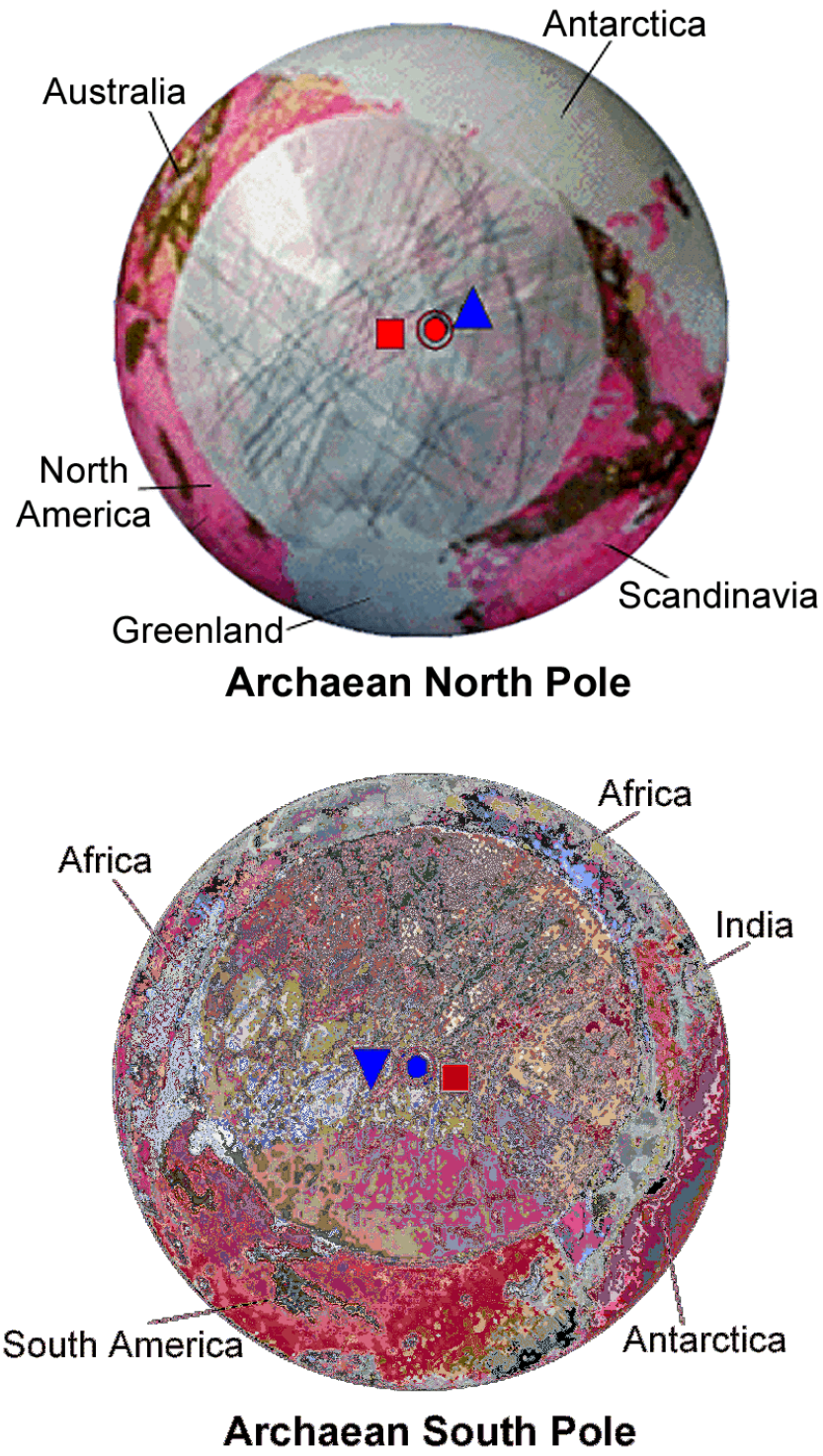

Figure 3.12 Archaean to Mesoproterozoic north and south poles. Poles are located by drawing small circle arcs (fine lines) equal to the actual palaeocolatitude, centred on the sample site location and visually meaning each cluster of arcs. Red squares are mean and projected north poles. Blue triangles are mean and projected south poles. Red bulls-eye: mean north pole. Blue bulls-eye: mean south pole. (Data after McElhinny & Lock, 1996; models after CGMW & UNESCO, 1990).

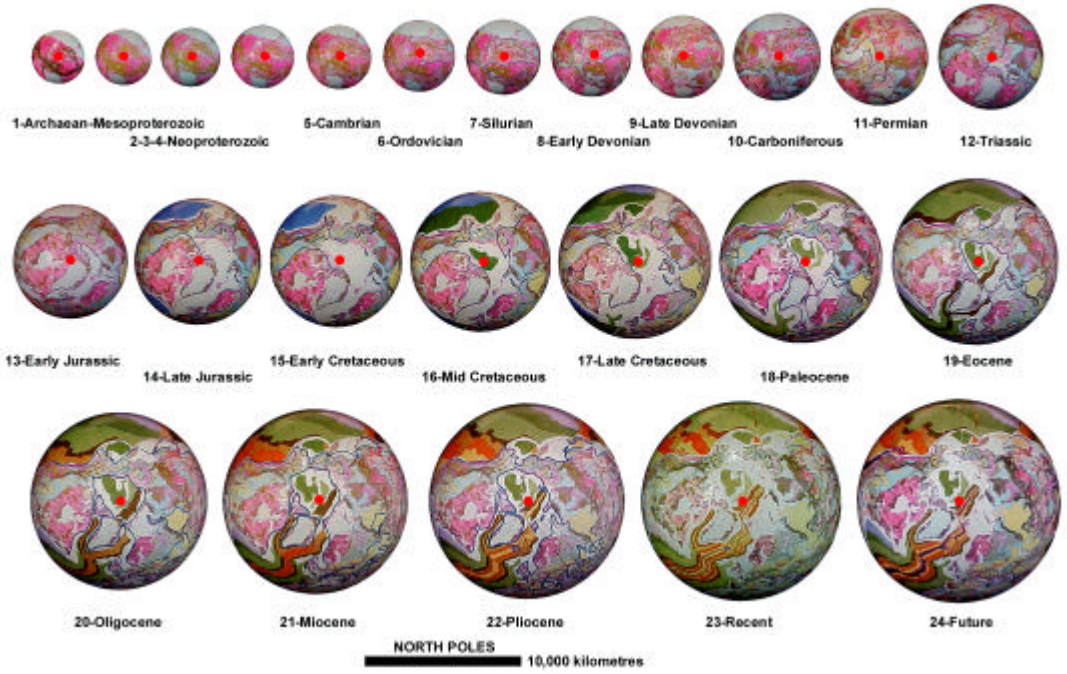

Figure 3.13 Expanding Earth Archaean to Future palaeomagnetic north poles (red dots). During the Precambrian and Palaeozoic the north pole is located within eastern Mongolia, prior to continental break-up and dispersal during the Mesozoic to Recent. Blue outlines represent palaeocoastlines (Section 3.3). (Palaeomagnetic data after McElhinny & Lock, 1996; models after CGMW & UNESCO, 1990).

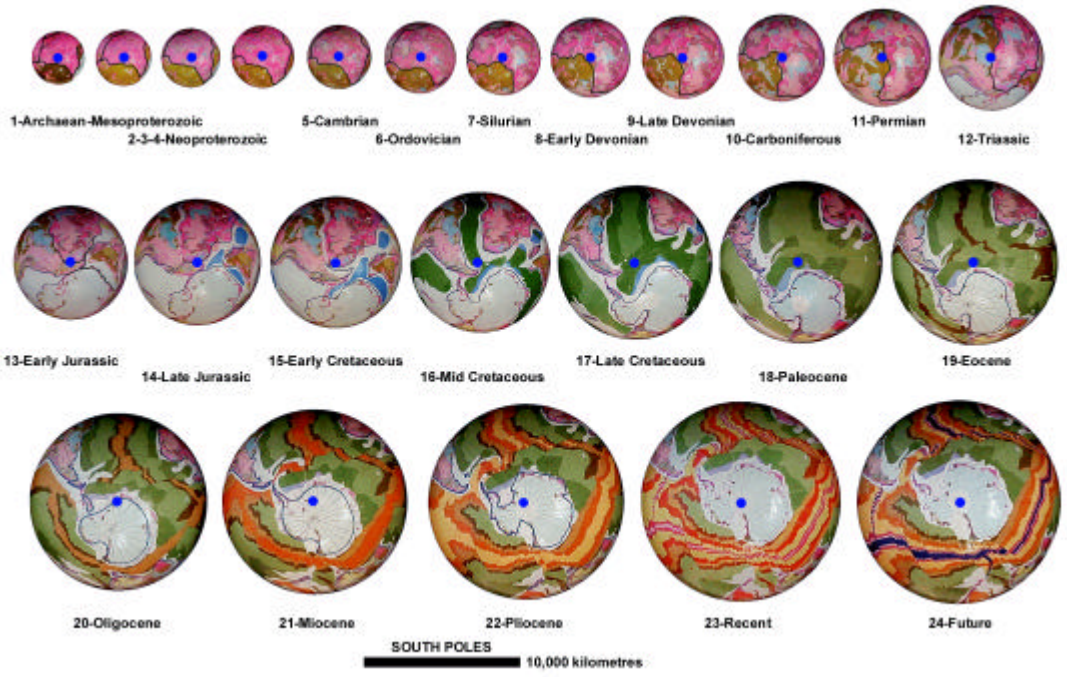

Figure 3.14 Expanding Earth Archaean to Future palaeomagnetic south poles (blue dots). During the Precambrian and Palaeozoic the south pole is located within west central Africa, prior to continental break-up and dispersal during the Mesozoic to Recent. Blue lines represent palaeocoastlines (Section 3.3) and black lines are continental outlines. (Models after CGMW & UNESCO, 1990).

The Precambrian and Palaeozoic north pole is located in eastern Mongolia-China and, as the continents slowly migrate south there is an apparent northward polar wander through Siberia to its present location within the Arctic Ocean. The Precambrian and Palaeozoic south pole is located in west central Africa and, as the continents slowly migrate north there is an apparent southward polar wander along the South American and west African coastlines to its present location in Antarctica.

3.2.6 Summary of Palaeomagnetic Results

Without the constraint of constancy of continental area, determining a palaeoradius of the Earth from conventional palaeomagnetic data becomes invalid and palaeomagnetic conclusions based on these calculations must be reconsidered. Without the constraint on Earth radius, derived palaeomagnetic quantities used to locate palaeopoles on a static radius Earth and establishment of apparent-polar-wander paths must also be re-evaluated.

To locate palaeopoles on expanding Earth models the published palaeomagnetic data of McElhinny & Lock (1996) are used to plot small circle arcs representing the actual palaeocolatitude from sample site to palaeopole. For each expanding Earth model this results in a cluster of diametrically opposed small circle arcs coinciding with north and south geocentric magnetic palaeopoles. The secular variation of the small circle arcs is shown to accord with the secular variation of poles for the Recent North Pole magnetic data (Figures 3.10 and 3.11). An equator is then plotted by scaling through 90° of latitude from each mean pole position and longitude established by adopting Greenwich as zero degrees longitude.

3.3 Palaeogeographic Data

Palaeogeography is a study of the physical and biological geography of the geologic past, including the configuration and latitudinal distribution of continental landmasses, their topographic relief, climate and biota (Ross, 1999). These studies impact directly on the driving forces behind geochemical signals contained in the rock record which are then used as a proxy for understanding the biogeochemical processes in Earth history (Ross, 1999).

Palaeogeographic reconstructions supply critical data towards constraining conventional palaeomagnetic-based plate tectonic reconstructions. Important

contributions include the global palaeogeographic reconstructions of Scotese *et al*. (1979), Ross & Ross (1981), Scotese (1994), Scotese & Golonka (1992), Smith A. G. *et al*. (1994), palaeogeographic reconstructions of Gondwana (eg. Lawver & Scotese, 1987; Grunow *et al*., 1987a, 1987b; DeWit *et al*., 1988; Wilson *et al*., 1989; Archbold, 1994), Pangaea (Veevers, 1994), the Tethys (Dercourt *et al*., 1993), Laurussia (Ziegler, 1989), Laurentia-Gondwana (Dalziel *et al*., 1994; Dalziel, 1997) and Rodinia (Torsvik *et al*., 1996).

Constraint on conventional palaeogeographic reconstructions is deduced from palaeomagnetic studies (eg. McElhinny & McFadden, 2000), the distribution of latitude-dependant sedimentary facies (eg. Caputo & Crowell, 1985; Witzke, 1990; Scotese & Barrett, 1990; Nie, 1991), latitudinal and provincial controls of certain faunas (eg. Meyerhoff *et al*., 1996) and comparisons of tectonostratigraphic histories (eg. Dalziel, 1991; Hoffman, 1991).

3.3.1 Palaeogeography on an Expanding Earth (Video A3.15)

Paleogeography on an expanding Earth has been established by transferring the palaeogeographic information of Scotese *et al*. (1979), Scotese (1994) and Smith A. G. *et al*. (1994) to expanding Earth models (Figure 3.15). These conventional palaeogeographic reconstructions include only the Cambrian to Recent. No attempt is made to reconstruct the geography beyond the Cambrian to include Precambrian expanding Earth models. Palaeogeographical grids have been established by adopting the palaeomagnetic palaeopole and palaeoequator locations determined in Section 3.2.5 and adopting Greenwich as zero degrees longitude for each model (Palaeozoic Video A3.15a; Mesozoic Video A3.15b; Cenozoic Video A3.15c).

The expanding Earth palaeogeographical information is used to display a generalised outline of palaeocoastlines, exposed land and mountainous regions throughout geological time. The information then forms a basis for defining the inter-relationships of exposed continental areas, intervening seaways, mountain building and orogenesis enabling the conventional Pangaea, Gondwana, Laurentia, Baltica, Laurussia and Rodinia continental configurations to be quantified on an expanding Earth. These models will also form the basis for further discussions on palaeobiogeography and palaeoclimate.

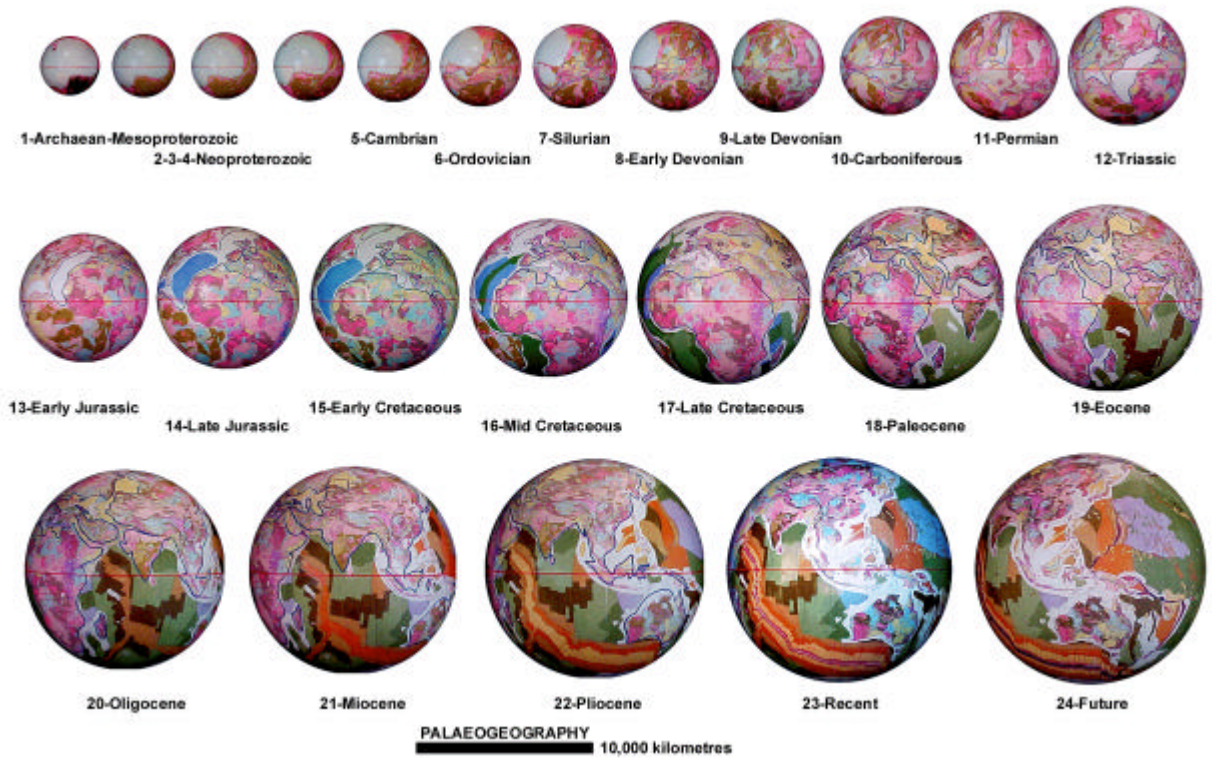

Figure 3.15 Palaeogeography on an Archaean to Future expanding Earth. Post-Proterozoic palaeocoastlines are shown as blue lines after Scotese *et al*., (1979), Scotese (1994) and Smith A. G. *et al*., (1994). Each image advances 15 degrees longitude throughout the sequence to show a broad coverage of geographical development during the Precambrian and Phanerozoic. (Models after CGMW & UNESCO, 1990).

3.3.2 Palaeocoastlines on an Expanding Earth (Video A3.15)

The conventional plate tectonic geographic maps of Smith A. G. *et al*. (1994) show a progressive closure of a Mesozoic to Cenozoic Tethys, Iapetus and Panthallassa Ocean and fragmentation, amalgamation and dispersal of continents to the Recent. The Palaeozoic maps of Scotese *et al*. (1979) and Scotese (1994) show a similar history of conventional crustal dispersal, collision and amalgamation. In each publication coastal information is simplistic and continents are shown dispersed, or fragmented, with intervening micro-continents inferred to represent remnant intracontinental cratonic or orogenic regions. The palaeocoastlines manually plotted on each expanding Earth model are shown as blue lines (Figure 3.15).

On each of the Recent to Cambrian expanding Earth models (Figure 3.15) the coastal geographic information of Scotese *et al*. (1979), Scotese (1994) and Smith A. G. *et al*. (1994) progressively interacts as palaeoradius is reduced backwards in time. In areas where the conventional coastal information overlaps the information is

merged on each expanding Earth model to maintain continuity of line-work. Over simplification of line-work is apparent in each publication and is adopted with minor modification as required. A disparity was also noted with timing of opening of the Atlantic Ocean in Smith A. G. *et al*. (1994), with reconstructions and timing modified according to the oceanic magnetic mapping (CGMW & UNESCO, 1990).

The coastal outlines on each of the Palaeozoic expanding Earth models (Figure 3.15) define emergent land surfaces coincident with cratonic and orogenic regions of each continent and a network of epi-continental seas surrounding emergent lands. These emergent land surfaces equate to the conventional Rodinia, Gondwana and Pangaean assemblages (Section 3.3.5). The network of seaways on each Phanerozoic model is coincident with intracratonic basin sedimentation, and sedimentary basins on each of the Precambrian models are inferred to represent epi-continental seas. Progressive interaction and development of the epi-continental seas defines a prolonged history of crustal spatial integrity, as distinct from the conventional requirement for random crustal amalgamation and dispersal.

Post-Permian coastal outlines on each expanding Earth model (Figure 3.15) coincide with Mesozoic and Cenozoic epi-continental basin sedimentation shown in CGMW & UNESCO (1990). The geographic history during the post-Permian is reflected in eustatic and transgressive-regressive marine cycles in response to opening of the modern oceans (Section 3.3.3). Distribution of coastlines defines a network of epi-continental seas throughout the Mesozoic, prior to regression of epi-continental seas during the Cenozoic to Recent. Regression of seas results in progressive exposure of continental basins to erosion and a shift in epi-continental sedimentary deposition to marginal continental basins as the modern oceans open.

The maintenance of coastal outlines throughout the Phanerozoic, coincident with distribution of epi-continental sedimentary basins, substantiates the premise that the volume of the hydrosphere has increased with time in sympathy with an increase in volume of oceanic lithosphere (Carey, 1988). The volume of hydrosphere is also shown to be influenced by glacio-eustatic changes in sea level during glacial times and transgressive-regressive marine cycles during successive opening of each of the modern oceans (Section 3.3.3).

The conventional Panthallassa (eg. Scotese, 1987), Tethys (eg. Ziegler, 1989) Iapetus (eg. McKerrow *et al.*, 1991) and minor oceans cannot be reconciled in their entirety with expanding Earth reconstructions. Instead, these are represented as a

primordial Panthallassa Sea located between Australia, Asia and North America, an epi-continental Tethys Sea located within the present Eurasian continent and an epi-continental Iapetus Sea located between the west African and North American cratons, possibly extending to South America and east Australia.

Coastal geography on expanding Earth models (Figures 2.22, 3.15) indicates that the early Panthallassan and Iapetus Seas developed during the Early Permian to Early Jurassic as extensional basins within the present northwest Pacific and north Atlantic Ocean regions respectively. These then progressively opened and extended throughout the Mesozoic and Cenozoic as the modern Pacific and Atlantic Oceans. In contrast, the Tethys Sea had its origins during the Early Proterozoic as an epi-continental sea, progressively enlarging and extending in area during the Proterozoic, Palaeozoic and Mesozoic. During Late Palaeozoic continental break-up the Tethys region was influenced by glacio-eustatic and transgressive-regressive marine cyclicity and formed the loci for continental Eurasia and intra-continental orogenesis during the Mesozoic and Cenozoic.

3.3.3 Marine Transgressive-Regressive History (Video A3.15)

The emergent continents, defined by coastal geography on expanding Earth models (Figure 3.15), show a complex history of eustatic and transgressive-regressive sea-level change. Conventional regional and global cycles are discussed in Miall (1990) in terms of cyclic and rhythmic stratigraphic events related to plate tectonic processes. Important effects influencing the geological history include changes in global climate, magmatism, ocean-water circulation patterns and biogenesis. Miall (1990) suggests these are preserved as three basic kinds of stratigraphic cycle spanning five orders of magnitude in time duration. These include: very long term cycles caused by the inferred assemblage and subsequent rifting and dispersal of supercontinents (Wilson cycles); convective overturn in the mantle; global changes to spreading rates; glacio-eustatic cycles (Milankovitch cycles) resulting from variation in the Earth's orbit; and variation in solar radiation.

Eustatic and transgressive-regressive changes in sea level throughout the Phanerozoic (Figure 3.16) are shown in relation to periods of glaciation and conventional global tectonic cycles. Sea-level change, relative to present sea level, steadily falls from a Cambrian-Ordovician peak to a minimum during the Triassic. A

rise from the Triassic to Late Cretaceous is then followed by a fall to the Recent. Superimposed on this first order eustatic cycle are second order transgressive-regressive cycles that approximate the major periods of Earth history and glacio-eustatic induced sea-level changes.

On an expanding Earth eustatic and transgressive-regressive marine cycles occur in response to climatic change, to a shift in the distribution of epi-continental seas, orogenesis, mountain building, erosion, and in response to opening of post-Permian modern oceans and production of new juvenile water. The variance of these changes is reflected in the palaeocoastal outlines (Figure 3.15) and results in a change in exposed continental land, coastal transgressive and regressive events, distribution of latitude-dependant sedimentary facies, latitudinal and provincial distribution of certain faunas and tectonostratigraphic histories.

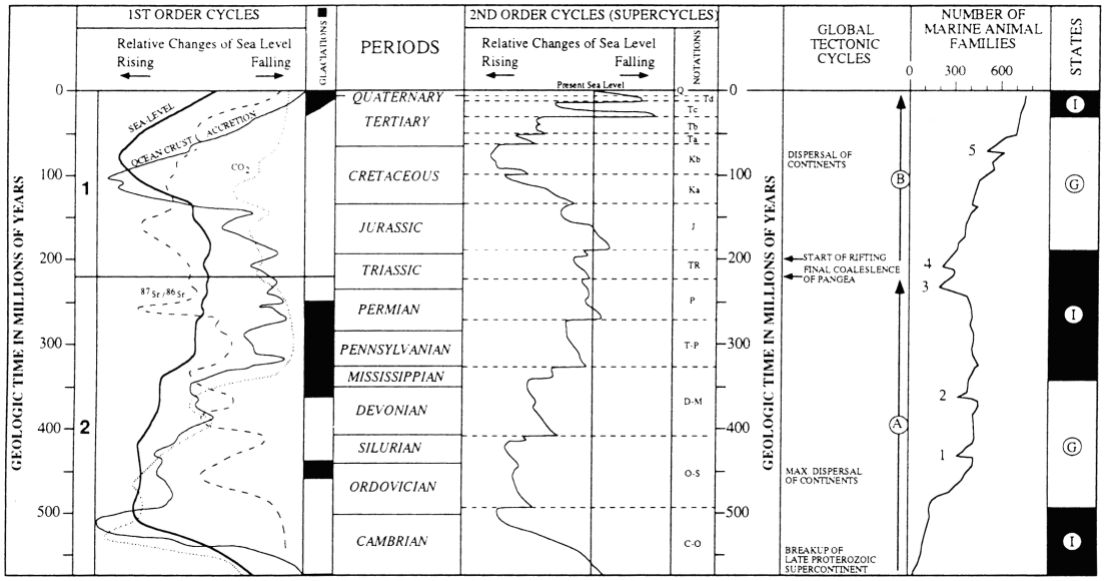

Figure 3.16 Changes in sea level and glacial record during the Phanerozoic. Periods of glaciation are shown as black fill, I represents icehouse state and G represents greenhouse state. (Figure 1.5 of Eyles & Young, 1994; sea level after Vail *et al*., 1977).

For example, sea-level change in Eurasia during Earth expansion (Figure 3.15) is defined by the variance in surficial area of the epi-continental Tethys Sea, and transgression and regression of palaeocoastlines. During the Palaeozoic to Triassic the surficial area of the Tethys Sea steadily reduces during periods of glaciation (Section 3.5.2), crustal extension and initial opening of the modern oceans. The area of the Tethys Sea then increases to a maximum during the Mid- to Late-

Cretaceous during a period of interglacial melting, rapid opening of modern oceans, continental break-up and increase in new juvenile water derived from mid-ocean-ridges, decreasing again to the present in conjunction with Cenozoic orogenesis, mountain building and Recent glaciation. The detail reflected in these changes is recorded in the tectonostratigraphic and erosional history of each continent.

3.3.4 Epi-continental Sedimentary Basins (Video A3.15)

The coastal outlines on expanding Earth models (Figure 3.15) define a prolonged history of crustal extension and sedimentation centred primarily on the complex Eurasian Tethys region, and Australian-American Panthallassa and Iapetus regions. These regions show complex transgressive-regressive histories related to polyphase basin extension, glacio-eustatic sea-level change, mountain building, erosion and continental break-up and dispersal.

On each expanding Earth model (Figure 3.15) the Eurasian and Australian-American basin regions represent zones of continental crustal extension and are important depocentres for continental sedimentation throughout the Precambrian and Palaeozoic. During the Late Palaeozoic, as continental break-up commences (Section 2.6), continental sedimentation then progressively shifts to marine basin settings within the opening North Pacific, South Pacific and Arctic Oceans, followed by the Atlantic and Indian Oceans during the Triassic to Early Jurassic and Southern Ocean during the Paleocene.

During the post-Permian, the long history of Precambrian and Palaeozoic epi-continental sedimentation is disrupted by continental rupture, break-up and dispersal. Sedimentation then shifts to continental marginal basin settings during rapid opening of the modern oceans, continuing to the Recent. Within the modern oceans the shift in sedimentation from Precambrian and Palaeozoic epi-continental to Mesozoic and Cenozoic marine and marginal basin settings is now preserved as marginal basin sediments along the continental coastlines and as remnant ocean plateau sediments within the modern oceans (eg. Dickins *et al*., 1992).

3.3.5 Palaeocontinents

The following brief descriptions of the Pangaea, Gondwana, Laurentia, Baltica, Laurussia and Rodinia crustal configurations on an expanding Earth differ

from conventional plate tectonic reconstructions. Conventional reconstructions require complex and extensive plate motion histories, such as described by Sadowski (1994) where assemblage of the Gondwana supercontinent resulted from a supercontinent dispersion-amalgamation cycle, commencing from a former Precambrian Rodinian supercontinent (Hoffman, 1991). The timing and formation of conventional assemblages is often contentious (Li & Powell, 1993) and are based on complex palaeomagnetic apparent polar wander constraints.

Geological expanding Earth reconstructions (Figure 2.10) show that a spatial intracratonic and intracontinental integrity is maintained throughout Earth history. The distinguishing feature of each expanding Earth reconstruction is the inter-relationships of intracratonic sedimentary basins, the network of epi-continental seas and the network of orogenic regions. Geographical reconstructions (Figure 3.15) show that the variance of each of these in time results in a change in exposed continental land. The supercontinent configuration is then a reflection of the palaeocoastal outlines, defined by eustatic and transgressive-regressive marine history. Each crustal assemblage is then progressive with no requirement for random dispersion-amalgamation cycles.

3.3.6 Rodinia (Video A3.18)

The conventional Neoproterozoic Rodinia supercontinent assemblage (eg. Dalziel, 1992) is based on palaeomagnetic evidence and formed at around 1100 Ma (Dalziel, 1991, 1992; Hoffman, 1991; Moores, 1991). Subsequent break-up occurred at 725-750 Ma, followed by final redistribution in Late Precambrian to Early Cambrian times (Powell *et al.*, 1993; Storey, 1993; Dalziel *et al.*, 1994). Reconstructions are shown in Torsvik *et al.* (1996) (Figure 3.17) with supportive palaeomagnetic palaeopole and apparent polar wander data in McMenamin & Schulte-McMenamin (1990).

Conventional intracontinental assemblages, such as Laurentia-Baltica-Siberia and Laurentia-Baltica-Amazonia (Figure 3.17), rely primarily on palaeomagnetic constraints and are restricted by the palaeolongitudinal limitations of Li *et al.* (1993). Beyond these defined assemblages the presence of large proto-oceans require cratons from remote continents to be fragmented and dispersed, resulting in a multitude of assemblage options (eg. Zhao *et al.*, 1999).

The Proterozoic expanding Earth reconstructions (Figure 3.18) agree in principle with the Rodinian intracontinental Laurentia-Baltica-Siberia and Laurentia-Baltica-Amazonia assemblages of Torsvik *et al.* (1996). No palaeocoastal information is available for the Precambrian and the expanding Earth Rodinian supercontinent is inferred from the distribution of Precambrian continental cratons and the network of orogens and basins. Each of the Precambrian cratons (Figure 3.18) are inferred to represent exposed land, and orogens and basins are inferred to represent epi-continental seas.

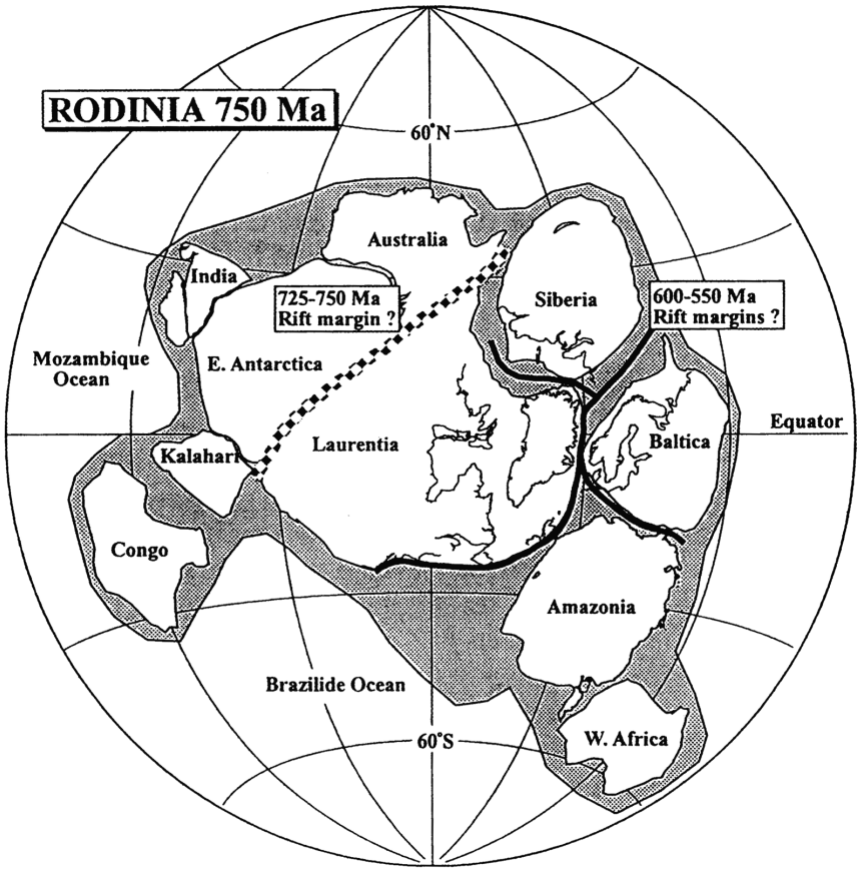

Figure 3.17 Conventional Rodinia supercontinent at 750 Ma. Reconstruction based on conventional palaeomagnetic evidence. Assemblage shows Laurentia in relation to Siberia, Baltica and Amazonia continents. Shaded area represents shelf outline. (From Torsvik *et al*., 1996, after Dalziel, 1992).

The spatial integrity of the expanding Earth Rodinian configuration is supported by the palaeomagnetic location of palaeopoles and palaeoequators (Section 3.2.5). The location of the Neoproterozoic palaeoequator and palaeopoles (Figure 3.18) agrees in principle with the distribution of glaciogenic deposits and location of the palaeoequator of Torsvik *et al.* (1996) (Figure 3.17). The expanding Earth

Rodinian North Pole is shown located in west central Africa, the South Pole in eastern Mongolia, and the equator passes through East Antarctica, central Australia, North America-southern Greenland (Laurentia), southern Scandinavia (Baltica) and central Europe.

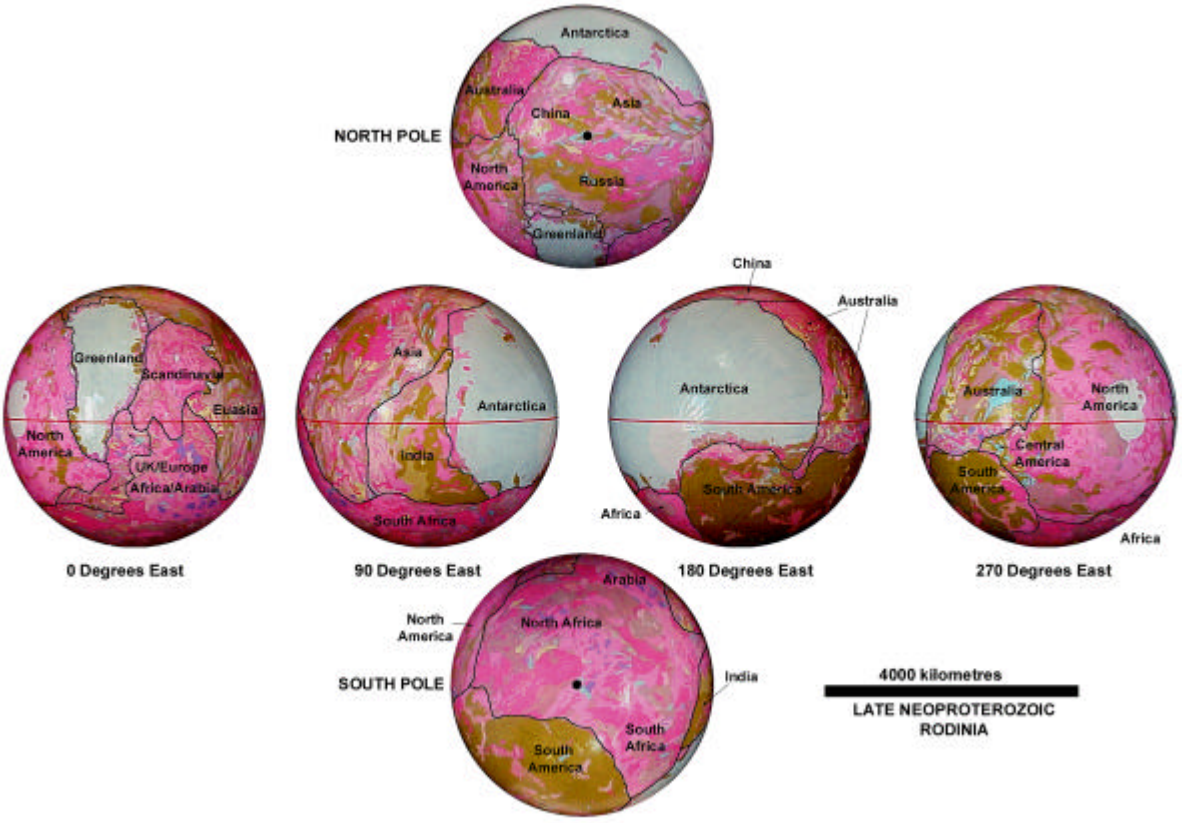

Figure 3.18 Late Neoproterozoic expanding Earth Rodinia supercontinent. Late Neoproterozoic model shows distribution of Precambrian cratons (pink and red) inferred to represent exposed land, and a network of orogens and basins (khaki and brown) inferred to represent epi-continental seas. Black lines represent outlines of remnant present-day continents. (Continental geology after CGMW & UNESCO, 1990).

The expanding Earth Rodinian assemblage (Figure 3.18) forms a pre-cursor to Gondwanan and Pangaean configurations, and demonstrates a spatial integrity of all proto-continents and tectonic elements during the Precambrian.

3.3.7 Gondwana (Video A3.20)

The conventional Gondwana palaeocontinental configuration comprises South America, Africa, Arabia, Madagascar, India, Australia and Antarctica, as well as Florida, southern and central Europe, Turkey, Iran, Afghanistan, Tibet and New Zealand (Scotese *et al.,* 1979). Conventional reconstruction (Figure 3.19) shows a large palaeocontinent forming during a Pan-African tectonic event at the end of the

Precambrian (Burke & Dewey, 1973), which remains intact throughout the Palaeozoic and Early Mesozoic (Scotese *et al.*, 1979). Li & Powell, (1993) note that past movements of Gondwana, based on palaeomagnetic, biogeographic and palaeoclimatic data, are both equivocal and contentious, despite the addition of new data from Africa and Australia.

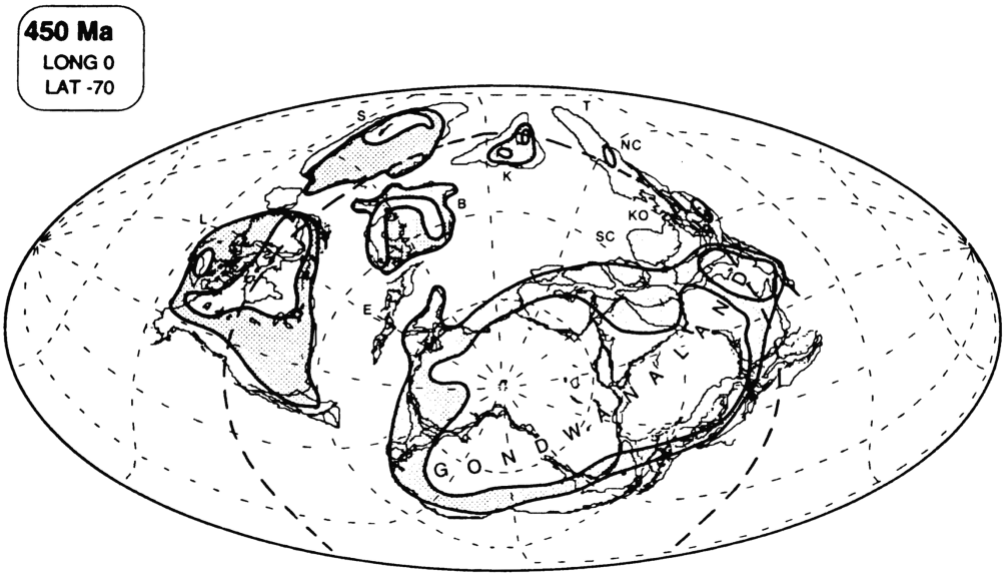

Figure 3.19 Conventional Gondwana assemblage at end Ordovician. Continents include Laurentia (L); Siberia (S); Baltica (B); England and others (E); Kazakhstania (K); North China (NC), including Tarim (T) and Korea (KO); and South China (SC). Shallow seas are shown as light stipple, palaeoequator is shown as heavy dashed line and South Pole is located in west central Africa. Lambert equal-area projection. (From Veevers, 1994).

On an expanding Earth (Figure 3.20) Gondwana is shown to be a successor of the Precambrian Rodinia supercontinent. The Gondwanan assemblage retains the same spatial integrity of cratons, orogens and basins throughout the Palaeozoic until initiation of continental break-up during the Early Permian and continental dispersal during the Mesozoic. The Gondwana, Laurentia, Baltica and Laurussia continents are each defined by the coastal information of Scotese *et al*. (1979) and Scotese (1994), shown as blue coastlines on the Ordovician expanding Earth model (Figure 3.20). The coastal information defines geographically distinct proto-continents, surrounded by a network of epi-continental seas coinciding in principle with conventional configurations.

Gondwana on an expanding Earth (Figures 3.20) comprises a joined North and South Gondwana, separated in part by a pre-cursor South Pacific Sea. North Gondwana comprises Australia, East and West Antarctica and India, and possibly

includes Tibet and Afghanistan. South Gondwana, joined at Madagascar, comprises Africa, Arabia and South America. Laurentia-Baltica comprises North America, Greenland, Scandinavia and Precambrian fragments of England and Ireland. Laurussia is centred on the Precambrian regions of Mongolia and northern Russia. Each of these exposed land surfaces are surrounded and interconnected by epi-continental seas, which are preserved as the Palaeozoic sedimentary basins of eastern Australia, North and South America, Eurasia and Africa.

The expanding Earth Gondwanan assemblage (Figure 3.20) differs from conventional reconstructions. Eastern Australia, proximal to both North and South America, is separated by a narrow epi-continental proto-South Pacific Sea as distinct from a wide conventional Panthallassa Ocean. This Australian-American tectono-stratigraphic association is acknowledged in Powell & Veevers (1994) and substantiated from distribution of marine taxa of Stevens (1990), but can only be maintained on an Earth of reduced palaeoradius.

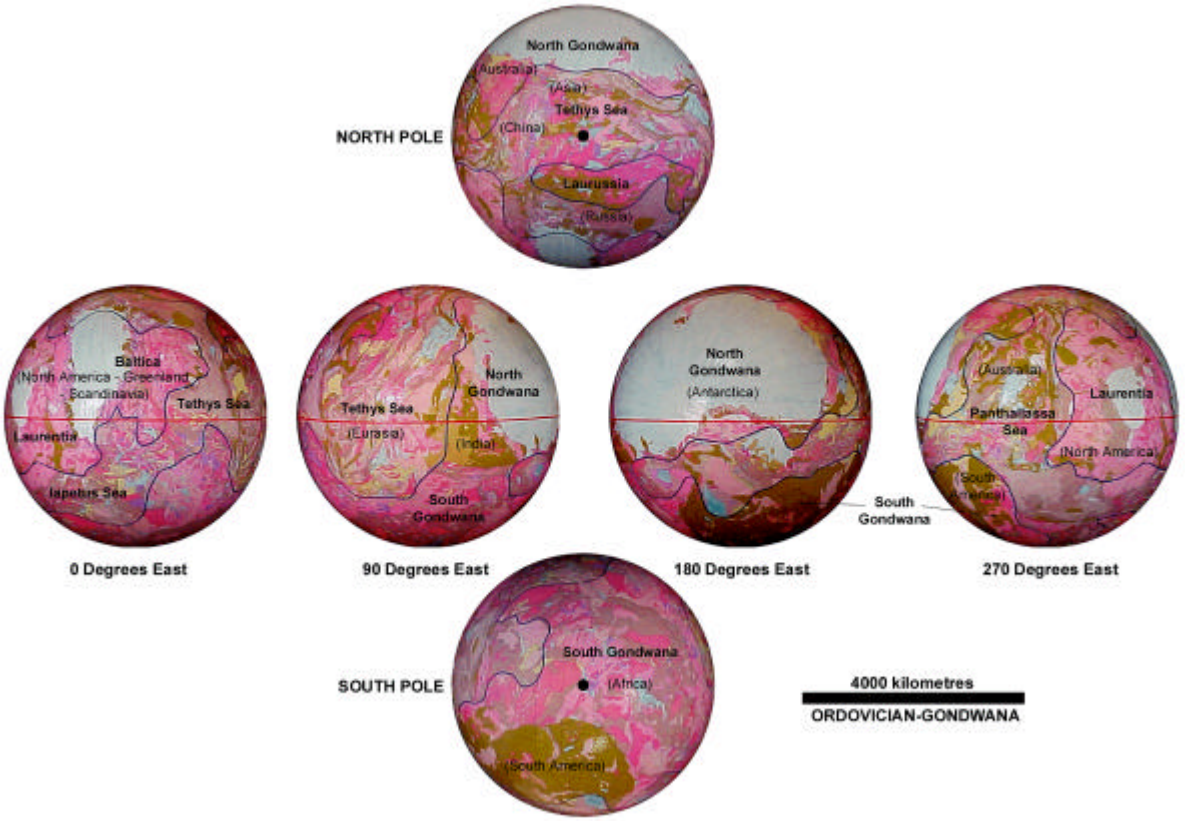

Figure 3.20 Ordovician expanding Earth Gondwana assemblage. Ordovician model shows palaeocoastline distribution (blue line) defining North and South Gondwana in relation to Laurentia, Baltica, and Laurussia. An intracratonic Tethys, Iapetus and Panthallassa Sea forms part of a global network surrounding each of the exposed supercontinents. (Continental geology after CGMW & UNESCO, 1990).

The South Pole on an expanding Earth during the Palaeozoic (Figure 3.20) is located within central west Africa (South Gondwana) and the palaeoequater passes through East Antarctica, central Australia, North America, central Eurasia and India (North Gondwana). This geographic configuration approximates conventional reconstructions (eg. Lawver & Scotese, 1987; Powell, 1993) but differs substantially in the South Pacific region because of the elimination of the Panthallassa Ocean.

During the Silurian and Devonian, expanding Earth coastal information (Figure 3.20) shows continental landlinks between north Australia and North America, and north Africa-Arabia to Scandinavia, forming two separate intervening seas. Models suggest that the eventual merger of these seas results in periods of transgressive-regressive sea-level change. This observation is substantiated by palaeobiogeographical extinction, sea level transgressive and regressive events and climatic changes occurring during the Late Ordovician to Devonian (eg. Briggs, 1995).

During the Late Palaeozoic the expanding Earth Gondwanan supercontinent progressively evolves into the Pangaean supercontinent. The Gondwanan continents then geographically merge with the smaller Laurentian, Baltican and Laurussian sub-continents as the epi-continental Tethys Sea, and narrow Panthallassa and Iapetus Seas regress during the Late Palaeozoic to Mesozoic era of continental break-up and dispersal.

3.3.8 Laurentia, Baltica, Laurussia (Video A3.20)

Laurentia and Baltica (Torsvik *et al*., 1996; Dalziel, 1997; 2000), Laurussia (Ziegler, 1989) and displaced continental fragments such as Kazakhstania and Southeast Asia (Metcalfe, 1993; Archbold, 1994) are described in conventional literature as sub-continents, or continental fragments periodically dispersing and amalgamating between the larger supercontinents.

On an expanding Earth (Figure 3.20) these sub-continents represent exposed cratonic or orogenic land surfaces, separated geographically from the supercontinents by the network of epi-continental seas. Their location is constrained by the spatial configuration of surrounding cratonic regions and development history of the epi-continental seas. Their geographical isolation results in a diversification of both marine and terrestrial biota and tectono-stratigraphic associations. Their progressive

merger with the supercontinents coincides with opening of the modern oceans during the Late Palaeozoic to Mesozoic and sea level regression during the Cenozoic.

3.3.9 Pangaea (Video A3.22)

A large Pangaea supercontinent assemblage was proposed by Wegener (1915). He presented evidence suggesting that the large continental areas of the modern world were united late in the Palaeozoic, prior to break-up and dispersal during the Cenozoic. Stanley (1989) describes a conventional Pangaea as fragmenting within the Tethyan region during the Mesozoic, with continental rifting beginning during the mid-Jurassic. During the subsequent period of continental break-up, dispersal and amalgamation, oceans were then created and destroyed during an extended mobile crustal history.

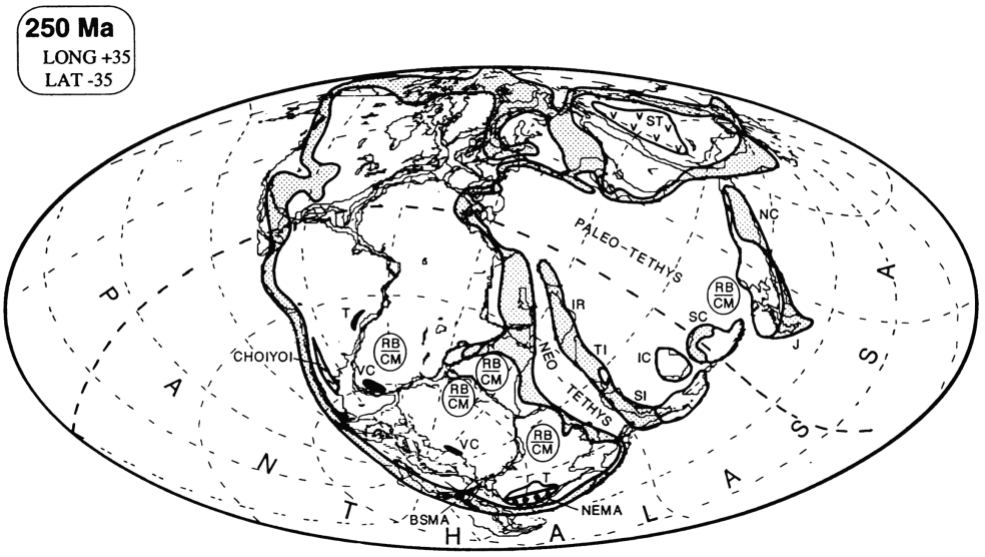

Figure 3.21 Conventional Permo-Triassic Pangaean assemblage. Continents shown define an emergent South Gondwanan province and a submergent northern or Laurasian province. Independent continents shown include North China (NC), including Japan (J); South China (SC); Indochina (IC); and a narrow Crimmerian continent comprising Iran (IR), Tibet (TI), and Sibumasu (China-Burma-Malaya-Sumatra) (SI). Shallow seas are shown as light stipple, and the palaeoequator is shown as a heavy dashed line. (From Veevers *et al*., 1994).

Conventional Pangaea was assembled during the mid-Carboniferous and began initial break-up during the mid-Jurassic (Veevers, 1994). Veevers (1994) describes Pangaea (Figure 3.21) as comprising two contrasting sedimentary provinces: an emergent southern (Gondwanan) province, with no more than 15% of the landmass covered by sea, dominated by non-marine facies and; a submergent

northern or Laurasian province, 25% or more covered by sea, dominated by marine facies. During the post- mid-Jurassic Pangaea then broke into fragments of the emergent Gondwana province and submergent Laurasia province. Final dispersal started when continental rifting was superseded by sea-floor spreading (Veevers, 1994).

Pangaea on the Early Permian expanding Earth model (Figure 3.22), coincides with the late Palaeozoic transitional period (Section 2.6), where Earth expansion progresses from continental extension to continental rupture, break-up and dispersal. The Permian expanding Earth had a palaeoradius approximately 50% of the present Earth radius. At that time modern oceans were starting to open and the network of epi-continental seas were rapidly extending and coastal outlines rapidly changing. This contrasts with the conventional requirement for closure of a large Tethys Ocean and reduction in surficial area of a Panthallassa Ocean during the Mesozoic.

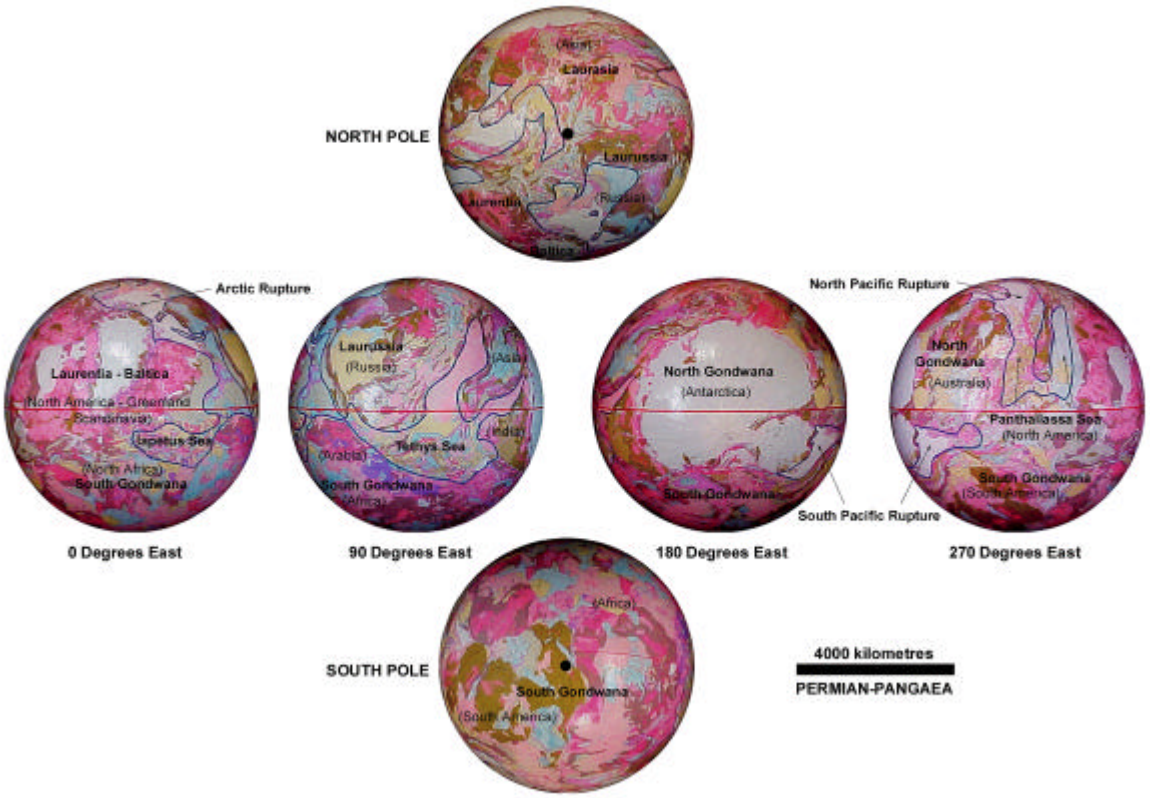

Figure 3.22 Early Permian expanding Earth Pangaean assemblage. Figure also shows continental rupture in the north and south Pacific and Arctic Ocean regions forming the modern oceans, prior to continental break-up and dispersal to the Recent. (Continental geology after CGMW & UNESCO, 1990).

During the Permian and post-Permian, Pangaea on an expanding Earth represents a progressive evolution of the Gondwanan assemblage prior to continental break-up and dispersal. This is defined by a progressive extension of epi-continental sedimentary basins, pulsed orogenesis and transgression-regression of epi-continental seas as modern oceans opened and rapidly expanded to the Recent. Large Panthallassa, Tethys and Iapetus Oceans are not required, instead, these are replaced by epi-continental Panthallassa, Tethys and Iapetus Seas which represent precursors to the modern Pacific and Atlantic Oceans and continental Europe and Asia.

3.3.10 Orogenesis

Orogeny was defined by Gilbert (1890) as representing a period of mountain building. With changing emphasis, orogeny now refers to folding of rocks in fold belts (Ollier & Pain, 2000) and represents an ill-defined tectonic concept "characterised by intense internal rock deformation along long linear mountain belts, and, at places, by associated regional synkinematic metamorphism" (Cebull & Shurbet, 1992, page 112). Burg & Ford (1997) conclude that "orogenesis encompasses all processes that result in crustal thickening, causing uplift and hence high topography" (Burg & Ford, 1997, page 13). Orogeny was further considered by Cebull & Shurbet (1992) to be a temporally discontinuous event, commonly diachronous and polyepisodic. These events generally occur at relatively shallow depths and their primary deformational characteristics were shown to be ill suited to the identification of presently active orogenic belts (Cebull & Shurbet, 1992).

Cebull & Shurbet (1992) discuss two distinctly different explanations for orogeny, referred to as noncollision and collisional orogeny. The noncollisional model of Cebull & Shurbet (1992) is depicted as being thermally induced by rising masses, or thermal fronts that originate from partial melting of a down-going lithospheric slab along subduction zones. The collisional model of Cebull & Shurbet (1992) portrays orogeny as being mechanically driven, mainly by the impact of colliding continents or island arcs. In this model interiors of orogenic belts are assumed to undergo extensive lateral shortening, principally as a product of horizontal compressive stress. Cebull & Shurbet (1992) conclude that neither conventional tectonic model is sufficiently comprehensive to explain the apparent complexities of orogenesis.

Conventional orogenesis, in conjunction with fold-mountain belts is depicted as sites of intra-continental collision and sites of major suturing between palaeocontinents (eg. Condie, 1989; Stanley, 1989; Cebull & Shurbet, 1992; Burg & Ford, 1997). These represent random global events, dependent on the plate motion and collisional history as a whole.

Models for relief of surface curvature and orogenesis on an expanding Earth were considered by Rickard (1969), Carey (1975, 1976, 1983a, 1988) and Glikson (1979). Orogenesis on an expanding Earth (Maxlow, 1995) was found to be related to intracratonic interaction during relief of surface curvature, resulting from expansion of the Earth. The radial and tangential vector components of this expansion process gives rise to a continuum of potential orogenic models. Earth expansion (Figures 2.1 and 2.10) empirically demonstrates the onset of orogenesis as continents extend, rupture, break-up and disperse under the action of an accelerating increase in surface area.

Both Rickard (1969) and Carey (1975, 1976, 1983a, 1988) put forward models for orogenesis and basin development under conditions of surface curvature adjustment and demonstrate that continental collision may not be required to promote orogenesis. The magnitude of both horizontal shortening and extension during isostatic re-equilibration of surface curvature (Maxlow, 1995) effectively demonstrates the potential for both tangential and radially directed motion acting within a continental plate during expansion of the Earth.

Conventional collisional orogenic models cannot be reconciled with an expanding Earth tectonic model. Observations from models suggest that orogenesis on an expanding Earth is represented by zones of intracratonic to intracontinental interaction, resulting from gravity induced collapse and partial rotation of cratons or proto-continents as they adjust for changing surface curvature. Geographical reconstructions (Figure 3.15) show that cratons and proto-continents are, in general, maintained in an elevated state throughout Earth history, with periodic gravity induced brittle fracture, collapse and isostatic re-equilibration and erosion maintaining the prevailing surface curvature. Tangentially directed motion during this collapse and re-equilibration is manifested as intracratonic to intracontinental rotation, localised within epi-continental sedimentary basins, and accompanied by regional synkinematic metamorphism and magmatism. This periodic rotation gives rise to long linear and interconnected orogenic belts surrounding each of the primary

cratons or proto-continents, with polyphase motion resulting in an extension-orogenesis-extension cyclicity. This observation is consistent with the fundamental definition for orogenesis of Cebull & Shurbet (1992).

Proterozoic and Palaeozoic orogenic zones are shown on each of the expanding Earth models (Figures 2.10, 2.13, 3.15). These orogenic zones form an intracratonic network coinciding with the network of epi-continental sedimentary basins. This orogenic network demonstrates that orogenesis on an expanding Earth occurs within zones of primary crustal weakness, rifting and crustal extension (Section 2.5.2, Figure 2.13). Observations from Proterozoic and Palaeozoic models (Figures 2.10, 3.15) suggest that orogenesis within this network involves predominantly intracratonic translational and rotational motion, resulting in linear fold-belts during changing surface curvature of the Earth with time.

During the post-Permian period of continental break-up and dispersal the established Palaeozoic and Precambrian orogenic belts (Figures 3.15) are also affected by break-up. Remnants of Palaeozoic and Precambrian orogenic belts remain accreted to the various primary cratons to form the modern continents. These orogenic remnants include the Grenville and Appalachian orogenic belts of North America, Australian Tasman and Lachlan orogenic belts, Hercynides of Europe, Caledonides of Scandinavia and Mauritanides of west Africa.

The onset of Mesozoic and Cenozoic Alpine-Himalayan orogenesis is shown on the Triassic to Mid Cretaceous expanding Earth models (Figure 3.23; Video A3.23) as pre-orogenic continental basin extension. The restoration of geologic detail on the models to a pre-orogenic configuration is graphically not possible and basin extension within the Eurasian orogenic belts is shown as white dilation spaces in Figure 3.23. This extension is followed by a progressive shortening of basin settings, shown on the Late Cretaceous to Eocene models as a progressive closure of the white dilation space (Figure 3.23). A return to post-orogenic basin extension then occurs from the Eocene to Recent.

The Alpine-Himalayan orogenic front is further complexed by clockwise rotation of both Europe and Asia relative to Africa, resulting in a return to post-orogenic basin extension within Asia during the Tertiary to Recent. This pulsed continental basin extension - translational orogenesis - basin extension scenario contrasts strongly with the conventional requirement for Africa to Europe and India to Asia collision (eg. Burg & Ford, 1997).

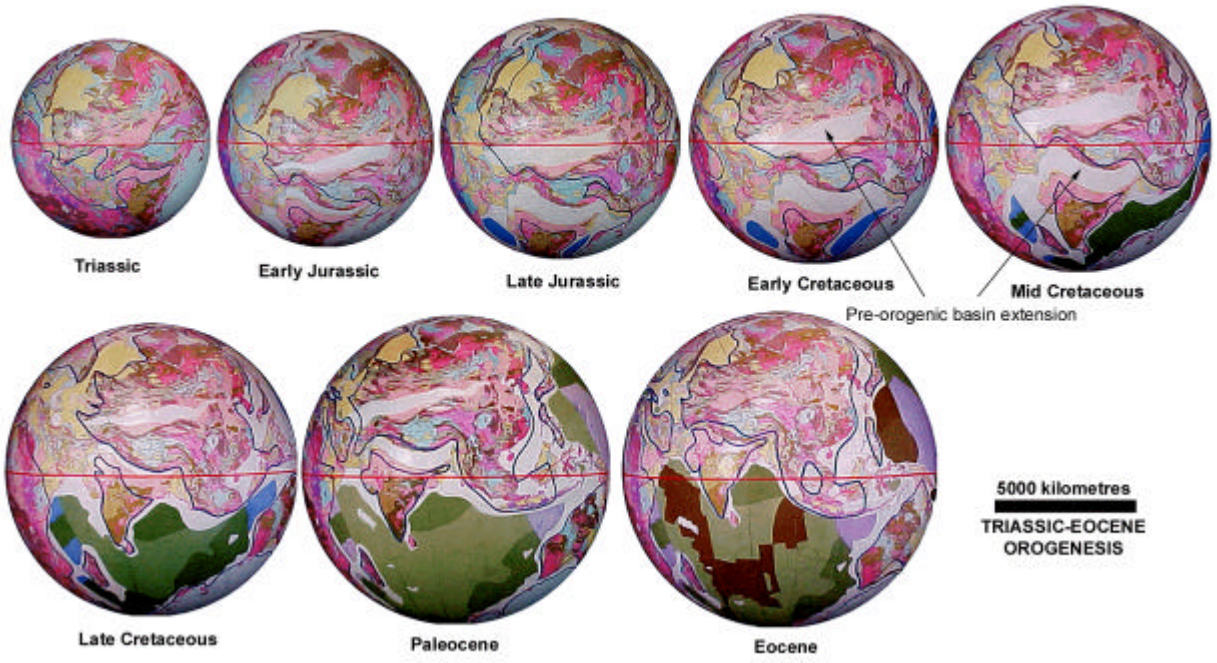

Figure 3.23 Triassic to Eocene expanding Earth Alpine-Himalayan orogenesis. White dilation space shown on each model represents pre-orogenic extension, prior to crustal shortening during the Cenozoic Alpine-Himalayan orogenic event. Blue lines represent palaeocoastlines. Each model is centred on 90 degrees east longitude. (Geology after CGMW & UNESCO, 1990).

3.3.11 Mountain Building and Erosion

Ollier (1985) and Ollier & Pain (2000) note that a distinction must be made between orogeny, which deals with formation of fold belts and mountain building, which results in vertical uplift to form plateaus. Ollier (1998) provides examples from major mountain ranges throughout the world to show that most mountains are eroded plateaus, once low-level planation surfaces that cut across older bedrock structures (Figure 3.24). This contrasts with the conventional view that vertical crustal movement must be derived from horizontal movement by collision or subduction (eg. Burg & Ford, 1997; Willett, 1999). Ollier (1998) concludes that any tectonic explanation though, must account for both the tectonic stability that permits planation and the rapid vertical uplift that exposes the plateaued land surfaces to erosion.

Ollier (1998) presents a model for passive margin development and erosion, based on extensive field-based observations, and concludes that continental rifting starts with a rift valley stage where the palaeoplain at the edge of the continent is downwarped. On-land changes to the drainage pattern occur and, as seafloor spreading begins, part of the palaeoplain sinks beneath the sea. Erosion is

concentrated on the steeper slopes between the axis of warping and the coast, often forming a great escarpment. Offshore sediments covering the sunken peneplain form a basal unconformity. This is graphically displayed in Yano & Wu (1995) (Figure 3.25) who present a conceptual cross section across the East Asian continental margin to explain continental scale arching, tectonics, and magmatism.

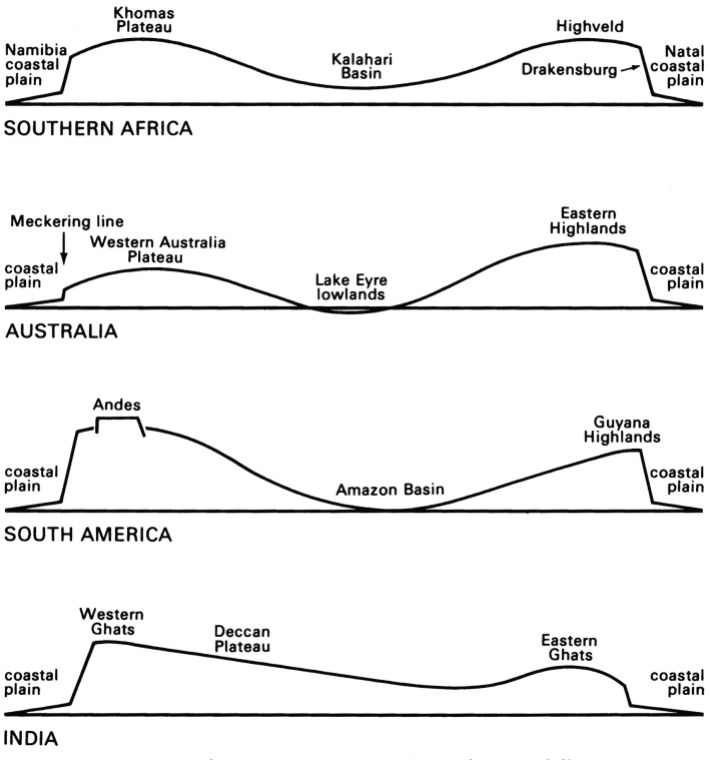

Figure 3.24 Schematic morphotectonic similarities between different continents. In each example Great Escarpments parallel the coasts, separating a high plateau from a coastal plain. Each continent has a central depression bounded by gentle rises to high plateaus. The plateaus are bounded by abrupt, outward-facing escarpments, beyond which are coastal plains. (From Ollier, 1985).

For an expanding Earth the Archaean to late Mesoproterozoic palaeoradius is shown to increase by about 60 kilometres during 3 billion years of Earth history (Section 2.4). It is inferred from model studies that the Archaean and Early Proterozoic was a time where exposed landsurfaces were subject to prolonged erosion and remained essentially of low relief and planated. Orogenesis (Figures 2.10, 2.13 and 3.15) is restricted to zones of intracratonic rotation manifested within extensional basins, forming linear fold belts. During the post-Mesoproterozoic the Earth undergoes a steady to rapidly accelerating expansion to the Recent. During this time the continental and oceanic crust undergoes extensive vertical adjustment for

changing surface curvature, resulting in intracratonic extension, intracratonic and intracontinental orogenesis, continental break-up and dispersal.

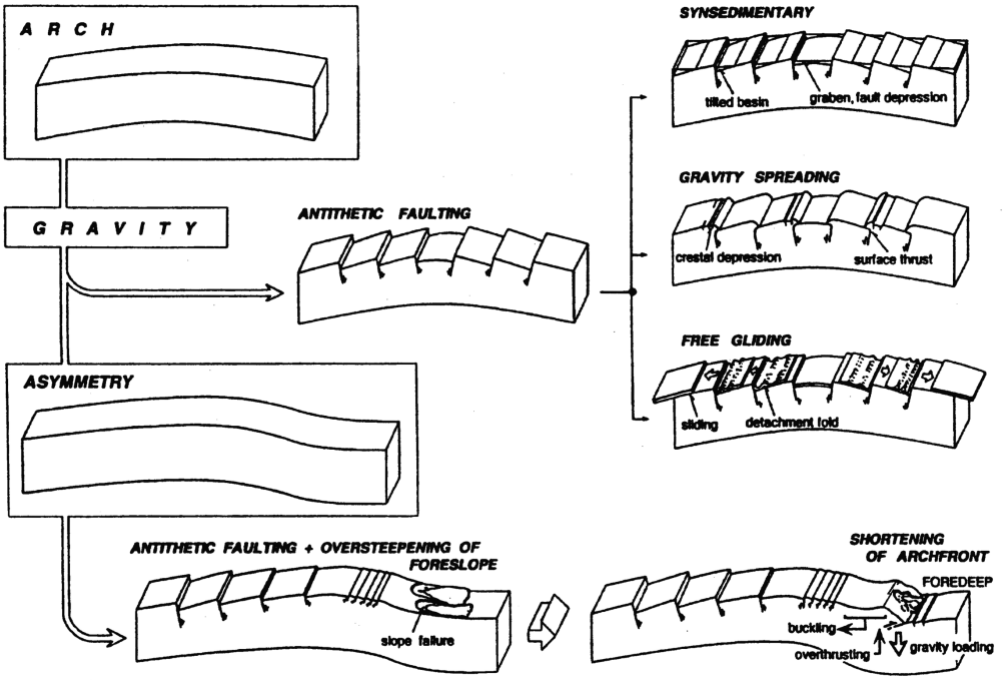

Figure 3.25 Conceptual cross-section of the East Asian continental margin. Yano & Wu (1995) describe the Late Jurassic to Early Cretaceous East Asian margin as comprising antithetic fault blocks, synsedimentary arching, grabens and half grabens. Gravity spreading results in near-surface thrusting, and free gliding of a sedimentary cover results in detachment folding. (After Yano & Wu, 1995).

Change in surface curvature during Earth expansion is considered a prime mechanism for the field-based mountain building observations presented by Ollier (1998). During expansion, continental interiors remain elevated, or arched relative to the intracratonic basins and margins are isostatically depressed or downwarped. During subsequent expansion, adjustment for changing surface curvature is achieved by: a) erosion and planation of the continental interior and; b) periodic gravitational collapse. Gravitational collapse of the continental interior results in isostatic uplift and associated block faulting of the continental margins, forming great escarpments. This process becomes cyclical during ongoing expansion, resulting in multiple and overlapping phases of mountain building, planation, sedimentation, uplift and erosion.

3.3.12 Summary of Palaeogeographic Results (Video A3.15)

Coastal outlines plotted on expanding Earth models (Figure 3.15) define emergent land surfaces coincident with proto-continental cratonic and orogenic regions. Coastal outlines also define a network of epi-continental seas surrounding emergent lands coincident with epi-continental sedimentary basins. Progressive interaction and development of the epi-continental seas defines a prolonged Precambrian and Palaeozoic history of crustal spatial integrity. The geographic history during the post-Permian is then reflected in eustatic and transgressive-regressive marine cycles in response to opening of the modern oceans.

Coastal geography on the Phanerozoic expanding Earth models (Figure 3.15) show that large Panthallassa, Tethys and Iapetus Oceans are not required, instead, these are replaced by epi-continental Panthallassa, Iapetus and Tethys Seas which represent precursors to the modern Pacific and Atlantic Oceans and continental Europe and Asia. Eustatic and transgressive-regressive marine cycles on an expanding Earth occur in response to climatic change, to a shift in the distribution of epi-continental seas, orogenesis, mountain building, erosion, opening of post-Permian oceans and production of new juvenile water at mid-ocean-ridges.

Reconstruction of the Rodinia, Gondwana and Pangaea supercontinents and smaller sub-continents (Figure 2.10, 3.15) demonstrates that each crustal assemblage is progressive, with no requirement for random dispersion-amalgamation cycles. Supercontinent configuration is then defined by a progressive extension of epi-continental sedimentary basins, pulsed orogenesis, and transgression-regression of epi-continental seas as modern oceans open and rapidly expand to the Recent.

3.4 Palaeobiogeographical Data

Palaeobiogeographic datasets are extensive and full coverage is beyond the scope of this thesis. Examples of fauna and floral distribution are discussed in this section to illustrate their distribution on expanding Earth palaeogeographic models defined by coastal geography (Section 3.3).

The recognition of palaeogeographic and palaeobiogeograhic inconsistencies within conventional palaeomagnetic based reconstructions is critically reviewed in Meyerhoff & Meyerhoff (1974), Meyerhoff *et al*. (1996), Smiley (1992), Shields (1997) and is acknowledged in Hallam (1994), Sluys (1994) and Briggs (1995). Smiley (1992) considers that late Palaeozoic, Mesozoic and Cenozoic distributions of

terrestrial plants, vertebrate tetrapods and contemporaneous marine faunal realms do not support conventional plate tectonics. Smiley (1992) (and Khudoley, 1974) consider the biogeographic data show continental and polar stability rather than random plate motion since late Palaeozoic times and conclude that conventional geophysical based theories that require significant past movements of major continental masses about rotational poles create biogeographic problems that would otherwise not exist.

Cox (1990) considers two different types of disjunct biotic patterns, which substantiated alternative theories such as Earth expansion. One of these is an east-west pattern of biotic distributions and includes three categories. Firstly, there are terrestrial biotic distributions where groups are found in both eastern Asia and North America, but are absent from the high latitudes of Siberia and Alaska. Secondly, there are terrestrial biotic distributions, which extend from Southeast Asia and Australia to South America. Thirdly, there are marine biotic patterns, especially in fossil organisms, which extend across the Pacific Ocean. The other major type is a north-south distribution pattern, where an antitropical disjunct pattern of distribution of organisms is found in both the northern and southern temperate regions, but not in the intervening tropics.

Similarly Meyerhoff *et al*. (1996), in considering the Phanerozoic faunal and floral realms of the Earth, consider that plate tectonic reconstructions and proposed movements of continents do not correspond to the known, or necessary migration routes and directions of biogeographical boundaries. In most cases the discrepancies are very large and no approximate match can be made. Meyerhoff *et al*. (1996) quoted numerous examples to substantiate their conclusions.

This is further substantiated by the continental reconstructions of Shields (1979, 1983b, 1996). Shields (1996) considered that none of the existing plate tectonic or Earth expansion (referring in particular to the partially expanding Earth reconstructions of Owen, 1983) Permo-Triassic assemblage of continents surrounding the Indian Ocean (Shields, 1996), and Pacific Ocean (Shields, 1998), appears to completely satisfy all of the constraints imposed by palaeobiogeography. This is supported by Sluys (1994) who considers that under a vicariance paradigm the classical predrift reconstruction of Pangaea cannot adequately explain trans Pacific tracks or faunal links.

Stevens (1990, 1997b), in discussing trans-Pacific faunal links, considers that a number of distinctive New Zealand taxa have very marked similarities with Mexico, seemingly without traditional linkages via West Antarctica or South America, plus strong Tethyan provincial and circum-Gondwana affinities. While circum-Gondwana links are comparable to conventional Gondwana reconstructions, Stevens (1990) considers that tighter palaeobiogeographic fits can be achieved by assuming an expanding Earth thesis. By reducing the Earth radius the Tethys is then dramatically reduced, making direct linkages between New Zealand and Central and South America a physical possibility, which simplifies the required migration routes.

In contrast, Hotton (1992) concludes, from a study of the distribution of terrestrial and aquatic tetrapods, that the evidence of cosmopolitanism is sufficiently strong in the Permian and Triassic to suggest that a conventional Pangaean configuration cannot be refuted. Molnar (1992), in a study of Australian Mesozoic tetrapods, also suggests that Australian fauna seem more closely related at the familial level to that of South America, rather than that of Africa.

What these various authors are suggesting with regard to palaeobiogeography and palaeobiogeographical reconstructions in particular is that:

- The combined palaeobiogeographical data are best explained by continental and polar stability, rather than significant past dislocations.
- With the possible exception of Australia, the cosmopolitan distribution of terrestrial tetrapods confirms a Pangaean configuration of continental landmasses.
- There is sufficient evidence to refute various aspects of the conventional plate tectonic based palaeobiogeographic reconstructions.
- There is opinion that alternatives to conventional plate tectonic constrained palaeobiogeographic reconstructions better fit the field evidence.

While modern physical datasets, such as oceanic magnetic isochron data, palaeomagnetics and space geodesy are further constraints to these observations, the context of supporting arguments regarding historical distribution of marine carbonates, latitudinal distribution of Cenozoic marine faunas, Late Palaeozoic, Mesozoic and Cenozoic tetrapod interchange routes, ecotonal admixtures of Late

Palaeozoic to Cenozoic plants and Late Palaeozoic to Recent latitudinal zonations of terrestrial vegetation is significant. This detailed information, outlined in Smiley (1992) and Meyerhof *et al*. (1996), is based on documented field evidence and must be accounted for on all plate reconstructions.

3.4.1 Palaeobiogeographic Data on an Expanding Earth

Palaeogeographic reconstructions (Figure 3.15) are used to plot the distribution of faunal and floral taxa to investigate the distributional patterns on models of an expanding Earth. Examples used, while nowhere complete, come from diverse disciplines such as distribution of Cambrian-Ordovician platform trilobite assemblages (Clarke & Cook, 1983; Cocks & Fortey, 1990; Hallam, 1994), distribution of Mesozoic Dinosauria (Weishampel *et al.*, 1990), distribution of New Zealand Jurassic marine taxa (Stevens, 1990) and global distribution of Late Palaeozoic *Glossopterous* flora (Plumstead, 1973; Stanley, 1989).

3.4.2 Mid- to Late Cambrian Agnostid Trilobites (Video A3.26)

The distribution of Mid- to Late-Cambrian agnostid trilobites (Clarke & Cook, 1983) are shown along with Early Ordovician faunas of Cocks & Fortey (1990) on the Ordovician expanding Earth model (Figure 3.26). These, predominantly pelagic trilobite faunas, together with a number of endemic molluscs and brachiopods (eg. Hallam, 1994) are traditionally used in conventional reconstructions to distinguish the main Cambrian and Early Ordovician Gondwana, Laurentia and Baltica continental faunas.

Briggs (1995) recognised clear evidence for biogeographic differentiation of the trilobite species throughout the Cambrian to Ordovician. During the Cambrian an Olenellid Province was recognised for much of Europe, Siberia and North America and a Redlichiid province included eastern Asia, China and Australia. For the Early Ordovician, Cocks & Fortey (1990) distinguish four cratonic faunas including: 1) Gondwana faunas characterised by certain Calymenacea and Dalmanitcea trilobites; 2) Laurentia faunas characterised by the trilobite family Bathyuridae; 3) Baltica faunas with distinctive asaphid and other trilobites and; 4) low latitude Gondwana regions including South China, Australia, the Himalayas and Bolivia characterised by Dikelokephalinid trilobites. During the Ordovician the dominant trilobite-rich

community (Briggs, 1995) was displaced by a new brachiopod-rich assemblage (Sepkoski & Miller, 1985) resulting in restriction of the trilobite fauna to deeper benthic waters and a pelagic habitat.

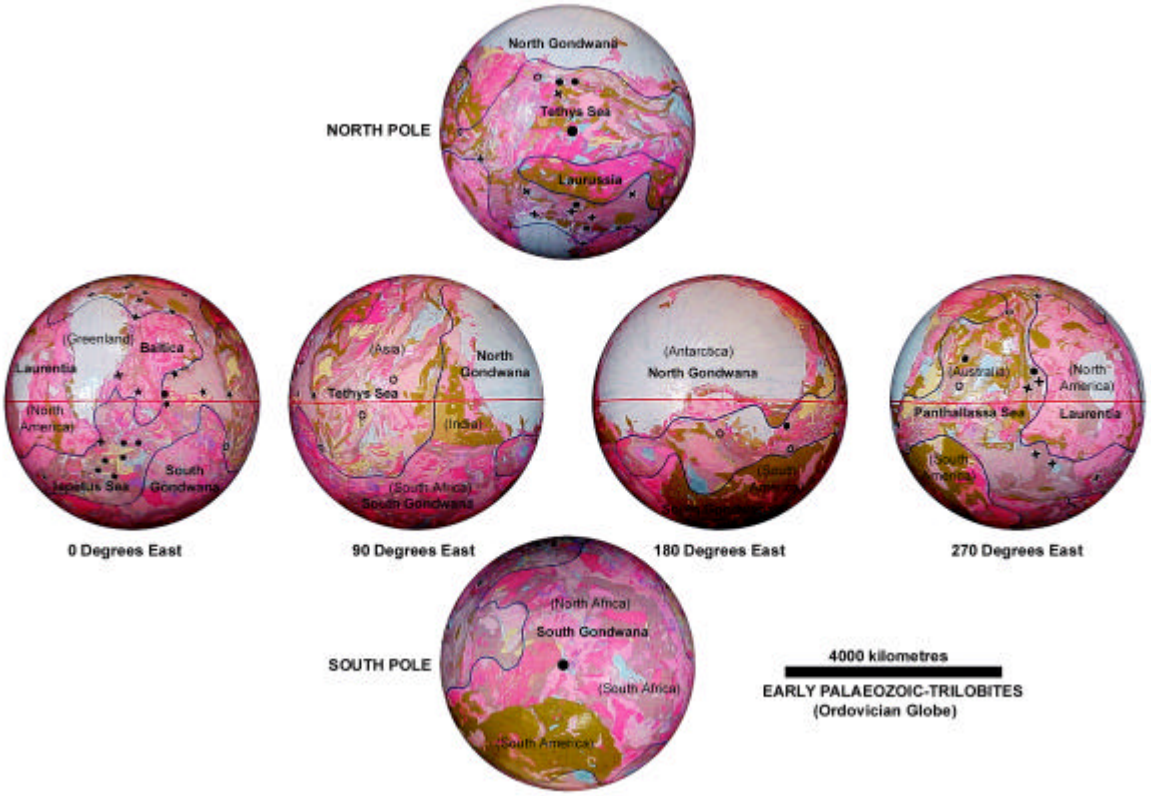

Figure 3.26 Mid- to Late-Cambrian agnostid trilobite and Early Ordovician platform trilobite faunas on an Ordovician expanding Earth. : Bathyuridae, ϑ Dikelokephalinid, H Ptychopygme/ Megalaspid, λ Calymenacean-Dalmanitacean, Ξ Mid- to Late-Cambrian agnostid trilobites. (Data after Clarke & Cook, 1983; Cocks & Fortey, 1990).

Cambrian and Ordovician trilobitic fauna on the Ordovician expanding Earth palaeogeographical model (Figure 3.26) coincide with epi-continental seas and Early Palaeozoic continental sedimentary basins. The distribution of Cambrian *Glyptagnostus reticulatus* throughout the entire epi-continental seas is consistent with the suggestion of Clarke & Cook (1983) for a cosmopolitan distribution, extending from equatorial to near polar regions. The distribution of Ordovician fauna of Cocks & Fortey (1990) confirms an increasing provincialism of the trilobites, with species located around the shelf margins of each of the main continental regions defined by palaeogeography (Figure 3.15). Latitudinal restrictions of Briggs (1995) are evident, with species from each family occurring predominantly in low-to-mid latitudes. A number of species also extend into high northern latitudes, possibly

reflecting a climatic differentiation dominated by an extensive south polar ice cap (Eyles & Young, 1994) located within central South Gondwana.

The faunal distributions (Figure 3.26) demonstrate the ease and simplification of migration and biogeographical development during the Palaeozoic, without the need for complex continental assemblage-dispersal requirements. Barriers to migration of trilobitic fauna on an expanding Earth are then deep-marine restrictions and, to a limited extent, latitude and climate.

3.4.3 Mesozoic Dinosauria (Video A3.27)

The origin, interrelationships, distribution and extinction of dinosaurs during the Mesozoic is extensively covered in Weishampel *et al*. (1990). Dinosauria form a well-defined group within the Archosauria and, among living vertebrates, birds and crocodiles are linked as sister groups within the Archosauria (Benton, 1990). The archosaurs form part of the Archosauromorpha group, a branch of the diapsid reptiles that include Trilophosaurus, the Rhynchosauria and the Prolacertiformes as successive outgroups to the Archosauria (Benton, 1990). The oldest known archosaur is *Archosaurus*, known from fragmentary remains in Late Permian strata from Russia. Archosaurs then radiated extensively during the Triassic and several distinct new lineages arose.

While most authors agree that Dinosauria are derived from a single line of decent, a number of Late Triassic dinosaurs do not fit into any of the major clades within the Dinosauria and are assumed by Benton (1990) to be primitive out-groups to the main dinosaurian clade. The true dinosaurs are divided into three monophyletic groups: 1) Ornthischia; 2) Theropoda and; 3) Sauropodomorpha, with the Theropoda and Sauropodomorpha thought to be sister groups, collectively known as Saurischia.

The disappearance of the dinosaurs is the most widely appreciated of all extinctions and the distribution of dinosaurs on global reconstructions must account for this extinction event. Questions of both the ascendance of dinosaurs during the Triassic and their extinction at the end of the Cretaceous have generally been explained by scenarios of competitive replacement of older groups by younger innovative ones. Dodson & Tatarinov (1990) consider that these explanations are currently rejected by most authors and preferred hypotheses link extinctions with abiotic factors or global catastrophes of cosmic origin. The discovery of an iridium

anomaly at the Cretaceous-Tertiary boundary has provided widespread evidence for a possible impact by an asteroid or comet. The detection of a supposed periodicity in mass extinctions during the Phanerozoic also implied an astronomical agent (Dodson & Tatarinov, 1990).

An alternative view to the terrestrial impact theory is the occurrence of major terrestrial volcanism tapping deep magma sources during the Cretaceous (Hallam 1987). This volcanism, such as the Deccan Traps of India, is thought to be an alternate source for the Cretaceous-Tertiary boundary iridium enrichment (Dodson & Tatarinov, 1990).

Dodson & Tatarinov (1990) further comment that the average duration of a dinosaur species was two to three million years and five to six million years for a genus. This typical rate of turnover of dinosaur genera suggested that extinctions of considerable magnitude occurred throughout the history of the dinosaurs. Only at the end of the Maastrichtian was there a failure to generate new taxa. The disappearance of the dinosaurs at end Cretaceous represented the loss of only a few species and represented a small aspect of the entire extinction (Dodson & Tatarinov, 1990).

The Maastrichtian extinctions considered by Dodson & Tatarinov (1990) were highly selective worldwide phenomenon. Dodson & Tatarinov (1990) reiterate that the Maastrichtian stage lasted approximately 8 million years and too much is attributed to the hypothesised impact or similar catastrophe. Many organisms were shown to dwindle over a significant portion of the Maastrichtian and were considered not to support a catastrophic extinction event. Dodson & Tatarinov (1990) conclude there has been too little resolution of the pattern of diversity of each of the affected groups within the Maastrichtian to determine the true cause of this extinction event.

The global Dinosaurian distributions are extensive and are known from localities of Late Triassic to Late Cretaceous age. The known Dinosaurian distribution is summarised in Weishampel (1990) and include skeletal remains, as well as footprints, trackways, eggs and coprolites. The Mesozoic distributions of Weishampel (1990) are plotted on the Triassic expanding Earth model (Figure 3.27) in conjunction with distribution of Permian reptiles (Colbert, 1965) to emphasise the common ancestry and migration in relation to the Mesozoic and Cenozoic transgressive sea-level history, continental break-up and dispersal.

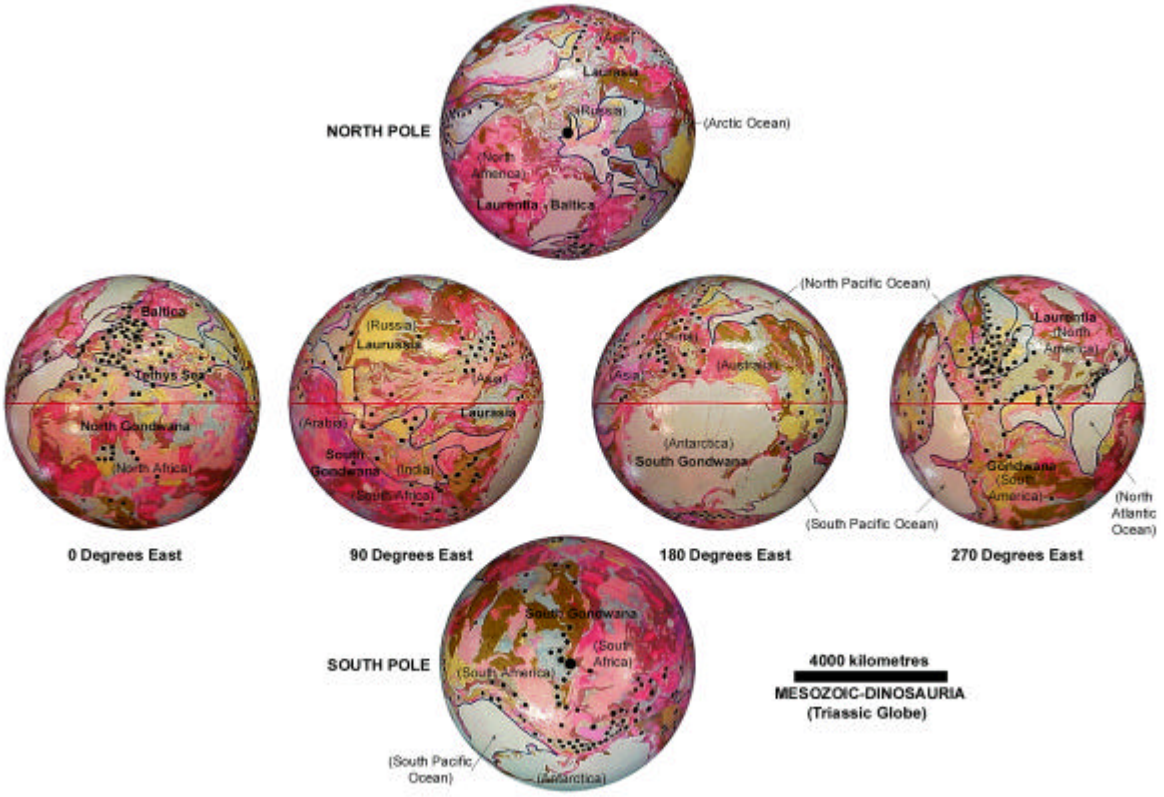

Figure 3.27 Permian reptile and Mesozoic Dinosaurian locations on the Triassic expanding Earth. Distribution shows provincial clusters within North America, Europe, South Africa and southern South America. Isolated occurrences are also shown in eastern Australia, southern China, and western South America. Ξ Permian reptiles, H Triassic Dinosauria, ν Jurassic Dinosauria, λ Cretaceous Dinosauria. Permian reptile distribution after Colbert (1965) and Mesozoic Dinosauria after Weishampel (1990).

The conventional plate tectonic palaeogeographic reconstructions of Scotese *et al*. (1979), Scotese (1994) and Smith A. G. *et al*. (1994) show Pangaea fragmenting and dispersing throughout the Mesozoic. Land connections existed between North America, South America, Africa, India, Australia and Antarctica during the Late Jurassic as part of the Pangaean assemblage. The major continents then fragmented during the Mesozoic and remained as island continents until amalgamation during the Cenozoic. Throughout the Mesozoic a large Tethys Ocean was inferred to have existed, separating the southern Gondwanan continents from the northern Laurussian, Baltican and Laurentian continents.

On an expanding Earth the palaeoradius during the Permian was approximately 50% of the present radius and continental crust covered the entire Earth surface. During this time a network of epi-continental seas existed, including the Tethys Sea, coinciding with intracratonic sedimentary basins (Figure 3.22).

During the Permian, continental break-up had commenced and the modern proto-oceans were starting to open forming the North and South Pacific, North Atlantic and Arctic Oceans. Each of the modern oceans then rapidly opened during the Triassic and Jurassic and continents dispersed to the Recent.

Dinosauria plotted on the Triassic expanding Earth model (Figure 3.27) demonstrate that Triassic distributions are clustered within three distinct provinces coinciding with Permian reptile distributions, including: 1) a low northern latitude Europe to Mediterranean region; 2) a low northern latitude central and eastern North American region, and; 3) a mid to high southern latitude South Africa and southern South American region, with links to India. Isolated occurrences are also shown in eastern Australia, south China, and western South America. Distribution though is possibly biased by favourable preservation and research effort in Europe and North America. Potential dinosaurian localities beneath the present Antarctican ice-sheet are not known.

During the Jurassic and Cretaceous, Dinosauria dispersed and radiated from each of the three main Triassic provinces (Figure 3.27). The migration routes are influenced by the Mesozoic transgressive sea-level history (Section 3.3.3), continental break-up (Figure 3.15) and rapid opening of the oceans. The European and Mediterranean dinosaurian province extends to include northern Africa and the eastern Mediterranean regions during the Cretaceous. The central North American province extends northeast to include western Canada and south to include Central America. An eastern North American sub-province is isolated during opening of the North Atlantic Ocean with links to central North America remaining. The African and South American province became separated during the Late Jurassic as the continents broke-up and the South Atlantic and Indian Oceans opened. Cretaceous dinosaurs dispersed throughout South America and disappeared within South Africa.

The south Pole on an expanding Earth migrated south from a Permian location along the emerging east Brazil and west African rift, through to South Africa during the Cretaceous (Figure 3.14) as the Indian and Southern Oceans opened and continents dispersed north. This apparent polar wander possibly explains the migration of dinosaurs away from South Africa to more equitable climates in South America and India.

The isolated Permian and Triassic reptile and dinosaurian occurrences located in Australia and southern China remained as small sub-provinces throughout the

Jurassic. During the Cretaceous the Australian dinosauria then extended throughout central and east Australia, during development of an extensive inland sea (Figure 3.15). Dinosaurian occurrences within the south China sub-province rapidly dispersed throughout China, Mongolia, Southeast Asia and eastern Asia during the Cretaceous, during a period of extensive basin development prior to the Cenozoic Alpine-Himalayan orogenic event (Section 3.3.10).

The distribution of Dinosauria and Permian ancestral reptiles on an expanding Earth demonstrate the close provincial links between Permian, Triassic and Jurassic fauna. This link is then disrupted during the Cretaceous during a period of prolonged marine transgression, continental break-up and dispersal, and disruption of climatic zones. During the Cretaceous, Dinosauria rapidly developed and dispersed from each of the provincial distributions. The European and Mediterranean Province in particular is retained with common links to Africa and possibly into Asia, without the plate tectonic requirement for a wide Tethyan Ocean. Faunal links between east Australia, northern New Zealand (Eagle, 1993) and North and Central America are suggested, as are links between China and Mongolia, and migration into Asia during the Cretaceous.

The extinction of the dinosaurs remains a contentious issue. On an expanding Earth a number of factors, previously not considered, may have contributed to the extinction event. As shown in Section 2.3, for an Earth expanding with an exponential increase in mass the surface gravity prevailing during the Triassic is approximately 50% of the present, increasing to approximately 75% during the Late Cretaceous. Considering the large size of many dinosaur genera, this increase in surface gravity may offer an alternative explanation for the turnover of dinosaur genera throughout the history of the dinosaurs, as noted by Dodson & Tatarinov (1990).

The Cretaceous also coincides with a period of continental basin extension accompanied by marine transgression, eustatic rise in sea level, increase in areal distribution of epi-continental seas and climatic disruption (Section 3.3.3). Marine transgression peaked during the Late Cretaceous and was followed by a rapid regression of epi-continental seas to the Recent. The Permian to Palaeocene expanding Earth models (Figure 3.15) suggest there may have been two or more separate oceans existing during the Mesozoic, with the possibility of separate sea levels. During the Triassic, rifting between Australia and North America occurred,

resulting in a mergence of the North and South Pacific Oceans. During the Palaeocene rifting between Australia and Antarctica also occurred, resulting in a merging of the Pacific, Indian and Atlantic Oceans and initiation of opening within the Southern Ocean.

Each of these rifting events coincide with the end Triassic and end Cretaceous faunal and floral extinction events. This suggests that the cause of extinction may ultimately be linked with periods of rapid transgressive-regressive sea level change, rather than inferred asteroidal or meteoric events.

3.4.4 Middle and Late Jurassic Marine Taxa (Video A3.28)

Stevens (1990) presented diagrammatic summaries of the affinities of representative New Zealand marine taxa of Middle and Late Jurassic age. While only relating to the New Zealand representatives of the named taxa and not representative of the entire range elsewhere in the world, they serve to illustrate Stevens (1990) (and Shields, 1996) claim that acceptance of even a moderate amount of Earth expansion would substantially close the Pacific and Tethyan gaps in conventional palaeogeographic reconstructions. Closing these gaps would then considerably shorten biotic dispersal routes. The occurrence of New Zealand marine taxa with strong Mexican affinities spread over 3300 metres of stratigraphic thickness (spanning Heterian-Puaroan), attests to the closeness and consistency of a New Zealand-Mexico link over time (Stevens, 1997b), suggesting a close geographical relationship.

New Zealand in conventional Jurassic reconstructions (eg. Smith A. G. *et al.*, 1994; Scotese, 1994) is shown as a proto-New Zealand continent, located in a high southern latitude Eastern Gondwana position, marginal to a large Panthallassa Ocean. It is closely linked to opening of the Tethys Ocean to the north, facilitating the opening and extension of Tethyan migration routes (Stevens, 1990). As Stevens (1980) notes, the absence of palaeoaustral (cool-temperate) faunas from the New Zealand Middle and Late Jurassic and the extensive distribution of Tethyan (warm-temperate) faunas support reconstructions that place southern New Zealand away from the South Pole. Isotopic and floral studies were considered to provide additional support for warm-temperate and hence a mid-latitude position for southern New

Zealand during the Jurassic, as did palaeomagnetic determinations from late Jurassic intrusives in Southland, New Zealand (Stevens, 1971).

The New Zealand-New Caledonia proto-continent on expanding Earth models (Figure 3.15) is located between the east coast of Australia and west coast of present-day Peru during the pre-Permian, in a low-southern latitude to equatorial position. During the Early Permian the South Pacific Ocean commenced opening between Australia and South America (Figure 3.22) as a small intracontinental sea and rapidly opened to its modern configuration during the Mesozoic to Recent. After separation from eastern Australia during the Late Permian, New Zealand-New Caledonia remained attached to Ecuador-Mexico throughout the Triassic until separation commenced during the Early Jurassic (precursory to the Late Jurassic Rangitata Orogeny, Stevens, 1990). From the Late Jurassic to Recent, both New Zealand and New Caledonia remained isolated within a rapidly opening central Pacific Ocean, forming part of a large proto-New Zealand continent. During this time both New Zealand and New Caledonia progressively shifted south and rotated anti-clockwise from a low- to mid-latitude position as the South Pacific Ocean opened.

An analysis of the extent of faunal radiation and extinction in response to environmental change during the Jurassic of New Zealand (Stevens, 1990) indicated to Stevens (1990) that the New Zealand Jurassic sequence was responsive to eustatic changes in sea level. This response is shown in the Late Jurassic expanding Earth model (Figure 3.28) where separate Panthallassa, Tethys, and Iapetus Seas merged during the Late Jurassic to form a single Ocean. This merging of separate seas exposed Jurassic marine faunas to the effects of global cycles of regression and transgression and opened up important ecological gateways.

Mid to Late Jurassic marine biota of Stevens (1990), plotted on the Late Jurassic expanding Earth palaeogeographical reconstruction (Figure 3.28), demonstrates the inter-relationships of Pacific, Indian and Tethyan faunal links to New Zealand. Similar distribution patterns are also shown by the progressive endemism in the Late Cretaceous ammonite family Kossmaticeratidae of Macellari (1987), and Krishna (1994) puts forward ammonoid evidence in support of a Jurassic to Cretaceous opening of the Trans-Gondwana (Pacific to Indian Ocean) corridor. By opening up the South Atlantic, Caribbean and possibly an Asian migration route, this enabled taxa endemic to the various regions to interact and extend their boundaries with time. The timing of ocean development in these areas, as noted by Stevens

(1990), is then reflected in eustacy and transgressive-regressive cycles facilitating faunal migration by extending and expanding immigration routes and moderating climatic differences.

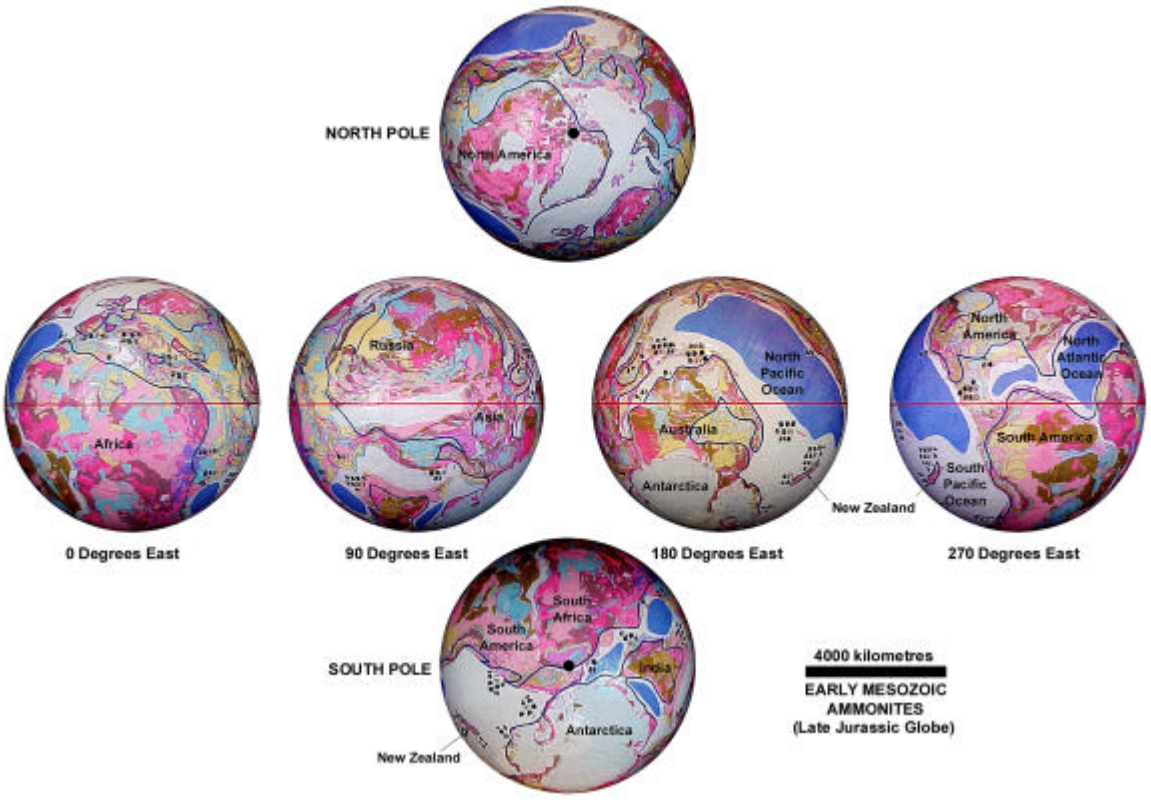

Figure 3.28 New Zealand Middle and Late Jurassic marine taxa on a Late Jurassic expanding Earth. Symbols for ammonite marine taxa shown are named in Stevens (1990). (Data after Stevens, 1990).

3.4.5 Late Palaeozoic *Glossopteris* Flora (Video A3.29)

During the nineteenth century, Late Palaeozoic coal deposits in India, South Africa, Australia and South America, and later Antarctica and possibly China were found to contain a group of fossil plants that were collectively designated the *Glossopteris* flora (Stanley, 1989) after a conspicuous variety of seed fern. The recognition that these flora, the most common fossil in the present southern hemisphere coal measures, differed completely from known flora from the European coal measures caused considerable interest (Plumstead, 1973). These Late Palaeozoic *Glossopteris* flora, their wide distribution and early association with glacial sediments offered supporting evidence for the existence of a Palaeozoic Gondwana supercontinent (Plumstead, 1973; Stanley, 1989), with characteristic rock units in each continent forming what is now known as the Gondwana Sequence.

The Gondwana Sequence is found in South America, South Africa, India, Antarctica and Australia, as well as the larger islands of the Southern Hemisphere (Plumstead, 1973). The South African sequence comprises a characteristic basal unit of Upper Carboniferous glacial tillites, alternating with interglacial sediments, including coals, that yield members of the *Glossopteris* flora and the reptile *Mesosaurus*, and carbonaceous shale. These are overlain by Permian clastic alluvial deposits, Triassic dune deposits and Jurassic basalt. The Gondwana sequence of Brazil, Antarctica, India, South America and Australia are similar, although *Mesosaurus* fossils are not always present (Plumstead, 1973).

Plumstead (1973) indicated that the Gondwana sequence has three successive but partly overlapping floras dominated by different plant species. The *Glossopteris* flora ranged throughout the whole of Gondwana during the Late Palaeozoic and was followed everywhere by a *Dicroidium* Triassic flora. In India an uppermost *Ptilophyllum* Jurassic flora is also preserved. Within Europe, Asia and North America three distinct northern Laurentian floras also existed, with the area occupied by the *Glossopteris* flora in Gondwana considerably larger than any of the three northern Late Palaeozoic floras.

The distribution of Late Palaeozoic *Glossopteris* flora was used by Du Toit (1937) as evidence to define a Palaeozoic Gondwanan continental assemblage. In conventional Gondwanan reconstructions (eg. Du Toit, 1937; Powell *et al*., 1988; and Veevers *et al*., 1994) the Permian-Jurassic south pole is positioned within eastern East Antarctica to eastern Australia, supported by the distribution of Palaeozoic glaciogenic occurrences.

On an expanding Earth the east coast of Australia is closed against South America during the Permian, eliminating the plate tectonic requirement for an extensive Panthallassa Ocean. The Permian-Jurassic South Pole (Section 3.2.5) migrates south along the opening South Atlantic rift, from a central west African Permian location to a South African Jurassic location. The palaeoequator during the Permian passes through India, East Antarctica and eastern Australia (Figure 3.15). This positioning of the South Pole and palaeoequator during the Late Palaeozoic contrasts strongly with plate tectonic reconstructions of Du Toit (1937), Powell *et al*. (1988) and Veevers *et al*. (1994).

The Late Palaeozoic *Glossopteris* flora shown on the Early Carboniferous expanding Earth model (Figure 3.29) straddle the established palaeoequator and

range from high northern to high-southern latitudes. This suggests that *Glossopteris* flora were tropical to cool temperate species, confirming the observations of Plumstead (1973) were Gondwana sequence rocks indicate a palaeoclimate commencing with an ice age and passing through a cold, but wet temperate to warm temperate climate during the Late Palaeozoic. Late Permian-Early Triassic sediments in South Africa indicate a wet temperate palaeoclimate (Faure *et al*., 1994), Triassic plants from the Sydney Basin New South Wales and Torlesse Supergroup New Zealand indicates a humid, cool temperate palaeoclimate.

Figure 3.29 *Glossopteris* flora on an Early Carboniferous expanding Earth. Locations suggest a high northern to high southern latitude distribution coinciding with the Palaeozoic Gondwana supercontinent. Blue lines represent palaeocoastlines. The symbol **G** represents *Glossopteris* locations plotted from Plumstead (1973).

The Carboniferous continental assemblage (Figure 3.29) suggests a strong provincialism of the *Glossopteris* flora, centred on the Karroo Basin type location of South Africa. East Antarctica, with its present ice cap, is located adjacent to South Africa and is surrounded by occurrences of *Glossopteris* flora in Australia, West Antarctica and India. This distribution suggests *Glossopteris* flora may have been more extensive beneath the present East Antarctican ice cap than is presently

exposed. The Laurentia-Baltica continent, characterised by a distinctive tropical flora is also shown (Figure 3.29), geographically isolated by epi-continental seas.

3.4.6 Summary of Palaeobiogeographic Results

The palaeobiogeographic faunal and floral examples used illustrate the ease and simplification of migration and biogeographical development on an expanding Earth. Cosmopolitan and provincial distributions and inter-relationships are maintained, without the need for complex conventional continental assemblage-dispersal requirements or incongruous migration routes.

During continental break-up and opening of the modern oceans on an expanding Earth established migration routes are disrupted, enabling taxa endemic to the various regions to interact and extend their boundaries with time. The timing of ocean development in these areas is reflected in eustacy and transgressive-regressive cycles, facilitating faunal migration by extending and expanding immigration routes, moderating climatic differences and providing a cause for extinction events.

3.5 Palaeoclimatic Data

Climate throughout Earth history is primarily affected by solar radiation and the major variables over geological time include the rate of insolation emitted by the Sun, chemical composition of the atmosphere and humidity (Barnes, 1999). The albedo of both the oceans and land is considered by Barnes (1999) to have changed with time by modifications to the biosphere, particularly the proportion of greenhouse gases, with the rate of insolation produced by the Sun over Earth's 4 billion year history increasing by about 30%. Changes to the Earth's eccentricity, obliquity and precession around the Sun also affected climate by producing regular Milankovitch cycles during much of Earth history (Imbrie *et al*., 1984; Miall, 1990).

Assumptions about palaeoclimate involve the study of all three complex systems of hydrosphere, atmosphere and lithosphere (Robinson, 1973). Ocean circulation, in particular the development of deep ocean currents during opening of the modern oceans, and hence climatic zonation on Earth, is strongly influenced by the presence of land barriers, and topographic relief on the continents influences precipitation (van der Voo, 1988). Correlation of coal swamps, thick clastic sequences and glacial tillites are considered by van der Voo (1988) to be excellent indicators of wet climates, while dry climates are indicated by evaporites and equatorial regions by coal, siliclastic and carbonate strata.

Comprehensive texts on palaeoclimate include Crowley & North (1991), Frakes *et al*. (1992) and Bigg (1996). Pangaean climate is reviewed in Crowley (1994) and Cretaceous climate reviewed in Francis & Frakes (1993).

The Late Palaeozoic palaeoclimates were considered by Barnes (1999) to be variable and complex. A Permian-Carboniferous glaciation lasted about 60 million years and considered by Klein (1994) to be related to Gondwanan palaeogeography and CO_2 drawdown during assemblage of Pangaea. The Permian climate is considered by Erwin (1993) to be related to an almost complete Pangaean continental assemblage at that time and the associated pattern of climate and glaciation was noted by Crowley & North (1991) to be related to an alternation of greenhouse and icehouse states.

Crowley (1994) showed that Pangaean climate involved a Late Palaeozoic glaciation, with subsequent transition to arid and nearly ice-free conditions during the Triassic and Jurassic. Geological studies indicated to Crowley (1994) that

Triassic and Jurassic aridity was extensive over much of Pangaea, with a peak in global evaporite formation. Other biotic and sedimentologic evidence, such as vegetation shifts, pointed to warming and drying during the Late Jurassic. Some changes were considered by Crowley (1994) to be associated with a rise in sea level accompanying the break-up of Pangaea.

Cretaceous climates are described by Barron (1983) as warm and equable. The polar regions in particular were considered to have been much warmer than today, with no evidence for polar ice, and warmth-loving floras and fauna were spread into high latitudes. In contrast, Francis & Frakes (1993) showed distinct variations and trends in warming and cooling during the Cretaceous, while van der Voo (1988) considered features of the Mesozoic and Cenozoic suggest that climate departed significantly from latitudinal predictions based on palaeomagnetism.

In addition to climate and biotic changes Crowley (1994) showed there were significant variations in the carbon cycle during Pangaean times, with organic carbon-rich layers found to be coincident with peaks in sea level highs (Jenkyns, 1988). The largest carbon sequestration event in the Phanerozoic reflected a time of major coal formation during the Permian-Carboniferous (Berner, 1987). The high carbon burial rates during this time suggested an absence of lignite-degrading organisms during the first terrestrial land plant occupation (Robinson, 1990). These carbon changes also contributed to estimated low atmospheric CO_2 levels at that time, with levels comparable to the present during the Carboniferous glaciations, increasing to levels of up to five times the present during the Late Jurassic (Berner, 1991).

3.5.1 Palaeoclimate Data on an Expanding Earth

Modelling palaeoclimatic data is limited to plotting selected latitude dependant lithofacies on expanding Earth palaeogeographic models (Figure 3.15). This information is then used to compare the resultant climate distribution patterns with the location of palaeomagnetic palaeopoles and palaeoequators (Section 3.2.5) to make an assessment of palaeoclimate zonation.

Expanding Earth palaeogeographic models are used to show the distribution of glaciation (Hambry & Harland, 1981) on Late Neoproterozoic, Ordovician, and Permian expanding Earth models. The distribution of Permo-Carboniferous coal and

carbonate reef deposits (Derry, 1980; Calder & Gibling, 1994; Flügel, 1994; Faure *et al.*, 1994) is shown on the Permian model, and the distribution of Carboniferous to Early Jurassic carbonate reefs (Flügel, 1994) on the Early Jurassic model. The distribution of Phanerozoic oil and gas (Derry, 1980; Tiratsoo, 1984; Meyer, 1986) is shown on the Mid Cretaceous model and the distribution of Early to Late Cretaceous coals (McCabe & Parrish, 1992) on the Late Cretaceous model.

Distribution of each of these lithofacies on conventional plate tectonic models is constrained by an inferred history of Rodinian to Gondwanan assemblage and break-up, followed by assemblage and dispersal of a Pangaean supercontinent. The approaching, apparently synchronous end-Triassic extinction event resulted in a rapid decline in the quantity of coal in sediments at the Permian-Triassic boundary (Faure *et al,* 1994), a change in frequency of reef types other than framework reefs (Flügel, 1994) and a coincidence of Late Triassic reef crises with major modifications to palaeogeography, palaeoceanography and climate.

3.5.2 Glacial Record

A summary of Earth's glacial record is given in Hambrey & Harland (1981) and geodynamic controls on glaciation in Deynoux *et al*. (1994) and Eyles & Young (1994). The preserved record of glaciation, summarised from Eyles & Young (1994), shows four major, well-documented glacial eras including the Palaeoproterozoic, Neoproterozoic, Early and Late Palaeozoic and Late Cenozoic.

Eyles & Young (1994) note that evidence for glaciation during the Archaean is scarce. The belief that Sun's luminosity was about 70% of the present value suggested that Earth surface temperatures may have been 30 degrees less than now and Eyles & Young (1994) argue for a weak solar luminosity for the early part of Earth history. Hoffman *et al.* (1998) in contrast, argues for a snowball Earth during the Neoproterozoic, where the oceans were effectively frozen prior to CO_2 levels reaching up to 350 times modern values. The abundance of waterlaid Archaean and Proterozoic sedimentary rocks is, however, testament to the presence of surface water rather than implied freezing surface temperatures.

DeWit *et al.* (1992) recorded diamictites and associated rocks interpreted as possible glacial products in the Archaean Witswatersrand Supergroup of South Africa, deposited between 3000 and 2700 Ma. Von Brunn & Gold (1993) reported

glaciclastic strata from the Pongola Sequence of Southern Africa, dated between 3100 and 2800 Ma and Archaean dropstones from the Stillwater Complex in western USA are ascribed to glacial transport (Page, 1981). Apart from these small occurrences, Eyles & Young (1994) consider the Archaean record to be essentially barren of glaciogenic deposits.

During the Paleoproterozoic there is evidence for widespread glaciation in several regions of North America, Karelia, South Africa, Australia, India and Scandinavia (eg. Okajangas, 1988). Eyles & Young (1994) describe clearly exposed deposits from the Gowganda Formation in Ontario, Canada, dated to about 2300 Ma (Young & Nesbitt, 1985) and less constrained deposits from the Northwest Territories (older than 2.1 Ga), Michigan (2100-2000 Ma) and Black Hills (2560-1620 Ma). Other deposits include the Griquatown Basin in southern Africa (*ca* 2300 Ma), the Bijawar Group in India (*ca* 1815 Ma) and the Meteoric Bore Member from Australia (*ca* 2500-2000 Ma). Diamictites of possible glaciogenic origin also occur in the Baltic shield and east-central and northern Russia (eg. Okajangas, 1988). In some palaeoproterozoic successions there is evidence of multiple glaciations separated by periods of intense chemical weathering (Nesbitt & Young, 1982).

The Mesoproterozoic is considered by Eyles & Young (1994) to be a non-glacial epoch. The only possible reported occurrence is from the Jena Formation, Russia, of uncertain age (Chumakov & Krasil'nikov, 1992).

Neoproterozoic glaciogenic deposits provide evidence for a widespread and long-ranging period of glaciation, extending from about 1.0 Ga to Early Cambrian. Most regions display evidence of several glaciations on a scale of tens of millions of years, similar to glaciations observed during the Paleoproterozoic. These are preceded, separated and followed by periods of relatively warm climate. Chumakov & Elston (1989) note that Late Proterozoic glaciers descended to sea level in low palaeolatitudes. Eyles & Young (1994) consider that most of the Neoproterozoic glacial deposits accumulated as glacially influenced marine strata along rifted continental margins or interiors, and dolomites underlying many glaciclastic strata were considered to record clastic-starved sedimentation in restricted warm-water basins prior to onset of uplift on the basin margins.

Neoproterozoic glaciogenic rocks are prominent in the Neoproterozoic stratigraphy of southeastern Australia (eg. Young & Gostin, 1991), with strong similarities to the northern Canadian Cordillera (eg. Young, 1992). This suggests that

Australia and Antarctica were juxtaposed against North America during the Neoproterozoic (eg. Hoffman, 1991). Elsewhere Late Proterozoic glacial deposits accumulated under extensional crustal regimes in Scotland, East Greenland and Scandinavia.

The known Precambrian glacial occurrences of Hambry & Harland (1981) are plotted on the Late Neoproterozoic expanding Earth palaeogeographic model (Figure 3.30). Figure 3.30 shows a uniform global distribution of glacial related deposits throughout each of the Archaean and Proterozoic terranes. This distribution qualifies the conclusions of Eyles & Young (1994) and, to a limited extent, the arguments of Hoffman *et al.* (1998) for a reduced insolation during the Neoproterozoic.

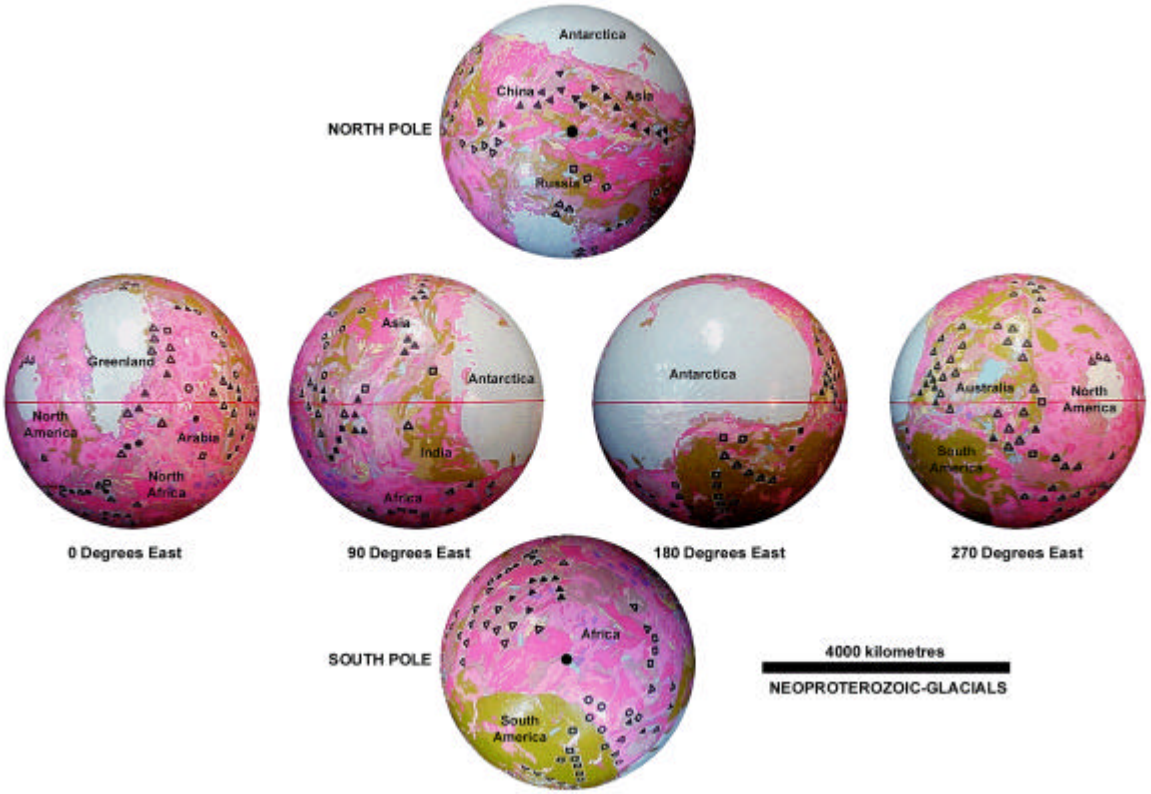

Figure 3.30 Precambrian glacial deposits on a Neoproterozoic expanding Earth. σGlacigenic rocks, well defined age (within the time span of a period in Phanerozoic time, or within 200 Ma in Precambrian time), D Glacigenic rocks, poorly-defined age, λ Non-glacigenic diamictites, well-defined age, m Non-glacigenic diamictites, poorly-defined age, ν Diamictites of uncertain origin, well-defined age, q Diamictites of uncertain origin, poorly-defined age (Data after Hambry & Harland, 1981).

The distribution of Precambrian glaciogenic rocks on an expanding Earth (Figure 3.30; Video A3.30) is considered in relation to the primordial Earth radius

(Section 2.2). The Archaean to Palaeozoic pole to equator distances vary from 2600 to 3400 kilometres during the Archaean to Ordovician respectively (27% to 34% of the present Earth radius). These distances are well within the bounds of sedimentary transport, or dissipation as glacio-marine ice sheets from polar ice caps located in west central Africa and Mongolia-China. Dissipation by sedimentary transport mechanisms provides a plausible explanation for the presence of low latitude glacial marine clastic strata, intercalated with warm water carbonate and iron sediments of Schermerhorn (1974).

Chemically weathered Proterozoic warm-water sediments intercalated with glacially influenced marine strata are discussed in Schermerhorn (1974), Eyles & Young (1994) and Fairchild (1994) and are reported from Australia, North America, Africa, Greenland, Scotland and Spitsbergen. During the Precambrian, these continents straddle the palaeoequator and are surrounded by Proterozoic epi-continental seas (Figure 3.30). The low latitude to equatorial location confirms the field-based observations of Schermerhorn (1974), suggesting cyclical deposition during glacio-eustatic changes in sea level and possible climatic fluctuation during drawdown or build-up of atmospheric CO_2 (eg. Crowley & Baum, 1992).

A major Early Palaeozoic glacial episode, peaking at approximately 440 Ma, is recorded from Late Ordovician strata in West Africa, Morocco and west-central Saudi Arabia. Less well-defined deposits occur in Scotland, Ireland, Normandy, South Africa, Spain and Portugal. Late Ordovician deposits, considered by Eyles & Young (1994) to represent small ice centres, also occur in eastern North America. In some areas the Late Ordovician glacial episode lasted into the Early Silurian, in particular those of South America and possibly Europe (Hambry & Harland, 1981).

The conventional distribution of Early Palaeozoic glaciation on the plate tectonic Late Ordovician Gondwanan reconstruction of Vaslet (1990) (Figure 3.31) shows the location of the Ordovician glacial South Pole and extent of a south polar ice cap. This can be compared with the distribution of Early Palaeozoic glacial occurrences of Hambry & Harland (1981), plotted on the Ordovician expanding Earth palaeogeographic model (Figure 3.32; Video A3.32). Both figures agree in principle, with the distribution of polar ice caps coincident with a palaeomagnetically derived west central Africa South Pole location (Section 3.2.5).

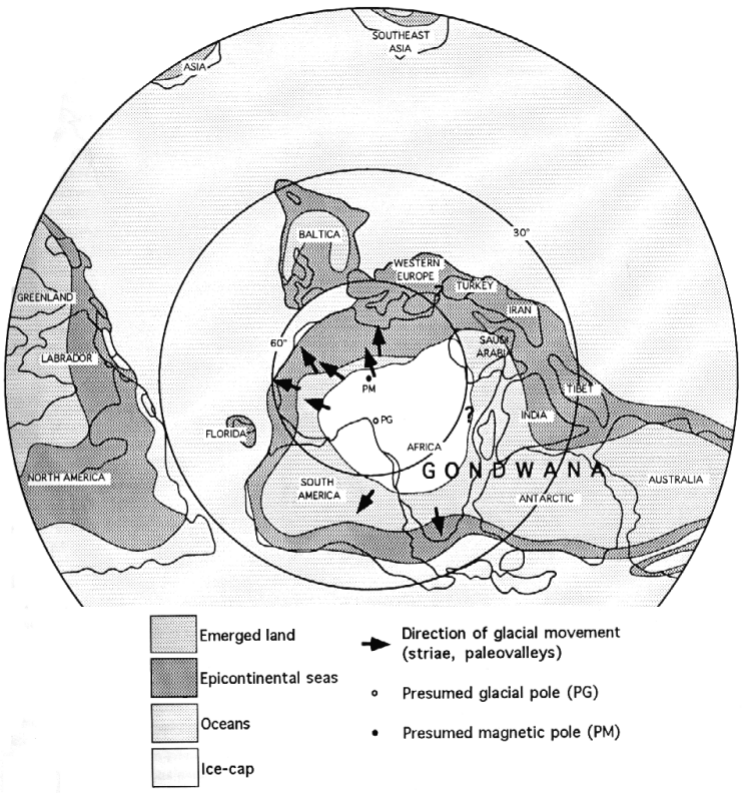

Figure 3.31 Plate tectonic reconstruction of the Late Ordovician ice-sheet. Figure shows Gondwanan and Laurentian continental assemblage, extent of polar ice cap, and presumed glacial and magnetic poles located within central west Africa. (After Vaslet, 1990)

The distribution of Early Palaeozoic expanding Earth glaciogenic deposits (Figure 3.32) is restricted to the southern hemisphere, with no significant deposits recorded by Hambry & Harland (1981) from the northern hemisphere. This distribution coincides with an emergent South Gondwanan continent, centred on the South Pole and an extensive Tethys Sea centred on the North Pole. The extensive Tethys Sea was open to equatorial latitudes during the Palaeozoic, suggesting that sea temperatures and northern climate were moderated by warm equatorial currents.

The distribution of Early Palaeozoic carbonate reef deposits in east Australia, North America, the Baltic region and central Europe, extending to west Australia and west Canada (Stanley, 1989) coincide with the established Ordovician palaeoequator.

This distribution of carbonate deposits, extending from low-southern to mid-northern latitudes, in conjunction with a southern hemisphere distribution of glaciogenic deposits, suggests a northward shift in climatic zonation, possibly reflecting changes to the Earth's eccentricity, obliquity and precession around the Sun.

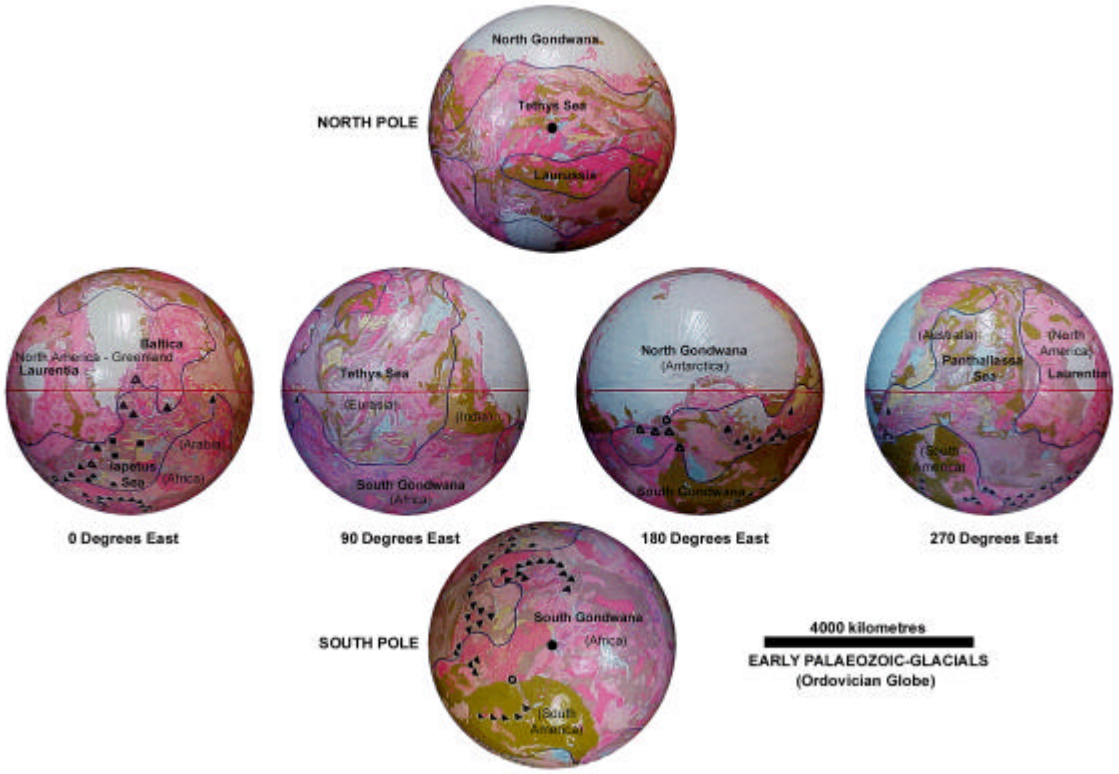

Figure 3.32 Early Palaeozoic glacial deposits on an Ordovician expanding Earth. σGlacigenic rocks, well defined age (within the time span of a period in Phanerozoic time), D Glacigenic rocks, poorly-defined age, m Non-glacigenic diamictites, poorly-defined age, ν Diamictites of uncertain origin, well-defined age, q Diamictites of uncertain origin, poorly-defined age (Data after Hambry & Harland, 1981).

The Late Silurian to Devonian is considered by Eyles & Young (1994) to be a non-glacial epoch. Renewed Late Devonian glaciation is recorded from three large intracratonic basins in Brazil and Bolivia, and by the Early Carboniferous glacial strata had accumulated in the sub-Andean basins of Bolivia, Argentina and Paraguay. By the mid-Carboniferous glaciation had spread to Antarctica, Australia, central and southern Africa, the Indian Sub-continent, Asia and the Arabian Peninsula. By the Late Carboniferous a very large area of the Gondwanan land mass was experiencing glacial conditions, persisting into the Late Permian (Eyles & Young, 1994).

The migration of Palaeozoic glacial centres across the conventional Gondwanan continental assemblage is considered by Caputo & Crowell (1985) and Eyes & Young (1994), based on palaeomagnetic determinations of apparent polar wander (Figure 3.33). The pattern of Early and Late Palaeozoic glaciations are explained by a migration of the Gondwanan supercontinent across the South Pole (Caputo & Crowell, 1985), with glacio-eustatic sea-level changes at about 440 Ma

responsible for a series of well-defined marine faunal extinction events (Brenchley, 1989). Eyles & Young (1994) conclude from poorly constrained glacially influenced deposits in Argentina, Bolivia, Peru and Brazil that during the Late Ordovician to Early Silurian the centre of glaciation had shifted from north Africa to south-west South America.

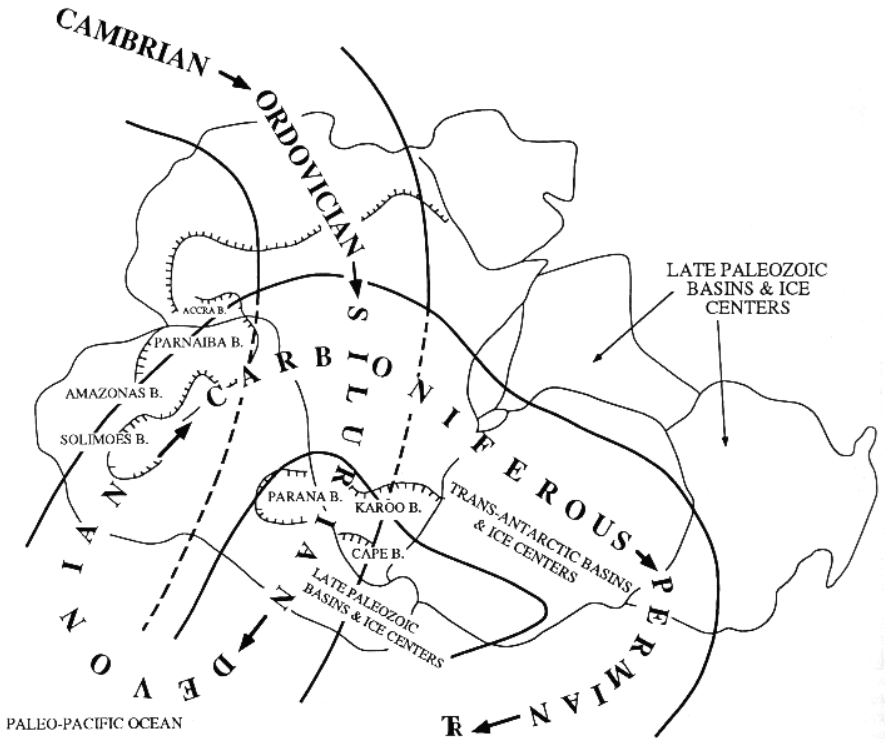

Figure 3.33 Plate tectonic Gondwanan migration of glacial centres. Migration routes across continents are based on conventional palaeomagnetic apparent polar wander data. (After Caputo & Crowell, 1985).

Palaeomagnetic derived pole locations on an expanding Earth (Section 3.2.5) show that the South Pole (Figure 3.14) remained approximately stationary within central west Africa, prior to shifting to east Brazil during the Permian and migration south, along the proto-Atlantic Ocean rift zone, during the Mesozoic. On an expanding Earth the South American Early Silurian glacio-marine deposits (Eyles & Young, 1994) possibly represent a waning of the African ice-sheet during the Silurian and low-latitude European deposits persisting to the Early Silurian (Hambry & Harland, 1981) represent small ice centres (Eyles & Young, 1994).

The distribution of Late Palaeozoic glacial deposits of Hambry & Harland (1981) are shown on the Permian expanding Earth palaeogeographic model (Figure

3.34; Video A3.34) in conjunction with Permian-Carboniferous coal and carbonate reef deposits (Sections 3.5.3, 3.5.4). These reconstructions contrast with conventional Palaeozoic reconstructions and distribution of glacial centres based on palaeomagnetic apparent polar wander data (Figure 3.33).

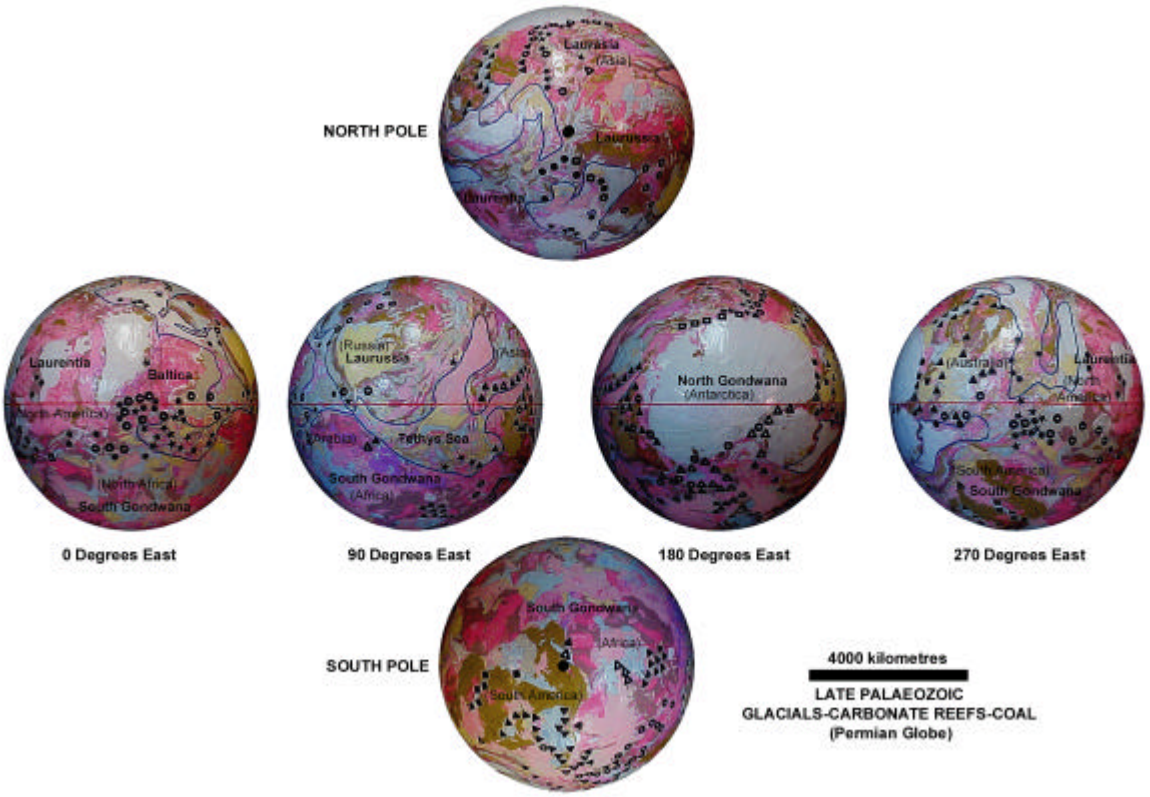

Figure 3.34 Late Palaeozoic glacial, carbonate and coal deposits on a Permian expanding Earth. ▲ Glacigenic rocks, well defined age (within the time span of a period in Phanerozoic time, or within 200 Ma in Precambrian time), D Glacigenic rocks, poorly-defined age, λ Non-glacigenic diamictites, well-defined age, ν Diamictites of uncertain origin, well-defined age, q Diamictites of uncertain origin, poorly-defined age (Data after Hambry & Harland, 1981). **C** represent Permo-Carboniferous coal deposits, Ξ represent Carboniferous carbonates and, H represent Permian carbonates. (Data after Derry, 1980; Calder & Gibling, 1994; Flügel, 1994; Fraure *et al*., 1994).

The distribution of Late Palaeozoic glaciogenic deposits on an expanding Earth (Figure 3.34) extend from high southern to high northern latitudes with a predominance of deposits in the southern hemisphere. The southern hemisphere deposits coincide with an exposed South Gondwana continent and deposits in the north polar region straddle the Laurussian and Laurentian continents (Figure 3.22). The distribution of both carbonate and coal deposits straddle and parallel the established Permian equator, suggesting a climatic zonation, with a northward shift in the climatic zonation suggesting a possible eccentricity in the Earth's obliquity and precession around the Sun.

No direct geological evidence of glaciation exists for the Triassic, Jurassic or Cretaceous, although Eyles & Young (1994) consider that ice-rafted horizons in Jurassic and Cretaceous strata of Siberia and Cretaceous strata of Australia indicate seasonally cold conditions at sea level.

Late Cenozoic Quaternary glaciations are relatively recent phenomena existing during the last 3.5 million years. Eyles & Young (1994) consider these to be the result of Cenozoic climatic change, beginning about 60 million years ago.

The distribution of glaciogenic deposits on an expanding Earth (Figures 3.30, 3.32 and 3.34) agree in principle with the location of palaeomagnetic derived poles and palaeoequators (Section 3.2.5). The distribution of Precambrian deposits in particular (Figure 3.30) demonstrate that low latitude glaciogenic deposits can occur, in conjunction with equatorial carbonate and iron-rich deposits, by considering the relatively short pole to equator distances existing during this time.

The distribution of Early Palaeozoic glacial deposits (Figure 3.32) and location of the well-documented west central Africa South Pole location is in good agreement with pole and equator locations of Vaslet (1990). The distributions of Late Palaeozoic orogenesis and mountain building (Sections 3.3.10 and 3.3.11) suggest that elevated topography influenced the distribution of isolated ice-centres, and glacio-eustatic and regressive-transgressive sea-level change may have influenced ocean current circulation and hence climate in the northern hemisphere.

The northward shift in climatic zonation and absence of a distinct north polar ice cap throughout the Phanerozoic is a prominent feature of glacial, carbonate and coal distributions shown in Figure 3.34. This northward shift suggests that an Earth rotational axis, inclined to the pole of the ecliptic, was well established by the beginning of the Palaeozoic and has been maintained to the Recent.

3.5.3 Late Palaeozoic to Triassic Coal (Video A3.35)

Calder & Gibling (1994) describe an extensive Late Palaeozoic peat forming ecosystem flourishing across the southern, equatorial and to a lesser degree, northern temperate lowlands of Euramerica as the landmass amalgamated with Gondwana to form the conventional Pangaean supercontinent. Preserved deposits of these tropical peat lands record the effects of climate, tectonism and eustacy, with many peats forming in foreland and intermontane basins associated with equatorial orogenic

belts or adjacent cratonic basins. Early Permian to Middle Triassic coal deposits of southern Africa, Australia, Antarctica, South America and China were deposited predominantly in foreland basins along the southern margins of the Gondwanan supercontinent during the Early Permian to Middle Triassic (Faure *et al.*, 1994). Faure *et al*. (1994) also indicate that Russian and Siberian coals occur in basins, flanked in the north, east and south by alleged subduction zones and associated regions of mountain building.

The Late Palaeozoic coal age of Calder & Gibling (1994) followed the evolution of vascular plants during the Late Silurian. The major phase of Euramerican peat formation on conventional Pangaean reconstructions is considered by Calder & Gibling (1994) to have resulted from the residence of a north-drifting Euramerica within an equatorial rainy belt. Repeated cyclotherms of coal, siliclastic and carbonate strata are inferred to have been deposited during periods of orbitally driven glacio-eustacy or associated climatic shifts. Evidence from stable isotope measurements suggest to Faure *et al*. (1994) that there was a decrease in the atmospheric $^{13}C/^{14}C$ ratio during the Permian-Triassic transition, which coincides with an abrupt world-wide coal hiatus.

The distribution of Late Palaeozoic to Triassic coal (Derry, 1980; Calder & Gibling, 1994; Faure *et al.*, 1994), in conjunction with Permian-Carboniferous carbonate reef deposits (Flügel, 1994) is shown on the Permian expanding Earth palaeogeographical model (Figure 3.35). Palaeogeographic reconstructions (Figure 3.15) demonstrate that the Carboniferous to Triassic is a transitional period of Earth history coinciding with opening of the modern oceans and regression of epi-continental seas. On an expanding Earth this period represents a major shift in sedimentary deposition, from epi-continental depocentres to marine and marginal continental basin depocentres.

During the Late Palaeozoic the south Gondwanan expanding Earth supercontinent, comprising Africa and South America is under the influence of a south polar ice cap, periodically melting and re-freezing during continental migration. Extensive areas of previously marine continental basins are exposed to erosion and terrestrial biotic colonisation. The distribution of coal and carbonate deposits (Figure 3.35) coincide with epi-continental seas and emergent Palaeozoic continental basins existing at the time.

Figure 3.35 Late Palaeozoic to Triassic coal and Permo-Carboniferous carbonate reefs on a Permian expanding Earth. υ represent Permo-Carboniferous coal deposits, Ξ represent Carboniferous carbonates and, H represent Permian carbonates. (Data after Derry, 1980; Calder & Gibling, 1994; Flügel, 1994; Fraure *et al*., 1994).

The distributions of coal and carbonate deposits (Figure 3.35) show two broad climatic zones paralleling the palaeoequator. Euramerican, east Australian, Antarctican, Indian, South African and South American coal deposits are located in a mid-southern to equatorial latitude belt while Russian, Siberian, Chinese and Western Australian deposits are located in a mid- to high-northern latitude belt.

The mid-southern and high-northern latitude distribution of coal, and equatorial to mid-northern latitude distribution of carbonate deposits on an expanding Earth suggests a northward shift in temperate and equatorial climatic zonation. This shift in climatic zonation coincides with observations from Late Palaeozoic glacial distributions (Section 3.5.2) where an inclined Earth rotational axis in conjunction with a south polar ice cap is suggested.

3.5.4 Carboniferous to Jurassic Carbonate Reefs (Video A3.36)

Conventional assemblage of a Lesser Pangaea during Early Carboniferous, the accretion of a Greater Pangaea during the Permian and the dispersal of Pangaea during the Triassic resulted in changes which controlled the expansion and reduction of biogenic carbonate production, the dispersal and distributional patterns of shelf biota and the development of reefs (Flügel, 1994). Flügel (1994) considers that the setting of Pangaean reefs is unusual, compared to the distribution of modern reefs, because most Pennsylvanian and many Permian reef build-ups formed in and around the margins of intracratonic basins. The growth of these Permian and Triassic reefs took place along the margins of, or in basins adjacent to an inferred east-west trending Tethys Ocean, located at the western end of an inferred Panthallassa Ocean.

Other important Permian and especially Triassic reef sites are inferred to be located on micro-continental fragments, now represented by exotic terranes in western North America, South East Asia and Japan (Flügel, 1994). The plate motion of these terranes is thought to produce a number of marginal seas favouring reef growth. Major evolutionary crises affecting reef biota from all sites correlate with extinction events, including an apparent synchronous end-Triassic reef extinction.

The distribution of Permian-Carboniferous carbonate reef deposits (Flügel, 1994) is shown on the Permian expanding Earth model (Figure 3.35), and Late Palaeozoic to Triassic carbonate reef deposits on the Early Jurassic expanding Earth palaeogeographical model (Figure 3.36). The carbonate reef deposits on each of these models coincide with distribution of epi-continental seas and the established palaeoequator. The Permian-Carboniferous deposits range from low southern to mid- to high-northern latitudes on the Permian model and Triassic to Jurassic deposits range from low southern to mid-northern latitudes on the Early Jurassic model.

On an expanding Earth the Carboniferous to Triassic represents a transitional period of Earth history, which results in opening and rapid development of the North and South Pacific and Arctic proto-Oceans. Large Tethys and Panthallassa Oceans did not exist and epi-continental seas steadily regressed as the modern oceans developed. By the Late Triassic a land connection between North America and Australia (Figure 3.15) is breached and the North and South Pacific Oceans merge to form the modern Pacific Ocean. This breaching coincides with the synchronous end-Triassic reef extinction event of Flügel (1994) and major transgressive-regressive changes in sea level (Vail *et al.*, 1977; Figure 3.16). By Early Jurassic the North Atlantic, Arctic and Indian Oceans also commenced opening.

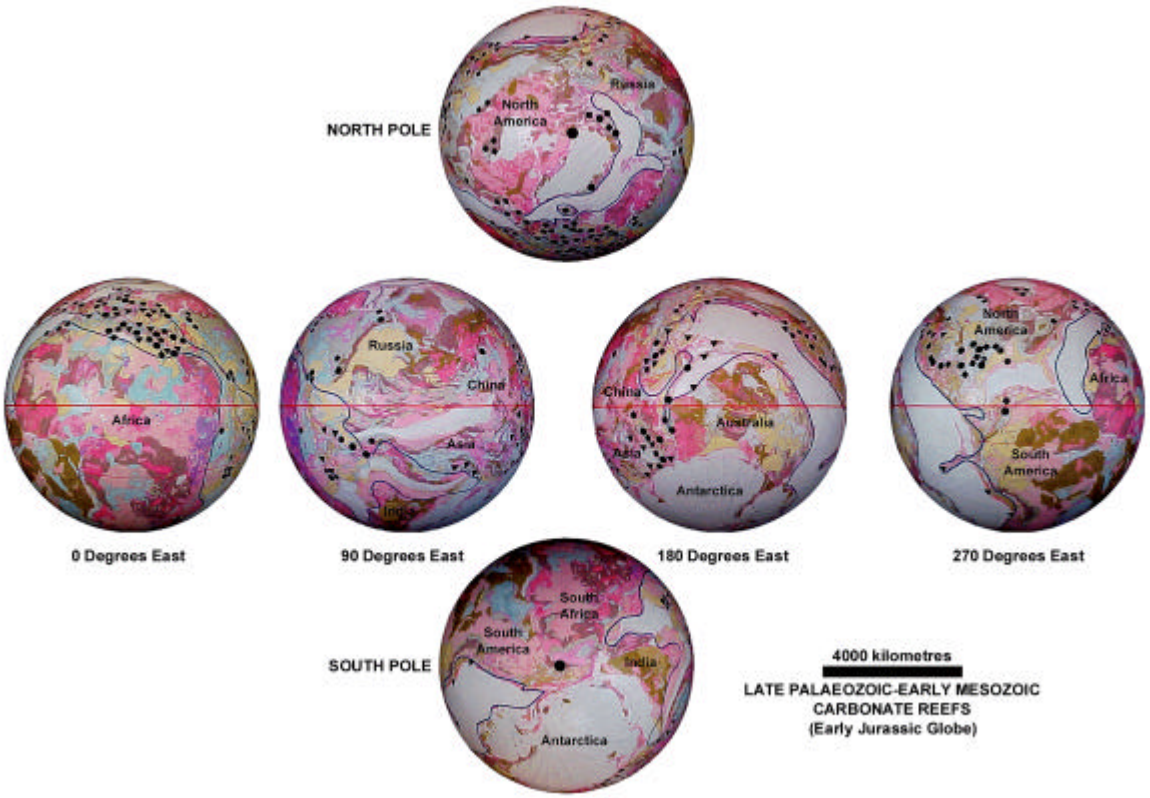

Figure 3.36 Permo-Carboniferous to Triassic carbonate reefs plotted on an Early Jurassic expanding Earth. Ξ represents Jurassic carbonate reefs, σ represents Triassic carbonate reefs, λ represents Permian carbonate reefs and, υ represents Carboniferous carbonate reefs. (Data after Flügel, 1994).

The expanding Earth Permian-Carboniferous reef distributions (Figure 3.35) show strong provincial reef occurrences within the emerging Caribbean, Mediterranean, Asian and North Canadian regions. These biota are lacking from the opening North and South Pacific Oceans. By the Early Jurassic (Figure 3.36) epi-continental seas partly regressed, exposing the Permo-Carboniferous deposits. Triassic to Jurassic deposits (Figure 3.36) coincide with epi-continental seas, suggesting that biotic migration kept pace with marine regression. By the Early Jurassic, reef biota migrated to and colonised each of the opening modern oceans.

The Permian-Carboniferous provincial reef clustering (Figure 3.35 and 3.36) suggests a biotic holdover from Early Palaeozoic carbonate reefs located in China, Europe, America and eastern Australia. These regions all coincide with equatorial locations on Early Palaeozoic expanding Earth models. The distribution of Carboniferous to Triassic carbonates (Figure 3.36) shows a northward displacement of climatic zonation. Biotic dispersal and latitudinal zonation within the opening modern ocean regions also parallel the established palaeoequator. The lack of a polar

ice cap and moderation of climatic extremes during the Mesozoic is evident from migration of biota to mid-southern latitudes, ranging to mid-northern latitudes.

3.5.5 Phanerozoic Hydrocarbons (Video A3.37)

Hydrocarbon deposits are generated by thermal processes from organic material of certain restricted types entombed in sedimentary rocks (North, 1990). For hydrocarbons to be generated and preserved within a depositional environment there must be suitable organic-rich source rocks and suitable reservoir rocks. North (1990) considers the most favoured source sediments to be early basin deposits, forming at the peak of transgression following a trans-basinal unconformity. The source sediments are commonly older than the main reservoir rocks and may be separated by entire formations devoid of recoverable hydrocarbons.

Studies of organic content of sedimentary rocks are shown by North (1990) to be at a maxima during the Cambrian-Ordovician, Carboniferous, Jurassic and Tertiary ages, and at a minima in Silurian-Devonian and Permian-Triassic rocks containing concentrations of evaporite deposits. Hydrocarbon occurrences are considered by North (1990) to correlate with source sediment maxima, with Tiratsoo (1984) showing that the worldwide percentage-by-weight distribution of crude oil and natural gas is greatest in Mesozoic reservoir rocks, followed by Cenozoic and Palaeozoic.

The first major Phanerozoic marine transgression recorded by Vail *et al*. (1977) (Figure 3.16) occurs during the Cambrian, before marine life is sufficiently abundant and diversified to provide rich accumulations of organic matter (North, 1990). North also describes transgressive events during the Ordovician, contributing effective source sediments in North America, and the Late Devonian transgression of Vail *et al*. (1977) contributes significant source sediments in the Ural-Volga and western Canadian basins, plus lesser basins in eastern and southern North America and North Africa.

An extensive marine transgressive period began during the Mid Jurassic and continued with minor setbacks until near the end Cretaceous. These formed the principle source sediments in the Middle East, western Siberia, North Sea and Central America and Peru. Smaller transgressions during the Oligocene-Miocene

also formed source sediments in the Californian, Caucasian, Carpathian and Indonesian provinces (North, 1990).

The widest distribution of gas not associated with oil occurs in Cretaceous molasse sediments, with important deposits located in northwestern Siberia and the western interior of North America. These also occur during the Permian-Triassic, associated with the spread of Pennsylvanian coal deposits (North, 1990). The Cretaceous is included within the time of greatest development of oil-source sediments and the Permian-Triassic coincides with an oil-source minimum.

The distribution of Palaeozoic, Mesozoic and Cenozoic oil and gas resources (Derry, 1980; Tiratsoo, 1984; Meyer, 1986) is shown on the Mid Cretaceous expanding Earth model (Figure 3.37) coinciding with peak Cretaceous development.

Figure 3.37 Palaeozoic, Mesozoic, and Cenozoic oil and gas on a Mid Cretaceous expanding Earth. λ represent oil resources and, ν represent gas resources. (Data after Derry, 1980; Tiratsoo, 1984; Meyer, 1986).

The distribution of both oil and gas deposits coincide with development of major Phanerozoic epi-continental to marginal basin settings, with deposits extending from high northern to high southern latitudes. A broad zonation of deposits

is evident, straddling the palaeoequator and extending from low southern to mid-northern latitudes, suggesting a northward shift in climatic zonation.

When viewed in context with eustatic and transgressive-regressive sea-level changes (Figure 3.16; Section 3.3.3) oil and gas development coincides with periods of sea-level transgression and maximum surficial areas of epi-continental seas. These conditions generate the most favoured early basin source sediments, forming at the peak of transgression following a trans-basinal unconformity (North, 1990). The Cretaceous in particular coincides with a period of post-Late Palaeozoic glacial melting, rapid opening of modern oceans, generally warm climatic conditions and rapid biotic diversification.

3.5.6 Early to Late Cretaceous Coal (Video A3.38)

Conventional plate tectonic reconstructions for the Cretaceous are dominated by the break-up of Pangaea. McCabe & Parrish (1992) indicate that, unlike the Palaeozoic, few Cretaceous coals accumulate in either associated rift basins or passive continental margins and occur on all continents with the exception of Antarctica. McCabe & Parrish (1992) indicate that extensive coal deposits occur in western North America and eastern Russia. Other areas include Europe, Japan, northern China, eastern Australia, New Zealand, northern Africa, Peru, Columbia and Argentina. The largest Cretaceous coal resources are located in foreland basins that stretched along the western margin of the Western Interior seaway of North America. These basins were created by thrusting and crustal loading within the Western Cordillera, extending from the Late Jurassic to latest Albian (McCabe & Parrish, 1992).

Cretaceous coals of the world are distributed in a similar fashion to modern peats and formed in mires in coastal regions, particularly near the equator where rainfall was presumably higher, or in high mid-latitudes where precipitation may have been relatively high and evaporation low (McCabe & Parrish, 1992). Examination of the global distribution of coals throughout the Phanerozoic indicated to McCabe & Parrish (1992) a striking latitudinal shift in coal deposition, from principally equatorial in the Carboniferous, to high-latitudes in Permian and later times. This shift was thought to have resulted from the onset of a Pangaean monsoon,

which disrupted climatic circulation in low- to mid-latitudes and led to drying of the equatorial regions.

Despite the apparent warming from the Early to Late Cretaceous, changes in the distribution of coals did not suggest to McCabe & Parrish (1992) any systematic climatic change. Changes in other factors, such as availability of basins with appropriate subsidence rates are considered by McCabe & Parrish (1992) to be more relevant.

Early to Late Cretaceous coal distribution is shown plotted on the Late Cretaceous expanding Earth palaeogeographic model (Figure 3.38). The distribution shows two broad temperate belts located north and south of the palaeoequator, with a predominance of deposits located in the northern hemisphere suggesting a northward offset in climatic zonation. By the Late Cretaceous, continental break-up, dispersal and opening of the modern oceans was well established with the spatial continental configuration similar to the Recent. Transgression of epi-continental seas was at its maximum (Figure 3.16), prior to regression during the Cenozoic.

Figure 3.38 Early to Late Cretaceous coal on a Late Cretaceous expanding Earth. λ represents Early Cretaceous coal, ϑ represents Mid Cretaceous coal and, H represents Late Cretaceous coal. (Data after McCabe & Parrish, 1992).

On an expanding Earth the latitudinal shift in Phanerozoic coal deposition noted by McCabe & Parrish (1992) is reflected in the rapid opening of each of the modern oceans, and northward migration of continents during the Mesozoic and Cenozoic. Late Palaeozoic to Triassic coal deposits (Figure 3.35) posses a latitudinal zonation coinciding with a north and south temperate belt, in conjunction with a southern polar ice cap. The predominance of coal deposits in the northern hemisphere (Figure 3.38) is attributed to the greater extent of landmass influencing rainfall and extent of remnant epi-continental basins suitable for coal formation.

3.5.7 Summary of Palaeoclimatic Results

The distribution of latitude dependent lithofacies such as glacials, coal, carbonate reef deposits and oil and gas resources on expanding Earth models coincides with palaeoequators and palaeopoles established from palaeomagnetic data and palaeocoastlines established from palaeogeographic data.

In each example a distinct latitudinal zonation paralleling the palaeoequator is evident, and a distinct northward shift in climatic zonation suggests that an inclined Earth rotational axis, inclined to the pole of the ecliptic, was well established during the Palaeozoic, persisting to the Recent.

3.6 Metallogenic Data

The assemblage of continents and crustal elements on an expanding Earth (Figures 2.10 and 3.15) provides a means to investigate the spatial and temporal distribution of metals across adjoining cratons and continents. Recognition and understanding of past metal distributions on the present Earth enables mineral search and genetic relationships to be extended beyond the known type locality. An investigation of the global spatial and temporal distribution of metal deposits on an expanding Earth represents the first time that such a study has been undertaken. Current plate tectonic continental reconstructions only extend to the Neoproterozoic (eg. Zhao *et al*., 1999) and metallogenic processes are speculated to the Archaean (eg. Barley & Groves, 1992).

Metallogeny on an expanding Earth is considered in the context of metallogenic epochs and metallogenic provinciality. A metallogenic epoch is a regularly recurring sequence of events that gives rise to a cyclicity in mineral

deposition during geological history (Smirnov 1984). A metallogenic province is a specific region possessing a notable concentration of a certain metal or metals (Evans, 1984) linked with common characteristic features (Vanecek, 1994). These characteristic features show genetical relations based on a common geological history, or on certain geological processes, which have influenced the origin of mineral, deposits in a given region. Metallogenic provinces are unified into global scale tectonic belts, divided into sub-provinces based on common occurrences of individual kinds or groups of minerals, or subdivided into metallogenic regions indicated by the existence of structural and tectonic units (Vanecek, 1994).

Mineral deposits of the world are extensively covered in standard texts including Edwards & Atkinson (1986), Cox & Singer (1992), Laznicka (1993) and Vanecek (1994). Individual countries are beyond the scope of this thesis and publications (eg. Australia: Solomon & Groves, 1994) were consulted as required. Published atlases of world mineral deposits include Derry (1980) and international databases include the Mineral Resources Data System (MRDS) available from the United States Geological Survey (USGS).

3.6.1 Metallogenic Epochs

Since the introduction and widespread application of radiometric dating techniques Gastil (1960) and Dearnley (1965) recognised that igneous and metamorphic mineral date abundance is periodic and roughly cyclic. The orogenic maxima indicated by these date abundances are considered by Evans (1984) to be closely related in time to metallogenic periodicities. The distribution of metal deposits and the nature and styles of mineralization in time and space (Figure 3.39) suggested to Anhaeusser (1981) that there has been an evolutionary trend in the concentration of metals, as well as diversity in morphological types of mineral occurrences. In contrast, Laznicka (1993) points out that when consideration is given to the preservation potential of deposits and the influence of giant metal accumulations, the metallogenic periodicities indicated by date abundances may be reduced to simple trends.

Time distribution patterns of mineralisation are considered from a recycling perspective by Veizer *et al.* (1989) suggesting that the patterns represent an evolutionary process of continental lithosphere, atmosphere, hydrosphere and

biospheric development. Meyer (1981, 1988) (Figure 3.39) considers the distribution in relation to various groups of metal deposits. Gaál (1992) and Vanecek (1994) consider the metallogeny in relation to global tectonic cycles and Barley & Groves (1992) attribute the distribution patterns to cyclic aggregation and break-up of large supercontinents.

Meyer (1981, 1988) recognises three main transitional periods from the metallogenic distribution of major groups of metal deposit types (Figure 3.39) representing changes in the characteristics and frequency of metal occurrences with time.

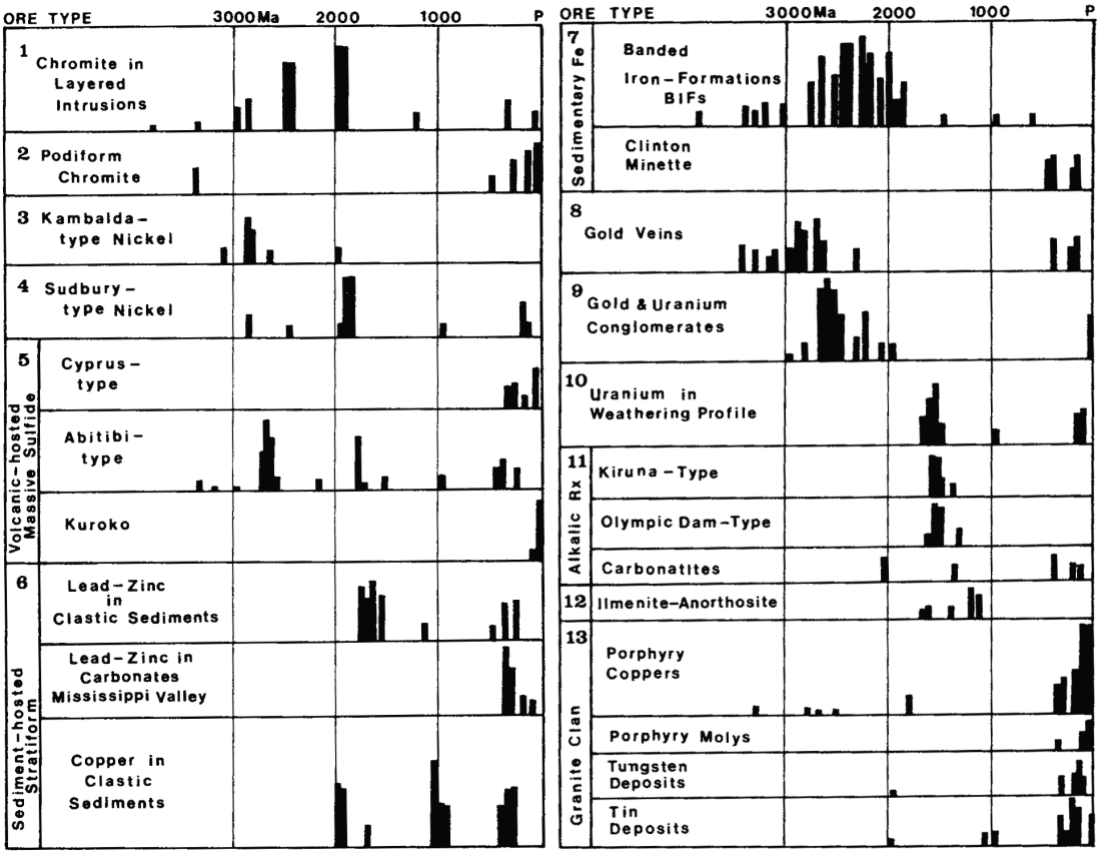

Figure 3.39 Styles of metal deposit distribution through geologic time. Width of each vertical bar represents approximately 50 million year interval, and length of each bar is the geological estimate of quantity of ore formed during the 50 million year interval as compared with total estimated tonnage for that style of deposit through geologic time. (From Meyer, 1988).

Characteristic peaks in the abundance of specific styles of metallic mineralization are also recognised and Barley & Groves (1992) considers the uneven temporal distribution to be related to three main factors:

1. The evolution of the hydrosphere and atmosphere.
2. A secular decrease in global heat flow.
3. Long-term tectonic trends.

This systematic temporal variation is considered by Barley & Groves (1992) in relation to a conventional plate tectonic model of cyclic aggregation and break-up of large continents throughout Earth history. In particular, metal deposits that formed in continental basins or associated with anorogenic magmatism are shown to be abundant in the Mesoproterozoic, corresponding to an inferred assemblage of a large proto-continent. Peaks in abundancy of continental metal deposits are also shown to coincide with a Late Proterozoic Rodinian supercontinent and a near maximum extent of a Pangaean assemblage during the Late Palaeozoic.

Barley & Groves (1992) further consider that metal deposits formed or preserved in convergent-margin orogens are abundant in the Late Archaean corresponding to periods of high global heat flow and rapid stabilisation of continental crust. This was also shown to be occurring during the past 200 million years, corresponding to a present tectonic cycle and similar mineralization styles were shown to be present in Early Proterozoic, Late Proterozoic and Phanerozoic orogens.

The relation between the abundance of specific metal deposit styles and long-term tectonic trends is less clear. Barley & Groves (1992) and Barnicoat *et al*. (1991) consider that major peaks in the abundance of metal deposits that formed, or were preserved in convergent-margin orogenic belts in the Late Archaean and metal deposits associated with either anorogenic magmatism or continental sedimentation in the Proterozoic are difficult to reconcile with the idea that plate tectonic processes have operated since the Late Archaean.

This metallogenic problem was explained in terms of an evolutionary trend in global tectonics from an Archaean pre-mobile regime, through a stable cratonic Proterozoic regime to the operation of plate tectonics during the Phanerozoic (Barley & Groves, 1992). The processes involved in the genesis of most metal deposits and their relation to tectonics are considered by Barley & Groves (1992) to have changed significantly through geologic time. The temporal variations in metallogeny are then related to tectonic cycles with wavelengths of several hundred million years, involving aggregation and break-up of supercontinents.

Metallogenic epochs on an expanding Earth are considered in relation to the continental and oceanic crustal development and subsequent tectonostratigraphic history (Section 2.6). The primary mechanism for crustal development on an expanding Earth is a process of crustal extension within established zones of crustal weakness (Section 2.5.2), orogenesis results from intracratonic motion during crustal extension (Section 3.3.10) and mountain building is related to isostatic uplift along continental margins with an associated collapse of continental interiors during changing Earth surface curvature with time (Section 3.3.11). On an expanding Earth these tectonic processes result in characteristic regional or tectonic settings, each reflecting a characteristic metallogeny.

Mathematical modelling of palaeoradius (Appendix A1) suggests that the increase in equatorial circumference during the Archaean to Palaeoproterozoic is approximately 21 kilometres, increasing to 474 kilometres during the Mesoproterozoic and 1716 kilometres during the Neoproterozoic. This increase provides a rational explanation for the changing crustal rheology with time. Expanding Earth models (Section 2.5) show that a granite-greenstone proto-crust encompassing the entire Earth at a primordial radius of approximately 1700 kilometres was established during the Archaean (Figure 2.13). A network of intracratonic sedimentary basins coinciding with Proterozoic basement rocks (Figure 2.13) also shows that primitive seas, an atmosphere and an erosive cycle were also well established during the Palaeoproterozoic.

The correlation of Precambrian metallogenic epochs and tectonic development on an expanding Earth is categorised in the following tectonic settings (adapted from Barley & Groves, 1992; Gaál, 1992):

1. Late Archaean stabilisation of continental crust (2.9 - 2.6 Ga) characterised by high global heat flow and magmatism.
2. Intracratonic rifting, extension and tensile fragmentation of the proto-Archaean crust (2.5 - 2.0 Ga) consisting of stages of early rifting (2.5 - 2.3 Ga) with Au-conglomerate basins, BIF basins, layered intrusions hosting PGE, Cr, V-Ti-Fe and Ni-Cu; Early Proterozoic greenstone belts (2.5 - 2.0 Ga) with vein Au, sulphide Cu-Au deposits; and late rifting (2.1 - 1.9 Ga) with layered intrusions hosting Ni-Cu, PGE and Cr.

3. Basement crustal extension and rifting (1.95 - 1.8 Ga) generating ophiolite associated Cu-Co-Zn massive sulphide deposits (~1.95 Ga), oceanic island arcs (1.93 - 1.85 Ga) with Ni-Cu deposits and continental arcs (1.9 - 1.8 Ga) with Zn-Cu-Pb-Ag-Au volcanogenic massive sulphide (VMS), porphyry Cu-Au-Mo, BIF and Kiruna-type Fe deposits.
4. Cratonisation, basement crustal extension and intracratonic rifting (1.8 - 1.6 Ga) characterised by rifted basins with sediment-hosted Zn-Pb-Cu and granitoids with Sn, Mo, W, Cu, Fe and REE.
5. Formation of vast, elongate, slowly sinking basins (0.8 - 0.6 Ga) characterised by metalliferous carbonaceous argillites and marls, often associated with bedded phosphorites, Cu-Pb and Zn-Pb base metals in a predominantly oxygenated hydrosphere.

On an expanding Earth each of these tectonic settings are global scale and metallogenic epochs correlate globally. Tectonostratigraphic development of continents (Section 2.6) suggests a common heritage for both lithosphere and metals and development is dominated by horizontal motion, including basement crustal extension and ensialic orogenesis accompanied by high heat flow. Crustal modelling suggests that the Archaean is an epoch where the lithosphere was stabilised into discrete cratons (Figure 2.13) that experienced limited internal deformation until the Proterozoic. Intracratonic crustal extension during the Proterozoic is then localised within a network of crustal weakness surrounding established cratons forming elongate basins and hosting ensialic orogeny.

Peaks in the abundance of specific styles of metallic mineralization on an expanding Earth (Figure 3.39) reflect the evolution of the continental crust, hydrosphere and atmosphere, the secular decrease in global heat flow and the changing crustal rheology with time. In particular, metal deposits abundant in the Early to Late Proterozoic form during a period of accelerating extension within intracratonic basins associated with anorogenic magmatism and ensialic orogeny. During the Late Palaeozoic, peaks in continental metal deposits coincide with initiation of continental break-up and during the Mesozoic and Cenozoic with continental dispersal and orogenesis.

3.6.2 Archaean Metallogenesis

Laznicka (1993) describes Early and Middle Archaean terranes as dominated by:

- Intrusions of monotonous tonolite to trondhjemitic granite-gneiss and migmatite;
- Local areas of the granulite-charnockite association;
- Layered or massive meta-gabbro, and anorthosite to peridotite intrusions;
- Amphibolite-facies supracrustal rocks, mostly amphibolite (metabasalt), gneiss and schist (metasediments) and minor conglomerate, calc-silicate gneiss and quartz-rich metamorphic rocks.

Laznicka (1993) considers the Early and Middle Archaean to be a pre-cratonic stage of Earth's history where metal mineralisation is absent to poorly developed. The amphibolite-facies greenstone associations host some banded siliceous iron deposits, minor stratabound massive copper sulphide deposits, layered and non-layered chromitite, and gold, arsenopyrite, minor chalcopyrite and locally significant antimony and mercury mineralisation. This metallic mineralization results from mainly sea-floor exhalations and crustal hydrothermal convection and metasomatism (Laznicka, 1993).

In contrast, the Late Archaean is a period where the granite-greenstone and greenstone belts in particular achieve their peak development (Laznicka, 1993). Greenstone assemblages throughout the world are important repositories for: iron as banded iron formation (BIF); manganese as bedded Mn ore; titanium, vanadium and chromium in differentiated mafic and ultramafic intrusions; nickel and cobalt associated with komatiites; copper, zinc and lead as volcanogenic massive sulphide (VMS) deposits; tin, mercury, uranium and gold in altered shear zones; silver associated with VMS and to a lesser extent in shears and veins; and platinum group elements (PGE) associated with nickel sulphides.

The proportion of ore deposits dependent on volcanic activity is considered by Meyer (1988) to be greater in the Archaean than during later geological times. The only sedimentary ore types are the banded iron formations and volcanic-hosted massive sulphide deposits. The abundance of gold, volcanic-hosted massive sulphide and Kambalda-type, komatiite-associated nickel sulphide mineralization in Late

Archaean greenstone belts and sedimentary basins is suggested by Barley & Groves (1992) to have resulted from a rapid growth and stabilisation of continental crust combined with high global heat flow.

Mineralization in the Archaean is considered by Anhaeusser (1981) to be extremely varied, with a direct relationship between metal type and host rock composition or environment of deposition. Mineral types are subdivided by Anhaeusser (1981) into those that favour development or association with ultramafic-mafic magmatic rocks (mainly gold, nickel, chrome, asbestos), those that occur predominantly in mafic to felsic magmatic successions (mainly massive sulphide deposits containing copper, zinc, silver, and gold, as well as iron-formations), those that favour development in sedimentary sequences (mainly iron-formations, limestone, barite, and placer deposits of gold and tin) and mineralization restricted to granitic rocks.

The greenstone and metasedimentary assemblages associated with Archaean cratons and sedimentary basins are considered by Barley & Groves (1992) to be similar to terranes in convergent margins of the present Pacific Ocean, hosting modern gold and volcanic-hosted massive-sulphide mineralization. In a conventional plate tectonic model cyclic, progressive accretion of volcanic-arc, marginal-basin, and related assemblages to protocratonic nuclei during the Late Archaean is considered by Barley & Groves (1992) to have resulted in the diachronous formation of cratons, with mineralization being a direct result of this tectonic regime.

On an Archaean expanding Earth, divergent structures, such as back-arc and marginal-basins within convergent plate tectonic settings cannot be reconciled. Instead, these same divergent settings represent zones of crustal extension and fragmentation of Archaean proto-cratonic nuclei (Figure 2.10). Geological expanding Earth models show that global-scale cratonization occurred during a prolonged period of stability during the Archaean to Mesoproterozoic (Figure 2.13). Mineralisation associated with this stable tectonic regime is reflected in the predominance of ultramafic to felsic magmatic associations, with an increase in accumulation of sediment and volcano-sediment associations during the Late Archaean as crustal extension commenced.

The spatial distribution of Archaean metal deposits on an expanding Earth is discussed in conjunction with Proterozoic and Phanerozoic deposits in Section 3.6.5.

3.6.3 Proterozoic Metallogenesis

The Archaean-Proterozoic boundary is considered by Meyer (1981) and Lambert & Groves (1981) to be a significant interface between two substantially different crust-forming regimes: a primitive Archaean and a more evolved Proterozoic. Vanecek (1994) describes the Upper Archaean to Palaeoproterozoic transition as an episodic event characterised by a change in the composition of granite rocks to potassium-rich granites displaying a negative europium-anomaly. During this time Archaean cratonic regions yielded enormous amounts of clastic sedimentary material to both platforms and continental margins, estimated at 43 kilometres thickness in places (Vanecek, 1994).

Laznicka (1993) summarised the Proterozoic as an era where there was:

- Cratonization of many Early Proterozoic regions;
- Initiation of epi-cratonic, shallow-water sedimentation and plateau greenstone belt volcanism;
- Emplacement of intracratonic mafic-ultramafic layered intrusions and alkaline complexes including kimberlites;
- Appearance of ophiolite associations;
- Proliferation of micro-organisms and algae resulting in an abundance of stromatolites and biogenic sediments including cherts and carbonates;
- Change of magmatic provenance including widespread intracrustal melting;
- A higher degree of magma evolution characterised by high K contents, high initial $^{87}Sr/^{86}Sr$ ratios and enrichment in incompatible elements.

Laznicka (1993) considers that the bulk of the Proterozoic greenstone belts and their depositional stage metallogeny retained the same characteristics as the Archaean greenstones, with some signs of maturity such as higher lead contents in some VMS deposits. Other volcano-sedimentary terranes departed substantially from the Archaean model, with a higher proportion of felsic volcanic rocks, meta-carbonate sediments, iron formations, and granitoids with a higher range of Na/K ratios. Laznicka (1993) attributes this to a significant involvement of continental crust as a source of some magma, to rifting regimes, to syn- and post-depositional regional metasomatism and to shallow water or subaerial deposition of sediments.

Meyer (1981) considers that vast, elongate, slowly sinking basins were the dominant tectonic feature of the Late Proterozoic, with metalliferous carbonaceous argillite and marl, often associated with bedded phosphorite, reaching a peak during 0.8 to 0.6 Ga (Laznicka, 1993). Sedimentation in these epi-continental basins and seas provided environments for concentration of base metals. The principle metals during this time are copper and lead, and zinc associated with lead, formed by local biogenic reduction of newly abundant sulphate supplied from a predominantly oxygenated hydrosphere. Elsewhere, mafic dykes were prevalent, alkaline complexes, including the first carbonatites became prominent, kimberlites were first emplaced and titanium-rich anorthosite massifs and layered complexes suggest an ongoing mantle-controlled differentiation and fracture history (Meyer, 1981; 1988).

The effect of abundant free oxygen on Earth's surface chemistry during the Palaeoproterozoic was gradual but irreversible (Meyer, 1981). This had major effects on chemical sedimentation, including the introduction of new types of sediment-hosted base-metal sulphide ores and sediment affiliated uranium concentrated along continental erosion surfaces. These new ore-types coincide with the introduction of bedded evaporites, red beds and carbonate sediments. The trigger for this change in ore-types is considered by Meyer (1981) to be tectonic by controlling the release of volcanic reducants from the Earth's interior and by providing stable shelves and shallow seas where photosynthesizing anaerobes could thrive and colonise. The generation of Proterozoic deposits is considered by Gaál (1992) to have taken place during extensional stages associated with upwelling thermal convection in the deep mantle.

The Proterozoic Era on an expanding Earth (Figure 2.10) is a period of steady to rapidly accelerating expansion (Figures 2.6) resulting in crustal extension and sediment accumulation within intracratonic sedimentary basins. This agrees with the observations of Meyer (1981) where vast, elongate, slowly sinking basins are the dominant tectonic feature of the Late Proterozoic. Archaean cratonic regions yielded clastic material to both platforms and proto-continental margins, and sedimentation in these epi-continental basins and seas provided environments for concentration of base metals and chemical sediments.

The spatial distribution of Proterozoic metal deposits on an expanding Earth is discussed in conjunction with Archaean and Phanerozoic deposits in Section 3.6.5.

3.6.4 Phanerozoic Metallogenesis

In most places of the world there is no break between the Proterozoic and Phanerozoic rock associations, with lithogenetic cycles continuing across the time boundary (Laznicka, 1993). The Neoproterozoic, characterised by heat dissipation through rifts and mobile zones, evolved into the Phanerozoic orogenic belts producing a variegated range of ore deposits (Meyers, 1981; 1988). Meyers (1981) notes that most Phanerozoic mineral deposits lie within orogenic belts, and Mesozoic and Cenozoic deposits in particular are aligned with present plate boundaries, supporting the ascendancy of new mechanisms of crustal behaviour during the Palaeozoic.

Meyers (1981) considers that large-scale plate tectonic recycling of oceanic crust during the Phanerozoic greatly increased the variety of ore-forming environments by generating long chains of volcanic island arcs around the margins of the continents and providing rift-bordered and back-arc basins, as well as large shallow epi-continental seas. Consequently, the Phanerozoic assemblage of ore types includes both Archaean volcanic types and Proterozoic sedimentalogic types, each modified in detail as chemical and tectonic evolution progressed (Meyers, 1981). Phanerozoic island arcs are considered by Meyers (1981) to be very similar, in a predominantly oxygenated regime, to many of the ore-forming systems of the Archaean.

Volcanogenic massive sulphide deposits are abundant during the Phanerozoic, locally containing lead as the principle metal and hosted by deformed volcanic rocks making up the cores of Phanerozoic mountain chains. This is considered by Meyers (1981) to be the result of second-generation recycling of basaltic oceanic crust along supposed subduction zones. Copper, silver and zinc deposits in black carbonaceous shales and lead in carbonate rocks are widespread during the Palaeozoic, becoming less abundant during later Eras. Uranium formed in continental sandstones within oxidation-reduction weathering fronts. Copper-pyrite deposits and podiform chromite deposits in ophiolite assemblages first appeared in the Phanerozoic, formed directly from primitive igneous assemblages at accreting plate margins (Meyers, 1981).

Large base and precious metal concentrations associated with quartz monzonite and granodiorite batholiths and subvolcanic plutons, including porphyry

deposits containing copper, silver, molybdenum, tin and tungsten are prominent during the Phanerozoic, reflecting a near-surface chemistry with abundant sulphate and moderate to strong hydrogen ion metasomatism (Meyers, 1981; 1988). Their alignment parallel to plate boundaries suggested to Meyers (1981) a genetic relationship to andesite-rhyolite volcanism and concentration of siliceous residues during magmatic recycling within supposed subduction zones along plate margins.

On an expanding Earth Precambrian and Palaeozoic continental crustal extension and epi-continental sedimentation culminated with the progressive break-up and dispersal of continents during the Mesozoic and Cenozoic (Figure 2.10). Palaeozoic sedimentation then shifted from epi-continental settings to marginal basins located around the perimeters of the newly formed continents. Long chains of volcanic island arcs around the margins of the continents are associated with initiation of mid-ocean-rifting (Figures 2.10 and 3.15), as well as rift-bordered and back-arc basins and large shallow epi-continental seas. As noted by Meyers (1981), most Phanerozoic mineral deposits lie within orogenic belts (discussed in Section 3.6.5) and Mesozoic and Cenozoic deposits in particular are aligned with present plate boundaries, supporting evidence for the ascendancy of new mechanisms of crustal behaviour during the Palaeozoic.

3.6.5 Metallogeny on an Expanding Earth (Videos A3.40 & A3.41)

Metallogenic modelling of selected Precambrian metal deposits is shown in Figure 3.40 (data after Derry, 1980; Laznicka, 1993; Vanecek, 1994) plotted on the Neoproterozoic expanding Earth model. Deposits within continental Greenland and Antarctica beneath present-day ice-sheets are unknown. Localities of mineral occurrences representative of each mining district are major, economically viable deposits only and a distributional bias may exist between developed and less developed countries.

Metals shown include (Figure 3.40; Video A3.40):

- Chromite in layered intrusions and ultramafic massifs;
- Nickel in ultramafic assemblages and gabbroic intrusions;
- Volcanic-associated and sediment-hosted base metals;
- Metamorphic associated sediment hosted and massive magnetite iron ores;

- Uranium in weathering profile sediments and roll-fronts;
- Alkali granite and porphyry hosted copper, tin and tantalum; and
- Vein and conglomerate associated gold.

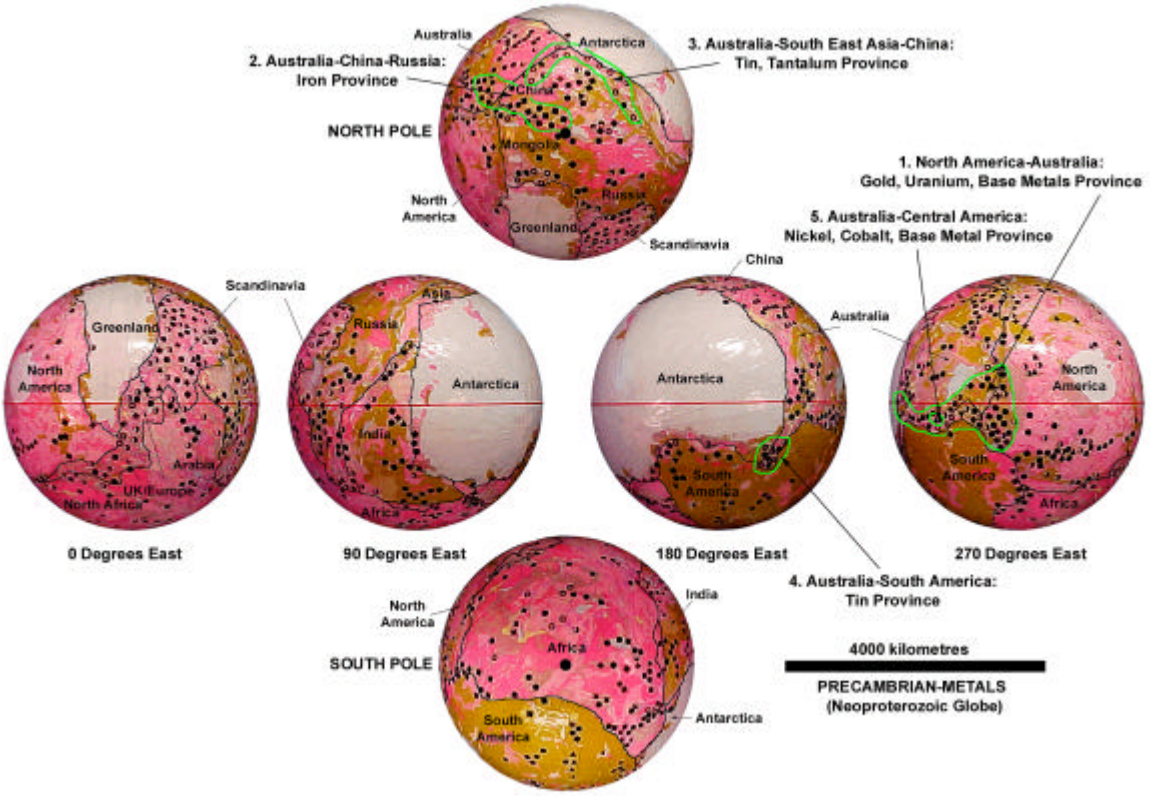

Figure 3.40 Precambrian metals on a Neoproterozoic expanding Earth. Symbols represent: σ chrome/nickel, ◑ zinc/lead, ⬣ copper, : uranium, λ gold, ϑ tin/tantalum, and ν iron. Examples of Australian metallogenic provinces are highlighted as green outlines. Black lines represent remnant present-day continents. (Data after Derry, 1980; Laznicka, 1993; Vanecek, 1994).

The metallogenic distribution on a Precambrian expanding Earth (Figure 3.40) can be broadly categorised as granite-greenstone associated deposits related to Archaean cratons, and rift, sediment, or granite associated deposits related to Proterozoic basement and intracratonic basin settings. Figure 3.40 shows a broad global metallogenic provinciality coinciding with cratons and intracratonic settings, and regional metallogenic settings are shown as clusters of specific metal deposits. The types of metal deposit occurring in each setting are related to the original tectonic regime and are subsequently modified by orogenic, magmatic and erosional processes.

A number of distinct intracontinental metallogenic provinces are highlighted whereby provinces from adjoining continents or tectonic regimes coincide, extending

across present-day geographical boundaries. Many of these provinces are now separated by intracratonic basins or large oceans during post-Permian continental break-up and dispersal.

Examples of Australian metallogenic provinces include (Figure 3.40):

1. The western North American Proterozoic gold (eg. Homestake) and base metal (eg. Sullivan) province is located adjacent to the north Australian Proterozoic uranium-gold (eg. Rum Jungle, Kakadu) and base metal (eg. McArthur River, Mt Isa) provinces. Each of these metal deposits are sediment hosted and together form a distinct intracratonic basin located between the South American Guyana Craton and Canadian Superior Provinces.
2. The Proterozoic sedimentary banded iron formations of the Hamersley Basin, Western Australia are located adjacent to Archaean to Proterozoic high-grade metamorphic and sedimentary iron deposits in northern China and southeastern Russia.
3. Palaeozoic granite-associated tin deposits in southern Asia and China coincide with the assembled continental margins of East Antarctica and Australia and are located adjacent to Archaean tin-tantalum pegmatite deposits in southwest Australia (Greenbushes) and the Pilbara Craton.
4. Palaeozoic tin deposits in Tasmania and east Australia are located adjacent to the Palaeozoic Bolivian tin deposits in South America.
5. Host rocks to nickel-cobalt-base metals in Queensland (Greenvale) and Central America (Honduras, Salvador and Guatemala) are adjacent during the Palaeozoic, and coincide with ophiolite-hosted deposits in Cuba and New Caledonia.

The distribution of selected mid- to late-Phanerozoic metals is shown in Figure 3.41 (data after Derry, 1980; McKelvey *et al*., 1984; Maslennikov, 1993; and Vanecek, 1994) plotted on the Triassic expanding Earth model. The Triassic model is chosen to highlight the distinct alignment of Mesozoic and Cenozoic metal deposits with present plate boundaries and to highlight the crosscutting of pre-existing Precambrian metallogenic provinces.

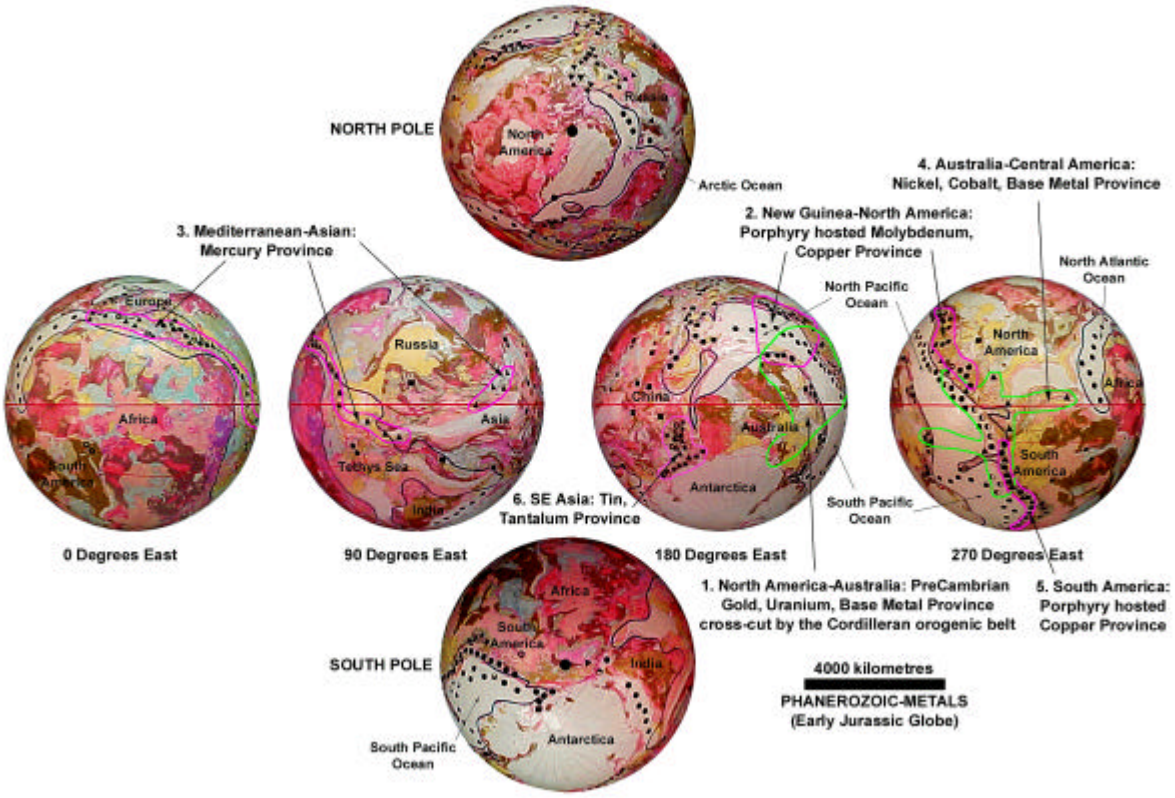

Figure 3.41 Mid- to late-Phanerozoic metals on an Early Jurassic expanding Earth. Symbols represent: λ nodular manganese, ◑ nodular manganese/chrome/nickel, σ mercury, ν Molybdenum, ⬣ Copper, H Tin, ϑ Tungsten. Examples of metallogenic provinces are highlighted. (Data after Derry, 1980; McKelvey *et al*., 1984; Maslennikov, 1993; and Vanecek, 1994)

Metals shown include (Figure 3.41; Video A3.41):

- Porphyry-associated copper, molybdenum, silver, gold, tungsten and tin mineralization abundant within Phanerozoic orogenic belts;
- Mercury associated with convergent margin settings; and
- Nodular manganese, nickel and chrome associated with sea-floor sediments.

The distributions of metals (Figure 3.41) represent deposits formed throughout the Mesozoic and Cenozoic during the period of continental crustal break-up and dispersal to the Recent. Distribution of sea-floor nodular metals is an indication of distribution only as deposition has occurred throughout the period of ocean development.

The mid- to late-Phanerozoic metallogenic distribution on an expanding Earth (Figure 3.41) highlights the abundance of porphyry-associated metals concentrated

within Phanerozoic orogenic belts, in particular the Cordilleran-Andean tectonic belt (Figure 3.42). On an expanding Earth these orogenic belts crosscut and displace pre-existing Palaeozoic and Precambrian metallogenic provinces and are considered to be related to isostatic uplift of continental margins during change in Earth surface curvature (Section 3.3.11). During break-up and dispersal a common mantle source for some metals is evident, forming time-dependant metallogenic provinces linking the original continents across the modern oceans.

Examples of Phanerozoic provinces include (Figures 3.41, 3.42):

1. The Proterozoic western North American and northern Australian sediment-hosted gold-uranium-base metal province (Figure 3.40) is now crosscut by the Cordilleran orogenic belt and is displaced during opening of the Pacific Ocean.
2. Porphyry hosted molybdenum-copper provinces in western Canada and New Guinea were previously adjacent during the Palaeozoic, prior to displacement during the Mesozoic opening of the North Pacific Ocean.
3. Mercury deposits in North Africa and the Mediterranean region occur within the Alpine orogenic belt and have since been displaced during opening of the Mediterranean Sea. This is consistent with a convergent orogenic origin proposed by Maslennikov (1993) and consistent with an expanding Earth post-Alpine divergence of Africa and Europe.
4. Distribution of manganese-nickel-cobalt sea-floor nodules within the central Pacific Ocean coincides with a pre-break-up nickel-cobalt-base metal province comprising Cuba, Central America, New Caledonia and Queensland. Nodules on the present sea floor are confined to sea floor located between New Caledonia, New Zealand and Central America.

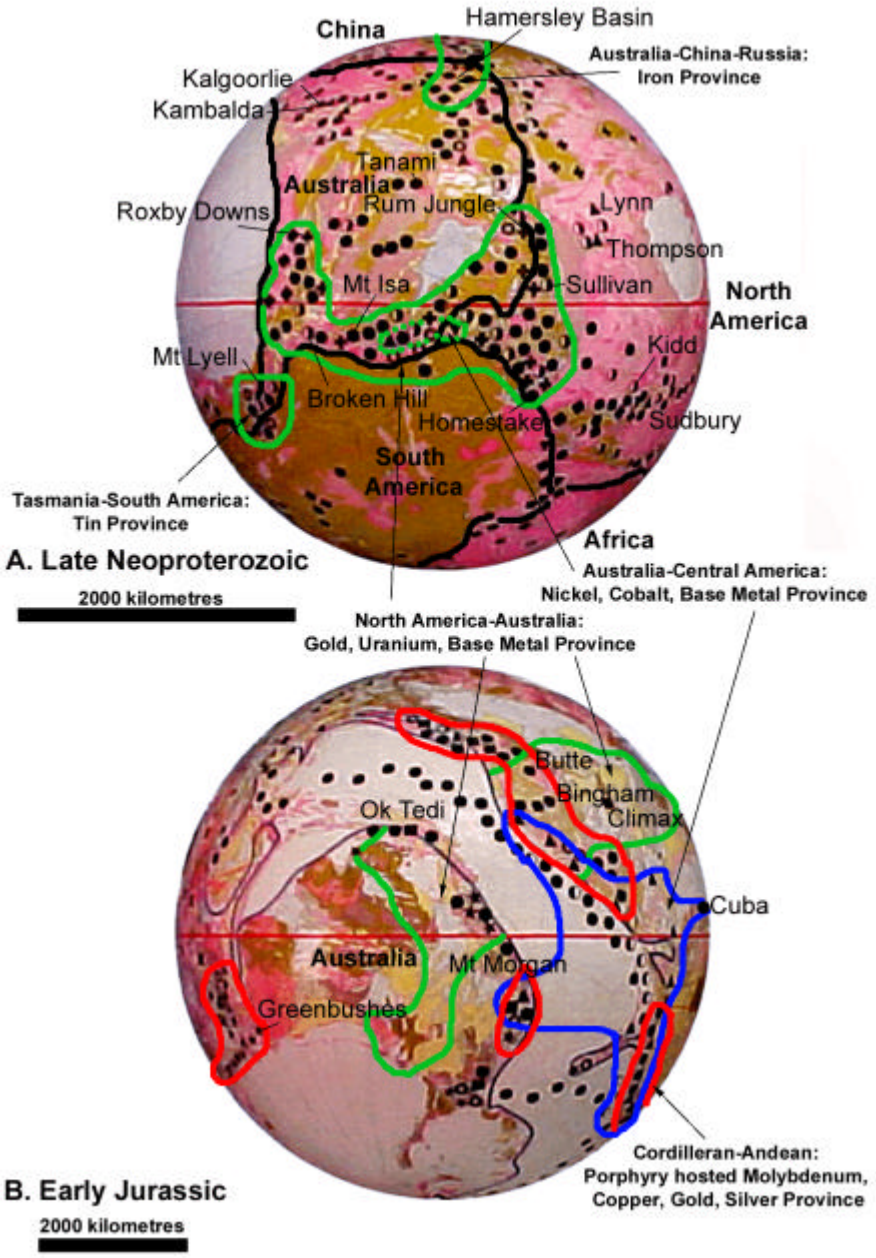

Figure 3.42 Australian Precambrian and Phanerozoic metallogenic provinces in relation to adjoining continents. **Figure A**: symbols represent: σ chrome/nickel, ◑ zinc/lead, ⬣ copper, : uranium, λ gold, ϑ tin/tantalum, and ν iron. (Data after Derry, 1980; Laznicka, 1993; Vanecek, 1994). **Figure B**: symbols represent: λ nodular manganese, ◑ nodular manganese/chrome/nickel, σ mercury, ν Molybdenum, ⬣ Copper, H Tin, ϑ Tungsten. (data after Derry, 1980; McKelvey *et al*., 1984; Maslennikov, 1993; and Vanecek, 1994)

3.6.6 Summary of Metallogenic Results

On an expanding Earth tectonic settings are global scale and characteristic metallogenic epochs correlate globally. Tectonic development suggests a common heritage for both lithosphere and metals and crustal development is dominated by

horizontal motion, including basement extension and ensialic orogenesis associated with high heat flow. Characteristic peaks in the abundance of specific styles of metallic mineralization (Figure 3.39) on an expanding Earth reflect the evolution of the hydrosphere and atmosphere, the secular decrease in global heat flow and the changing crustal rheology with time.

Metallogenic modelling of prominent Precambrian and Phanerozoic metal deposits (Figures 3.40, 3.41, and 3.42) show a broad Precambrian global metallogenic provinciality coinciding with cratons and intracratonic settings, to regional settings shown as a clustering of specific metal deposits. The Phanerozoic metallogenic distribution highlights the abundance of porphyry-associated metals concentrated within Phanerozoic orogenic belts. On an expanding Earth these Phanerozoic orogenic belts crosscut and displace pre-existing Palaeozoic and Precambrian metallogenic provinces and a common time-dependant mantle source for some metals is evident.

3.7 Integration of Geological and Geophysical Data Modelling

Archaean to Future expanding Earth models have been used in this chapter to investigate the spatial and temporal distribution of global geological and geophysical data within a conceptual expanding Earth tectonic framework. This information forms the basis for comprehensive studies in space geodetics, palaeomagnetics, palaeogeography, palaeobiogeography, palaeoclimate and metallogeny.

The 1992 to 1997 period of global space geodetic measurement was used to study vertical trends in Earth radii from selected observation sites. Measurement precision is routinely quoted to sub-centimetre accuracy, yet large fluctuations in Earth radii for each observation site (Figures 3.1 to 3.4 and Appendix A2) confirm the conclusions of space geodetists where space geodetic solutions are not as sufficiently well constrained in the vertical as they are in the horizontal. For horizontal plate motion the published results for current-day horizontal motion of the major plates is close to the million year average motion vectors determined from oceanic magnetic mapping. Empirical expanding Earth modelling of oceanic mapping (Figure 3.5) confirms these observations.

The application of palaeomagnetism to Earth expansion has been investigated by reconsidering the conventional palaeomagnetic dipole formula in conjunction

with an exponential increase in Earth radius to derive a modified formula applicable to an expanding Earth. The modified dipole formula (Equation 3.8) is used to determine the actual palaeocolatitude to the ancient pole located on the present Earth. This results in an actual ancient palaeopole that is located closer to the sample site but is not representative of the geographical palaeolatitude. Only when site location data is transferred to a sphere of palaeoradius representative of the age of the site data do geographical grid systems and palaeopoles coincide.

The published palaeomagnetic data of McElhinny & Lock (1996) is used to plot small circle arcs representing the actual palaeocolatitude from sample site to palaeopole on each expanding Earth model. For each model this results in a cluster of diametrically opposed small circle arcs defining the location of the north and south geocentric magnetic palaeopoles (Figure 3.12). Mean pole positions were then determined and an equator established by scaling through 90° of latitude from each mean pole position and longitude established by adopting Greenwich as zero degrees longitude (Figures 3.13 and 3.14).

Palaeogeographic maps of Scotese *et al*. (1979), Scotese (1994) and Smith A. G. *et al*. (1994) form the basis for defining the inter-relationships of exposed continental areas, intervening seaways, mountain building and orogenesis. The coastal outlines plotted on each Palaeozoic expanding Earth model (Figure 3.15) define emergent land surfaces coincident with cratonic and orogenic regions, and a network of epi-continental seas surrounding emergent lands is coincident with epi-continental sedimentary basins.

Coastal geography on expanding Earth models (Figure 3.15) show that large Panthallassa, Tethys and Iapetus Oceans are not required during reconstruction. These oceans are replaced by epi-continental Panthallassa, Iapetus and Tethys Seas, which represent precursors to the modern Pacific and Atlantic Oceans and emergent Eurasian continent. Emergent land surfaces equate to the conventional Rodinia, Gondwana and Pangaea supercontinents and smaller sub-continents (Figure 2.10, 3.15), and demonstrate a spatial intracratonic and intracontinental integrity throughout Earth history. Each crustal assemblage is progressive with no requirement for random dispersion-amalgamation cycles. Supercontinent configuration is then defined by a progressive extension of epi-continental sedimentary basins, pulsed orogenesis and transgression-regression of epi-continental seas as modern oceans open and rapidly expand to the Recent.

Eustatic and transgressive-regressive marine cycles on an expanding Earth are shown to occur in response to climatic change, to a shift in the distribution of epi-continental seas, orogenesis, mountain building, erosion, opening of post-Permian modern oceans and production of new water at mid-ocean-ridges. The variance of these changes is reflected in the palaeocoastal outlines (Figure 3.15) and results in a change in exposed continental land, coastal transgressive and regressive events, distribution of latitude-dependant sedimentary facies, latitudinal and provincial distribution of certain faunas and tectonostratigraphic histories.

Orogenesis on an expanding Earth is represented by zones of intracratonic to intracontinental interaction, resulting from gravity induced collapse and partial rotation of cratons and proto-continents as they adjust for changing surface curvature. Tangentially directed crustal motion during this collapse and re-equilibration is manifested as intracratonic to intracontinental rotation, localised within epi-continental sedimentary basins and accompanied by regional synkinematic metamorphism and magmatism. This periodic rotation gives rise to long linear and interconnected orogenic belts surrounding each of the primary cratons or proto-continents, with polyphase motion resulting in an extension-orogenesis-extension cyclicity.

A distinction is made between orogeny, which deals with formation of fold belts and mountain building, which results in vertical uplift to form plateaus. Change in surface curvature during Earth expansion gives a prime mechanism for mountain building where continental interiors remain elevated, or arched relative to the intracratonic basins and margins are isostatically depressed or downwarped. Periodic gravitational collapse of the continental interiors results in isostatic uplift and associated block faulting of the continental margins, forming escarpments. This process becomes cyclical during ongoing expansion, resulting in multiple and overlapping phases of mountain building, planation, sedimentation, uplift and erosion.

Palaeogeographic expanding Earth models (Figure 3.15) are used to plot the distribution of selected faunal and floral taxa to demonstrate the distribution in relation to established palaeogeography, palaeopoles and palaeoequators. Examples used include the distribution of Cambrian-Ordovician platform trilobite assemblages (Figure 3.26), distribution of Mesozoic Dinosauria (Figure 3.27), distribution of

Pacific Ocean Jurassic marine taxa in relation to New Zealand (Figure 3.28) and global distribution of Late Palaeozoic *Glossopterous* flora (Figure 3.29).

The palaeobiogeographic faunal and floral examples illustrate the ease and simplification of migration and biogeographical development on an expanding Earth. Cosmopolitan and provincial distributions and inter-relationships are maintained without the need for complex conventional continental assemblage-dispersal requirements. During continental break-up and opening of the modern oceans traditional migration routes are then disrupted, enabling taxa endemic to the various regions to interact and extend their boundaries with time. The timing of ocean development is reflected in eustacy and transgressive-regressive cycles, facilitating faunal migration by extending and expanding immigration routes, moderating climatic differences and providing a causal relationship to extinction events.

Palaeoclimate on an expanding Earth was investigated by plotting selected latitude dependant lithofacies on expanding Earth palaeogeographic models (Figure 3.15) and comparing the resultant distribution patterns with the location of palaeomagnetic palaeopoles and palaeoequators. Climatic indicators include the distribution of glaciation on Late Neoproterozoic (Figure 3.30), Ordovician (Figure 3.32) and Permian (Figure 3.34) expanding Earth models, the distribution of Permian-Carboniferous coal and carbonate reef deposits (Figure 3.35), Carboniferous to Early Jurassic carbonate reefs (Figure 3.36), Phanerozoic oil and gas (Figure 3.37 and the distribution of Early to Late Cretaceous coals (Figure 3.38).

The distribution of latitude dependent lithofacies on expanding Earth models is shown to coincide with palaeopoles and palaeoequators established from palaeomagnetic data and palaeogeography established from coastal outlines. For each climatic indicator a distinct latitudinal zonation paralleling the palaeoequator is evident, and a distinct northward shift in climatic zonation suggests that an inclined Earth rotational axis, inclined to the pole of the ecliptic was well established during the Palaeozoic, persisting to the Recent.

Metallogeny on an expanding Earth is considered in the context of metallogenic epochs and metallogenic provinciality and is used as an example where recognition of ancient metallogenic provinces on the present Earth enable mineral search and genetic relationships to be extended beyond the known type locality. The distribution of metal deposits and the nature and styles of mineralization in time and space (Figure 3.39) suggests that there has been an evolutionary trend in the

concentration of metals, as well as a diversity in morphological types of mineral occurrences.

Metallogenic modelling of selected Precambrian and Phanerozoic metal deposits shows a broad global Precambrian metallogenic provinciality coinciding with cratons and intracratonic settings, to regional settings shown as a clustering of specific metal deposits (Figures 3.40). The Phanerozoic metallogenic distribution highlights the abundance of porphyry-associated metals concentrated within Phanerozoic orogenic belts (Figure 3.42). On an expanding Earth these Phanerozoic orogenic belts crosscut and displace pre-existing Palaeozoic and Precambrian metallogenic provinces and a common mantle source for various metals is evident.

The spatial and temporal distribution of global geological and geophysical data considered in this chapter highlight two important points:

1. Conventional palaeomagnetic determinations of palaeoradius conclude that the Earth has undergone minimal expansion during the past 400 Ma. These observations are confirmed by space geodetic measurements where increase in radius is constrained to less than 5 ± 3 mm/year. An interrogation of these data sets show that: a) determining palaeoradius from palaeomagnetic data is dependant on the premise that the surface area of continents has remained constant; b) palaeomagnetic formulae used to determine palaeopole locations are dependant on the premise that Earth radius is constant and; c) space geodetic observational data is constrained to a constant radius Earth.
2. Palaeogeographic and palaeobiogeograhic inconsistencies with conventional palaeomagnetic based reconstructions are acknowledged by Meyerhoff *et al.* (1974; 1996), Smiley (1992), Shields (1997), Hallam (1994), Sluys (1994) and Briggs (1995). Late Palaeozoic, Mesozoic and Cenozoic distributions of terrestrial plants, vertebrate tetrapods and contemporaneous marine faunal realms were concluded not to support conventional plate tectonics, nor conventional geophysical based theories which require significant past movements of major continental masses about rotational poles.

By removing the imposed constant surface area and constant radius premises from geophysical observations the geophysical data sets, when applied to an expanding Earth model, demonstrate that the data is consistent with an expanding

Earth. Similarly, geographical and biogeographical data sets, when applied to expanding Earth models, quantify Earth expansion and quantify the location of palaeopoles and palaeoequators determined from unconstrained geophysical data.

4. TECTONIC DEVELOPMENT OF AUSTRALIA ON AN EXPANDING EARTH

In this chapter the geological evolution of Australia on an expanding Earth is reviewed to demonstrate the application of Earth expansion to the stratigraphic and tectonic development of a continent. The geological evolution of Australia is extensively covered in Brown *et al.* (1968), Plumb (1979) and the following descriptions are summarised in part from Rutland *et al*. (1990) and Solomon & Groves (1994).

Myers (1990a), in summarising the Precambrian geological evolution of Western Australia, concluded that west Australia has a long record of continental growth and fragmentation extending from 3.7 Ga and possibly from 4.3 Ga. Myers (1990a) considered west Australia to be a collage of accreted crustal fragments where the main episodes and processes of crustal generation are a consequence of the amalgamation of rafts of sialic crust and destruction of intervening oceanic crust. This interpretation is reflected in Early Proterozoic plate tectonic reconstructions based on Precambrian collisional orogenic belts (eg. Zhao *et al*., 1999; Figure 4.1) where Australian cratons and Proterozoic terranes are fragmented and assembled separately as part of two proposed pre-Rodinian supercontinents.

These conventional Early Proterozoic plate tectonic reconstructions of Australia (Figure 4.1) place west Australian Archaean cratons adjacent to South Africa and southern South America within a southern pre-Rodinia supercontinent. Central Australian Proterozoic terranes are located adjacent to Alaska and East Antarctica within a separate northern pre-Rodinia supercontinent (Zhao *et al*., 1999). During the Neoproterozoic, the Australian cratons are then assembled as part of Rodinia, located adjacent to East Antarctica and Alaska (Hoffman, 1991; Lawver *et al*., 1991). From the Neoproterozoic to Mid Palaeozoic, Australia remains in contact with East Antarctica as part of Gondwana (Lawver & Scotese, 1987; Powell, 1993; Unrug, 1993; Scotese, 1994) and during the Late Palaeozoic as part of Pangaea (Scotese *et al*., 1988; Smith A. G. *et al*., 1994; Scotese, 1994). Once the central and west Australian Precambrian terranes were assembled during the Proterozoic, Australian terranes remain intact and Australia is located adjacent to East Antarctica until rifting commences during the Paleocene. Throughout the Palaeozoic Australia

is inferred to be bordered by large Panthallassa and Neo Tethys Oceans to the west, north and east, and during the Mesozoic to Recent Australia is bordered by the Indian, Pacific and Southern Oceans.

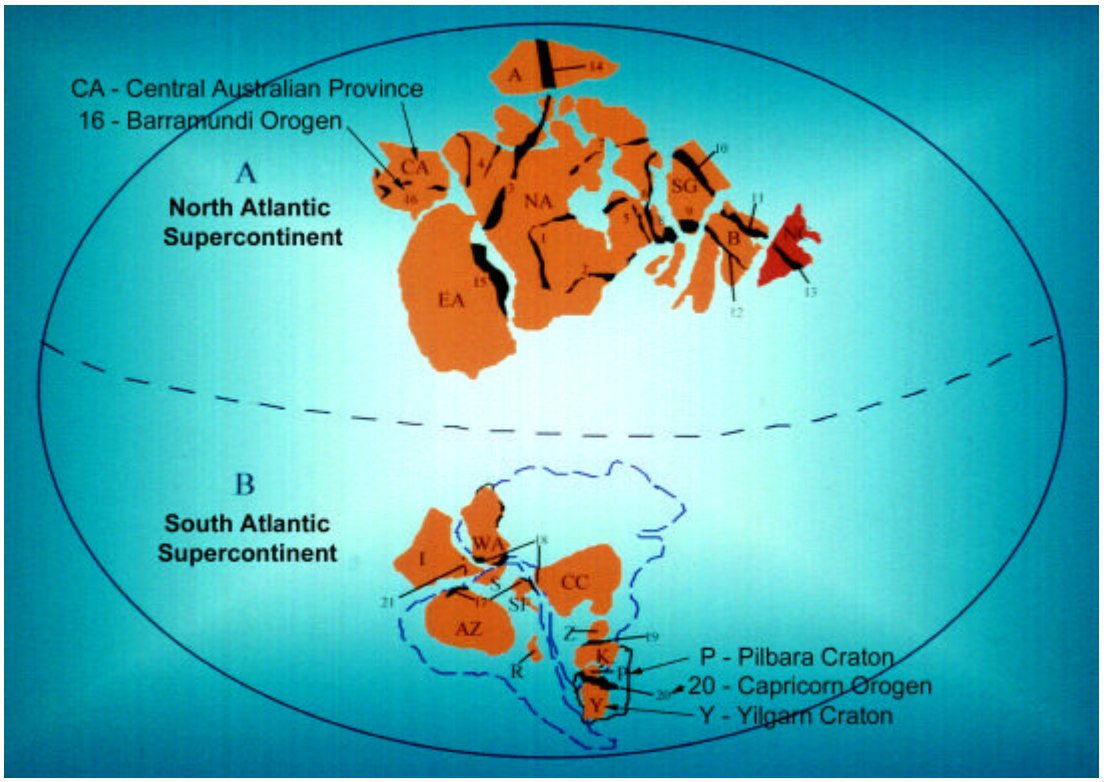

Figure 4.1 A proposed reconstruction of conventional pre-Rodinia supercontinents. Abbreviations: A-Aldan Shield, AZ-Amazon Craton; B-Baltic Shield; CA-Central Australia; CC-Congo-Chailu Craton; EA-East Antarctica; I-Indian Shield; K-Kaapvaal Craton; NA-North American Shield; NC-North China Craton; P-Pilbara Craton; R-Rio de la Plata Craton; S-São Luis Craton; SF-São Fransisco Craton; SG-South Greenland Craton; WA-West African Craton; Y-Yilgarn Craton. For additional abbreviations see Figure 1 of Zhao *et al*. (1999). (After Zhao *et al*., 1999).

The interpretation of Myers (1990a) contrasts with evidence, which suggests that west Australia, and much of Australia, has been largely intact since about 2.5 Ga and that most subsequent orogenic activity has been ensialic (Rutland, 1973; Etheridge *et al*., 1987; Wyborn, 1988). This interpretation also contrasts with Earth expansion modelling where it is shown (Section 2.6.1, Figure 2.15) that Australia originates from an Archaean cratonic and Palaeoproterozoic basin assemblage, comprising central and west Australian cratons and orogens located adjacent to cratons and Proterozoic terranes of China, North America, South America and East Antarctica.

On Precambrian and Palaeozoic expanding Earth models (Figure 4.2) the Proterozoic basins and terranes of north and central Australia form part of an

intracratonic network extending to include an assemblage of Proterozoic basins from north Russia, Asia, North America, Central America, South America and Antarctica. During the Proterozoic and Palaeozoic the spatial integrity of each basin is maintained during basin extension, rifting, orogenesis and Palaeozoic sedimentary basin development. Palaeozoic sedimentary basins primarily develop within east Australia as an extensive epi-continental basin intracontinental to South America, North America and Antarctica. Epi-continental intracratonic basins also include the Officer and Canning Basins located in west Australia.

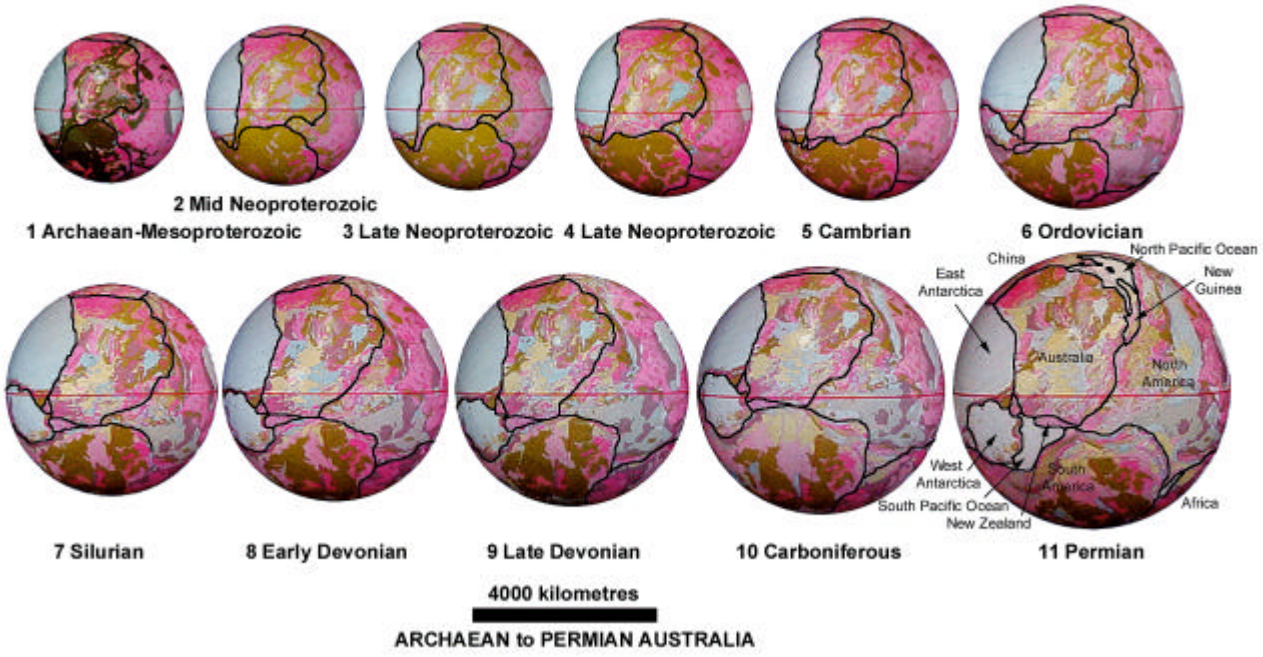

Figure 4.2 Tectonostratigraphic development of Australia and adjoining continents. Continental assemblage shown in Permian model is the same for all remaining models. Red lines represent palaeoequator derived from McElhinny & Lock (1996). White lines are continental outlines. (Geology after CGMW & UNESCO, 1990).

The spatial integrity of Australia, in relation to adjoining continents on an expanding Earth, is retained throughout the Precambrian and Palaeozoic until continental break-up and dispersal during the Mesozoic and Cenozoic (Figure 2.15). Intra-continental rupture, initiating continental break-up and development of the modern oceans, occurred adjacent to the Pilbara Craton and Kimberley Basin, and adjacent to east Australia during the Early Permian (Figure 4.2). These sites represent initiation of the North Pacific Ocean and South Pacific Ocean, respectively. The early North and South Pacific Oceans rapidly extended as separate oceans throughout the Permian and Early Triassic, merging during the Triassic and

separating Australia from North America. Opening of the Indian Ocean commenced during the Jurassic, separating Australia from China. Rifting between Australia and East Antarctica commenced during the Paleocene and has continued to the Recent.

Since the Paleocene Australia has remained geographically isolated, rotating anticlockwise during the Permian and Triassic to its present east-west orientation and migrating from a mid northern latitude to the present low to mid southern latitude.

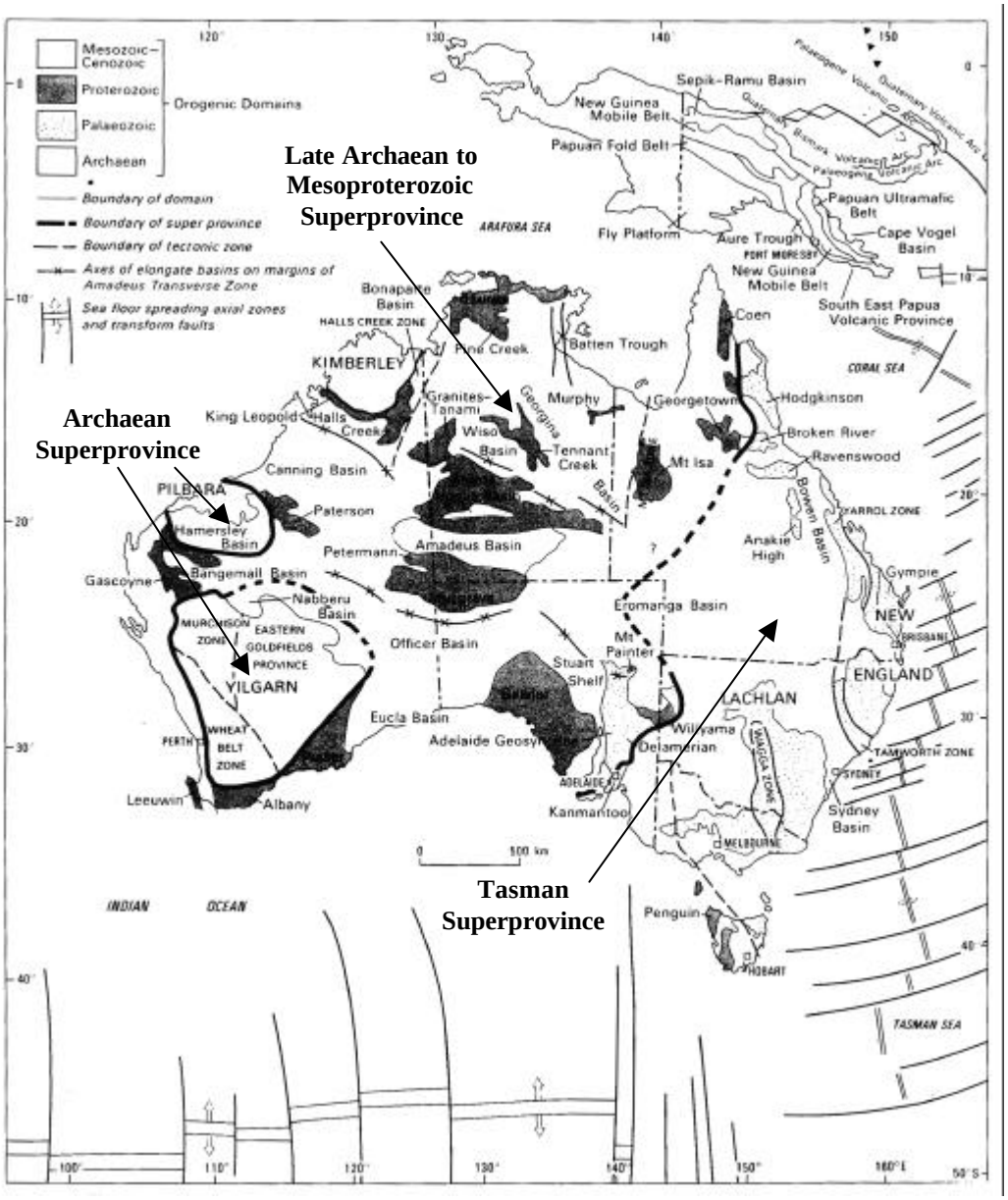

Figure 4.3 Principal orogenic domains of Australia and Papua New Guinea. Map shows the Archaean superprovince, the Late Archaean to Mesoproterozoic superprovince and the Palaeozoic Tasman superprovince. The locations of the principal sedimentary basins, of varying age, are also shown (after Rutland *et al*., 1990)

Rutland *et al.* (1990) subdivide Australia into three tectonic superprovinces (Figure 4.3): the Archaean, the Late Archaean to Mesoproterozoic and the Neoproterozoic and Palaeozoic Tasman. The Australian Archaean superprovince of Rutland *et al.* (1990) comprises the older Pilbara Craton (3600 to 3000 m.y.) and younger Yilgarn Craton (3000 to 2600 m.y.) granite-greenstone domains. The Late Archaean to Mesoproterozoic superprovince includes separate provinces in west, north, central and southern Australia. The Tasman superprovince includes the east Australian orogenic province of Late Proterozoic and Palaeozoic age, and Rutland *et al.* (1990) also includes the Mesozoic and Cenozoic New Guinea orogenic province.

4.1 Australian Archaean Superprovinces

On models of an expanding Earth (Figure 4.2) the Archaean to Mesoproterozoic provinces from adjoining continents are assembled by removing Phanerozoic and Late Proterozoic sediments and magmatism. Basins and orogens are then restored to a pre-extension, pre-rift or pre-orogenic configuration (Section 2.5). During the Precambrian the Australian Palaeozoic Canning and Officer Basins in west Australia, and east Australian Late Proterozoic and Palaeozoic Tasman Superprovince did not exist and each of the remaining Proterozoic basins are reduced in surficial area to allow for Precambrian crustal extension.

The tectonic assemblage of Australia on an expanding Earth then comprises the Yilgarn and Pilbara Cratons assembled against the Kimberley and north Australian Proterozoic terranes, and the Gawler Craton and central Australian Proterozoic terranes (Figure 4.4). The Pilbara Craton, Kimberley Basin and north Australian Proterozoic terranes are assembled against the Canadian Slave, Churchill and Superior Provinces. The Yilgarn Craton is assembled against remnant Archaean cratons and Proterozoic terranes in China, South East Asia and Korea. The Yilgarn and Gawler Cratons and central Australian Proterozoic terranes are assembled against Wilkes Land in East Antarctica, and central Australian Proterozoic terranes against the Amazon Craton of South America (Figure 4.4).

These assemblages are consistent with tectonostratigraphic correlations of Li *et al.* (1996) who suggest that the Tibetan and North China Palaeoproterozoic to Mesoproterozoic terranes were attached to northwest Australia and Siberia during the Palaeoproterozoic. The assemblage of central Australian Proterozoic terranes against

East Antarctica is consistent with Zhao *et al*. (1999) and consistent with a proposed west Canada, Australia and China connection during the Proterozoic, based on stratigraphic, metallogenic, tectonic and palaeomagnetic similarities (Bell & Jefferson, 1987).

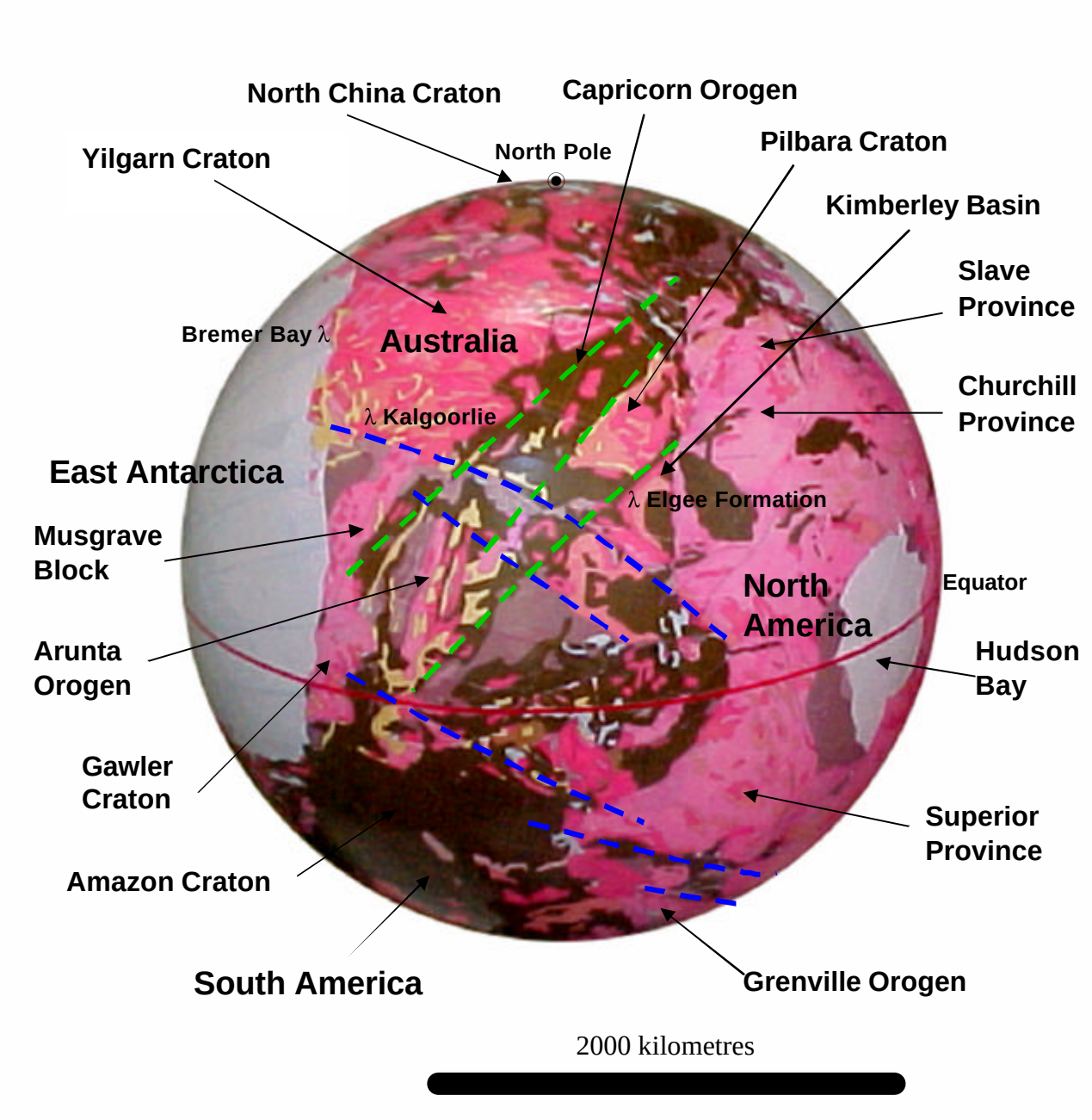

Figure 4.4 Archaean-Mesoproterozoic expanding Earth reconstruction of Australia and adjoining continents. Palaeomagnetic sample sites are shown for Bremer Bay (Li, 1999) and the Elgee Formation (Pisarevsky & Harris, 1999). Dashed green lines represent Barramundi orogenic orientation. Dashed blue lines represent Grenville orogenic orientation. (Geology after CGMW & UNESCO, 1990).

Palaeomagnetic evidence places the Kimberley Basin at 8° (north) latitude during the Palaeoproterozoic (after Li, 1999) and Bremer Bay within the southwest Australian Albany-Fraser Mobile Belt at 58° (north) latitude during the Mesoproterozoic (after Pisarevsky & Harris, 1999) (Figure 4.4). These palaeomagnetic measurements are consistent with an Early Proterozoic and Archaean palaeoequator passing through central and northern Australia determined from global palaeomagnetic data (Section 3.2.5, Figure 2.10).

Rocks older than 2500 Ma are widely exposed in the Yilgarn, Pilbara and Gawler Cratons and Pine Creek Inlier, and are suspected to underlie Proterozoic terranes in the Kimberley, Ashburton and Bangemall Basins and central Australian terranes (Solomon & Groves, 1994). The granite-greenstone assemblages of the Yilgarn and Pilbara Cratons are very similar, however the Pilbara Craton lacks the distinct directional grain of the Yilgarn and is older (Rutland *et al*., 1990). This directional grain has a similar orientation to the directional grain shown in the Canadian Churchill and Superior Provinces (Figure 4.4), which implies a compatible stress regime prior to intracratonic ensialic basin extension during the Proterozoic.

Apart from granitoids the Pilbara Craton consists largely of greenstones, mainly mafic volcanic and sedimentary rocks, dating from about 3.5 to pre-3.0 Ga (Blake & McNaughton, 1984). The Pilbara Craton was then intruded by granitoids ranging in age from 3.5 to 3.3 Ga and 3.05 to 2.85 Ga (Solomon & Groves, 1994). The oldest rocks in the Yilgarn Craton are about 3.75 to 3.5 Ga (Myers, 1990b) and consist of high-grade gneiss, mafic rocks, and metasedimentary rocks in the west and southwest regions (Solomon & Groves, 1994). Greenstone belts elsewhere in the Yilgarn Craton comprise older (*ca* 2.95 Ga) and younger (*ca* 2.7 Ga) successions. Later granitoid intrusion, deformation and metamorphism are dated between 2.7 and 2.6 Ga making stabilisation of the Yilgarn Craton considerably later than the Pilbara Craton (Solomon & Groves, 1994).

The Pilbara Craton and much of the Yilgarn Craton are underlain by continental crust about 30 kilometres thick, with velocities in the lower part typical of felsic granulites (Drummond & Collins, 1986; Solomon & Groves, 1994). Other Archaean terranes show similar patterns suggesting that Archaean granulite-facies rocks are generally representative of the lower crust (Solomon & Groves, 1994). Solomon & Groves (1994) suggest that by the Late Archaean the continental crust had completed a substantial part of its chemical development, having an average

composition represented by a mixture of the dominant Archaean igneous rocks; basalt and tonalite-trondhjemite granite.

According to Patchett & Arndt (1986) the Archaean Pilbara and Yilgarn crust had reached 40 percent of its present crustal volume by 2.7 Ga and 75 percent by 1.7 Ga, while Veizer *et al*. (1989) suggest that by 1.8 Ga it had reached a steady-state size close to the present day size. By the close of the Archaean the crust of the Pilbara and Yilgarn Cratons, and by inference the Gawler Craton, underwent little change in volume. By the Early Proterozoic ensialic basement extension (Etheridge *et al*., 1987) was well established, forming the loci for intracratonic extension, basin formation and orogenesis during the Proterozoic within the northern and central Australian Proterozoic terranes.

Barley *et al*. (1989) suggest that deformation of the older greenstone belts at about 2.65 to 2.60 Ga reflects a westward propagation of stresses associated with compression of the Norseman-Wiluna greenstone belts in the southeast Yilgarn Craton. The younger greenstones of the Yilgarn Craton were formed in linear belts related to this stress regime and include abundant felsic and ultramafic volcanic rocks, compared to the generally basalt-dominated older sequences elsewhere (Barley *et al*., 1989). On an expanding Earth this compressional phase is related to oblique basement extension and anticlockwise translation and rotation between the Canadian provinces, plus Pilbara Craton and northern Australian terranes, relative to the Yilgarn Craton. This oblique ensialic basement extension and rotational stress regime is consistent with a pre- and post-Barramundi orogenic event affecting Proterozoic terranes throughout northern Australia during the Early Proterozoic (Etheridge *et al*., 1987).

There is a marked concentration of major gold and base metal deposits within the younger granite-greenstone belts of the Yilgarn Craton (Rutland *et al*., 1990). Groves (1982) suggests this might be related to a progressive increase in oblique crustal extension during greenstone development within the Pilbara Craton through to the western Yilgarn Craton including the Norseman-Wiluna belt. This extension is consistent with extension between the Australian and Canadian Precambrian cratons on an expanding Earth, with rifting and crustal extension resulting in areas of subsidence and sub-aerial eruption of komatiites and formation of nickel-copper sulphide deposits, such as in the Norseman-Wiluna belt.

Volcanogenic copper-zinc sulphide deposits occur in association with felsic volcanic centres in the Murchison zone of the Yilgarn Craton and also in a zone along the northeast margin of the Norseman-Wiluna belt (Rutland *et al*., 1990). Other notable mineralisation is associated with pegmatites in the Western Gneiss Terrain, including rare metal pegmatite at Greenbushes located adjacent to Precambrian cratons of China and remnant fragments from South East Asia.

Gold mineralisation was intense within the greenstones of the Norseman-Wiluna belt and is related to a Yilgarn-wide period of tectonism between 2.7 and 2.65 Ga (McNaughton & Dahl, 1987). Many of the gold deposits are shear hosted and Groves (1988) suggests that the distribution is controlled by kilometre scale, oblique-slip, reverse or normal faults, linked to crustal scale strike-slip shear zones that also appear to have focused mantle derived carbonation and emplacement of I- and A-type granitoids, felsic porphyries and calc-alkaline lamprophyres.

4.2 Late Archaean to Mesoproterozoic Superprovince

Etheridge *et al.* (1987) describe the Late Archaean to Mesoproterozoic Australian superprovince (Figure 4.3) as an ensialic basin-forming episode that resulted from local extension of pre-existing Archaean continental crust. Rutland *et al.* (1990) note that each of the provinces making up the superprovince show uniformity in their older age patterns, in particular evidence for widespread pre-1.8 Ga Barramundi and younger orogenic and plutonic events. These periods of tectonic activity are considered by Rutland *et al.* (1990) to have been important in defining the present structure of the cratonic areas, which then controlled later tectonic reactivation during the Late Proterozoic and Palaeozoic.

The Hamersley Province of the Pilbara Craton represents a preserved transition from Archaean to Early Proterozoic, displaying banded iron formations dated at about 2.5 Ga conformably overlying basalts and sandstones of the Fortescue Group, dated at 2.75 Ga (Solomon & Groves, 1994; Trendall, 1990). Early Proterozoic rocks older than 2.0 Ga are also recognised in the Pine Creek, Granites-Tanami and Gawler regions. Elsewhere Proterozoic rocks cover a large part of central and west Australia and occur in a number of discrete tectonic provinces overlain in part by Phanerozoic sediments.

On an expanding Earth the ensialic basin formation event of Etheridge *et al.* (1987) and tectonism of Rutland *et al.* (1990) is consistent with oblique east-west (Precambrian orientation, Figures 4.2 and 4.4) crustal extension between the Australian Archaean Superprovinces and the Canadian Archaean Slave, Churchill and Superior Provinces, accompanied by ensialic translational motion during the Palaeoproterozoic Barramundi and later orogenic events.

The Pilbara and Yilgarn Cratons of Australia and the Slave, Churchill and Superior Provinces of Canada are inferred to represent exposed low-relief land surfaces supplying sediment to the Proterozoic basins as part of an extensive global network of epi-continental seas. Griffin & Grey (1990) record extensive clastic sediments and intrusive dolerite sills overlain by Late Proterozoic glaciogenic rocks in the Kimberley Basin of northern Australia, and strong unidirectional longshore currents flowing south south-east suggested to Plumb *et al*. (1981) landmasses to the west and north-east. On an expanding Earth these are consistent with an exposed Canadian Churchill Province located adjacent to the Kimberley Basin.

Throughout the Precambrian and Palaeozoic the central Australian basins on an expanding Earth (Figure 4.2) are located in equatorial to low-northern latitudes, extending to mid- to high-northern latitudes in west Australian cratonic regions. This is supported by the occurrence of Late Proterozoic marine glaciogenic deposits intercalated with warm-water carbonate sediments in the central Australian basins (Schermerhorn, 1974; Fairchild, 1994) and palaeomagnetic studies confirm deposition in low-latitudes (Williams, 1994). This contrasts with a plate tectonic high southern latitude location during the Neoproterozoic Rodinian assemblage (Torsvik *et al*., 1996).

The Proterozoic orogenic provinces of Australia all have similar tectonostratigraphic histories (Etheridge *et al*., 1987) with very little evidence for activity between 2.5 and 2.1 Ga. Most of the provinces record a major basin forming event probably initiated by lithospheric extension between 2.1 and 1.9 Ga (Rutland *et al*., 1990). Deposition within each basin was then abruptly terminated by the Barramundi orogenic event between 1.88 and 1.84 Ga which was uniform in style and age across the whole continent and whole globe (Rutland *et al*., 1990).

The Early Proterozoic basins (summarised from Rutland *et al*., 1990) are typified by three tectonostratigraphic sequences. A basal sequence is dominated by clastic and/or volcaniclastic units of limited lateral extent and considered to be a rift

facies sequence. This is overlain by more laterally extensive units dominated by finer clastics, carbonates and other chemical sediments, considered to be a thermal subsidence facies sequence. The youngest sequence is dominated by quartz-rich to volcaniclastic flysch and indicated a phase of rapid basin collapse prior to onset of the Barramundi Orogeny.

The Barramundi Orogeny is characterised by horizontal shortening, low-pressure metamorphism and voluminous, late orogenic, high-level felsic intrusives and comagmatic ignimbrites of uniform composition (Rutland *et al*., 1990). The Barramundi igneous suite is I-type, potassium rich, uniformly enriched in incompatible elements with respect to Archaean granitoids and were generally emplaced between about 1.88 to 1.84 Ga (Wyborn, 1988).

The period immediately following the Barramundi Orogeny was one of renewed crustal extension and basin formation in many of the Proterozoic provinces. Basins largely overlie Early Proterozoic rather than Archaean basement and are characterised by a basal sequence dominated by bimodal volcanics and quartz-rich clastics, overlain by finer clastics, carbonates and evaporites (Rutland *et al*., 1990). Renewed extension and transtension in the eastern Central Australian Proterozoic provinces between 1.7 and 1.6 Ga led to further basin formation, comprising widespread felsic-dominated bimodal volcanism and thick carbonate-rich to quartzo-feldspathic turbiditic sequences (Rutland *et al*., 1990).

On an expanding Earth (Figure 4.4) Proterozoic platform sequences in north Australia are located adjacent to Proterozoic sequences in western North America. In Australia, these represent post-Barramundi basin forming episodes and are interpreted by Rutland *et al*. (1990) as facies deposited as a result of extensive thermal subsidence beyond the active central Australian rifts and orogenies. A distinction between platform cover and mobile belts was made by Rutland *et al*. (1990), reflecting the localisation of Middle Proterozoic orogenic events rather than a waning of older continental tectonic activity.

The expanding Earth Mesoproterozoic assemblage (Figure 4.4) demonstrates that north and east Australian Middle Proterozoic orogenic events are aligned with the Grenville Orogenic event of eastern North America. The Albany-Fraser and parts of the Musgrave provinces are also considered by Solomon & Groves (1994) to form an extension of the Grenvillian fold belt, although Figure 4.4 suggests that these are two parallel zones. In Australia this event is accompanied by widespread intrusion

and extrusion of a highly fractionated I-type felsic igneous suite between 1.6 and 1.45 Ga (Wyborn *et al*., 1987) and intrusion of diamond-bearing pipes in the Halls Creek fold belt at 1.2 Ga (Pidgeon *et al*., 1989).

The metallogeny of the Proterozoic superprovince was considered to be distinct from the preceding Archaean and subsequent Phanerozoic superprovinces (Rutland *et al*., 1990; Solomon & Groves, 1994). The Proterozoic superprovince is characterised by large, stratiform, banded iron formations, sediment hosted base metal sulphide deposits, and commonly polymetallic, high-level, hydrothermal deposits that are structurally controlled and up to 300 m.y. younger than their Barramundian host rocks (Rutland *et al*., 1990). These include iron in the Hamersley province, gold in the Telfer, Tanami, Tennant Creek and Pine Creek regions, giant sediment hosted lead-zinc-silver deposits at Broken Hill, Mount Isa and MacArthur River, high-grade uranium in the East Alligator and Pine Creek province, copper at Mount Isa and polymetallic deposits at Olympic Dam.

4.3 Neoproterozoic and Palaeozoic Tasman Superprovince

The Neoproterozoic and Palaeozoic Tasman Superprovince involves a history of orogenic fold belt development along the eastern margin of Australia. The Tasman Superprovince (Tasman Fold Belt of Solomon & Groves, 1994) is made up of the Kanmantoo, Lachlan, Thomson, Hodgkinson-Broken River and New England fold belts (Figure 4.5), which form part of an orogenic belt extending south to the Borchgrevink Orogen in Antarctica and north to Papua New Guinea (Solomon & Groves, 1994). Reference is also be made to continued sedimentation in the Officer and Canning Basins, intracratonic to the Precambrian Pilbara and Yilgarn Cratons and Kimberley Basin in west Australia.

In east Australia the fold belts, tectonism and granitoid plutonism in the Tasman Superprovince progressively youngs from west to east (north-west to south-east on expanding Earth models, Figure 4.6). Deformation in the Adelaide and Kanmantoo fold belts is Late Cambrian (Delmamerian Orogeny); in the Lachlan Fold Belt the major deformations are Late Ordovician (Benambran Orogeny), mid-Devonian (Tabberabberan Orogeny) and mid-Cretaceous (Kanimblan Orogeny), while in the New England Fold Belt deformation is mid-Carboniferous to Late Permian and younger (Rutland *et al*., 1990).

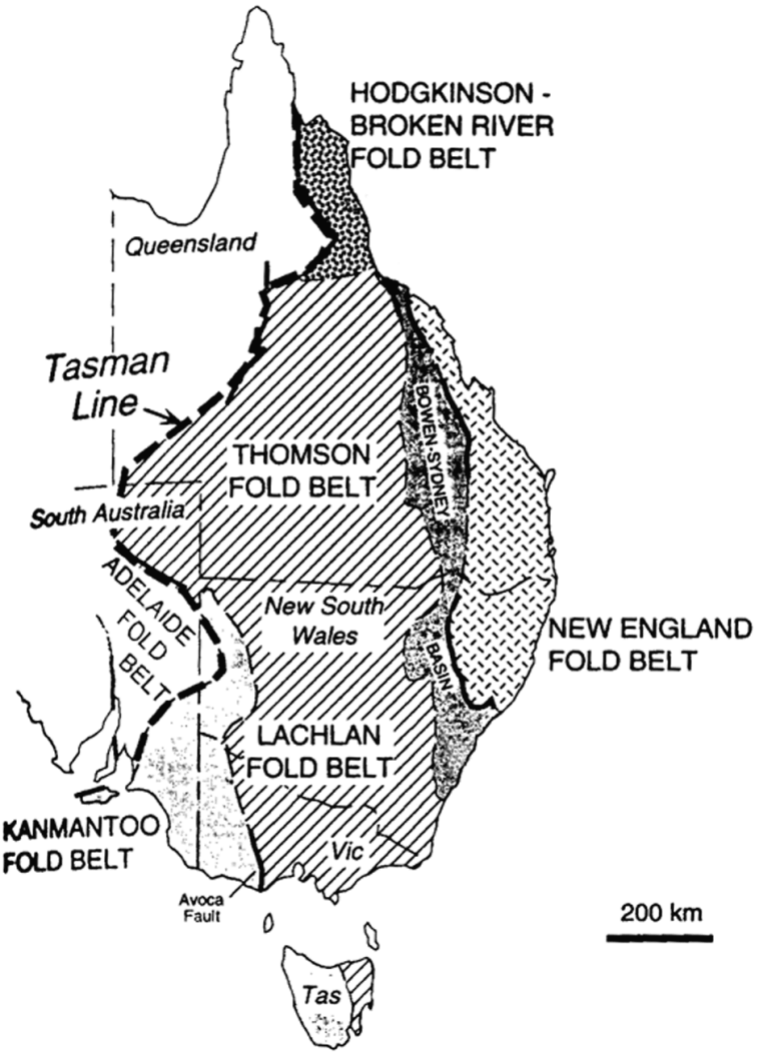

Figure 4.5 The Neoproterozoic and Palaeozoic Tasman Superprovince of east Australia. The superprovince extends south to include the Borchgrevink Orogen in Antarctica and north to Papua New Guinea. (After Walshe *et al*., 1995)

Solomon & Groves (1994) describe the Tasman Fold Belt system as representing an eastward growth of the Indo-Australian plate from the Early Cambrian to Early Mesozoic, during which successive fold belts, island arcs or terranes were incorporated into the Australian craton from west to east and north-east. It was suggested by Solomon & Groves (1994) that growth of the Australian craton was by mostly westward subduction and terrane accretion preceded and followed by orogenic movements. Although isotopic evidence from granitoids provided evidence for the occurrence of Proterozoic basement in the region (eg. Chappell *et al*., 1988) which suggested to Rutland *et al*. (1990) that orogeny cannot be solely the consequence of lateral accretion.

This conventional plate history for the Tasman Superprovince cannot be reconciled with an expanding Earth. On an expanding Earth (Figure 4.6) the Tasman Superprovince is intracratonic to the central Australian Proterozoic terranes, the Amazon Craton of South America and remnant terranes in Central America, and extends east (Palaeozoic orientation, Figure 4.6) to include Palaeozoic basins in south-east North America and south to include basins in West Antarctica and southern South America. Development of the superprovince represents an extended period of crustal divergence and intracratonic basin sedimentation between Australia, North America and South America during Earth expansion.

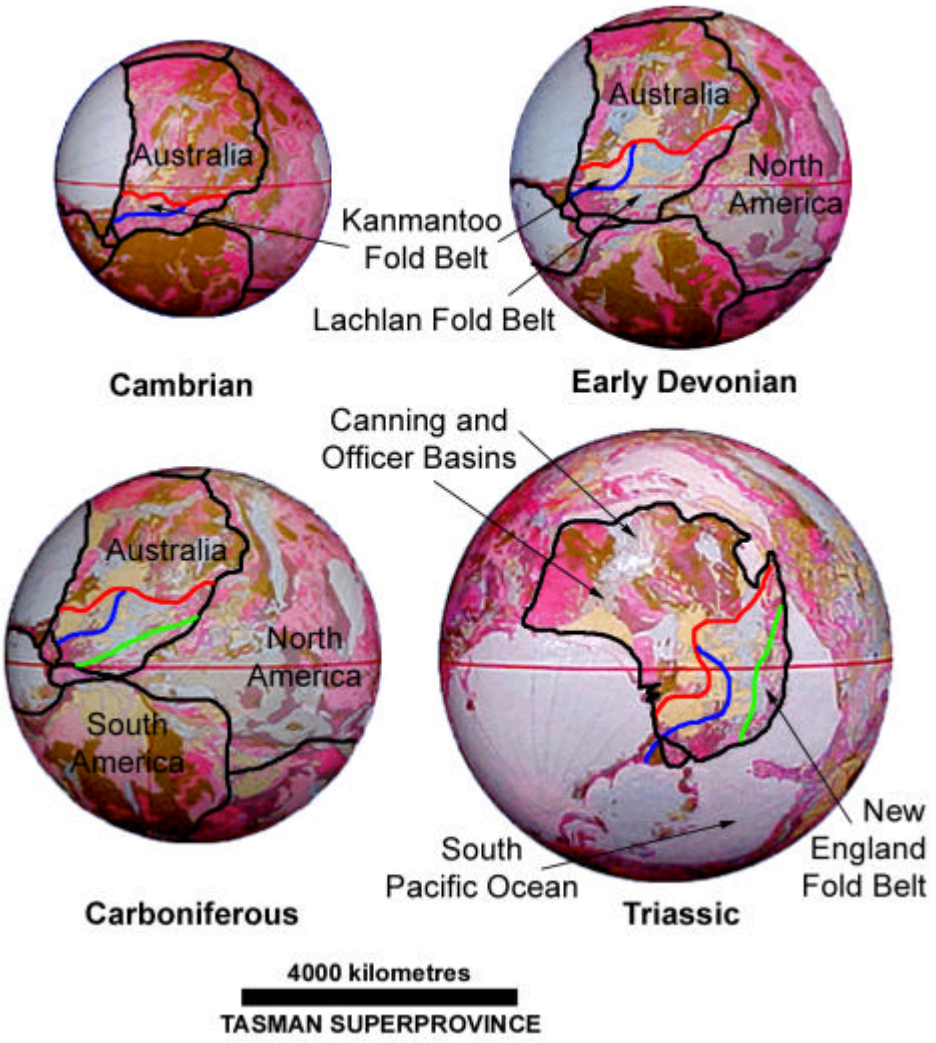

Figure 4.6 The Neoproterozoic and Palaeozoic Tasman Superprovince on an expanding Earth. Red, blue and green lines represent margins of the Kanmantoo, Lachlan and New England fold belts (after Walshe et al., 1995). (Geology after CGMW & UNESCO, 1990).

This Australian-American tectono-stratigraphic association is acknowledged in Brown *et al*. (1968) and Powell & Veevers (1994). New Zealand on conventional reconstructions forms part of Gondwana and is located adjacent to Australia (eg. Powell & Li, 1994). This is confirmed by Retallack (1987) who noted the similarity between Triassic vegetation from coal measures in the Torlesse Supergroup of New Zealand and the Sydney Basin of east Australia. The occurrence of New Zealand Mesozoic marine taxa with strong Mexican affinities spread over 3300 metres of stratigraphic thickness (spanning Heterian-Puaroan), suggested to Stevens (1997b) a close and consistent link between New Zealand and Mexico over time. This tectono-stratigraphic link between Australia and South America via New Zealand is consistent with expanding Earth reconstructions (Figure 2.29).

The lithostratigraphic and tectonic history of the Tasman Superprovince on an expanding Earth is influenced by the relative plate motions between the Australian, North American and South American cratons. Rifting during the Proterozoic Grenvillian and Palaeozoic Appalachian Orogenic events initiated basin extension in both southeast North America and east Australia and initiated magmatism related to the Andean-Cordilleran magmatic arc. During basin development South America is displaced south (Palaeozoic orientation, Figure 4.6) relative to North America and Australia, resulting in large strike-slip inter-terrane movements (eg. Rutland *et al*., 1990) within the Tasman Superprovince, and southeast extension and growth of the superprovince between successive orogenic events.

On the Late Carboniferous to Early Permian expanding Earth (Figure 4.2) continental rupture between east Australia and South America results in opening of the South Pacific Ocean, merging with the opening North Pacific Ocean during the Late Triassic to Jurassic (Figure 2.29). During this event the Andean-Cordilleran magmatic arc separates from east Australia and remains part of South America and North America. The New England fold belt remains as a remnant within east Australia and other remnants fragment to form New Zealand. Following widespread deformation and granitoid intrusion during the Carboniferous Kanimblan Orogeny, the Lachlan fold belt stabilises to form a regional platform (eg. Solomon and Groves, 1994), persisting to the Recent.

The Canning (Iasky, 1990) and Officer (Middleton, 1990) Basins in west Australia contain Phanerozoic sediments interpreted as interior or intracratonic sag

basins (Cockbain & Hocking, 1990) forming part of Gondwana. On an expanding Earth (Figure 4.6) these basins are intracratonic to the Yilgarn and Pilbara Cratons and the Proterozoic Kimberley and Central Australian basins, and together represent an intracratonic epi-continental extensional basin. This interpretation is unique to Earth expansion and represents a period of Palaeozoic crustal break-up and dispersal of the Australian cratonic regions, masked by accumulation of Phanerozoic sediments. Stabilisation of the basins is maintained during the Mesozoic and Cenozoic during opening of the Indian and Southern Oceans.

The metallogeny of the Tasman Superprovince includes volcanic-hosted massive sulphide deposits, porphyry-granitoid related copper-gold and gold deposits, and granitoid-associated tin and wolfram deposits as well as structurally controlled gold and copper-lead-zinc deposits (Walshe *et al*., 1995). Walshe *et al*. (1995) indicate that magmatism associated with this metallogeny originated in the mantle as crust-mantle interactions, with crystal fractionation and prevalence of major north-south trending fault systems forming an important metallogenetic process. Solomon & Groves (1994) consider that the porphyry copper-molybdenum, skarn, and tin-wolfram deposits are indicative of an Andean-type continental margin.

On an expanding Earth this spatial link to both the Andean and Cordilleran Orogenic belts is maintained throughout the Neoproterozoic and Palaeozoic, forming a magmatic arc located between Australia and the Americas. Continental rupture between Australia and the Americas during the Permian, and rapid opening of the Pacific Ocean during the Mesozoic to Recent then terminated the established continental link.

5. PROPOSED CAUSAL MODEL FOR EARTH EXPANSION

In previous chapters spherical Earth models were used to demonstrate the viability of an Earth expansion process, extending from the Archaean to Recent and extrapolated to the future. In this chapter it is intended to present a proposed causal model for Earth expansion, drawing on observations from both the spherical modelling studies and the interrogation of geological and geophysical data. The proposed causal model is speculative and commences during the pre-Archaean, prior to the beginning of recorded geological Earth history.

The potential causes of Earth expansion have been addressed in Egyed (1963), Wesson (1973), Carey (1983a) and Maxlow (1995). Scenarios, such as a constant Earth mass, a pulsating Earth, meteoric and asteroidal accretion, or a variation in the universal gravity constant G were considered and, while possibly contributing in part, were shown to be contrary to the dynamics of the present Solar System (Carey, 1983a; Maxlow, 1995).

A study of the kinematics of Earth expansion (Section 2.3; Appendix A1) suggests that Earth expansion is caused by an exponential increase in mass with time, confirming the conclusions of Hilgenberg (1933) and Carey (1983a). Where the excess mass comes from is considered at length by Carey (1983a; 1996) who concludes that matter is the antithesis of energy and is being created deep within the Earth's core in sympathy with creation and expansion of matter within the Universe.

The proposed causal model for Earth expansion involves an increase in mass by condensation, or segregation of new matter from energy within the Earth's core. This new matter accumulates at the core-mantle interface and the increase in volume results in swelling of the mantle. Mantle swell is then manifested in the outer crust as crustal extension and is currently occurring as extension along the mid-ocean-rift zones. Matter generation within the Earth's core is seen as an endothermic reaction, which will ultimately result in a decay of matter formation in the core and cessation of expansion with time.

5.1 Pre-Archaean Earth

The cosmological origins of the Earth and Solar System are beyond the scope of this thesis. Speculation is made on the pre-Archaean origins of Earth, prior to presenting

a causal model for Earth expansion from the Archaean to Recent. The conventional Kant-LaPlace accretional model for the creation of the Solar System (eg. Silk, 1980), originating from accretion of a dense cloud of post-Big Bang interstellar debris, is contrary to the physical evidence shown by geological reconstructions of continents on the Archaean to Mesoproterozoic expanding Earth model (Figure 2.13).

Conventional plate tectonics considers that formation of the Earth by accretion of interstellar debris occurred during the pre-Archaean. Continental crust was then either fully developed by approximately 4 Ga and has since been recycled through the mantle throughout geological time with no net change in crustal mass, or that the earliest continental crust occurred in small, localised patches where juvenile continental crust was cratonised and not returned to the mantle in bulk (Moorbath, 1982).

Shuldiner (1982) presented evidence from high-grade metamorphic terranes to suggest that the surface temperature of Earth during the pre-Archaean was 300 ± 100°C. Evidence from glacial studies suggested to Eyles & Young (1994) that, during the Late Archaean and Early Proterozoic, Earth surface temperatures may have been 30 degrees less than now and Sun's luminosity was about 70% of the present value, even though upper mantle temperatures on Earth were still up to 150°C higher than the present (Kröner, 1982). A reduced luminosity of the Sun during the Archaean and Early Proterozoic then implies that high pre-Archaean Earth surface temperatures are attributed to a higher geothermal gradient. Low Archaean temperatures were then possibly the result of an insulating effect caused by development of a primitive crust in conjunction with a declining geothermal gradient.

In contrast, it is speculated that for an Earth that is expanding in sympathy with the Solar System and Universe, the Earth-Moon system had a high surface temperature during the pre-Archaean because it was located much closer to a primitive young Sun than it is now. By the Archaean and Early Proterozoic the Earth-Moon system had moved away from the influence of the Sun's surface temperature and gravity, sufficiently far to lower Earth surface temperatures enough to retain liquid water on a primitive crust while still retaining a high residual geothermal gradient.

It is further speculated that a combined Earth-Moon, as well as each of the solar planets, originated from the surface of the primitive young Sun during the very

early pre-Archaean, ejected as incandescent plasmoidal, or similar material at regular, periodic intervals, similar to solar flare activity on the present Sun's surface. The Earth-Moon and each of the solar planets in turn then gradually moved away from the direct influence of the Sun's surface temperature and gravity during transferral of angular momentum from the Sun to each of the planets.

During this pre-Archaean phase the Earth and Moon were separated as a result of gravitational instability of the primitive incandescent Earth-Moon mass, forming a binary planet. An incandescent sialic layer is thought to have been stripped from the surface of the primitive Earth-Moon body to form the Moon. During this process the primitive core and remnants of a simatic outer layer remained intact, forming the proto-Earth. Surface temperatures then gradually cooled sufficiently to form a juvenile mantle on the proto-Earth, segregating to form a primitive outer crust, hydrosphere and atmosphere with an accompanying reduction in geothermal gradient with time.

It is inferred that a primitive Moon composed essentially of sialic material would undergo minimal expansion since formation. By combining the volume of the present Moon and the volume of the Archaean Earth, the pre-Archaean Earth plus Moon is then calculated to have been approximately 2100 kilometres radius prior to separation.

A schematic representation of cross sections of the Earth from the pre-Archaean to Recent (Figure 5.2) shows the proposed development of the core, mantle, crust and continental break-up and dispersal throughout Earth history. Empirical modelling studies indicate that the primordial Earth radius during the Early Proterozoic, Archaean and possibly pre-Archaean was approximately 1700 kilometres. During the pre-Archaean to Mesoproterozoic, the Earth's radius remained relatively static, prior to a steady to rapidly accelerating increase in radius during the Late Proterozoic and Palaeozoic, resulting in continental crustal rupture, break-up and dispersal during the Mesozoic to Recent (Section 2.2).

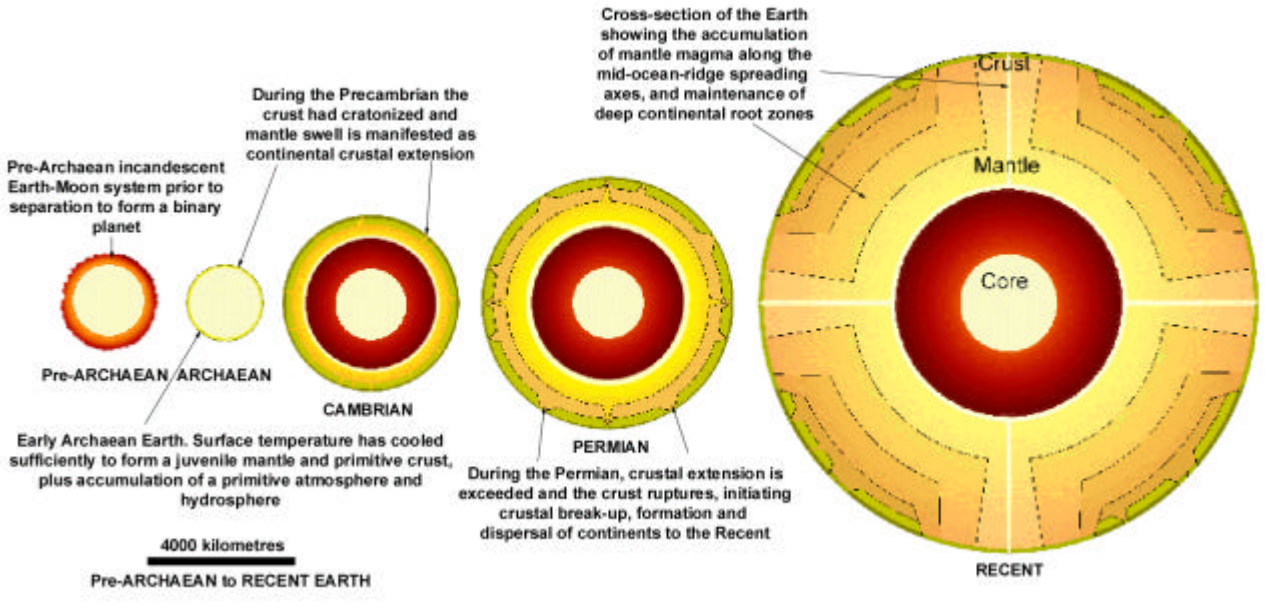

Figure 5.1 Proposed development of the core, mantle, crust and continental break-up and dispersal throughout Earth history. Cross sections show the development of the mantle and brittle-ductile reaction of the crust during mantle swell. The accumulation of matter at the core-mantle boundary results in maintenance of deep continental root zones throughout Earth history, aging away from the core to the crust. Accumulation of magma at the mid-ocean-rift zones represents exposure and preservation of a mantle-derived crust.

5.2 Primitive Lithosphere

Empirical expanding Earth models demonstrate that a primitive Archaean lithosphere enclosed the primordial Earth with a complete shell at a palaeoradius of approximately 1700 kilometres (Figure 5.2). It is speculated that segregation of the core to form a primitive mantle occurred during the pre-Archaean, prior to formation of a primitive simatic crust through surface cooling by convection and surface radiation, and solidification of a primitive mantle melt. Early Archaean geological history commences with the stabilisation and preservation of the thin outer primitive crust, prior to extensive cratonization during the Mid to Late Archaean.

Lambert (1982) suggests that the main products of fractional crystallisation of melts produced in the primitive outer Earth crust would have been ultramafic cumulates and mafic rocks. The constraints on the formation of granitic and anorthositic rocks from a peridotitic source (Lambert, 1982) suggest that the volume of sialic rocks in the primitive Archaean crust was considerably less than in the present continental crust, with primordial sialic material accumulating in a surface layer of not more than two to three kilometres thick. Lambert (1982) considers the high geothermal gradient existing during the pre- to Early Archaean suggests that the

lower crust would have comprised mafic rocks extending to depths of 30 to 100 kilometres thick. Beneath these were possibly ultramafic cumulates and depleted peridotitic mantle containing entrapped melt, overlying unmelted mantle peridotite (Lambert, 1982).

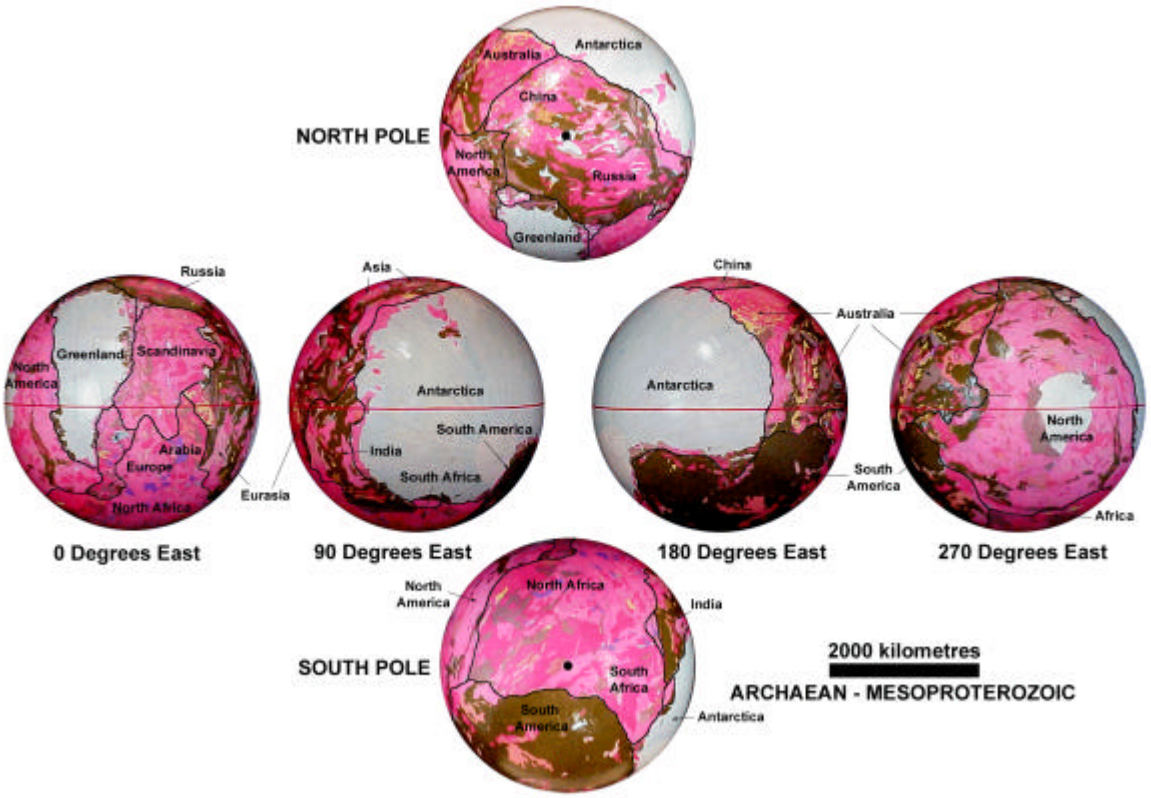

Figure 5.2 Primordial Archaean to Mesoproterozoic expanding Earth model. Cratons are shown as pink and red, Proterozoic basement rocks are shown as khaki, present Antarctic and Greenland ice-caps are shown as pale blue. An Archaean lithosphere encloses the primordial Earth with a complete shell at a palaeoradius of approximately 1700 kilometres. Early Archaean geological history commences with the stabilization and preservation of a thin outer primitive crust, prior to extensive cratonization during the Mid to Late Archaean.

On an expanding Earth model the core represents remnant plasmoidal, or similar material and generation of matter to form the mantle occurs by condensation of energy (eg. Carey, 1996). The mantle represents a segregation or condensation of the core during cooling, prior to chemical differentiation to form an outer crust (Figure 5.1). Fractionation of the mantle during an extended period of high geothermal gradient gives rise to peridotitic, ultramafic and mafic melts, forming a primitive mantle and crust with a surface accumulation of sialic rocks.

Earth expansion during the pre-Archaean is then initiated by phase changes and fractionation of the molten upper mantle as the Earth moves away from the

influence of gravitational and temperature extremes near the surface of the primitive Sun. Once a pre-Archaean core-mantle-crust is established further segregation or condensation of matter at the core-mantle interface occurs, steadily accelerating during the Late Proterozoic to Recent. Matter generation at the core-mantle interface results in mantle swell, which is transferred to the primitive outer crust as crustal extension.

5.3 Primitive Atmosphere and Hydrosphere

The primitive atmosphere and hydrosphere is considered by Lambert (1982) to have formed largely from juvenile components degassed from the Earth's interior and subsequently modified by physical, chemical and biological processes. Rubey (1975) proposed that degassing has been a continuous or recurrent process, which is still occurring. While others (eg. Fanale, 1971) argue that degassing was essentially complete at a very early stage in Earth history, and there is also suggestion of input from comets. Geochemical arguments (eg. Lambert, 1982) based on the oxidation state of the mantle and fluid inclusion studies suggest that a reduced atmosphere was established during the Archaean, comprising mainly H_2O and CO_2, with lesser CO, N_2, H_2S, SO_2, HCL and small amounts of NH_3 and CH_4. The absence of a juvenile O_2 source implied to Lambert (1982) that oxygen was not a stable component of the early atmosphere but was generated by secondary processes.

Early Archaean surface temperatures were too high for the existence of liquid water and resulted in a water-rich atmosphere (Lambert, 1982). Lambert (1982) suggests that the presence of surface water is evident from sub-aqueous sedimentation by 3.8 Ga and suggested also that hydrospheric development is a pre-requisite for preservation of the primitive crust.

The main controls on the chemistry of the Archaean hydrosphere are considered by Lambert (1982) to be reactions with hot igneous rocks, sea floor weathering, and additions of new juvenile water with minor input from fluvial systems. Oxygen isotope studies (Lambert, 1982) from Archaean hydrothermal talc-bearing sediments implied the existence of fluids isotopically similar to modern seawater. Lower $\delta^{18}O$ values from Archaean cherts and carbonates also suggested to Lambert (1982) that Archaean hydrospheric temperatures were up to 70°C.

On an expanding Earth model the primitive atmosphere and hydrosphere developed progressively throughout Earth history by a process of devolitilisation of the mantle during a variation in Earth's temperature, pressure and surface gravity conditions (Maxlow, 1995). This was initiated once the Earth-Moon system had migrated away from the influence of the Sun's surface temperature and gravity.

The production of new juvenile water on an expanding Earth during the Palaeozoic and Precambrian occurs within zones of intracratonic crustal extension (eg. Figure 5.2), and for the Mesozoic to Recent production occurs along the mid-oceanic-rift zones. Geographical studies (Section 3.3) show this to be an accelerating process, particularly during the Phanerozoic, occurring during continental break-up and generation of new mantle-derived oceanic lithosphere. As Lambert (1982) demonstrates, the primitive Archaean hydrosphere had a low NaCl content and devolitilisation to form the hydrosphere and atmosphere during Earth history results in enrichment in sedimentary iron, silica and carbonate species.

5.4 Archaean Expanding Earth Crust-Mantle Evolution

The formation of localised cratonised patches of juvenile crust to form primitive continents, as suggested by Moorbath (1982), is consistent with a pre- to Early Archaean expanding Earth model. During the Archaean the primitive continental crust progressively stabilised, enclosing the entire primordial Earth with continental crust, and tectonic and magmatic events are globally synchronous (Figure 5.2). The following proposal for crust-mantle evolution and development of greenstone-granite-gneiss terranes during the Archaean is based on Kröner (1982).

The pre- to Early Archaean on an expanding Earth (Figure 5.1) represents an Era where surface temperatures are sufficiently low to allow solidification of a thin ultramafic crust on a mantle retaining a high global geothermal gradient and where hot, mantle-derived surface water pools in low-lying depressions. As cooling progresses the early crust thickens and extends as komatiitic to basaltic volcanism becomes widespread. Volcanic activity covered the entire primordial Earth surface, as indicated by Early Archaean heat flow measurements (eg. Smith, 1981) and volcanic activity occurs over a complex system of mantle thermal plumes.

This early ultramafic crust and overlying komatiitic volcanism may not have fully survived the extensive plume activity and may have been, in part, subsequently

resorbed into the mantle, reducing surface temperatures in the process. By about 4 Ga mantle temperatures and heat flow had decreased sufficiently to maintain a komatiite-dominated crust, allowing volcanic centres to rapidly increase in height and thickness. Growth of volcanic piles through partial fractionation of the underlying subcrustal mantle resulted in basalt depletion and cooling to form a primitive subcrustal root zone, further stabilising the overlying crust. Regions away from the volcanic centres maintained a relatively thin lithosphere, which may have ultimately formed the loci for ongoing crustal extension and basin formation during Proterozoic Earth expansion.

The onset of mantle swell and fractionation of the upper mantle during the pre- to Early Archaean produced tholeiitic magmas, with a large proportion accumulating at the base of the crust, forming a reservoir for bimodal volcanic suites and tonalite-trondhjemite granitoid diapirs. As the overlying volcanic pile thickens its lower part and underlying ultramafic protocrust may also melt to form a vast reservoir for further differentiated magmas. The continued growth of the volcanic pile gradually reduces the overall density of the evolving crust through partial melting at its base, establishing a two-layered structure, with the lower part transformed into high-grade metamorphic assemblages and the upper part consisting of both primitive and differentiated volcanics and granitoid intrusives.

During the Early Archaean the crustal surface is made up of predominantly sialic, early upper crust comprising a mixture of granitoid intrusives and differentiated volcanics. Emergent surfaces are then exposed to mechanical and chemical erosion, in particular erosion by hot juvenile waters from volcanic eruptions, forming early calc-alkaline sediments deposited in low lying regions which reflect the composition of the parent rocks. Early sedimentary basins are small and isolated, becoming more extensive by about 3.8 Ga. This early-differentiated sialic crust now forms the oldest preserved crustal remnants on Earth (eg. Moorbath, 1982).

The survival of a 30 to 40 kilometre thick Archaean crust implies the presence of a stable subcrustal root-zone not less than 200 kilometres thick (Wells, 1981). This is further substantiated by geotherms deduced from kimberlite pyroxenes (Davies & Strebeck 1982). The growth of subcrustal lithosphere and development of a stable root-zone on an expanding Earth occurs during repeated periods of basalt extraction from the mantle, leaving a less dense peridotitic residue over an

undepleted mantle. This is then incorporated into the crust and thickens the crustal lithosphere from below. Cratonisation of continental crust during the Early Archaean is then a consequence of the early formation of a thick lithosphere.

Kröner (1982) envisaged that by about 3.6 Ga sialic continental crust had attained sufficient thickness and rigidity to support large basins. On an expanding Earth this crust is then subjected to crustal attenuation during the initial phases of expansion, resulting in crustal fracture, fissuring and rifting above mantle plumes, generating ovoid to elongate basins or sharply bounded, fault controlled graben systems. These basins collect water, shallow-water sediments and mafic to ultramafic lavas produced from melting in the subcrustal mantle. A small proportion of these melts reach the surface as Mg-rich lava while a much larger volume remains near the base of the crust to become the source for bimodal volcanic assemblages and tonalite-trondhjemite granitoid intrusives.

The Archaean high-grade metamorphic terranes represent largely pre-greenstone sialic crust, together with predominantly shallow water sedimentary deposits and granitoids produced during various stages of incomplete crustal fissuring and subsidence (eg. Kröner, 1982). Periodic subcrustal mantle decoupling during Earth expansion provides a mechanism for sub-horizontal ductile flow and extension within the Archaean lower crust. Crustal extension accompanied by a high heat flow from rising plumes then results in formation of high-grade gneiss terranes.

Ongoing crustal extension in the lower crust during Earth expansion results in crustal fracture and formation of listric fault systems in the upper crust. Faulting and rifting results in basin extension accompanied by deposition and accumulation of thick sequences of volcanic rocks and intercalated sedimentary sequences. Subsidence within these proto-greenstone basins, along with crustal thinning results in a rise in the crust-mantle boundary. Further crustal extension results in spreading and decoupling of the lower crust and dense residues of earlier underplated material. This is accompanied by production of large volumes of basaltic rock. Crustal fusion and crust-mantle mixing results in the production and emplacement of calc-alkaline suites and crustal-derived granitoids.

The final phase of Archaean basin extension during expansion results in formation of large, stable platforms and shallow seas with a low elevation contrast between continents and seas. Continental sedimentary input is limited and calc-silicate cherts and banded iron formation are laterally extensive during the Mid to

Late Archaean (eg. Goodwin, 1982). Intracratonic motion during changing Earth surface curvature results in early recumbent folding and shallow thrusts, which may lead to stratigraphic repetition or obliteration of original depositional relationships. These early structures are later modified and possibly steepened during the emplacement of granitoid batholiths, accompanied by translational shortening within the greenstone piles.

These areally extensive granitoid and volcano-sedimentary greenstone successions represent Late Archaean to Early Proterozoic global events (Figure 5.2), which result in substantial cratonisation of the Archaean crust, crustal thickening and formation of a deep crustal root-zone persisting to the Recent. Zones of intracratonic mantle derived magmatism remain tectonically mobile during the Archaean and Proterozoic, resulting in extensive tectonic reworking during large-scale intracratonic transform motion (eg. Katz, 1976).

5.5 Proterozoic Expanding Earth Tectonostratigraphic Evolution

The Proterozoic represents an Epoch of comparative crustal stability and increasing mobility. Condie (1981) concludes from a review of Early and Middle Proterozoic successions that the period prior to about 1.7 Ga was dominated by stable continental margin or intracratonic basins, while later assemblages suggest more mobile environments. In southern Africa, crustal stability had been achieved by about 3 Ga while elsewhere in India and west Australia; for instance, stability was achieved by 2.6 to 2.4 Ga (Kröner, 1982).

On an expanding Earth Proterozoic volcanic and sedimentary sequences were deposited in elongate, well-defined basins representing a global network of intracratonic basin extension (Figure 5.2). The initial stability and increasing mobility during the Proterozoic is reflected in the mathematical modelling of palaeoradius on an expanding Earth (Figure 2.6) where, during the pre-Neoproterozoic, expansion amounted to approximately 60 kilometres increase in radius over a 3 billion year history prior to a steady to rapidly accelerating expansion during the Neoproterozoic to Recent.

The model for Proterozoic tectonic evolution on an expanding Earth involves crustal extension within established zones of intracratonic basement weakness and an increase in intracratonic translational mobility during change in surface curvature.

Ongoing condensation, or segregation of new matter at the core-mantle interface results in mantle swell, which is transferred to the outer crust as extension. Crustal extension then becomes an ongoing and accelerating process throughout Earth history and results in (Figure 5.1):

1. Brittle fracture of the sialic crust providing mantle-tapping conduits for transferral of mantle derived magma, volatiles and metal products;
2. Crustal extension, basement thinning and underplating accompanied by high heat flow and regional metamorphism;
3. Intrusion of granitoids by melting and fractionation of crust during crustal fracture, extension or underplating.

During expansion, the surface of the cratonised Archaean crust is maintained in an elevated or domal state as surface curvature progressively decreases with time. The surrounding intracratonic zones remain isostatically depressed and represent the loci for ongoing basement extension and sedimentation. Erosion of the elevated cratonic regions maintains a low to medium elevation contrast and turbiditic sediments accumulate within an extensive network of intracratonic sedimentary basins. Rift and platform volcanism diminishes with time and the proportion of differentiated volcanics, including andesites, as well as immature sediments is higher than in Archaean suites.

Tectonics during the Proterozoic is ensialic, resulting from intracratonic mobility during differential extension of basins and intracratonic motion during adjustment for change in surface curvature (Section 3.3.10). This occurs along narrow, elongate orogenic zones and is accompanied by bimodal volcanics and granite intrusions. During orogeny the subcrustal mantle may delaminate, causing rifting, heating and post-orogenic extension of the crust during lithospheric thinning over a pre-existing but previously subdued mantle plume. The rise of the asthenosphere enhances gravitational instabilities within the lithosphere resulting in further fracture, crustal stretching and delamination. Hot asthenospheric material rises to replace or mix with the existing lithosphere, resulting in sub-crustal thickening of the crust. The thickened crust is partially melted at depth, intruded by syn- and post-orogenic granites, and is periodically uplifted and subjected to erosion.

The Proterozoic orogenic zones coincide with the established network of intracratonic sedimentary basins and represent a global network of intracratonic crustal weakness (Figure 5.2). Proterozoic extension during Earth expansion is confined to this network and is accompanied by high heat flow from mantle-derived plumes. Polyphase extension-mobility-extension is a prime feature of the expanding Earth tectonic model, extending through to the Palaeozoic, prior to continental crustal rupture during the Early Permian and continental break-up and dispersal during the Mesozoic and Cenozoic to the Recent.

5.6 Phanerozoic Expanding Earth Tectonostratigraphic Evolution

Laznicka (1993) notes that there is no tectono-stratigraphic break between the Proterozoic and Phanerozoic. The Phanerozoic on conventional plate tectonic reconstructions is dominated by the break-up of a Late Proterozoic Rodinia supercontinent, its reassemblage as Gondwana and Pangaea during the Palaeozoic and its subsequent break-up and dispersal to the Recent (Barley & Groves, 1992). The near maximum assembly of Pangaea corresponds with a period of widespread cratonic subsidence and the development of extensive intracontinental sedimentary basins (Kominz & Bond, 1991).

Conventional continental assembly-dispersal-reassembly cyclicity cannot be reconciled on an expanding Earth (Section 2.6; Figures 2.15 to 2.21, and Section 2.7; Figures 2.23 to 2.30). On an expanding Earth the transition from Late Proterozoic to Palaeozoic represents an era of accelerating increase in crustal extension, caused by an increase in matter generation at the core-mantle interface and subsequent increase in mantle swell (Figure 5.1). A limit to crustal extension is reached during the Early Permian resulting in crustal rupture, initiating break-up of Pangaea, formation of distinct continents and continental dispersal during the Mesozoic and Cenozoic. The Phanerozoic tectonostratigraphic history is further complexed by a variance of coastal outlines during eustatic and transgressive-regressive sea-level changes (Section 3.3.3), ensialic orogenesis (Section 3.3.10), mountain building and erosion (Section 3.3.11), and biotic development (Section 3.4).

On an expanding Earth basin sedimentation and tectonism during the Palaeozoic is ensialic and coincides with the established Precambrian intracratonic network of epi-continental basins, orogens and zones of crustal weakness. During the

Palaeozoic pulsed orogenesis increases, caused by periodic gravitationally induced collapse and fragmentation of cratons and Proterozoic orogens during change in surface curvature of the Earth. Intracratonic interaction and translational motion during collapse results in formation of linear orogenic fold belts, mantle plume related orogenic magmatism and metamorphism, prior to a return to basin extension. Continental crustal collapse results in isostatic uplift of orogenic zones, accompanied by underplating, high heat flow, bimodal magmatism and crustal thickening.

During expansion, continental rupture and initiation of continental scale rifting during the Late Palaeozoic is accompanied by a shift in sedimentary deposition from epi-continental to shallow marine and marginal continental basin settings (Section 3.3.4). The influx and admixture of sediments within rift related magmatic zones gives rise to alkaline to perialkaline magmatism and the initiation of island arcs along the emerging continent to oceanic crustal interface. Ongoing extension and continental rupture results in opening of the modern oceans, formation of marginal sedimentary basins, initiation of anorogenic magmatism, orogenesis and mountain building.

Island arcs on an expanding Earth represent Late Palaeozoic to Early Mesozoic zones of continental rupture and break-up and are analogous to modern mid-ocean-rift zones. Initiation is marked by ophiolite related mafic and ultramafic magmatism (eg. Ishiwatari, 1994; Yakubchuk *et al.*, 1994) and calc-silicate chemical sedimentation. The location of island arcs coincides with the global network of Palaeozoic crustal weakness and basin formation established during the Precambrian (Figure 5.2), and represent divergent structures located over a network of mantle plumes. Crustal thickening at island arcs results from an increasing sedimentary input during a shift in sedimentary depocentres (Section 3.3.4) and syn-kinematic magmatic admixture during crustal fracture and extension.

Continental break-up and opening of the modern oceans during the Mesozoic and Cenozoic initiates preservation of mantle derived mafic magmatism along well-defined mid-ocean-rift zones. During the initial break-up phase the sea-floor spreading process is masked by sedimentary input within marginal sedimentary basins. As break-up progresses the mid-ocean-rift magmatism is then preserved as sea-floor crust and oceanic sedimentation is minimal. During sea-floor extension the mantle-derived magmas are intruded along mid-ocean-rift zones and are quenched on contact with seawater to form sub-vertical dyke-like structures within a tensile

tectonic regime. These mid-ocean-rift zones coincide with zones of high heat flow within a global network of mantle plumes.

Figure 5.1 illustrates the mechanics of Phanerozoic Earth expansion. As matter is added at the core-mantle interface mantle swell causes the oceanic crust to extend and fracture along the mid-ocean-rift zones, located over rising mantle plumes. The oceanic magmatism represents exposed upper mantle, which is continuously intruded by fresh mantle-derived magma. The plumes also represent a conduit for mantle-derived volatiles and metal enriched fluids. New mantle magma added during expansion ages radially outwards from the core-mantle interface towards the surface, preserving and adding to deep continental root zones.

Conventional interpretations of convergent margin subduction zones cannot be reconciled on an expanding Earth. On an expanding Earth spherical geometry dictates that divergence at mid-ocean-rift zones is transferred to the continents as convergence. Continental margins represent a significant rheology contrast between thick continental crust and relatively thin oceanic crust. The interaction at continental margins is complex and involves:

1. Formation of elongate trenches along some margins during isostatic depression of the continental margin;
2. Extension of the oceanic lithosphere during expansion, forming back-arc basins;
3. Translational to transpressive crustal interaction between oceanic and continental crust during change in surface curvature;
4. Local obduction or subduction of oceanic crust during collapse of continental interiors accompanied by isostatic uplift of continents along continental margins;
5. Translational fault movement along the crustal plate margins;
6. Elevated heat flow over established mantle plumes;
7. Syn-kinematic magma intrusion and admixture of sediments from marginal basins.

Recent Earth expansion is predominantly confined to mid-ocean-rift zones with minor basin extension and continental rifting during adjustment for change in surface curvature. Elongation of mid-ocean-rift zones continues to break-up both oceanic and continental crust (Section 2.8), focusing seismic activity, heat-flow and magmatism along well-defined zones of crustal weakness.

5.7 Earth Expansion into the Future

A causal model for Earth expansion into the future is speculative and based on observations from mathematical modelling of the kinematics of Earth expansion (Appendix A1). Extrapolation of Earth radius to the future indicates that Earth will approach the radius of the planets Jupiter and Saturn by approximately 500 million years (Appendix A1; Table 1.2). It is speculated that during this time condensation of plasmoidal, or similar material from within the Earth core will decline and degassing of volatiles from the mantle will result in establishment of a giant gaseous planet, devoid of high-order sustainable life forms. During this time Earth, along with all solar planets, will continue to increase its solar radius as angular momentum continues to be transferred from the Sun to the planets.

Expanding Earth modelling studies suggest that in the near future (Figure 2.31) spreading and elongation of mid-ocean-ridge spreading axes will continue, consistent with an increase in Earth circumference with time. Continental crust will continue to break-up and disperse while retaining the same spatial integrity of continents and crustal elements as during the Cenozoic. Seismic activity will remain active during break-up of continental crust and ongoing elongation of spreading axes. Mantle plumes along mid-ocean-rift zones will continue to focus mantle-derived heat, along with magma and volatiles. It is speculated that the atmosphere may eventually extend to form planetary ring structures, similar to the giant planets.

6.0 SUMMARY

The primary objective of this thesis has been to investigate the concept of Earth expansion as an explanation for observed global geological and geophysical data. To achieve this a series of 24 spherical models of an expanding Earth have been created to display and present this global data in an expanding Earth framework. The objectives of the Archaean to Recent expanding Earth models have been to display oceanic and continental geology; to investigate the mathematical constraints of a potential Archaean to Recent Earth expansion; to speculate on expansion of the Earth to the future; to display global geological and geophysical data sets; to apply this information to investigate the geological history of Australia; and to speculate on a proposed causal model for Archaean to future Earth expansion.

A set of twenty four spherical models have been constructed, twenty three covering the Archaean to Recent and one projected to five million years into the future. The primary base map used for construction of each model is the *Geological Map of the World* (CGMW & UNESCO, 1990) (Figure 2.1), which provides a comprehensive global coverage of both continental and oceanic time-based geology. The construction of these models relies on the fundamental premise that crustal lithosphere is cumulative with time, and historical markers preserved in the oceanic and continental geology represent a means to accurately constrain both palaeoradius and plate reconstruction from the Archaean to Recent.

Post-Triassic oceanic magnetic mapping demonstrates that all oceans are increasing their surface areas away from the mid-ocean-ridges, including the Pacific Ocean, which has traditionally been considered a sink for disposal of excess lithosphere generated within each of the remaining oceans. Conventional plate reconstructions on a static radius Earth (eg. Scotese *et al*., 1988; Müller *et al*., 1997) consistently show an increasing misfit, moving backwards in time, along each of the mid-ocean-ridge plate margins with a requirement for the introduction of presumed, pre-existing lithosphere to maintain a constant surface area.

Post-Triassic models of an expanding Earth have been reconstructed by successive removal of older geological Periods paralleling the active mid-oceanic spreading ridges and restoring plates to a pre-spreading, or pre-extension configuration along each plate or continental margin respectively, at a reduced Earth

radius. During the Triassic, continents envelope the Earth as a complete continental shell and marginal and epi-continental sedimentary basins merge to form a global network surrounding continental cratons and orogenic zones. Reconstructing post-Triassic oceanic lithosphere on expanding Earth models results in a plate fit-together along each mid-ocean-ridge plate margin at better than 99% fit. This unique fit-together empirically demonstrates that post-Triassic Earth expansion is a viable process and justifies extending modelling to the Archaean.

Quantification of an Earth expansion process back to the Archaean requires an extension of the fundamental cumulative lithospheric premise to include continental crust. Continental crust is reconstructed on Pre-Jurassic models using the primary crustal elements cratons, orogens and basins, with expansion primarily manifested as crustal extension within an established network of epi-continental rifts, orogens and sedimentary basins. Moving backwards in time, extension is progressively restored to a pre-extension, pre-orogenic or pre-rift configuration by removing young sedimentary rocks and continental magmatism. During this process the integrity of orogens is retained until restoration to a pre-orogenic configuration is required and the integrity of cratons is retained until all pre-orogenic and non-orogenic basin sediments and continental magmatism are removed. By removing all basin and pre-orogenic sediments a primordial proto-Earth at a palaeoradius of approximately 1700 kilometres is achieved during the Mesoproterozoic, comprising assembled cratons and Proterozoic basement rocks.

Pre-Jurassic expanding Earth models demonstrate that each of the continental tectonic regimes comprising cratons, orogens and basins has maintained spatial integrity throughout the Precambrian and Palaeozoic, prior to Late Palaeozoic continental rupture, break-up and dispersal of continents to the Recent. From an Archaean and Early Proterozoic crustal assemblage of cratons and orogenic basement rocks, a network of Proterozoic intracratonic sedimentary basins coinciding with orogenic basement rocks is established (Figure 5.1). This network represents zones of primary crustal weakness and forms the loci for ongoing continental crustal extension, basin sedimentation and intracratonic mobility during the Proterozoic and Palaeozoic, and represents the loci for continental break-up and opening of the modern oceans during the post-Permian.

Mathematical modelling of oceanic and continental surface area data demonstrates that the Earth is undergoing an exponential increase in palaeoradius,

commencing from a primordial Earth of approximately 1700 kilometres radius during the Early Proterozoic. The current rate of increase in Earth radius is calculated to be 22 mm/year. Earth expansion during the Archaean to Late Mesoproterozoic is shown to increase by approximately 60 kilometres during 3 billion years of Earth history, prior to a steady to rapidly accelerating increase in Earth radius during the Neoproterozoic to Recent. Extrapolating Earth expansion to the future demonstrates that expansion to 5 million years in the future is consistent with a continued spreading and elongation of all present-day mid-ocean-ridge axes.

In contrast to conventional geophysical constrained plate tectonic reconstructions Precambrian and Palaeozoic expanding Earth reconstructions are geologically constrained by the spatial configuration of continental tectonic regimes. Similarly, during the Mesozoic and Cenozoic all continents are latitudinally and longitudinally constrained by oceanic geology, which can be further extrapolated to the future. To quantify an Earth expansion process, comprehensive studies in space geodetics, palaeomagnetics, palaeogeography, palaeobiogeography, palaeoclimate and metallogeny have been used to investigate the spatial and temporal distribution of global geological and geophysical data within a conceptual expanding Earth tectonic framework.

Modelling of palaeomagnetic and space geodetic data shows that, by removing the imposed constant surface area and constant radius premises from geophysical observations the data is consistent with Earth expansion. In particular the published palaeomagnetic data of McElhinny & Lock (1996), when used to plot palaeopoles on expanding Earth models, results in a cluster of diametrically opposed north and south geocentric magnetic palaeopoles for each expanding Earth model (Figures 3.13 and 3.14). These show that the north palaeopole was located in eastern Mongolia-China during the Precambrian and Palaeozoic and, as the continents slowly migrated south during expansion there was an apparent northward polar wander through Siberia to its present location within the Arctic Ocean. The Precambrian and Palaeozoic south palaeopole was located in west central Africa and, as the continents slowly migrated north there was an apparent southward polar wander along the South American and west African coastlines to its present location in Antarctica.

Geographical and biogeographical data sets, when applied to expanding Earth models quantify the location of palaeopoles and palaeoequators determined from

unconstrained palaeomagnetic data. The distribution of latitude dependent lithofacies including glacials, carbonates and coal, and faunal and floral species is shown to coincide precisely with established palaeopoles and palaeoequators for all expanding Earth models. For climatic and biotic indicators a distinct latitudinal zonation paralleling the established palaeoequator is evident and a distinct northward shift in climatic zonation suggests that an inclined Earth rotational axis, inclined to the pole of the ecliptic, was well established during the Palaeozoic, persisting to the Recent.

Coastal geography on expanding Earth models shows that large Panthallassa, Tethys and Iapetus Oceans are not required during reconstruction. These oceans are replaced by epi-continental Panthallassa, Iapetus and Tethys Seas, which represent precursors to the modern Pacific and Atlantic Oceans and present Eurasian continent. Emergent land surfaces during the Precambrian and Phanerozoic equate to the conventional Rodinian, Gondwanan and Pangaean supercontinents and smaller sub-continents, and demonstrate a spatial intracratonic and intracontinental integrity throughout Earth history. On each model proto-continental development is progressive, with no requirement for random dispersion-amalgamation cycles. Supercontinent configuration is then defined by a progressive extension of epi-continental sedimentary basins, pulsed orogenesis, eustatic and transgression-regression of epi-continental seas, and opening of modern oceans during the Mesozoic to Recent.

Eustatic and transgressive-regressive marine sea-level cycles on an expanding Earth are shown to occur in response to climatic change, to a shift in the distribution of epi-continental seas, orogenesis, mountain building, erosion, opening of post-Permian modern oceans and generation of new juvenile water at mid-ocean-ridges. The variance of these changes to the palaeocoastal outlines results in a change in exposed continental land, coastal transgressive and regressive events, distribution of latitude-dependant sedimentary facies, latitudinal and provincial distribution of biotic taxa and tectonostratigraphic histories.

Orogenesis on an expanding Earth is represented by zones of intracratonic to intracontinental interaction, resulting from gravity induced collapse and partial rotation of cratons and proto-continents as they adjust for changing surface curvature. Tangentially directed crustal motion during this collapse and re-equilibration is manifested as intracratonic to intracontinental rotation, localised within epi-continental sedimentary basins and accompanied by regional

synkinematic metamorphism and magmatism. This periodic rotational motion gives rise to long linear and interconnected orogenic belts surrounding each of the primary cratons or proto-continents, with polyphase motion resulting in an extension-orogenesis-extension cyclicity.

A distinction is made between orogeny, which deals with formation of fold belts, and mountain building, which results in vertical uplift to form plateaus. Change in surface curvature during Earth expansion gives a prime mechanism for mountain building where continental interiors initially remain elevated, or arched relative to the intracratonic basins or continental margins. Periodic gravitational collapse of the continental interiors results in isostatic uplift and associated block faulting of the continental margins, forming mountain escarpments. This process becomes cyclical during ongoing expansion, resulting in multiple and overlapping phases of mountain building, planation, sedimentation, uplift and erosion.

The distribution of selected faunal and floral taxa on palaeogeographic expanding Earth models demonstrates the distribution in relation to established palaeogeography, palaeopoles and palaeoequators. The palaeobiogeographic faunal and floral examples used illustrate the ease and simplification of migration and biogeographical development on an expanding Earth. Cosmopolitan and provincial distributions and inter-relationships are maintained, without the need for conventional continental assemblage-dispersal requirements. During continental break-up and opening of the modern oceans traditional migration routes are then disrupted, enabling taxa endemic to the various regions to interact and extend their boundaries with time. The timing of faunal and floral development is then reflected in eustatic and transgressive-regressive sea-level cycles, facilitating evolution, migration or extinction by extending or destroying habitats and migration routes and modifying climate.

Metallogeny on an expanding Earth is considered in the context of metallogenic epochs and metallogenic provinciality. The distribution of ore deposits and the nature and styles of mineralization in time and space suggests that there has been an evolutionary trend in the concentration of metals, as well as diversity in morphological types of mineral occurrences. Metallogenic modelling of Precambrian and Phanerozoic metal deposits shows a broad global Precambrian metallogenic provinciality coinciding with cratons and intracratonic settings, to regional provinces clustering as specific metal associations. The Phanerozoic metallogenic distribution

highlights the abundance of porphyry and granite associated metals concentrated within Phanerozoic orogenic belts. On an expanding Earth these Phanerozoic orogenic belts crosscut and displace pre-existing Palaeozoic and Precambrian metallogenic provinces and a common mantle source for various metal associations is evident.

The conceptual expanding Earth framework established from modelling is used to investigate the spatial and temporal tectonostratigraphic history of Australia. Australia is located adjacent to Archaean cratons and Proterozoic and Phanerozoic terranes from China, North America, South America and East Antarctica. Much of Australia has been largely intact since about 2.5 Ga and most subsequent orogenic activity has been ensialic (Rutland, 1973; Etheridge *et al*., 1987; Wyborn, 1988). A distinct tectonic directional grain recognised in the Yilgarn Craton (Rutland *et al.*, 1990) parallels the directional grain in the Canadian Churchill and Superior Provinces. This is consistent with oblique east-west (Precambrian orientation) crustal extension between the Australian Archaean Superprovinces and the Canadian Archaean Slave, Churchill and Superior Provinces, followed by oblique ensialic translational motion during a global-wide Palaeoproterozoic Barramundi and later orogenic events.

North and east Australian Middle Proterozoic orogenic events are aligned with the Grenville Orogenic event of eastern North America and the Tasman event of eastern Australia. On an expanding Earth, the Tasman Superprovince is intracratonic to the Central Australian Proterozoic terranes, the Amazon Craton of South America and remnant terranes in Central America, and extends to include Palaeozoic basins in southeast North America, West Antarctica and southern South America. Development of the superprovince represents an extended period of crustal divergence and intracratonic basin sedimentation between Australia and South America during Earth expansion.

A causal model for Earth expansion is based on a study of the kinematics of the Earth (Section 2.3 and Appendix A1), which suggests that expansion is caused by an exponential increase in mass with time. Carey (1983a, 1996) concludes that matter is being created deep within Earth's core, in sympathy with creation and expansion of matter within the Universe. The proposed causal model for Earth expansion involves an increase in mass by condensation, or segregation of new matter from the Earth's core. This new matter accumulates at the core-mantle

interface and the increase in volume results in a swelling of the mantle. Mantle swell is then manifested in the outer crust as continental crustal extension and extension along the mid-ocean-rift zones. Matter generation within the Earth's core is seen as an endothermic reaction, which will ultimately result in a decay of the matter formation process within the core and cessation of expansion with time.

On an expanding Earth causal model the pre-Archaean Earth-Moon was an incandescent mass ejected from the surface of a primitive young Sun. Gravitational instability resulted in separation of the Earth and Moon, forming a binary planet with high surface temperatures and elevated geothermal gradients. By the Early Archaean surface temperatures were sufficiently low to allow solidification of a thin sialic crust on Earth. During the Early Archaean the Earth mantle retains a high global geothermal gradient and hot, mantle-derived surface water pools within low-lying surface depressions. The survival of a 30 to 40 kilometre thick Archaean crust on the present Earth implies the stabilisation of a subcrustal root-zone not less than 200 kilometres thick during the Early Archaean (Wells, 1981).

By the Late Archaean cratonisation of the Earth's crust was complete and basin extension during expansion results in large, stable platforms with a low elevation contrast between continents and seas. The Proterozoic represents an epoch of comparative crustal stability and increasing mobility, with volcanic and sedimentary sequences deposited within well defined, elongate basins representing a global network of intracratonic basin extension. Polyphase extension-mobility-extension is a prime feature of the Precambrian Earth causal model, extending through to the Palaeozoic, prior to continental crustal rupture during the Early Permian and continental break-up and dispersal during the Mesozoic and Cenozoic to the Recent.

7. CONCLUSIONS

While the extensive spherical model studies presented in this thesis empirically demonstrate that the concept of an expanding Earth is a viable global tectonic process, the problem of where the excess mass comes from remains a very real enigma. These conclusions, therefore, are simply based on the observations made from the published global geological and geophysical data.

Reconstructions of oceanic and continental geology on models of an expanding Earth demonstrate that crustal plates can be latitudinally and longitudinally constrained with only one plate fit-option on an Earth at reduced palaeoradii. Post-Triassic reconstructions of crustal plates constrained by oceanic magnetic mapping consistently show a plate fit-together at better than 99% fit for all plates. Pre-Jurassic crustal reconstructions demonstrate that all continental tectonic regimes retain a spatial integrity throughout a Precambrian and Palaeozoic phase of crustal extension, prior to Late Palaeozoic continental rupture, Mesozoic continental break-up and dispersal to the Recent.

Mathematical modelling of crustal surface area data provides a means to accurately qualify a rate of change of palaeoradius from the Archaean to Recent. The Earth is shown to be undergoing an exponential increase in palaeoradius, commencing from a primordial Earth of approximately 1700 kilometres radius during the Early Proterozoic. The current rate of increase in Earth radius is calculated to be 22 millimetres per year. Extrapolation of radius to the future suggests that the Earth will increase to the size of Jupiter within approximately 500 million years.

The use of published palaeomagnetic data to locate palaeopoles demonstrates that, by removing imposed constant surface area and constant radius premises from observational data, palaeomagnetic pole data plot as diametrically opposed north and south palaeopoles for each expanding Earth model. Throughout the Precambrian and Palaeozoic, the North Pole is located in Mongolia-China and the South Pole is located in west Africa, prior to migration of continents to their present locations.

Modelling of the published space geodetic data shows that horizontal plate motion is consistent with plate motion on an expanding Earth and consistent with plate motion defined by oceanic magnetic mapping. Vertical plate motion studies of observation stations show that large periodic adjustments to Earth radius are not

consistent with published estimates of plate motion, quoted to sub-centimetre accuracy and cannot be used to determine Earth expansion.

The distribution of global geological and geophysical data in relation to reconstructed geology, established palaeoequators and palaeogeographical grids demonstrate that palaeogeographic, palaeobiogeographic, palaeoclimatic and metallogenic data collectively quantify an Earth expansion process. Each geological and geophysical discipline is shown to be inter-related, with no cross-discipline inconsistencies.

Palaeogeographic data quantify the distribution of epi-continental Panthallassa, Iapetus and Tethys Seas and surrounding emergent Rodinia, Gondwana and Pangaea supercontinents and smaller sub-continents during the Precambrian and Phanerozoic. Palaeobiogeographic studies demonstrate a consistency in cosmopolitan and provincial biotic distribution coincident with geographic and climatic constraints. Palaeoclimatic indicators demonstrate a climatic zonation consistent with palaeomagneticly-determined palaeopoles and palaeoequators, with a northward zonal offset suggesting an inclined Earth rotational axis. Metallogeny demonstrates a provincial distribution of metal associations consistent with distribution of tectonostratigraphic terranes and consistent with post-Palaeozoic tectonism and continental break-up.

The geological history of Australia in relation to adjacent continents is consistent with intracontinental palaeomagnetic, tectonostratigraphic and lithostratigraphic constraints. Intracratonic and intracontinental tectonostratigraphic relationships are maintained and metallogenic distribution demonstrates a spatial and temporal provincialism of metal associations across continental boundaries.

A proposed causal mechanism for Earth expansion, from the pre-Archaean to Recent, suggests that cooling of an incandescent pre-Archaean Earth enabled a primitive crust, hydrosphere and atmosphere to form during the Early Archaean. It is speculated that Earth expansion results from matter generation at the core-mantle interface. The increase in matter results in mantle swell, which in turn causes crustal extension. During the Late Palaeozoic the capacity for the crust to extend was exceeded causing rupture, continental break-up and dispersal to the Recent.

Despite the enigmatic origin for the excess mass required for expansion global geological and geophysical data quantify and substantiate an Archaean to Recent Earth expansion process. This cannot be mere coincidence.

REFERENCES

AHMAD F. 1988. Estimates of palaeodiameters of the Earth through geological time. *Journal of the Geological Society of India* **31**, 386-397.

ANDERSON A. T. 1975. Some basaltic and andesitic gases. *Reviews of Geophysics and Space Physics* **13**, number 1, 37-55.

ANHAEUSSER C. R. 1981. The relationships of mineral deposits to early crustal evolution. *Economic Geology*, 75th Anniversary Volume, 42-62.

ARCHBOLD N. W. 1994. Gondwana and the complex of Asia during the Permian: The importance of palaeobiogeographical studies. *Ninth International Gondwana Symposium, Hyderabad, India*, 479-489.

ARGUS D. F. 1996. Postglacial rebound from VLBI geodesy: on establishing vertical reference. *Geophysical Research Letter*, **23**, 973-976.

AUDLEY-CHARLES M. G., BALLANTYNE P. D. & HALL R. 1988. Mesozoic Cenozoic rift-drift sequence of Asian fragments from Gondwanaland. *Tectonophysics* **155**, 317-330.

BARLEY M. E., EISENLOHR B., GROVES D. I., PERRING C. S. & VEARCOMBE J. R. 1989. Late Archaean convergent margin tectonics and gold mineralisation: a new look at the Norseman-Wiluna Belt, Western Australia. *Geology* **17**, 826-829.

BARLEY M. E. & GROVES D. I. 1992. Supercontinent cycles and the distribution of metal deposits through time. *Geology* **20**, 291-294.

BARNETT C. H. 1962. A suggested reconstruction of the land masses of the Earth as a complete crust. *Nature* **195**, 447-448.

BARNETT C. H. 1969. Oceanic rises in relation to the expanding Earth hypothesis. *Nature* **221**, 1043-1044.

BARNICOAT A. C., FARE R. J., GROVES D. J. & McNAUGHTON N. J., 1991. Synmetamorphic Code-gold deposits in high-grade Archaean settings. *Geology* **19**, 921-924.

BARNES C. R. 1999. Paleoceanography and paleoclimatology: an Earth system perspective. *Chemical Geology* **161**, 17-35.

BARRON E. J. 1983. A warm, equable Cretaceous: the nature of the problem. *Earth Science Reviews* **19**, 305-338.

BELL R. T. & JEFFERSON C. W. 1987. An hypothesis for an Australian-Canadian connection in the Late Proterozoic and the birth of the Pacific Ocean. Pacific Rim Congress 87. *Australasian Institute of Mining and Metallurgy*. 39-50.

BENTON M. J. 1990. Origin and interrelationships of dinosaurs. *In*: Weishampel D. B., Dodson P. & Osmólska H. eds. 1990. *The Dinosauria*. University of California Press, Los Angeles, 11-30.

BERNER R. A. 1987. Models for carbon and sulphur cycles and atmospheric oxygen: Application to Paleozoic geologic history. *American Journal of Science* **287**, 177-196.

BERNER R. A. 1991. A model for atmospheric CO_2 over Phanerozoic time. *American Journal of Science* **291**, 339-376.

BEUTLER G., HEIN G. W., MELBOURNE W. G. & SEEBER G. 1995. eds. GPS trends in precise terrestrial, airborne, and spaceborne applications. *Symposium* No. **115**, Boulder, USA.

BIANCO G., DEVOTI R., FERMI M., LUCERI V., RUTIGLIANO P. & SCIARRETTA C. 1998. A contribution in the estimation of tectonic motion in crutial areas: the CGS96 SLR solution. *Tectonophysics* **294**, 225-236.

BLAKE T. S. & McNAUGHTON N. J. 1984. A geochronological framework for the Pilbara region. *In:* Muhling J. R., Groves D. I. & Blake T. S. eds. *Archaean and Proterozoic Basins of the Pilbara, Western Australia: Evolution and mineralization potential.* University of Western Australia Geology Department and University Extension Publication **9**, 1-22.

BLATT H. & JONES R. L. 1975. Proportions of exposed igneous, metamorphic and sedimentary rocks. *Geological Society of America Bulletin* **86**, 1085-1088.

BLEWITT G. 1993. Advances in global positioning system technology for geodynamics investigations: 1978-1992. *In*: Smith D. E. & Turcotte D. L. eds. *Contributions of space geodesy to geodynamics: technology*. Geodynamics Series **25**, American Geophysical Union, Washington, USA, 195- 213.

BLINOV V. F. 1973. Problems of possible Earth evolution (a discussion). Academy of Science, Ukraine S.S.R., *Geophysical Series* **54**, 85. (in Russian).

BLINOV V. F. 1983. Spreading rate and rate of expansion of the Earth. *In:* Carey S.W. ed. *Expanding Earth Symposium, Sydney, 1981*. University of Tasmania, 297-304.

BIGG G. R. 1996. *The oceans and climate.* Cambridge University Press, Cambridge.

BRENCHLEY P. J. 1989. The Late Ordovician extinction. *In*: Donovan S. K. ed. *Mass Extinctions*. Columbia University Press, New York, 104-132.

BRIGGS J. C. 1995. *Global Biogeography.* Developments in Palaeontology and Stratigraphy **14**, Elsevier, Amsterdam.

BROWN D. A., CAMPBELL K. S. W. & CROOK K. A. W. 1968. *The geological evolution of Australia & New Zealand.* Pergamon Press, London.

BURG J-P. & FORD M. 1997. Orogeny through time: an overview. In: Burg J-P. & Ford M. eds. *Orogeny through time.* Geological Society Special Publication **121**, 1-17.

BURKE K. & DEWEY J. F. 1973. An outline of Precambrian plate development. *In*: Tarling D. H., & Runcorn S. K. eds. *Implications of continental drift to the Earth sciences*, Volume 2. Academic Press, 1035-1045.

BUTLER R. F. 1992. *Paleomagnetism: Magnetic Domains to Geologic Terranes.* Blackwell Scientific Publications, USA.

CALDER J. H. & GIBLING M. R. 1994. The Euramerican coal province: controls on Late Paleozoic peat accumulation. *Palaeogeography, Palaeoclimatology, Palaeoecology* **106**, 1-21.

CAPUTO M. V. & CROWELL J. C. 1985. Migration of glacial centres across Gondwana during Paleozoic Era. *Geological Society of America Bulletin* **96**, 1020-1036.

CAREY S. W. 1958. The tectonic approach to continental drift. *In: Continental Drift, a Symposium.* University of Tasmania, Hobart, 177-355.

CAREY S. W. 1975. The expanding Earth - an essay review. *Earth Science Reviews* **11**, 105-143.

CAREY S. W. 1976. *The Expanding Earth.* Elsevier, Amsterdam.

CAREY S. W. 1983a. Earth expansion and the null Universe. *In:* Carey S.W. ed. *Expanding Earth Symposium, Sydney, 1981*. University of Tasmania, 365-372.

CAREY S. W. 1983b. The necessity for Earth expansion. *In:* Carey S.W. ed. *Expanding Earth Symposium, Sydney, 1981*. University of Tasmania, 375-393.

CAREY S. W. 1988. *Theories of the Earth and Universe*: A History of Dogma in the Earth Sciences. Stanford University press, Stanford, California.

CAREY S. W. 1996. *Earth, Universe, Cosmos.* University of Tasmania, Hobart.

CEBULL S. E. & SHURBET D. H. 1992. Conventional plate tectonics and orogenic models. *In:* Chatterjee S. & Hotton N (III) eds. *New Concepts in Global Tectonics.* Texas Technical Press, USA, 111-117.

CGMW & UNESCO 1990. *Geological Map of the World*. Commission for the Geological Map of the World, Paris.

CHAPPELL B. W., WHITE A. J. R. & HINE R. 1988. Granite provinces and basement terranes in the Lachlan Fold Belt, southeastern Australia. *Australian Journal of Earth Sciences* **35**, 505-521.

CHATTERJEE S. 1992. A kinematic model for the evolution of the Indian plate since the Late Jurassic. *In*: Chatterjee S. & Hotton N. (III) eds. 1992. *New Concepts in Global Tectonics.* Texas Technical Press, USA, 33-62.

CHATTERJEE S. & HOTTON N. (III) eds. 1992. *New Concepts in Global Tectonics.* Texas Technical Press, USA.

CHUMAKOV N. M. & ELSTON D. P. 1989. The paradox of Late Proterozoic glaciations at low latitudes. *Episodes* **12**, 115-1120.

CHUMAKOV N. M. & KRASIL'NIKOV S. S. 1992. Lithology of Riphean tilloids: Urinsk uplift area, Lena region. *Lithology and Mineral Resources* **26**, 249 264.

CIRIC B. M. 1983. The Mediterranean Tethys in Alpine time - evidence for Earth expansion. *In:* Carey S. W. (ed), *Expanding Earth Symposium, Sydney, 1981*. University of Tasmania, 149-160.

CLARKE I.F. & COOK B.J. 1983. *Perspectives of the Earth.* Australian Academy of Sciences, Canberra.

COCKBAIN A. E. & HOCKING R. M. 1990. Phanerozoic. *In: Geology and mineral resources of Western Australia.* Western Australia Geological Survey, Memoir **3**, 750-756.

COCKS L. R. M. & FORTEY R. A. 1990. Biogeography of Ordovician and Silurian faunas. *In*: McKerrow W. S. & Scotese C. R. eds. *Palaeozoic palaeogeography and biogeography*, Geological Society Memoir **12**, 97-104.

COLBERT E. H. 1965. The age of the reptiles. W. W. Norton & Company, Inc. USA.

CONDIE K. C. 1981. Geochemical and isotopic constraints on the origin and source of Archaean granites. Special Publication **7**, *Geological Survey of Australia*, 469-480.

CONDIE K. C. 1989. *Plate Tectonics and Crustal Evolution.* Third edition. Pergamon Press.

COX A. & DOELL R. R. 1961. Palaeomagnetic evidence relevant to a change in the Earth's radius. *Nature* **189**, 45-47.

COX C. B. 1990. New geological theories and old biogeographical problems. *Journal of Biogeography* **17**, 117-130.

COX D. P. & SINGER D. A. 1992. eds. *Mineral deposit models*. U. S. Geological Survey Bulletin **1693**. United States Government printing office, Washington.

CREER K. M., IRVING E. & RUNCORN S. K. 1954. The direction of the geomagnetic field in remote epochs in Great Britain. *Journal of Geomagnetics and Geoelectricity* **6**, 163-168.

CRÉTAUX J-F., SOUDARIN L., CAZENAVE A. & BOUILLÉ F. 1998. Present day tectonic plate motions and crustal deformations from DORIS space system. *Journal of Geophysical Research* **103**, 30167-30181.

CROSSLEY D. J. & STEVENS R. K. 1976. Expansion of the Earth due to a secular decrease in G - evidence from Mercury. *Canadian Journal of Earth Science* **13**, 1723-1725.

CROWLEY T. J. & BAUM S. K. 1992. Modeling late Paleozoic glaciation. *Geology* **20**, 507-510.

CROWLEY T. J. & NORTH G. R. 1991. *Paleoclimatology*. New York, Oxford University Press.

CROWLEY T. J. 1994. Pangean climates. *In*: Klein G. D. ed. Pangea: paleoclimate, tectonics, and sedimentation during accretion, zenith, and breakup of a supercontinent. *Geological Society of America Special Paper* **288**, 25-39.

DACHILLE F. 1977. Meteorites - little and big: from shooting stars to Earth shaking catastrophes. *Earth and Mineral Sciences* **46**, 49-52.

DACHILLE F. 1983. Great meteorite impacts and global geological responses. *In:* Carey S. W. ed, *Expanding Earth Symposium, Sydney, 1981*. University of Tasmania.

DALZIEL I. W. D. 1991. Pacific margins of Laurentia and East Antarctica-Australia as a conjugate rift pair: Evidence and implications for an Eocambrian supercontinent. *Geology* **19**, 598-601.

DALZIEL I. W. D. 1992. On the organization of American plates in the Neoproterozoic and the breakout of Laurentia. *Geological Survey of America Today* **2**, 237-241.

DALZIEL I. W. D. 1997. Neoproterozoic-Paleozoic geography and tectonics: review, hypothesis, environmental speculation. *Geological Society of America Bulletin* **109**, 16-42.

DALZIEL I. W. D., DALLA SALDA H. & GAHAGEN L. M. 1994. Paleozoic Laurentia-Gondwana interaction and the origin of the Appalachian-Andean mountain system. *Geological Society of America Bulletin* **106**, 243-252.

DALZIEL I. W. D., MOSHERS S. & GAHAGAN L. M. 2000. Laurentia-Kalahari collision and the assembly of Rodinia. *The Journal of Geology* **108**, 499-513.

DAVIDSON J. K. 1983. Tethys and Pacific stratigraphic evidence for an expanding Earth. *In:* Carey S. W. (ed), *Expanding Earth Symposium, Sydney, 1981*. University of Tasmania, 191-197.

DAVIES R. D. & STREBECK J. W. 1982. Old continental geotherms: Constraints on heat production and thickness of continental plates. *Geophysical Journal of the Royal Astrological Society* **69**, 623-634.

DEARNLEY R. 1965. Orogenic fold-belts and continental drift. *Nature* **206**, 1083 1087.

DEGNAN J. J. 1993. Millimeter accuracy Satellite Laser Ranging: a review. *In*: Smith D. E. & Turcotte D. L. eds. *Contributions of space geodesy to geodynamics: Technology*. Geodynamics Series, Volume **25**. American Geophysical Union, 133-162.

DeMETS C., GORDON R. G., ARGUS D. F. & STEIN S. 1990. Current plate motions. *Geophysical Journal International* **101**, 425-478.

DERCOURT J., RICOU L. E. & VRIELYNCK B. eds. 1993. *Atlas Tethys palaeoenvironmental maps*. Gauthier-Villars, Paris.

DERRY D. R. 1980. *A concise world atlas of geology and mineral deposits.* Mining Journal Books Ltd, London.

De WIT M., JEFFERY M., BERGH H. & NICOLASEN L. 1988. Geological map of sectors of Gondwana reconstructed to their disposition 150 Ma ago: Lambert equal area projection. *American Association of Petroleum Geologists.*

De WIT M. J., ROERING C., HART R. J., ARMSTRONG R. A., De RONDE C. E., GREEN R. W. E., TREDOUX M., PEBERDY E. & HART R. A. 1992. Formation of an Archaean continent. *Nature* **357**, 553-556.

DEYNOUX M., MILLER J. M. G., DOMACK E. W., EYLES N., FAIRCHILD I. J. & YOUNG G M. eds. 1994. International Geological Correlation Program Project 260: *Earth's Glacial Record*. Cambridge University Press.

DICKE R.H. 1962. The Earth and cosmology. *Science* **138**, 653-664.

DICKINS J. M., CHOI D. R. & Yeates A. T. 1992. Past distribution of oceans and continents. *In:* Chatterjee S. & Hotton N (III) eds. *New Concepts in Global Tectonics.* Texas Technical Press, USA, 193-199.

DODSON P. & TATARINOV L. P. 1990. Dinosaur extinction. *In*: Weishampel D. B., Dodson P. & Osmólska H. eds. 1990. *The Dinosauria*. University of California Press, Los Angeles, 55-62.

DRUMMOND B. J. & COLLINS C. D. N. 1986. Seismic evidence for underplating of the lower continental crust of Australia. *Earth and Planetary Science Letters* **79**. 361-372.

Du TOIT A. L. 1937. *Our wandering continents, an hypothesis of continental drifting*. Oliver & Boyd Ltd., Edinburgh.

DUNN P. J. & TORRENCE M. H. 1993. Vertical positioning at laser observatories. *In*: Smith D. E. & Turcotte D. L. eds. Contributions of Space Geodesy to Geodynamics: Crustal Dynamics. Geodynamics Series, Volume **23**. *American Geophysical Union.*

EAGLE M. K. 1993. A dinosaur? record. Geological Society of New Zealand Newsletter 101, 40-43.

EDWARDS R. & ATKINSON K. 1986. *Ore deposit geology and its influence on mineral exploration*. Chapman and Hall Ltd. University Press, Cambridge.

EGGLER D. H. 1987. Solubility of major and trace elements in mantle metasomatic fluids: experimental constraints. *In:* Menzies M. A. & Hawkesworth C. J. eds, *Mantle Metasomatism*. Academic Press, London. 21-41.

EGYED L. 1956. The change in the Earth's dimensions determined from palaeogeographical data. *Geofisica Pura Applica* **33**, 42-48.

EGYED L. 1960. Some remarks on continental drift. *Geofisica Pura Applica* **45**, 115-116.

EGYED L. 1963. The expanding Earth? *Nature* **197**, 1059-1060.

ERWIN D. H. 1993. *The great dying: life and death in the Permian*. Columbia University Press, New York.

ETHERIDGE M. A., RUTLAND R. W. R. & WYBORN L. A. I. 1987. Orogenesis and tectonic processes in the Early to Middle Proterozoic of Northern Australia. *In:* Kröner A. ed. *Proterozoic lithospheric evolution, Geodynamics Series* **17**, Geological Society of America, 131-147.

EVANS A. M. 1984. *An introduction to ore geology*. Blackwell Scientific Publications, Oxford.

EYLES N. & YOUNG G. M. 1994. Geodynamic controls on glaciation in Earth history. *In*: Deynoux M., Miller J. M. G., Domack E. W., Eyles N., Fairchild I. J. & Young G. M. eds. International Geological Correlation Program Project 260: *Earth's Glacial Record.* Cambridge University Press, 1-28.

FAIRCHILD I. J. 1994. Balmy shores and icy wastes: the paradox of carbonates associated with glacial deposits in Neoproterozoic times. *In*: Wright V. P. ed. *Sedimentology Review* **1**, 1-15.

FANALE F. P. 1971. A case for catastrophic early degassing of the Earth. *Chemical Geology* **8**, 79-105.

FAURE K., DeWIT M. J. & WILLIS J. P. 1994. Late Permian global coal discontinuity and Permian-Triassic boundary "events". *Ninth International Gondwana Symposium*. Hyderabad, India, 1994, 1075-1089.

FLÜGEL E. 1994. Pangean shelf carbonates: Controls and paleoclimatic significance of Permian and Triassic reefs. *In*: Klein, G. D. ed. *Pangea: paleoclimate, tectonics, and sedimentation during accretion, zenith, and breakup of a supercontinent.* Geological Society of America Special Paper **288**, 247-266.

FRAKES L. A., FRAKES J. E. & SYKTUS J. I. 1992. Climate models of the Phanerozoic. Cambridge, Cambridge University Press.

FRANCIS J. E. & FRAKES L. A. 1993. Cretaceous climates. *Sedimentology Review* 1993. 17-28.

GAÁL G. 1992. Global Proterozoic tectonic styles and Early Proterozoic metallogeny. *South African Journal of Geology* **95**, 80-87.

GAHAGAN L. M., SCOTESE C. R., ROYER J. Y., SANDWELL D. T., WINN J. K., TOMLINS R. L., ROSS M. I., NEWMAN J. S., MULLER R. D., MAYES C. L., LAWVER L. A. & HEUBECK C. E. 1988. Tectonic fabric map of the ocean basins from satellite altimetry data. *Tectonophysics* **155**, 1-26.

GARFUNKEL Z. 1975. Growth, shrinking, and long-term evolution of plates and their implications for the flow pattern in the mantle. *Journal of Geophysical Research* **80**, 4425-4432.

GASTIL G. 1960. The distribution of mineral dates in time and space. *American Journal of Science* **258**, 1-35.

GEALEY W. K. 1988. Plate tectonic evolution of the Mediterranean-Middle East region. *Tectonophysics* **155**, 285-306.

GILBERT G. K. 1890. *Lake Bonneville*. United States Geological Survey, Monograph 1.

GLIKSON A. Y. 1979. The missing Precambrian crust. *Geology* **7**, 449-454.

GLIKSON A. Y. 1993. Asteroids and early Precambrian crustal evolution. *Earth Science Reviews* **35**, 285-319.

GOODWIN A. M. 1982. Distribution and origin of Precambrian banded iron formation. *Revista Brasileira de Geociências* **12**, 457-462.

GRANT A. C. 1992. Intracratonic tectonism: key to the mechanism of diastrophism. *In:* Chatterjee S. & Hotton N. (III). eds. *New Concepts in Global Tectonics.* Texas Technical University Press, 65-73.

GRAY G. G. & NORTON I. O. 1988. A palinspastic Mesozoic plate reconstruction of New Zealand. *Tectonophysics* **155**, 391-399.

GRIFFIN T. J. & GREY K. 1990. Kimberley Basin. *In: Geology and mineral resources of Western Australia.* Western Australia Geological Survey, Memoir **3**, 293-304.

GROVES D. I. 1982. The Archaean and earliest Proterozoic evolution and metallogeny of Australia. *Revista Brasileira de Geociências* **12**, 135-148.

GROVES D. I. 1988. (Abstract) Tectonic setting and genesis of Archaean gold deposits in the Western Australian Shield. Australian Bicentenary Meeting, Geological Society of London.

GRUNOW A. M., DALZIEL I. W. D. & KENT D. V. 1987a. Ellsworth-Whitmore Mountains crustal block, Western Antarctica: new paleomagnetic results and

their tectonic significance. *In*: McKenzie G. D. ed. Gondwana Six. *American Geophysical Union, Geophysical Monograph* **40**, 161-171.

GRUNOW A. M., KENT D. V. & DALZIEL I. W. D., 1987b. Mesozoic evolution of West Antarctica and the Weddell Sea Basin: new paleomagnetic constraints. *Earth and Planetary Science Letters* **86**, 16-26.

HALLAM A. 1987. End-Cretaceous mass extinction event: Argument for terrestrial causation. *Science* **238**, 1232-1244.

HALLAM A. 1994. *An Outline of Phanerozoic Biogeography*. Oxford University Press, Oxford.

HAMBRY M. J. & HARLAND W. B. eds. 1981. *Earth's Pre-Pleistocene glacial record*. Cambridge: Cambridge University Press, London.

HEFTY J. & GONTIER A-M. 1997. Sensitivity of UT1 determined by single baseline VLBI to atmospheric delay model, terrestrial and celestrial reference frames. *Journal of Geodesy* **71**, 253-261.

HEKI K. 1990. Three approaches to improve the estimation accuracies of the vertical VLBI station positions. *Journal of Geodesy Society of Japan* **36**, 143-154.

HEKI K. 1996. Horizontal and vertical crustal movements from three-dimensional very long baseline interferometry kinematic reference frame: Implications for the reversal time scale revision. *Journal of Geophysical Research* **101**, 3187-3198.

HERRING T. & PEARLMAN M. R. 1993. Future developments and synergism of space geodetic measurement techniques. *In*: Smith D. E. & Turcotte D. L. eds. *Contributions of Space Geodesy to Geodynamics: Technology. Geodynamics Series*, Volume **25**. American Geophysical Union, 21-25.

HILGENBERG O. C. 1933. *Vom wachsenden Erdball*. Selbstverlag, Berlin.

HILGENBERG O. C. 1962. Paläopollagen der Erde. Neues *Jahrb. Geol. und Paläontol.*, Abhandl **116**, Struttgart.

HOFFMAN P. F. 1991. Did the break-out of Laurentia turn Gondwanaland inside out? *Science* **252**, 1409-1412.

HOFFMAN P. F., KAUFFMAN A. J., HALVERSON G. P. & SCHRAG D. P. 1998. A Neoproterozoic snowball earth. *Science* **281**, 1342-1346.

HOLMES D. L. 1965. *Principles of Physical Geology*, third edition. Thomas Nelson and Sons Ltd. pp 701-708.

HOOIJBERG M. 1997. *Practical Geodesy using computers*. Springer.

HORA H. 1983. Degenerate plasma phases to explain the expansion of the Earth while releasing energy. *In:* Carey S. W. ed, *Expanding Earth Symposium, Sydney, 1981*. University of Tasmania, 363-364.

HOSPERS J. & VAN ANDEL S. I. 1967. Palaeomagnetism and the hypothesis of an expanding Earth. *Tectonophysics* **5**, 5-24.

HOTTON N. (III) 1992. Global distribution of terrestrial and aquatic tetrapods, and its relevance to the position of continental masses. *In:* Chatterjee S. & Hotton N. (III) eds. *New Concepts in Global Tectonics.* Texas Technical Press, USA, 267-285.

IASKY R. P. 1990. Officer Basin. *In: Geology and mineral resources of Western Australia.* Western Australia Geological Survey, Memoir **3**, 362-380.

IMBRIE J., HAYS J. D., MARTINSON D., McINTYRE A., MIX A., MORLEY J., PISIAS N., PRELL W. & SHACKLETON N.J. 1984. The orbital theory of Pleistocene climate: support from a revised chronology of the marine? ^{18}O record. *In*: Berger A. L. ed. *Milankovitch and climate*, Part 1:D. Reidel, Dordrecht, 269-305.

IRVING E. 1956. Paleomagnetic and paleoclimatological aspects of polar wandering. *Geofisica Pura Applica* **33**, 23-41.

IRVING E. 1964. *Paleomagnetism and its application to geological and geophysical problems.* John Wiley and Sons, New York.

ISHIWATARI A. 1994. Circum-Pacific Phanerozoic multiple ophiolite belts. *Proceedings of the 29th International Geological Conference*, Part D, 7-28.

IVANENKO D. D. & SAGITOV M. V. 1961. *O gipoteze rassheryayushchcusya Zemli.* (The hypothesis of an expanding Earth). *Vestnik Moskovskaia Universiteta*, third series, **6**, 83p. (in Russian).

IVANKIN V. P. 1990. Time increase of the Earth mass and dimensions - determinant of the Earth's development. *In*: *Critical Aspects of the Plate Tectonics Theory; Volume II, Alternative Theories.* Theophrastus Publishers, Athens, Greece, 95-113.

JACKSON M. J. & POLLACK H. N. 1987. Mantle devolatilization and convection: implications for the thermal history of the Earth. *Geophysical Research Letters* **14**, number 7, 737-740.

JENKYNS H. C. 1988. The early Toacian (Jurassic) anoxic event: Stratigraphic, sedimentary, and geochemical evidence. *American Journal of Science* **288**, 101-151.

JORDAN P. 1969. On the possibility of avoiding Ramsay's hypothesis in formulating a theory of Earth expansion. *In:* Runcorn S. K. ed. *The Application of Modern Physics to Earth and Planetary Interiors.* Wiley and Sons, London, 55-63.

KATZ M. B. 1976. Early Precambrian granulite-greenstones, transform mobile belts and their tectonic setting. *In:* Sidorenko A. V. ed. *Correlation of the Precambrian* **1**, Nauka Publication Office, Moscow, 26-39.

KHAIN V. Y. 1974. Modern ideas on causes and mechanisms of tectogenesis. An experiment in critical analysis and conclusions. *International Geological Reviews* **16**, 169.

KHUDOLEY K. M. 1974. Circum-Pacific ammonoid distribution: relation to hypotheses of continental drift, polar wandering, and Earth expansion. *In*: Kahle C. F. ed. Plate Tectonics assessments and reassessments. *American Association of Petroleum Geologists*, Memoir **23**, 295-330.

KIRILLOV I. B. 1958. A hypothesis of the development of the Earth and continents and ocean basins. (in Russian).

KLEIN G. D. 1994. Pangea: paleoclimate, tectonics, and sedimentation during accretion, zenith, and breakup of a supercontinent. *Geological Society of America Special Paper* **288**,

KOMINZ M. A. & BOND G. C. 1991. Unusually large subsidence and sea-level events during middle Paleozoic time: New evidence supporting mantle convection models for supercontinent assembly. *Geology* **19**, 56-60.

KOZIAR J. 1980. Ekspansja den oceanicznych I jej zwiazek z hipotaza ekspansji Ziemi. Sprawozdania Wroclawskiego Towarzystwa Naukowego, **35**, 13-19.

KREMP G. O. W. 1983. Precambrian events indicative of Earth expansion. *In:* Carey S. W. ed, *Expanding Earth Symposium, Sydney, 1981*. University of Tasmania, 91-99.

KRISHNA J. 1994. Origin of the Gondic (Trans-Gondwana) corridor: the ammonoid evidence. *Ninth International Gondwana Symposium*. Hyderabad, India, 1091-1099.

KRÖNER A. 1982. Archaean to Early Proterozoic tectonics and crustal evolution: A review. *Revista Brasileira de Geociências* **12**, 15-31.

KUSZNIR N. J. & PARK R. G. 1987. The extensional strength of the continental lithosphere: its dependence on geothermal gradient, and crustal composition and thickness. *In*: Coward M. P., Dewey J. F. & Hancock P. L. eds. *Continental Extensional Tectonics*. Geological Society Special Publication **28**, 35- 64.

LAMBECK K. 1988. *Geophysical Geodesy: The slow deformations of the Earth.* Oxford Science Publications, Clarendon Press, London.

LAMBERT I. B. 1982. Early geobiochemical evolution of the Earth. *Revista Brasileira de Geociências* **12**, 32-38.

LAMBERT I. B. & GROVES D. I. 1981. Early Earth evolution and metallogeny. *In:* K. H. Wolf ed. *Handbook of stratabound and stratiform ore deposits* **8**, Elsevier Co, Amsterdam, 339-447.

LARSON K. M., FREYMUELLER J. T. & PHILIPSEN S. 1997. Global plate velocities from the Global Positioning System. *Journal of Geophysical Research* **102**, 9961-9981.

LARSON R. L. & PITMAN W. C.(III). 1972. World-wide correlation of Mesozoic magnetic anomalies, and its implications. *Geological Society of America Bulletin* **83**, 3645-3662.

LARSON R. L., PITMAN W. C. (III)., GOLOVCHENKO X., CANDE S. C., DEWEY J. F., HAXBY W. F. & LaBRECQUE (mapcompilers) 1985. *The Bedrock Geology of the World.* Freeman & Co., New York.

LAWVER L. A. & SCOTESE C. R. 1987. A revised reconstruction of Gondwanaland. *In*: McKenzie G. D. ed. *Gondwana 6: structure, tectonics, and geophysics*. Geophysical Monograph **40**, 17-22.

LAWVER L. A., SANDWELL D. A., ROYER J-Y. & SCOTESE C. R. 1991. Evolution of the Antarctic continental margins. *In*: Thomson M. R. A., Crames J. A. & Thomson J. W. eds. *Geological evolution of Antarctica*. Cambridge University Press, Cambridge, England.

LAZNICKA P. 1993. *Precambrian empirical metallogeny: precambrian lithologic associations and metallic ores*. Volume 2 of empirical metallogeny, part a & b. Developments in economic geology, 29. Elsevier. Amsterdam.

LINDERMAN B. 1927. *Kettengebirge, Kontinentale Zerspaltung und Erdexpansion.* Gustav Fischer Publishers, Jena. 186p.

LI Z. X. 1999. Palaeomagnetic evidence for an united north and west Australian cratons by *ca*. 1.7 Ga. *In:* Watts G. R. & Evans D. A. D. eds. Two billion years of tectonics and mineralisation. *Geological Society of Australia Abstracts* **56**, 25.

LI Z. X. & POWELL C. McA. 1993. Late Proterozoic to Early Paleozoic palaeomagnetism and the formation of Gondwanaland. *In*: Findley R. H., Unrug R., Banks M. R. & Veevers J. J. eds. *Gondwana Eight. Assembly, evolution and dispersal*. Balkema, Rotterdam, 9-21.

LI Z. X., POWELL C. McA. & TRENCH A. 1993. Palaeozoic global reconstructions. *In*: Long J. A. ed. *Palaeozoic vertabrate biostratigraphy and biogeography*. Belhaven Press, London, 25-45.

LI Z. X., ZHANG L. & POWELL C. McA. 1996. Positions of the East Asian cratons in the Neoproterozoic supercontinent Rodinia. *Australian Journal of Earth Sciences* **43**, 593-604.

LYNCH H. D. & MORGAN P. 1987. The tensile strength of the lithosphere and the localization of extension. *In*: Coward M. P., Dewey J. F. & Hancock P. L. eds. *Continental Extensional Tectonics*. Geological Society Special Publication **28**, 53-64.

MA C. & RYAN J. W. 1998. *NASA Space Geodesy Program - GSFC DATA Analysis - August 1998, VLBI geodetic results 1979-1998*.

MACELLARI C. E. 1987. Progressive endemism in the Late Cretaceous ammonite family Kossmaticeratidae and the breakup of Gondwanaland. *In*: McKenzie G. D. ed. *Gondwana Six. Structure, Tectonics and Geophysics*. American Geophysical Union, Geophysical Monograph **40**, 85-92.

MASCLE J., BLAREZ E. & MARINHO M. 1988. The shallow structures of the Guinea and Ivory Coast-Guana transform margins: their bearing on the equatorial Atlantic evolution. *Tectonophysics* **155**, 193-209.

MASLENNIKOV V. V. 1993. Cyclicity in the formation of mercury deposits. *Proceedings of the 8th Quadrennial IAGOD Symposium*, 695-699.

MAXLOW J. 1995. *Global Expansion Tectonics: the geological implications of an expanding Earth.* Unpublished thesis, Curtin University of Technology, Perth, Western Australia.

McCABE P. J. & PARRISH J. T. 1992. Tectonic and climatic controls on the distribution and quality of Cretaceous coals. *In*: McCabe P. J. & Parrish J. T. eds. *Controls on the distribution and quality of Cretaceous coals*. Geological Society of America Special Paper **267**, 1- 15.

McELHINNY M. W. & BROCK A. 1975. A new paleomagnetic result from East Africa and estimates of the Mesozoic paleoradius. *Earth and Planetary Science Letters* **27**, 321-328.

McELHINNY M. W. & LOCK J. 1996. IAGA paleomagnetic databases with Access. *Surveys in Geophysics,* **17**, 575-591.

McELHINNY M. W. & McFADDEN P. L. 2000. *Paleomagnetism: Continents and oceans*. International Geophysics Series **73**. Academic Press, San Diego.

McKELVEY V. E., WRIGHT N. A. & BOWEN R. W. 1984. World distribution of metal-rich subsea manganese nodules: a summary. *Proceedings of the 27th International Geological Congress* **12**, Metallogenesis and Mineral Ore Deposits, VNU Science Press, 311-339.

McKERROW W. S., DEWEY J. F. & SCOTESE C. F. 1991. The Ordovician and Silurian development of the Iapetus Ocean. *Special Papers in Palaentology* **44**, 165-178.

McMENAMIN M. A. S. & SCHULTE-McMENAMIN D. L. 1990. *The emergence of animals; the Cambrian breakthrough.* Columbia University Press, New York.

McNAUGHTON N. J. & DAHL N. 1987. A geochronological framework for gold mineralisation in the Yilgarn Block, Western Australia. *In:* Ho S. E. & Groves D. I. eds. *Recent advances in understanding Precambrian gold deposits* **11**, 29-49.

MENZIES M. A. & HAWKESWORTH C. J., 1987 eds. *Mantle metasomatism*. Academic Press, London, 472p.

METCALFE I. 1993. Southeast Asian terranes: Gondwanaland origins and evolution. *In*: Findley R. H., Unrug R., Banks M. R. & Veevers J. J. eds. *Gondwana Eight. Assembly, evolution and dispersal*. Balkema, Rotterdam, 181-199.

MEYER C. 1981. Ore-forming processes in geologic history. *Economic Geology,* 75th Anniversary Volume, 6-41.

MEYER C. 1988. Ore deposits as guides to geologic history of the Earth. *Annual Reviews in Earth and Planetary Sciences* **16**, 147-171.

MEYERHOFF A. A. & MEYERHOFF H. A. 1974. Tests of plate tectonics. *In*: Kahle C. H. ed. Plate Tectonics - Assessments and reassessments. *American Association of Petroleum Geologists,* Memoir **23**, 43

MEYERHOFF A. A., BOUCOT A. J., MEYERHOFF-HULL D. & DICKINS J. M. 1996. Phanerozoicfaunal and floral realms of the Earth: The intercalary relations of the Milvinokaffric and Gondwana faunal realms with the Tethyan faunal realm. *Geological Society of America,* Memoir **189**.

MEYER R. F. 1986. *Shallow Oil and Gas Resources*. Proceedings of the first International Conference. The United Nations Institute for Training and Research.

MIALL A. D. 1990. *Principles of sedimentary basin analysis.* Springer-Verlag, New York.

MIDDLETON M. F. 1990. Canning Basin. *In: Geology and mineral resources of Western Australia.* Western Australia Geological Survey, Memoir **3**, 425 453.

MILANOVSKY E. E. 1980. Problems of the tectonic development of the Earth in the light of concept on its pulsations and expansion. R*evue de Geologique et de Geographie Physique* **22**, 15-27.

MINSTER J. B. & JORDAN T. H. 1978. Present-day plate motions. *Journal of Geophysical Research* **83**, 5331-5354.

MOLNAR R. E. 1992. Paleozoogeographic relationships of Australian Mesozoic tetrapods. *In:* Chatterjee S. & Hotton N (III) eds. *New Concepts in Global Tectonics.* Texas Technical Press, USA, 259-265.

MONTAG H. & REIGBER C. 1992. eds. *Geodesy and Physics of the Earth.* Geodetic contributions to geodynamics, 7th International Symposium, No. **112**, Potsdam. Springer-Verlag, Berlin.

MOORBATH S. 1982. Crustal evolution in the Early Precambrian. *Revista Brasileira de Geociências* **12**, 39-44.

MOORES E. M., 1991. Southwest U.S.-East Antarctic (SWEAT) connection: a hypothesis. *Geology* **19**, 425-428.

MORLEY L. W. & LAURCHELLE A. 1964. Paleomagnetism as a means of dating geological events. *Royal Society of Canada Special Publication* **8**, 39-51.

MÜLLER R. D., ROEST W. R., ROYER J.-Y., GAHAGAN L. M. & SLATER J. G. 1997. The World's ocean floor. *Journal of Geophysical Research* **102**, 3211-3214.

MYERS J. S. 1990a. Precambrian. *In: Geology and mineral resources of Western Australia.* Western Australia Geological Survey, Memoir **3**, 737-749.

MYERS J. S. 1990b. Precambrian tectonic evolution of part of Gondwana, southwestern Australia. *Geology* **18**, 537-540.

NEIMAN V. B. 1984. Geological and geophysical proofs and possible causes of the Earth's expansion. Nauka, M., 116-173.

NEIMAN V. B. 1990. An alternative to Wegener's mobilism. *In*: *Critical Aspects of the Plate Tectonics Theory; Volume II, Alternative Theories.* Theophrastus Publishers, Athens, Greece, 3-18.

NESBITT H. W. & YOUNG G. M. 1982. Early Proterozoic climates and plate motions inferred from major element chemistry of lutites. *Nature* **299**, 715-717.

NIE S-Y. 1991. Paleoclimatic and paleomagnetic constraints on the Paleozoic reconstructions of south China, north China and Tarim. *Tectonophysics* **196**, 279-308.

NORTH F. K. 1990. *Petroleum geology*. Unwin Hyman Inc., Boston.

OKAJANGAS R. W. 1988. Glaciation: an uncommon 'mega-event' as a key to intracontinental and intercontinental correlation of Early Proterozoic basinfill, North American and Baltic Cratons. *In*: Kleinspehn K. L. & Paola C eds. *New Perspectives in Basin Analysis.* Springer-Verlag, New York, 431-444.

OLLIER C. D. 1985. Morphotectonics of passive continental margins: Introduction. *Z. Geomorphology Suppl. Bd. N. F*. **54**, 1-9.

OLLIER C. D. 1998. Geomorphology and mountain building. Fourth International conference on geomorphology - Italy 1997. *Suppl. Geogr. Fis. Dinam Quat* III, T. 3, 1-12.

OLLIER C. D. & PAIN C. F. 2000. The origin of mountains. Routledge, London.

OWEN H. G. 1976. Continental displacement and expansion of the Earth during the Mesozoic and Cenozoic. *Philosophical Transactions of the Royal Society,* London **281**. 223-291.

OWEN H. G. 1983. *Atlas of Continental Displacement, 200 Million Years to the Present.* Cambridge Earth Series, Cambridge University Press, Cambridge.

PAGE N. J. 1981. The Precambrian diamictite below the base of the Stillwater Complex, Montana. *In*: Hambrey M. J. & Harland W. B. *Earth's Pre Pleistocene Glacial Record.* Cambridge University Press, Cambridge, 821-825.

PARSONS B. 1982. Causes and consequences of the relation between area and age of the ocean floor. *Journal of Geophysical Research* **87**, 289-302.

PATCHETT P. J. & ARNDT N. T. 1986. Nd isotopes and tectonics of 1.9-1.7 Ga crustal genesis. *Earth and Planetary Science Letters* **78**, 329-338.

PIDGEON R. T., SMITH C. B. & FANNING C. M. 1989. Kimberlite and lamproite emplacement ages in Western Australia. *Geological Society of Australia Special Publication* **14**, 369-381.

PINDELL J. L. & BARRETT S. F. 1987. Geological evolution of the Caribbean region: a plate-tectonic perspective. *In*: Dengo G. & Case J. E., (eds), *The Geology of North America, Volume H, The Caribbean Region.* Geological Society of America, Boulder, Colorado.

PINDELL J. L., CANDE S .C., PITMAN W. C. (III), ROWLEY D. B., DEWEY J. F., LABRECQUE J. & HAXBY W. 1988. A plate-kinematic framework for models of Caribbean evolution. *Tectonophysics* **155**, 121-138.

PIPER J. D. A. 1989. Palaeomagnetism. *In*: Jacobs J.A. ed. Academic Press Ltd. 31-147.

PISAREVSKY S. & HARRIS L. 1999. Rock magnetic and palaeomagnetic results from high-grade metamorphic and intrusive rocks: Determination of magnetic anisotropy and a 1.2 Ga palaeomagnetic pole from the Bremer Bay area, Albany Mobile Belt, Western Australia. *In:* Watts G. R. & Evans D. A. D. eds. Two billion years of tectonics and mineralisation. *Geological Society of Australia Abstracts* **56**, 34-38.

PLUMB K. A. 1979. The tectonic evolution of Australia. *Earth-Science Reviews* **14**, 205-249.

PLUMB K. A ., DERRICK. G. M., NEEDHAM R. S. & SHAW R. D. 1981. The Proterozoic of Northern Australia. *In*: Hunter D. R. ed. *Precambrian of the Southern Hemisphere.* Elsevier, Amsterdam, 205-308.

PLUMSTEAD E. P. 1973. The Late Palaeozoic Glossopteris flora. *In*: Hallam A. ed. *Atlas of palaeobiogeography*. Elsevier Scientific Publishing Company, Amsterdam, 187-205.

POWELL C. McA. 1993. Assembly of Gondwanaland - Open forum. *In*: Findlay R. H., Unrug R., Banks M. R., & Veevers J. J. eds. *Gondwana eight. Assembly, evolution and dispersal.* Proceedings of the Eigth Gondwana Symposium, Hobart. A. A. Balkema, Rotterdam, 219-237.

POWELL C. McA & LI Z. X. 1994. Reconstruction of the Panthalassan margin of Gondwanaland. *In*: Veevers J. J. & Powell C. McA. eds. Permian-Triassic Pangean basins and foldbelts along the Panthalassan margin of Gondwanaland. *Geological Society of America* Memoir **184**, 5-9.

POWELL C. McA. & VEEVERS J. J. 1994. Introduction. *In:* Veevers J. J. & POWELL C. McA. eds. Permian Triassic Pangean basins and foldbelts along the Panthalassan margin of Gondwanaland. Boulder, Colorado, *Geological Society of America Memoir* **184**, 1-3.

POWELL C. McA., JOHNSON B. D. & VEEVERS J. J. 1980. A revised fit of east and west Gondwanaland. *Tectonophysics* **63**, 13-29.

POWELL C. McA., LI Z. X., McELHINNY M. W., MEERT J. G. & PARK J. K. 1993. Paleomagnetic constraints on timing of the Neoproterozoic breakup of Rodinia and the Cambrian formation of Gondwana. *Geology* **21**, 889-892.

POWELL C. McA., ROOTS S. R. & VEEVERS J. J. 1988. Pre-breakup continental extension in East Gondwanaland and the early opening of the eastern Indian ocean. *Tectonophysics* **155**, 261-283.

RAY J. R. 1996. Measurements of length of day using the Global Positioning System. *Journal of Geophysical Research* **101**, 20141-20149.

RETALLACK G. J. 1987. Triassic vegetation and geography of the New Zealand portion of the Gondwana Supercontinent. *In*: McKenzie G. D. ed. Gondwana Six. *American Geophysical Union, Geophysical Monograph* **40**, 29-39.

RICKARD M. J. 1969. Relief of curvature on expansion - a possible mechanism of geosynclinal formation and orogenesis. *Tectonophysics* **8**, 129-144.

ROBAUDO S. & HARRISON C. G. A. 1993. Plate tectonics from SLR and VLBI global data. *In*: Smith D. E., & Turcotte D. L. eds. *Contributions of Space Geodesy to Geodynamics: Crustal Dynamics*. Geodynamics Series, Volume **23**. American Geophysical Union.

ROBBINS J. W., SMITH D. E. & MA C. 1993. Horizontal crustal deformation and large scale plate motions inferred from space geodetic techniques. *In*: Smith D. E. & Turcotte D. L. eds. *Contributions of space geodesy to geodynamics. Crustal Dynamics, Geodynamics Series* **23**, 21-36.

ROBINSON J. M. 1973. Palaeoclimatology and continental drift. *In*: Tarling D. H., & Runcorn S. K. eds. *Implications of continental drift to Earth sciences* **1**. Academic Press, New York, 451-476.

ROBINSON J. M. 1990. Lignin, land plants, and fungi: Biological evolution evolution affecting Phanerozoic oxygen balance. *Geology* **15**, 607-610.

ROGERS A. E. E., CAPPALLO R. J., COREY B. E., HINTEREGGER H. F., NEILL A. E., PHILLIPS R. B., SMYTHE D. L., WHITNEY A. R., HERRING T. A., BOSWORTH J. M., CLARK T. A., MA C., RYAN J. W., DAVIS J. L., SHAPIRO I. I., ELGERED G., JALDEHAG K., JOHANSSON J. M., RÖNNÄNG B. O., CARTER W. E., RAY J. R., ROBERTSON D. S., EUBANKS T. M., KINGHAM K. A., WALKER R. C., HIMWICH W. E., KUEHN C. E., MACMILLAN D. S., POTASH R. I., SHAFFER D. B., VANDENBERG N. R., WEBBER J. C., ALLSHOUSE R. L., SCHUPLER B. R. & GORDON D. 1993. Improvements in the accuracy of geodetic VLBI. *In*: Smith D. E. & Turcotte D. L. eds. *Contributions of Space Geodesy to Geodynamics: Technology*. Geodynamics Series, Volume **25**. American Geophysical Union, USA, 47-63.

ROSS C. A. & ROSS J. R. P. 1981. Biogeographical influences on Late Paleozoic faunal distributions. *In*: Larwood G. P. & Nielsen C. eds. *Recent and fossil bryzoa*. Fredensborg, Denmark, Olsen & Olsen Printers, 199-212.

ROSS G. M. 1999. Paleogeography: an earth systems perspective. *Chemical Geology* **161**, 5-16.

ROSS M. I. & SCOTESE C. R. 1988. A hierarchical tectonic model of the Gulf of Mexico and Caribbean region. *Tectonophysics* **155**, 139-168.

ROWLEY D. B. & LOTTES A. L. 1988. Plate-kinematic reconstructions of the North Atlantic and Arctic: Late Jurassic to Present. *Tectonophysics* **155**, 73 120.

ROYER J-Y., PATRIAT P., BERGH H. W. & SCOTESE C.R. 1988. Evolution of the Southwest Indian ridge from the Late Cretaceous (anomaly 34) to the Middle Eocene (anomaly 20). *Tectonophysics* **155**, 235-260.

RUBEY W. W. 1975. Geologic history of sea water; an attempt to state the problem. *In:* Kitano Y. ed. *Geochemistry of Water*. Dowden, Hutchinson & Ross Inc., Stroudsburg, Pennsylvania.

RUNCORN S. K. 1956. Paleomagnetic comparisons between North America and Europe. *Proceedings of the Geological Association of Canada* **8**, 77-85.

RUTLAND R. W. R. 1973. The tectonic map of Australia and New Guinea in the context of tectonic theory. *Geological Society of Australia,* Tectonics Structural Newsletter **2**, 47-52.

RUTLAND R. W. R., ETHERIDGE M. A. & SOLOMON M. 1990. The stratigraphic and tectonic setting of the ore deposits of Australia. *In*: Hughes F. E. ed. *Geology of the mineral deposits of Australia and Papua New Guinea*, 15-26.

SADOWSKI G. R. 1994. The Gondwana supercontinent cycle and the Salvador Congo Craton. *Ninth International Gondwana Symposium*, Hyderabad, India, 1994. 999-1001.

SAVOSTOVIN L. A., SIBUET J. C., ZONENSHAIN L. P., LePICHON X. & ROULET M. J. 1986. Kinematic evolution of the Tethys belt from the Atlantic Ocean to the Pamirs since the Triassic. *In:* Auboin J., LePichon X. & Monin A. S. eds. Evolution of the Tethys. *Tectonophysics* **123**, 1-35.

SCHERMERHORN L. J. G. 1974. Late Precambrian mixtites: glacial and/or non glacial. *American Journal of Science* **274**, 673-824.

SCOTESE C.R. 1987. Development of the circum-Pacific Panthallassic Ocean during the Early Paleozoic. *In*: Monger J. W. H. & Francheteau J. eds. *Circum-Pacific orogenic belts and evolution of the Pacific Ocean basin.* Geodynamic Series **18**, 49-57.

SCOTESE C. R. 1994. Paleogeographic maps. *In*: Klein, G. D. ed. *Pangea: paleoclimate, tectonics, and sedimentation during accretion, zenith, and breakup of a supercontinent.* Geological Society of America Special Paper **288**.

SCOTESE C. R. & BARRETT S. F. 1990. Gondwana's movement over the South Pole during the Palaeozoic: evidence from lithological indicators of climate. *In*: McKerrow W. S., & Scotese C. R. eds. *Palaeozoic Palaeogeography and Biogeography*. The Geological Society of London Memoir **12**, 75-85.

SCOTESE C. R. & GOLONKA J. 1992. *Paleogeographic atlas*. Arlington University of Texas Arlington, Paleomap project.

SCOTESE C. R., BAMBACH R. K., BARTON C., Van Der VOO R. & ZIEGLER A. M. 1979. Paleozoic basemaps. *Journal of Geology* **87**, 217-277.

SCOTESE C. R., GAHAGAN L. M. & LARSON R. L. 1988. Plate tectonic reconstructions of the Cretaceous and Cenozoic ocean basins. *Tectonophysics* **155**, 27-48.

SENO T. & MARUYAMA S. 1984. Paleogeographic reconstruction and origin of the Philippine Sea. *Tectonophysics* **102**, 53-84.

SEPKOSKI J. J. & MILLER A. I. 1985. Evolutionary faunas and the distribution of Paleozoic marine communities in time and space. *In:* Valentine J. W. ed. *Phanerozoic diversity patterns*. Princeton University Press, Princeton New Jersey, 153-180.

SHIELDS O. 1979. Evidence for initial opening of the Pacific ocean in the Jurassic. *Palaeontology, Palaeoclimatology, Palaeoecology* **26**, 181-220.

SHIELDS O. 1983a. The role of gravity and asteroid impacts in Earth expansion. *In:* Carey S. W. ed, *Expanding Earth Symposium, Sydney, 1981*. University of Tasmania, 277-282.

SHIELDS O. 1983b. Trans-Pacific biotic links that suggest Earth expansion. *In:* Carey S.W. ed. *Expanding Earth Symposium, Sydney, 1981*. University of Tasmania, 199-205.

SHIELDS O. 1988. Post-Triassic Earth expansion perhaps caused by a cometary impact in Tibet. *Journal of the Geological Society of India* **32**, 506-512.

SHIELDS O. 1996. Geologic significance of land organisms that crossed over the Eastern Tethys "Barrier" during the Permo-Triassic. *Palaeobotanist* **43**, 85-95.

SHIELDS O. 1997. Is plate tectonics withstanding the test of time? *Annali di Geofisica*, Vol XL, 1-8.

SHIELDS O. 1998. Upper Triassic Pacific vicariance as a test of geological theories. *Journal of Biogeography* **25**, 203-211.

SHULDINER V. I. 1982. The oldest high grade terranes: Possible relicts of primeval Earth crust. *Revista Brasileira de Geociências* **12**, 45-52.

SILK J. 1980. *The Big Bang: The creation and evolution of the Universe*. Freeman and Company, San Francisco.

SLUYS R. 1994. Explanations for biogeographic tracks across the Pacific Ocean: a challenge for paleogeography and historical biogeography. *Progress in Physical Geography* **18**, 42-58.

SMILEY C. J. 1992. Paleofloras, faunas, and continental drift: some problem areas. *In:* Chatterjee S. & Hotton N. (III) eds. *New Concepts in Global Tectonics.* Texas Technical Press, USA, 241-257.

SMIRNOFF L. S. 1992. The contracting-expanding Earth and the binary system of its megacyclicity. *In:* Chatterjee S. & Hotton N. (III). eds. *New Concepts in Global Tectonics*. Texas Technical University Press, USA, 441-449.

SMIRNOV V. I. 1984. Periodicity of ore formation in geological history. Proceedings of the 27th International Geological Congress, Volume 12, *Metallogenesis and mineral ore deposits*, 1-15.

SMITH A. G., SMITH D. G. & FUNNELL B. M. 1994. *Atlas of Mesozoic and Cenozoic coastlines.* Cambridge University Press.

SMITH D. E. & TURCOTTE D. L. eds. 1993. *Contributions of space geodesy to dynamics:crustal dynamics.* Geodynamic Series volume **23**. American Geophysical Union, Washington, D. C.

SMITH D. E., CHRISTODOULIDIS D. C., KOLENKIEWICZ R., DUNN P. J., KLOSKO S. M. & TORRENCE M. H. 1985. A Global Geodetic Reference Frame From LAGEEOS Ranging (Sl5.1AP). *Journal of Geophysical Research*. **90**, 9221-9233.

SMITH D. E., KOLENKIEWICZ R., DUNN P. J., ROBBINS J. W., TORRENCE M. H., KLOSKO S. M., WILLIAMSON R. G., PAVLIS E. C. & DOUGLAS N. B. 1990. Tectonic motion and deformation from satellite laser ranging to LAGEOS. *Journal of Geophysical Research* **90**, 22013-22041.

SMITH D. E., KOLENKIEWICZ R., NEREM R. S., DUNN P. J., TORRENCE M. H., ROBBINS J. W., KLOSKO S. M. WILLIAMSON R. G. & PAVLIS E. C. 1994. Conteporary global horizontal crustal motion. *Geophysical Journal International* **119**, 511-520.

SMITH J. V. 1981. The first 800 million years of Earth's history. *Philosophical Transactions of the Royal society of London* **A301**, 401-422.

SOLOMON M. & GROVES D. I. 1994. *The geology and origins of Australia's mineral deposits.* Oxford University press, Melbourne.

SOUDARIN L., CRÉTAUX J-F. & CAZENAVE A. 1999. Vertical crustal motions from the DORIS space-geodesy system. *Geophysical Research Letters* **26**, 1207-1210.

SRIVASTAVA S. P. & TAPSCOTT C. 1986. *In*: Tucholke B.E., & VOGT P.R., eds. *The Geology of North America. Volume M. The Western Atlantic Region.* Geological Society of America, Boulder, Colorado, 379-404.

STACEY F. D. 1977. *Physics of the Earth.* (second edition), John Wiley & Sons, New York, 414p.

STANLEY S. M. 1989. *Earth and life through time.* W. H. Freeman and Company, New York.

STEINER J. 1967. The sequence of geological events and the dynamics of the Milky Way Galaxy. *Geological Society of Australia* **14**, pp 99-131.

STEINER J. 1977. An expanding Earth on the basis of sea-floor spreading and subduction rates. *Geology* **5**, 313-318.

STEVENS G. R. 1971. Relationship of isotopic temperatures and faunal realms to Jurassic and Cretaceous palaeogeography, particularly of the Southwest Pacific. *Journal of the Royal Society of New Zealand* **1**, 145-158.

STEVENS G. R. 1980. Southwest Pacific faunal palaeobiogeography in Mesozoic and Cenozoic times: a review. *Palaeogeograaphy, Palaeoclimatology, Palaeoecology* **31**, 153-196.

STEVENS G. R. 1990. The influences of paleogeography, tectonism and eustacy on faunal development in the Jurassic of New Zealand. *In*: Pallini G., Cecca F., Cresta S. & Santantonio M. eds. Atti del secondo convegno internazionale. *Fossili, evoluzione, ambiente.* Pergola, 1987, 441-457.

STEVENS G. R. 1997a. The Late Jurassic ammonite fauna of New Zealand. *Institute of Geological & Nuclear Sciences,* monograph **18**, 110-115.

STEVENS G. R. 1997b. The paleobiogeography of New Zealand Late Jurassic ammonites. *Geological Society of New Zealand*, Annual Conference.

STEWART A. D. 1977. Quantitative limits to palaeogravity. *Journal of the Geological Society of London* **133**, 281-291.

STEWART A. D. 1978. Limits to palaeogravity since the late Precambrian. *Nature* **271**, 153-155.

STEWART A. D. 1983. Quantitative limits to the palaeoradius of the Earth. *In:* Carey S. W. ed, *Expanding Earth Symposium, Sydney, 1981*. University of Tasmania, 305-319.

STOCKLIN J. 1983. Himalayan orogeny and Earth expansion. *In:* Carey S. W. ed. *Expanding Earth Symposium, Sydney, 1981*. University of Tasmania, 119 130.

STOREY B. B. 1993. The changing face of late Precambrian and early Palaeozoic reconstructions. *Journal of the Geological Society of London Special Paper*, 665-668.

SUNDVIK M. T. & LARSON R. L. 1988. Seafloor spreading history of the western North Atlantic Basin derived from the Keathley sequence and computor graphics. *Tectonophysics* **155**, 49-71.

TANNER W. F. 1983. Absolute motion of North America, and the development of the middle America "arc". *In:* Carey S.W. ed. *Expanding Earth Symposium, Sydney, 1981*. University of Tasmania, 219-223.

TAPLEY B. D., SCHUTZ B. E. & EANES R. J. 1985. Station Coordinates, Baselines, and Earth Rotation from LAGEOS Laser Ranging: 1976-1984. *Journal of Geophysical Research* **90**,9235-9248.

TARLING D. H. 1983. *Paleomagnetism.* Chapman & Hall, London.

TARNEY J., WEAVER B. L. & WINDLEY B. F. 1982. Geological and geochemical evolution of the Archaean continental crust. *Revista Brasileira de Geociências* **12**, 53-59.

TIRATSOO E. N. 1984. *Oilfields of the World*. Scientific Press Ltd, England.

TORSVIK T. H., SMETHURST M. A., MEERT J. G., VAN DER VOO R., McKERROW W. S., BRASIER M. D., STURT B. A. & WALDERHAUG H. J. 1996. Continental break-up and colloision in the Neoproterozoic and Paleozoic - A tale of Baltica and Laurentia. *Earth Science Reviews* **40**, 229-258.

TRENDALL A. F. 1990. Introduction. *In*: *Geology and mineral resources of Western Australia.* Western Australia Geological Survey, Memoir **3**, 1-7.

TURNELL H. B. 1988. Mesozoic evolution of Greek microplates from palaeomagnetic measurements. *Tectonophysics* **155**, 307-316.

UNRUG R. 1993. The Gondwana supercontinent: Middle Proterozoic crustal fragments, Late Proterozoic assembly, and unresolved problems. *In*: Findlay

R. H., Unrug R., Banks M. R. & Veevers J. J. eds. *Gondwana eight. Assembly, evolution and dispersal.* Proceedings of the Eigth Gondwana Symposium, Hobart. A. A. Balkema, Rotterdam, 3-8.

UNTERNEHR P., CURIE D., OLIVET J. L., GOSLIN J. & BEUZART P. 1988. South Atlantic fits and interplate boundaries in Africa and South America. *Tectonophysics* **155**, 169-179.

VAIL P. R., MITCHUM R. M. & THOMPSON S. 1977. Seismic stratigraphy and global changes in sea-level. *American Association of Petroleum Geologists Memoir* **26**, 83-97.

VALDIYA K. S. 1984. Evolution of the Himalaya. *Tectonophysics* **105**, 229-248.

VAN ANDEL S. I. & HOSPERS J. 1968. Palaeomagnetic calculations of the radius of the ancient Earth by means of the palaeomeridian method. *Physics of the Earth and Planetary Interiors* **1**, 155-163.

VAN DER VOO R. 1988. Paleozoic paleogeography of North America, Gondwana, and intervening displaced terranes: comparisons of palaeomagnetism with paleoclimatology and biogeographical patterns. *Geological Society of America Bulletin* **100**, 311-324.

VAN DER VOO R. 1993. *Paleomagnetism of the Atlantic, Tethys and Iapetus Oceans*. Cambridge University Press.

VANECEK M. 1994. *Mineral deposits of the world*. Ores, industrial minerals and rocks. Developments in economic geology, 28. Elsevier, Amsterdam.

VAN HILTEN D. 1963. Palaeomagnetic indications of an increase in the Earth's radius. *Nature* **200**, 1277-1279.

VAN HILTEN D. 1968. Global expansion and palaeomagnetic data. *Tectonophysics* **5**, 191-210.

VASLET D. 1990. Upper Ordovician glacial deposits in Saudi Arabia. *Episodes* **13**, 147-161.

VEEVERS J. J. 1994. Pangea: Evolution of a supercontinent and its consequences for Earth's paleoclimate and sedimentary environments. *In*: Klein, G. D. ed. *Pangea: paleoclimate, tectonics, and sedimentation during accretion, zenith, and breakup of a supercontinent*. Geological Society of America Special Paper **288**, 13-23.

VEEVERS J.J., POWELL C. McA., COLLINSON J. W. & LOPEZ-GAMUNDI O. R. 1994. Synthesis. *In:* Veevers J. J. & POWELL C. McA. eds. Permian

Triassic Pangean basins and foldbelts along the Panthalassan margin of Gondwanaland. Boulder, Colorado, *Geological Society of America Memoir* **184**, 331-353.

VEIZER J., LAZNICKA P. & JANSEN S. L. 1989. Mineralization through geologic time: recycling perspective. *American Journal of Science* **289**, 484-524.

VINE F. J. & MATHEWS D. H. 1963. Magnetic anomalies over oceanic ridges. *Nature* **199**, 947-949.

VISSER J. N. J. & PRAEKELT H. E. 1998. Late Palaeozoic crustal block rotations within the Gondwana sector of Pangea. *Tectonophysics* **287**, 201-212.

VOGEL K. 1983. Global models and Earth expansion. *In:* Carey S.W. ed. *Expanding Earth Symposium, Sydney, 1981*. University of Tasmania, 17-27.

VOGEL K. 1984. Beitrage zur frage der expansion der Erde auf der grundlage von globenmodellen. *Z. geol. Wiss. Berlin* **12**. 563-573.

VOGEL K. 1990. The expansion of the Earth - an alternative model to the plate tectonics theory. *In*: *Critical Aspects of the Plate Tectonics Theory; Volume II, Alternative Theories.* Theophrastus Publishers, Athens, Greece, 14-34.

VON BRUNN V. & GOLD D. J. C. 1993. Diamictites in the Archean Pongola Sequence of southern Africa. *Journal of African Earth Sciences* **16**, 367-374.

VYSKOCIL P., REIGBER C. & CROSS P. A. eds. 1989. *Global and regional dynamics, Symposium No. 101*, Edinburgh, Scotland. Springer-Verlag, New York.

WALSHE J. L., HEITHERSAY P. S. & MORRISON G. W. 1995. Toward an understanding of the metallogeny of the Tasman Fold Belt System. *Economic Geology* **90**, 1382-1401.

WARD M. A. 1963. On detecting changes in the Earth's radius. *Geophysical Journal* **8**, 217-225.

WEGENER A. 1915. *Die Eutstehung der Kontinents und Ozeane*. F Vieweg und Sohn, Brunswick, Germany.

WEIJERMARS R. 1989. Global tectonics since the breakup of Pangea 180 million years ago: evolution maps and lithospheric budget. *Earth-Science Reviews* **26**, 113-162.

WEISHAMPEL D. B. 1990. Dinosaurian distribution. *In*: Weishampel D. B., Dodson P. & Osmólska H. eds. 1990. *The Dinosauria*. University of California Press, Los Angeles.

WEISHAMPEL D. B., DODSON P. & OSMÓLSKA H. eds. 1990. *The Dinosauria.* University of California Press, Los Angeles.

WELLS P. R. A. 1981. Accretion of continental crust: Thermal and geochemical consequences. *Philosophical Transactions of the Royal society of London* **A301**, 347-357.

WESSON P. S. 1973. The implications for geophysics of modern cosmologies in which G is variable. *Quarterley Journal of the Royal Astrological Society* **14**, 9-64.

WEZEL F. C. 1992. Global change: shear dominated geotectonics modulated by rhythmic Earth pulsations. *In:* Chatterjee S. & Hotton N (III) (eds), *New Concepts in Global Tectonics.* Texas Technical Press, USA, 421-439.

WILLETT S. D. 1999. Orogeny and orography: The effects of erosion on the structure of mountain belts. *Journal of Geophysical Research* **104/B12**, 28,957-28,981.

WILLIAMS G. E. 1994. The enigmatic Late Proterozoic glacial climate: an Australian perspective. *In*: Deynoux M., Miller J. M. G., Domack E. W., Eyles N., Fairchild I. J. & Young G. M. eds. International Geological Correlation Program Project 260: *Earth's Glacial Record.* Cambridge University Press,

WILSON K. M., ROSOL M. J. & HAY W. W. 1989. Global Mesozoic reconstructions using revised continental data and terrane histories: a progress report. *American Geophysical Union* Monograph **50**, 1-40.

WITZKE B. J. 1990. Palaeoclimatic constraints for Palaeozoic palaeolatitudes of Laurentia and Euramerica. *In*: McKerrow W. S. & Scotese C. R. eds. *Palaeozoic Palaeogeography and Biogeography.* The Geological Society of London Memoir **12**, 57-73.

WYBORN L. A. I. 1988. Petrology, geochemistry and origin of a major Australian 1880-1840 Ma felsic volcano-plutonic suite: a model for intracontinental felsic magma generation. *Precambrian Research* **40/41**, 37-60.

WYBORN L. A. I., PAGE R. W. & PARKER A. J. 1987. Geochemical and geochronological signatures in Australian Proterozoic rocks. *In*: Pharoah T. C., Beckinsale R. D. & Rickard D. eds. Geochemistry and mineralization of Proterozoic volcanic suites. *Geological Society of London, Special Publication* **33**, 377-394.

WYLLIE P. J. 1979. Magmas and volatile components. *American Mineralogist* **64**, 469-500.

YAKUBCHUK A. S., NIKISHIN A. M. & ISHIWATARI A. 1994. A Late Proterozoic ophiolite pulse. *Proceedings of the 29th International Geological Conference*, Part D, 273-286.

YANO T. & WU G. 1995. Middle Jurassic to Early Cretaceous arch tectonics in East Asian continental margin. *Proceedings of 15th International Symposium of Kyungpook National University (1995)*, 177-192.

YOUNG G. M. 1992. Late Proterozoic stratigraphy and the Canada-Australia connection. *Geology* **20**, 215-218.

YOUNG G. M. & GOSTIN V. A. 1991. Late Proterozoic (Sturtian) succession of the North Flinders Basin, South Australia: an example of temperate glaciation in an active rift setting. *In*: Anderson J. B. & Ashley G. M. eds. *Glacial marine sedimentation: paleoclimatic significance*. Geological Society of America Special Paper **261**, 207-223.

YOUNG G. M. & NESBITT H. W. 1985. The Gowganda Formation in the southern part of the Huronian outcrop belt, Ontario, Canada: Stratigraphy, depositional environments and regional tectonic significance. *Precambrian Research* **29**, 265-301.

ZHAO G., CAWOOD P. A. & WILDE S. A. 1999. Reconstructions of global 2.1-1.8 Ga collisional orogens and associated cratons: implications for two pre Rodinia supercontinents? *In:* Watts G. R. & Evans D. A. D. eds. Two billion years of tectonics and mineralisation. *Geological Society of Australia Abstracts* **56**, 60-64.

ZIEGLER P. A. 1989. *Evolution of Laurussia. A study in Late Palaeozoic plate tectonics*. Kluwer Academic Publishers, Dordrecht.

CONTENTS

LIST OF FIGURES

LIST OF TABLES

A1. KINEMATICS OF EARTH EXPANSION

An investigation into the kinematics of an Earth expansion with time uses the equation for palaeoradius:

$$R_a = (R_0 - R_p)e^{kt} + R_p \qquad \text{(Equation 2.6)}$$

which was derived in Section 2.2 from empirical oceanic surface area data (Table A1.1) and continental surface area based on a primordial Earth of radius 1700 kilometres. Equation 2.6 is a mathematical expression for exponential change in the palaeoradius of the Earth from the Archaean to the Recent, and assumes that oceanic and continental lithosphere is fully fixed in the rock record with little or no requirement for removal of lithosphere by subduction.

Table A1.1 Empirical surface area data derived from Larson *et al*. (1985). Areas digitized and calculated using a CAD based Graphical Design System software package. Arbitrarily assigned errors are ±5% (from Maxlow, 1995).

Age		Surface Area			Palaeoradius
Chron	**Years (x10^6)**	**dS (x10^7 km^2)**	**S dS (x10^7 km^2)**	**S_a=S_0-S dS (x10^7 km^2)**	**R_a (km)**
0	0	0	0	51.0000	6370.80
C2	0-1.9	0.5342	0.5342	50.4658	6337.15
C3a	1.9-5.9	1.3328	1.8670	49.3300	6265.43
C6b	5.9-23.0	4.9213	6.7883	44.2117	5931.49
C15	23.0-37.7	4.1624	10.9507	40.0493	5645.37
C25	37.7-59.2	4.1649	15.1156	35.8844	5343.77
C29	59.2-66.2	1.0462	16.1618	34.8382	5265.30
C34	66.2-84.0	4.7956	20.9574	30.0426	4889.49
M0	84.0-118.7	5.6758	26.6332	24.3668	4403.46
M17	118.7-143.8	1.9348	28.5680	22.4320	4225.02
M38	143.8-205	1.9386	30.5066	20.4934	4038.31

S_0 = present surface area = 5.1x10^8 km^2 (Stacey, 1977), S_a = ancient surface area, dS = surface area of chron interval, ΣdS = cumulative chron interval surface areas, R_a = ancient palaeoradius.

Known parameters of the present Earth at time t_0 are (Stacey, 1977):

$R_0 = 6.3708 \times 10^6$ m

$S_0 = 5.1000 \times 10^{14}$ m^2

$V_0 = 1.0830 \times 10^{21}$ m^3

$M_0 = 5.9730 \times 10^{24}$ kg

$D_0 = 5.5150 \times 10^3$ kg/m^3

$G_0 = 6.6732 \times 10^{-11}$ m^3 kg^{-1} sec^{-2}

$g_0 = 9.780317$ m sec^{-2}

Where: R = palaeoradius, S = surface area, V = volume, M = mass, D = mean density, G = universal gravitation, g = surface gravity of the Earth

A1.1 Radius, Circumference, Surface Area, Volume

Derived quantities for the variables radius, circumference, surface area and volume are calculated for the time interval t_0 (present) to t_{3800} (Archaean) using the following equations:

Ancient Radius	$R_a = (R_0-R_p)e^{kt}+R_p$
Ancient Circumference	$C_a = 2\pi R_a = 2\pi((R_0-R_p)e^{kt}+R_p)$
Ancient Surface Area	$S_a = 4\pi R_a^2 = 4\pi((R_0-R_p)e^{kt}+R_p)^2$
Ancient Volume	$V_a = (4/3)\pi(R_a)^3 = (4/3)\pi((R_0-R_p)e^{kt}+R_p)^3$

Where: R_a = past Earth palaeoradius, R_0 = present mean Earth radius = 6370.8 km (Stacey 1977), R_p = primordial Earth radius = 1700 km, e = an exponent, k = 4.5366×10^{-9}/year (Section 2.2), t = time before present (negative)

Derived quantities for radius, circumference, surface area and volume are listed in Table A1.2 and shown in Figure 2.7 (Section 2.3).

Table A1.2 Derived quantities for the variables radius, circumference, surface area and volume. Calculated from palaeoradius Equation 2.6.

Geologic Time Scale		Kinematics			
Chron	**Age**	**Radius**	**Circumference**	**Area**	**Volume**
	(m.y.)	(km)	($kmx10^4$)	(km^2x10^5)	(km^3x10^8)
Future	300	19916.4	12513.81	49845.91	330916.26
Future	200	13272.8	8339.54	22137.79	97943.42
Future	100	9052.2	5687.64	10297.07	31070.24
Future	5	6478.0	4070.22	5273.35	11386.84
C0 Present	0.0	6370.8	4002.89	5100.32	10831.05
C2 Quaternary	-1.9	6330.7	3977.70	5036.34	10627.87
C3A Pliocene	-5.9	6247.4	3925.38	4904.72	10213.97
C6B Miocene	-23.0	5908.0	3712.11	4386.23	8637.94
C15 Oligocene	-37.7	5636.5	3541.54	3992.39	7501.08
C25 Eocene	-59.2	5270.7	3311.68	3490.97	6133.29
C29 Paleocene	-66.2	5159.1	3241.55	3344.69	5751.85
C34 Late Cretaceous	-84.0	4890.7	3072.94	3005.79	4900.19
M0 Mid Cretaceous	-118.7	4426.0	2780.93	2461.68	3631.79
M17 Early Cretaceous	-143.8	4132.6	2596.59	2146.14	2956.38
M29 Late Jurassic	-160.0	3960.2	2488.29	1970.84	2601.67
M38 Early Jurassic	-205.0	3542.9	2226.05	1577.32	1862.74
Triassic	-245.0	3237.0	2033.89	1316.75	1420.79
Permian	-286.0	2976.2	1869.98	1113.07	1104.22
Carboniferous	-360.0	2612.2	1641.32	857.50	746.66
Devonian	-408.0	2433.7	1529.16	744.31	603.82
Silurian	-438.0	2340.4	1470.50	688.30	536.96
Ordovician	-505.0	2172.5	1365.04	593.11	429.52
Cambrian	-570.0	2051.9	1289.22	529.06	361.85
Neoproterozoic	-900.0	1778.7	1117.61	397.59	235.74
Mesoproterozoic	-1,600.0	1703.3	1070.21	364.57	206.99
Palaeoproterozoic	-2,500.0	1700.1	1068.18	363.19	205.82
Archaean	-3,800.0	1700.0	1068.14	363.17	205.8

A1.2 Mass Density and Surface Gravity

The kinematics of mass, density and surface gravity, assuming a simplistic spherical Earth model with a homogeneous mass and density distribution is governed by the standard equations:

Density $D = Mass / Volume$

and:

Surface gravity $g = GM/R^2$

In the density equation, volume is calculated from Equation 2.6 and the variables mass M and density D are unknown. In the surface gravity equation, universal gravitation G is assumed to be constant. Three possible scenarios exist for an expression representing the kinematics of mass, density and surface gravity with time:

1. Mass remains constant requiring density to decrease exponentially as volume increases throughout geological time.
2. Density remains constant requiring mass to increase exponentially as volume increases throughout geological time.
3. Both mass and density are variable as volume increases throughout geological time.

Derived quantities for the variables mass, density and surface gravity for conditions of a) constant mass and b) constant density are calculated by incorporating Equation 2.6 for the time interval t_0 to t_{3800} using the following equations:

a) Constant Mass: $M = M_0$

$$D = M/V = M_0/(4/3)\pi((R_0-R_p)e^{kt}+R_p)^3$$

$$g = GM/R^2 = GM_0/((R_0-R_p)e^{kt}+R_p)^2$$

b) Constant Density: $D = D_0$

$$M = DV = D_0(4/3)\pi((R_0-R_p)e^{kt}+R_p)^3$$

$$g = GM/R^2 = GD_0(4/3)\pi((R_0-R_p)e^{kt}+R_p)^3/((R_0-R_p)e^{kt}+R_p)^2$$

$$= GD_0(4/3)\pi((R_0-R_p)e^{kt}+R_p)$$

Each of these variables is shown graphically in Figure 2.8 (Section 2.3).

A1.3 Secular Rate of Earth expansion

The secular rate of Earth expansion is defined as an incremental increase in the physical dimensions of the Earth throughout geological time and may be quantified by considering the variables radius, circumference, surface area and volume. Mass, density and surface gravity are considered speculative and mass is assumed to

increase with time (Section 2.3). The application of Equation 2.6 enables the secular rate of Earth expansion to be determined for the following variables between times t_1 and t_2:

$dR/dt = (R_1-R_2)/(t_1-t_2) = (((R_0-R_p)e^{kt1}+R_p)-((R_0-R_p)e^{kt2}+R_p))/(t_1-t_2)$

$dC/dt = (C_1-C_2)/(t_1-t_2)= ((2\pi((R_0-R_p)e^{kt1}+R_p)-(2\pi((R_0-R_p)e^{kt2}+R_p))/t_1-t_2)$

$dS/dt = (S_1-S_2)/(t_1-t_2) = ((4\pi((R_0-R_p)e^{kt1}+R_p)^2-(4\pi((R_0-R_p)e^{kt2}+R_p)^2)/(t_1-t_2)$

$dV/dt = (V_1-V_2)/(t_1-t_2) = ((4\pi/3)((R_0-R_p)e^{kt1}+R_p)^3-(4\pi/3)((R_0-R_p)e^{kt2}+R_p)^3/(t1-t2)$

Assuming a constant Earth density and variable mass and surface gravity:

$dD/dt = 0$

$dM/dt = (M_1-M_2)/(t_1-t_2)$

$= (D_0(4/3)\pi((R_0-R_p)e^{kt1}+R_p)^3-D_0(4/3)\pi((R_0-R_p)e^{kt2}+R_p)^3)/(t_1-t_2)$

$dg/dt = (g_1-g_2)/(t_1-t_2)$

$= (GD_0(4/3)\pi((R_0-R_p)e^{kt1}+R_p)-GD_0(4/3)\pi((R_0-R_p)e^{kt2}+R_p))/(t_1-t_2)$

The present secular rates of Earth expansion derived from the above formulae at time t_0 are:

Radius	$dR/dt_0 = 22$ mm/year
Circumference	$dC/dt_0 = 140$ mm/year
Surface Area	$dS/dt_0 = 3.50$ km^2/year
Volume	$dV/dt_0 = 11{,}000$ km^3/year
Mass	$dM/dt_0 = 60 \times 10^{12}$tonnes/year
Density	$dD/dt_0 = 0$
Surface Gravity	$dg/dt_0 = 3.4 \times 10^{-8}$ msec^{-2}/year

A2. SPACE GEODETIC CHARTS

The following contains charted and tabulated information on 88 VLBI, SLR, GPS and LLR observation sites used by the International Earth Rotation Service (ITRF) during the period 1992 to 1997 inclusive. Charts are organised into Appendix A2.1: VLBI; Appendix A2.2: SLR; Appendix A2.3: GPS and; Appendix A2.4: LLR. Within each appendix, charts are arranged in numerical order according to the observation site location number. Charts represent plots of the variation of actual Earth radius of a particular observing site, derived from published International Earth Rotation Service geodetic solutions for 1992, 1993, 1994, 1996 and 1997 (http://lareg.ensg.ign.fr/ITRF/). Site position geocentric co-ordinates and velocity vectors for VLBI, SLR, GPS and LLR (one observation only) solutions are tabulated with each chart. Graphs shown on all charts represent plots of Earth radii relative to the geocentric centre of the Earth for each year of publication, followed by radii derived from published velocity vectors projected in yearly increments to 1999.

Earth radii are derived using the following equation:

$$\text{Earth radius} = v(X^2 + Y^2 + Z^2) \qquad \text{(Equation A2.1)}$$

Where: X, Y, and Z represent the published site co-ordinates in ITRF cartesian co-ordinates relative to the centre of the Earth's mass.

Projected time variant Earth radii are derived using:

$$\text{Projected Earth radius} = v((X+Vx)^2 + (Y+Vy)^2 + (Z+Vz)^2) \qquad \text{(Equation A2.2)}$$

Where: Vx, Vy, and Vz represent the published site velocities in ITRF cartesian co-ordinates relative to the centre of the Earth's mass.

Predicted Earth expansion is derived using:

$$\text{Earth radius} = v(X^2 + Y^2 + Z^2) + 0.022 \qquad \text{(Equation A2.3)}$$

Where: 0.022 represents the radial increase in Earth expansion in millimetres per year determined from Equation 2.6 (Section 2.2, and Appendix A1).

For each chart the 1992 solution is adopted as a starting point for plotting predicted Earth expansion. Actual radius variation is shown as a thick line by joining the published solutions for each year shown. For each of the VLBI sites in Appendix 2.1, GSFC solution 1102g 1998 is also included for reference only. Part of this VLBI solution is constrained within the ITRF97 global solution.

A2.1 VLBI Space Geodetic Charts

10002M003 GRASSE - VLBI (FRANCE)

	Site Co-ordinates			Site Velocity			Derived Earth Radius							
Data	**X**	**Y**	**Z**	**Vx**	**Vy**	**Vz**	**1992**	**1993**	**1994**	**1995**	**1996**	**1997**	**1998**	**1999**
Source	**m**	**m**	**m**	**m/y**	**m/y**	**m/y**	6369272.747	6369272.769	6369272.791	6369272.813	6369272.835	6369272.857	6369272.879	6369272.901
ITRF 1992	4581697.792	556125.612	4389351.315	-0.0179	0.0185	0.0018	6369272.747	6369272.737	6369272.727	6369272.716	6369272.706	6369272.696	6369272.686	6369272.676
ITRF 1993	4581697.715	556125.69	4389351.416	-0.0116	0.0208	0.0074		6369272.768	6369272.766	6369272.765	6369272.763	6369272.762	6369272.760	6369272.759
ITRF 1994	4581697.718	556125.694	4389351.406	-0.0125	0.019	0.0087			6369272.763	6369272.762	6369272.761	6369272.759	6369272.758	6369272.757
ITRF 1996	4581697.68	556125.772	4389351.462	-0.012	0.0189	0.0106					6369272.781	6369272.782	6369272.782	6369272.782
ITRF 1997	4581697.669	556125.765	4389351.446	-0.0118	0.0185	0.009						6369272.762	6369272.761	6369272.760
GSFC 1998	4581697.663	556125.766	4389351.455	-0.0123	0.0188	0.0104							6369272.764	6369272.764
							6369272.747	6369272.768	6369272.763	6369272.772	6369272.781	6369272.762	6369272.764	

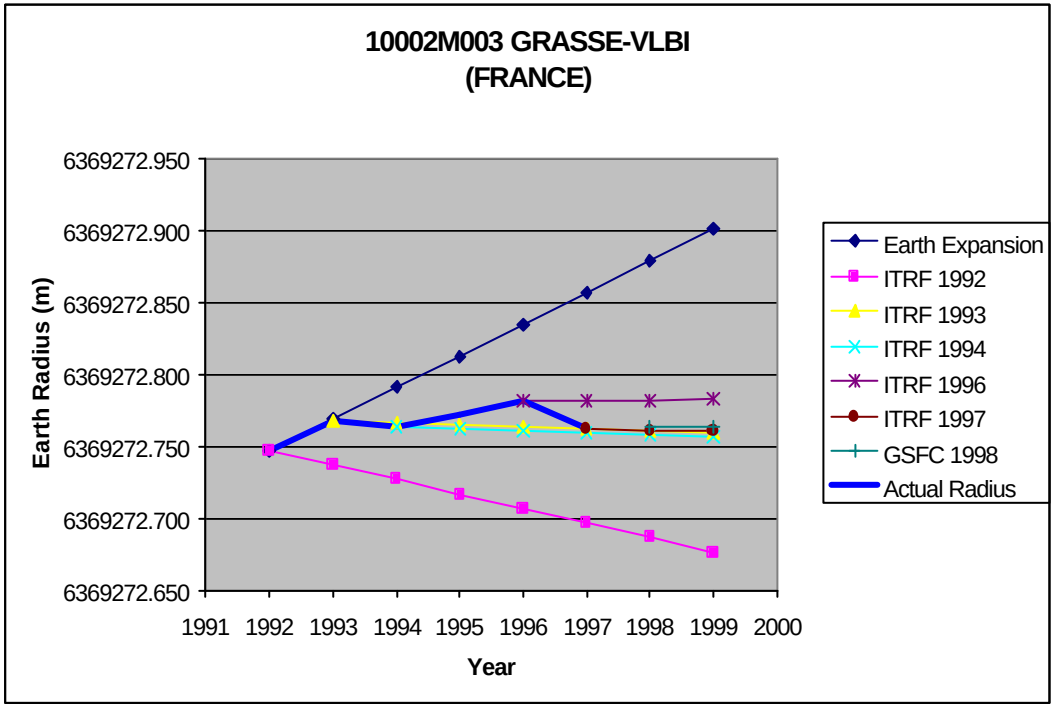

10302M002 TROMSO-VLBI (NORWAY)

	Site Co-ordinates			Site Velocity			Derived Earth Radius							
Data	X	Y	Z	Vx	Vy	Vz	1992	1993	1994	1995	1996	1997	1998	1999
Source	m	m	m	m/y	m/y	m/y	6359487.284	6359487.306	6359487.328	6359487.350	6359487.372	6359487.394	6359487.416	6359487.438
ITRF 1992	2102904.226	721602.401	5958201.264	-0.0173	0.0131	0.0045	6359487.284	6359487.284	6359487.284	6359487.284	6359487.284	6359487.284	6359487.284	6359487.284
ITRF 1993	2102904.121	721602.481	5958201.294	-0.0167	0.0125	0.0039		6359487.286	6359487.286	6359487.285	6359487.285	6359487.284	6359487.284	6359487.283
ITRF 1994	2102904.131	721602.491	5958201.291	-0.0191	0.0153	0.0042			6359487.288	6359487.287	6359487.286	6359487.286	6359487.285	6359487.285
ITRF 1996	2102904.058	721602.508	5958201.318	-0.0182	0.0074	0.0047					6359487.291	6359487.290	6359487.289	6359487.289
ITRF 1997	2102904.056	721602.517	5958201.315	-0.0175	0.0076	0.005						6359487.288	6359487.288	6359487.288
GSFC 1998	2102904.053	721602.61	5958201.344	-0.0176	0.0233	0.0105							6359487.325	6359487.332
							6359487.284	6359487.286	6359487.288	6359487.290	6359487.291	6359487.288	6359487.325	

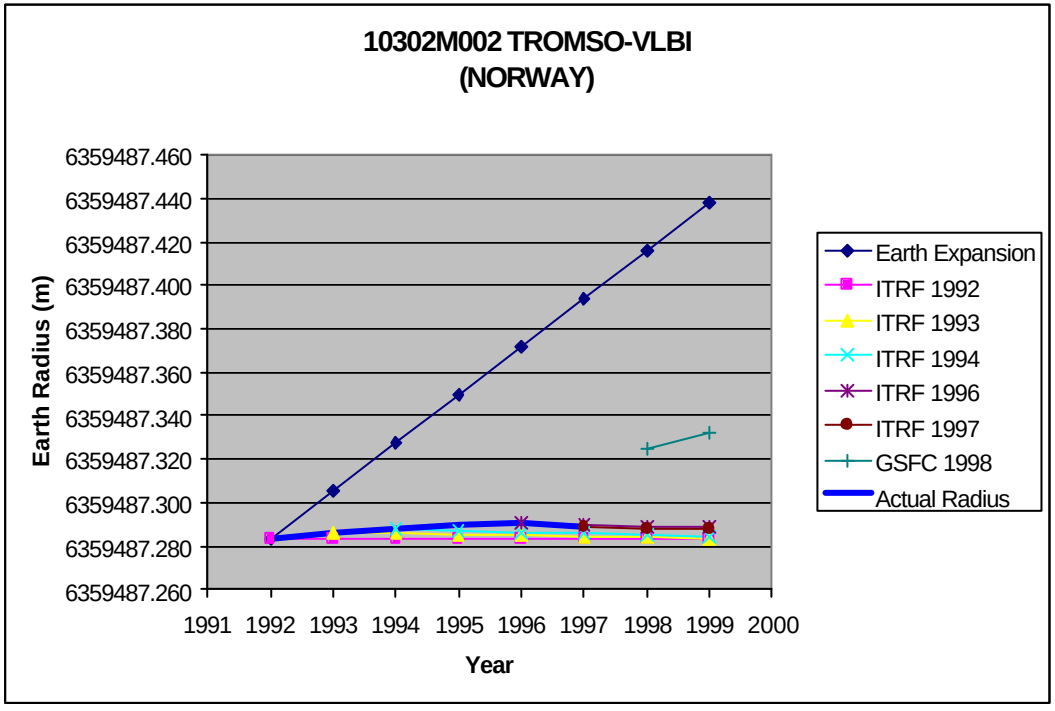

10503M002 METSAHOVI-VLBI (FINLAND)

	Site Co-ordinates			Site Velocity			Derived Earth Radius							
Data	X	Y	Z	Vx	Vy	Vz	1992	1993	1994	1995	1996	1997	1998	1999
Source	m	m	m	m/y	m/y	m/y	6362113.423	6362113.445	6362113.467	6362113.489	6362113.511	6362113.533	6362113.555	6362113.577
ITRF 1992	2890652.901	1310295.212	5513958.602	-0.0181	0.0152	0.0059	6362113.423	6362113.423	6362113.423	6362113.423	6362113.423	6362113.423	6362113.423	6362113.423
ITRF 1993	2890652.805	1310295.288	5513958.67	-0.0174	0.0145	0.0055		6362113.454	6362113.453	6362113.453	6362113.453	6362113.453	6362113.453	6362113.453
ITRF 1994	2890652.817	1310295.278	5513958.671	-0.0169	0.0129	0.0052			6362113.458	6362113.457	6362113.457	6362113.456	6362113.456	6362113.455
ITRF 1996	2890652.755	1310295.341	5513958.711	-0.0171	0.0135	0.0062					6362113.477	6362113.478	6362113.478	6362113.478
ITRF 1997	2890652.753	1310295.341	5513958.707	-0.0176	0.0139	0.0049						6362113.473	6362113.472	6362113.471
GSFC 1998	2890652.731	1310295.337	5513958.683	-0.0173	0.0146	0.0056							6362113.441	6362113.441
							6362113.423	6362113.454	6362113.458	6362113.468	6362113.477	6362113.473	6362113.441	

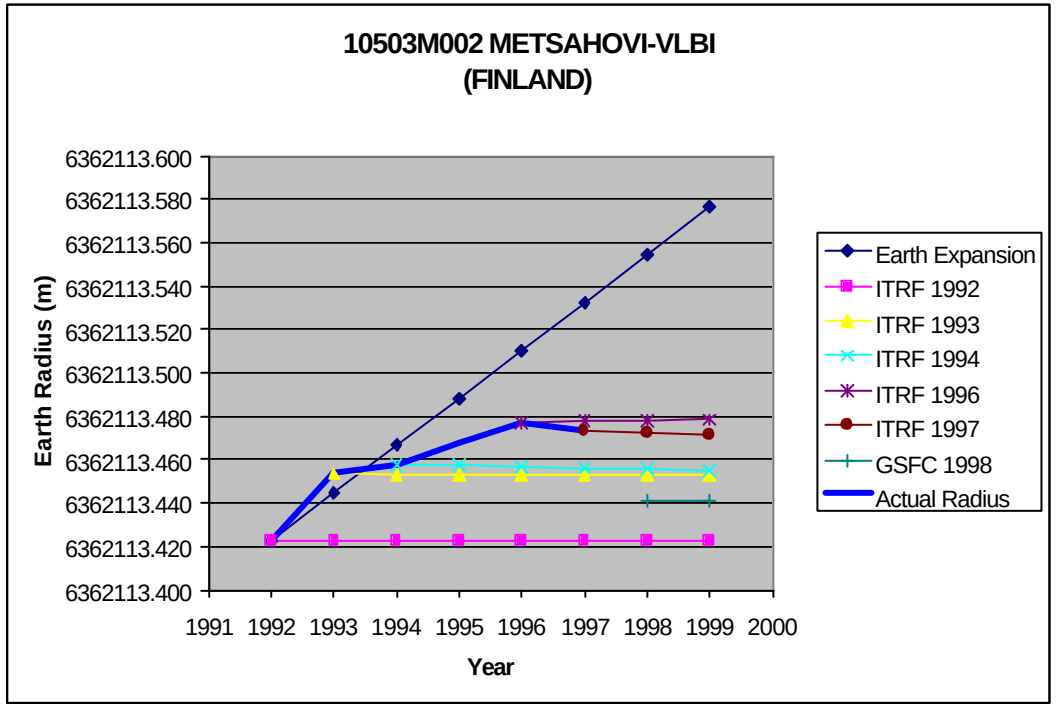

14209S001 EFFELSBERG-VLBI (GERMANY)

	Site Co-ordinates			Site Velocity			Derived Earth Radius							
Data	**X**	**Y**	**Z**	**Vx**	**Vy**	**Vz**	**1992**	**1993**	**1994**	**1995**	**1996**	**1997**	**1998**	**1999**
Source	**m**	**m**	**m**	**m/y**	**m/y**	**m/y**	6365855.306	6365855.328	6365855.350	6365855.372	6365855.394	6365855.416	6365855.438	6365855.460
ITRF 1992	4033947.6	486990.364	4900430.687	-0.0162	0.0166	0.0084	6365855.306	6365855.303	6365855.301	6365855.298	6365855.296	6365855.293	6365855.290	6365855.288
ITRF 1993	4033947.502	486990.45	4900430.741	-0.0169	0.0166	0.0075		6365855.292	6365855.288	6365855.284	6365855.281	6365855.277	6365855.273	6365855.270
ITRF 1994	4033947.524	486990.447	4900430.748	-0.0167	0.0168	0.006			6365855.311	6365855.306	6365855.301	6365855.297	6365855.292	6365855.287
ITRF 1996	4033947.46	486990.521	4900430.776	-0.0153	0.0175	0.006					6365855.297	6365855.294	6365855.290	6365855.286
ITRF 1997	4033947.469	486990.519	4900430.782	-0.0138	0.0174	0.0078						6365855.308	6365855.306	6365855.305
GSFC 1998	4033947.473	486990.523	4900430.788	-0.0136	0.018	0.0085							6365855.315	6365855.314
							6365855.306	6365855.292	6365855.311	6365855.304	6365855.297	6365855.308	6365855.315	

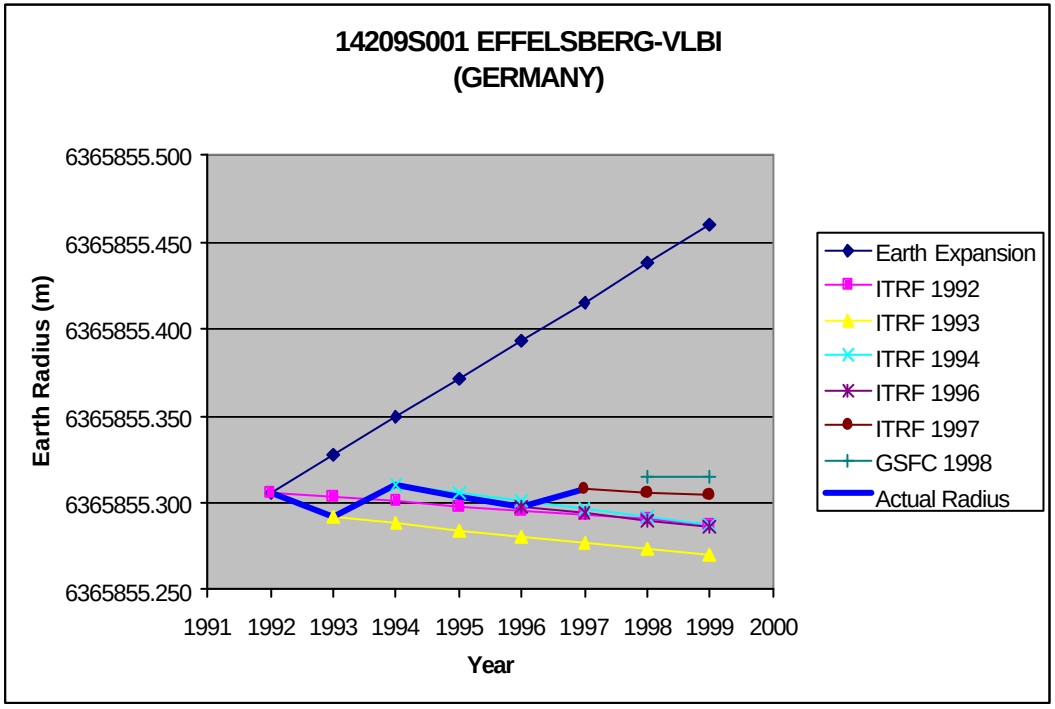

21701S001 KASHIMA-VLBI (JAPAN)

	Site Co-ordinates			Site Velocity			Derived Earth Radius							
Data	**X**	**Y**	**Z**	**Vx**	**Vy**	**Vz**	**1992**	**1993**	**1994**	**1995**	**1996**	**1997**	**1998**	**1999**
Source	**m**	**m**	**m**	**m/y**	**m/y**	**m/y**	6370885.703	6370885.725	6370885.747	6370885.769	6370885.791	6370885.813	6370885.835	6370885.857
ITRF 1992	-3997892.25	3276581.252	3724118.349	-0.0005	0.0021	-0.012	6370885.703	6370885.697	6370885.691	6370885.686	6370885.680	6370885.675	6370885.669	6370885.663
ITRF 1993	-3997892.27	3276581.289	3724118.274	-0.0022	-0.0001	-0.0084		6370885.690	6370885.687	6370885.683	6370885.680	6370885.676	6370885.673	6370885.669
ITRF 1994	-3997892.27	3276581.262	3724118.288	-0.0018	0.0014	-0.0144			6370885.682	6370885.676	6370885.669	6370885.663	6370885.656	6370885.649
ITRF 1996	-3997892.26	3276581.277	3724118.22	-0.0013	0.0024	-0.0129					6370885.647	6370885.642	6370885.636	6370885.631
ITRF 1997	-3997892.27	3276581.288	3724118.216	-0.0021	0.0036	-0.0135						6370885.654	6370885.649	6370885.645
GSFC 1998	-3997892.27	3276581.28	3724118.222	-0.0003	0.0065	-0.0116							6370885.651	6370885.648
							6370885.703	6370885.690	6370885.682	6370885.665	6370885.647	6370885.654	6370885.651	

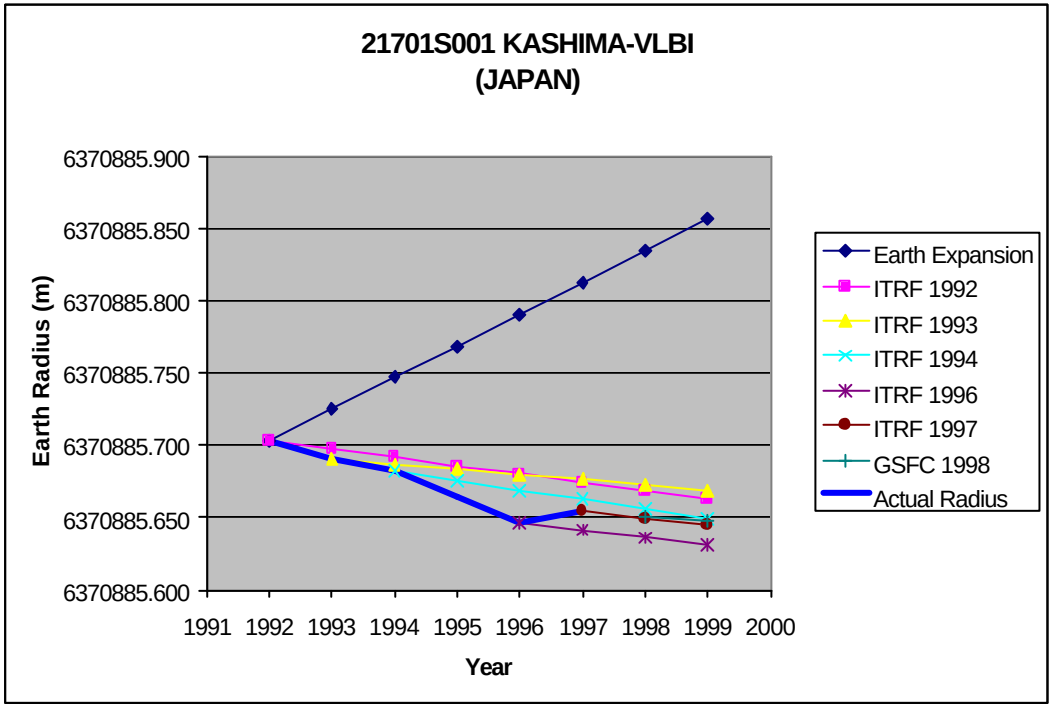

21725S001 NOBEYAMA-VLBI (JAPAN)

	Site Co-ordinates			Site Velocity			Derived Earth Radius							
Data	**X**	**Y**	**Z**	**Vx**	**Vy**	**Vz**	**1992**	**1993**	**1994**	**1995**	**1996**	**1997**	**1998**	**1999**
Source	**m**	**m**	**m**	**m/y**	**m/y**	**m/y**	6372199.833	6372199.855	6372199.877	6372199.899	6372199.921	6372199.943	6372199.965	6372199.987
ITRF 1992	-3871168.22	3428273.995	3723697.72	-0.0134	-0.0004	-0.0137	6372199.833	6372199.832	6372199.832	6372199.832	6372199.832	6372199.832	6372199.832	6372199.832
ITRF 1993	-3871168.32	3428273.986	3723697.641	-0.0068	0.0041	-0.0093		6372199.837	6372199.838	6372199.839	6372199.840	6372199.841	6372199.842	6372199.843
ITRF 1994	-3871168.32	3428273.957	3723697.655	-0.0169	-0.0086	-0.0139			6372199.830	6372199.827	6372199.825	6372199.823	6372199.820	6372199.818
ITRF 1996	-3871168.43	3428273.937	3723697.582	-0.0274	-0.0049	-0.0134					6372199.845	6372199.851	6372199.858	6372199.864
ITRF 1997	-3871168.6	3428274.139	3723697.749	-0.0581	0.0302	0.0174						6372200.154	6372200.215	6372200.277
GSFC 1998	-3871168.56	3428274.263	3723697.835	-0.0463	0.0493	0.0273							6372200.247	6372200.318
							6372199.833	6372199.837	6372199.830	6372199.838	6372199.845	6372200.154	6372200.247	

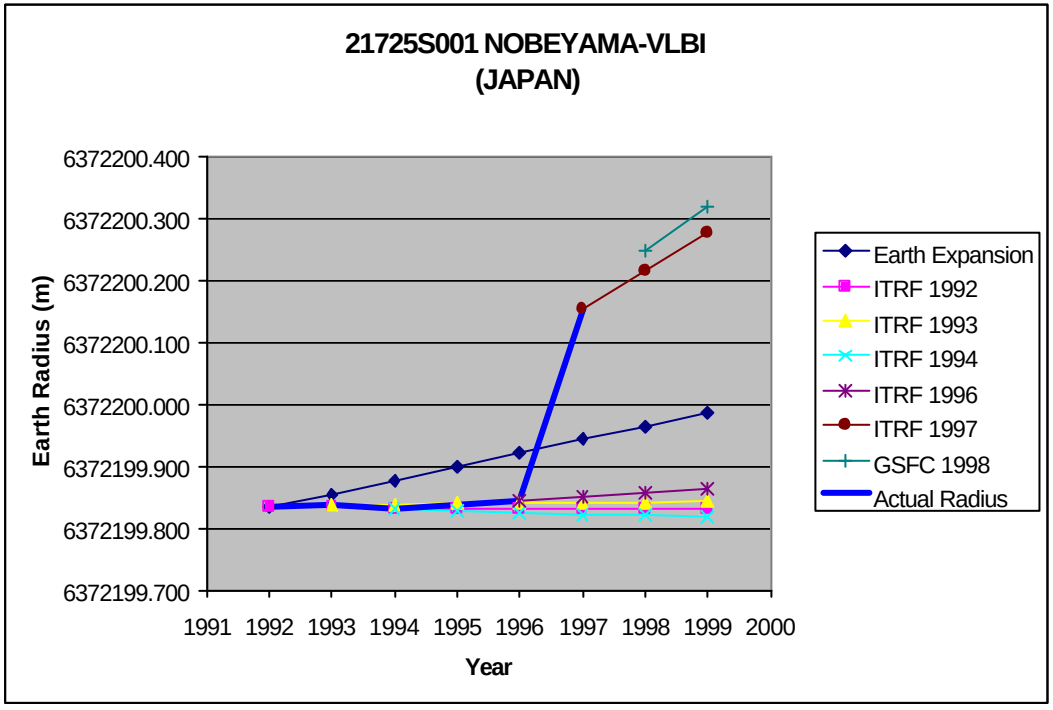

21730S001 TSUKUBA-VLBI (JAPAN)

	Site Co-ordinates			Site Velocity			Derived Earth Radius							
Data	**X**	**Y**	**Z**	**Vx**	**Vy**	**Vz**	**1992**	**1993**	**1994**	**1995**	**1996**	**1997**	**1998**	**1999**
Source	**m**	**m**	**m**	**m/y**	**m/y**	**m/y**								
ITRF 1992	-3957172.89	3310237.922	3737709.034	-0.0037	0.0021	-0.0111	6370821.078	6370821.075	6370821.072	6370821.069	6370821.066	6370821.063	6370821.060	6370821.056
ITRF 1993	-3957172.92	3310237.968	3737708.976	-0.0046	0.0022	-0.0053		6370821.089	6370821.090	6370821.091	6370821.091	6370821.092	6370821.093	6370821.094
ITRF 1994	-3957172.93	3310237.934	3737709.015	-0.0046	0.0015	-0.0111			6370821.096	6370821.094	6370821.091	6370821.088	6370821.085	6370821.082
ITRF 1996	-3957172.93	3310237.956	3737708.939	-0.0005	0.0025	-0.0118					6370821.062	6370821.057	6370821.051	6370821.046
ITRF 1997	-3957172.93	3310237.963	3737708.933	-0.0017	0.0043	-0.013						6370821.066	6370821.062	6370821.057
GSFC 1998	-3957172.92	3310237.954	3737708.923	-0.001	0.0064	-0.011							6370821.046	6370821.043
							6370821.078	6370821.089	6370821.096	6370821.079	6370821.062	6370821.066	6370821.046	

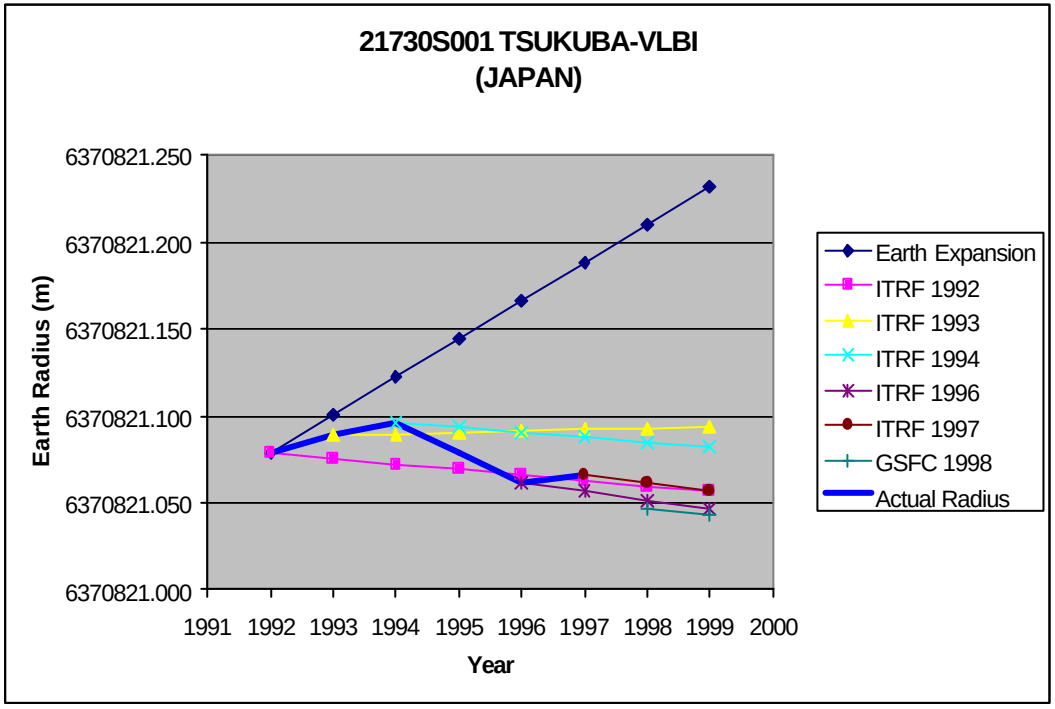

21732S001 CHICHIJIMA-VLBI (JAPAN)

	Site Co-ordinates			Site Velocity			Derived Earth Radius							
Data	**X**	**Y**	**Z**	**Vx**	**Vy**	**Vz**	**1992**	**1993**	**1994**	**1995**	**1996**	**1997**	**1998**	**1999**
Source	**m**	**m**	**m**	**m/y**	**m/y**	**m/y**	6373828.221	6373828.243	6373828.265	6373828.287	6373828.309	6373828.331	6373828.353	6373828.375
ITRF 1992	-4489356.68	3482989.525	2887931.223	0.0141	0.017	0.0014	6373828.221	6373828.221	6373828.221	6373828.221	6373828.221	6373828.221	6373828.221	6373828.221
ITRF 1993	-4489356.63	3482989.621	2887931.217	0.0135	0.0163	0.0013		6373828.236	6373828.236	6373828.236	6373828.236	6373828.236	6373828.236	6373828.236
ITRF 1994	-4489356.62	3482989.589	2887931.231	0.0188	0.016	-0.0005			6373828.219	6373828.214	6373828.209	6373828.204	6373828.200	6373828.195
ITRF 1996	-4489356.6	3482989.625	2887931.246	0.0111	0.0124	0.004					6373828.229	6373828.230	6373828.230	6373828.231
ITRF 1997	-4489356.52	3482989.612	2887931.171	0.0113	0.0158	-0.0021						6373828.130	6373828.130	6373828.129
GSFC 1998	-4489356.57	3482989.663	2887931.215	0.0169	0.0208	0.0011							6373828.211	6373828.211
							6373828.221	6373828.236	6373828.219	6373828.224	6373828.229	6373828.130	6373828.211	

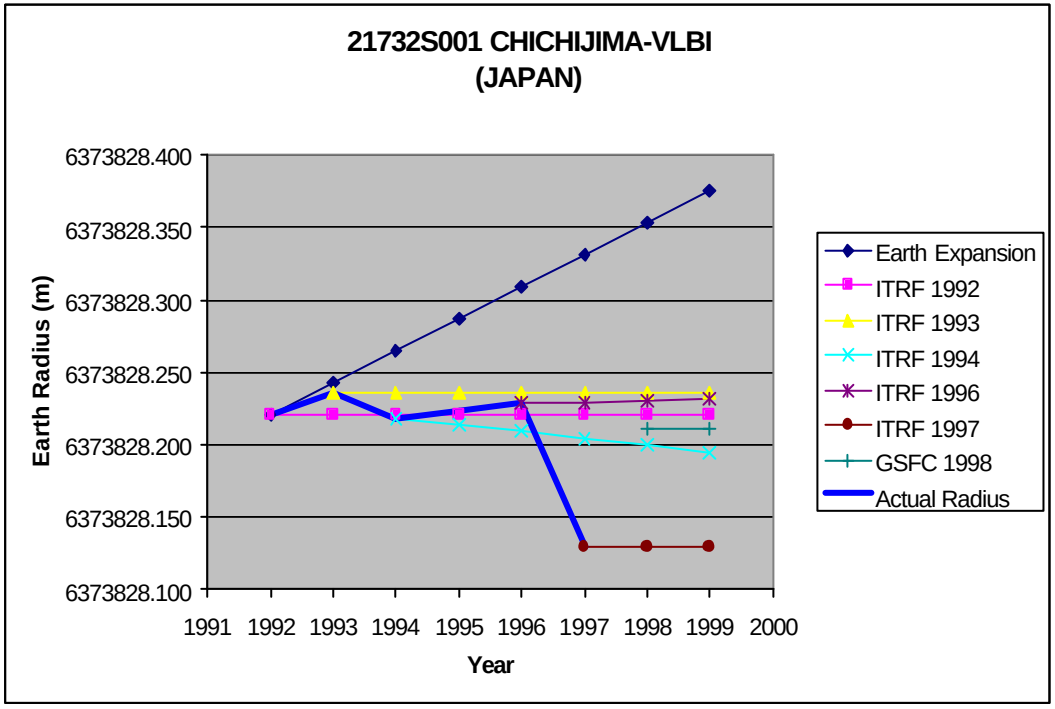

31906M001 SAO MIGUEL-VLBI (BRAZIL)

	Site Co-ordinates			Site Velocity			Derived Earth Radius							
Data	**X**	**Y**	**Z**	**Vx**	**Vy**	**Vz**	**1992**	**1993**	**1994**	**1995**	**1996**	**1997**	**1998**	**1999**
Source	**m**	**m**	**m**	**m/y**	**m/y**	**m/y**	6370225.664	6370225.686	6370225.708	6370225.730	6370225.752	6370225.774	6370225.796	6370225.818
ITRF 1992	4552174.65	-2186664.82	3882779.666	-0.0036	0.015	0.0127	6370225.664	6370225.664	6370225.664	6370225.664	6370225.664	6370225.664	6370225.664	6370225.664
ITRF 1993	4552174.618	-2186664.76	3882779.756	-0.0034	0.0144	0.0121		6370225.675	6370225.675	6370225.675	6370225.675	6370225.675	6370225.675	6370225.675
ITRF 1994	4552174.646	-2186664.76	3882779.749	-0.0013	0.0175	0.0136			6370225.690	6370225.691	6370225.693	6370225.694	6370225.695	6370225.697
ITRF 1996	4552174.608	-2186664.68	3882779.801	-0.0024	0.0165	0.014					6370225.669	6370225.670	6370225.671	6370225.673
ITRF 1997	4552174.615	-2186664.69	3882779.79	-0.0026	0.0159	0.012						6370225.669	6370225.669	6370225.669
GSFC 1998	4552174.616	-2186664.67	3882779.791	-0.0024	0.0181	0.0131							6370225.666	6370225.666
							6370225.664	6370225.675	6370225.690	6370225.679	6370225.669	6370225.669	6370225.666	

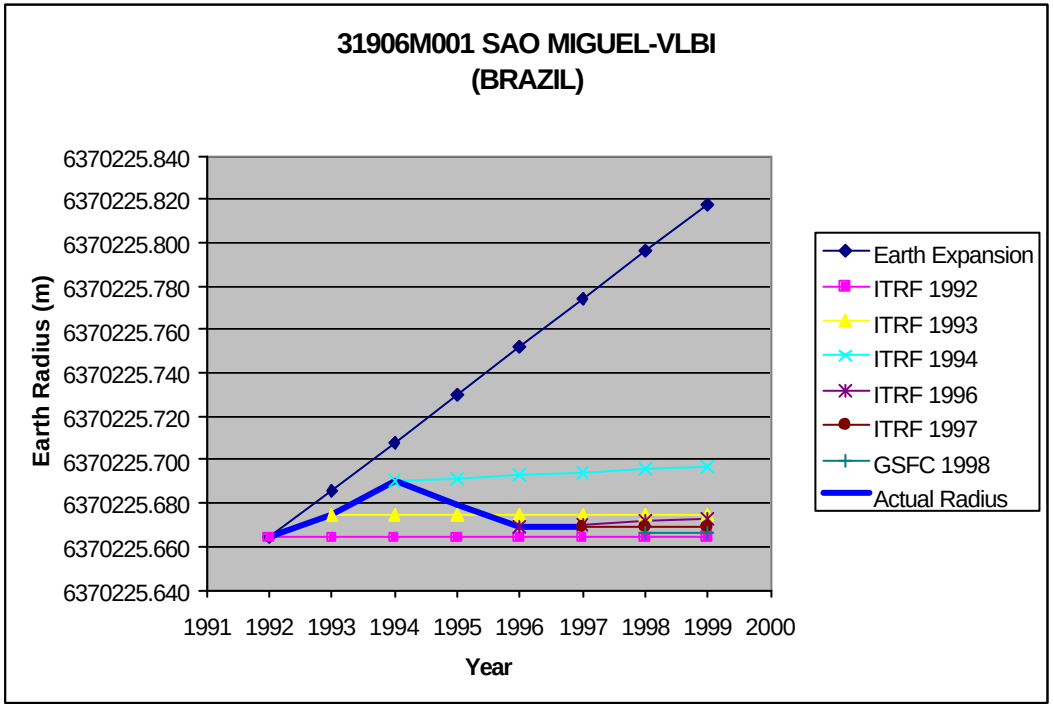

40127M001 YELLOWKNIFE-VLBI (CANADA)

	Site Co-ordinates			Site Velocity			Derived Earth Radius							
Data	**X**	**Y**	**Z**	**Vx**	**Vy**	**Vz**	**1992**	**1993**	**1994**	**1995**	**1996**	**1997**	**1998**	**1999**
Source	**m**	**m**	**m**	**m/y**	**m/y**	**m/y**	6361525.176	6361525.198	6361525.220	6361525.242	6361525.264	6361525.286	6361525.308	6361525.330
ITRF 1992	-1224124.44	-2689530.68	5633555.419	-0.0216	-0.0013	-0.0053	6361525.176	6361525.176	6361525.176	6361525.176	6361525.176	6361525.176	6361525.176	6361525.176
ITRF 1993	-1224124.57	-2689530.66	5633555.377	-0.0212	-0.0026	-0.0023		6361525.157	6361525.160	6361525.163	6361525.166	6361525.169	6361525.172	6361525.176
ITRF 1994	-1224124.55	-2689530.69	5633555.38	-0.0203	-0.005	-0.0022			6361525.166	6361525.170	6361525.174	6361525.178	6361525.182	6361525.186
ITRF 1996	-1224124.64	-2689530.69	5633555.374	-0.0196	-0.003	-0.0048					6361525.181	6361525.182	6361525.183	6361525.184
ITRF 1997	-1224124.64	-2689530.69	5633555.355	-0.0204	-0.0054	-0.0022						6361525.164	6361525.168	6361525.172
GSFC 1998	-1224124.64	-2689530.68	5633555.341	-0.021	-0.0038	0.0014							6361525.144	6361525.151
							6361525.176	6361525.157	6361525.166	6361525.174	6361525.181	6361525.164	6361525.144	

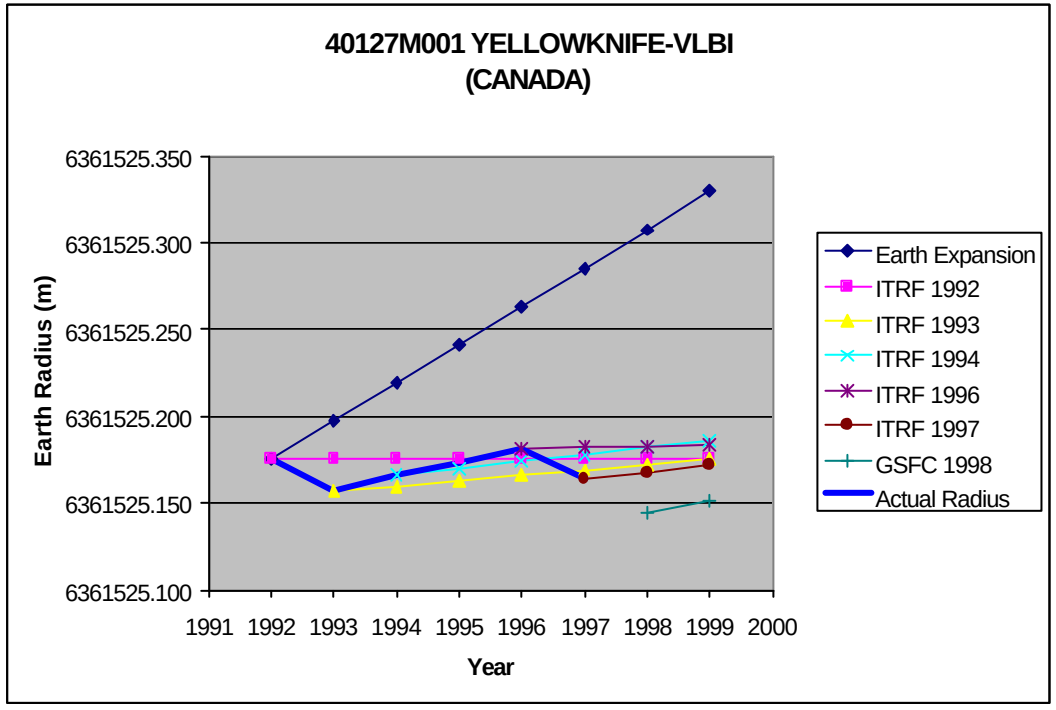

40129M001 VICTORIA-VLBI (WASHINGTON USA)

	Site Co-ordinates			Site Velocity			Derived Earth Radius							
Data	**X**	**Y**	**Z**	**Vx**	**Vy**	**Vz**	**1992**	**1993**	**1994**	**1995**	**1996**	**1997**	**1998**	**1999**
Source	**m**	**m**	**m**	**m/y**	**m/y**	**m/y**	6366252.022	6366252.044	6366252.066	6366252.088	6366252.110	6366252.132	6366252.154	6366252.176
ITRF 1992	-2341310.01	-3539083.87	4745768.389	-0.0184	-0.0009	-0.0097	6366252.022	6366252.022	6366252.022	6366252.022	6366252.022	6366252.022	6366252.022	6366252.022
ITRF 1993	-2341310.13	-3539083.86	4745768.366	-0.0177	-0.0011	-0.0091		6366252.045	6366252.045	6366252.046	6366252.046	6366252.046	6366252.047	6366252.047
ITRF 1994	-2341310.1	-3539083.88	4745768.353	-0.0107	-0.0078	-0.0019			6366252.034	6366252.040	6366252.047	6366252.054	6366252.061	6366252.068
ITRF 1996	-2341310.14	-3539083.89	4745768.339	-0.0095	-0.0041	-0.0038					6366252.042	6366252.044	6366252.047	6366252.050
ITRF 1997	-2341310.14	-3539083.89	4745768.324	-0.0105	-0.0033	-0.007						6366252.033	6366252.034	6366252.034
GSFC 1998	-2341310.17	-3539083.89	4745768.295	-0.0176	-0.0008	-0.0093							6366252.022	6366252.022
							6366252.022	6366252.045	6366252.034	6366252.038	6366252.042	6366252.033	6366252.022	

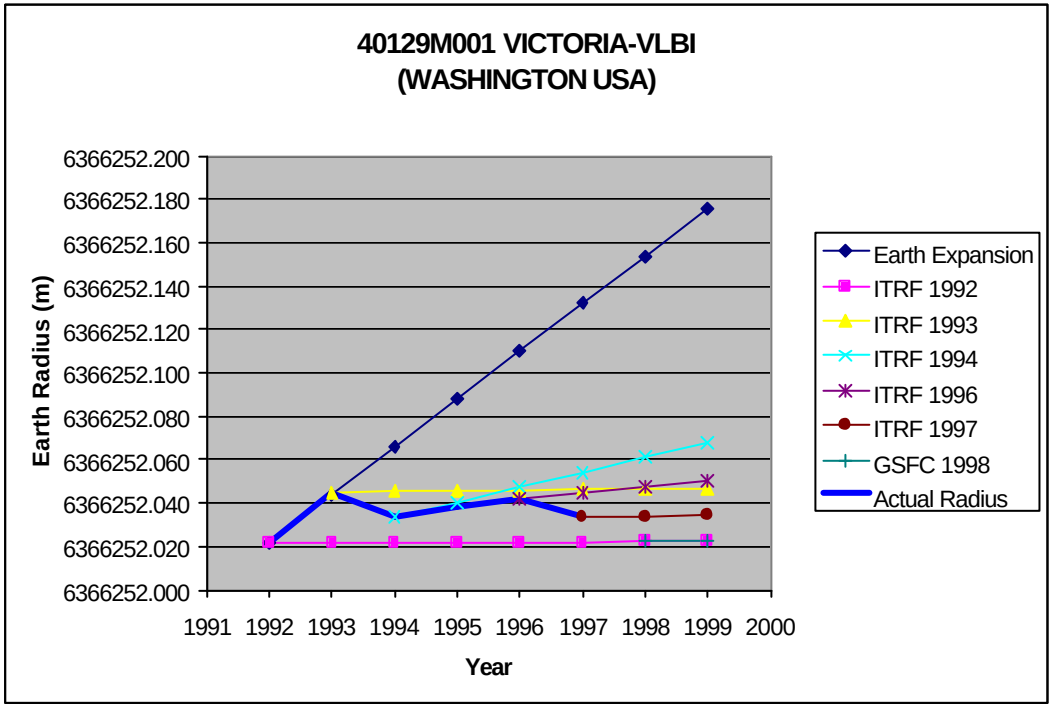

40403M001 PALOS VERDES-VLBI (CALIFORNIA)

	Site Co-ordinates			Site Velocity			Derived Earth Radius							
Data	**X**	**Y**	**Z**	**Vx**	**Vy**	**Vz**	**1992**	**1993**	**1994**	**1995**	**1996**	**1997**	**1998**	**1999**
Source	**m**	**m**	**m**	**m/y**	**m/y**	**m/y**	6371646.254	6371646.276	6371646.298	6371646.320	6371646.342	6371646.364	6371646.386	6371646.408
ITRF 1992	-2525452.71	-4670035.68	3522886.784	-0.0296	0.0241	0.0125	6371646.254	6371646.255	6371646.256	6371646.257	6371646.258	6371646.259	6371646.260	6371646.261
ITRF 1993	-2525452.89	-4670035.54	3522886.862	-0.0297	0.0246	0.014		6371646.266	6371646.268	6371646.269	6371646.270	6371646.272	6371646.273	6371646.275
ITRF 1994	-2525452.87	-4670035.57	3522886.851	-0.0282	0.027	0.0103			6371646.265	6371646.263	6371646.260	6371646.257	6371646.254	6371646.251
ITRF 1996	-2525452.98	-4670035.43	3522886.908	-0.0276	0.0275	0.0127					6371646.240	6371646.238	6371646.236	6371646.234
ITRF 1997	-2525453	-4670035.45	3522886.918	-0.0304	0.0253	0.0147						6371646.269	6371646.271	6371646.272
GSFC 1998	-2525452.95	-4670035.36	3522886.838	-0.0256	0.0385	0.0058							6371646.143	6371646.128
							6371646.254	6371646.266	6371646.265	6371646.253	6371646.240	6371646.269	6371646.143	

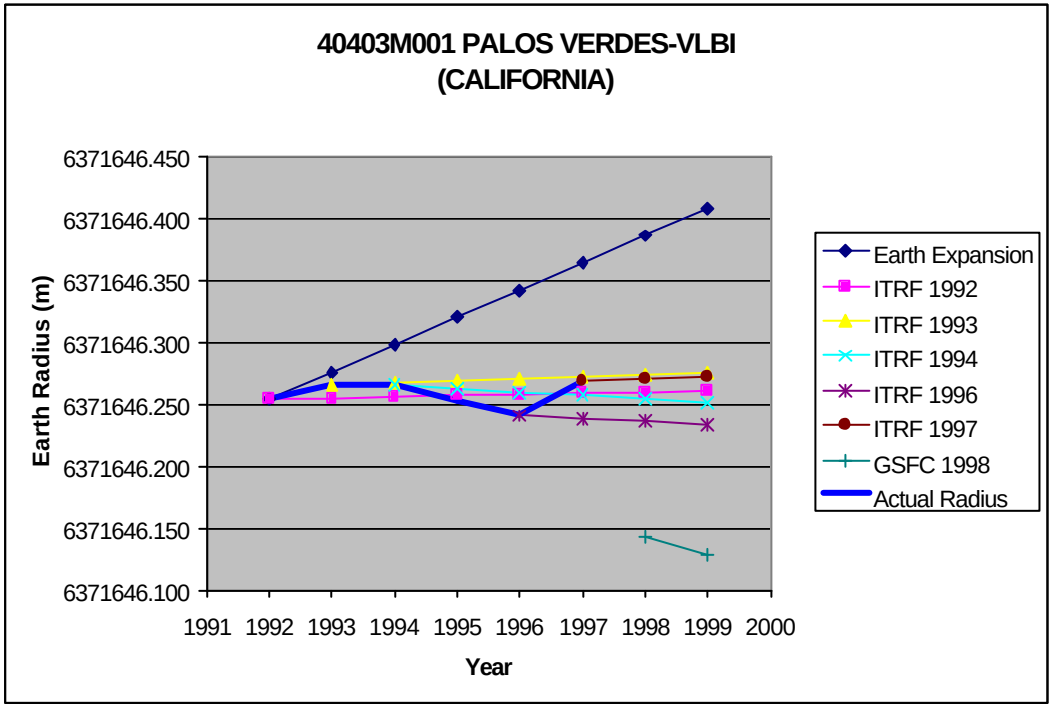

40404M001 PEARBLOSSOM-VLBI (CALIFORNIA)

	Site Co-ordinates			Site Velocity			Derived Earth Radius							
Data	X	Y	Z	Vx	Vy	Vz	1992	1993	1994	1995	1996	1997	1998	1999
Source	m	m	m	m/y	m/y	m/y	6372202.336	6372202.358	6372202.380	6372202.402	6372202.424	6372202.446	6372202.468	6372202.490
ITRF 1992	-2464070.85	-4649425.66	3593905.739	-0.0228	0.0134	0.0032	6372202.336	6372202.337	6372202.338	6372202.338	6372202.339	6372202.340	6372202.341	6372202.342
ITRF 1993	-2464070.99	-4649425.58	3593905.768	-0.0228	0.0137	0.0046		6372202.343	6372202.345	6372202.346	6372202.348	6372202.349	6372202.350	6372202.352
ITRF 1994	-2464070.97	-4649425.59	3593905.759	-0.0224	0.0146	0.003			6372202.342	6372202.341	6372202.341	6372202.341	6372202.341	6372202.340
ITRF 1996	-2464071.05	-4649425.49	3593905.758	-0.0213	0.0165	0.0025					6372202.295	6372202.293	6372202.290	6372202.288
ITRF 1997	-2464071.06	-4649425.5	3593905.755	-0.0234	0.0162	0.0022						6372202.308	6372202.307	6372202.305
GSFC 1998	-2464071.03	-4649425.43	3593905.712	-0.0206	0.0259	-0.0012							6372202.219	6372202.207
							6372202.336	6372202.343	6372202.342	6372202.319	6372202.295	6372202.308	6372202.219	

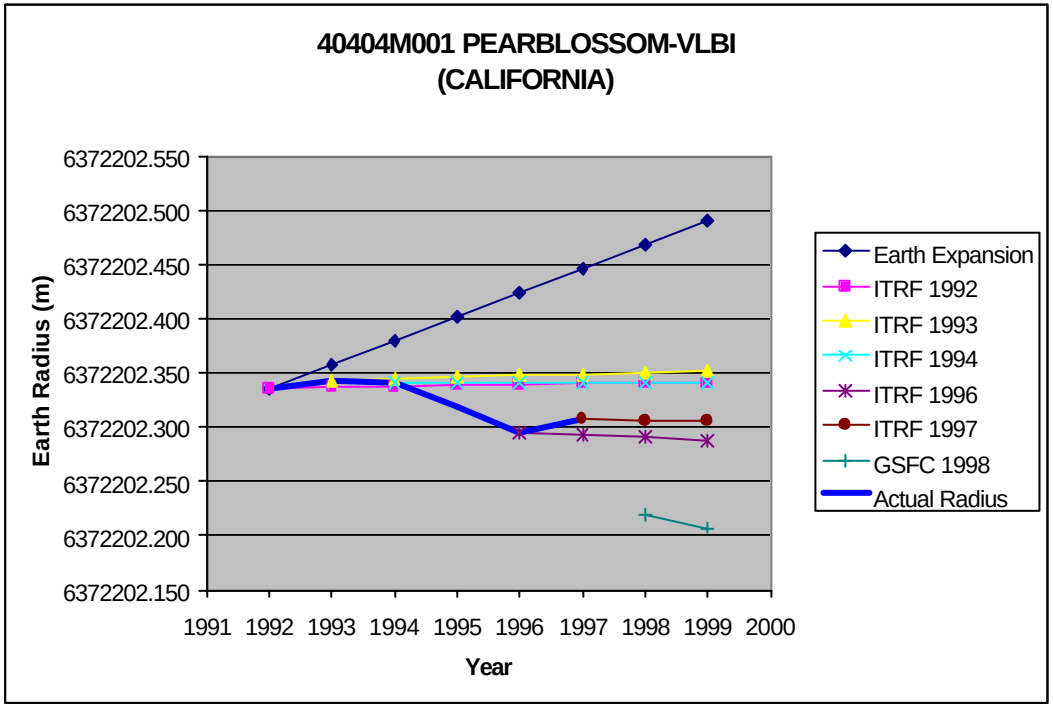

40406M001 PRESIDIO-VLBI (CALIFORNIA)

	Site Co-ordinates			Site Velocity			Derived Earth Radius							
Data	**X**	**Y**	**Z**	**Vx**	**Vy**	**Vz**	**1992**	**1993**	**1994**	**1995**	**1996**	**1997**	**1998**	**1999**
Source	**m**	**m**	**m**	**m/y**	**m/y**	**m/y**	6370114.513	6370114.535	6370114.557	6370114.579	6370114.601	6370114.623	6370114.645	6370114.667
ITRF 1992	-2707704.79	-4257609.62	3888374.212	-0.0218	0.0204	0.0082	6370114.513	6370114.514	6370114.515	6370114.515	6370114.516	6370114.517	6370114.517	6370114.518
ITRF 1993	-2707704.93	-4257609.49	3888374.259	-0.0215	0.0205	0.0098		6370114.516	6370114.517	6370114.519	6370114.520	6370114.522	6370114.523	6370114.525
ITRF 1994	-2707704.9	-4257609.55	3888374.223	-0.0222	0.0106	0.0002			6370114.519	6370114.522	6370114.524	6370114.527	6370114.529	6370114.532
ITRF 1996	-2707704.96	-4257609.37	3888374.206	-0.0177	0.0259	0.0004					6370114.412	6370114.402	6370114.393	6370114.383
ITRF 1997	-2707704.98	-4257609.37	3888374.214	-0.0201	0.0265	0.0012						6370114.428	6370114.419	6370114.411
GSFC 1998	-2707704.97	-4257609.38	3888374.253	-0.0204	0.0281	0.0058							6370114.457	6370114.450
							6370114.513	6370114.516	6370114.519	6370114.466	6370114.412	6370114.428	6370114.457	

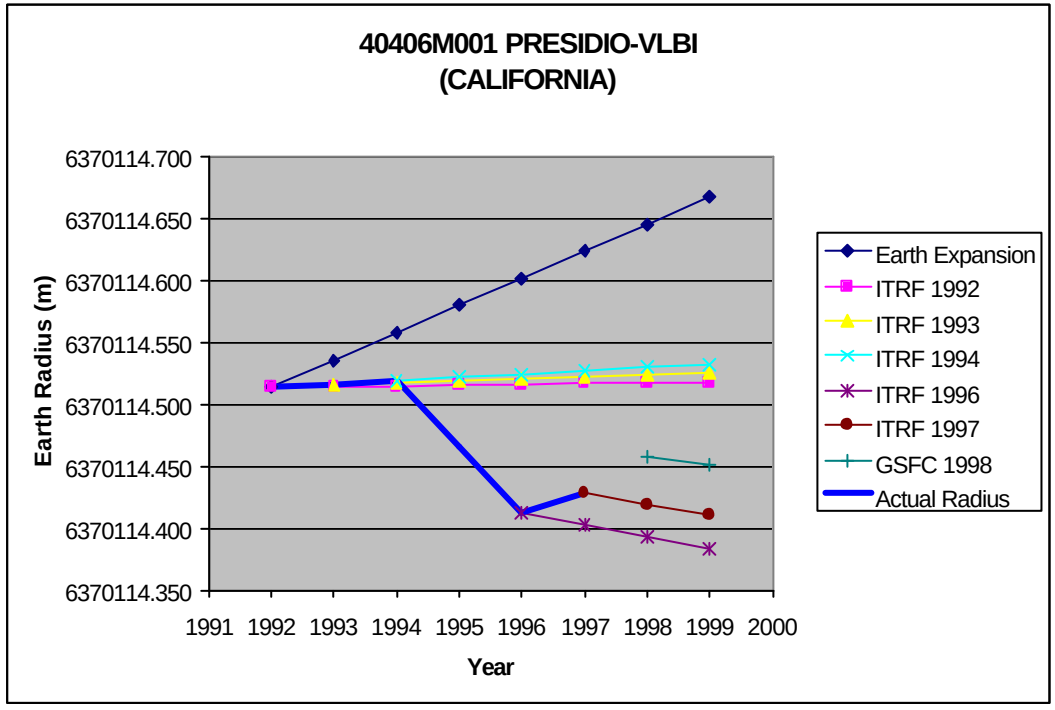

40407M001 PINYON FLATS-VLBI (CALIFORNIA)

	Site Co-ordinates			Site Velocity			Derived Earth Radius							
Data	**X**	**Y**	**Z**	**Vx**	**Vy**	**Vz**	**1992**	**1993**	**1994**	**1995**	**1996**	**1997**	**1998**	**1999**
Source	**m**	**m**	**m**	**m/y**	**m/y**	**m/y**	6372858.544	6372858.566	6372858.588	6372858.610	6372858.632	6372858.654	6372858.676	6372858.698
ITRF 1992	-2369635.87	-4761324.93	3511116.17	-0.0238	0.0136	0.0042	6372858.544	6372858.545	6372858.546	6372858.547	6372858.548	6372858.549	6372858.550	6372858.551
ITRF 1993	-2369636.02	-4761324.84	3511116.205	-0.0238	0.0144	0.006		6372858.552	6372858.554	6372858.555	6372858.557	6372858.558	6372858.559	6372858.561
ITRF 1994	-2369635.99	-4761324.86	3511116.195	-0.0232	0.0146	0.0037			6372858.551	6372858.551	6372858.551	6372858.551	6372858.550	6372858.550
ITRF 1996	-2369636.04	-4761324.77	3511116.266	-0.0187	0.0165	0.0087					6372858.541	6372858.540	6372858.540	6372858.539
ITRF 1997	-2369636.1	-4761324.81	3511116.201	-0.0253	0.0125	0.0038						6372858.552	6372858.554	6372858.556
GSFC 1998	-2369636.09	-4761324.77	3511116.199	-0.0249	0.0191	0.0042							6372858.518	6372858.516
							6372858.544	6372858.552	6372858.551	6372858.546	6372858.541	6372858.552	6372858.518	

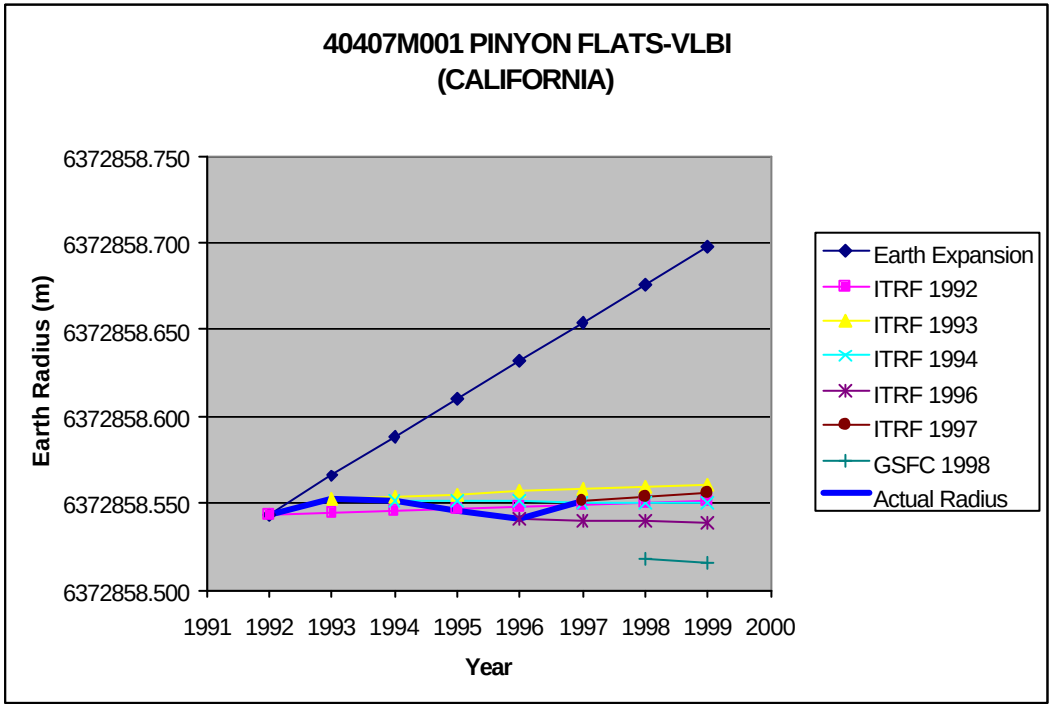

40410M001 POINT REYES-VLBI (CALIFORNIA)

	Site Co-ordinates			Site Velocity			Derived Earth Radius							
Data	**X**	**Y**	**Z**	**Vx**	**Vy**	**Vz**	**1992**	**1993**	**1994**	**1995**	**1996**	**1997**	**1998**	**1999**
Source	**m**	**m**	**m**	**m/y**	**m/y**	**m/y**	6370033.631	6370033.653	6370033.675	6370033.697	6370033.719	6370033.741	6370033.763	6370033.785
ITRF 1992	-2732333.02	-4217634.92	3914491.082	-0.0221	0.0266	0.0144	6370033.631	6370033.631	6370033.632	6370033.633	6370033.634	6370033.634	6370033.635	6370033.636
ITRF 1993	-2732333.17	-4217634.77	3914491.174	-0.0221	0.0267	0.0162		6370033.655	6370033.657	6370033.658	6370033.660	6370033.662	6370033.664	6370033.665
ITRF 1994	-2732333.15	-4217634.79	3914491.169	-0.021	0.0305	0.0156			6370033.652	6370033.651	6370033.649	6370033.648	6370033.646	6370033.644
ITRF 1996	-2732333.27	-4217634.71	3914491.265	-0.0261	0.0208	0.0206					6370033.716	6370033.727	6370033.737	6370033.747
ITRF 1997	-2732333.3	-4217634.74	3914491.278	-0.0299	0.0184	0.0225						6370033.753	6370033.767	6370033.782
GSFC 1998	-2732333.27	-4217634.71	3914491.276	-0.0278	0.0239	0.0231							6370033.721	6370033.731
							6370033.631	6370033.655	6370033.652	6370033.684	6370033.716	6370033.753	6370033.721	

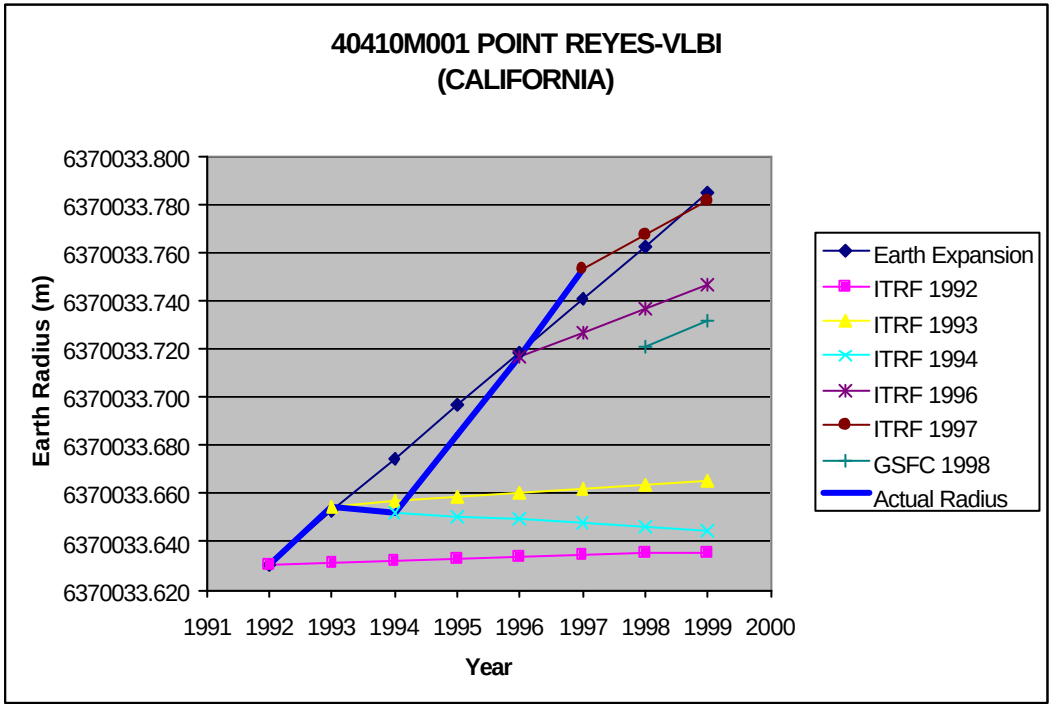

40416M001 YAKATAGA-VLBI (ALASKA)

	Site Co-ordinates			Site Velocity			Derived Earth Radius							
Data	**X**	**Y**	**Z**	**Vx**	**Vy**	**Vz**	**1992**	**1993**	**1994**	**1995**	**1996**	**1997**	**1998**	**1999**
Source	**m**	**m**	**m**	**m/y**	**m/y**	**m/y**	6362126.757	6362126.779	6362126.801	6362126.823	6362126.845	6362126.867	6362126.889	6362126.911
ITRF 1992	-2529744.13	-1942091.3	5505027.966	-0.0087	0.0277	0.0055	6362126.757	6362126.757	6362126.757	6362126.757	6362126.756	6362126.756	6362126.756	6362126.756
ITRF 1993	-2529744.2	-1942091.14	5505028.001	-0.0086	0.0267	0.0076		6362126.769	6362126.771	6362126.772	6362126.774	6362126.776	6362126.778	6362126.780
ITRF 1994	-2529744.19	-1942091.17	5505027.993	-0.0086	0.0288	0.0003			6362126.765	6362126.760	6362126.754	6362126.749	6362126.744	6362126.739
ITRF 1996	-2529744.28	-1942091.09	5505028.1	-0.0145	0.0237	0.0122					6362126.870	6362126.879	6362126.888	6362126.897
ITRF 1997	-2529744.29	-1942091.06	5505028.078	-0.0159	0.0266	0.0109						6362126.846	6362126.854	6362126.861
GSFC 1998	-2529744.35	-1942091.14	5505028.272	-0.0214	0.0211	0.0316							6362127.060	6362127.090
							6362126.757	6362126.769	6362126.765	6362126.818	6362126.870	6362126.846	6362127.060	

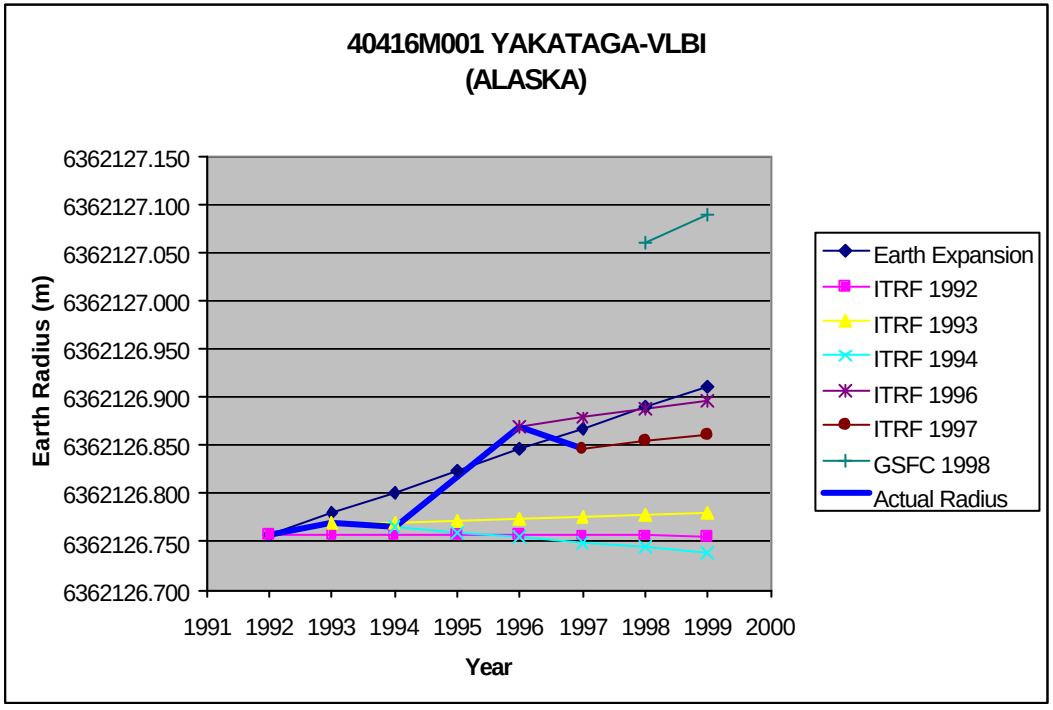

40419M001 KODIAK-VLBI (ALASKA)

	Site Co-ordinates			Site Velocity			Derived Earth Radius							
Data	**X**	**Y**	**Z**	**Vx**	**Vy**	**Vz**	**1992**	**1993**	**1994**	**1995**	**1996**	**1997**	**1998**	**1999**
Source	**m**	**m**	**m**	**m/y**	**m/y**	**m/y**	6362912.693	6362912.715	6362912.737	6362912.759	6362912.781	6362912.803	6362912.825	6362912.847
ITRF 1992	-3026940.1	-1575911.8	5370362.521	-0.0177	0.0045	-0.0093	6362912.693	6362912.692	6362912.692	6362912.691	6362912.690	6362912.690	6362912.689	6362912.689
ITRF 1993	-3026940.22	-1575911.75	5370362.491	-0.0178	0.0029	-0.0067		6362912.714	6362912.716	6362912.718	6362912.720	6362912.722	6362912.724	6362912.726
ITRF 1994	-3026940.19	-1575911.78	5370362.485	-0.0174	0.0052	-0.0085			6362912.703	6362912.703	6362912.703	6362912.703	6362912.702	6362912.702
ITRF 1996	-3026940.33	-1575911.79	5370362.57	-0.026	-0.0005	0.0076					6362912.844	6362912.863	6362912.882	6362912.901
ITRF 1997	-3026940.28	-1575911.74	5370362.454	-0.0198	0.0056	-0.0057						6362912.710	6362912.713	6362912.716
GSFC 1998	-3026940.29	-1575911.75	5370362.476	-0.0204	0.0074	-0.0031							6362912.735	6362912.740
							6362912.693	6362912.714	6362912.703	6362912.774	6362912.844	6362912.710	6362912.735	

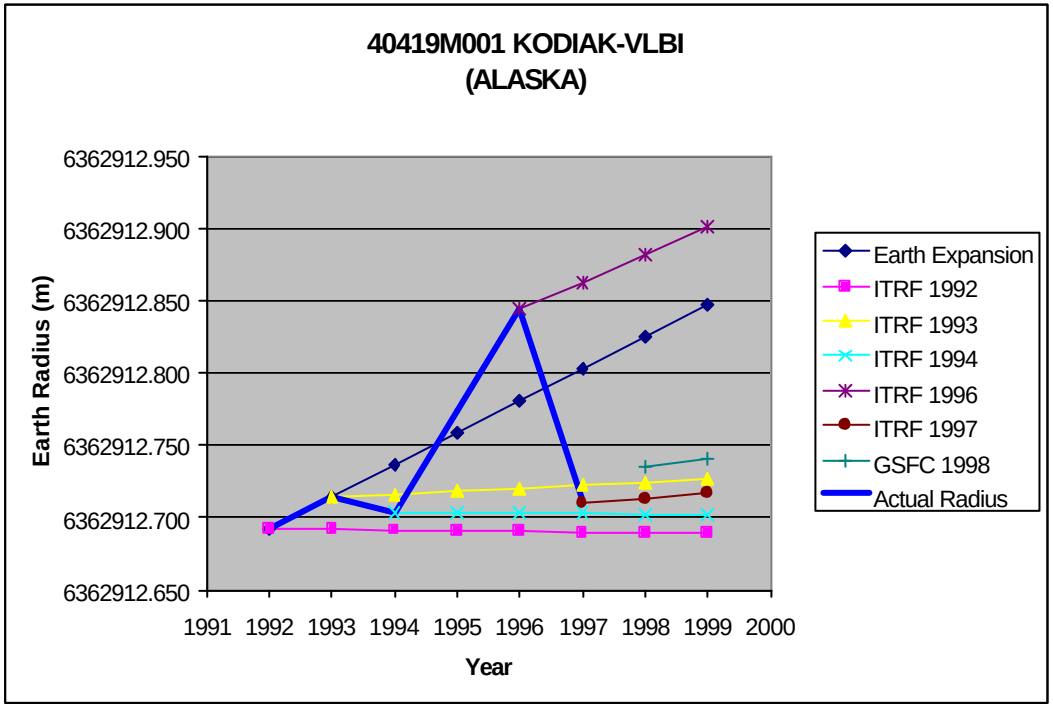

40420M002 VANDENBERG AFB-VLBI (CALIFORNIA)

	Site Co-ordinates			Site Velocity			Derived Earth Radius							
Data	**X**	**Y**	**Z**	**Vx**	**Vy**	**Vz**	**1992**	**1993**	**1994**	**1995**	**1996**	**1997**	**1998**	**1999**
Source	**m**	**m**	**m**	**m/y**	**m/y**	**m/y**	6371283.717	6371283.739	6371283.761	6371283.783	6371283.805	6371283.827	6371283.849	6371283.871
ITRF 1992	-2678094.66	-4525450.84	3597410.165	-0.0281	0.0302	0.0177	6371283.717	6371283.717	6371283.717	6371283.718	6371283.718	6371283.718	6371283.719	6371283.719
ITRF 1993	-2678094.85	-4525450.68	3597410.279	-0.029	0.0297	0.0202		6371283.749	6371283.751	6371283.754	6371283.756	6371283.759	6371283.761	6371283.764
ITRF 1994	-2678094.82	-4525450.7	3597410.264	-0.0292	0.0295	0.0189			6371283.738	6371283.740	6371283.742	6371283.744	6371283.746	6371283.748
ITRF 1996	-2678094.92	-4525450.54	3597410.309	-0.028	0.0324	0.0157					6371283.693	6371283.691	6371283.688	6371283.686
ITRF 1997	-2678094.94	-4525450.56	3597410.312	-0.0302	0.0304	0.0164						6371283.718	6371283.718	6371283.719
GSFC 1998	-2678094.94	-4525450.57	3597410.348	-0.0314	0.0315	0.0215							6371283.745	6371283.748
							6371283.717	6371283.749	6371283.738	6371283.716	6371283.693	6371283.718	6371283.745	

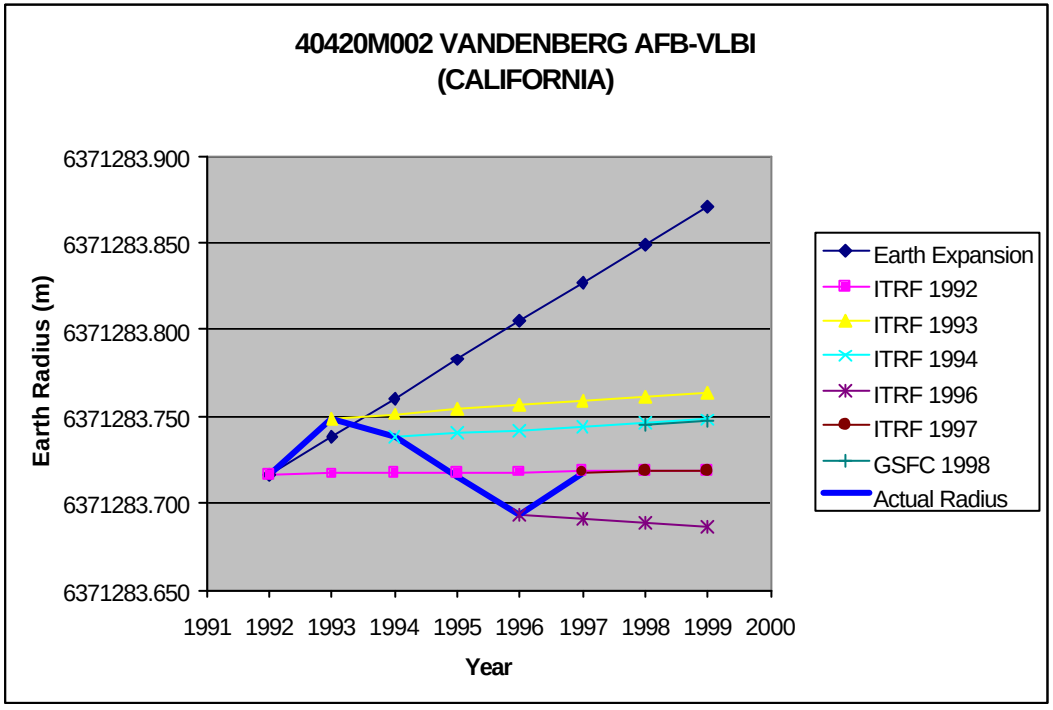

40421M001 NOME-VLBI (ALASKA)

	Site Co-ordinates			Site Velocity			Derived Earth Radius							
Data	**X**	**Y**	**Z**	**Vx**	**Vy**	**Vz**	**1992**	**1993**	**1994**	**1995**	**1996**	**1997**	**1998**	**1999**
Source	**m**	**m**	**m**	**m/y**	**m/y**	**m/y**	6361056.250	6361056.272	6361056.294	6361056.316	6361056.338	6361056.360	6361056.382	6361056.404
ITRF 1992	-2658150.37	-693821.909	5737236.653	-0.0206	-0.0057	-0.011	6361056.250	6361056.249	6361056.249	6361056.248	6361056.247	6361056.247	6361056.246	6361056.245
ITRF 1993	-2658150.5	-693821.924	5737236.609	-0.021	-0.0083	-0.0085		6361056.270	6361056.272	6361056.274	6361056.276	6361056.278	6361056.280	6361056.282
ITRF 1994	-2658150.48	-693821.95	5737236.604	-0.0216	-0.0073	-0.0125			6361056.259	6361056.258	6361056.256	6361056.255	6361056.253	6361056.252
ITRF 1996	-2658150.64	-693821.991	5737236.645	-0.0299	-0.0107	0.0006					6361056.365	6361056.379	6361056.393	6361056.407
ITRF 1997	-2658150.59	-693821.957	5737236.538	-0.0237	-0.0063	-0.0117						6361056.244	6361056.244	6361056.244
GSFC 1998	-2658150.57	-693821.959	5737236.548	-0.0218	-0.0038	-0.0098							6361056.247	6361056.248
							6361056.250	6361056.270	6361056.259	6361056.312	6361056.365	6361056.244	6361056.247	

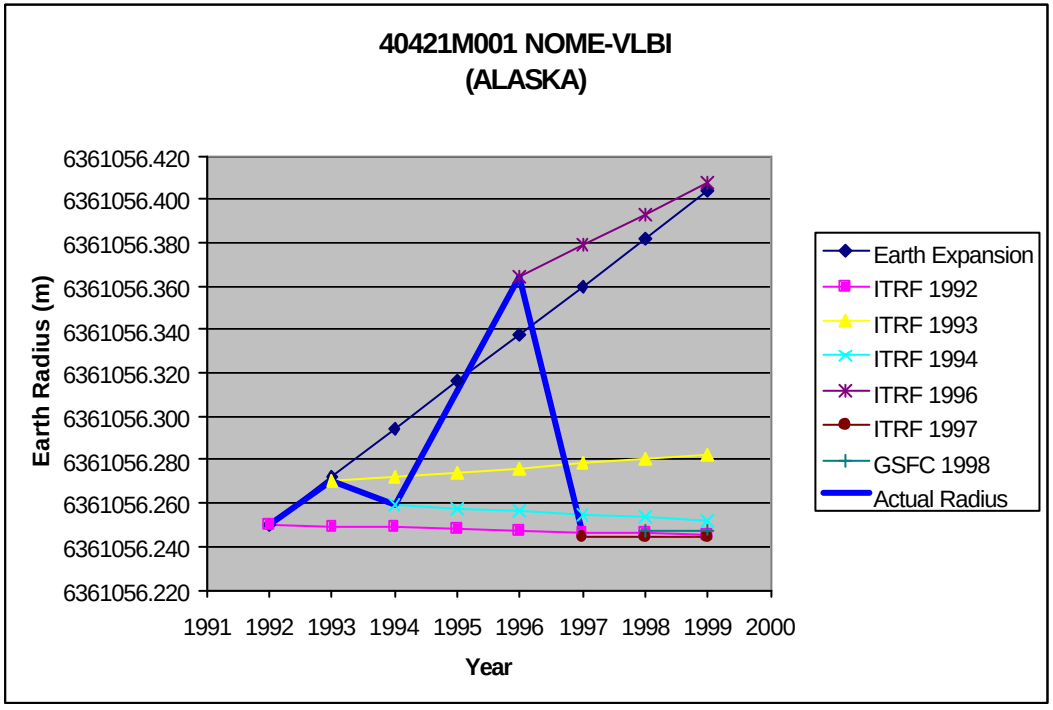

40423M001 SANDPOINT-VLBI (ALASKA)

	Site Co-ordinates			Site Velocity			Derived Earth Radius							
Data	**X**	**Y**	**Z**	**Vx**	**Vy**	**Vz**	**1992**	**1993**	**1994**	**1995**	**1996**	**1997**	**1998**	**1999**
Source	**m**	**m**	**m**	**m/y**	**m/y**	**m/y**	6363796.454	6363796.476	6363796.498	6363796.520	6363796.542	6363796.564	6363796.586	6363796.608
ITRF 1992	-3425461.83	-1214669.14	5223858.292	-0.0202	0.0037	-0.0135	6363796.454	6363796.453	6363796.452	6363796.451	6363796.450	6363796.449	6363796.448	6363796.447
ITRF 1993	-3425461.96	-1214669.09	5223858.229	-0.0203	0.0024	-0.0104		6363796.463	6363796.465	6363796.467	6363796.469	6363796.471	6363796.473	6363796.475
ITRF 1994	-3425461.94	-1214669.12	5223858.226	-0.0192	0.0044	-0.0154			6363796.455	6363796.452	6363796.448	6363796.445	6363796.442	6363796.439
ITRF 1996	-3425462.01	-1214669.1	5223858.17	-0.02	0.0022	-0.0121					6363796.447	6363796.447	6363796.448	6363796.448
ITRF 1997	-3425462.03	-1214669.08	5223858.156	-0.0219	0.0054	-0.0138						6363796.442	6363796.442	6363796.441
GSFC 1998	-3425461.98	-1214669.07	5223858.105	-0.016	0.0101	-0.0193							6363796.371	6363796.362
							6363796.454	6363796.463	6363796.455	6363796.451	6363796.447	6363796.442	6363796.371	

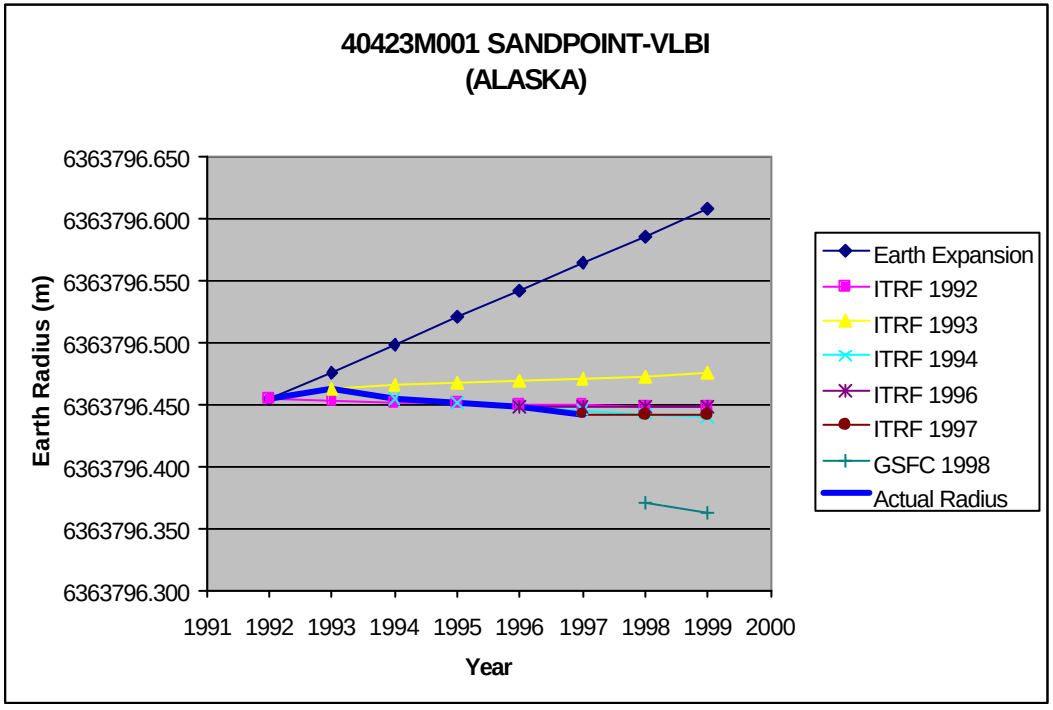

40428M001 SANTA PAOLA-VLBI (CALIFORNIA)

	Site Co-ordinates			Site Velocity			Derived Earth Radius							
Data	**X**	**Y**	**Z**	**Vx**	**Vy**	**Vz**	**1992**	**1993**	**1994**	**1995**	**1996**	**1997**	**1998**	**1999**
Source	**m**	**m**	**m**	**m/y**	**m/y**	**m/y**	6371539.228	6371539.250	6371539.272	6371539.294	6371539.316	6371539.338	6371539.360	6371539.382
ITRF 1992	-2554476.59	-4608627.4	3582138.326	-0.0301	0.023	0.0098	6371539.228	6371539.229	6371539.230	6371539.231	6371539.232	6371539.233	6371539.234	6371539.235
ITRF 1993	-2554476.78	-4608627.27	3582138.397	-0.0304	0.0236	0.0114		6371539.253	6371539.255	6371539.256	6371539.258	6371539.259	6371539.261	6371539.262
ITRF 1994	-2554476.75	-4608627.29	3582138.38	-0.0299	0.0239	0.0089			6371539.244	6371539.243	6371539.243	6371539.243	6371539.242	6371539.242
ITRF 1996	-2554476.92	-4608627.26	3582138.464	-0.0353	0.0138	0.0153					6371539.335	6371539.348	6371539.361	6371539.373
ITRF 1997	-2554476.93	-4608627.24	3582138.455	-0.0374	0.0157	0.0148						6371539.325	6371539.337	6371539.349
GSFC 1998	-2554476.92	-4608627.24	3582138.472	-0.0368	0.0184	0.0174							6371539.328	6371539.339
							6371539.228	6371539.253	6371539.244	6371539.290	6371539.335	6371539.325	6371539.328	

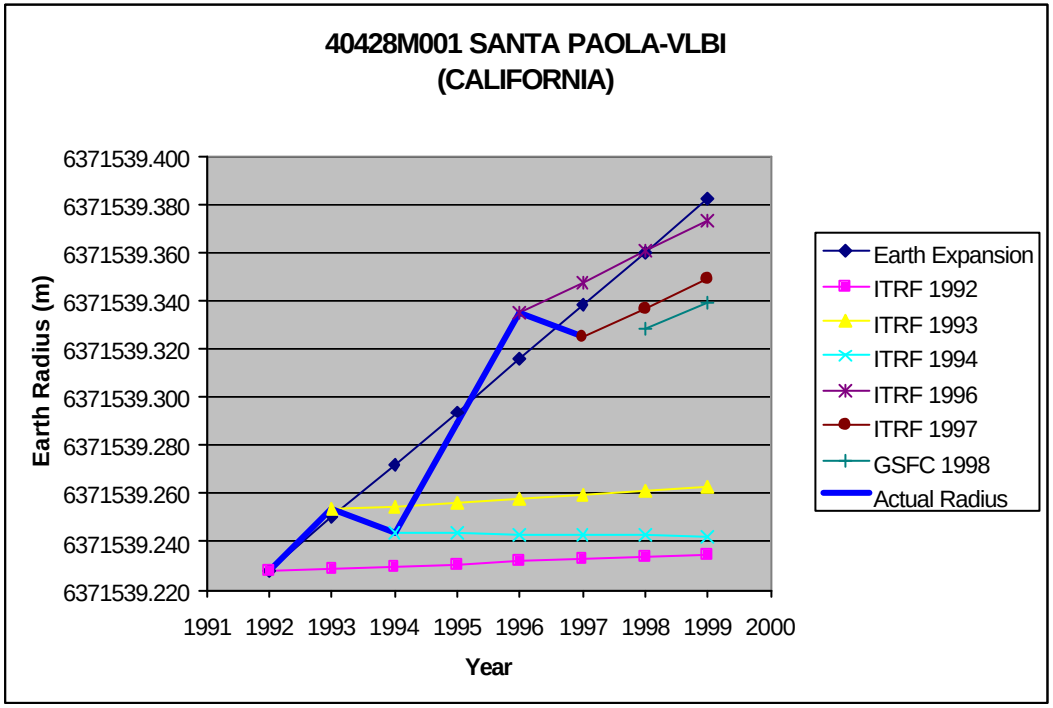

40430M001 BLACK BUTTE-VLBI (CALIFORNIA)

	Site Co-ordinates			Site Velocity			Derived Earth Radius							
Data	**X**	**Y**	**Z**	**Vx**	**Vy**	**Vz**	**1992**	**1993**	**1994**	**1995**	**1996**	**1997**	**1998**	**1999**
Source	**m**	**m**	**m**	**m/y**	**m/y**	**m/y**	6372093.764	6372093.786	6372093.808	6372093.830	6372093.852	6372093.874	6372093.896	6372093.918
ITRF 1992	-2306306.87	-4787914.45	3515736.452	-0.0178	0.0012	-0.0082	6372093.764	6372093.765	6372093.766	6372093.767	6372093.768	6372093.769	6372093.770	6372093.771
ITRF 1993	-2306307	-4787914.42	3515736.427	-0.0179	0.0018	-0.0068		6372093.776	6372093.778	6372093.779	6372093.781	6372093.782	6372093.783	6372093.785
ITRF 1994	-2306306.97	-4787914.44	3515736.415	-0.0171	0.003	-0.0088			6372093.774	6372093.773	6372093.772	6372093.771	6372093.770	6372093.769
ITRF 1996	-2306307	-4787914.34	3515736.325	-0.0126	0.0102	-0.014					6372093.657	6372093.646	6372093.635	6372093.625
ITRF 1997	-2306307.07	-4787914.43	3515736.382	-0.0197	0.0013	-0.0084						6372093.786	6372093.787	6372093.789
GSFC 1998	-2306307.02	-4787914.34	3515736.323	-0.0159	0.0128	-0.0135							6372093.667	6372093.655
							6372093.764	6372093.776	6372093.774	6372093.716	6372093.657	6372093.786	6372093.667	

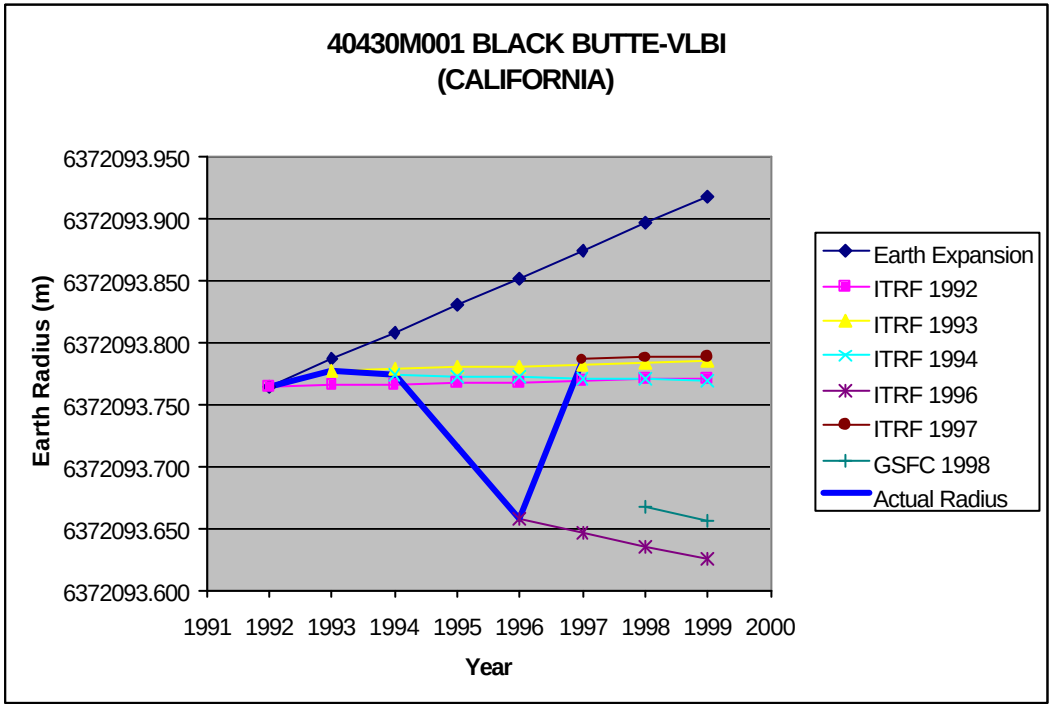

40431M001 DEADMAN LAKE-VLBI (CALIFORNIA)

	Site Co-ordinates			Site Velocity			Derived Earth Radius							
Data	**X**	**Y**	**Z**	**Vx**	**Vy**	**Vz**	**1992**	**1993**	**1994**	**1995**	**1996**	**1997**	**1998**	**1999**
Source	**m**	**m**	**m**	**m/y**	**m/y**	**m/y**	6372233.641	6372233.663	6372233.685	6372233.707	6372233.729	6372233.751	6372233.773	6372233.795
ITRF 1992	-2336819.57	-4732586.97	3570330.011	-0.018	0.003	-0.0061	6372233.641	6372233.642	6372233.643	6372233.644	6372233.645	6372233.646	6372233.647	6372233.648
ITRF 1993	-2336819.68	-4732586.96	3570329.982	-0.0178	0.0035	-0.0044		6372233.654	6372233.655	6372233.657	6372233.658	6372233.660	6372233.661	6372233.663
ITRF 1994	-2336819.67	-4732586.96	3570329.99	-0.0175	0.0049	-0.0066			6372233.658	6372233.657	6372233.656	6372233.655	6372233.654	6372233.653
ITRF 1996	-2336819.71	-4732586.98	3570329.927	-0.0138	-0.0023	-0.0092					6372233.649	6372233.650	6372233.652	6372233.653
ITRF 1997	-2336819.73	-4732587.01	3570329.939	-0.0162	-0.0041	-0.008						6372233.683	6372233.688	6372233.692
GSFC 1998	-2336819.98	-4732587.4	3570330.269	-0.0438	-0.0437	0.0281							6372234.250	6372234.315
							6372233.641	6372233.654	6372233.658	6372233.654	6372233.649	6372233.683	6372234.250	

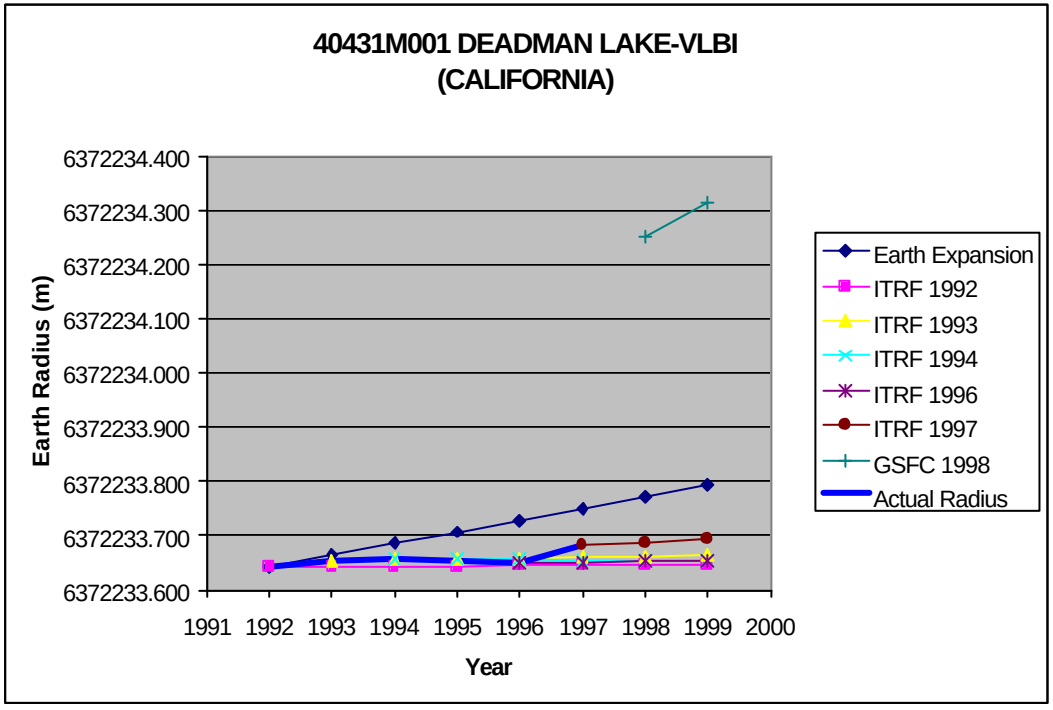

40432M001 ELY-VLBI (NEVADA)

	Site Co-ordinates			Site Velocity			Derived Earth Radius							
Data	**X**	**Y**	**Z**	**Vx**	**Vy**	**Vz**	**1992**	**1993**	**1994**	**1995**	**1996**	**1997**	**1998**	**1999**
Source	**m**	**m**	**m**	**m/y**	**m/y**	**m/y**	6371489.886	6371489.908	6371489.930	6371489.952	6371489.974	6371489.996	6371490.018	6371490.040
ITRF 1992	-2077236.23	-4486712.73	4018753.78	-0.0173	-0.0017	-0.0091	6371489.886	6371489.888	6371489.889	6371489.890	6371489.891	6371489.892	6371489.893	6371489.894
ITRF 1993	-2077236.35	-4486712.72	4018753.751	-0.0171	-0.0014	-0.008		6371489.902	6371489.903	6371489.905	6371489.906	6371489.908	6371489.909	6371489.911
ITRF 1994	-2077236.33	-4486712.74	4018753.736	-0.0169	0.0003	-0.0109			6371489.897	6371489.895	6371489.894	6371489.892	6371489.891	6371489.889
ITRF 1996	-2077236.39	-4486712.7	4018753.671	-0.0156	0.0023	-0.0128					6371489.848	6371489.843	6371489.839	6371489.834
ITRF 1997	-2077236.41	-4486712.73	4018753.687	-0.0191	-0.0016	-0.0105						6371489.893	6371489.894	6371489.894
GSFC 1998	-2077236.4	-4486712.72	4018753.693	-0.0189	0.0019	-0.0091							6371489.887	6371489.886
							6371489.886	6371489.902	6371489.897	6371489.873	6371489.848	6371489.893	6371489.887	

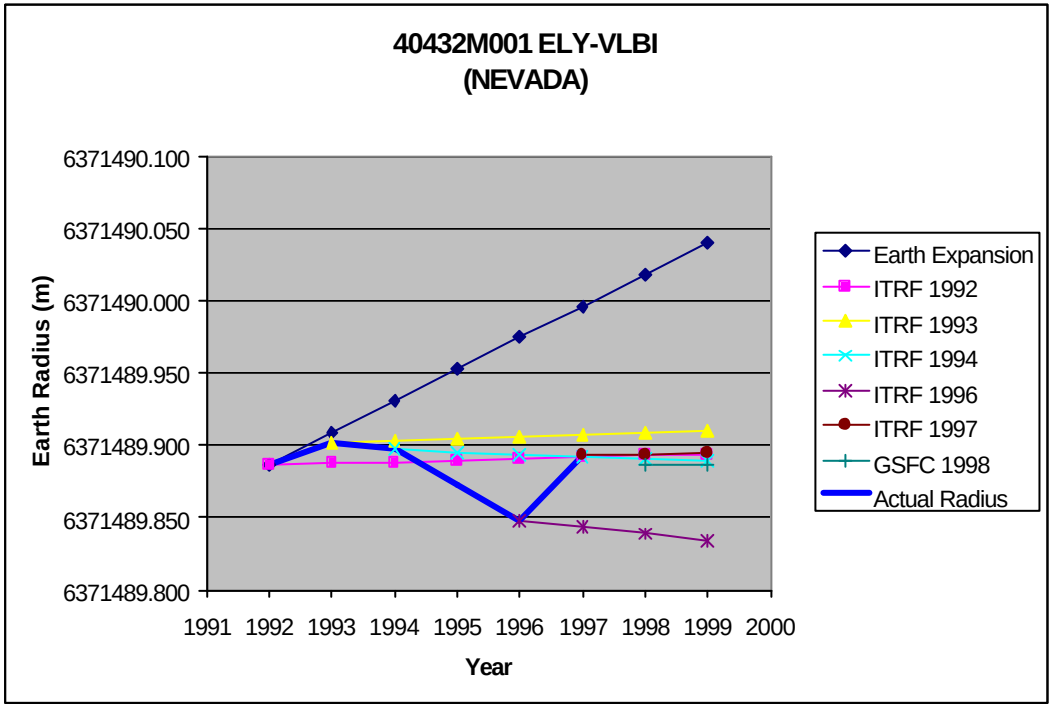

40437M001 MAMMOTH LAKES-VLBI (CALIFORNIA)

	Site Co-ordinates			Site Velocity			Derived Earth Radius							
Data	**X**	**Y**	**Z**	**Vx**	**Vy**	**Vz**	**1992**	**1993**	**1994**	**1995**	**1996**	**1997**	**1998**	**1999**
Source	**m**	**m**	**m**	**m/y**	**m/y**	**m/y**	6372513.445	6372513.467	6372513.489	6372513.511	6372513.533	6372513.555	6372513.577	6372513.599
ITRF 1992	-2448246.69	-4426738.33	3875435.92	-0.0219	0.0078	-0.0036	6372513.445	6372513.446	6372513.447	6372513.448	6372513.448	6372513.449	6372513.450	6372513.451
ITRF 1993	-2448246.81	-4426738.31	3875435.899	-0.0199	0.0034	-0.0059		6372513.468	6372513.470	6372513.471	6372513.473	6372513.475	6372513.476	6372513.478
ITRF 1994	-2448246.81	-4426738.28	3875435.904	-0.0213	0.0103	-0.0051			6372513.452	6372513.449	6372513.447	6372513.445	6372513.443	6372513.441
ITRF 1996	-2448246.89	-4426738.41	3875435.887	-0.0251	-0.0097	-0.0013					6372513.562	6372513.577	6372513.593	6372513.608
ITRF 1997	-2448246.89	-4426738.43	3875435.875	-0.0229	-0.0095	-0.0043						6372513.568	6372513.581	6372513.594
GSFC 1998	-2448246.77	-4426737.99	3875435.692	-0.0118	0.034	-0.0202							6372513.103	6372513.072
							6372513.445	6372513.468	6372513.452	6372513.507	6372513.562	6372513.568	6372513.103	

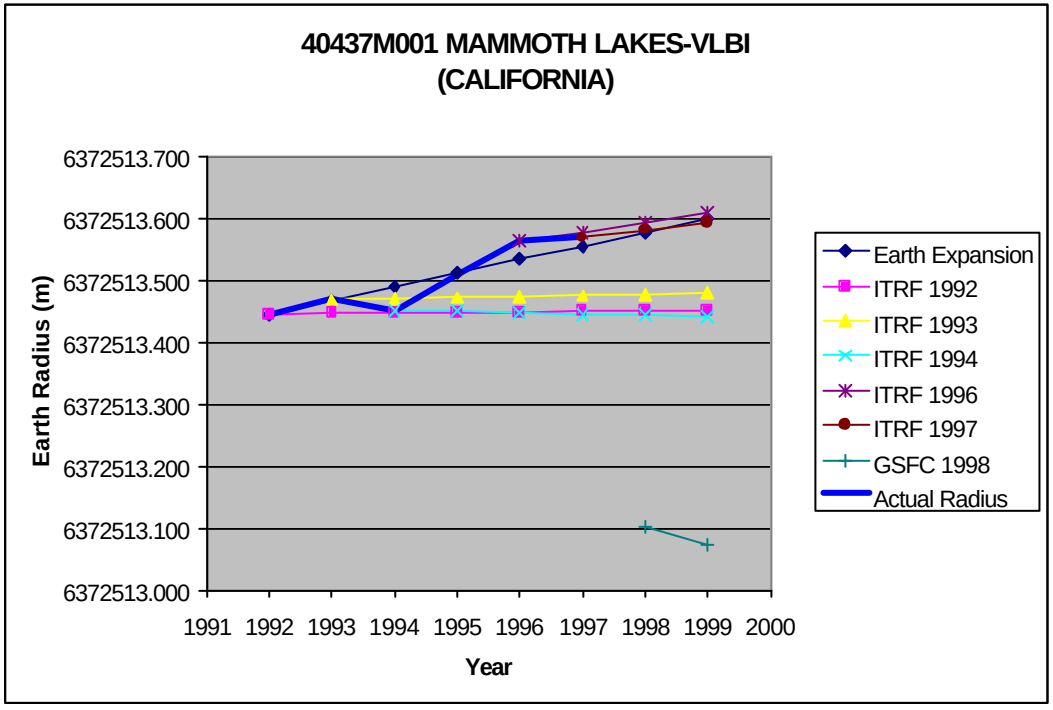

40441S001 GREENBANK-VLBI (WEST VIRGINIA)

	Site Co-ordinates			Site Velocity			Derived Earth Radius							
Data	X	Y	Z	Vx	Vy	Vz	1992	1993	1994	1995	1996	1997	1998	1999
Source	m	m	m	m/y	m/y	m/y	6370727.574	6370727.596	6370727.618	6370727.640	6370727.662	6370727.684	6370727.706	6370727.728
ITRF 1992	882880.037	-4924482.31	3944130.664	-0.0144	-0.0034	0.0027	6370727.574	6370727.577	6370727.579	6370727.581	6370727.584	6370727.586	6370727.588	6370727.590
ITRF 1993	882879.932	-4924482.32	3944130.699	-0.0154	-0.0017	0.0007		6370727.592	6370727.591	6370727.591	6370727.590	6370727.590	6370727.590	6370727.589
ITRF 1994	882879.96	-4924482.32	3944130.689	-0.0142	-0.0004	0.0005			6370727.588	6370727.587	6370727.586	6370727.584	6370727.583	6370727.582
ITRF 1996	882879.894	-4924482.31	3944130.691	-0.0143	-0.0005	-0.0004					6370727.573	6370727.571	6370727.569	6370727.567
ITRF 1997	882879.893	-4924482.31	3944130.678	-0.0146	-0.0009	-0.0011						6370727.569	6370727.567	6370727.565
GSFC 1998	882879.896	-4924482.3	3944130.688	-0.0152	0.0006	0.0011							6370727.569	6370727.567
							6370727.574	6370727.592	6370727.588	6370727.581	6370727.573	6370727.569	6370727.569	

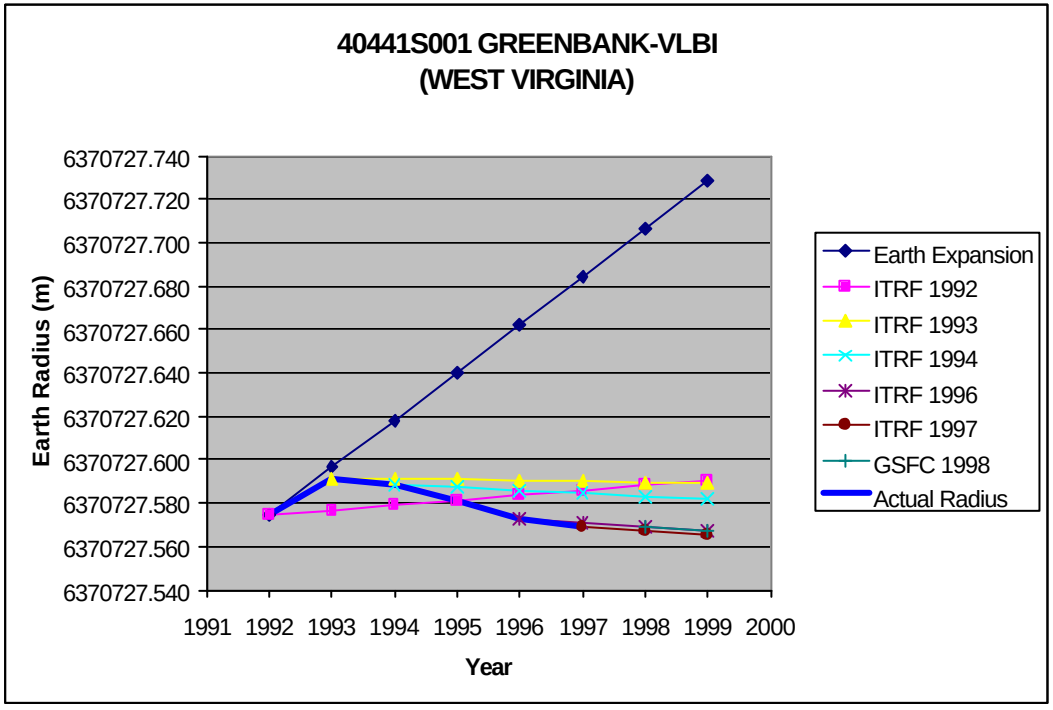

40449M001 OCOTILLO-VLBI (MEXICO)

	Site Co-ordinates			Site Velocity			Derived Earth Radius							
Data	**X**	**Y**	**Z**	**Vx**	**Vy**	**Vz**	**1992**	**1993**	**1994**	**1995**	**1996**	**1997**	**1998**	**1999**
Source	**m**	**m**	**m**	**m/y**	**m/y**	**m/y**	6371865.406	6371865.428	6371865.450	6371865.472	6371865.494	6371865.516	6371865.538	6371865.560
ITRF 1992	-2335601.08	-4832244.16	3434392.635	-0.033	0.0298	0.0195	6371865.406	6371865.406	6371865.406	6371865.406	6371865.406	6371865.406	6371865.406	6371865.406
ITRF 1993	-2335601.26	-4832243.98	3434392.718	-0.0316	0.0285	0.0186		6371865.385	6371865.385	6371865.385	6371865.385	6371865.385	6371865.385	6371865.385
ITRF 1994	-2335601.23	-4832244.03	3434392.725	-0.0286	0.0281	0.0162			6371865.417	6371865.415	6371865.413	6371865.410	6371865.408	6371865.406
ITRF 1996	-2335601.36	-4832243.88	3434392.774	-0.0313	0.0247	0.0193					6371865.371	6371865.375	6371865.378	6371865.381
ITRF 1997	-2335601.38	-4832243.9	3434392.781	-0.0324	0.0265	0.0171						6371865.401	6371865.402	6371865.403
GSFC 1998	-2335601.36	-4832243.94	3434392.793	-0.0307	0.0276	0.018							6371865.429	6371865.429
							6371865.406	6371865.385	6371865.417	6371865.394	6371865.371	6371865.401	6371865.429	

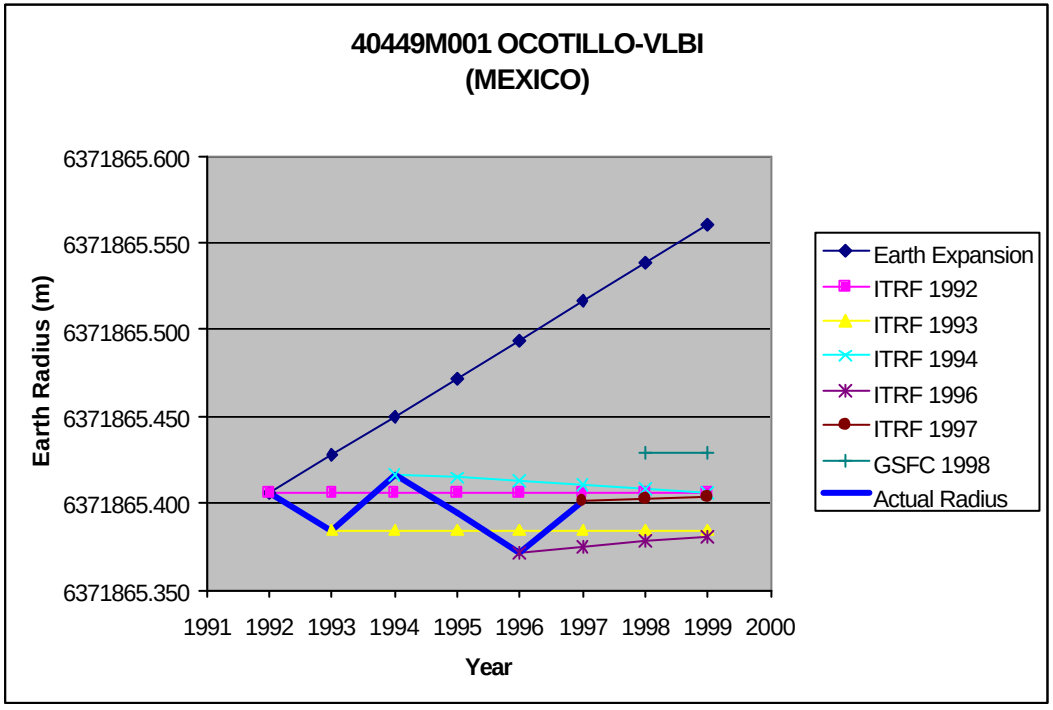

40463S001 LOS ALAMOS-VLBI (CALIFORNIA)

	Site Co-ordinates			Site Velocity			Derived Earth Radius							
Data	X	Y	Z	Vx	Vy	Vz	1992	1993	1994	1995	1996	1997	1998	1999
Source	m	m	m	m/y	m/y	m/y	6372831.266	6372831.288	6372831.310	6372831.332	6372831.354	6372831.376	6372831.398	6372831.420
ITRF 1992	-1449752.23	-4975298.59	3709123.985	-0.0094	0.0087	-0.0128	6372831.266	6372831.254	6372831.242	6372831.230	6372831.218	6372831.206	6372831.194	6372831.182
ITRF 1993	-1449752.32	-4975298.58	3709123.968	-0.0126	0.0024	-0.0072		6372831.271	6372831.268	6372831.264	6372831.261	6372831.258	6372831.255	6372831.252
ITRF 1994	-1449752.3	-4975298.61	3709123.958	-0.0121	0.0009	-0.0078			6372831.275	6372831.273	6372831.270	6372831.268	6372831.265	6372831.263
ITRF 1996	-1449752.35	-4975298.59	3709123.925	-0.0123	-0.0001	-0.0084					6372831.258	6372831.256	6372831.254	6372831.251
ITRF 1997	-1449752.36	-4975298.59	3709123.916	-0.0136	0	-0.0082						6372831.255	6372831.254	6372831.252
GSFC 1998	-1449752.35	-4975298.59	3709123.927	-0.0141	0.0027	-0.0063							6372831.256	6372831.253
							6372831.266	6372831.271	6372831.275	6372831.267	6372831.258	6372831.255	6372831.256	

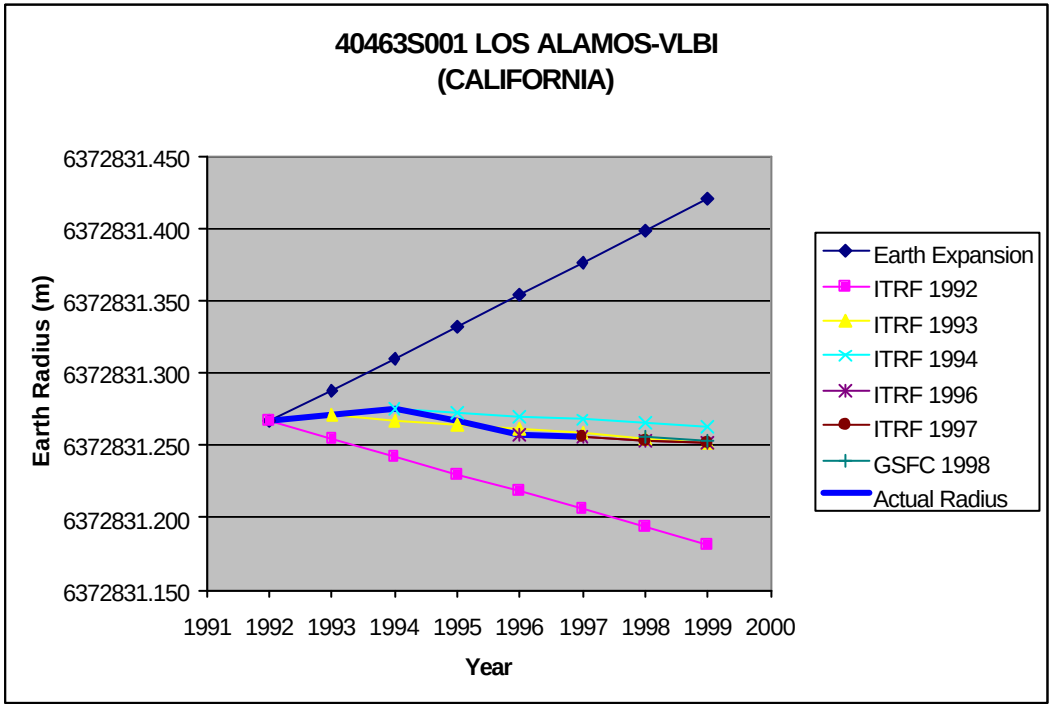

40466S001 KITT PEAK-VLBI (ARIZONA)

	Site Co-ordinates			Site Velocity			Derived Earth Radius							
Data	**X**	**Y**	**Z**	**Vx**	**Vy**	**Vz**	**1992**	**1993**	**1994**	**1995**	**1996**	**1997**	**1998**	**1999**
Source	**m**	**m**	**m**	**m/y**	**m/y**	**m/y**	6374084.630	6374084.652	6374084.674	6374084.696	6374084.718	6374084.740	6374084.762	6374084.784
ITRF 1992	-1995678.5	-5037317.7	3357328.193	-0.0135	-0.0006	-0.0088	6374084.630	6374084.630	6374084.630	6374084.630	6374084.630	6374084.630	6374084.630	6374084.631
ITRF 1993	-1995678.59	-5037317.71	3357328.176	-0.0111	-0.0015	-0.0068		6374084.656	6374084.657	6374084.658	6374084.659	6374084.661	6374084.662	6374084.663
ITRF 1994	-1995678.57	-5037317.73	3357328.166	-0.012	0.005	-0.0115			6374084.661	6374084.654	6374084.648	6374084.642	6374084.636	6374084.629
ITRF 1996	-1995678.62	-5037317.72	3357328.122	-0.0122	-0.0022	-0.0121					6374084.645	6374084.644	6374084.643	6374084.642
ITRF 1997	-1995678.63	-5037317.72	3357328.118	-0.0131	0	-0.0096						6374084.645	6374084.644	6374084.643
GSFC 1998	-1995678.62	-5037317.72	3357328.133	-0.0137	0.0028	-0.0077							6374084.649	6374084.647
							6374084.630	6374084.656	6374084.661	6374084.653	6374084.645	6374084.645	6374084.649	

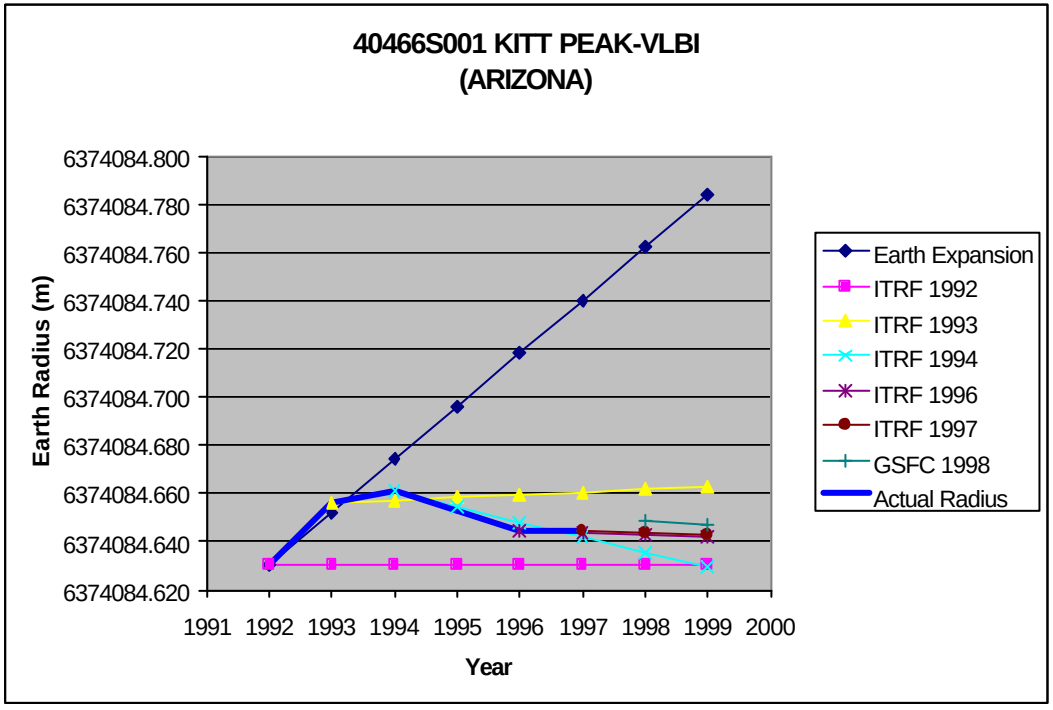

40490S001 MARYLAND POINT-VLBI (MARYLAND USA)

	Site Co-ordinates			Site Velocity			Derived Earth Radius							
Data	**X**	**Y**	**Z**	**Vx**	**Vy**	**Vz**	**1992**	**1993**	**1994**	**1995**	**1996**	**1997**	**1998**	**1999**
Source	**m**	**m**	**m**	**m/y**	**m/y**	**m/y**	6369924.666	6369924.688	6369924.710	6369924.732	6369924.754	6369924.776	6369924.798	6369924.820
ITRF 1992	1106629.456	-4882907.18	3938086.963	-0.0139	-0.0016	0.0016	6369924.666	6369924.666	6369924.665	6369924.665	6369924.665	6369924.665	6369924.665	6369924.664
ITRF 1993	1106629.347	-4882907.19	3938086.997	-0.0149	-0.0003	0		6369924.671	6369924.669	6369924.666	6369924.664	6369924.662	6369924.659	6369924.657
ITRF 1994	1106629.373	-4882907.18	3938086.967	-0.0151	0.0018	-0.0009			6369924.650	6369924.646	6369924.641	6369924.636	6369924.632	6369924.627
ITRF 1996	1106629.299	-4882907.17	3938086.961	-0.0152	0.0014	-0.0024					6369924.629	6369924.624	6369924.619	6369924.613
ITRF 1997	1106629.295	-4882907.19	3938086.979	-0.0159	-0.0004	-0.0003						6369924.652	6369924.650	6369924.647
GSFC 1998	1106629.307	-4882907.15	3938086.961	-0.016	0.0042	-0.0007							6369924.613	6369924.606
							6369924.666	6369924.671	6369924.650	6369924.640	6369924.629	6369924.652	6369924.613	

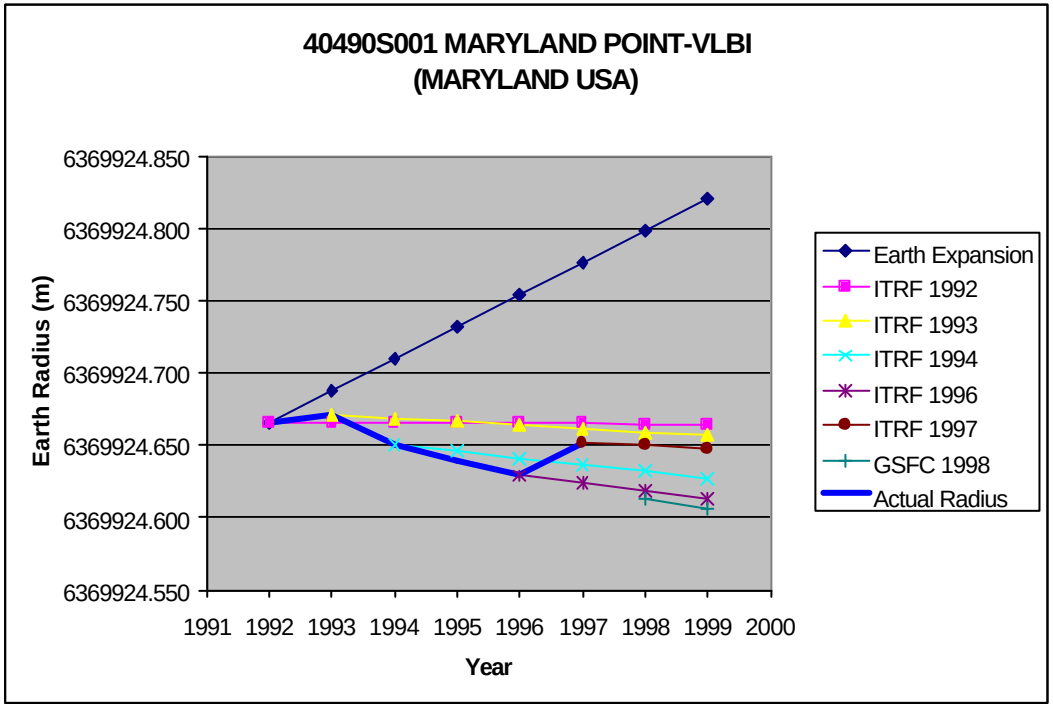

40493M001 YUMA-VLBI (ARAZONA)

	Site Co-ordinates			Site Velocity			Derived Earth Radius							
Data	**X**	**Y**	**Z**	**Vx**	**Vy**	**Vz**	**1992**	**1993**	**1994**	**1995**	**1996**	**1997**	**1998**	**1999**
Source	**m**	**m**	**m**	**m/y**	**m/y**	**m/y**	6372090.178	6372090.200	6372090.222	6372090.244	6372090.266	6372090.288	6372090.310	6372090.332
ITRF 1992	-2196777.84	-4887337.07	3448425.26	-0.0129	-0.0021	-0.0092	6372090.178	6372090.179	6372090.180	6372090.181	6372090.182	6372090.183	6372090.184	6372090.185
ITRF 1993	-2196777.94	-4887337.06	3448425.237	-0.0133	-0.0015	-0.0079		6372090.197	6372090.199	6372090.200	6372090.202	6372090.203	6372090.205	6372090.206
ITRF 1994	-2196777.91	-4887337.08	3448425.22	-0.012	-0.0003	-0.0103			6372090.190	6372090.189	6372090.188	6372090.187	6372090.185	6372090.184
ITRF 1996	-2196777.99	-4887337.15	3448425.238	-0.0152	-0.0093	-0.004					6372090.280	6372090.290	6372090.300	6372090.310
ITRF 1997	-2196778.03	-4887337.19	3448425.26	-0.0193	-0.0135	-0.0012						6372090.336	6372090.353	6372090.369
GSFC 1998	-2196778.02	-4887337.18	3448425.264	-0.0193	-0.0094	-0.0002							6372090.327	6372090.340
							6372090.178	6372090.197	6372090.190	6372090.235	6372090.280	6372090.336	6372090.327	

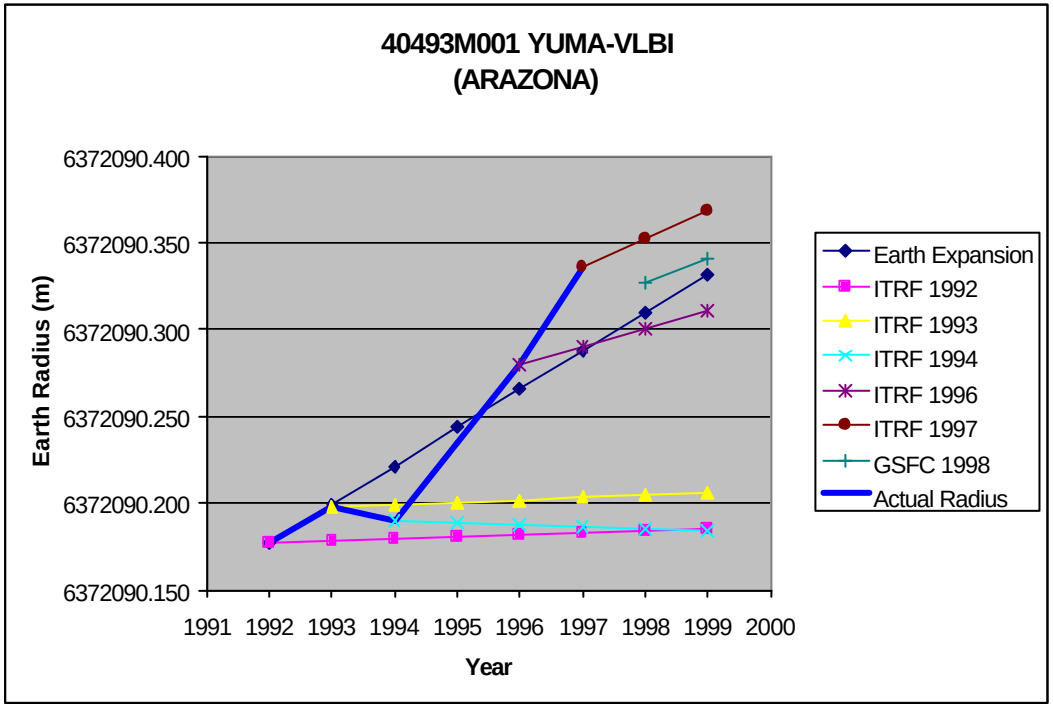

41709S001 SEST-VLBI (CHILE)

	Site Co-ordinates			Site Velocity			Derived Earth Radius							
Data	**X**	**Y**	**Z**	**Vx**	**Vy**	**Vz**	**1992**	**1993**	**1994**	**1995**	**1996**	**1997**	**1998**	**1999**
Source	**m**	**m**	**m**	**m/y**	**m/y**	**m/y**	6375475.438	6375475.460	6375475.482	6375475.504	6375475.526	6375475.548	6375475.570	6375475.592
ITRF 1992	1838237.884	-5258699.2	-3100588.87	0.0001	-0.0051	0.0086	6375475.438	6375475.438	6375475.438	6375475.438	6375475.438	6375475.438	6375475.438	6375475.438
ITRF 1993	1838237.867	-5258699.27	-3100588.8	0.0001	-0.0048	0.0082		6375475.463	6375475.463	6375475.463	6375475.463	6375475.463	6375475.463	6375475.463
ITRF 1994	1838237.872	-5258699.24	-3100588.82	-0.0076	-0.0035	0.0057			6375475.451	6375475.449	6375475.447	6375475.445	6375475.443	6375475.441
ITRF 1996	1838237.888	-5258699.29	-3100588.76	-0.0003	-0.0084	0.0099					6375475.465	6375475.467	6375475.469	6375475.471
ITRF 1997	1838237.892	-5258699.32	-3100588.79	-0.0017	-0.0078	0.0073						6375475.504	6375475.506	6375475.509
GSFC 1998	1838237.894	-5258699.25	-3100588.77	0.0001	-0.0048	0.0082							6375475.441	6375475.441
							6375475.438	6375475.463	6375475.451	6375475.458	6375475.465	6375475.504	6375475.441	

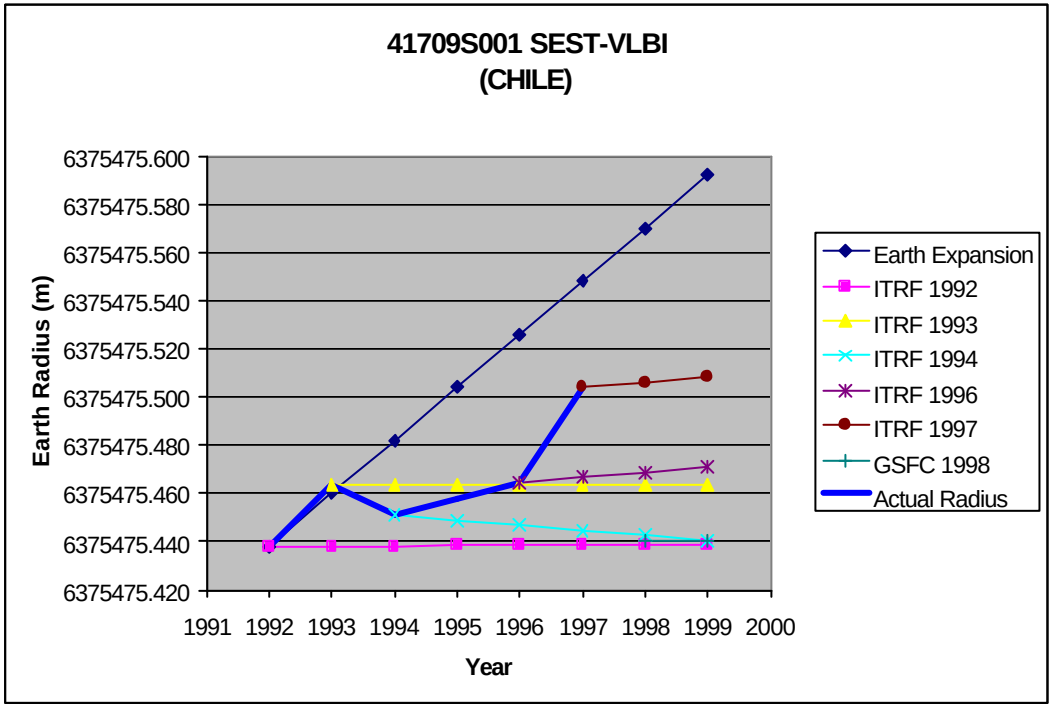

A2.2 SLR Space Geodetic Charts

12205S001 BOROWIEC-SLR (RUSSIA)

	Site Co-ordinates			Site Velocity			Derived Earth Radius							
Data	**X**	**Y**	**Z**	**Vx**	**Vy**	**Vz**	**1992**	**1993**	**1994**	**1995**	**1996**	**1997**	**1998**	**1999**
Source	**m**	**m**	**m**	**m/y**	**m/y**	**m/y**	6364922.201	6364922.223	6364922.245	6364922.267	6364922.289	6364922.311	6364922.333	6364922.355
ITRF 1992	3738332.837	1148246.354	5021815.661	-0.0167	0.0174	0.0076	6364922.201	6364922.200	6364922.199	6364922.199	6364922.198	6364922.197	6364922.197	6364922.196
ITRF 1993	3738332.861	1148246.426	5021816.257	-0.0156	0.0167	0.0078		6364922.698	6364922.698	6364922.698	6364922.698	6364922.698	6364922.698	6364922.698
ITRF 1994	3738332.915	1148246.437	5021815.995	-0.0165	0.0167	0.0067			6364922.525	6364922.524	6364922.522	6364922.521	6364922.520	6364922.518
ITRF 1996	3738332.844	1148246.5	5021816.021	-0.0158	0.0153	0.0083					6364922.515	6364922.515	6364922.515	6364922.515
ITRF 1997	3738332.844	1148246.498	5021816.023	-0.0175	0.0152	0.0054						6364922.517	6364922.513	6364922.510
GSFC 1998														
							6364922.201	6364922.698	6364922.525	6364922.520	6364922.515	6364922.517		

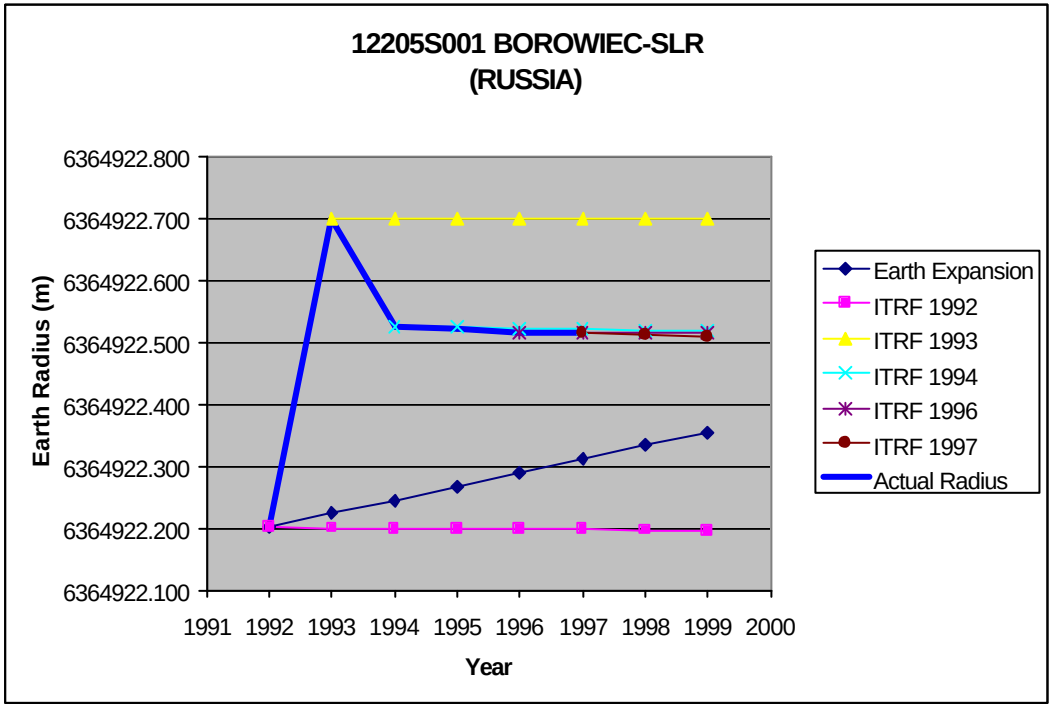

12612M001 ASKITES-SLR (EUROPE)

	Site Co-ordinates			Site Velocity			Derived Earth Radius							
Data	**X**	**Y**	**Z**	**Vx**	**Vy**	**Vz**	**1992**	**1993**	**1994**	**1995**	**1996**	**1997**	**1998**	**1999**
Source	**m**	**m**	**m**	**m/y**	**m/y**	**m/y**	6369185.891	6369185.913	6369185.935	6369185.957	6369185.979	6369186.001	6369186.023	6369186.045
ITRF 1992	4353444.885	2082666.283	4156506.67	-0.0181	0.023	0.0069	6369185.891	6369185.890	6369185.890	6369185.890	6369185.889	6369185.889	6369185.889	6369185.888
ITRF 1993	4353444.803	2082666.396	4156506.724	-0.0173	0.0247	0.0085		6369185.907	6369185.909	6369185.910	6369185.912	6369185.914	6369185.916	6369185.918
ITRF 1994	4353444.808	2082666.387	4156506.736	-0.0141	0.0209	0.0099			6369185.915	6369185.919	6369185.923	6369185.926	6369185.930	6369185.933
ITRF 1996	4353444.687	2082666.497	4156506.751	-0.0237	0.0227	0.009					6369185.878	6369185.875	6369185.872	6369185.870
ITRF 1997	4353444.729	2082666.494	4156506.743	-0.017	0.0225	0.0054						6369185.901	6369185.900	6369185.899
GSFC 1998														
							6369185.891	6369185.907	6369185.915	6369185.897	6369185.878	6369185.901		

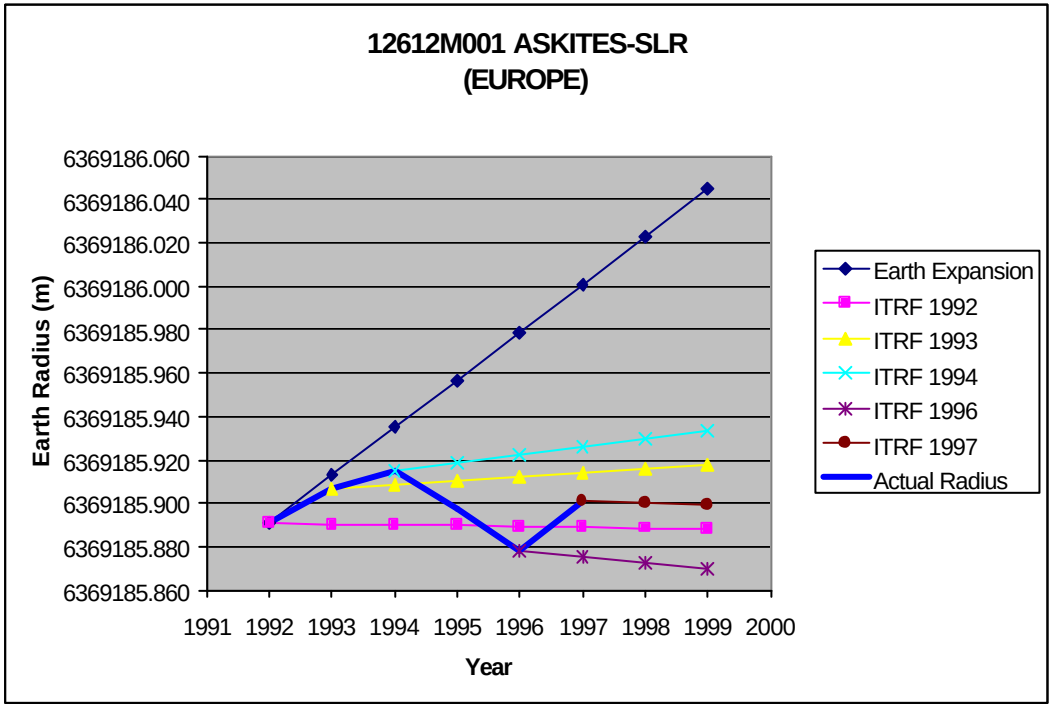

12613M001 ROUMELLI-SLR (EUROPE)

	Site Co-ordinates			Site Velocity			Derived Earth Radius							
Data	**X**	**Y**	**Z**	**Vx**	**Vy**	**Vz**	**1992**	**1993**	**1994**	**1995**	**1996**	**1997**	**1998**	**1999**
Source	**m**	**m**	**m**	**m/y**	**m/y**	**m/y**	6371101.891	6371101.913	6371101.935	6371101.957	6371101.979	6371102.001	6371102.023	6371102.045
ITRF 1992	4728694.664	2174373.368	3674572.973	0.0254	-0.0004	-0.0059	6371101.891	6371101.906	6371101.921	6371101.937	6371101.952	6371101.967	6371101.983	6371101.998
ITRF 1993	4728694.685	2174373.423	3674572.909	0.0109	0.0142	-0.0074		6371101.888	6371101.897	6371101.906	6371101.914	6371101.923	6371101.932	6371101.940
ITRF 1994	4728694.705	2174373.443	3674572.937	0.0095	0.0135	-0.0088			6371101.926	6371101.933	6371101.939	6371101.946	6371101.952	6371101.959
ITRF 1996	4728694.684	2174373.471	3674572.879	0.0003	0.0102	-0.0104					6371101.887	6371101.884	6371101.882	6371101.880
ITRF 1997	4728694.721	2174373.48	3674572.882	0.0064	0.0113	-0.0123						6371101.919	6371101.920	6371101.922
GSFC 1998														
							6371101.891	6371101.888	6371101.926	6371101.907	6371101.887	6371101.919		

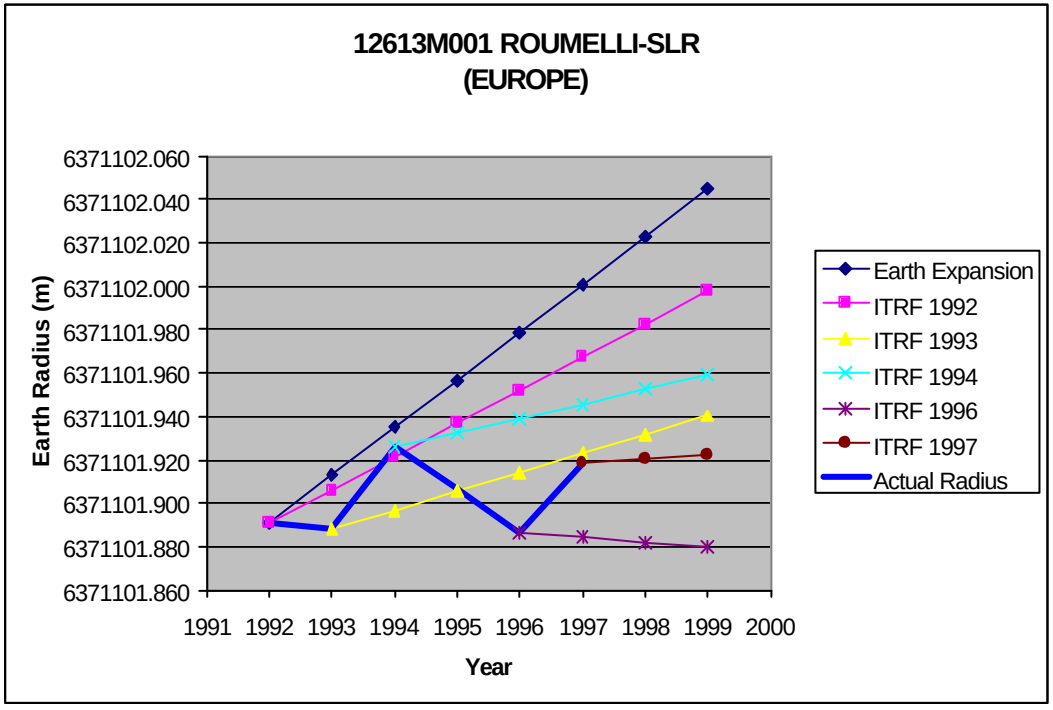

12614M001 KARITSA-SLR (EUROPE)

	Site Co-ordinates			Site Velocity			Derived Earth Radius							
Data	**X**	**Y**	**Z**	**Vx**	**Vy**	**Vz**	**1992**	**1993**	**1994**	**1995**	**1996**	**1997**	**1998**	**1999**
Source	**m**	**m**	**m**	**m/y**	**m/y**	**m/y**	6370040.900	6370040.922	6370040.944	6370040.966	6370040.988	6370041.010	6370041.032	6370041.054
ITRF 1992	4596042.613	1733476.756	4055720.861	-0.0062	-0.0168	0.0102	6370040.900	6370040.897	6370040.895	6370040.892	6370040.890	6370040.887	6370040.885	6370040.882
ITRF 1993	4596042.614	1733476.683	4055720.93	-0.0036	-0.0161	0.0096		6370040.925	6370040.924	6370040.923	6370040.922	6370040.921	6370040.920	6370040.919
ITRF 1994	4596042.559	1733476.818	4055720.933	-0.0143	0.019	0.0103			6370040.924	6370040.925	6370040.926	6370040.928	6370040.929	6370040.931
ITRF 1996	4596042.475	1733476.892	4055720.977	-0.0191	0.0176	0.0115					6370040.911	6370040.910	6370040.908	6370040.906
ITRF 1997	4596042.499	1733476.884	4055720.967	-0.0155	0.0166	0.0071						6370040.920	6370040.918	6370040.916
GSFC 1998														
							6370040.900	6370040.925	6370040.924	6370040.918	6370040.911	6370040.920		

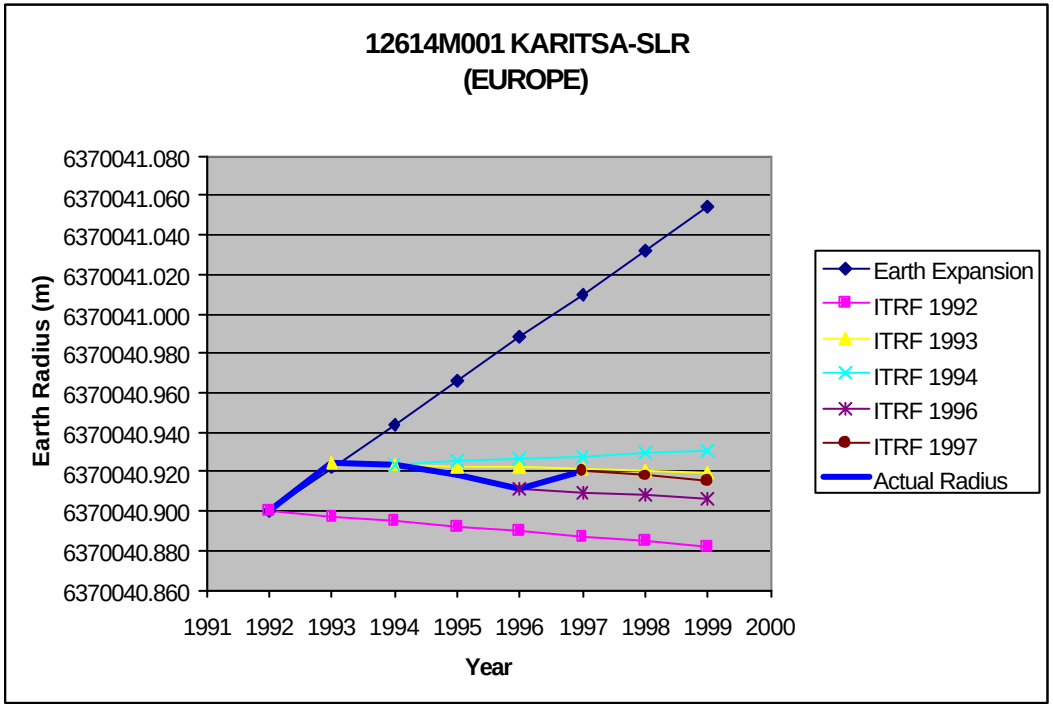

12615M001 KATAVIA-SLR (EUROPE)

	Site Co-ordinates			Site Velocity			Derived Earth Radius							
Data	**X**	**Y**	**Z**	**Vx**	**Vy**	**Vz**	**1992**	**1993**	**1994**	**1995**	**1996**	**1997**	**1998**	**1999**
Source	**m**	**m**	**m**	**m/y**	**m/y**	**m/y**	6370880.376	6370880.398	6370880.420	6370880.442	6370880.464	6370880.486	6370880.508	6370880.530
ITRF 1992	4573400.02	2409322.211	3723881.78	0.0021	0.0186	-0.008	6370880.376	6370880.380	6370880.384	6370880.388	6370880.392	6370880.396	6370880.400	6370880.403
ITRF 1993	4573400.033	2409322.29	3723881.724	0.0042	0.0198	-0.0073		6370880.383	6370880.389	6370880.395	6370880.402	6370880.408	6370880.414	6370880.420
ITRF 1994	4573400.053	2409322.317	3723881.75	0.0061	0.0197	-0.0077			6370880.423	6370880.430	6370880.437	6370880.445	6370880.452	6370880.459
ITRF 1996	4573400.012	2409322.371	3723881.694	-0.0043	0.016	-0.0106					6370880.381	6370880.378	6370880.374	6370880.371
ITRF 1997	4573400.059	2409322.377	3723881.7	0.0032	0.0174	-0.011						6370880.420	6370880.423	6370880.425
GSFC 1998														
							6370880.376	6370880.383	6370880.423	6370880.402	6370880.381	6370880.420		

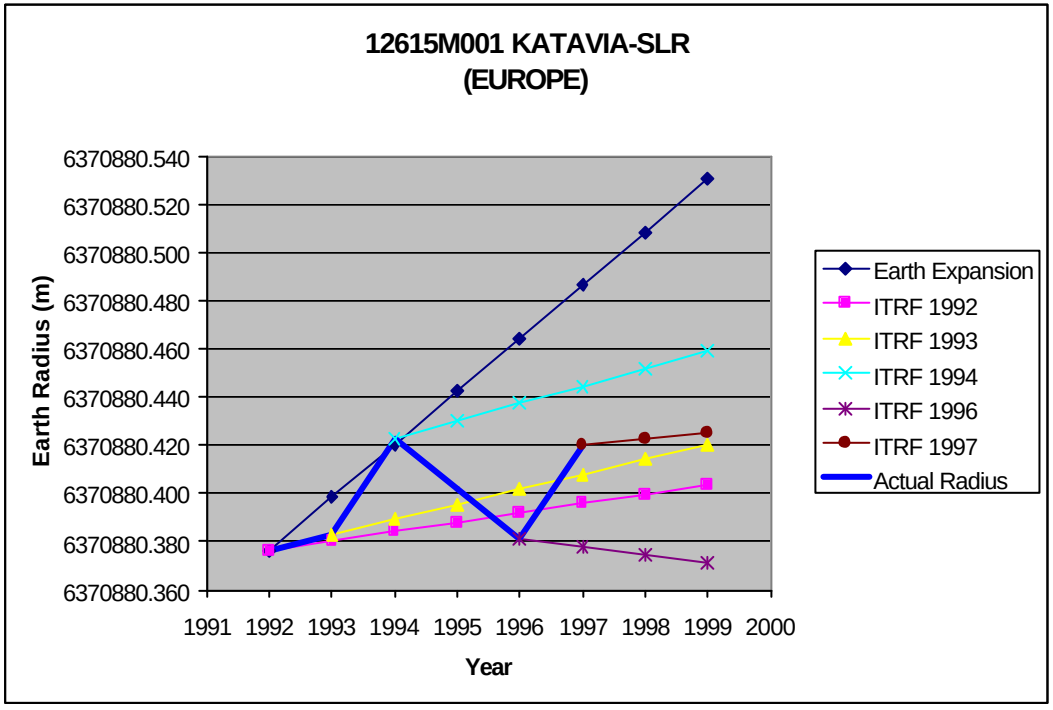

12616M001 XRISOKALARIA-SLR (EUROPE)

	Site Co-ordinates			Site Velocity			Derived Earth Radius							
Data	**X**	**Y**	**Z**	**Vx**	**Vy**	**Vz**	**1992**	**1993**	**1994**	**1995**	**1996**	**1997**	**1998**	**1999**
Source	**m**	**m**	**m**	**m/y**	**m/y**	**m/y**	6370984.043	6370984.065	6370984.087	6370984.109	6370984.131	6370984.153	6370984.175	6370984.197
ITRF 1992	4745949.535	1905705.936	3799169.064	0.0057	-0.0097	-0.0118	6370984.043	6370984.038	6370984.032	6370984.026	6370984.021	6370984.015	6370984.009	6370984.003
ITRF 1993	4745949.569	1905705.964	3799169.027	0.0054	0.0069	-0.009		6370984.055	6370984.056	6370984.056	6370984.057	6370984.058	6370984.059	6370984.059
ITRF 1994	4745949.569	1905705.969	3799169.04	0.0072	0.0069	-0.0078			6370984.064	6370984.067	6370984.070	6370984.073	6370984.075	6370984.078
ITRF 1996	4745949.569	1905705.992	3799169.018	0.0019	0.0056	-0.0055					6370984.058	6370984.058	6370984.058	6370984.057
ITRF 1997	4745949.584	1905705.991	3799169.003	0.0052	0.0057	-0.0096						6370984.060	6370984.060	6370984.060
GSFC 1998														
							6370984.043	6370984.055	6370984.064	6370984.061	6370984.058	6370984.060		

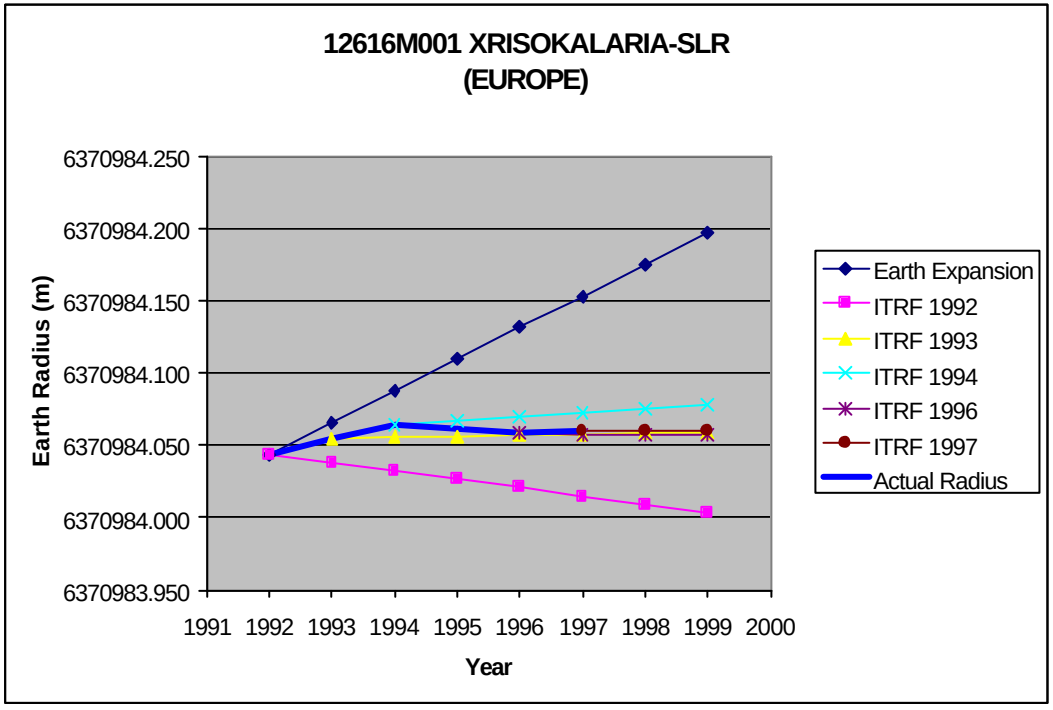

12706M001 LAMPEDUSA-SLR (MEDITERRANEAN)

	Site Co-ordinates			Site Velocity			Derived Earth Radius							
Data	**X**	**Y**	**Z**	**Vx**	**Vy**	**Vz**	**1992**	**1993**	**1994**	**1995**	**1996**	**1997**	**1998**	**1999**
Source	**m**	**m**	**m**	**m/y**	**m/y**	**m/y**	6371071.463	6371071.485	6371071.507	6371071.529	6371071.551	6371071.573	6371071.595	6371071.617
ITRF 1992	5072831.987	1130886.238	3684836.975	-0.0153	0.0186	0.0186	6371071.463	6371071.465	6371071.467	6371071.468	6371071.470	6371071.472	6371071.474	6371071.476
ITRF 1993	5072831.93	1130886.331	3684837.078	-0.0124	0.0199	0.0197		6371071.493	6371071.499	6371071.504	6371071.509	6371071.514	6371071.519	6371071.524
ITRF 1994	5072831.946	1130886.341	3684837.084	-0.009	0.0205	0.0181			6371071.511	6371071.518	6371071.525	6371071.532	6371071.539	6371071.546
ITRF 1996	5072831.846	1130886.437	3684837.146	-0.0198	0.0213	0.0157					6371071.485	6371071.482	6371071.479	6371071.476
ITRF 1997	5072831.886	1130886.415	3684837.144	-0.0132	0.0187	0.0135						6371071.512	6371071.512	6371071.513
GSFC 1998														
							6371071.463	6371071.493	6371071.511	6371071.498	6371071.485	6371071.512		

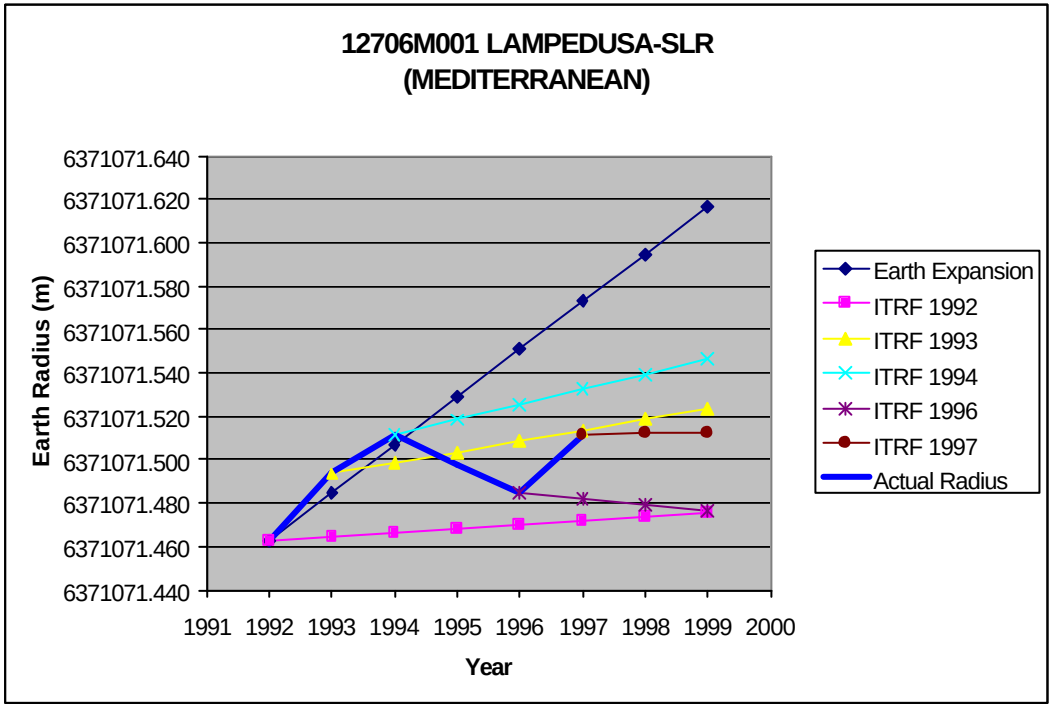

12711M002 BOLOGNA-SLR (ITALY)

	Site Co-ordinates			Site Velocity			Derived Earth Radius							
Data	**X**	**Y**	**Z**	**Vx**	**Vy**	**Vz**	**1992**	**1993**	**1994**	**1995**	**1996**	**1997**	**1998**	**1999**
Source	**m**	**m**	**m**	**m/y**	**m/y**	**m/y**	6367718.150	6367718.172	6367718.194	6367718.216	6367718.238	6367718.260	6367718.282	6367718.304
ITRF 1992	4461399.704	919566.761	4449510.545	-0.0184	0.0189	0.0102	6367718.150	6367718.147	6367718.144	6367718.141	6367718.138	6367718.135	6367718.132	6367718.129
ITRF 1993	4461399.586	919566.849	4449510.594	-0.0199	0.0185	0.0085		6367718.114	6367718.109	6367718.104	6367718.098	6367718.093	6367718.088	6367718.082
ITRF 1994	4461399.597	919566.849	4449510.594	-0.0187	0.019	0.0084			6367718.122	6367718.117	6367718.113	6367718.108	6367718.104	6367718.099
ITRF 1996	4461399.528	919566.936	4449510.64	-0.0142	0.0214	0.0118					6367718.118	6367718.120	6367718.121	6367718.122
ITRF 1997	4461399.525	919566.931	4449510.636	-0.018	0.0199	0.0081						6367718.113	6367718.109	6367718.104
GSFC 1998														
							6367718.150	6367718.114	6367718.122	6367718.120	6367718.118	6367718.113		

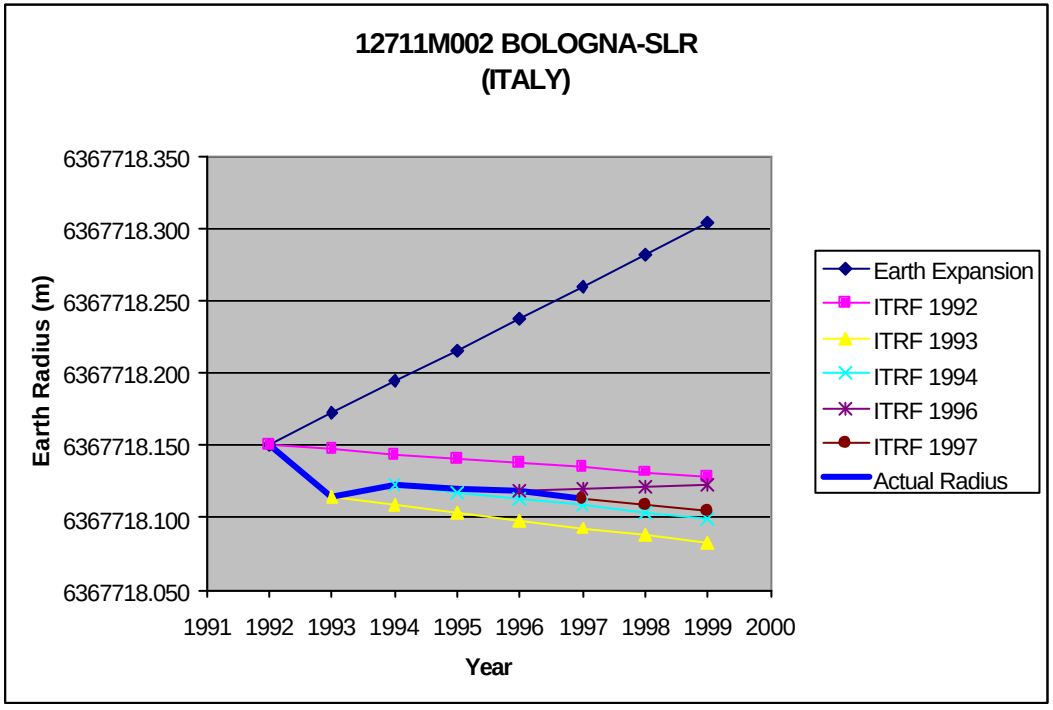

12717M001 NOTO-SLR (SOUTH AFRICA)

	Site Co-ordinates			Site Velocity			Derived Earth Radius							
Data	**X**	**Y**	**Z**	**Vx**	**Vy**	**Vz**	**1992**	**1993**	**1994**	**1995**	**1996**	**1997**	**1998**	**1999**
Source	**m**	**m**	**m**	**m/y**	**m/y**	**m/y**	6370603.117	6370603.139	6370603.161	6370603.183	6370603.205	6370603.227	6370603.249	6370603.271
ITRF 1992	4934529.05	1321133.208	3806522.583	-0.0211	0.016	0.0152	6370603.117	6370603.113	6370603.109	6370603.105	6370603.101	6370603.097	6370603.093	6370603.089
ITRF 1993	4934528.938	1321133.282	3806522.638	-0.0237	0.016	0.0127		6370603.078	6370603.071	6370603.063	6370603.056	6370603.049	6370603.041	6370603.034
ITRF 1994	4934528.959	1321133.288	3806522.65	-0.0192	0.0167	0.0136			6370603.103	6370603.100	6370603.097	6370603.093	6370603.090	6370603.087
ITRF 1996	4934528.888	1321133.371	3806522.725	-0.0163	0.0188	0.0157					6370603.110	6370603.111	6370603.111	6370603.112
ITRF 1997	4934528.891	1321133.369	3806522.722	-0.0162	0.0184	0.014						6370603.110	6370603.110	6370603.109
GSFC 1998														
							6370603.117	6370603.078	6370603.103	6370603.107	6370603.110	6370603.110		

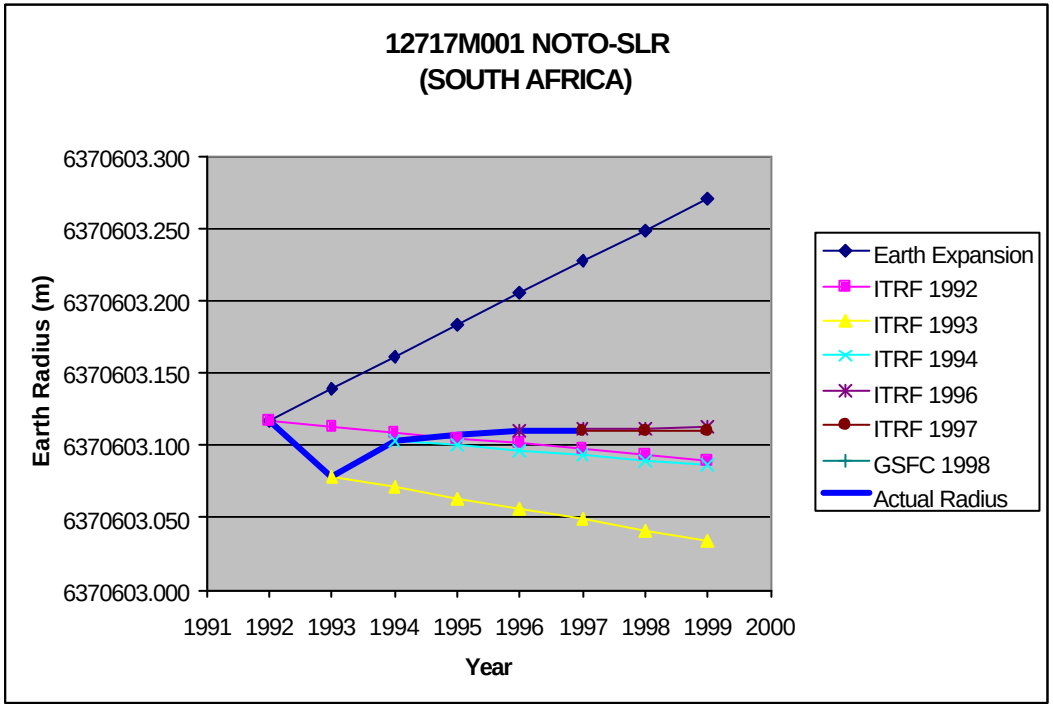

12718M002 TRIESTE-SLR (ITALY)

	Site Co-ordinates			Site Velocity			Derived Earth Radius							
Data	**X**	**Y**	**Z**	**Vx**	**Vy**	**Vz**	**1992**	**1993**	**1994**	**1995**	**1996**	**1997**	**1998**	**1999**
Source	**m**	**m**	**m**	**m/y**	**m/y**	**m/y**	6367696.658	6367696.680	6367696.702	6367696.724	6367696.746	6367696.768	6367696.790	6367696.812
ITRF 1992	4336738.58	1071271.474	4537911.044	-0.0139	0.019	0.0111	6367696.658	6367696.659	6367696.661	6367696.663	6367696.664	6367696.666	6367696.668	6367696.669
ITRF 1993	4336738.525	1071271.559	4537911.121	-0.014	0.0181	0.0096		6367696.689	6367696.690	6367696.690	6367696.691	6367696.691	6367696.691	6367696.692
ITRF 1994	4336738.518	1071271.571	4537911.131	-0.0147	0.02	0.0136			6367696.694	6367696.697	6367696.700	6367696.703	6367696.706	6367696.709
ITRF 1996	4336738.338	1071271.567	4537910.835	-0.0294	0.0091	-0.0244					6367696.360	6367696.324	6367696.288	6367696.252
ITRF 1997	4336738.424	1071271.633	4537911.093	-0.0178	0.0155	-0.0028						6367696.613	6367696.602	6367696.590
GSFC 1998														
							6367696.658	6367696.689	6367696.694	6367696.527	6367696.360	6367696.613		

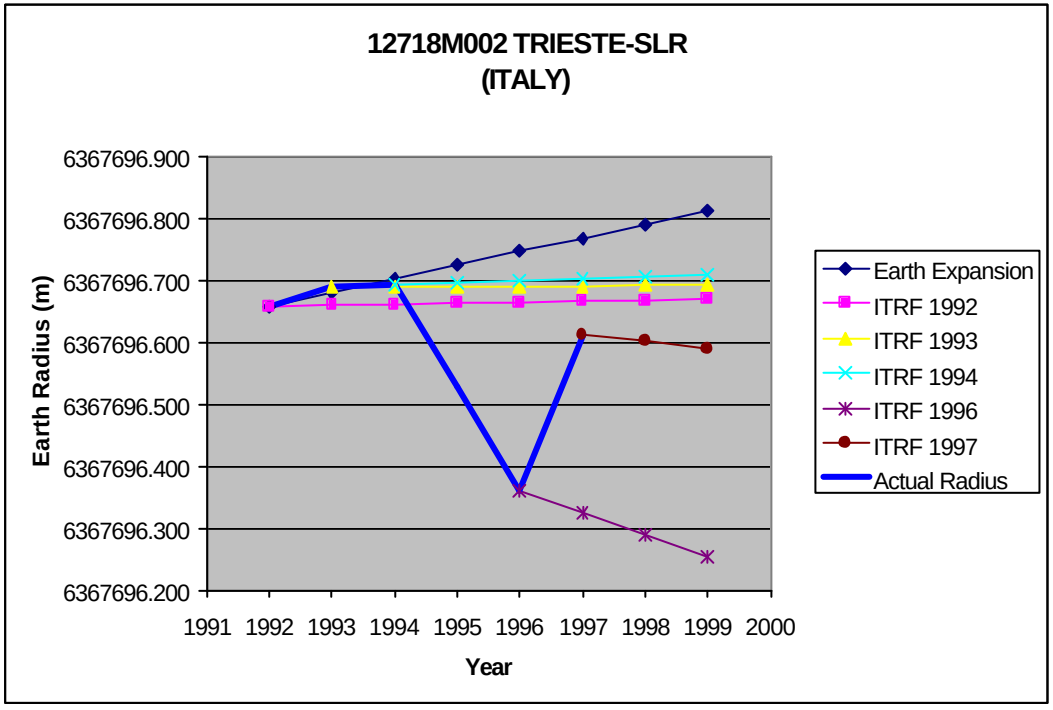

12725M002 CAGLIARI-SLR (ITALY)

	Site Co-ordinates			Site Velocity			Derived Earth Radius							
Data	**X**	**Y**	**Z**	**Vx**	**Vy**	**Vz**	**1992**	**1993**	**1994**	**1995**	**1996**	**1997**	**1998**	**1999**
Source	**m**	**m**	**m**	**m/y**	**m/y**	**m/y**	6369891.191	6369891.213	6369891.235	6369891.257	6369891.279	6369891.301	6369891.323	6369891.345
ITRF 1992	4893398.079	772673.297	4004140.982	-0.0104	0.02	0.0119	6369891.191	6369891.193	6369891.195	6369891.197	6369891.199	6369891.201	6369891.203	6369891.205
ITRF 1993	4893398.033	772673.387	4004141.07	-0.0083	0.0193	0.015		6369891.222	6369891.227	6369891.233	6369891.238	6369891.244	6369891.249	6369891.254
ITRF 1994	4893398.013	772673.4	4004141.042	-0.0164	0.0182	0.0115			6369891.191	6369891.188	6369891.184	6369891.181	6369891.178	6369891.175
ITRF 1996	4893397.984	772673.477	4004141.107	-0.0071	0.0127	0.0079					6369891.219	6369891.220	6369891.221	6369891.222
ITRF 1997	4893397.983	772673.475	4004141.104	-0.0108	0.0194	0.0105						6369891.216	6369891.216	6369891.217
GSFC 1998														
							6369891.191	6369891.222	6369891.191	6369891.205	6369891.219	6369891.216		

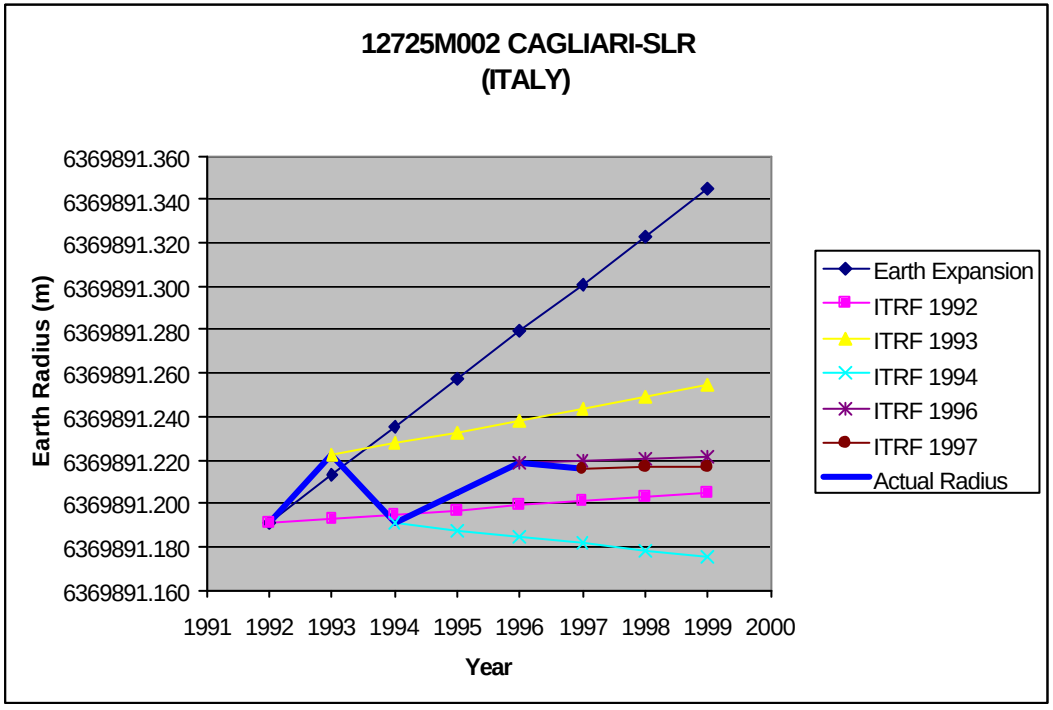

12734M004 MATERA-SLR (ITALY)

	Site Co-ordinates			Site Velocity			Derived Earth Radius							
Data	**X**	**Y**	**Z**	**Vx**	**Vy**	**Vz**	**1992**	**1993**	**1994**	**1995**	**1996**	**1997**	**1998**	**1999**
Source	**m**	**m**	**m**	**m/y**	**m/y**	**m/y**	6369634.721	6369634.743	6369634.765	6369634.787	6369634.809	6369634.831	6369634.853	6369634.875
ITRF 1992	4641990.303	1393042.292	4133231.869	-0.0217	0.0171	0.0119	6369634.721	6369634.717	6369634.713	6369634.708	6369634.704	6369634.700	6369634.695	6369634.691
ITRF 1993	4641990.243	1393042.392	4133231.916	-0.0226	0.0186	0.0116		6369634.730	6369634.725	6369634.720	6369634.715	6369634.710	6369634.706	6369634.701
ITRF 1994	4641990.233	1393042.404	4133231.945	-0.0184	0.02	0.0122			6369634.744	6369634.743	6369634.742	6369634.741	6369634.740	6369634.739
ITRF 1996	4641990.155	1393042.48	4133232.002	-0.0189	0.0192	0.0136					6369634.741	6369634.740	6369634.739	6369634.739
ITRF 1997	4641990.153	1393042.475	4133232.003	-0.0179	0.0192	0.0129						6369634.739	6369634.739	6369634.738
GSFC 1998														
							6369634.721	6369634.730	6369634.744	6369634.743	6369634.741	6369634.739		

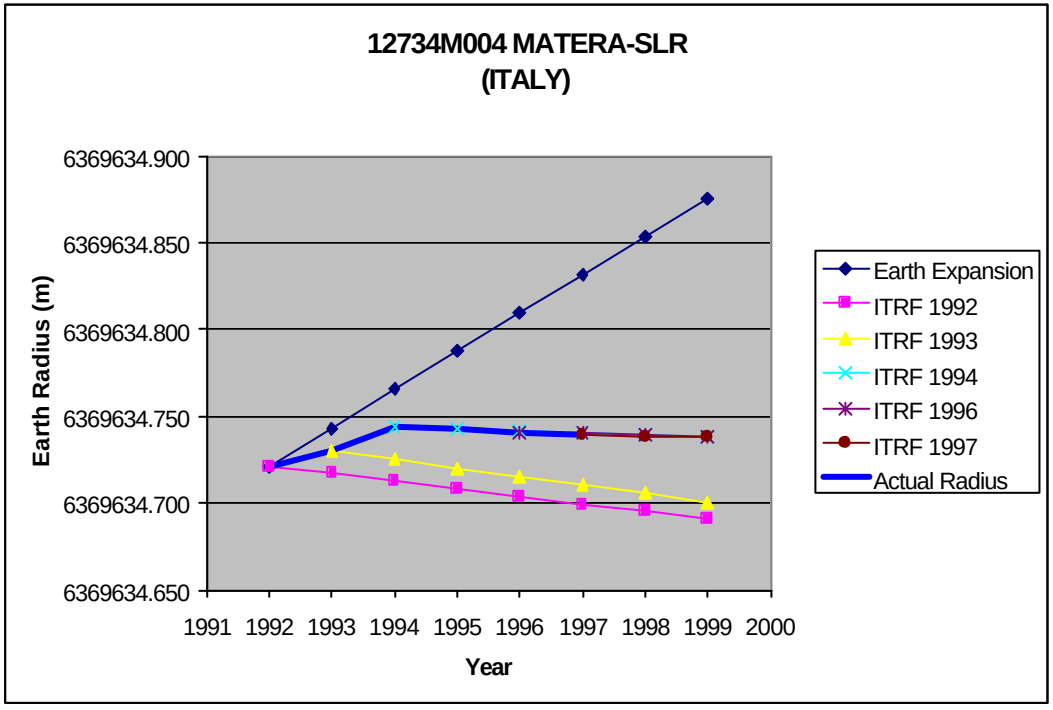

13504M002 KOOTWIJK-SLR (NETHERLANDS)

	Site Co-ordinates			Site Velocity			Derived Earth Radius							
Data	X	Y	Z	Vx	Vy	Vz	1992	1993	1994	1995	1996	1997	1998	1999
Source	m	m	m	m/y	m/y	m/y	6364924.236	6364924.258	6364924.280	6364924.302	6364924.324	6364924.346	6364924.368	6364924.390
ITRF 1992	3899237.85	396769.173	5015055.228	-0.0143	0.017	0.0074	6364924.236	6364924.234	6364924.232	6364924.230	6364924.228	6364924.226	6364924.225	6364924.223
ITRF 1993	3899237.762	396769.263	5015055.275	-0.0147	0.0179	0.007		6364924.225	6364924.222	6364924.220	6364924.217	6364924.215	6364924.213	6364924.210
ITRF 1994	3899237.774	396769.253	5015055.278	-0.0146	0.0172	0.0085			6364924.234	6364924.232	6364924.231	6364924.230	6364924.229	6364924.228
ITRF 1996	3899237.717	396769.32	5015055.32	-0.0132	0.0163	0.01					6364924.236	6364924.237	6364924.238	6364924.238
ITRF 1997	3899237.717	396769.316	5015055.317	-0.013	0.0158	0.0092						6364924.233	6364924.234	6364924.234
GSFC 1998														
							6364924.236	6364924.225	6364924.234	6364924.235	6364924.236	6364924.233		

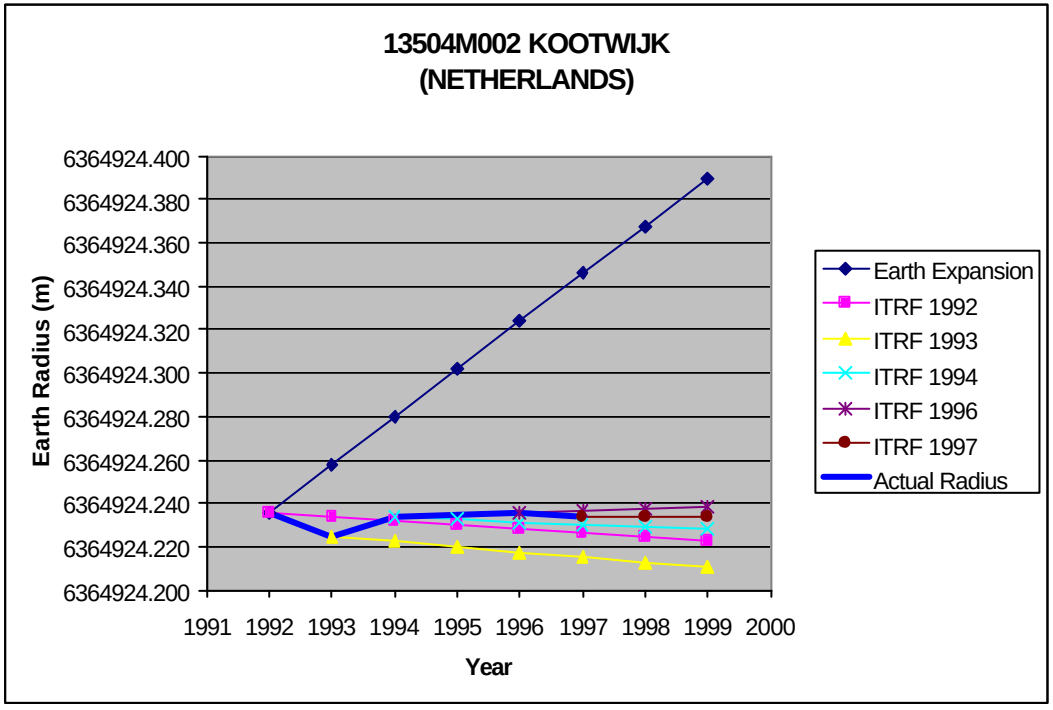

14106S001 POTSDAM-SLR (GERMANY)

	Site Co-ordinates			Site Velocity			Derived Earth Radius							
Data	**X**	**Y**	**Z**	**Vx**	**Vy**	**Vz**	**1992**	**1993**	**1994**	**1995**	**1996**	**1997**	**1998**	**1999**
Source	**m**	**m**	**m**	**m/y**	**m/y**	**m/y**	6364910.357	6364910.379	6364910.401	6364910.423	6364910.445	6364910.467	6364910.489	6364910.511
ITRF 1992	3800621.302	882005.313	5028859.533	-0.028	0.0127	-0.0113	6364910.357	6364910.333	6364910.309	6364910.286	6364910.262	6364910.238	6364910.214	6364910.190
ITRF 1993	3800621.17	882005.374	5028859.467	-0.0272	0.0146	-0.0079		6364910.235	6364910.214	6364910.194	6364910.173	6364910.153	6364910.132	6364910.112
ITRF 1994	3800621.186	882005.377	5028859.529	-0.0136	0.0152	0.0058			6364910.294	6364910.292	6364910.291	6364910.289	6364910.288	6364910.287
ITRF 1996	3800621.169	882005.514	5028859.568	-0.0128	0.0175	0.012					6364910.333	6364910.338	6364910.342	6364910.346
ITRF 1997	3800621.128	882005.483	5028859.546	-0.0154	0.0166	0.0078						6364910.287	6364910.286	6364910.286
GSFC 1998														
							6364910.357	6364910.235	6364910.294	6364910.314	6364910.333	6364910.287		

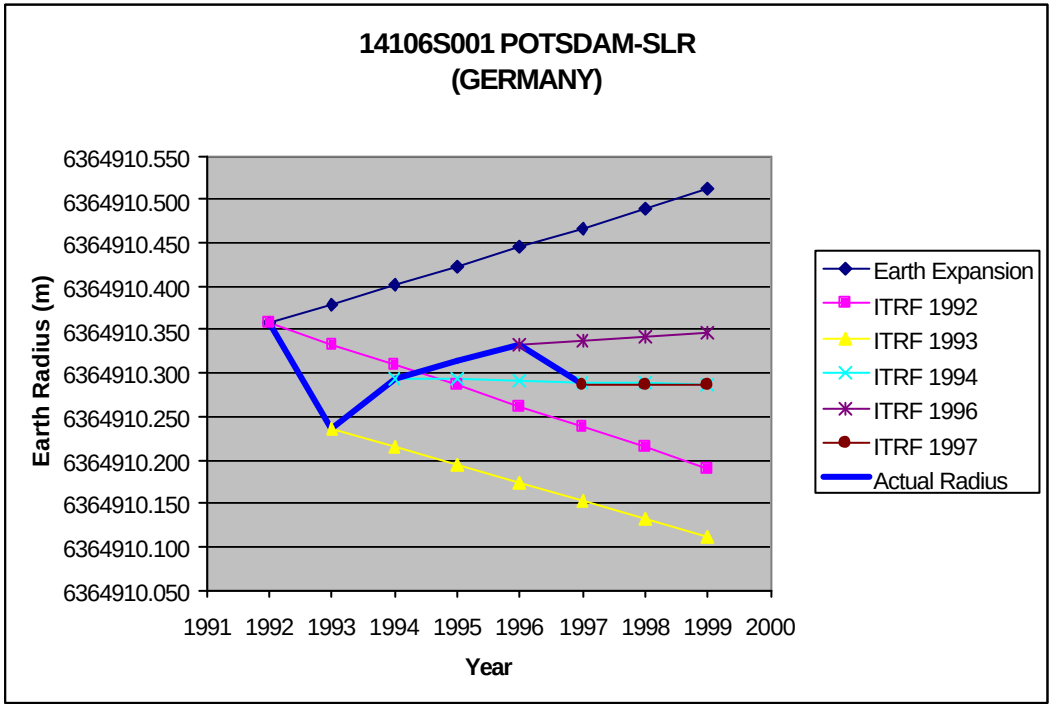

14201M004 WETTZELL-SLR (GERMANY)

	Site Co-ordinates			Site Velocity			Derived Earth Radius							
Data	**X**	**Y**	**Z**	**Vx**	**Vy**	**Vz**	**1992**	**1993**	**1994**	**1995**	**1996**	**1997**	**1998**	**1999**
Source	**m**	**m**	**m**	**m/y**	**m/y**	**m/y**	6366605.951	6366605.973	6366605.995	6366606.017	6366606.039	6366606.061	6366606.083	6366606.105
ITRF 1992	4075582.606	931837.182	4801559.874	-0.0169	0.0161	0.0092	6366605.951	6366605.950	6366605.948	6366605.946	6366605.945	6366605.943	6366605.942	6366605.940
ITRF 1993	4075582.502	931837.27	4801559.909	-0.0184	0.0159	0.0071		6366605.924	6366605.920	6366605.916	6366605.911	6366605.907	6366605.903	6366605.899
ITRF 1994	4075582.518	931837.266	4801559.918	-0.0167	0.0171	0.0065			6366605.940	6366605.937	6366605.934	6366605.930	6366605.927	6366605.924
ITRF 1996	4075582.449	931837.337	4801559.948	-0.0159	0.0174	0.007					6366605.929	6366605.927	6366605.924	6366605.922
ITRF 1997	4075582.452	931837.333	4801559.947	-0.0158	0.0171	0.0071						6366605.930	6366605.927	6366605.925
GSFC 1998														
							6366605.951	6366605.924	6366605.940	6366605.935	6366605.929	6366605.930		

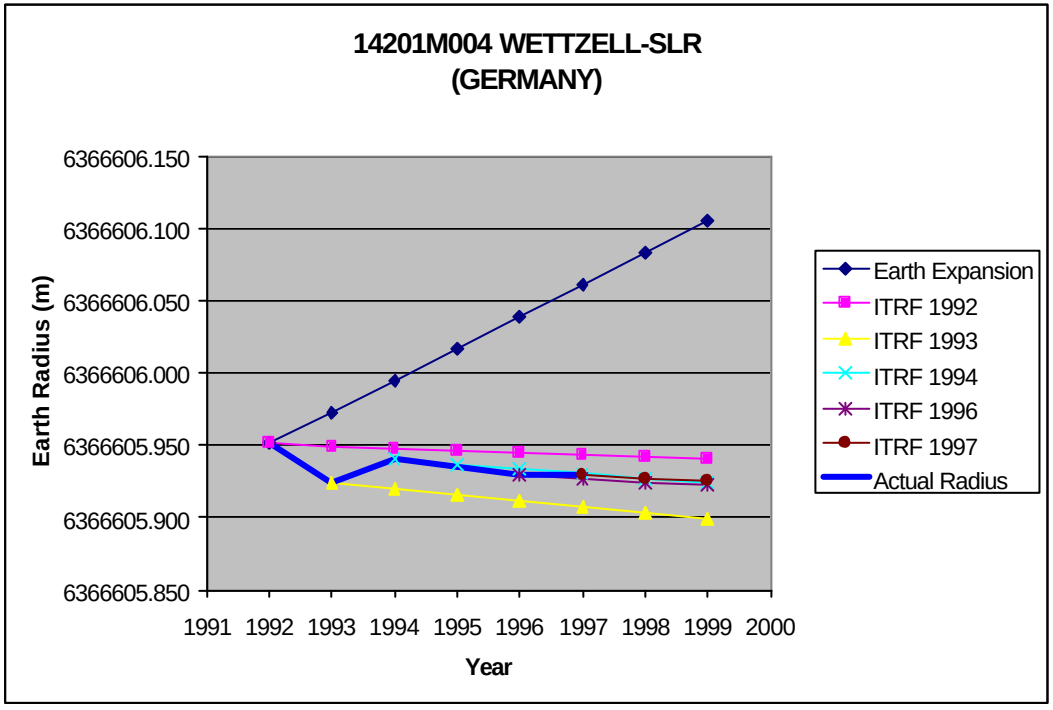

20702M001 BAR GIYYORA-SLR (NORTH AFRICA)

	Site Co-ordinates			Site Velocity			Derived Earth Radius							
Data	**X**	**Y**	**Z**	**Vx**	**Vy**	**Vz**	**1992**	**1993**	**1994**	**1995**	**1996**	**1997**	**1998**	**1999**
Source	**m**	**m**	**m**	**m/y**	**m/y**	**m/y**	6373034.983	6373035.005	6373035.027	6373035.049	6373035.071	6373035.093	6373035.115	6373035.137
ITRF 1992	4443967.253	3121945.386	3334694.432	-0.0217	0.0168	0.0185	6373034.983	6373034.986	6373034.988	6373034.991	6373034.994	6373034.997	6373035.000	6373035.002
ITRF 1993	4443965.888	3121945.26	3334693.739	-0.0252	0.0193	0.0156		6373033.607	6373033.607	6373033.607	6373033.607	6373033.607	6373033.607	6373033.607
ITRF 1994	4443965.873	3121945.272	3334693.732	-0.0127	0.0193	0.0187			6373033.599	6373033.609	6373033.619	6373033.630	6373033.640	6373033.650
ITRF 1996	4443965.778	3121945.343	3334693.829	-0.0287	0.0142	0.0177					6373033.618	6373033.614	6373033.610	6373033.606
ITRF 1997	4443965.85	3121945.341	3334693.823	-0.0139	0.0184	0.0182						6373033.664	6373033.673	6373033.682
GSFC 1998														
							6373034.983	6373033.607	6373033.599	6373033.609	6373033.618	6373033.664		

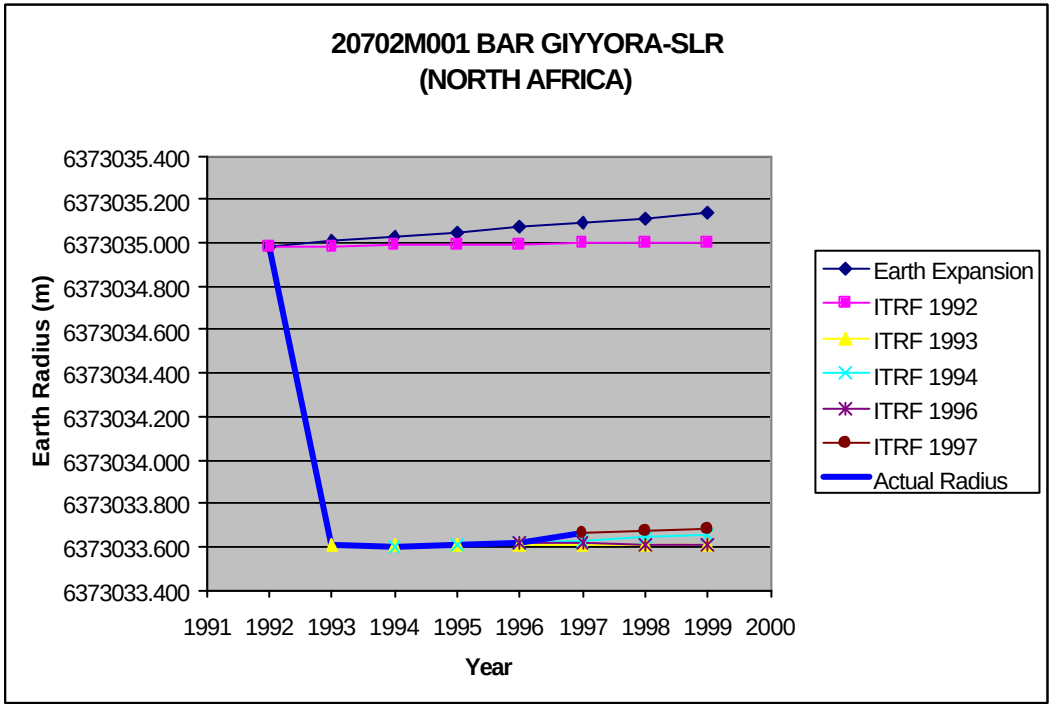

20801M001 DIYARBAKIR-SLR (TURKEY)

	Site Co-ordinates			Site Velocity			Derived Earth Radius							
Data	**X**	**Y**	**Z**	**Vx**	**Vy**	**Vz**	**1992**	**1993**	**1994**	**1995**	**1996**	**1997**	**1998**	**1999**
Source	**m**	**m**	**m**	**m/y**	**m/y**	**m/y**	6370827.352	6370827.374	6370827.396	6370827.418	6370827.440	6370827.462	6370827.484	6370827.506
ITRF 1992	3848635.953	3251760.908	3898909.263	-0.0367	0.0016	0.0026	6370827.352	6370827.332	6370827.312	6370827.292	6370827.272	6370827.253	6370827.233	6370827.213
ITRF 1993	3848635.829	3251760.958	3898909.331	-0.0346	0.004	0.0055		6370827.344	6370827.328	6370827.313	6370827.297	6370827.282	6370827.266	6370827.251
ITRF 1994	3848635.796	3251760.898	3898909.335	-0.0289	-0.0051	0.0125			6370827.296	6370827.283	6370827.271	6370827.258	6370827.246	6370827.234
ITRF 1996	3848635.69	3251760.972	3898909.373	-0.0334	0.0015	0.0091					6370827.293	6370827.279	6370827.265	6370827.251
ITRF 1997	3848635.722	3251760.911	3898909.412	-0.0251	-0.0024	0.0141						6370827.305	6370827.297	6370827.289
GSFC 1998														
							6370827.352	6370827.344	6370827.296	6370827.295	6370827.293	6370827.305		

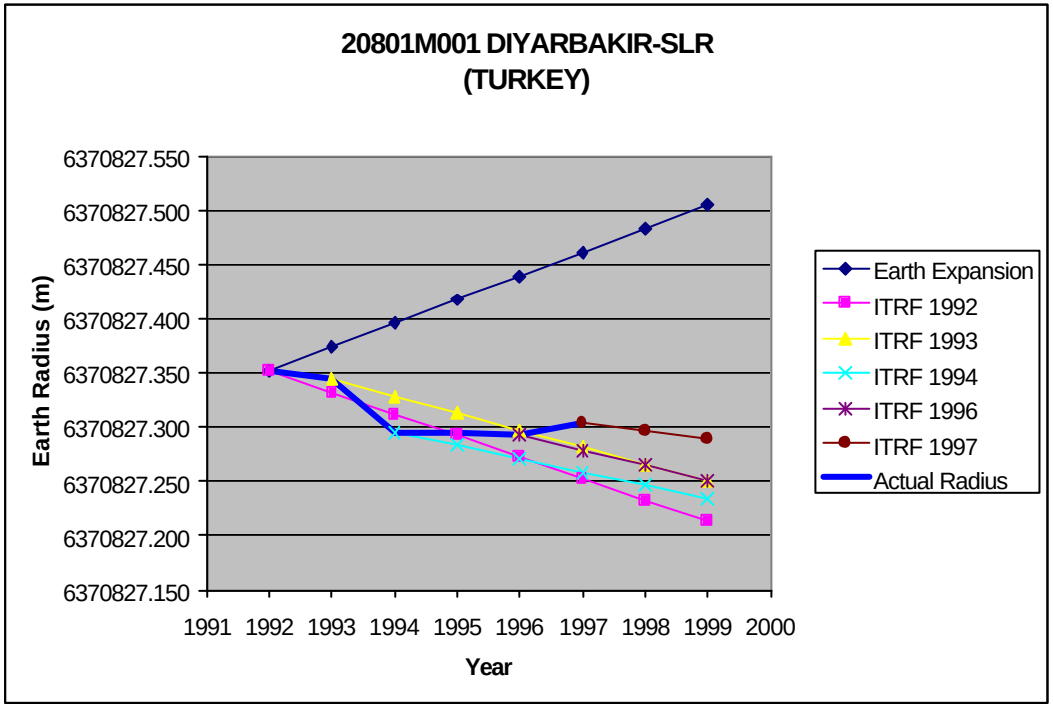

20802M001 YOZGAT-SLR (TURKEY)

	Site Co-ordinates			Site Velocity			Derived Earth Radius							
Data	**X**	**Y**	**Z**	**Vx**	**Vy**	**Vz**	**1992**	**1993**	**1994**	**1995**	**1996**	**1997**	**1998**	**1999**
Source	**m**	**m**	**m**	**m/y**	**m/y**	**m/y**	6371095.083	6371095.105	6371095.127	6371095.149	6371095.171	6371095.193	6371095.215	6371095.237
ITRF 1992	4029730.653	2802093.294	4062068.019	-0.015	-0.0139	0.0061	6371095.083	6371095.071	6371095.059	6371095.048	6371095.036	6371095.024	6371095.013	6371095.001
ITRF 1993	4029730.586	2802093.256	4062068.091	-0.0125	-0.006	0.0132		6371095.070	6371095.068	6371095.065	6371095.063	6371095.061	6371095.059	6371095.057
ITRF 1994	4029730.574	2802093.269	4062068.097	-0.0116	-0.0024	0.0142			6371095.072	6371095.072	6371095.073	6371095.074	6371095.074	6371095.075
ITRF 1996	4029730.481	2802093.255	4062068.17	-0.0196	-0.0041	0.0186					6371095.053	6371095.051	6371095.049	6371095.046
ITRF 1997	4029730.542	2802093.203	4062068.143	-0.0095	-0.0105	0.0115						6371095.052	6371095.048	6371095.045
GSFC 1998														
							6371095.083	6371095.070	6371095.072	6371095.062	6371095.053	6371095.052		

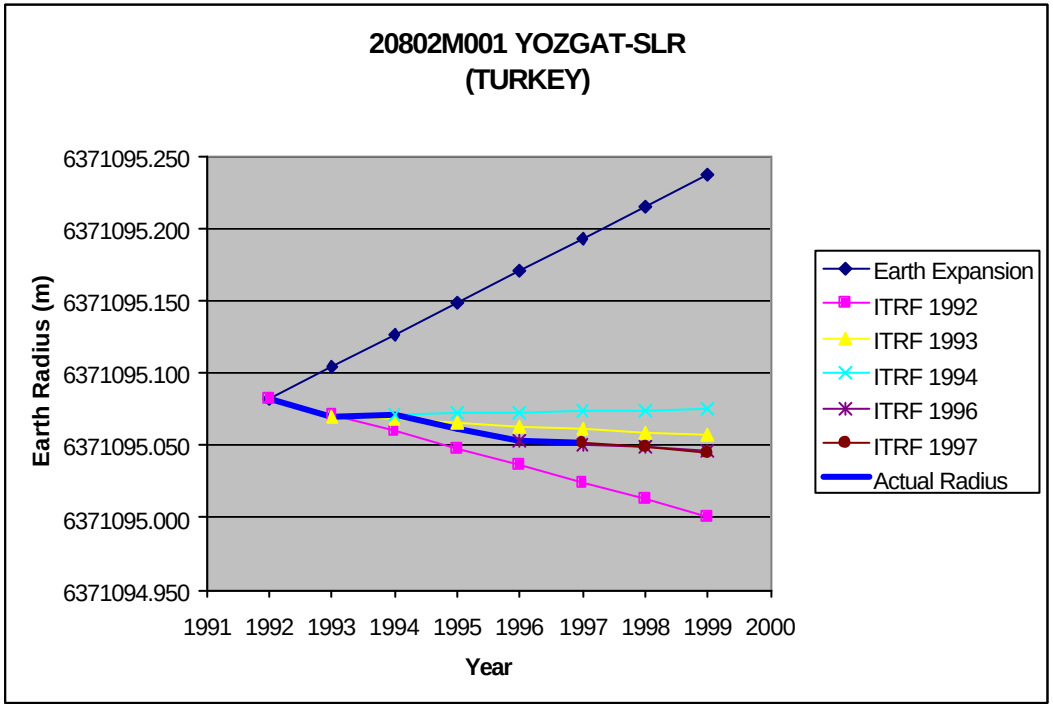

20803M001 MELENGICLICK-SLR (TURKEY)

	Site Co-ordinates			Site Velocity			Derived Earth Radius							
Data	**X**	**Y**	**Z**	**Vx**	**Vy**	**Vz**	**1992**	**1993**	**1994**	**1995**	**1996**	**1997**	**1998**	**1999**
Source	**m**	**m**	**m**	**m/y**	**m/y**	**m/y**	6371655.585	6371655.607	6371655.629	6371655.651	6371655.673	6371655.695	6371655.717	6371655.739
ITRF 1992	4247620.482	2778638.975	3851607.532	-0.0191	-0.012	0.0016	6371655.585	6371655.568	6371655.551	6371655.534	6371655.517	6371655.500	6371655.483	6371655.466
ITRF 1993	4247620.42	2778638.988	3851607.57	-0.017	0.0008	0.0066		6371655.572	6371655.565	6371655.558	6371655.551	6371655.544	6371655.537	6371655.530
ITRF 1994	4247620.407	2778638.992	3851607.585	-0.0133	0.004	0.0103			6371655.574	6371655.573	6371655.573	6371655.572	6371655.571	6371655.570
ITRF 1996	4247620.32	2778638.995	3851607.628	-0.0187	0.0011	0.0118					6371655.544	6371655.539	6371655.534	6371655.529
ITRF 1997	4247620.363	2778638.97	3851607.603	-0.0124	-0.0019	0.0064						6371655.546	6371655.541	6371655.536
GSFC 1998														
							6371655.585	6371655.572	6371655.574	6371655.559	6371655.544	6371655.546		

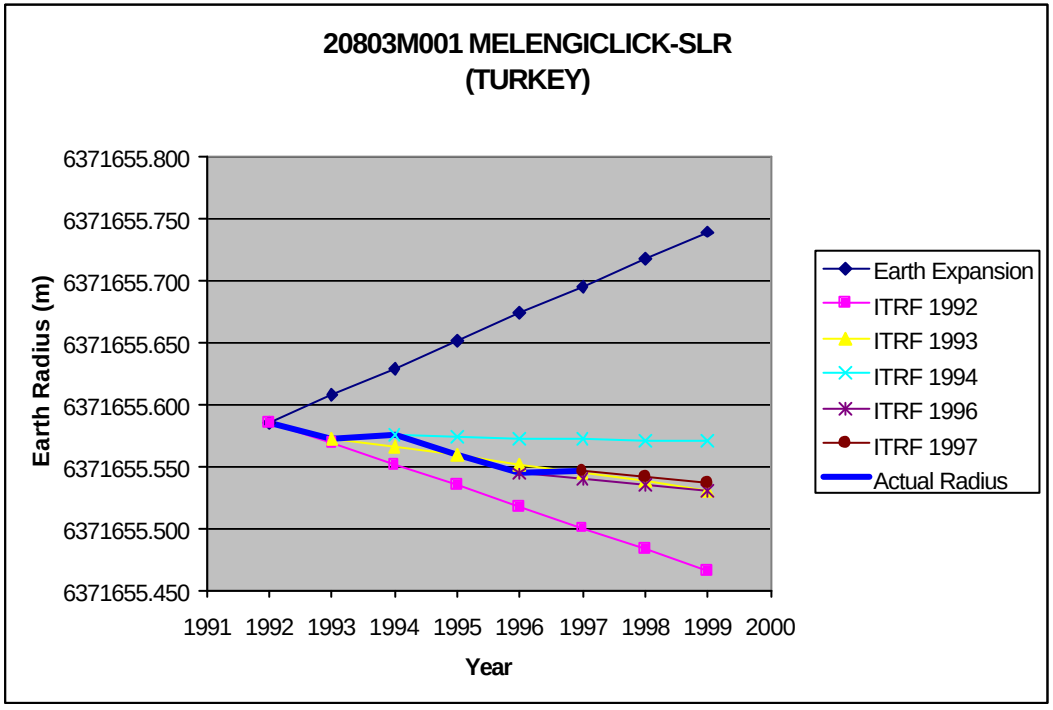

20804M001 YIGILCA-SLR (TURKEY)

	Site Co-ordinates			Site Velocity			Derived Earth Radius							
Data	**X**	**Y**	**Z**	**Vx**	**Vy**	**Vz**	**1992**	**1993**	**1994**	**1995**	**1996**	**1997**	**1998**	**1999**
Source	**m**	**m**	**m**	**m/y**	**m/y**	**m/y**	6369822.661	6369822.683	6369822.705	6369822.727	6369822.749	6369822.771	6369822.793	6369822.815
ITRF 1992	4117361.982	2517076.836	4157679.069	-0.0203	-0.0049	0.0079	6369822.661	6369822.651	6369822.641	6369822.631	6369822.621	6369822.611	6369822.601	6369822.591
ITRF 1993	4117361.896	2517076.91	4157679.119	-0.0181	0.0134	0.0082		6369822.667	6369822.666	6369822.665	6369822.664	6369822.663	6369822.662	6369822.661
ITRF 1994	4117361.896	2517076.91	4157679.134	-0.0169	0.015	0.0117			6369822.677	6369822.680	6369822.682	6369822.685	6369822.687	6369822.690
ITRF 1996	4117361.828	2517076.972	4157679.228	-0.0189	0.0142	0.0186					6369822.719	6369822.724	6369822.730	6369822.735
ITRF 1997	4117361.85	2517076.934	4157679.186	-0.0146	0.0103	0.0114						6369822.691	6369822.693	6369822.695
GSFC 1998														
							6369822.661	6369822.667	6369822.677	6369822.698	6369822.719	6369822.691		

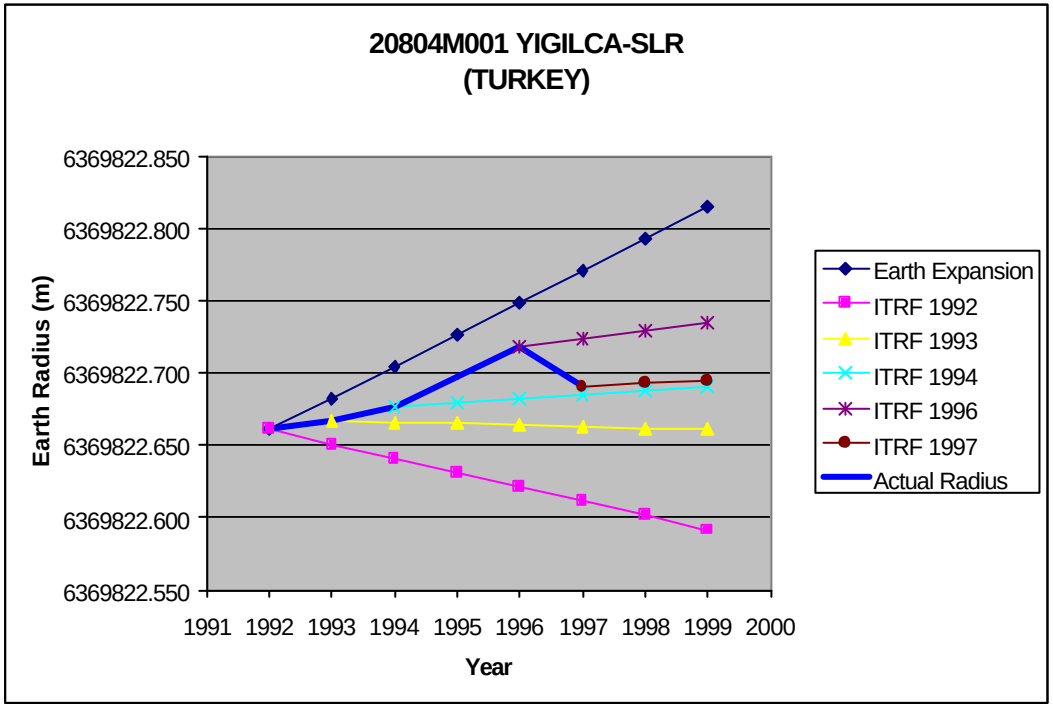

21602S003 WUHAN-SLR (CHINA)

	Site Co-ordinates			Site Velocity			Derived Earth Radius							
Data	**X**	**Y**	**Z**	**Vx**	**Vy**	**Vz**	**1992**	**1993**	**1994**	**1995**	**1996**	**1997**	**1998**	**1999**
Source	**m**	**m**	**m**	**m/y**	**m/y**	**m/y**	6372687.705	6372687.727	6372687.749	6372687.771	6372687.793	6372687.815	6372687.837	6372687.859
ITRF 1992	-2266555.56	5009079.321	3222266.106	-0.0246	-0.0041	-0.0108	6372687.705	6372687.705	6372687.705	6372687.705	6372687.705	6372687.705	6372687.705	6372687.705
ITRF 1993	-2266555.68	5009079.468	3222266.155	-0.0235	-0.004	-0.0104		6372687.888	6372687.888	6372687.888	6372687.888	6372687.888	6372687.888	6372687.888
ITRF 1994	-2266555.7	5009079.469	3222266.178	-0.0269	-0.0042	-0.0078			6372687.909	6372687.911	6372687.914	6372687.916	6372687.918	6372687.921
ITRF 1996	-2266555.84	5009079.404	3222266.134	-0.035	-0.0114	-0.0061					6372687.887	6372687.887	6372687.888	6372687.888
ITRF 1997	-2266555.82	5009079.423	3222266.115	-0.0354	-0.0074	-0.0127						6372687.884	6372687.884	6372687.884
GSFC 1998														
							6372687.705	6372687.888	6372687.909	6372687.898	6372687.887	6372687.884		

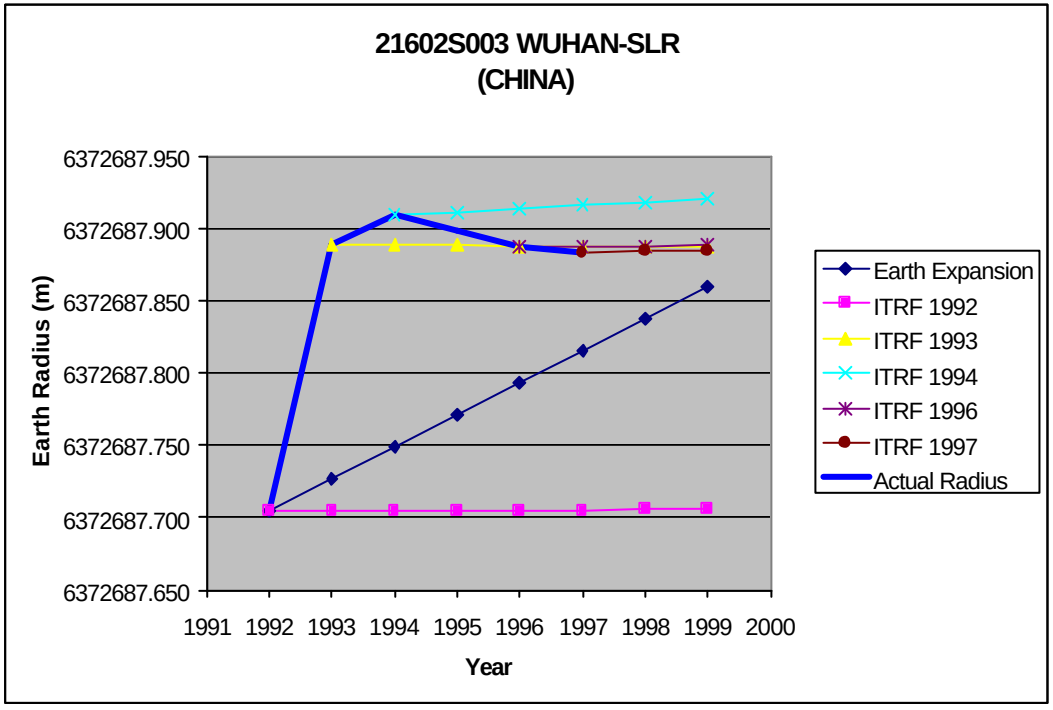

21605S001 SHANGHAI-SLR (CHINA)

	Site Co-ordinates			Site Velocity			Derived Earth Radius							
Data	**X**	**Y**	**Z**	**Vx**	**Vy**	**Vz**	**1992**	**1993**	**1994**	**1995**	**1996**	**1997**	**1998**	**1999**
Source	**m**	**m**	**m**	**m/y**	**m/y**	**m/y**	6372495.081	6372495.103	6372495.125	6372495.147	6372495.169	6372495.191	6372495.213	6372495.235
ITRF 1992	-2831087.77	4676203.416	3275172.849	-0.0276	-0.0126	-0.0126	6372495.081	6372495.077	6372495.074	6372495.070	6372495.067	6372495.063	6372495.060	6372495.056
ITRF 1993	-2831087.91	4676203.346	3275172.746	-0.0306	-0.0131	-0.0094		6372495.038	6372495.038	6372495.037	6372495.036	6372495.035	6372495.034	6372495.033
ITRF 1994	-2831087.92	4676203.334	3275172.78	-0.0264	-0.0212	-0.015			6372495.050	6372495.039	6372495.027	6372495.016	6372495.004	6372494.993
ITRF 1996	-2831088.11	4676203.358	3275172.834	-0.0309	-0.0117	-0.012					6372495.180	6372495.179	6372495.178	6372495.177
ITRF 1997	-2831088.1	4676203.354	3275172.81	-0.0323	-0.0116	-0.0143						6372495.161	6372495.160	6372495.158
GSFC 1998														
							6372495.081	6372495.038	6372495.050	6372495.115	6372495.180	6372495.161		

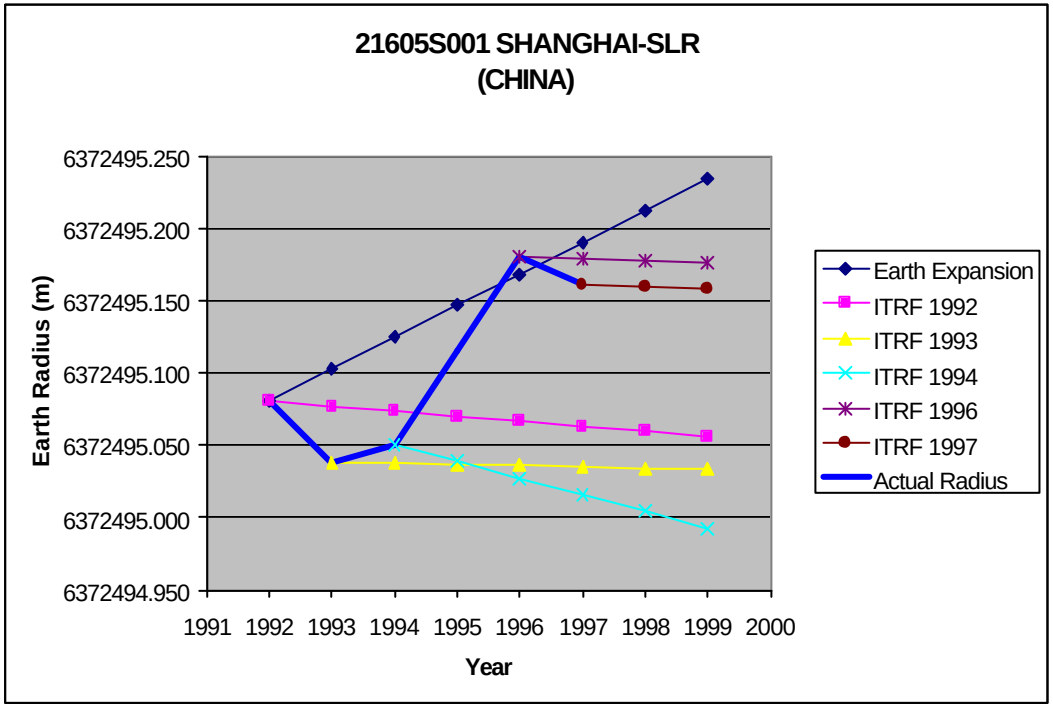

30101S001 HELWAN-SLR (TURKEY)

	Site Co-ordinates			Site Velocity			Derived Earth Radius							
Data	**X**	**Y**	**Z**	**Vx**	**Vy**	**Vz**	**1992**	**1993**	**1994**	**1995**	**1996**	**1997**	**1998**	**1999**
Source	**m**	**m**	**m**	**m/y**	**m/y**	**m/y**	6373001.634	6373001.656	6373001.678	6373001.700	6373001.722	6373001.744	6373001.766	6373001.788
ITRF 1992	4728283.588	2879670.295	3156894.54	-0.0399	0.0083	0.0076	6373001.634	6373001.612	6373001.590	6373001.568	6373001.546	6373001.524	6373001.502	6373001.480
ITRF 1993	4728283.459	2879670.358	3156894.63	-0.0179	0.0172	0.0231		6373001.612	6373001.618	6373001.624	6373001.630	6373001.636	6373001.641	6373001.647
ITRF 1994	4728283.466	2879670.372	3156894.649	-0.0198	0.0197	0.0148			6373001.633	6373001.634	6373001.636	6373001.637	6373001.639	6373001.640
ITRF 1996	4728283.35	2879670.437	3156894.718	-0.029	0.0152	0.016					6373001.610	6373001.604	6373001.597	6373001.590
ITRF 1997	4728283.387	2879670.409	3156894.717	-0.02	0.0095	0.0185						6373001.625	6373001.623	6373001.622
GSFC 1998														
							6373001.634	6373001.612	6373001.633	6373001.622	6373001.610	6373001.625		

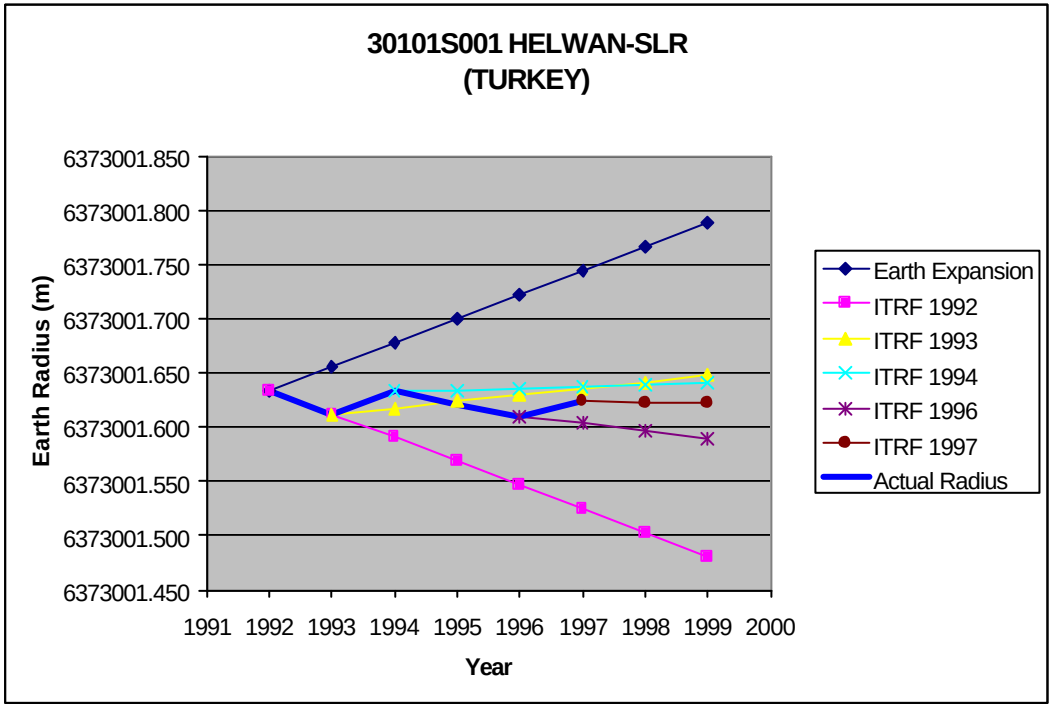

40405M001 GOLDSTONE-SLR (CALIFORNIA)

	Site Co-ordinates			Site Velocity			Derived Earth Radius							
Data	**X**	**Y**	**Z**	**Vx**	**Vy**	**Vz**	**1992**	**1993**	**1994**	**1995**	**1996**	**1997**	**1998**	**1999**
Source	**m**	**m**	**m**	**m/y**	**m/y**	**m/y**	6371957.959	6371957.981	6371958.003	6371958.025	6371958.047	6371958.069	6371958.091	6371958.113
ITRF 1992	-2353394.1	-4641529.57	3676899.199	-0.0139	0.0038	-0.0055	6371957.959	6371957.958	6371957.957	6371957.956	6371957.955	6371957.955	6371957.954	6371957.953
ITRF 1993	-2353394.22	-4641529.53	3676899.193	-0.0144	0.0042	-0.0041		6371957.974	6371957.973	6371957.973	6371957.973	6371957.973	6371957.973	6371957.973
ITRF 1994	-2353394.19	-4641529.54	3676899.174	-0.0145	0.0047	-0.0051			6371957.957	6371957.956	6371957.955	6371957.954	6371957.953	6371957.952
ITRF 1996	-2353394.25	-4641529.52	3676899.16	-0.0145	0.004	-0.004					6371957.954	6371957.954	6371957.954	6371957.954
ITRF 1997	-2353394.26	-4641529.52	3676899.146	-0.0156	0.0043	-0.006						6371957.956	6371957.955	6371957.954
GSFC 1998														
							6371957.959	6371957.974	6371957.957	6371957.956	6371957.954	6371957.956		

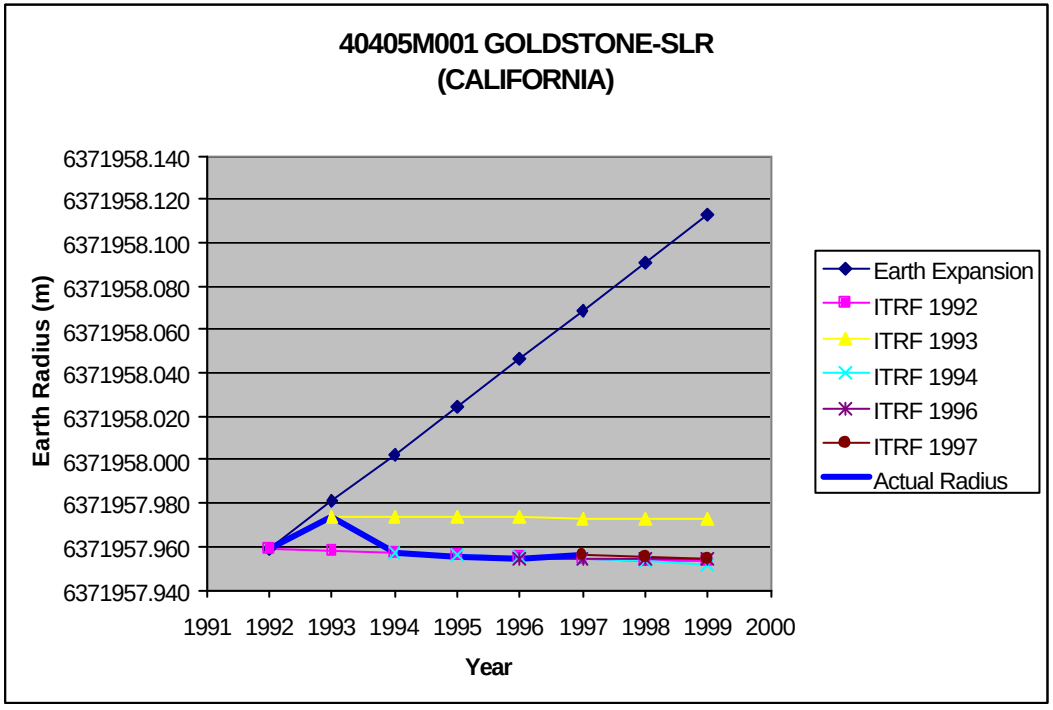

40433M001 QUINCY-SLR (CALIFORNIA)

	Site Co-ordinates			Site Velocity			Derived Earth Radius							
Data	**X**	**Y**	**Z**	**Vx**	**Vy**	**Vz**	**1992**	**1993**	**1994**	**1995**	**1996**	**1997**	**1998**	**1999**
Source	**m**	**m**	**m**	**m/y**	**m/y**	**m/y**	6370414.595	6370414.617	6370414.639	6370414.661	6370414.683	6370414.705	6370414.727	6370414.749
ITRF 1992	-2516893.13	-4198845.07	4076411.559	-0.0193	0.0045	-0.0052	6370414.595	6370414.597	6370414.598	6370414.599	6370414.601	6370414.602	6370414.603	6370414.605
ITRF 1993	-2516893.26	-4198845.03	4076411.551	-0.0197	0.0052	-0.003		6370414.616	6370414.618	6370414.621	6370414.623	6370414.626	6370414.628	6370414.630
ITRF 1994	-2516893.23	-4198845.03	4076411.536	-0.0209	0.0058	-0.0052			6370414.594	6370414.595	6370414.596	6370414.597	6370414.598	6370414.599
ITRF 1996	-2516893.31	-4198845	4076411.515	-0.0195	0.0065	-0.0052					6370414.592	6370414.592	6370414.592	6370414.592
ITRF 1997	-2516893.31	-4198845	4076411.504	-0.0204	0.0055	-0.0059						6370414.589	6370414.590	6370414.590
GSFC 1998														
							6370414.595	6370414.616	6370414.594	6370414.593	6370414.592	6370414.589		

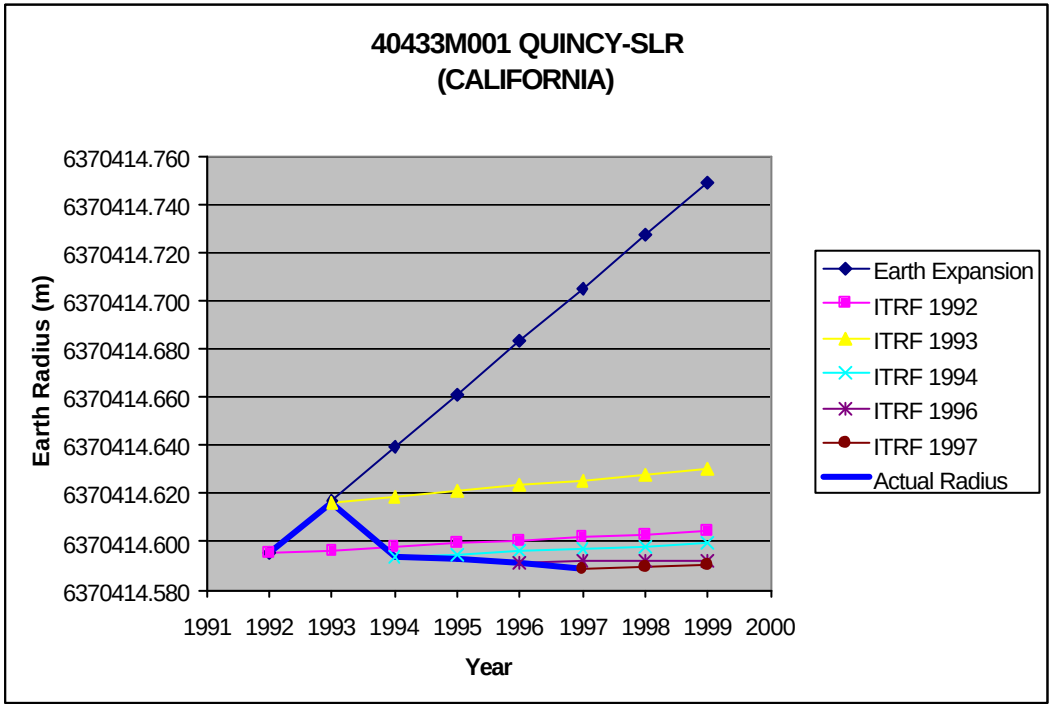

40436M002 SAN DIEGO-SLR (CALIFORNIA)

	Site Co-ordinates			Site Velocity			Derived Earth Radius							
Data	**X**	**Y**	**Z**	**Vx**	**Vy**	**Vz**	**1992**	**1993**	**1994**	**1995**	**1996**	**1997**	**1998**	**1999**
Source	**m**	**m**	**m**	**m/y**	**m/y**	**m/y**	6372954.790	6372954.812	6372954.834	6372954.856	6372954.878	6372954.900	6372954.922	6372954.944
ITRF 1992	-2428825.85	-4799750.51	3417272.71	-0.0342	0.0276	0.0212	6372954.790	6372954.794	6372954.798	6372954.801	6372954.805	6372954.809	6372954.812	6372954.816
ITRF 1993	-2428826.06	-4799750.35	3417272.802	-0.0326	0.0239	0.0156		6372954.793	6372954.796	6372954.799	6372954.801	6372954.804	6372954.807	6372954.810
ITRF 1994	-2428826	-4799750.38	3417272.804	-0.0309	0.0254	0.0186			6372954.801	6372954.804	6372954.806	6372954.809	6372954.811	6372954.814
ITRF 1996	-2428826.11	-4799750.27	3417272.849	-0.0281	0.0242	0.0139					6372954.785	6372954.785	6372954.785	6372954.785
ITRF 1997	-2428826.12	-4799750.25	3417272.875	-0.0297	0.0268	0.0174						6372954.784	6372954.784	6372954.785
GSFC 1998														
							6372954.790	6372954.793	6372954.801	6372954.793	6372954.785	6372954.784		

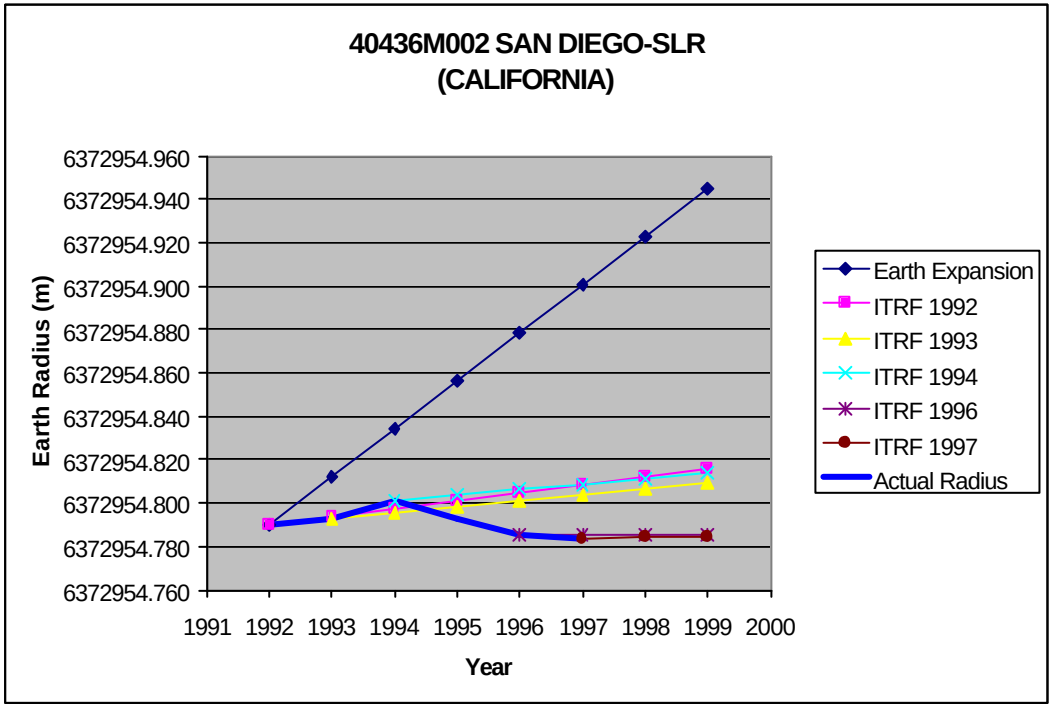

40438M001 BEAR LAKE-SLR (USA)

	Site Co-ordinates			Site Velocity			Derived Earth Radius							
Data	**X**	**Y**	**Z**	**Vx**	**Vy**	**Vz**	**1992**	**1993**	**1994**	**1995**	**1996**	**1997**	**1998**	**1999**
Source	**m**	**m**	**m**	**m/y**	**m/y**	**m/y**	6370594.318	6370594.340	6370594.362	6370594.384	6370594.406	6370594.428	6370594.450	6370594.472
ITRF 1992	-1735997.15	-4425048.36	4241430.521	-0.0154	0.0013	-0.0121	6370594.318	6370594.313	6370594.308	6370594.304	6370594.299	6370594.294	6370594.289	6370594.285
ITRF 1993	-1735997.19	-4425048.31	4241430.394	-0.0154	0.0003	-0.0085		6370594.206	6370594.204	6370594.203	6370594.201	6370594.199	6370594.198	6370594.196
ITRF 1994	-1735997.24	-4425048.37	4241430.48	-0.0187	-0.0055	-0.0083			6370594.323	6370594.327	6370594.330	6370594.333	6370594.337	6370594.340
ITRF 1996	-1735997.32	-4425048.39	4241430.44	-0.018	-0.0045	-0.0104					6370594.326	6370594.327	6370594.328	6370594.329
ITRF 1997	-1735997.3	-4425048.38	4241430.433	-0.0156	-0.0026	-0.0107						6370594.312	6370594.311	6370594.310
GSFC 1998														
							6370594.318	6370594.206	6370594.323	6370594.325	6370594.326	6370594.312		

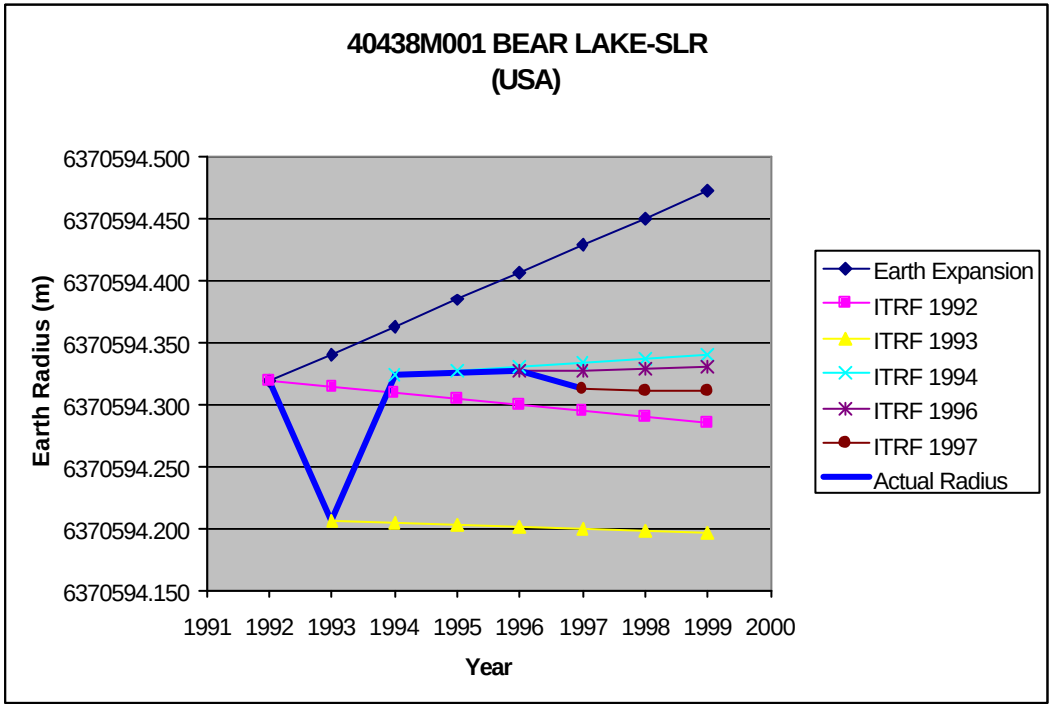

40439M001 OWENS VALLEY-SLR (CALIFORNIA)

	Site Co-ordinates			Site Velocity			Derived Earth Radius							
Data	**X**	**Y**	**Z**	**Vx**	**Vy**	**Vz**	**1992**	**1993**	**1994**	**1995**	**1996**	**1997**	**1998**	**1999**
Source	**m**	**m**	**m**	**m/y**	**m/y**	**m/y**	6371527.983	6371528.005	6371528.027	6371528.049	6371528.071	6371528.093	6371528.115	6371528.137
ITRF 1992	-2410422.37	-4477802.69	3838686.739	-0.0168	0.0044	-0.0058	6371527.983	6371527.983	6371527.983	6371527.982	6371527.982	6371527.982	6371527.982	6371527.981
ITRF 1993	-2410422.49	-4477802.65	3838686.731	-0.0161	0.0059	-0.0051		6371527.992	6371527.991	6371527.990	6371527.989	6371527.987	6371527.986	6371527.985
ITRF 1994	-2410422.46	-4477802.67	3838686.714	-0.0153	0.0088	-0.0092			6371527.984	6371527.978	6371527.972	6371527.966	6371527.960	6371527.954
ITRF 1996	-2410422.51	-4477802.69	3838686.58	-0.0135	0.0024	-0.0182					6371527.935	6371527.927	6371527.920	6371527.912
ITRF 1997	-2410422.53	-4477802.64	3838686.66	-0.0166	0.0071	-0.0086						6371527.956	6371527.952	6371527.948
GSFC 1998														
							6371527.983	6371527.992	6371527.984	6371527.960	6371527.935	6371527.956		

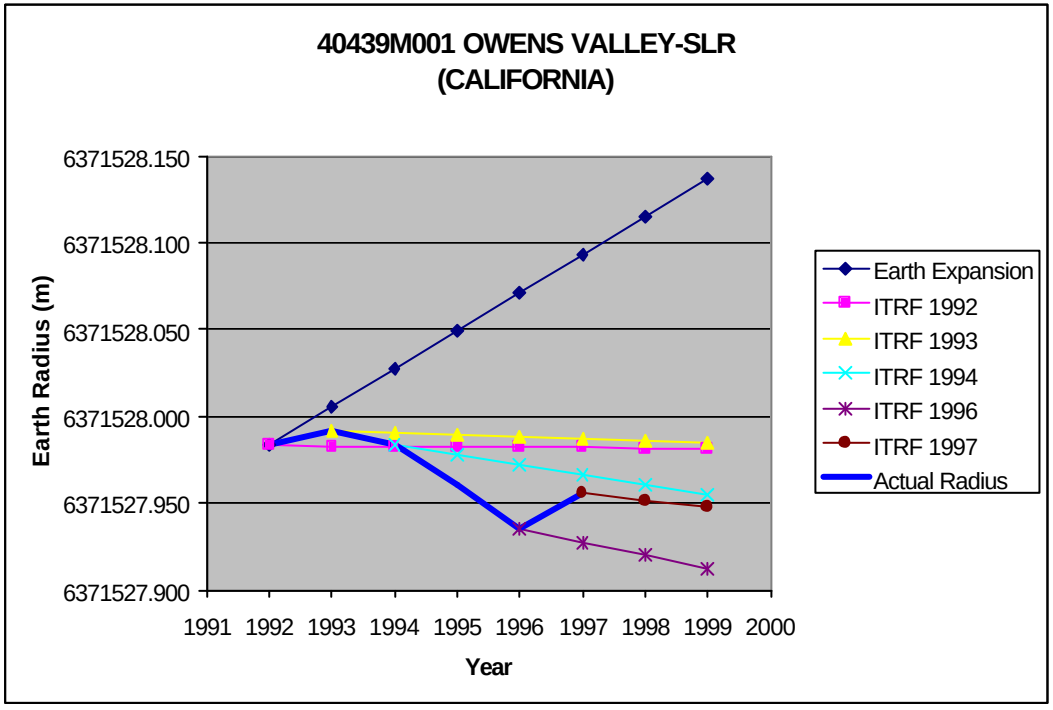

40445M001 MAUI-SLR (HAWAII)

	Site Co-ordinates			Site Velocity			Derived Earth Radius							
Data	**X**	**Y**	**Z**	**Vx**	**Vy**	**Vz**	**1992**	**1993**	**1994**	**1995**	**1996**	**1997**	**1998**	**1999**
Source	**m**	**m**	**m**	**m/y**	**m/y**	**m/y**	6378550.430	6378550.452	6378550.474	6378550.496	6378550.518	6378550.540	6378550.562	6378550.584
ITRF 1992	-5466006.47	-2404427.98	2242187.534	-0.0123	0.0604	0.0304	6378550.430	6378550.429	6378550.427	6378550.426	6378550.424	6378550.422	6378550.421	6378550.419
ITRF 1993	-5466006.58	-2404427.66	2242187.684	-0.0154	0.0589	0.0338		6378550.456	6378550.459	6378550.461	6378550.464	6378550.467	6378550.470	6378550.473
ITRF 1994	-5466006.57	-2404427.67	2242187.64	-0.0111	0.0611	0.0289			6378550.433	6378550.429	6378550.426	6378550.423	6378550.419	6378550.416
ITRF 1996	-5466006.6	-2404427.41	2242187.753	-0.0122	0.0609	0.0303					6378550.406	6378550.404	6378550.402	6378550.400
ITRF 1997	-5466006.62	-2404427.42	2242187.749	-0.015	0.06	0.0293						6378550.425	6378550.425	6378550.426
GSFC 1998														
							6378550.430	6378550.456	6378550.433	6378550.420	6378550.406	6378550.425		

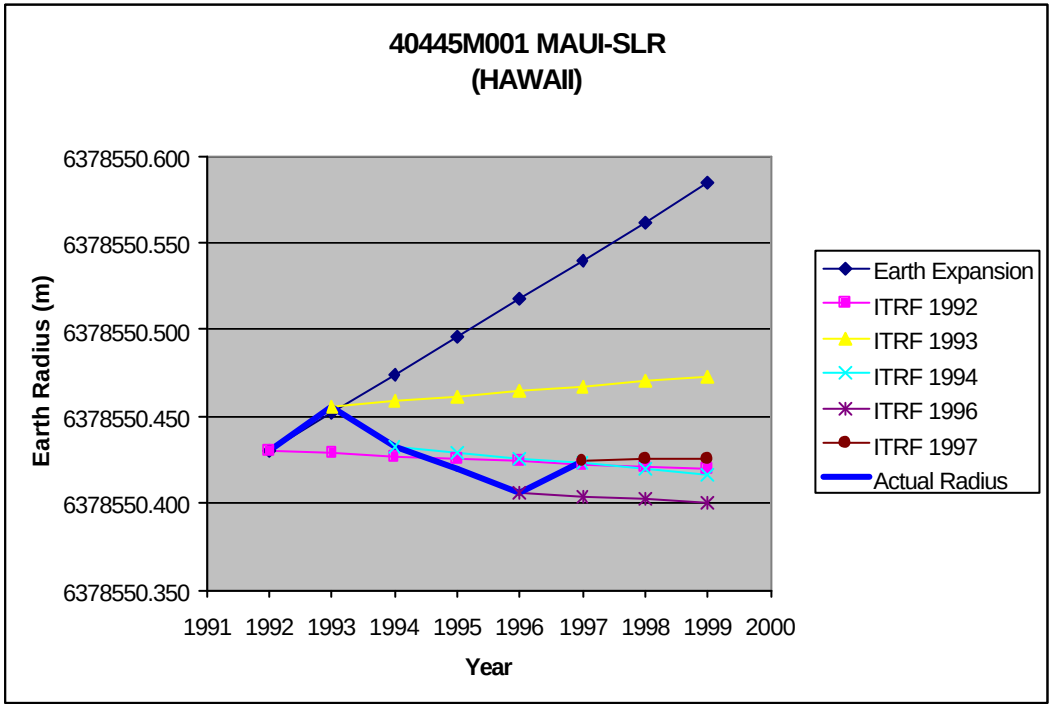

40451M101 WASHINGTON-SLR (USA)

	Site Co-ordinates			Site Velocity			Derived Earth Radius							
Data	**X**	**Y**	**Z**	**Vx**	**Vy**	**Vz**	**1992**	**1993**	**1994**	**1995**	**1996**	**1997**	**1998**	**1999**
Source	**m**	**m**	**m**	**m/y**	**m/y**	**m/y**	6369711.494	6369711.516	6369711.538	6369711.560	6369711.582	6369711.604	6369711.626	6369711.648
ITRF 1992	1131240.36	-4831179.75	3994148.475	-0.0131	-0.0036	0.0035	6369711.494	6369711.497	6369711.500	6369711.502	6369711.505	6369711.507	6369711.510	6369711.513
ITRF 1993	1131240.258	-4831179.74	3994148.509	-0.014	-0.001	0.0034		6369711.491	6369711.492	6369711.492	6369711.493	6369711.493	6369711.493	6369711.494
ITRF 1994	1131240.281	-4831179.75	3994148.488	-0.0148	-0.0014	0.0003			6369711.490	6369711.489	6369711.487	6369711.486	6369711.484	6369711.483
ITRF 1996	1131240.204	-4831179.74	3994148.494	-0.0178	0.0009	0.0001					6369711.477	6369711.473	6369711.469	6369711.466
ITRF 1997	1131240.216	-4831179.76	3994148.491	-0.0144	-0.0023	0.0009						6369711.488	6369711.488	6369711.487
GSFC 1998														
							6369711.494	6369711.491	6369711.490	6369711.484	6369711.477	6369711.488		

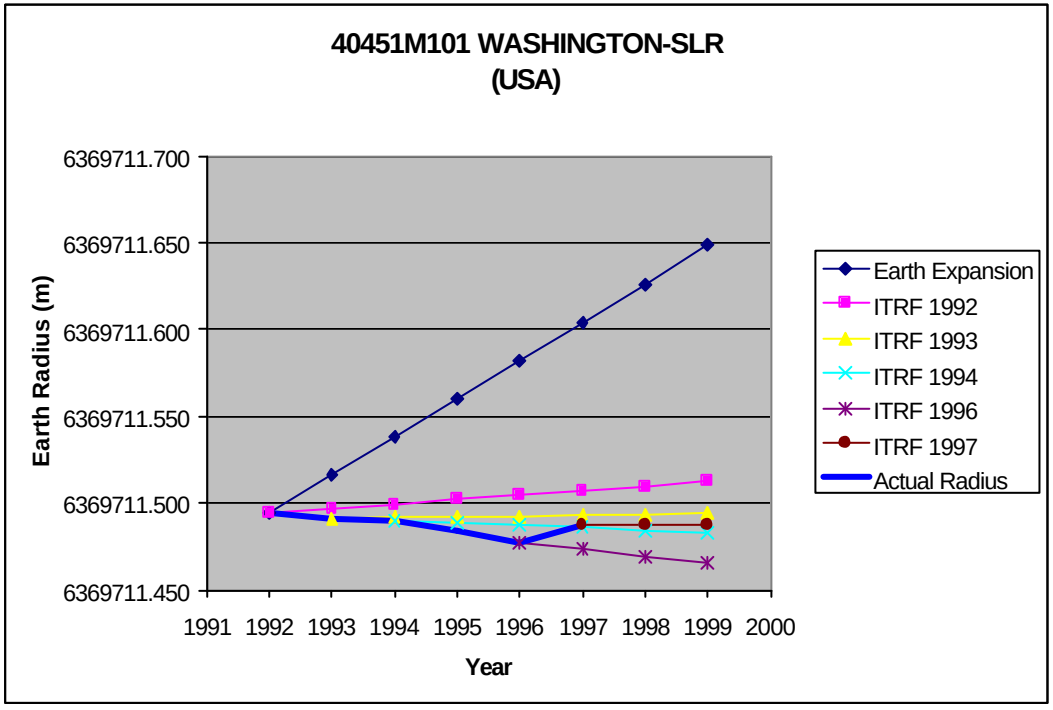

40496M001 PLATTVILLE-SLR (COLORADO USA)

	Site Co-ordinates			Site Velocity			Derived Earth Radius							
Data	**X**	**Y**	**Z**	**Vx**	**Vy**	**Vz**	**1992**	**1993**	**1994**	**1995**	**1996**	**1997**	**1998**	**1999**
Source	**m**	**m**	**m**	**m/y**	**m/y**	**m/y**	6370779.275	6370779.297	6370779.319	6370779.341	6370779.363	6370779.385	6370779.407	6370779.429
ITRF 1992	-1240678.15	-4720463.39	4094480.641	-0.0143	-0.0034	-0.0061	6370779.275	6370779.276	6370779.277	6370779.279	6370779.280	6370779.282	6370779.283	6370779.284
ITRF 1993	-1240678.26	-4720463.39	4094480.631	-0.0148	-0.0025	-0.0051		6370779.294	6370779.296	6370779.297	6370779.299	6370779.300	6370779.302	6370779.303
ITRF 1994	-1240678.24	-4720463.4	4094480.609	-0.0155	-0.0017	-0.0077			6370779.281	6370779.280	6370779.280	6370779.279	6370779.278	6370779.278
ITRF 1996	-1240678.29	-4720463.38	4094480.574	-0.0138	-0.0004	-0.0088					6370779.258	6370779.255	6370779.252	6370779.250
ITRF 1997	-1240678.3	-4720463.38	4094480.577	-0.0146	-0.0002	-0.008						6370779.261	6370779.259	6370779.257
GSFC 1998														
							6370779.275	6370779.294	6370779.281	6370779.270	6370779.258	6370779.261		

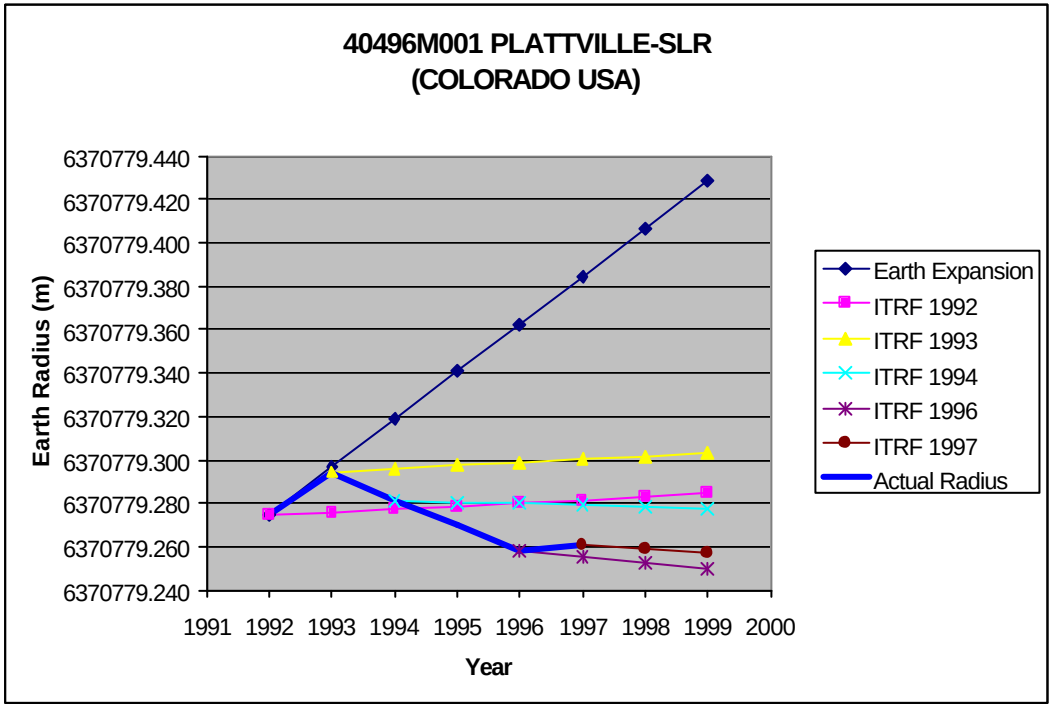

40497M001 MONUMENT PEAK-SLR (CALIFORNIA)

	Site Co-ordinates			Site Velocity			Derived Earth Radius							
Data	**X**	**Y**	**Z**	**Vx**	**Vy**	**Vz**	**1992**	**1993**	**1994**	**1995**	**1996**	**1997**	**1998**	**1999**
Source	**m**	**m**	**m**	**m/y**	**m/y**	**m/y**	6373706.787	6373706.809	6373706.831	6373706.853	6373706.875	6373706.897	6373706.919	6373706.941
ITRF 1992	-2386277.93	-4802354.37	3444881.47	-0.0332	0.0241	0.0117	6373706.787	6373706.788	6373706.789	6373706.789	6373706.790	6373706.790	6373706.791	6373706.792
ITRF 1993	-2386278.13	-4802354.24	3444881.554	-0.0335	0.0247	0.0141		6373706.807	6373706.808	6373706.810	6373706.811	6373706.813	6373706.814	6373706.816
ITRF 1994	-2386278.09	-4802354.25	3444881.535	-0.032	0.025	0.0141			6373706.786	6373706.787	6373706.787	6373706.788	6373706.789	6373706.790
ITRF 1996	-2386278.21	-4802354.14	3444881.596	-0.0308	0.0263	0.0138					6373706.785	6373706.785	6373706.784	6373706.783
ITRF 1997	-2386278.21	-4802354.15	3444881.59	-0.0318	0.0236	0.0141						6373706.792	6373706.794	6373706.796
GSFC 1998														
							6373706.787	6373706.807	6373706.786	6373706.786	6373706.785	6373706.792		

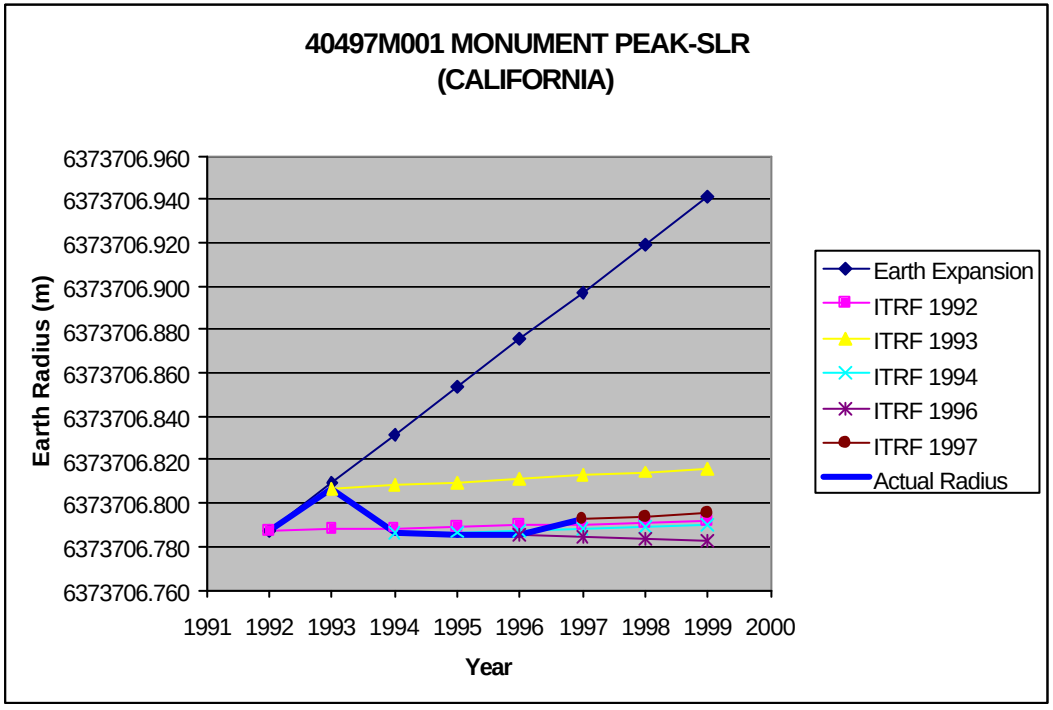

40504M001 MAZATLAN-SLR (MEXICO)

	Site Co-ordinates			Site Velocity			Derived Earth Radius							
Data	**X**	**Y**	**Z**	**Vx**	**Vy**	**Vz**	**1992**	**1993**	**1994**	**1995**	**1996**	**1997**	**1998**	**1999**
Source	**m**	**m**	**m**	**m/y**	**m/y**	**m/y**	6374834.193	6374834.215	6374834.237	6374834.259	6374834.281	6374834.303	6374834.325	6374834.347
ITRF 1992	-1660089.29	-5619100.43	2511637.896	-0.0122	-0.0096	-0.0048	6374834.193	6374834.203	6374834.213	6374834.222	6374834.232	6374834.242	6374834.252	6374834.261
ITRF 1993	-1660089.38	-5619100.42	2511637.896	-0.0112	-0.0037	-0.0034		6374834.213	6374834.217	6374834.222	6374834.227	6374834.232	6374834.237	6374834.242
ITRF 1994	-1660089.35	-5619100.44	2511637.871	-0.0114	-0.0015	-0.007			6374834.210	6374834.212	6374834.213	6374834.215	6374834.217	6374834.218
ITRF 1996	-1660089.39	-5619100.43	2511637.832	-0.0097	0.0002	-0.0083					6374834.196	6374834.196	6374834.195	6374834.194
ITRF 1997	-1660089.4	-5619100.45	2511637.84	-0.0107	-0.0018	-0.0072						6374834.215	6374834.216	6374834.218
GSFC 1998														
							6374834.193	6374834.213	6374834.210	6374834.203	6374834.196	6374834.215		

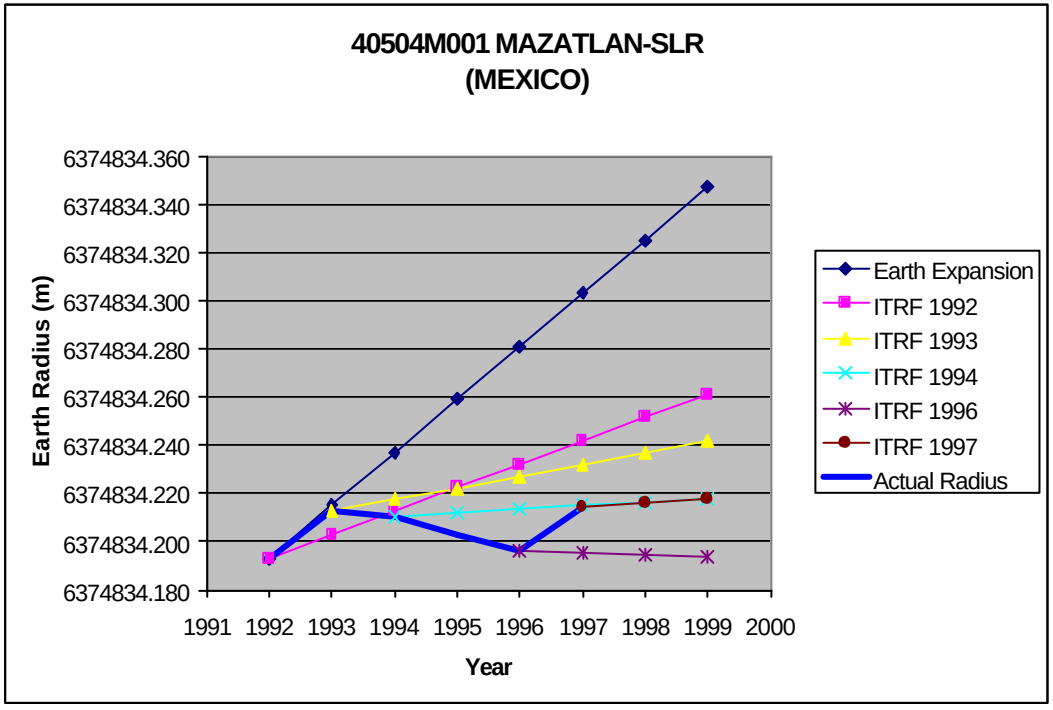

40505M001 CABO SAN LUCA-SLR (CALIFORNIA)

	Site Co-ordinates			Site Velocity			Derived Earth Radius							
Data	**X**	**Y**	**Z**	**Vx**	**Vy**	**Vz**	**1992**	**1993**	**1994**	**1995**	**1996**	**1997**	**1998**	**1999**
Source	**m**	**m**	**m**	**m/y**	**m/y**	**m/y**	6375028.839	6375028.861	6375028.883	6375028.905	6375028.927	6375028.949	6375028.971	6375028.993
ITRF 1992	-1997241.74	-5528041.27	2468355.286	-0.0456	0.0305	0.0153	6375028.839	6375028.833	6375028.826	6375028.820	6375028.814	6375028.808	6375028.801	6375028.795
ITRF 1993	-1997242.01	-5528041.16	2468355.387	-0.0447	0.0233	0.0161		6375028.861	6375028.862	6375028.862	6375028.862	6375028.862	6375028.862	6375028.862
ITRF 1994	-1997241.97	-5528041.19	2468355.372	-0.0484	0.0046	0.0227			6375028.869	6375028.889	6375028.909	6375028.929	6375028.949	6375028.968
ITRF 1996	-1997242.14	-5528041.09	2468355.411	-0.0423	0.0194	0.0123					6375028.855	6375028.856	6375028.857	6375028.858
ITRF 1997	-1997242.14	-5528041.06	2468355.405	-0.042	0.0276	0.0107						6375028.823	6375028.816	6375028.809
GSFC 1998														
							6375028.839	6375028.861	6375028.869	6375028.862	6375028.855	6375028.823		

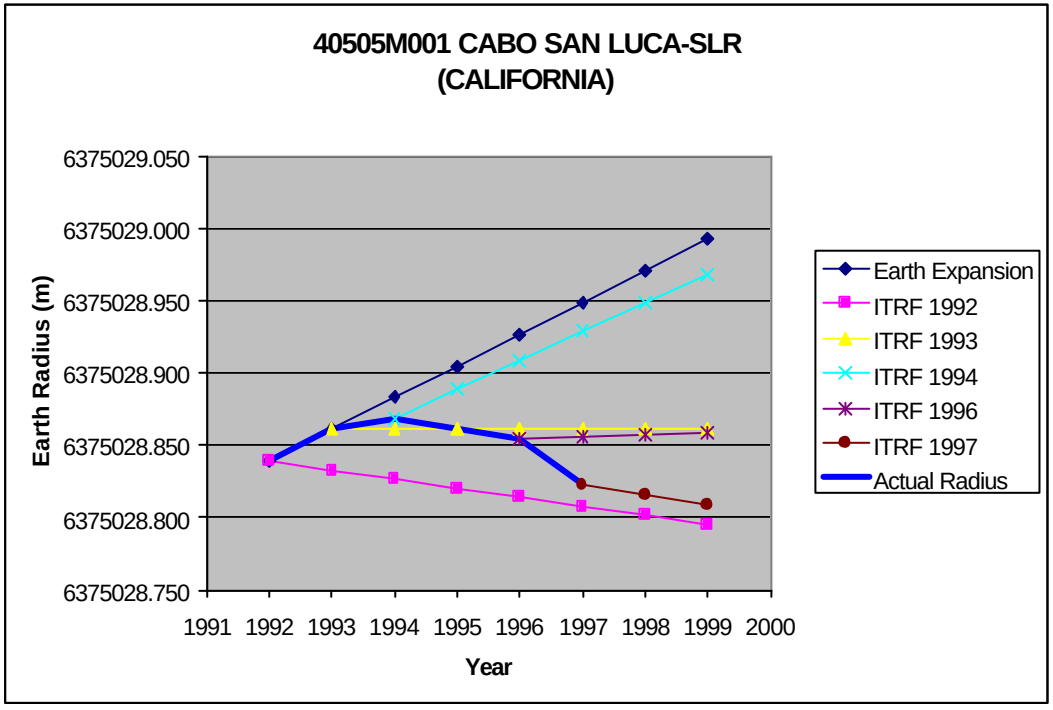

40506M001 ENSENADA-SLR (CALIFORNIA)

	Site Co-ordinates			Site Velocity			Derived Earth Radius							
Data	**X**	**Y**	**Z**	**Vx**	**Vy**	**Vz**	**1992**	**1993**	**1994**	**1995**	**1996**	**1997**	**1998**	**1999**
Source	**m**	**m**	**m**	**m/y**	**m/y**	**m/y**	6372579.837	6372579.859	6372579.881	6372579.903	6372579.925	6372579.947	6372579.969	6372579.991
ITRF 1992	-2406126.75	-4898368.4	3290336.591	-0.0342	0.0252	0.0211	6372579.837	6372579.841	6372579.846	6372579.850	6372579.855	6372579.859	6372579.863	6372579.868
ITRF 1993	-2406126.96	-4898368.26	3290336.714	-0.0334	0.0283	0.0195		6372579.868	6372579.869	6372579.870	6372579.871	6372579.872	6372579.873	6372579.874
ITRF 1994	-2406126.93	-4898368.28	3290336.698	-0.0264	0.0268	0.0185			6372579.867	6372579.866	6372579.865	6372579.864	6372579.863	6372579.862
ITRF 1996	-2406127.05	-4898368.19	3290336.767	-0.0298	0.0248	0.017					6372579.877	6372579.878	6372579.879	6372579.880
ITRF 1997	-2406127.03	-4898368.16	3290336.754	-0.0264	0.0291	0.0156						6372579.845	6372579.841	6372579.837
GSFC 1998														
							6372579.837	6372579.868	6372579.867	6372579.872	6372579.877	6372579.845		

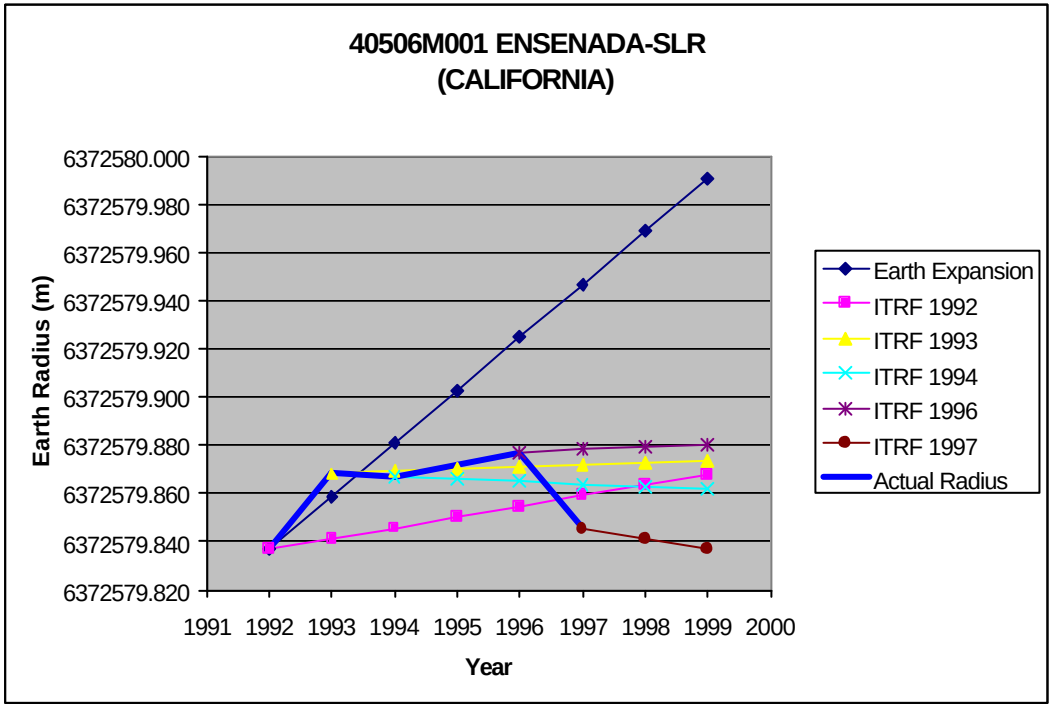

41705M001 SANTIAGO-SLR (CHILE)

	Site Co-ordinates			Site Velocity			Derived Earth Radius							
Data	**X**	**Y**	**Z**	**Vx**	**Vy**	**Vz**	**1992**	**1993**	**1994**	**1995**	**1996**	**1997**	**1998**	**1999**
Source	**m**	**m**	**m**	**m/y**	**m/y**	**m/y**	6372502.117	6372502.139	6372502.161	6372502.183	6372502.205	6372502.227	6372502.249	6372502.271
ITRF 1992	1769699.542	-5044612.88	-3468260.03	0.0009	-0.0054	0.0083	6372502.117	6372502.117	6372502.117	6372502.117	6372502.117	6372502.117	6372502.118	6372502.118
ITRF 1993	1769699.541	-5044612.95	-3468259.95	0.0174	-0.0044	0.0202		6372502.131	6372502.129	6372502.126	6372502.123	6372502.121	6372502.118	6372502.115
ITRF 1994	1769699.567	-5044612.94	-3468259.97	0.0224	-0.0066	0.0148			6372502.137	6372502.140	6372502.144	6372502.147	6372502.151	6372502.154
ITRF 1996	1769699.649	-5044612.98	-3468259.92	0.0219	-0.0074	0.007					6372502.158	6372502.166	6372502.174	6372502.182
ITRF 1997	1769699.657	-5044612.98	-3468259.93	0.0216	-0.0072	0.0069						6372502.166	6372502.174	6372502.182
GSFC 1998														
							6372502.117	6372502.131	6372502.137	6372502.148	6372502.158	6372502.166		

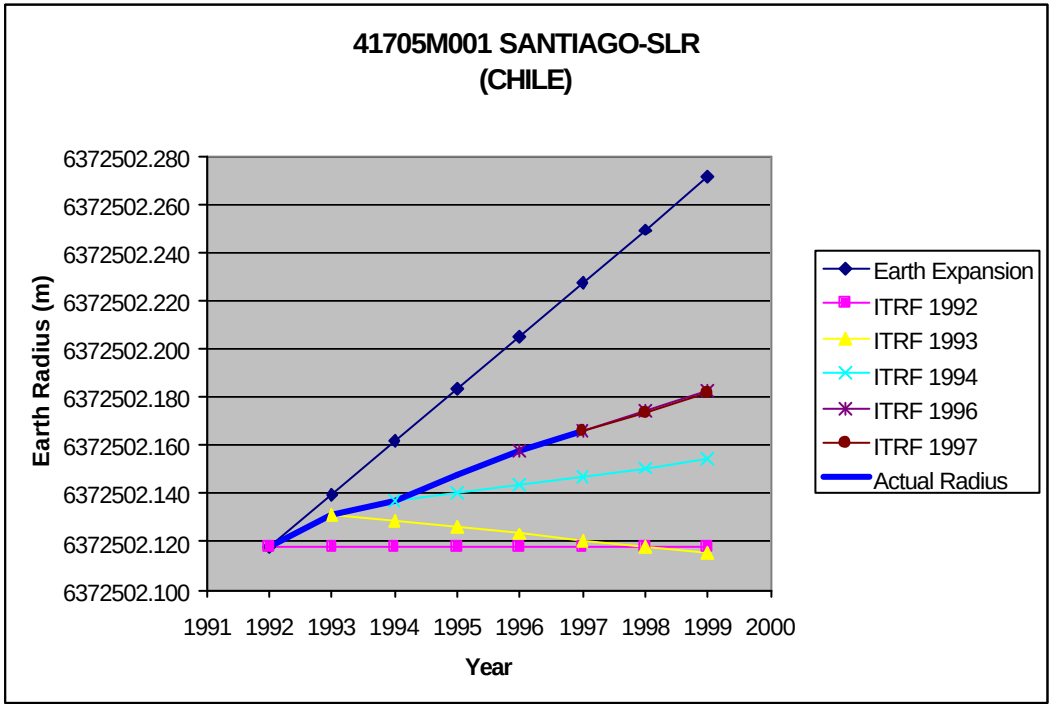

41706M001 CERRO TOLOLO-SLR (CHILE)

	Site Co-ordinates			Site Velocity			Derived Earth Radius							
Data	**X**	**Y**	**Z**	**Vx**	**Vy**	**Vz**	**1992**	**1993**	**1994**	**1995**	**1996**	**1997**	**1998**	**1999**
Source	**m**	**m**	**m**	**m/y**	**m/y**	**m/y**	6374924.159	6374924.181	6374924.203	6374924.225	6374924.247	6374924.269	6374924.291	6374924.313
ITRF 1992	1815517.221	-5213464.83	-3187999.33	0.0209	0.0075	0.0195	6374924.159	6374924.149	6374924.139	6374924.129	6374924.119	6374924.109	6374924.099	6374924.089
ITRF 1993	1815517.316	-5213464.83	-3187999.19	0.0186	0.0014	0.0152		6374924.119	6374924.116	6374924.113	6374924.109	6374924.106	6374924.102	6374924.099
ITRF 1994	1815517.344	-5213464.8	-3187999.22	0.0227	0.0054	0.019			6374924.116	6374924.108	6374924.101	6374924.093	6374924.086	6374924.078
ITRF 1996	1815517.455	-5213464.89	-3187999.19	0.0233	-0.0076	0.0119					6374924.206	6374924.213	6374924.220	6374924.227
ITRF 1997	1815517.459	-5213464.89	-3187999.19	0.0251	-0.0106	0.0103						6374924.206	6374924.217	6374924.228
GSFC 1998														
							6374924.159	6374924.119	6374924.116	6374924.161	6374924.206	6374924.206		

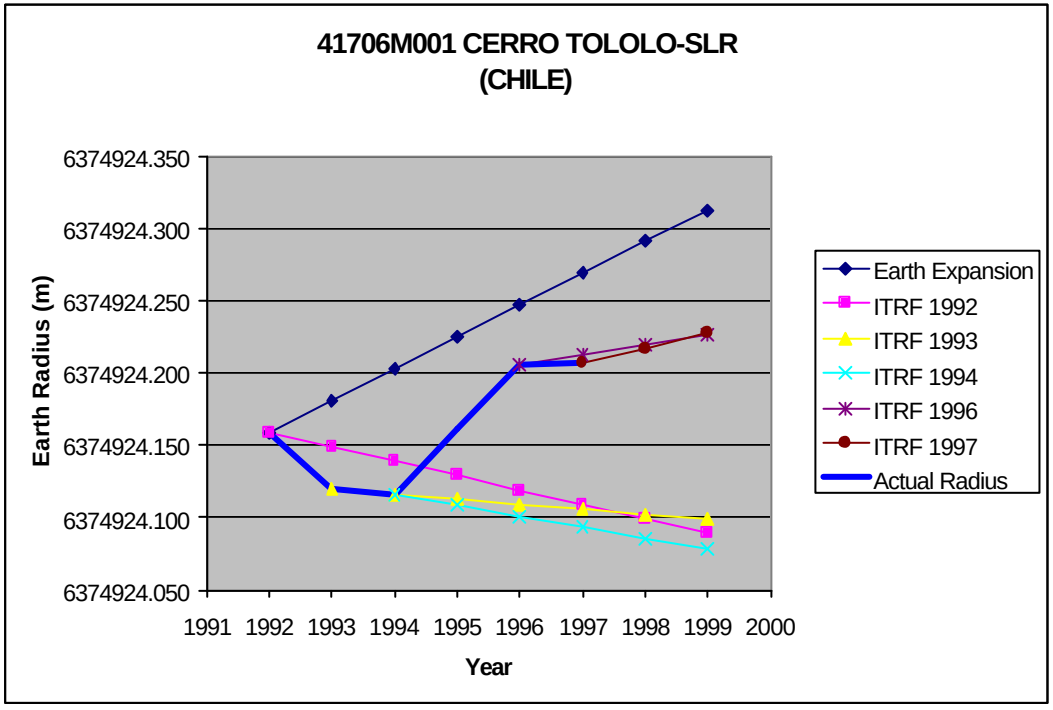

42202M003 AREQUIPA-SLR (PERU)

	Site Co-ordinates			Site Velocity			Derived Earth Radius							
Data	**X**	**Y**	**Z**	**Vx**	**Vy**	**Vz**	**1992**	**1993**	**1994**	**1995**	**1996**	**1997**	**1998**	**1999**
Source	**m**	**m**	**m**	**m/y**	**m/y**	**m/y**	6378921.060	6378921.082	6378921.104	6378921.126	6378921.148	6378921.170	6378921.192	6378921.214
ITRF 1992	1942808.005	-5804069.71	-1796915.61	0.0121	0.0113	0.0147	6378921.060	6378921.049	6378921.038	6378921.028	6378921.017	6378921.006	6378920.995	6378920.985
ITRF 1993	1942808.049	-5804069.71	-1796915.5	0.0128	0.0043	0.0134		6378921.035	6378921.031	6378921.027	6378921.024	6378921.020	6378921.016	6378921.012
ITRF 1994	1942808.077	-5804069.7	-1796915.53	0.0134	-0.0012	0.0076			6378921.044	6378921.047	6378921.050	6378921.053	6378921.056	6378921.059
ITRF 1996	1942808.115	-5804069.7	-1796915.47	0.0114	0.0013	0.0123					6378921.042	6378921.041	6378921.040	6378921.038
ITRF 1997	1942808.121	-5804069.71	-1796915.49	0.0122	-0.002	0.01						6378921.055	6378921.058	6378921.061
GSFC 1998														
							6378921.060	6378921.035	6378921.044	6378921.043	6378921.042	6378921.055		

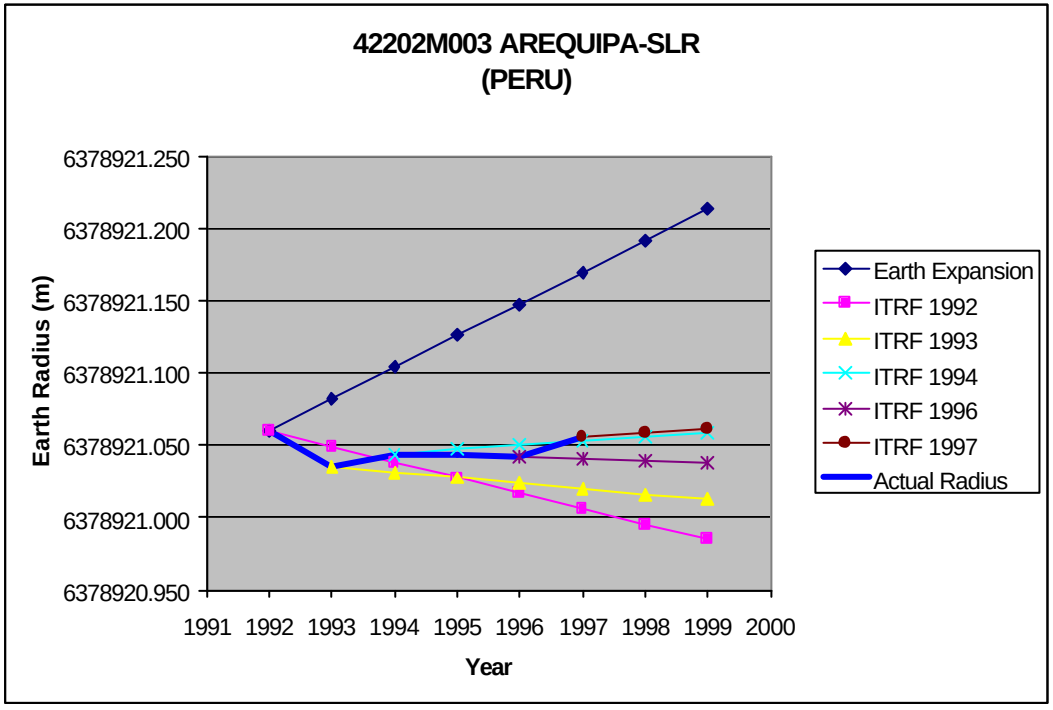

50107M001 YARRAGADEE-SLR (WESTERN AUSTRALIA)

	Site Co-ordinates			Site Velocity			Derived Earth Radius							
Data	**X**	**Y**	**Z**	**Vx**	**Vy**	**Vz**	**1992**	**1993**	**1994**	**1995**	**1996**	**1997**	**1998**	**1999**
Source	**m**	**m**	**m**	**m/y**	**m/y**	**m/y**	6373369.642	6373369.664	6373369.686	6373369.708	6373369.730	6373369.752	6373369.774	6373369.796
ITRF 1992	-2389006.52	5043329.274	-3078525.34	-0.0451	0.0078	0.0528	6373369.642	6373369.640	6373369.637	6373369.635	6373369.632	6373369.630	6373369.628	6373369.625
ITRF 1993	-2389006.73	5043329.303	-3078525.12	-0.0498	0.011	0.0466		6373369.635	6373369.640	6373369.645	6373369.650	6373369.655	6373369.659	6373369.664
ITRF 1994	-2389006.74	5043329.316	-3078525.09	-0.0485	0.0124	0.049			6373369.637	6373369.641	6373369.645	6373369.650	6373369.654	6373369.658
ITRF 1996	-2389006.94	5043329.339	-3078524.91	-0.0498	0.0056	0.0491					6373369.638	6373369.638	6373369.637	6373369.637
ITRF 1997	-2389006.93	5043329.354	-3078524.91	-0.0477	0.0087	0.0459						6373369.651	6373369.653	6373369.656
GSFC 1998														
							6373369.642	6373369.635	6373369.637	6373369.638	6373369.638	6373369.651		

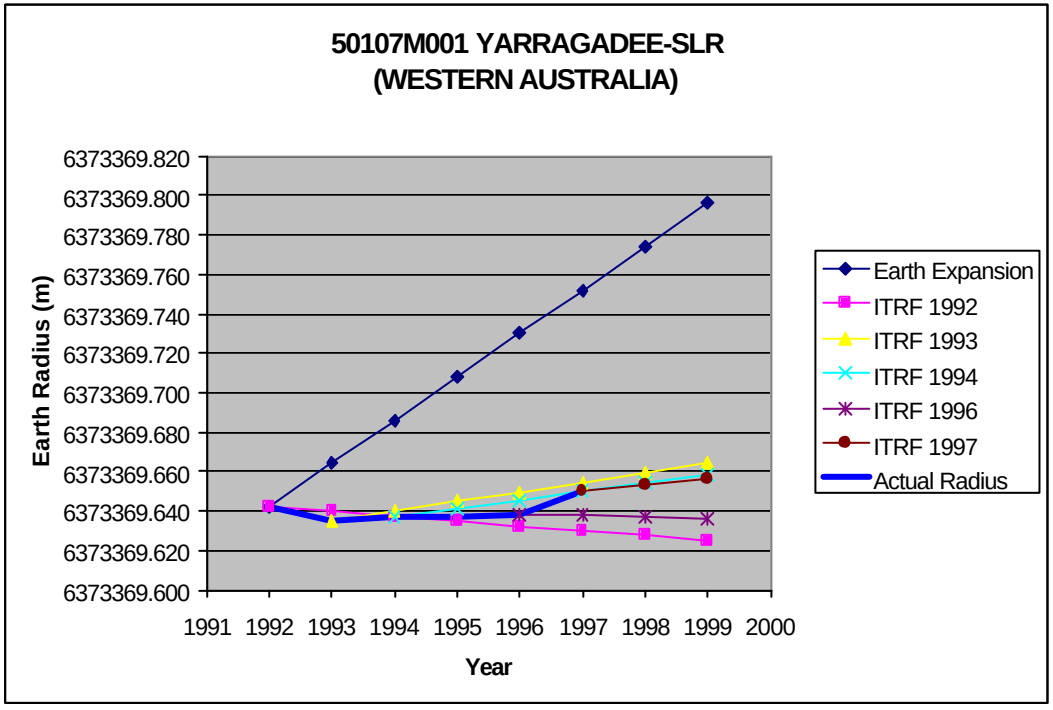

92202M002 HUAHINE-SLR (TAHITI)

	Site Co-ordinates			Site Velocity			Derived Earth Radius							
Data	**X**	**Y**	**Z**	**Vx**	**Vy**	**Vz**	**1992**	**1993**	**1994**	**1995**	**1996**	**1997**	**1998**	**1999**
Source	**m**	**m**	**m**	**m/y**	**m/y**	**m/y**	6376421.489	6376421.511	6376421.533	6376421.555	6376421.577	6376421.599	6376421.621	6376421.643
ITRF 1992	-5345865.28	-2958246.68	-1824623.8	-0.0378	0.0523	0.0295	6376421.489	6376421.488	6376421.487	6376421.486	6376421.485	6376421.484	6376421.483	6376421.482
ITRF 1993	-5345865.48	-2958246.42	-1824623.64	-0.0401	0.0509	0.0304		6376421.492	6376421.494	6376421.495	6376421.496	6376421.498	6376421.499	6376421.500
ITRF 1994	-5345865.48	-2958246.39	-1824623.66	-0.0384	0.053	0.0276			6376421.486	6376421.486	6376421.486	6376421.485	6376421.485	6376421.485
ITRF 1996	-5345865.69	-2958246.21	-1824623.53	-0.0432	0.0499	0.0316					6376421.539	6376421.543	6376421.547	6376421.551
ITRF 1997	-5345865.68	-2958246.2	-1824623.56	-0.0434	0.0504	0.0266						6376421.534	6376421.539	6376421.545
GSFC 1998														
							6376421.489	6376421.492	6376421.486	6376421.513	6376421.539	6376421.534		

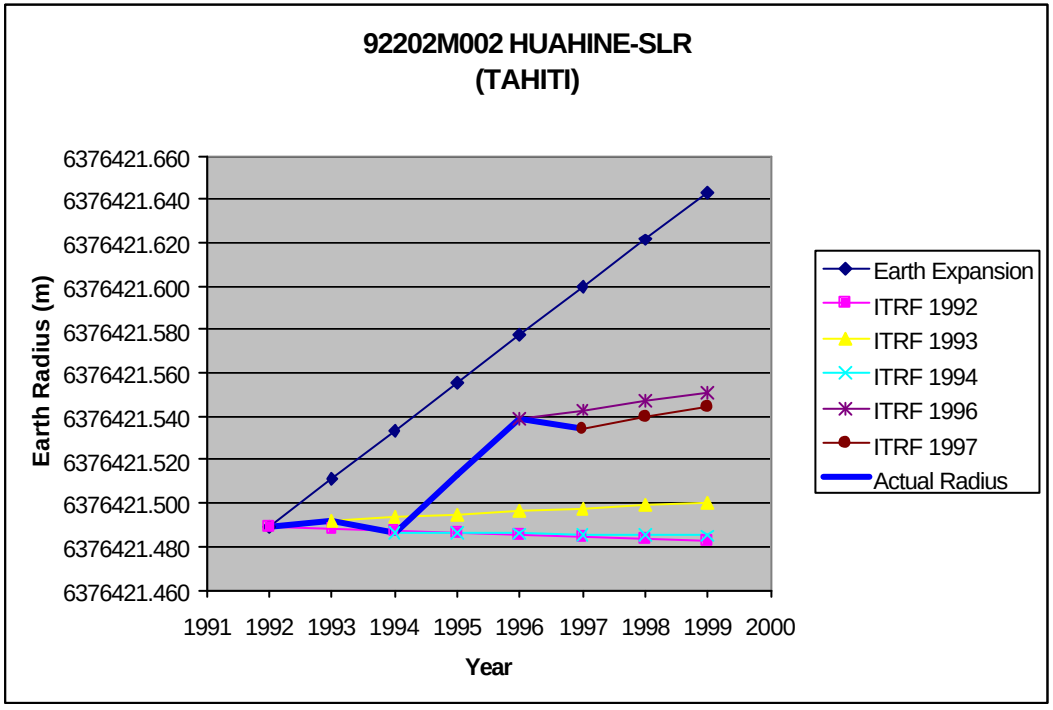

A2.3 GPS Space Geodetic Charts

10402M004 ONSALA-GPS (SWEDEN)

	Site Co-ordinates			Site Velocity			Derived Earth Radius							
Data	**X**	**Y**	**Z**	**Vx**	**Vy**	**Vz**	**1992**	**1993**	**1994**	**1995**	**1996**	**1997**	**1998**	**1999**
Source	**m**	**m**	**m**	**m/y**	**m/y**	**m/y**	6363043.942	6363043.964	6363043.986	6363044.008	6363044.030	6363044.052	6363044.074	6363044.096
ITRF 1992	3370658.81	711876.901	5349786.787	-0.0136	0.0136	0.0118	6363043.942	6363043.946	6363043.950	6363043.954	6363043.958	6363043.963	6363043.967	6363043.971
ITRF 1993	3370658.716	711876.978	5349786.83	-0.0152	0.0133	0.0091		6363043.937	6363043.938	6363043.939	6363043.940	6363043.941	6363043.942	6363043.943
ITRF 1994	3370658.732	711876.975	5349786.833	-0.015	0.0151	0.0061			6363043.947	6363043.946	6363043.945	6363043.944	6363043.943	6363043.942
ITRF 1996	3370658.674	711877.032	5349786.866	-0.0143	0.0147	0.0072					6363043.951	6363043.951	6363043.951	6363043.951
ITRF 1997	3370658.676	711877.029	5349786.868	-0.0136	0.0147	0.0084						6363043.953	6363043.954	6363043.956
GSFC 1998														
							6363043.942	6363043.937	6363043.947	6363043.949	6363043.951	6363043.953		

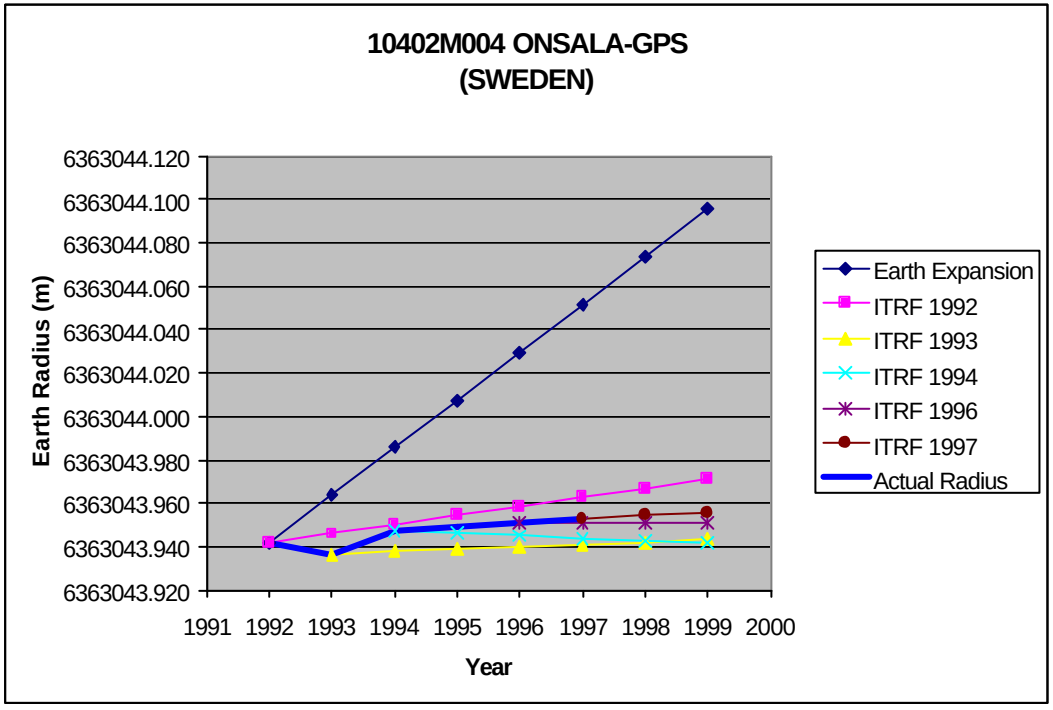

11001M002 GRAZ-GPS (AUSTRIA)

	Site Co-ordinates			Site Velocity			Derived Earth Radius							
Data	**X**	**Y**	**Z**	**Vx**	**Vy**	**Vz**	**1992**	**1993**	**1994**	**1995**	**1996**	**1997**	**1998**	**1999**
Source	**m**	**m**	**m**	**m/y**	**m/y**	**m/y**	6367256.766	6367256.788	6367256.810	6367256.832	6367256.854	6367256.876	6367256.898	6367256.920
ITRF 1992	4194424.122	1162702.404	4647245.219	-0.019	0.0176	0.0094	6367256.766	6367256.763	6367256.761	6367256.758	6367256.756	6367256.754	6367256.751	6367256.749
ITRF 1993	4194424.034	1162702.49	4647245.279	-0.0177	0.02	0.0097		6367256.767	6367256.766	6367256.765	6367256.764	6367256.764	6367256.763	6367256.762
ITRF 1994	4194424.04	1162702.484	4647245.282	-0.0166	0.0184	0.0098			6367256.772	6367256.772	6367256.771	6367256.771	6367256.771	6367256.770
ITRF 1996	4194423.971	1162702.56	4647245.319	-0.0154	0.0187	0.0104					6367256.768	6367256.769	6367256.769	6367256.770
ITRF 1997	4194423.972	1162702.556	4647245.317	-0.0163	0.0182	0.0081						6367256.766	6367256.765	6367256.763
GSFC 1998														
							6367256.766	6367256.767	6367256.772	6367256.770	6367256.768	6367256.766		

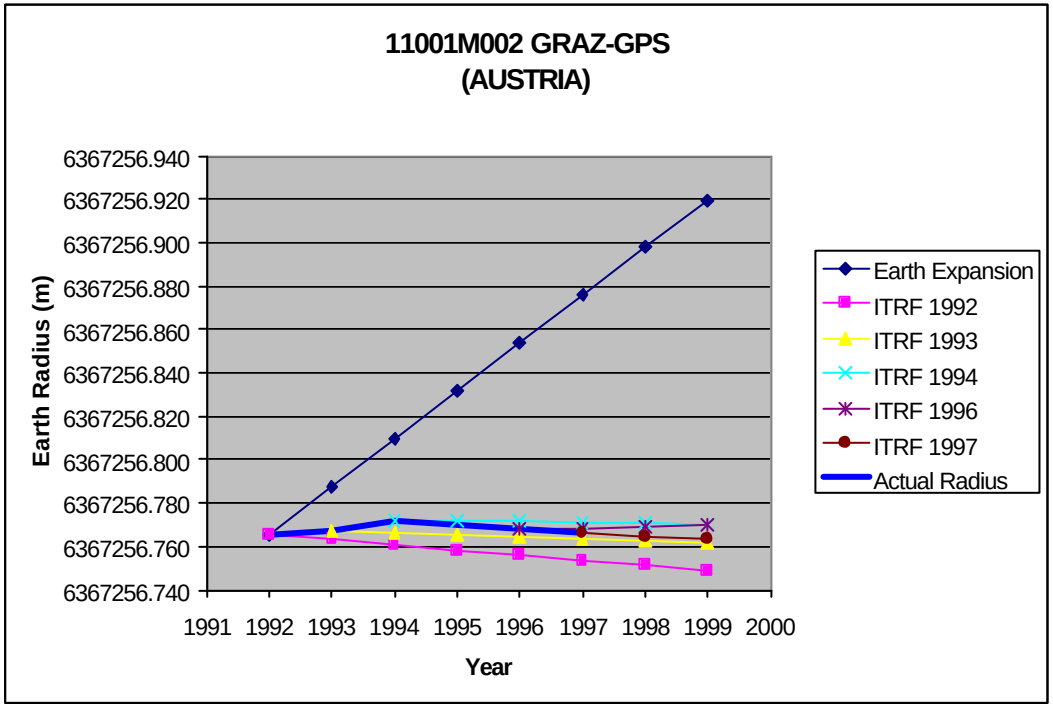

13212M007 HERSTMONCEUX-GPS (ENGLAND)

	Site Co-ordinates			Site Velocity			Derived Earth Radius							
Data	**X**	**Y**	**Z**	**Vx**	**Vy**	**Vz**	**1992**	**1993**	**1994**	**1995**	**1996**	**1997**	**1998**	**1999**
Source	**m**	**m**	**m**	**m/y**	**m/y**	**m/y**	6365389.606	6365389.628	6365389.650	6365389.672	6365389.694	6365389.716	6365389.738	6365389.760
ITRF 1992	4033470.343	23672.61	4924301.111	-0.014	0.0175	0.0102	6365389.606	6365389.605	6365389.604	6365389.603	6365389.602	6365389.601	6365389.600	6365389.599
ITRF 1993	4033470.271	23672.698	4924301.178	-0.0137	0.0187	0.0112		6365389.612	6365389.612	6365389.612	6365389.612	6365389.612	6365389.612	6365389.613
ITRF 1994	4033470.281	23672.691	4924301.176	-0.0107	0.0175	0.011			6365389.617	6365389.619	6365389.621	6365389.622	6365389.624	6365389.626
ITRF 1996	4033470.236	23672.761	4924301.225	-0.0102	0.0182	0.0128					6365389.627	6365389.630	6365389.634	6365389.637
ITRF 1997	4033470.233	23672.756	4924301.219	-0.0113	0.017	0.0099						6365389.620	6365389.621	6365389.621
GSFC 1998														
							6365389.606	6365389.612	6365389.617	6365389.622	6365389.627	6365389.620		

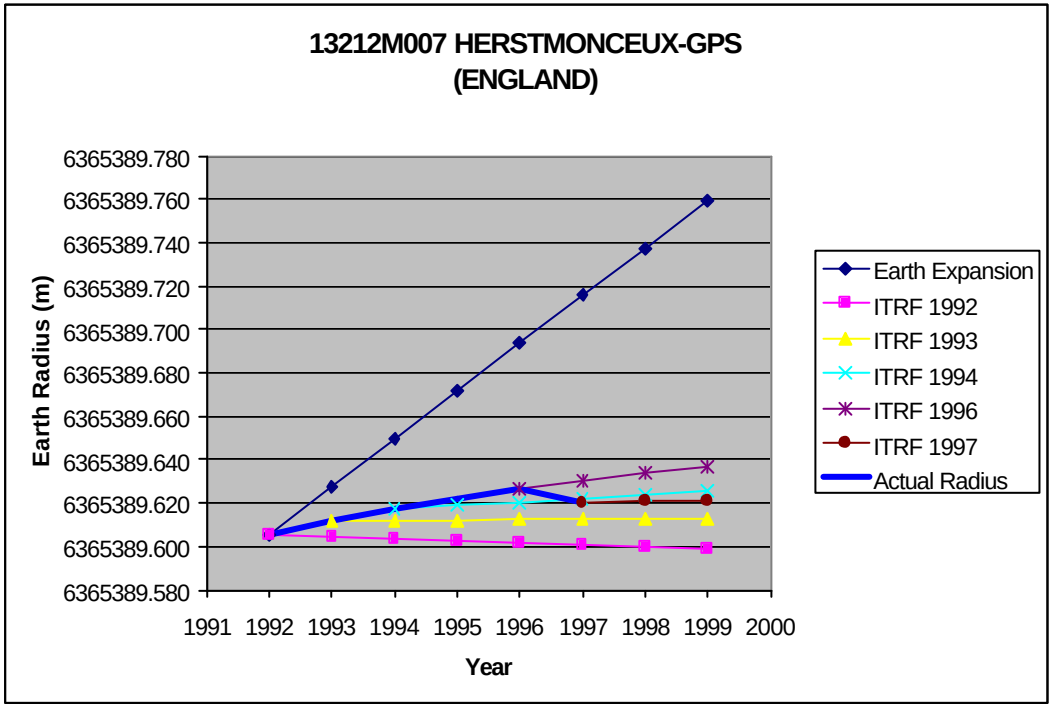

23601M001 TAIPEI-GPS (TAIWAN)

	Site Co-ordinates			Site Velocity			Derived Earth Radius							
Data	**X**	**Y**	**Z**	**Vx**	**Vy**	**Vz**	**1992**	**1993**	**1994**	**1995**	**1996**	**1997**	**1998**	**1999**
Source	**m**	**m**	**m**	**m/y**	**m/y**	**m/y**	6374381.769	6374381.791	6374381.813	6374381.835	6374381.857	6374381.879	6374381.901	6374381.923
ITRF 1992	-3024781.78	4928936.927	2681234.588	-0.0229	-0.0072	-0.0126	6374381.769	6374381.769	6374381.769	6374381.769	6374381.769	6374381.769	6374381.769	6374381.769
ITRF 1993	-3024781.88	4928936.917	2681234.49	-0.0219	-0.007	-0.0121		6374381.770	6374381.770	6374381.770	6374381.770	6374381.770	6374381.769	6374381.769
ITRF 1994	3024781.87	4928936.897	2681234.506	-0.0215	-0.0186	0.0004			6374381.756	6374381.732	6374381.707	6374381.683	6374381.658	6374381.634
ITRF 1996	-3024781.98	4928936.823	2681234.453	-0.031	-0.0192	-0.0125					6374381.728	6374381.723	6374381.717	6374381.712
ITRF 1997	-3024781.98	4928936.829	2681234.445	-0.0324	-0.0188	-0.0163						6374381.732	6374381.726	6374381.720
GSFC 1998														
							6374381.769	6374381.770	6374381.756	6374381.742	6374381.728	6374381.732		

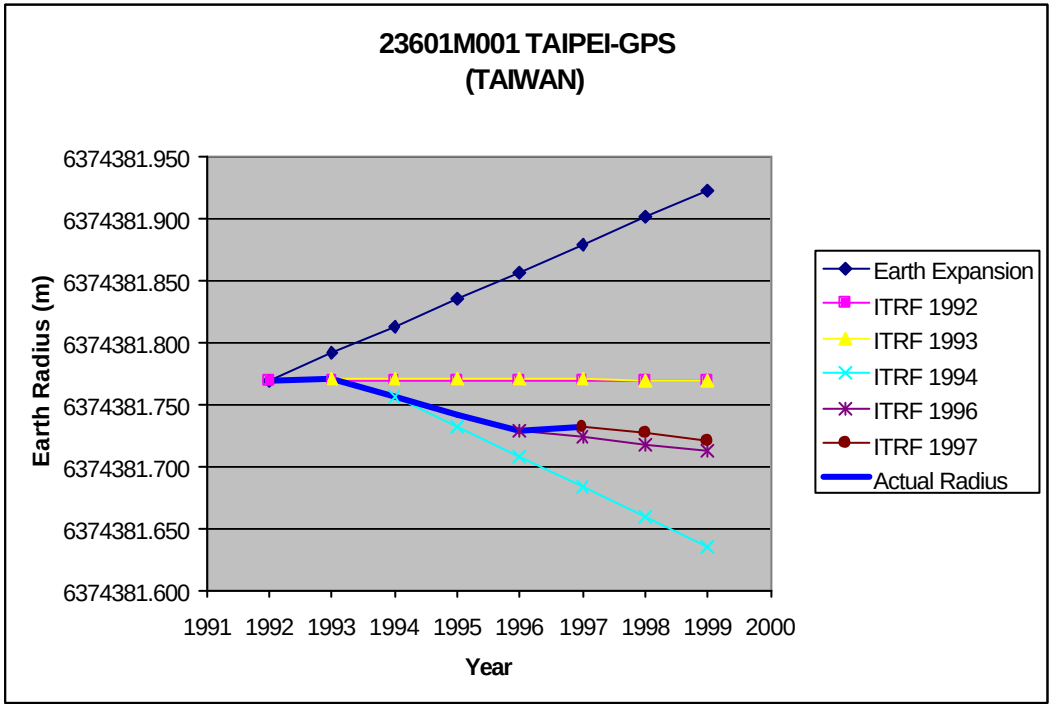

30302M002 HARTEBEESTHOEK-GPS (SOUTH AFRICA)

	Site Co-ordinates			Site Velocity			Derived Earth Radius							
Data	**X**	**Y**	**Z**	**Vx**	**Vy**	**Vz**	**1992**	**1993**	**1994**	**1995**	**1996**	**1997**	**1998**	**1999**
Source	**m**	**m**	**m**	**m/y**	**m/y**	**m/y**	6375643.703	6375643.725	6375643.747	6375643.769	6375643.791	6375643.813	6375643.835	6375643.857
ITRF 1992	5084625.453	2670366.458	-2768494.11	-0.0027	0.0187	0.0151	6375643.703	6375643.702	6375643.701	6375643.700	6375643.699	6375643.699	6375643.698	6375643.697
ITRF 1993	5084625.442	2670366.508	-2768494.03	-0.009	0.0187	0.016		6375643.684	6375643.678	6375643.671	6375643.665	6375643.659	6375643.652	6375643.646
ITRF 1994	5084625.454	2670366.541	-2768494.01	-0.0015	0.0164	0.018			6375643.696	6375643.694	6375643.692	6375643.690	6375643.687	6375643.685
ITRF 1996	5084625.441	2670366.601	-2768493.94	0.0007	0.0192	0.0164					6375643.682	6375643.683	6375643.685	6375643.686
ITRF 1997	5084625.46	2670366.609	-2768493.95	0.0001	0.0209	0.014						6375643.704	6375643.706	6375643.709
GSFC 1998														
							6375643.703	6375643.684	6375643.696	6375643.689	6375643.682	6375643.704		

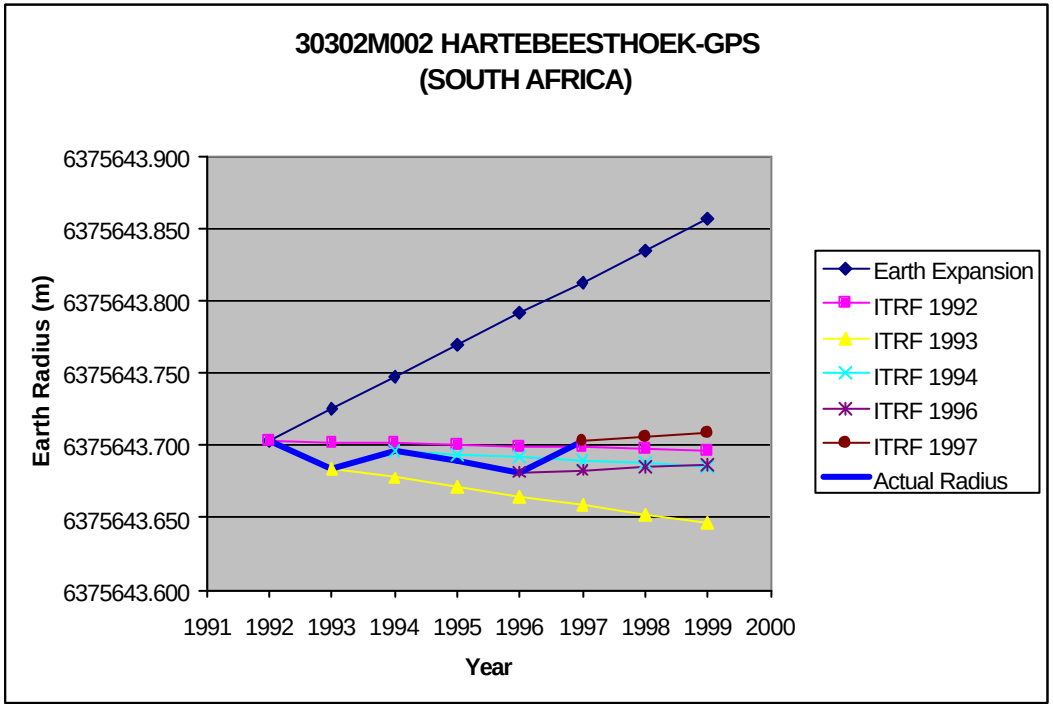

31303M001 MASPALOMAS-GPS (CANARY ISLANDS)

	Site Co-ordinates			Site Velocity			Derived Earth Radius							
Data	**X**	**Y**	**Z**	**Vx**	**Vy**	**Vz**	**1992**	**1993**	**1994**	**1995**	**1996**	**1997**	**1998**	**1999**
Source	**m**	**m**	**m**	**m/y**	**m/y**	**m/y**	6373725.820	6373725.842	6373725.864	6373725.886	6373725.908	6373725.930	6373725.952	6373725.974
ITRF 1992	5439189.208	-1522054.96	2953464.119	-0.0033	0.0195	0.0162	6373725.820	6373725.821	6373725.821	6373725.821	6373725.821	6373725.821	6373725.821	6373725.821
ITRF 1993	5439189.145	-1522054.85	2953464.214	-0.0033	0.0187	0.0154		6373725.786	6373725.786	6373725.786	6373725.785	6373725.785	6373725.785	6373725.785
ITRF 1994	5439189.154	-1522054.85	2953464.209	0.0001	0.0154	0.0152			6373725.791	6373725.794	6373725.797	6373725.801	6373725.804	6373725.808
ITRF 1996	5439189.146	-1522054.78	2953464.275	0.0002	0.0176	0.0153					6373725.798	6373725.801	6373725.804	6373725.807
ITRF 1997	5439189.145	-1522054.78	2953464.269	-0.0021	0.0171	0.0128						6373725.795	6373725.795	6373725.795
GSFC 1998														
							6373725.820	6373725.786	6373725.791	6373725.795	6373725.798	6373725.795		

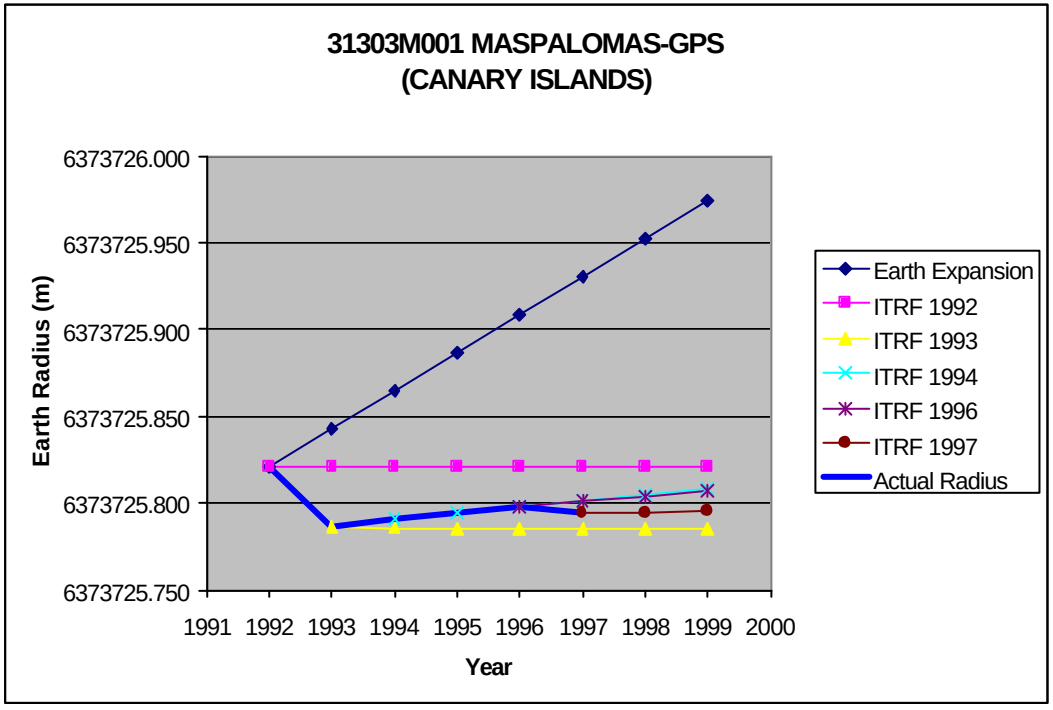

40101M001 ST. JOHNS-GPS (ENGLAND)

	Site Co-ordinates			Site Velocity			Derived Earth Radius							
Data	**X**	**Y**	**Z**	**Vx**	**Vy**	**Vz**	**1992**	**1993**	**1994**	**1995**	**1996**	**1997**	**1998**	**1999**
Source	**m**	**m**	**m**	**m/y**	**m/y**	**m/y**	6366674.708	6366674.730	6366674.752	6366674.774	6366674.796	6366674.818	6366674.840	6366674.862
ITRF 1992	2612631.412	-3426807	4686757.698	-0.0182	-0.0017	0.0089	6366674.708	6366674.708	6366674.708	6366674.708	6366674.708	6366674.708	6366674.708	6366674.708
ITRF 1993	2612631.296	-3426807.01	4686757.776	-0.0173	-0.0017	0.0087		6366674.720	6366674.721	6366674.721	6366674.721	6366674.721	6366674.722	6366674.722
ITRF 1994	2612631.316	-3426807.01	4686757.76	-0.0195	-0.0034	0.0127			6366674.721	6366674.724	6366674.727	6366674.730	6366674.733	6366674.737
ITRF 1996	2612631.24	-3426807.02	4686757.797	-0.0171	-0.0025	0.0061					6366674.719	6366674.718	6366674.717	6366674.716
ITRF 1997	2612631.239	-3426807.03	4686757.792	-0.0158	-0.0038	0.006						6366674.719	6366674.719	6366674.719
GSFC 1998														
							6366674.708	6366674.720	6366674.721	6366674.720	6366674.719	6366674.719		

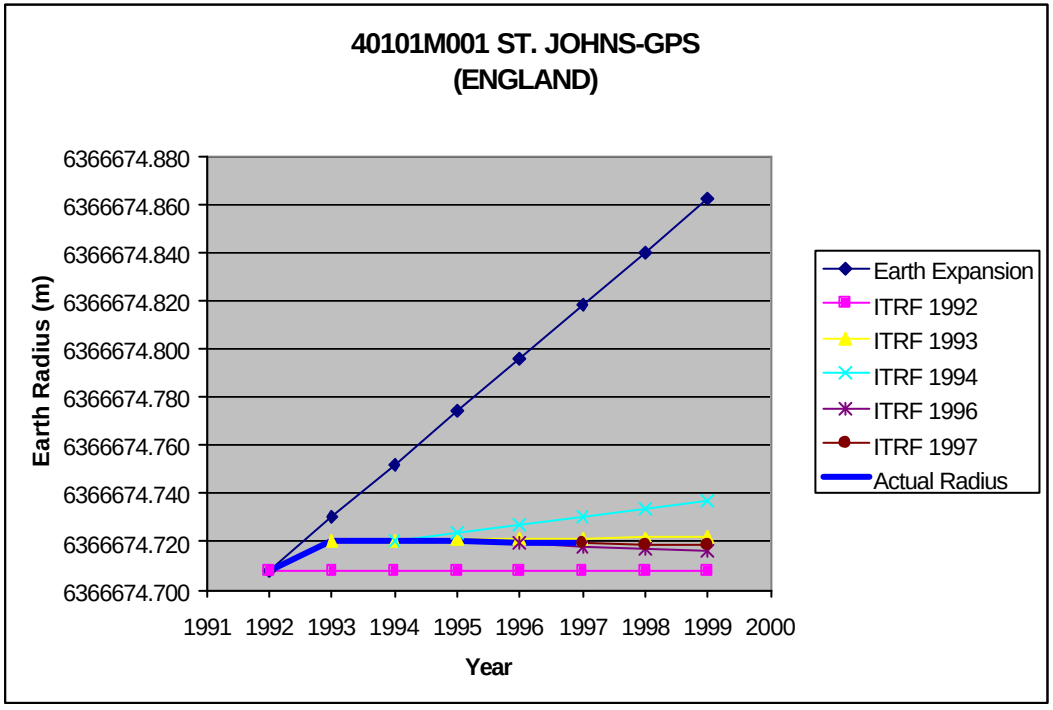

40104M002 ALGONQUIN-GPS (ILLINOIS USA)

	Site Co-ordinates			Site Velocity			Derived Earth Radius							
Data	**X**	**Y**	**Z**	**Vx**	**Vy**	**Vz**	**1992**	**1993**	**1994**	**1995**	**1996**	**1997**	**1998**	**1999**
Source	**m**	**m**	**m**	**m/y**	**m/y**	**m/y**	6367333.703	6367333.725	6367333.747	6367333.769	6367333.791	6367333.813	6367333.835	6367333.857
ITRF 1992	918129.667	-4346071.21	4561977.801	-0.0148	-0.0063	0.0045	6367333.703	6367333.709	6367333.714	6367333.719	6367333.725	6367333.730	6367333.735	6367333.741
ITRF 1993	918129.553	-4346071.22	4561977.833	-0.0157	-0.0049	0.0028		6367333.721	6367333.724	6367333.727	6367333.730	6367333.733	6367333.736	6367333.739
ITRF 1994	918129.576	-4346071.23	4561977.811	-0.0158	-0.0051	0.0035			6367333.712	6367333.715	6367333.719	6367333.723	6367333.726	6367333.730
ITRF 1996	918129.509	-4346071.23	4561977.818	-0.0157	-0.0023	0.0003					6367333.708	6367333.708	6367333.707	6367333.707
ITRF 1997	918129.507	-4346071.24	4561977.811	-0.016	-0.0042	0.0005						6367333.708	6367333.709	6367333.710
GSFC 1998														
							6367333.703	6367333.721	6367333.712	6367333.710	6367333.708	6367333.708		

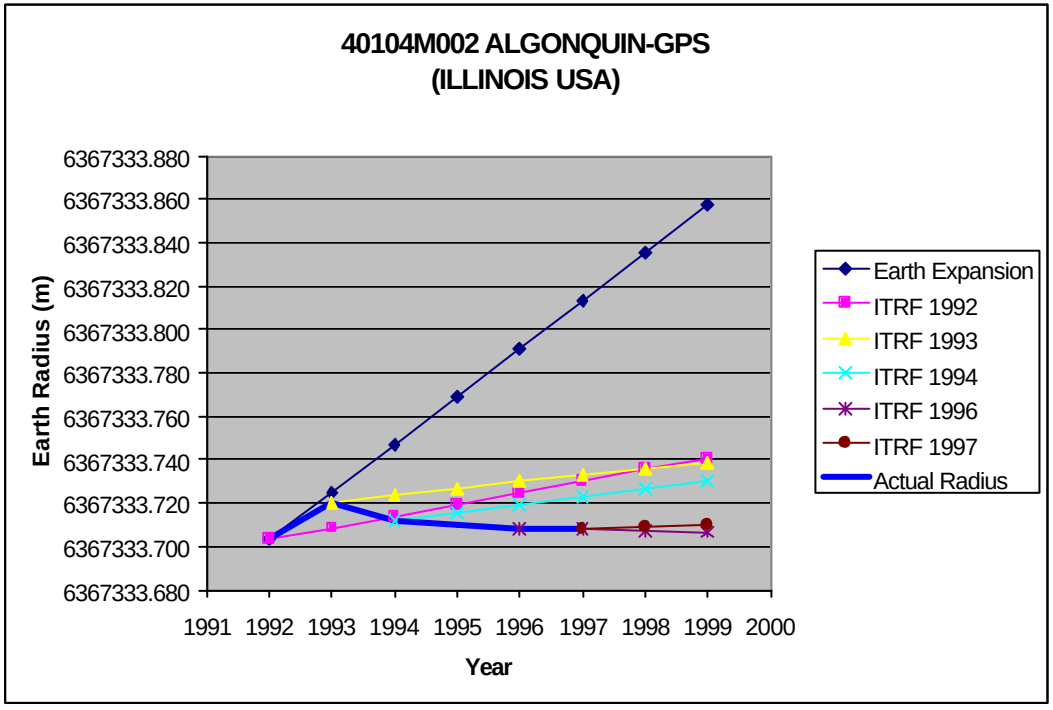

40408M001 FAIRBANKS-GPS (ALASKA)

	Site Co-ordinates			Site Velocity			Derived Earth Radius							
Data	**X**	**Y**	**Z**	**Vx**	**Vy**	**Vz**	**1992**	**1993**	**1994**	**1995**	**1996**	**1997**	**1998**	**1999**
Source	**m**	**m**	**m**	**m/y**	**m/y**	**m/y**	6360923.478	6360923.500	6360923.522	6360923.544	6360923.566	6360923.588	6360923.610	6360923.632
ITRF 1992	-2281621.22	-1453595.76	5756961.999	-0.0206	-0.0039	-0.0098	6360923.478	6360923.477	6360923.477	6360923.476	6360923.476	6360923.475	6360923.474	6360923.474
ITRF 1993	-2281621.37	-1453595.76	5756961.965	-0.0205	-0.0051	-0.0078		6360923.498	6360923.499	6360923.500	6360923.502	6360923.503	6360923.505	6360923.506
ITRF 1994	-2281621.35	-1453595.78	5756961.969	-0.0208	-0.0031	-0.0117			6360923.500	6360923.498	6360923.496	6360923.493	6360923.491	6360923.488
ITRF 1996	-2281621.43	-1453595.79	5756961.923	-0.0215	-0.0042	-0.0097					6360923.490	6360923.490	6360923.489	6360923.489
ITRF 1997	-2281621.43	-1453595.79	5756961.911	-0.0226	-0.0046	-0.0101						6360923.481	6360923.481	6360923.481
GSFC 1998														
							6360923.478	6360923.498	6360923.500	6360923.495	6360923.490	6360923.481		

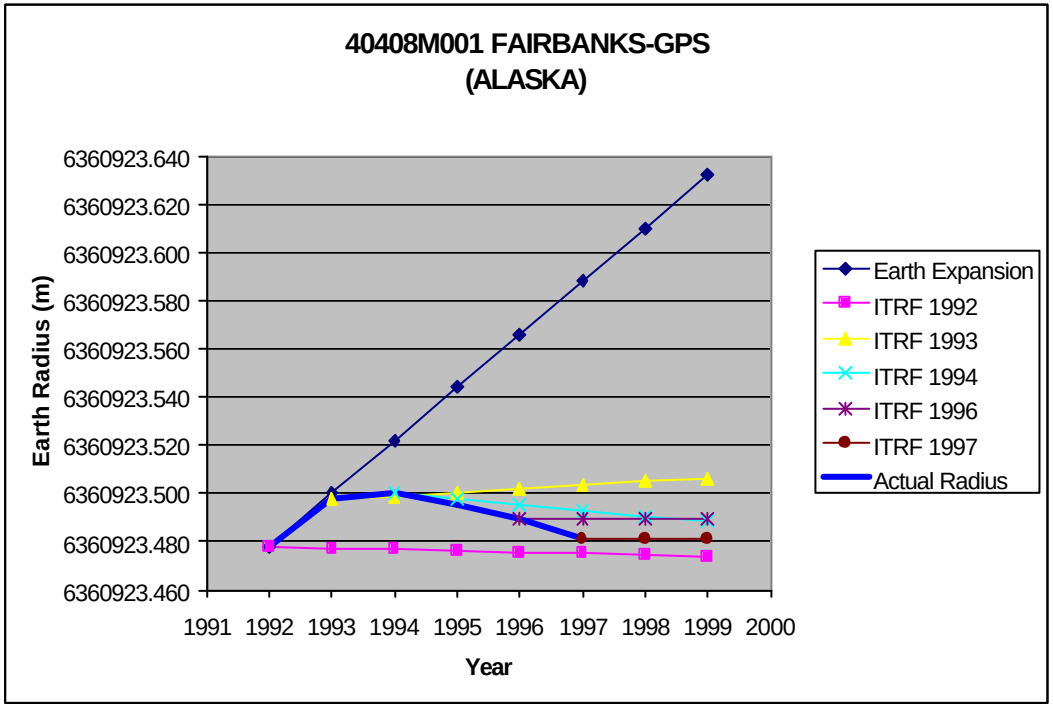

40424M004 KAUAI-GPS (HAWAII)

	Site Co-ordinates			Site Velocity			Derived Earth Radius							
Data	**X**	**Y**	**Z**	**Vx**	**Vy**	**Vz**	**1992**	**1993**	**1994**	**1995**	**1996**	**1997**	**1998**	**1999**
Source	**m**	**m**	**m**	**m/y**	**m/y**	**m/y**	6376292.421	6376292.443	6376292.465	6376292.487	6376292.509	6376292.531	6376292.553	6376292.575
ITRF 1992	-5543838.03	-2054587.82	2387809.429	-0.0083	0.0625	0.0305	6376292.421	6376292.419	6376292.418	6376292.416	6376292.415	6376292.413	6376292.412	6376292.410
ITRF 1993	-5543838.1	-2054587.49	2387809.584	-0.0098	0.0606	0.0358		6376292.436	6376292.439	6376292.441	6376292.444	6376292.446	6376292.448	6376292.451
ITRF 1994	-5543838.08	-2054587.52	2387809.589	-0.0079	0.06	0.0305			6376292.430	6376292.429	6376292.428	6376292.427	6376292.425	6376292.424
ITRF 1996	-5543838.11	-2054587.25	2387809.703	-0.0081	0.0618	0.0302					6376292.411	6376292.409	6376292.408	6376292.406
ITRF 1997	-5543838.12	-2054587.26	2387809.689	-0.0109	0.0611	0.0292						6376292.415	6376292.415	6376292.416
GSFC 1998														
							6376292.421	6376292.436	6376292.430	6376292.421	6376292.411	6376292.415		

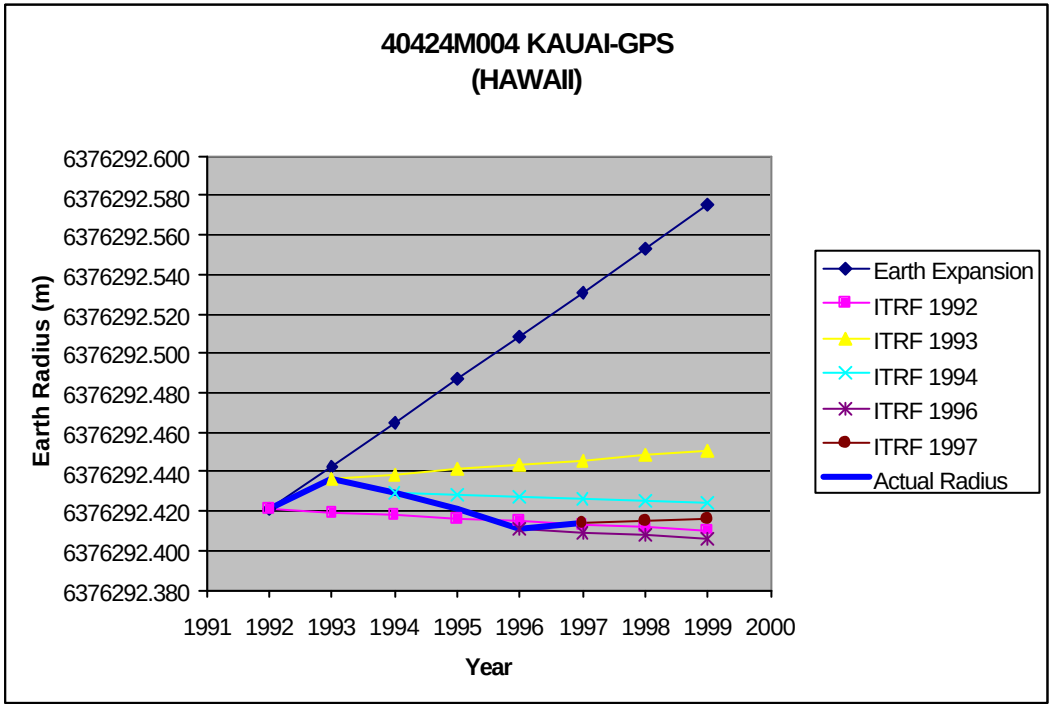

40499M002 RICHMOND-GPS (FLORIDA USA)

	Site Co-ordinates			Site Velocity			Derived Earth Radius							
Data	**X**	**Y**	**Z**	**Vx**	**Vy**	**Vz**	**1992**	**1993**	**1994**	**1995**	**1996**	**1997**	**1998**	**1999**
Source	**m**	**m**	**m**	**m/y**	**m/y**	**m/y**	6374145.088	6374145.110	6374145.132	6374145.154	6374145.176	6374145.198	6374145.220	6374145.242
ITRF 1992	961319.033	-5674090.97	2740489.563	-0.0079	-0.0036	0.0029	6374145.088	6374145.092	6374145.095	6374145.098	6374145.101	6374145.105	6374145.108	6374145.111
ITRF 1993	961318.948	-5674090.99	2740489.609	-0.0099	-0.0026	0.0021		6374145.119	6374145.121	6374145.123	6374145.125	6374145.126	6374145.128	6374145.130
ITRF 1994	961318.976	-5674090.99	2740489.601	-0.0104	-0.0014	0.004			6374145.120	6374145.122	6374145.123	6374145.124	6374145.126	6374145.127
ITRF 1996	961318.936	-5674091.02	2740489.627	-0.0079	-0.0059	0.0041					6374145.148	6374145.154	6374145.160	6374145.166
ITRF 1997	961318.931	-5674091.01	2740489.604	-0.0093	-0.0042	0.0014						6374145.130	6374145.133	6374145.136
GSFC 1998														
							6374145.088	6374145.119	6374145.120	6374145.134	6374145.148	6374145.130		

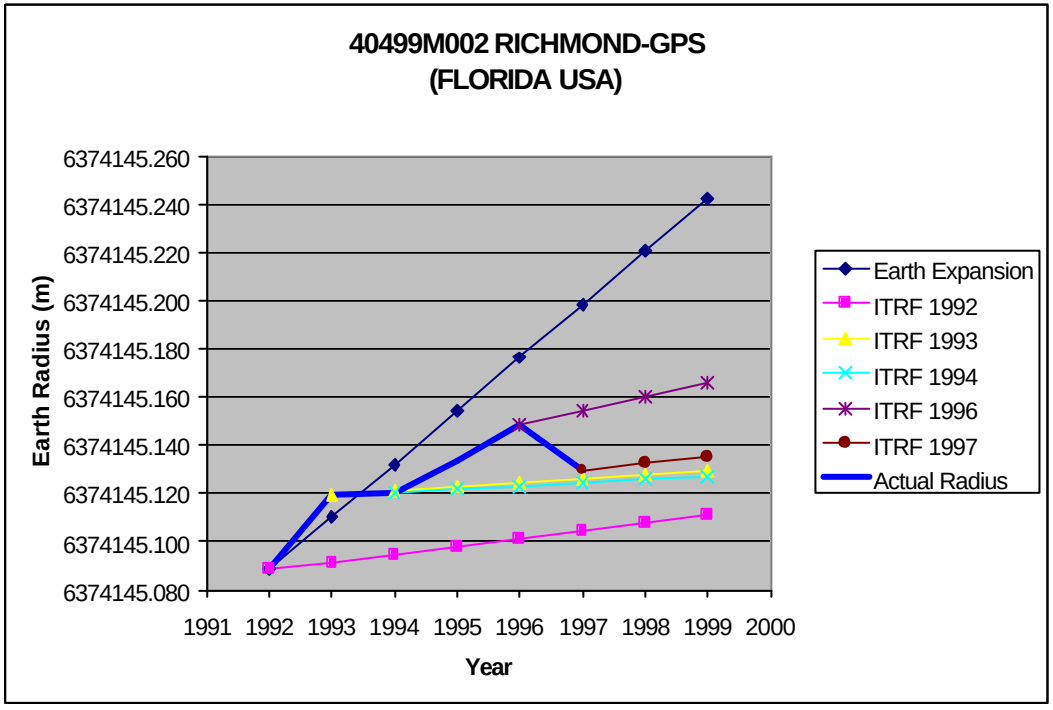

50103M108 TIDBINBILLA-GPS (EASTERN AUSTRALIA)

	Site Co-ordinates			Site Velocity			Derived Earth Radius							
Data	**X**	**Y**	**Z**	**Vx**	**Vy**	**Vz**	**1992**	**1993**	**1994**	**1995**	**1996**	**1997**	**1998**	**1999**
Source	**m**	**m**	**m**	**m/y**	**m/y**	**m/y**	6371666.670	6371666.692	6371666.714	6371666.736	6371666.758	6371666.780	6371666.802	6371666.824
ITRF 1992	-4460995.83	2682557.118	-3674444.13	-0.0393	0.0043	0.0418	6371666.670	6371666.675	6371666.680	6371666.685	6371666.690	6371666.696	6371666.701	6371666.706
ITRF 1993	-4460996.03	2682557.122	-3674443.93	-0.0403	0.0008	0.049		6371666.695	6371666.695	6371666.696	6371666.696	6371666.696	6371666.696	6371666.697
ITRF 1994	-4460995.98	2682557.093	-3674443.88	-0.0366	-0.003	0.0442			6371666.624	6371666.622	6371666.621	6371666.620	6371666.619	6371666.618
ITRF 1996	-4460996.13	2682557.08	-3674443.7	-0.0368	-0.0045	0.0479					6371666.620	6371666.616	6371666.612	6371666.609
ITRF 1997	-4460996.13	2682557.087	-3674443.72	-0.0364	-0.0011	0.0427						6371666.628	6371666.628	6371666.629
GSFC 1998														
							6371666.670	6371666.695	6371666.624	6371666.622	6371666.620	6371666.628		

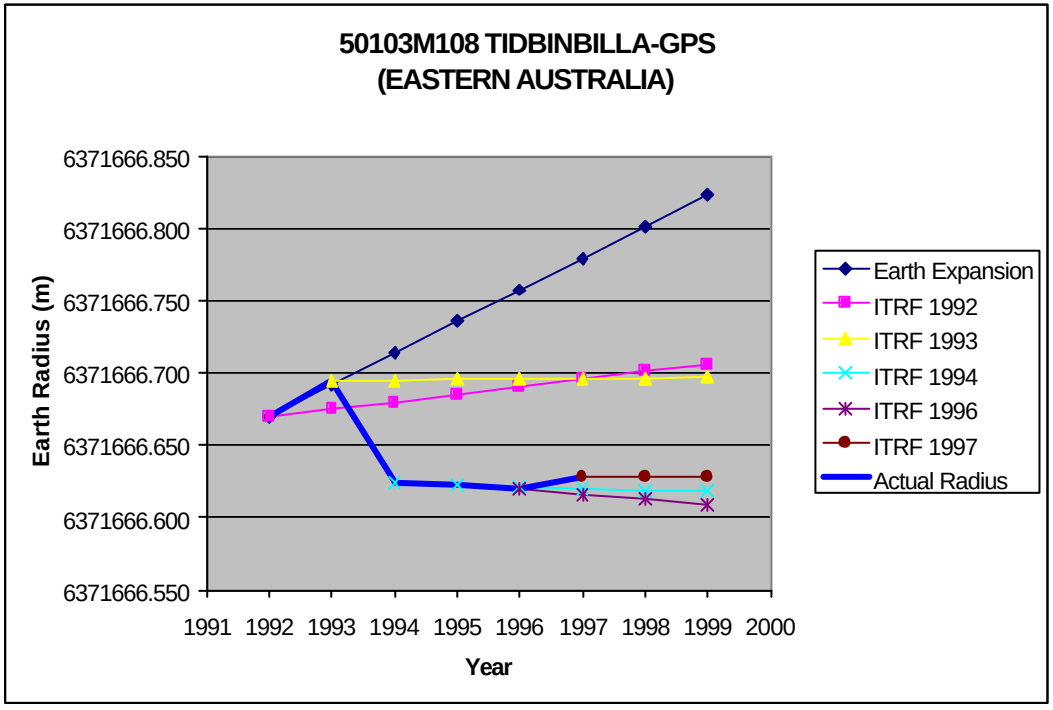

92201M003 PAMATAI-GPS (TAHITI)

	Site Co-ordinates			Site Velocity			Derived Earth Radius							
Data	**X**	**Y**	**Z**	**Vx**	**Vy**	**Vz**	**1992**	**1993**	**1994**	**1995**	**1996**	**1997**	**1998**	**1999**
Source	**m**	**m**	**m**	**m/y**	**m/y**	**m/y**	6376541.674	6376541.696	6376541.718	6376541.740	6376541.762	6376541.784	6376541.806	6376541.828
ITRF 1992	-5245194.95	-3080472.63	-1912825.66	-0.0418	0.0517	0.0314	6376541.674	6376541.674	6376541.674	6376541.674	6376541.674	6376541.674	6376541.674	6376541.674
ITRF 1993	-5245195.18	-3080472.36	-1912825.51	-0.0404	0.0492	0.0299		6376541.687	6376541.687	6376541.688	6376541.688	6376541.689	6376541.689	6376541.690
ITRF 1994	-5245195.16	-3080472.38	-1912825.5	-0.0374	0.0463	0.0339			6376541.675	6376541.674	6376541.672	6376541.670	6376541.668	6376541.667
ITRF 1996	-5245195.34	-3080472.19	-1912825.39	-0.0424	0.0432	0.0289					6376541.693	6376541.698	6376541.704	6376541.709
ITRF 1997	-5245195.34	-3080472.19	-1912825.41	-0.0423	0.0416	0.0266						6376541.703	6376541.710	6376541.716
GSFC 1998														
							6376541.674	6376541.687	6376541.675	6376541.684	6376541.693	6376541.703		

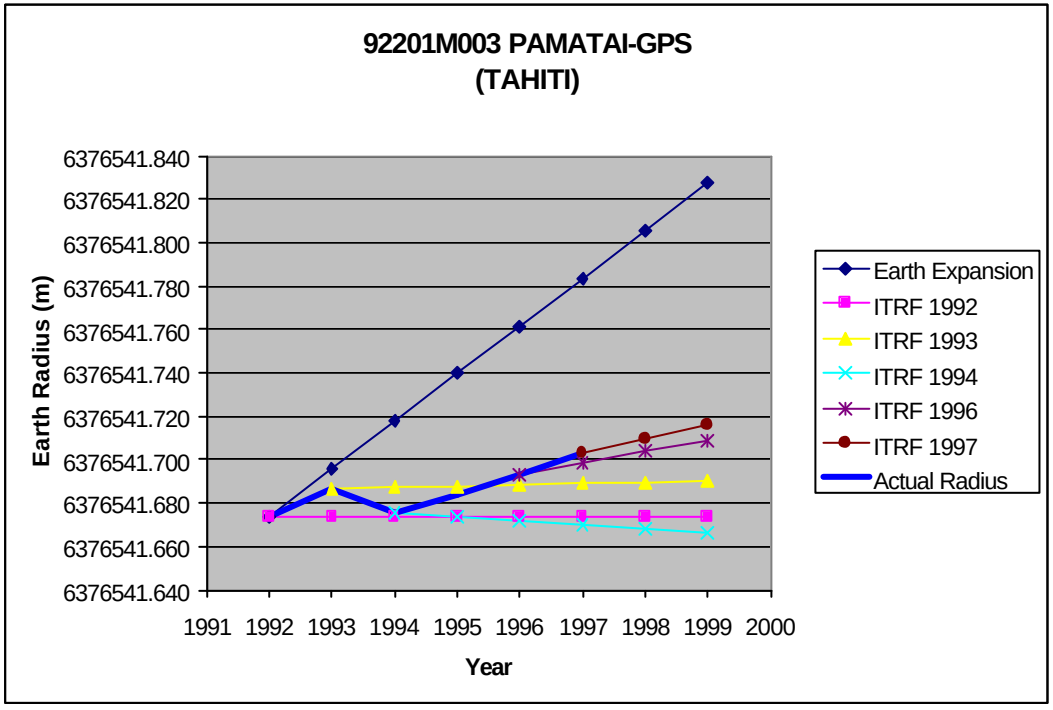

97301M210 KOUROU-GPS (BRAZIL)

	Site Co-ordinates			Site Velocity			Derived Earth Radius							
Data	**X**	**Y**	**Z**	**Vx**	**Vy**	**Vz**	**1992**	**1993**	**1994**	**1995**	**1996**	**1997**	**1998**	**1999**
Source	**m**	**m**	**m**	**m/y**	**m/y**	**m/y**	6377933.516	6377933.538	6377933.560	6377933.582	6377933.604	6377933.626	6377933.648	6377933.670
ITRF 1992	3839591.474	-5059567.51	579956.772	-0.0055	-0.0029	0.0116	6377933.516	6377933.516	6377933.516	6377933.516	6377933.516	6377933.516	6377933.516	6377933.516
ITRF 1993	3839591.42	-5059567.55	579956.874	-0.005	-0.0031	0.0111		6377933.521	6377933.522	6377933.522	6377933.523	6377933.523	6377933.523	6377933.524
ITRF 1994	3839591.447	-5059567.54	579956.867	0.0027	-0.0041	0.0133			6377933.530	6377933.537	6377933.543	6377933.549	6377933.555	6377933.561
ITRF 1996	3839591.428	-5059567.54	579956.924	-0.001	0.0001	0.0114					6377933.526	6377933.526	6377933.527	6377933.527
ITRF 1997	3839591.433	-5059567.55	579956.916	-0.0022	-0.0024	0.0103						6377933.537	6377933.538	6377933.540
GSFC 1998														
							6377933.516	6377933.521	6377933.530	6377933.528	6377933.526	6377933.537		

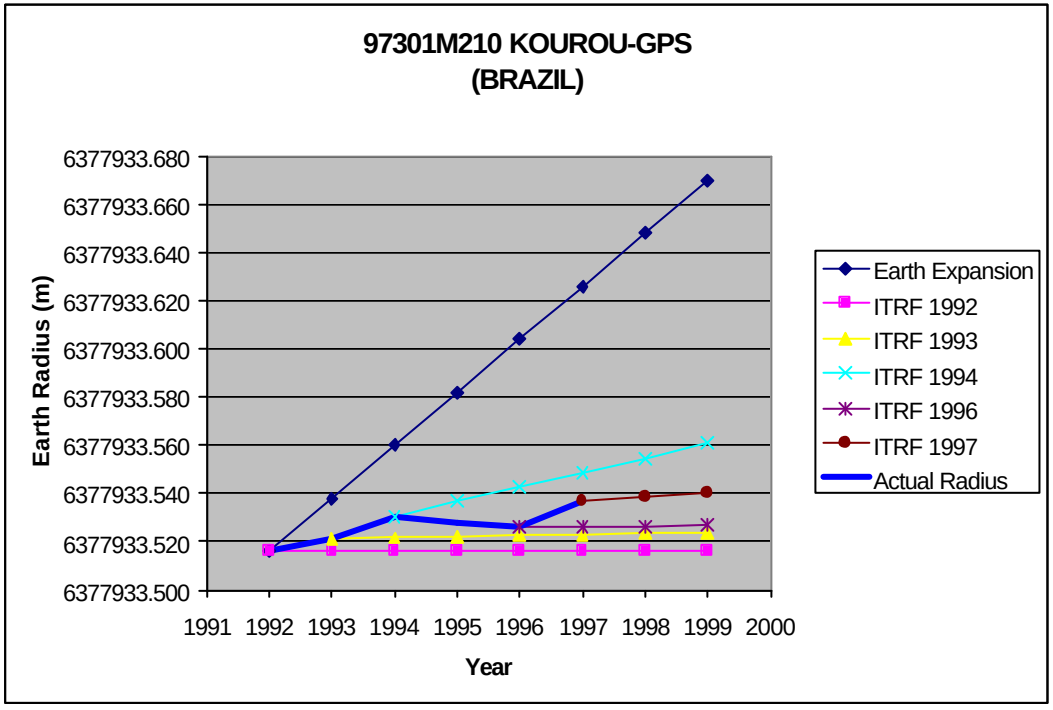

A2.4 LLR Space Geodetic Chart

40442M001 FORT DAVIS-LLR (TEXAS)

	Site Co-ordinates			Site Velocity			Derived Earth Radius							
Data	**X**	**Y**	**Z**	**Vx**	**Vy**	**Vz**	**1992**	**1993**	**1994**	**1995**	**1996**	**1997**	**1998**	**1999**
Source	**m**	**m**	**m**	**m/y**	**m/y**	**m/y**	6374566.496	6374566.518	6374566.540	6374566.562	6374566.584	6374566.606	6374566.628	6374566.650
ITRF 1992	-1330125.27	-5328526.64	3236150.281	-0.0106	0.0005	-0.0081	6374566.496	6374566.494	6374566.492	6374566.489	6374566.487	6374566.485	6374566.483	6374566.480
ITRF 1993	-1330125.37	-5328526.6	3236150.253	-0.0126	-0.0009	-0.0053		6374566.473	6374566.473	6374566.474	6374566.475	6374566.476	6374566.476	6374566.477
ITRF 1994	-1330125.34	-5328526.67	3236150.259	-0.0118	-0.0036	-0.0074			6374566.525	6374566.527	6374566.528	6374566.530	6374566.532	6374566.534
ITRF 1996	-1330125.39	-5328526.66	3236150.227	-0.0117	-0.0034	-0.0064					6374566.507	6374566.509	6374566.511	6374566.513
ITRF 1997	-1330125.39	-5328526.64	3236150.217	-0.0127	-0.0025	-0.007						6374566.491	6374566.492	6374566.494
GSFC 1998														
							6374566.496	6374566.473	6374566.525	6374566.516	6374566.507	6374566.491		

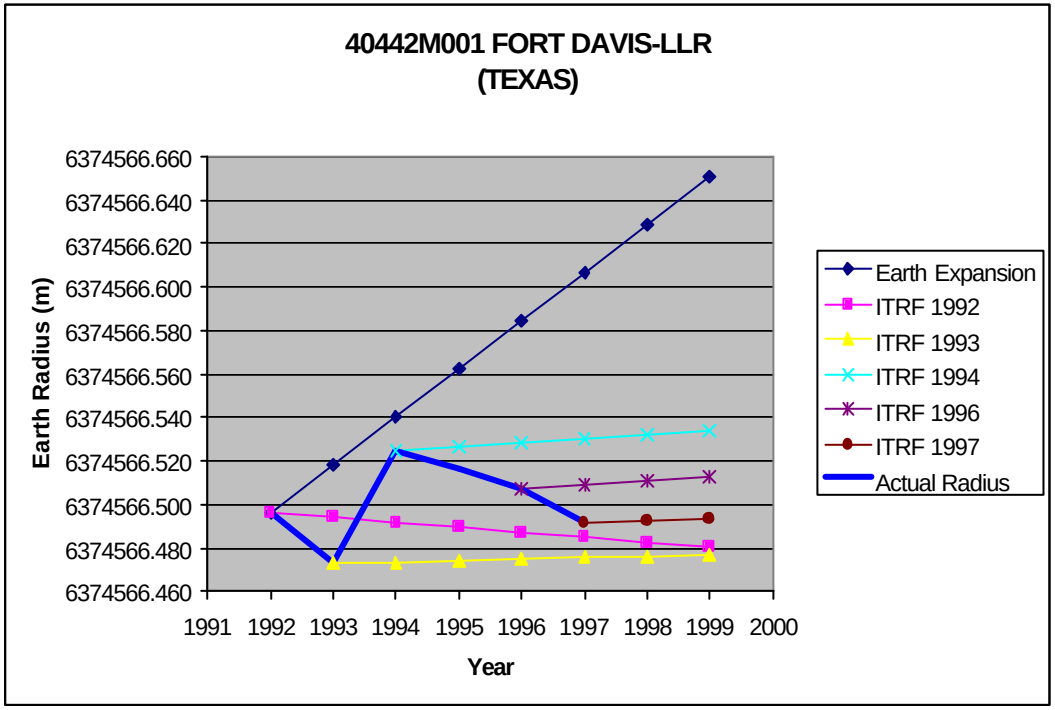

A3. PALAEOMAGNETIC FORMULAE

A3.1 Magnetic Dipole Equations

The geocentric axial dipole model is central to the principles of palaeomagnetism (Figure A3.1). In this conventional Earth model a magnetic field produced by a single magnetic dipole **M**, located at the centre of the Earth and aligned with the rotation axis, is considered.

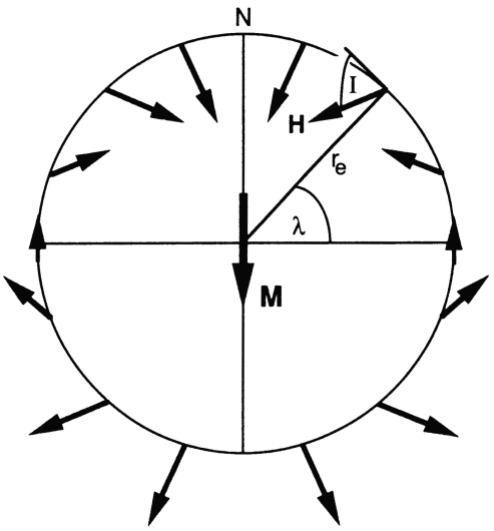

Figure A3.1. Geocentric axial dipole model. A magnetic dipole **M** is located at the centre of the Earth and aligned with the rotation axis. The geographic latitude is l, the mean Earth radius is $\mathbf{r_e}$, the magnetic field directions at the Earth's surface, produced by the geocentric axial dipole are schematically shown, inclination **I** is shown for one location and **N** is the North geographic pole. (from Butler, 1992)

The derivation of the conventional dipole equation is given in Butler (1992) and defined as:

$$\mathbf{\tan I = 2 \tan} \, l \, \mathbf{= 2 \cot p} \qquad \text{(Equation A3.1)}$$

Where:

I is the mean inclination of the magnetic field, increasing from -90° at the geographic south pole to +90° at the geographic north pole

l is the geographic latitude determined from I

p is the geographic colatitude determined from I

Rearranging the dipole equation gives colatitude **p** as:

$$\mathbf{p = \cot^{-1}(\tan I/2) = \tan^{-1}(2/\tan I)} \qquad \text{(Equation A3.2)}$$

Equation A3.2 represents a measure of the great-circle angular distance from the mean sample site to the magnetic pole and, like latitude is independent of any radial or time constraints imposed by the sample. The dipole equation is a general equation applicable to any sized magnetic sphere that obeys the geocentric axial dipole model (Figure A3.1). On this sphere the magnetic lines of force behave in exactly the same manner, irrespective of scale and, for a given site inclination, the colatitude (or latitude) calculated using the dipole equation will always remain the same.

Figure A3.2 demonstrates this very important characteristic of the dipole equation where, for a given site value I, the dipole equation remains true for an infinite number of sites along a radius vector R, passing through the centre of the Earth to the site location and beyond. Colatitude (Equation A3.2) calculated from an inclination I at sites S_1.....S_n, located along the radius vector R, is equal to a constant angular measurement p. At site S_1 this colatitude p represents an arcuate distance D_1 which is not equal to distances D_2.....D_n for sites S_2.....S_n using the identical values of inclination I and colatitude p.

For a simplistic radial expansion of the Earth from R_1 to R_2.....R_n the palaeopole positions P_1, P_2.....P_n calculated from the conventional dipole equation (Equation A3.2) are shown (Figure A3.2). Because the conventional dipole equation uses angular measurements and has no provision for either a radial or time component to compensate for the shift in actual palaeopole position with expansion, the calculated pole positions will always coincide with the geomagnetic pole N.

To determine the ancient palaeopole position P_a on the present day Earth with palaeoradius varying exponentially with time, consider Figure A3.3. At site S_0 located at the present radius R_0, using the conventional palaeocolatitude equation (Equation A3.2) an inclination I gives a colatitude p_0 which equates with the palaeocolatitude p_a locked into the rock record from site S_a at palaeoradius R_a.

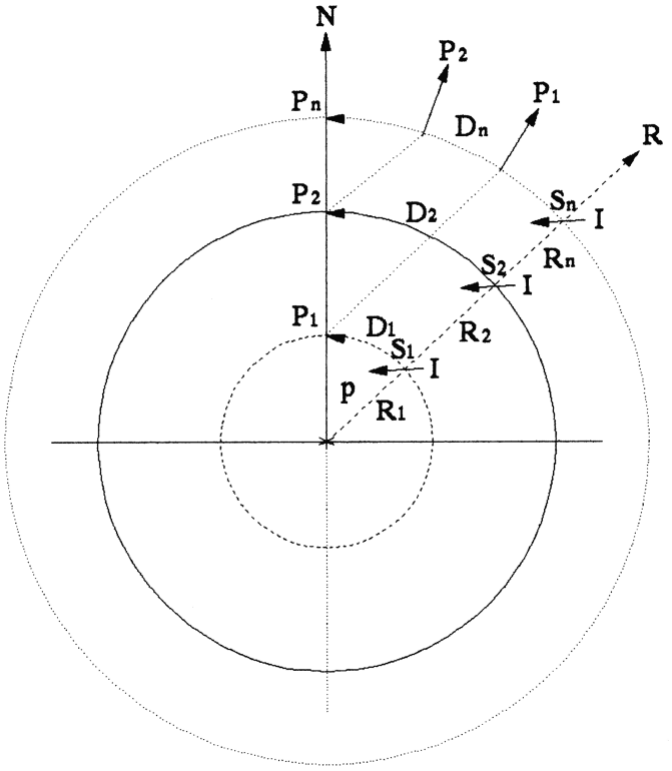

Figure A3.2. Palaeopoles determined using the conventional dipole equation. Cross section showing a number geocentric axial dipolar spheres. For a given site value **I** the dipole equation remains true for an infinite number of sample sites $\mathbf{S_1}$ to $\mathbf{S_n}$ along a radius vector **R**. The colatitude calculated from inclination **I** at sites $\mathbf{S_1}$ to $\mathbf{S_n}$ is equal to a constant angular measurement **p**. At sites $\mathbf{S_1}$ this colatitude **p** represents an arcuate distance $\mathbf{D_1}$ which is not equal to distances $\mathbf{D_2}$ to $\mathbf{D_n}$ for sites $\mathbf{S_2}$ to $\mathbf{S_n}$. No provision is made in the dipole equation for a variation in palaeoradius with time in determining the actual palaeopole positions $\mathbf{P_1}$ to $\mathbf{P_n}$.

At site S_a the arc distance D_a is equal to:

$$D_a = R_a p_a$$

Where p_a is in radians. Rearranging:

$$p_a = (D_a/R_a)$$

To determine the palaeopole position P_a located on the present radius Earth, which equates to the ancient palaeopole position P_a determined from site S_a, palaeocolatitude:

$$p = (D_a/R_0) \times 180/\pi = (R_a p_a \times (\pi/180)/R_0) \times 180/\pi = R_a p_a / R_0$$

Where p is in degrees.

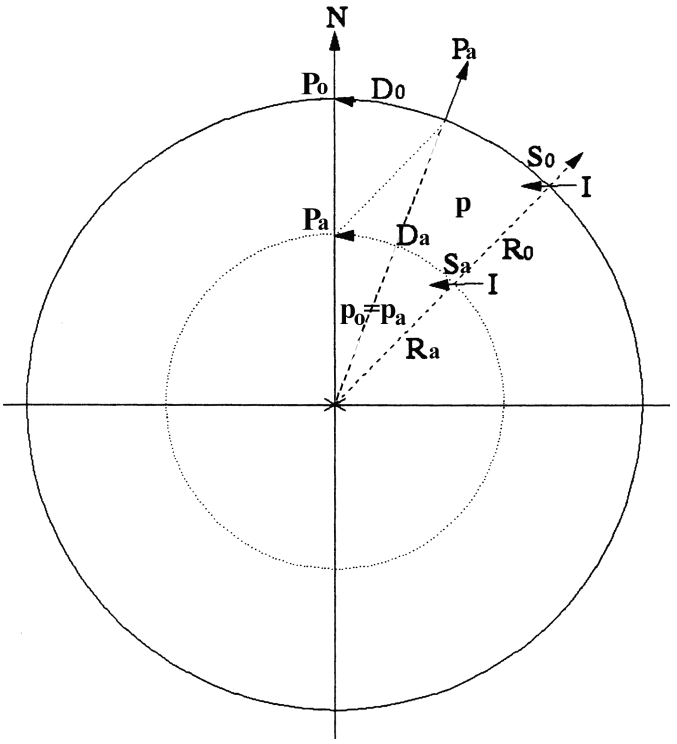

Figure A3.3. Determining the actual palaeopole position on the present Earth. Cross section shows an ancient Earth at palaeoradius $\mathbf{R_a}$ and a present Earth at present radius $\mathbf{R_0}$. For an inclination **I**, site $\mathbf{S_0}$, and present radius $\mathbf{R_0}$, the arcuate distance to palaeopole **P** is $\mathbf{D_0}$, and colatitude $\mathbf{p_0}$. For site $\mathbf{S_a}$, palaeoradius $\mathbf{R_a}$ and arcuate distance $\mathbf{D_a}$, the colatitude $\mathbf{p_a}$ is the same for site $\mathbf{S_0}$, but the actual palaeopole position on the present Earth is located at position $\mathbf{P_a}$ determined from $\mathbf{D_a}$.

The mathematical relationship for an exponential increase in the Earth's palaeoradius, derived from empirical measurements of oceanic and continental surface area data was previously found to be (Equation 2.6) (Section 2.3):

$$R_a = (R_0 - R_p)e^{kt} + R_p \qquad \text{(Equation 2.6)}$$

Incorporating Equation 2.6 for R_a gives:

$$p = ((R_0 - R_p)e^{kt} + R_p)p_a/R_0$$

and incorporating Equation A4.2 for p_a gives:

$$p = ((R_0 - R_p)e^{kt} + R_p)) (\tan^{-1} (2/\tan I))/R_0)$$

For any site sample, constrained by the age of the rock sequence containing the site data, the palaeocolatitude from site to the ancient palaeopole position on an Earth of present radius is equal to:

$$\mathbf{p = ((R_0 - R_p)e^{kt} + R_p)) (\tan^{-1} (2/\tan I))/R_0} \qquad \text{(Equation A3.3)}$$

The application of this modified dipole equation to palaeomagnetic site data (Section 3.2.2) enables palaeocolatitude to be converted to the present geographical grid system. This correctly locates the ancient palaeopole position on the present Earth. To determine palaeolatitude and establish latitudinal zonation, the conventional dipole equation (Equation A3.2) is used.

The modified dipole Equation A3.3 can now be used to develop formulae to convert ancient palaeopole geographical coordinates to present geographical coordinates from ancient site mean data located on the present Earth. This enables palaeopoles to be correctly located on the present Earth, constrained by both time and palaeoradius.

A3.2 Modified Dipole Formulae

Site mean data determined from a set of site samples are assumed by palaeomagneticians to represent a time-averaged field which compensates for any secular variation caused by non-dipole components (Tarling, 1983). For a geocentric axial dipole field (Figure A3.1) the time-averaged and structurally corrected inclination I, determined from site data establishes the palaeocolatitude existing at the site when the site data were locked into the rock-record and a time-average declination D determines the direction along a palaeomeridian to the palaeopole.

Calculation of the palaeomagnetic pole position on the present Earth surface uses spherical trigonometry, based on the dipole Equation 3.1, to determine the distance traveled from the observing locality to the pole position (Figure A3.4).

Details and derivation of the following conventional palaeomagnetic equations, sign conventions and symbols for geographic locations, are adopted from Butler (1992):

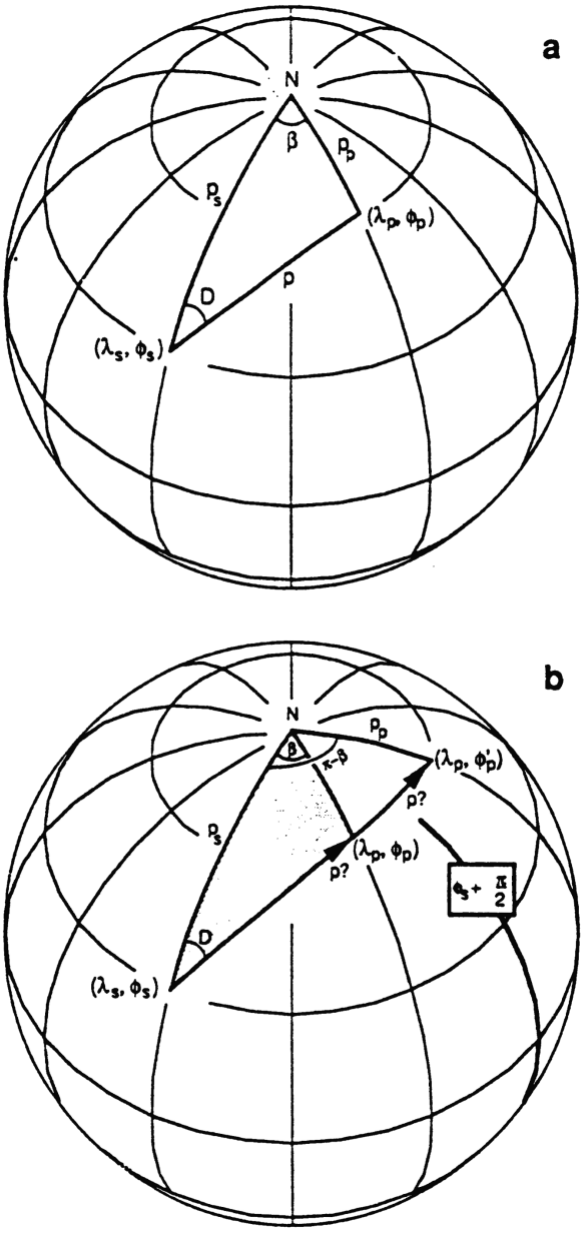

Figure A3.4. Determination of a magnetic pole from a magnetic field direction, using the palaeomagnetic dipole equation. Orthorhombic projection with latitude and longitude grid in 30° increments. Figure A3.4a: the site latitude and longitude is (λ_s, ϕ_s); the palaeomagnetic pole is located at (λ_p, ϕ_p); site colatitude is p_s; colatitude of the magnetic pole is p_p; and the longitudinal difference between the magnetic pole and site is β. Figure A3.4b: illustrates the ambiguity in magnetic pole longitude. The pole may be at either (λ_p, ϕ_p) or (λ_p, ϕ'_p); the longitude at $\phi_s + \pi/2$ is shown by the heavy meridian line. (From Butler, 1992).

- latitudes increase from -90° at the south geographic pole to 0° at the equator and +90° at the north geographic pole;
- longitudes east of the Greenwich meridian are positive, while westerly longitudes are negative and;
- (λ_p, ϕ_p) is the pole position calculated from a site-mean direction (I_m, D_m) measured at site location (λ_s, ϕ_s).

The pole latitude derived from spherical trigonometry (Figure A3.4) is:

$$\lambda_p = \sin^{-1} (\sin\lambda_s \cos p + \cos\lambda_s \sin p \cos D_m) \qquad \text{(Equation A3.4)}$$

The longitudinal difference between pole and site, denoted by β, is positive towards the east, negative towards the west and is:

$$\beta = \sin^{-1} (\sin p \sin D_m / \cos\lambda_p) \qquad \text{(Equation A3.5)}$$

where if:

$$\cos p \geq \sin\lambda_s \sin\lambda_p \qquad \text{(Equation A3.6)}$$

then the pole longitude:

$$\phi_p = \phi_s + \beta \qquad \text{(Equation A3.7)}$$

but if:

$$\cos p \leq \sin\lambda_s \sin\lambda_p \qquad \text{(Equation A3.8)}$$

then the pole longitude:

$$\phi_p = \phi_s + 180° - \beta \qquad \text{(Equation A3.9)}$$

For any site-mean direction (I_m, D_m) the associated circular confidence limit (α_{95}) is transformed into an ellipse of confidence about the calculated pole position with semi-axes of angular length given by (Figure A3.5):

$$d_p = \alpha_{95} ((1 + 3\cos^2 p)/2) = 2\,\alpha_{95} (1/ (1 + 3\cos^2 I_m)) \qquad \text{(Equation A3.10)}$$

and:

$$d_m = \alpha_{95} (\sin p / \cos I_m) \qquad \text{(Equation A3.11)}$$

While Equations A3.4 to A3.11 represent the basis for conventional plate tectonic determination of pole positions and derived apparent polar wander paths, they do not and cannot acknowledge any variation in angular dimension of palaeogeographical grids as a result of a variable palaeoradius or time constraint. What is assumed by these equations is that the angular dimension of the palaeogeographical co-ordinate system, indicated by the site-data, equals the angular dimension of the geographical co-ordinate system represented by the present site location. By using these conventional palaeomagnetic equations to determine the palaeopole position the two systems are then simply added, using spherical trigonometry to give a palaeopole latitude and longitude.

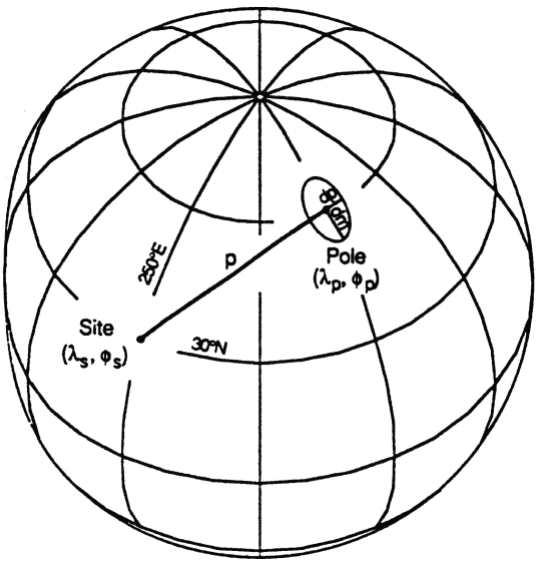

Figure A3.5. Ellipse of confidence about a magnetic pole position, determined using the palaeomagnetic dipole equation. For a magnetic colatitude p, d_p is the semi-axis of a confidence ellipse along the great-circle path from site to pole; dm is the semi-axis perpendicular to that great-circle path. Orthorhombic projection, with latitude and longitude grid in 30° increments. (From Butler, 1992)

To determine actual palaeopole locations on the present Earth each site sample must be qualified by a time constraint to convert the palaeogeographical co-ordinate system to the present system. For an Earth undergoing an exponential increase in palaeoradius from the Archaean to the Recent, derivation of palaeocolatitude from site data is (Equation A3.3):

$$\mathbf{p = ((R_0 - R_p)e^{kt} + R_p))\ (\tan^{-1}\ (2/\tan\ I))/R_0} \qquad \text{(Equation A3.3)}$$

By incorporating palaeocolatitude Equation A3.3 into the pole coordinate Equations A3.4 to A3.11 of Butler (1992), equations that constrain the palaeocolatitude arcuate distances to the present geographical co-ordinates are established. These are then used to determine the actual palaeopole location on the present Earth surface.

Palaeopole latitude becomes:

$$l_p = \mathbf{\sin^{-1}\ (\sin} l_s \mathbf{\cos[((R_0 - R_p)e^{kt} + R_p))\ (\tan^{-1}\ (2/\tan\ I))/R_0] + \cos} l_s \mathbf{\sin[((R_0 - R_p)e^{kt} + R_p))\ (\tan^{-1}\ (2/\tan\ I))/R_0]\ \cos D_m)} \qquad \text{(Equation A3.12)}$$

longitudinal difference becomes:

$$b = \mathbf{\sin^{-1}\ (\sin[((R_0 - R_p)e^{kt} + R_p))\ (\tan^{-1}\ (2/\tan\ I))/R_0]\ \sin D_m/\cos} l_p\mathbf{)} \qquad \text{(Equation A3.13)}$$

where if:

$$\mathbf{\cos[((R_0 - R_p)e^{kt} + R_p))\ (\tan^{-1}\ (2/\tan\ I))/R_0]\ \geq\ \sin} l_s \mathbf{\sin} l_p \qquad \text{(Equation A3.14)}$$

then the palaeopole longitude:

$$f_p = f_s + b \qquad \text{(Equation A3.15)}$$

but if:

$$\mathbf{\cos[((R_0 - R_p)e^{kt} + R_p))\ (\tan^{-1}\ (2/\tan\ I))/R_0]\ \leq\ \sin} l_s \mathbf{\sin} l_p \qquad \text{(Equation A3.16)}$$

then the palaeopole longitude:

$$f_p = f_s + \mathbf{180°} - b \qquad \text{(Equation A3.17)}$$

and ellipse of confidence:

$$\mathbf{d_p = a_{95}\ ((1 + 3\cos^2[((R_0 - R_p)e^{kt} + R_p))\ (\tan^{-1}\ (2/\tan I))/R_0])/2)}$$

$$\mathbf{= 2\ a_{95}\ (1/\ (1 + 3\cos^2\ I_m))} \qquad \text{(Equation A3.18)}$$

and:

$$\mathbf{d_m = a_{95}\ (\sin[((R_0 - R_p)e^{kt} + R_p))\ (\tan^{-1}\ (2/\tan I))/R_0]/\cos I_m)} \qquad \text{(Equation A3.19)}$$

A4. PALAEOMAGNETIC DATA

Actual palaeopole locations derived from the structurally corrected palaeomagnetic data of McElhinny & Lock (1996) using modified palaeomagnetic Equations A3.12 to A3.19.

Table A4.1 Recent Palaeomagnetic Data

Site Details						Structure Corrected		Derived Actual Paleomagnetic Data				
Number	Age	Age	Age	Site	Site	Correct	Correct	Paleo	Paleo	Palaeo	Pole	Pole
Result	Low Mag	High Mag	Mean	Lat	Long	Dec	Inc	Radius	Colatitude	Latitude	Latitude	Longitude
340	0	1	0.5	**37.7**	**-118.9**	359.4	55.8	6360.22	53.57	**36.3**	**88.64**	**81.97**
345	0	1	0.5	**2.5**	**98.7**	0.8	6.6	6360.22	86.55	**3.3**	**88.75**	**138.60**
392	0	1	0.5	**35.9**	**-106.6**	358.2	43.9	6360.22	64.20	**25.7**	**79.78**	**82.58**
608	0	1	0.5	**41.7**	**-121.7**	3.8	49.3	6360.22	59.73	**30.2**	**78.17**	**42.09**
628	0	1	0.5	**38.6**	**179.3**	353.0	55.0	6360.22	54.38	**35.5**	**83.67**	**423.35**
780	0	1	0.5	**50.4**	**7.3**	5.2	66.6	6360.22	40.81	**49.1**	**86.43**	**115.09**
791	0	1	0.5	**50.2**	**6.7**	14.7	67.8	6360.22	39.16	**50.8**	**80.65**	**87.09**
795	0	1	0.5	**-2.0**	**36.0**	184.9	0.8	6360.22	89.45	**0.4**	**-84.89**	**289.56**
1054	0	1	0.5	**35.2**	**138.1**	355.4	49.8	6360.22	59.29	**30.6**	**84.08**	**360.06**
1147	0	1	0.5	**-38.0**	**140.7**	357.0	-57.0	6360.22	-52.32	**-37.6**	**-87.61**	**237.45**
1148	0	1	0.5	**-38.0**	**140.7**	9.0	-55.0	6360.22	-54.38	**-35.5**	**-82.42**	**395.16**
1150	0	1	0.5	**-36.8**	**174.9**	0.2	-61.7	6360.22	-47.04	**-42.9**	**-83.84**	**173.54**
1151	0	1	0.5	**-38.1**	**176.2**	182.9	40.6	6360.22	66.69	**23.2**	**-75.00**	**366.54**
1238	0	1	0.5	**19.0**	**-99.0**	357.0	31.4	6360.22	72.91	**17.0**	**86.57**	**137.71**
1258	0	1	0.5	**34.5**	**135.5**	11.3	47.7	6360.22	61.11	**28.8**	**78.88**	**252.69**
1259	0	1	0.5	**43.7**	**-79.2**	3.9	45.6	6360.22	62.85	**27.0**	**73.16**	**88.74**
1367	0	1	0.5	**18.5**	**-72.5**	358.0	32.0	6360.22	72.53	**17.4**	**87.84**	**169.41**
1537	0	1	0.5	**-63.0**	**-60.6**	247.0	-82.0	6360.22	-15.67	**-74.3**	**-54.09**	**-35.51**
1538	0	1	0.5	**-63.0**	**-60.6**	8.0	-69.0	6360.22	-37.45	**-52.5**	**-78.73**	**145.06**
1833	0	1	0.5	**-37.0**	**147.0**	17.0	-65.0	6360.22	-42.93	**-47.0**	**-73.91**	**101.06**
1834	0	1	0.5	**-33.0**	**149.0**	1.0	-67.0	6360.22	-40.26	**-49.7**	**-73.25**	**146.76**
1835	0	1	0.5	**-37.0**	**150.0**	15.0	-64.0	6360.22	-44.21	**-45.7**	**-75.76**	**102.78**
1899	0	1	0.5	**-4.0**	**150.0**	0.0	-16.0	6360.22	-81.71	**-8.2**	**-85.71**	**150.00**
1963	0	1	0.5	**-34.0**	**144.0**	353.7	-56.1	6360.22	-53.26	**-36.7**	**-84.18**	**204.12**
1987	0	1	0.5	**50.3**	**-118.9**	5.8	67.6	6360.22	39.43	**50.5**	**86.30**	**-35.24**

2016	0	1	0.5	**45.0**	**-111.0**	1.8	65.9	6360.22	41.75	**48.2**	**86.52**	**-90.84**
2043	0	1	0.5	**-5.0**	**119.7**	178.0	18.0	6360.22	80.64	**9.2**	**-85.21**	**144.04**
2159	0	1	0.5	**52.5**	**-2.8**	6.0	70.0	6360.22	35.99	**53.9**	**86.11**	**62.03**
2160	0	1	0.5	**52.5**	**-2.8**	13.0	73.0	6360.22	31.39	**58.6**	**80.47**	**42.24**
2185	0	1	0.5	**11.6**	**42.5**	358.9	19.2	6360.22	79.99	**9.9**	**88.08**	**256.81**
2186	0	1	0.5	**11.6**	**42.5**	87.3	12.0	6360.22	83.79	**6.1**	**3.88**	**126.95**
2232	0	1	0.5	**64.1**	**-21.1**	269.9	-80.5	6360.22	-18.47	**-71.5**	**58.59**	**16.34**
2241	0	1	0.5	**-27.1**	**-109.2**	357.9	-43.4	6360.22	-64.59	**-25.3**	**-87.47**	**22.18**
2290	0	1	0.5	**50.5**	**7.0**	3.7	67.7	6360.22	39.30	**50.6**	**87.64**	**90.59**
2315	0	1	0.5	**39.8**	**115.9**	7.1	54.8	6360.22	54.58	**35.3**	**82.88**	**241.60**
2324	0	1	0.5	**-12.1**	**49.2**	3.9	-33.9	6360.22	-71.31	**-18.6**	**-82.41**	**19.99**
2325	0	1	0.5	**-19.9**	**47.0**	340.7	-40.9	6360.22	-66.47	**-23.4**	**-71.72**	**122.07**
2396	0	1	0.5	**43.5**	**-81.8**	0.7	42.4	6360.22	65.35	**24.5**	**71.14**	**96.23**
2397	0	1	0.5	**44.2**	**-81.2**	3.2	35.8	6360.22	70.05	**19.8**	**65.60**	**91.50**
2449	0	1	0.5	**38.5**	**-110.8**	10.4	60.2	6360.22	48.80	**41.1**	**81.58**	**-42.80**
2451	0	1	0.5	**38.6**	**-110.7**	357.7	48.7	6360.22	60.25	**29.6**	**80.94**	**82.09**
2468	0	1	0.5	**-37.8**	**77.8**	3.2	-58.0	6360.22	-51.25	**-38.7**	**-87.31**	**9.52**
2469	0	1	0.5	**-21.1**	**55.5**	357.2	-40.2	6360.22	-66.98	**-22.9**	**-86.77**	**108.53**
2470	0	1	0.5	**38.7**	**-27.2**	358.2	52.5	6360.22	56.82	**33.1**	**84.29**	**168.13**
2486	0	1	0.5	**-46.5**	**52.2**	7.5	-61.7	6360.22	-47.04	**-42.9**	**-83.61**	**291.27**
2487	0	1	0.5	**-46.5**	**51.7**	4.0	-62.0	6360.22	-46.68	**-43.2**	**-85.74**	**274.80**
2488	0	1	0.5	**-46.5**	**51.9**	5.9	-61.8	6360.22	-46.92	**-43.0**	**-84.59**	**284.75**
2507	0	1	0.5	**4.5**	**9.5**	4.6	4.3	6360.22	87.70	**2.2**	**84.91**	**124.96**
2508	0	1	0.5	**3.5**	**9.0**	359.9	-3.0	6360.22	-88.35	**-1.5**	**-84.85**	**10.11**
2587	0	1	0.5	**-11.6**	**43.3**	359.8	-21.6	6360.22	-78.67	**-11.2**	**-89.67**	**187.44**
2593	0	1	0.5	**35.0**	**-3.0**	173.0	-33.0	6360.22	-71.89	**-18.0**	**72.00**	**199.01**
2621	0	1	0.5	**47.5**	**-80.7**	338.8	73.0	6360.22	31.39	**58.6**	**73.23**	**-121.44**
2650	0	1	0.5	**42.1**	**-82.1**	9.6	42.6	6360.22	65.20	**24.7**	**70.97**	**70.24**
2655	0	1	0.5	**66.5**	**-85.0**	55.0	72.0	6360.22	32.96	**57.0**	**63.36**	**-1.19**
2695	0	1	0.5	**-38.8**	**77.5**	347.3	-55.1	6360.22	-54.28	**-35.6**	**-79.44**	**180.52**
2696	0	1	0.5	**-38.3**	**77.5**	356.3	-57.0	6360.22	-52.32	**-37.6**	**-87.02**	**178.34**

2725	0	1	0.5	**-46.9**	**37.8**	11.9	-67.1	6360.22	-40.13	**-49.8**	**-81.57**	**-27.19**
2726	0	1	0.5	**-46.7**	**45.0**	5.4	-62.2	6360.22	-46.44	**-43.5**	**-85.06**	**277.43**
2728	0	1	0.5	**18.1**	**145.7**	1.9	32.1	6360.22	72.47	**17.4**	**88.10**	**252.77**
2743	0	1	0.5	**42.4**	**-81.9**	7.4	47.2	6360.22	61.53	**28.4**	**74.84**	**72.45**
2744	0	1	0.5	**43.7**	**-79.2**	336.4	60.6	6360.22	48.34	**41.6**	**72.59**	**-167.73**
2745	0	1	0.5	**43.6**	**-79.2**	5.8	44.3	6360.22	63.88	**26.0**	**71.89**	**83.83**
2803	0	1	0.5	**40.7**	**13.9**	9.0	47.9	6360.22	60.94	**29.0**	**76.23**	**158.83**
2822	0	1	0.5	**38.5**	**-109.5**	1.8	54.3	6360.22	55.08	**34.8**	**86.14**	**47.99**
2865	0	1	0.5	**79.5**	**13.3**	25.0	83.0	6360.22	13.77	**76.2**	**83.88**	**122.57**
2931	0	1	0.5	**21.3**	**-157.8**	359.9	32.1	6360.22	72.47	**17.4**	**86.23**	**23.65**
2932	0	1	0.5	**44.3**	**-121.9**	2.2	49.6	6360.22	59.47	**30.4**	**76.12**	**50.18**
2963	0	1	0.5	**31.0**	**-115.0**	19.0	57.0	6360.22	52.32	**37.6**	**72.99**	**-53.27**
2969	0	1	0.5	**8.5**	**-71.2**	6.0	4.0	6360.22	87.85	**2.0**	**81.28**	**65.23**
2971	0	1	0.5	**36.0**	**136.0**	356.1	49.3	6360.22	59.73	**30.2**	**83.41**	**346.76**
2986	0	1	0.5	**-0.8**	**-89.5**	357.6	3.0	6360.22	88.35	**1.5**	**86.57**	**-133.93**
3054	0	1	0.5	**44.6**	**3.5**	357.8	60.3	6360.22	48.68	**41.2**	**86.35**	**210.39**
3079	0	1	0.5	**-63.0**	**-60.7**	6.0	-72.0	6360.22	-32.96	**-57.0**	**-83.33**	**148.63**
3080	0	1	0.5	**-63.0**	**-60.7**	11.0	-73.0	6360.22	-31.39	**-58.6**	**-83.08**	**174.90**
3085	0	1	0.5	**-57.1**	**-26.8**	7.0	-64.0	6360.22	-44.21	**-45.7**	**-77.89**	**177.09**
3086	0	1	0.5	**-59.4**	**-27.3**	20.0	-71.0	6360.22	-34.50	**-55.4**	**-78.61**	**231.44**
3087	0	1	0.5	**-58.0**	**-27.0**	15.0	-68.0	6360.22	-38.88	**-51.1**	**-78.95**	**210.98**
3088	0	1	0.5	**-63.0**	**-60.7**	17.0	-75.0	6360.22	-28.14	**-61.8**	**-82.07**	**208.66**
3096	0	1	0.5	**53.0**	**-168.0**	350.5	64.7	6360.22	43.32	**46.6**	**81.21**	**59.83**
3097	0	1	0.5	**53.5**	**-168.1**	6.9	70.6	6360.22	35.10	**54.8**	**85.73**	**-100.02**
3098	0	1	0.5	**51.9**	**-177.1**	355.9	65.3	6360.22	42.54	**47.4**	**84.83**	**35.34**
3099	0	1	0.5	**54.0**	**-167.0**	0.9	69.1	6360.22	37.31	**52.6**	**88.59**	**-9.70**
3100	0	1	0.5	**57.0**	**-135.7**	334.6	77.4	6360.22	24.05	**65.9**	**75.10**	**-178.51**
3101	0	1	0.5	**58.3**	**-155.3**	330.2	76.7	6360.22	25.26	**64.7**	**74.59**	#####
3102	0	1	0.5	**51.9**	**-177.1**	1.1	72.2	6360.22	32.65	**57.3**	**84.51**	**-170.88**
3105	0	1	0.5	**44.4**	**-121.7**	178.1	-60.9	6360.22	-47.99	**-41.9**	**87.24**	**89.09**
3106	0	1	0.5	**52.0**	**-177.0**	352.2	69.7	6360.22	36.43	**53.5**	**85.03**	**-245.56**

3115	0	1	0.5	**50.3**	**16.9**	357.4	65.8	6360.22	41.88	**48.0**	**87.24**	**235.81**
3131	0	1	0.5	**9.0**	**-68.1**	5.0	27.0	6360.22	75.58	**14.3**	**82.70**	**-26.48**
3157	0	1	0.5	**19.5**	**-155.6**	354.8	24.1	6360.22	77.26	**12.6**	**81.59**	**61.61**
3183	0	1	0.5	**-37.4**	**173.8**	2.0	-63.1	6360.22	-45.34	**-44.6**	**-82.59**	**162.71**
3188	0	1	0.5	**45.0**	**3.0**	231.0	-65.0	6360.22	-42.93	**-47.0**	**55.17**	**70.93**
3189	0	1	0.5	**45.0**	**3.0**	234.0	-71.5	6360.22	-33.73	**-56.2**	**54.97**	**54.51**
3190	0	1	0.5	**45.0**	**3.0**	114.0	57.0	6360.22	52.32	**37.6**	**11.81**	**50.61**
3191	0	1	0.5	**45.0**	**3.0**	354.2	83.8	6360.22	12.24	**77.7**	**57.16**	**0.74**
3192	0	1	0.5	**45.0**	**3.0**	295.5	66.5	6360.22	40.94	**49.0**	**47.19**	**-57.50**
3216	0	1	0.5	**15.0**	**122.0**	356.0	28.5	6360.22	74.69	**15.2**	**86.13**	**37.15**
3227	0	1	0.5	**-46.8**	**37.9**	353.2	-68.0	6360.22	-38.88	**-51.1**	**-83.79**	**81.28**
3228	0	1	0.5	**-54.5**	**3.3**	17.6	-73.3	6360.22	-30.91	**-59.0**	**-79.37**	**-54.05**
3262	0	1	0.5	**15.0**	**-24.4**	358.2	0.8	6360.22	89.45	**0.4**	**75.44**	**162.78**
3284	0	1	0.5	**-21.0**	**55.5**	6.3	-39.2	6360.22	-67.70	**-22.2**	**-84.00**	**-20.85**
3315	0	1	0.5	**-29.5**	**30.8**	340.5	-64.5	6360.22	-43.58	**-46.4**	**-67.26**	**67.34**
3323	0	1	0.5	**42.2**	**2.5**	356.0	54.0	6360.22	55.37	**34.5**	**81.81**	**206.25**
3342	0	1	0.5	**38.1**	**-28.1**	4.0	64.0	6360.22	44.21	**45.7**	**81.76**	**-8.25**
3343	0	1	0.5	**39.0**	**-28.0**	346.0	45.0	6360.22	63.33	**26.6**	**73.00**	**199.68**
3348	0	1	0.5	**-27.0**	**-109.3**	357.0	-48.0	6360.22	-60.86	**-29.0**	**-86.59**	**-59.02**
3423	0	1	0.5	**-21.0**	**-175.0**	357.0	-38.0	6360.22	-68.55	**-21.3**	**-87.17**	**-94.72**
3440	0	1	0.5	**19.5**	**-155.5**	5.7	31.1	6360.22	73.09	**16.8**	**84.00**	**-40.81**
3476	0	1	0.5	**71.1**	**-8.2**	339.5	82.5	6360.22	14.73	**75.2**	**82.81**	**-53.53**
3483	0	1	0.5	**-37.0**	**-13.0**	359.0	-46.0	6360.22	-62.52	**-27.4**	**-80.44**	**161.65**
3486	0	1	0.5	**-37.0**	**-13.0**	2.1	-52.5	6360.22	-56.82	**-33.1**	**-85.81**	**191.85**
3574	0	1	0.5	**-58.0**	**-26.0**	19.0	-69.0	6360.22	-37.45	**-52.5**	**-77.94**	**225.32**
3588	0	1	0.5	**19.5**	**-155.5**	10.2	36.3	6360.22	69.72	**20.2**	**80.38**	**-71.90**
3597	0	1	0.5	**23.0**	**5.0**	345.0	32.0	6360.22	72.53	**17.4**	**74.89**	**256.28**
3617	0	1	0.5	**35.7**	**139.8**	357.0	46.0	6360.22	62.52	**27.4**	**81.39**	**337.87**
3618	0	1	0.5	**52.0**	**-1.0**	3.0	58.0	6360.22	51.25	**38.7**	**76.59**	**168.87**
3657	0	1	0.5	**52.0**	**0.0**	0.0	66.5	6360.22	40.94	**49.0**	**87.06**	**180.00**
3665	0	1	0.5	**45.5**	**3.0**	353.0	62.0	6360.22	46.68	**43.2**	**84.55**	**251.90**

3666	0	1	0.5	**45.5**	**3.0**	206.0	-63.5	6360.22	-44.84	**-45.1**	**71.80**	**84.74**
3668	0	1	0.5	**37.0**	**10.0**	359.0	54.5	6360.22	54.88	**35.0**	**87.95**	**213.57**
3669	0	1	0.5	**35.7**	**139.8**	356.0	53.0	6360.22	56.34	**33.6**	**86.13**	**379.13**
3705	0	1	0.5	**37.7**	**15.0**	4.3	55.8	6360.22	53.57	**36.3**	**86.34**	**123.98**
3706	0	1	0.5	**63.0**	**18.0**	355.2	73.1	6360.22	31.23	**58.7**	**85.17**	**229.01**
3707	0	1	0.5	**43.0**	**-73.0**	355.0	51.0	6360.22	58.21	**31.7**	**78.11**	**128.08**
3709	0	1	0.5	**64.0**	**-19.0**	2.0	75.0	6360.22	28.14	**61.8**	**87.67**	**137.07**
3718	0	1	0.5	**-38.0**	**176.0**	350.0	-65.0	6360.22	-42.93	**-47.0**	**-78.34**	**211.80**
3806	0	1	0.5	**57.0**	**161.0**	4.0	62.0	6360.22	46.68	**43.2**	**76.09**	**328.82**
3807	0	1	0.5	**49.0**	**154.0**	345.0	65.0	6360.22	42.93	**47.0**	**79.80**	**418.75**
3808	0	1	0.5	**69.0**	**88.5**	273.0	83.0	6360.22	13.77	**76.2**	**65.67**	**53.25**
3809	0	1	0.5	**43.5**	**42.5**	13.0	59.0	6360.22	50.15	**39.8**	**79.64**	**148.69**
3811	0	1	0.5	**45.0**	**36.0**	8.0	75.0	6360.22	28.14	**61.8**	**72.51**	**48.62**
3812	0	1	0.5	**45.0**	**36.0**	1.0	74.0	6360.22	29.78	**60.2**	**74.77**	**37.89**
3813	0	1	0.5	**45.0**	**35.0**	6.0	70.0	6360.22	35.99	**53.9**	**80.19**	**56.14**
3814	0	1	0.5	**45.0**	**36.0**	5.0	74.0	6360.22	29.78	**60.2**	**74.50**	**45.32**
3815	0	1	0.5	**47.0**	**39.0**	8.0	72.0	6360.22	32.96	**57.0**	**78.84**	**62.03**
3816	0	1	0.5	**47.0**	**39.0**	5.0	73.0	6360.22	31.39	**58.6**	**78.01**	**51.63**
3817	0	1	0.5	**47.0**	**39.0**	6.0	73.0	6360.22	31.39	**58.6**	**77.85**	**53.99**
3818	0	1	0.5	**50.0**	**30.0**	4.0	67.0	6360.22	40.26	**49.7**	**87.41**	**124.28**
3820	0	1	0.5	**46.0**	**31.0**	340.0	76.0	6360.22	26.46	**63.5**	**69.20**	**5.58**
3821	0	1	0.5	**45.0**	**28.0**	7.0	69.0	6360.22	37.45	**52.5**	**81.16**	**56.84**
3822	0	1	0.5	**45.0**	**28.0**	9.0	70.0	6360.22	35.99	**53.9**	**79.28**	**57.62**
3823	0	1	0.5	**45.0**	**28.0**	3.0	73.0	6360.22	31.39	**58.6**	**76.27**	**34.60**
3824	0	1	0.5	**45.0**	**28.0**	337.0	75.0	6360.22	28.14	**61.8**	**68.51**	**-2.21**
3825	0	1	0.5	**45.0**	**28.0**	1.0	72.0	6360.22	32.96	**57.0**	**77.95**	**30.61**
3827	0	1	0.5	**50.5**	**105.0**	8.0	68.0	6360.22	38.88	**51.1**	**84.91**	**184.86**
3829	0	1	0.5	**57.0**	**99.0**	8.0	72.0	6360.22	32.96	**57.0**	**85.65**	**185.15**
3837	0	1	0.5	**47.0**	**23.0**	355.0	70.0	6360.22	35.99	**53.9**	**82.31**	**0.50**
3839	0	1	0.5	**41.0**	**44.0**	348.0	53.0	6360.22	56.34	**33.6**	**77.98**	**280.20**
3840	0	1	0.5	**40.5**	**44.5**	355.0	50.0	6360.22	59.11	**30.8**	**79.57**	**248.90**

3845	0	1	0.5	**40.0**	**45.5**	5.0	66.0	6360.22	41.61	**48.3**	**80.89**	**66.93**
3848	0	1	0.5	**40.0**	**45.0**	0.0	58.0	6360.22	51.25	**38.7**	**88.75**	**225.00**
3849	0	1	0.5	**40.0**	**45.5**	357.0	61.0	6360.22	47.87	**42.1**	**86.89**	**-0.23**
3851	0	1	0.5	**56.0**	**53.0**	8.0	70.0	6360.22	35.99	**53.9**	**85.00**	**163.16**
3852	0	1	0.5	**55.0**	**55.0**	10.0	67.0	6360.22	40.26	**49.7**	**81.95**	**181.71**
3853	0	1	0.5	**58.0**	**56.0**	10.0	65.0	6360.22	42.93	**47.0**	**77.52**	**202.82**
3854	0	1	0.5	**65.0**	**54.0**	351.0	73.0	6360.22	31.39	**58.6**	**82.34**	**271.68**
3855	0	1	0.5	**55.7**	**159.3**	356.0	70.0	6360.22	35.99	**53.9**	**87.14**	**394.63**
3870	0	1	0.5	**53.0**	**108.0**	351.0	75.0	6360.22	28.14	**61.8**	**79.92**	**83.06**
3871	0	1	0.5	**53.0**	**108.0**	3.0	82.0	6360.22	15.67	**74.3**	**68.64**	**110.22**
3872	0	1	0.5	**53.0**	**108.0**	353.0	77.0	6360.22	24.74	**65.2**	**77.25**	**94.64**
3874	0	1	0.5	**54.1**	**159.7**	10.0	67.0	6360.22	40.26	**49.7**	**82.46**	**280.95**
3875	0	1	0.5	**53.8**	**82.2**	6.0	68.0	6360.22	38.88	**51.1**	**85.47**	**205.99**
3898	0	1	0.5	**47.0**	**38.0**	359.0	65.0	6360.22	42.93	**47.0**	**89.32**	**-45.91**
3911	0	1	0.5	**48.0**	**22.5**	357.0	64.0	6360.22	44.21	**45.7**	**86.98**	**246.39**
3921	0	1	0.5	**56.2**	**161.0**	358.0	66.0	6360.22	41.61	**48.3**	**82.09**	**350.70**
3925	0	1	0.5	**54.0**	**56.0**	24.0	71.0	6360.22	34.50	**55.4**	**76.14**	**130.04**
3926	0	1	0.5	**54.0**	**56.0**	6.0	71.0	6360.22	34.50	**55.4**	**86.23**	**120.09**
3927	0	1	0.5	**54.0**	**56.0**	22.0	71.0	6360.22	34.50	**55.4**	**77.27**	**130.31**
3928	0	1	0.5	**42.0**	**45.0**	352.0	59.0	6360.22	50.15	**39.8**	**83.59**	**298.06**
3929	0	1	0.5	**45.0**	**147.7**	347.0	63.0	6360.22	45.46	**44.5**	**80.77**	**59.42**
5708	0	1	0.5	**46.0**	**-121.8**	0.2	65.2	6360.22	42.67	**47.3**	**88.66**	**-115.98**
5953	0	1	0.5	**43.7**	**-79.2**	2.7	43.3	6360.22	64.66	**25.2**	**71.50**	**93.09**
5955	0	1	0.5	**67.9**	**-139.8**	351.0	71.0	6360.22	34.50	**55.4**	**76.92**	**63.25**
5956	0	1	0.5	**67.8**	**-139.8**	1.0	73.5	6360.22	30.59	**59.4**	**81.60**	**36.72**
5957	0	1	0.5	**50.1**	**-118.8**	1.2	67.2	6360.22	39.99	**49.9**	**89.22**	**-22.74**
6061	0	1	0.5	**35.2**	**139.2**	4.9	47.7	6360.22	61.11	**28.8**	**82.45**	**284.51**
6062	0	1	0.5	**35.2**	**139.2**	51.8	46.7	6360.22	61.95	**27.9**	**45.81**	**223.46**
6254	0	1	0.5	**19.8**	**-155.5**	4.7	27.2	6360.22	75.46	**14.4**	**83.08**	**-16.69**
6283	0	1	0.5	**19.0**	**-109.0**	359.2	28.3	6360.22	74.81	**15.1**	**86.12**	**82.48**
6298	0	1	0.5	**22.1**	**-99.0**	357.8	31.9	6360.22	72.59	**17.3**	**84.87**	**105.19**

6313	0	1	0.5	**37.0**	**14.0**	1.0	54.0	6360.22	55.37	**34.5**	**87.49**	**174.83**
6375	0	1	0.5	**38.5**	**15.0**	356.6	54.9	6360.22	54.48	**35.4**	**85.97**	**238.37**
6389	0	1	0.5	**-37.0**	**174.5**	0.9	-57.9	6360.22	-51.36	**-38.6**	**-88.21**	**151.37**
6445	0	1	0.5	**72.0**	**-125.6**	180.0	-73.0	6360.22	-31.39	**-58.6**	**76.61**	**54.40**
6446	0	1	0.5	**49.1**	**-113.5**	354.0	73.0	6360.22	31.39	**58.6**	**79.86**	**-131.52**
6447	0	1	0.5	**49.1**	**-113.5**	150.0	-53.0	6360.22	-56.34	**-33.6**	**62.99**	**132.88**
6457	0	1	0.5	**50.7**	**-107.9**	194.9	-54.8	6360.22	-54.58	**-35.3**	**71.31**	**31.25**
6463	0	1	0.5	**50.1**	**-120.8**	10.6	65.7	6360.22	42.01	**47.9**	**82.74**	**-17.94**
6655	0	1	0.5	**-41.5**	**175.5**	176.0	53.0	6360.22	56.34	**33.6**	**-81.55**	**332.24**
6683	0	1	0.5	**40.3**	**49.9**	201.0	-45.0	6360.22	-63.33	**-26.6**	**67.91**	**171.53**
6983	0	1	0.5	**37.2**	**128.8**	357.3	58.1	6360.22	51.14	**38.8**	**87.30**	**77.59**
7241	0	1	0.5	**40.3**	**16.3**	180.5	-55.3	6360.22	-54.08	**-35.8**	**85.61**	**191.01**
7440	0	1	0.5	**19.4**	**-115.4**	2.4	31.6	6360.22	72.78	**17.1**	**86.85**	**17.96**
7516	0	1	0.5	**40.3**	**15.6**	351.3	56.1	6360.22	53.26	**36.7**	**82.32**	**260.76**
7557	0	1	0.5	**38.1**	**140.5**	6.1	56.9	6360.22	52.42	**37.5**	**85.15**	**234.84**
7558	0	1	0.5	**-35.3**	**-70.5**	2.5	-50.5	6360.22	-58.66	**-31.2**	**-85.52**	**137.99**
7579	0	1	0.5	**-21.1**	**55.5**	355.1	-47.6	6360.22	-61.19	**-28.7**	**-81.11**	**84.46**
7593	0	1	0.5	**45.8**	**85.5**	0.1	69.5	6360.22	36.73	**53.2**	**82.53**	**85.96**
7750	0	1	0.5	**19.6**	**-99.0**	1.2	34.0	6360.22	71.24	**18.6**	**88.59**	**27.49**
7792	0	1	0.5	**64.0**	**-21.1**	13.9	71.2	6360.22	34.19	**55.8**	**79.29**	**112.31**
7802	0	1	0.5	**34.0**	**138.0**	2.6	52.9	6360.22	56.44	**33.5**	**87.80**	**238.70**
7810	0	1	0.5	**-39.3**	**175.5**	18.9	-54.4	6360.22	-54.98	**-34.9**	**-74.38**	**435.53**
7811	0	1	0.5	**19.3**	**-99.2**	359.2	32.9	6360.22	71.96	**17.9**	**88.53**	**112.04**
7813	0	1	0.5	**46.0**	**3.0**	356.5	60.1	6360.22	48.91	**41.0**	**84.47**	**211.54**
7814	0	1	0.5	**63.5**	**-19.7**	11.3	76.0	6360.22	26.46	**63.5**	**84.97**	**64.78**
7816	0	1	0.5	**64.0**	**-21.0**	8.8	73.3	6360.22	30.91	**59.0**	**83.55**	**114.58**
7817	0	1	0.5	**28.7**	**-17.8**	359.8	38.8	6360.22	67.99	**21.9**	**83.31**	**163.79**
7822	0	1	0.5	**42.5**	**-116.5**	0.6	58.3	6360.22	50.92	**39.0**	**86.55**	**55.74**
8073	0	1	0.5	**26.6**	**106.7**	0.7	51.8	6360.22	57.47	**32.4**	**84.04**	**112.40**
8119	0	1	0.5	**-0.2**	**37.3**	1.0	-5.0	6360.22	-87.35	**-2.5**	**-87.35**	**15.11**
8120	0	1	0.5	**-0.2**	**37.3**	1.0	-13.0	6360.22	-83.28	**-6.6**	**-83.40**	**28.63**

8176	0	1	0.5	**19.3**	**-100.5**	0.0	39.1	6360.22	67.77	**22.1**	**87.07**	**-100.50**
8193	0	1	0.5	**38.4**	**15.0**	9.3	52.2	6360.22	57.10	**32.8**	**80.66**	**138.26**
8198	0	1	0.5	**-6.5**	**146.8**	117.6	5.9	6360.22	86.90	**3.0**	**-27.76**	**236.71**
8199	0	1	0.5	**-6.5**	**146.8**	85.8	6.3	6360.22	86.70	**3.2**	**3.79**	**233.03**
8200	0	1	0.5	**-6.5**	**146.8**	341.3	1.6	6360.22	89.05	**0.8**	**69.90**	**77.89**
8201	0	1	0.5	**-6.5**	**146.8**	191.5	-0.7	6360.22	-89.50	**-0.4**	**76.56**	**205.84**
8205	0	1	0.5	**44.8**	**4.3**	346.8	60.9	6360.22	47.99	**41.9**	**80.03**	**262.72**
119	0	2	1	**35.8**	**109.2**	180.7	-53.7	6349.66	-55.57	**-34.2**	**88.51**	**266.36**
761	0	2	1	**32.5**	**-5.0**	14.5	50.0	6349.66	59.01	**30.8**	**77.59**	**88.13**
831	0	2	1	**32.3**	**70.7**	358.6	29.7	6349.66	73.84	**15.9**	**73.81**	**255.53**
1115	0	2	1	**15.2**	**145.8**	358.7	26.0	6349.66	76.04	**13.7**	**88.23**	**371.34**
1189	0	2	1	**31.4**	**35.8**	352.8	30.8	6349.66	73.16	**16.6**	**74.04**	**241.66**
1227	0	2	1	**46.0**	**-105.0**	348.0	62.0	6349.66	46.61	**43.2**	**81.09**	**152.31**
1355	0	2	1	**19.5**	**-97.0**	359.1	30.6	6349.66	73.28	**16.5**	**87.09**	**100.23**
1586	0	2	1	**-17.7**	**168.4**	9.6	-33.0	6349.66	-71.77	**-18.0**	**-80.85**	**83.18**
1786	0	2	1	**37.0**	**14.5**	358.0	58.0	6349.66	51.16	**38.7**	**87.58**	**-25.56**
2015	0	2	1	**45.0**	**-111.0**	184.5	-64.0	6349.66	-44.14	**-45.7**	**86.73**	**-37.80**
2097	0	2	1	**28.1**	**-16.5**	4.1	34.7	6349.66	70.67	**19.1**	**80.46**	**139.47**
2221	0	2	1	**10.5**	**12.3**	4.7	15.4	6349.66	81.89	**7.8**	**84.78**	**129.13**
2234	0	2	1	**0.0**	**36.0**	1.8	-2.4	6349.66	-88.50	**-1.2**	**-87.66**	**-14.27**
2330	0	2	1	**-19.1**	**46.7**	351.0	-46.9	6349.66	-61.68	**-28.1**	**-77.64**	**86.75**
2495	0	2	1	**53.0**	**-172.0**	359.4	70.4	6349.66	35.34	**54.5**	**88.30**	**-183.80**
2516	0	2	1	**28.0**	**-16.0**	4.8	39.1	6349.66	67.66	**22.1**	**82.87**	**125.45**
2574	0	2	1	**-17.7**	**-149.4**	358.6	-32.5	6349.66	-72.09	**-17.7**	**-88.65**	**-68.51**
2588	0	2	1	**-12.2**	**44.4**	4.5	-22.0	6349.66	-78.32	**-11.4**	**-85.57**	**308.15**
2611	0	2	1	**27.8**	**17.3**	3.0	38.0	6349.66	68.43	**21.3**	**83.20**	**173.04**
2797	0	2	1	**12.0**	**43.0**	356.0	10.0	6349.66	84.68	**5.0**	**82.24**	**253.95**
2923	0	2	1	**13.7**	**107.1**	357.4	18.8	6349.66	80.07	**9.7**	**85.45**	**321.37**
2955	0	2	1	**65.5**	**-20.5**	3.6	73.7	6349.66	30.22	**59.7**	**84.05**	**141.76**
3077	0	2	1	**9.0**	**-72.0**	38.2	-5.6	6349.66	-86.90	**-2.8**	**-50.05**	**-146.08**
3179	0	2	1	**35.9**	**-106.5**	359.0	48.0	6349.66	60.75	**29.0**	**83.29**	**80.99**

3289	0	2	1	**-21.0**	**55.5**	4.7	-38.0	6349.66	-68.43	**-21.3**	**-85.58**	**-26.29**
3294	0	2	1	**37.0**	**128.5**	26.0	45.0	6349.66	63.22	**26.6**	**65.78**	**235.96**
3324	0	2	1	**39.4**	**-31.2**	2.8	58.5	6349.66	50.62	**39.2**	**87.84**	**58.43**
3381	0	2	1	**25.2**	**121.8**	16.2	30.8	6349.66	73.16	**16.6**	**72.74**	**237.62**
3390	0	2	1	**-16.0**	**168.0**	1.1	-22.2	6349.66	-78.21	**-11.5**	**-85.66**	**362.38**
3543	0	2	1	**35.0**	**139.0**	337.9	51.6	6349.66	57.56	**32.2**	**71.48**	**407.35**
3600	0	2	1	**41.0**	**-84.0**	356.5	59.0	6349.66	50.07	**39.8**	**87.13**	**165.29**
3659	0	2	1	**34.5**	**131.5**	0.0	59.0	6349.66	50.07	**39.8**	**84.57**	**131.50**
3660	0	2	1	**37.0**	**-122.0**	7.0	58.0	6349.66	51.16	**38.7**	**84.18**	**-52.52**
3664	0	2	1	**36.0**	**138.0**	359.0	49.5	6349.66	59.46	**30.3**	**84.48**	**326.99**
3671	0	2	1	**43.0**	**-115.0**	0.0	62.0	6349.66	46.61	**43.2**	**89.61**	**-115.00**
3672	0	2	1	**46.0**	**-120.0**	5.0	68.5	6349.66	38.10	**51.8**	**83.26**	**-92.74**
3673	0	2	1	**44.0**	**-103.0**	66.0	69.0	6349.66	37.39	**52.5**	**46.85**	**-48.79**
3675	0	2	1	**41.5**	**-108.5**	355.0	63.0	6349.66	45.39	**44.5**	**85.20**	**-156.40**
3676	0	2	1	**44.5**	**-109.0**	351.5	63.5	6349.66	44.77	**45.1**	**83.93**	**-189.10**
3677	0	2	1	**40.0**	**-110.0**	2.0	65.0	6349.66	42.86	**47.0**	**82.72**	**-99.21**
3678	0	2	1	**39.0**	**-109.0**	349.0	63.0	6349.66	45.39	**44.5**	**80.08**	**-161.03**
3679	0	2	1	**37.0**	**-111.5**	4.0	50.0	6349.66	59.01	**30.8**	**83.13**	**38.48**
3708	0	2	1	**35.5**	**138.5**	343.0	51.0	6349.66	58.11	**31.7**	**75.42**	**399.01**
3710	0	2	1	**64.6**	**-22.0**	181.0	-75.2	6349.66	-27.76	**-62.1**	**87.60**	**146.82**
3714	0	2	1	**-38.0**	**-70.0**	1.0	-61.0	6349.66	-47.79	**-42.1**	**-85.72**	**-79.98**
3717	0	2	1	**61.0**	**-134.0**	349.0	75.0	6349.66	28.09	**61.8**	**84.67**	**-209.41**
3783	0	2	1	**49.9**	**17.5**	10.9	72.9	6349.66	31.50	**58.4**	**79.32**	**49.72**
3826	0	2	1	**39.0**	**53.0**	7.0	52.0	6349.66	57.19	**32.6**	**81.61**	**188.41**
3838	0	2	1	**40.0**	**44.5**	355.0	52.0	6349.66	57.19	**32.6**	**81.76**	**255.25**
3841	0	2	1	**40.5**	**44.0**	338.0	51.0	6349.66	58.11	**31.7**	**70.34**	**294.99**
3842	0	2	1	**40.5**	**44.0**	347.0	56.0	6349.66	53.27	**36.5**	**79.18**	**297.77**
3843	0	2	1	**40.5**	**44.2**	348.0	53.0	6349.66	56.25	**33.6**	**78.31**	**282.76**
3844	0	2	1	**40.0**	**45.0**	2.0	45.0	6349.66	63.22	**26.6**	**76.67**	**217.23**
3846	0	2	1	**40.0**	**45.0**	1.0	47.0	6349.66	61.60	**28.2**	**78.38**	**220.63**
3847	0	2	1	**40.5**	**45.0**	356.0	57.0	6349.66	52.23	**37.6**	**85.87**	**274.91**

3850	0	2	1	**40.1**	**45.1**	0.0	56.0	6349.66	53.27	**36.5**	**86.63**	**225.10**
3865	0	2	1	**52.5**	**83.5**	358.0	66.0	6349.66	41.55	**48.3**	**85.76**	**281.74**
3876	0	2	1	**53.5**	**83.5**	348.0	65.0	6349.66	42.86	**47.0**	**80.06**	**318.55**
3877	0	2	1	**53.5**	**83.5**	4.0	71.0	6349.66	34.44	**55.4**	**86.90**	**130.28**
3878	0	2	1	**53.5**	**82.5**	356.0	68.0	6349.66	38.81	**51.1**	**86.64**	**310.70**
3879	0	2	1	**53.6**	**82.9**	358.0	68.0	6349.66	38.81	**51.1**	**87.30**	**290.55**
3880	0	2	1	**53.0**	**50.0**	359.0	64.0	6349.66	44.14	**45.7**	**82.83**	**235.59**
3881	0	2	1	**47.0**	**47.0**	8.0	59.0	6349.66	50.07	**39.8**	**80.86**	**184.77**
3882	0	2	1	**47.0**	**47.0**	349.0	56.0	6349.66	53.27	**36.5**	**76.89**	**269.38**
3883	0	2	1	**47.0**	**47.0**	0.0	58.0	6349.66	51.16	**38.7**	**81.84**	**227.00**
3884	0	2	1	**42.0**	**44.0**	359.0	70.0	6349.66	35.93	**53.9**	**77.91**	**41.20**
3885	0	2	1	**42.0**	**44.0**	359.0	60.0	6349.66	48.94	**40.9**	**88.80**	**262.76**
3886	0	2	1	**42.5**	**44.5**	13.0	45.0	6349.66	63.22	**26.6**	**71.03**	**186.34**
3887	0	2	1	**42.2**	**44.2**	5.0	59.0	6349.66	50.07	**39.8**	**85.60**	**163.57**
3888	0	2	1	**42.0**	**44.0**	359.0	47.0	6349.66	61.60	**28.2**	**76.38**	**227.74**
3889	0	2	1	**41.0**	**44.0**	6.0	60.0	6349.66	48.94	**40.9**	**85.47**	**131.32**
3890	0	2	1	**41.0**	**44.0**	4.0	58.0	6349.66	51.16	**38.7**	**86.25**	**167.90**
3891	0	2	1	**41.4**	**44.3**	3.0	67.0	6349.66	40.20	**49.7**	**81.34**	**57.26**
3892	0	2	1	**41.3**	**44.1**	3.0	58.0	6349.66	51.16	**38.7**	**86.63**	**180.15**
3906	0	2	1	**49.0**	**33.0**	2.0	65.0	6349.66	42.86	**47.0**	**87.71**	**176.56**
3907	0	2	1	**47.0**	**30.0**	357.0	71.0	6349.66	34.44	**55.4**	**81.24**	**18.80**
3908	0	2	1	**47.0**	**30.0**	356.0	64.0	6349.66	44.14	**45.7**	**87.02**	**278.97**
3909	0	2	1	**47.0**	**30.0**	357.0	68.0	6349.66	38.81	**51.1**	**85.37**	**6.00**
3922	0	2	1	**52.7**	**47.0**	15.0	61.0	6349.66	47.79	**42.1**	**75.46**	**177.20**
3923	0	2	1	**47.3**	**47.0**	9.0	51.0	6349.66	58.11	**31.7**	**73.13**	**199.77**
3924	0	2	1	**43.0**	**47.4**	20.0	40.0	6349.66	67.02	**22.8**	**64.03**	**181.43**
5954	0	2	1	**62.8**	**-136.8**	179.0	-71.5	6349.66	-33.68	**-56.2**	**83.50**	**48.11**
6118	0	2	1	**64.2**	**-21.6**	350.7	76.3	6349.66	25.91	**64.0**	**85.95**	**-108.90**
6134	0	2	1	**9.6**	**8.8**	341.6	-8.8	6349.66	-85.29	**-4.4**	**-66.74**	**61.61**
6345	0	2	1	**23.5**	**121.3**	184.4	-23.5	6349.66	-77.48	**-12.3**	**78.26**	**279.71**
6347	0	2	1	**23.0**	**121.2**	190.0	-31.2	6349.66	-72.91	**-16.8**	**78.91**	**241.58**

6382	0	2	1	**34.4**	**-119.1**	199.8	-52.0	6349.66	-57.19	**-32.6**	**73.46**	**-29.16**
6656	0	2	1	**-38.5**	**175.5**	178.7	64.4	6349.66	43.63	**46.2**	**-82.08**	**182.02**
6674	0	2	1	**2.7**	**98.9**	185.4	-4.7	6349.66	-87.36	**-2.4**	**84.61**	**189.36**
6684	0	2	1	**41.1**	**71.7**	182.0	-54.0	6349.66	-55.28	**-34.5**	**83.43**	**237.19**
6984	0	2	1	**35.0**	**139.0**	3.3	49.0	6349.66	59.89	**29.9**	**84.37**	**288.48**
6991	0	2	1	**32.9**	**128.9**	8.8	54.2	6349.66	55.08	**34.7**	**82.43**	**201.04**
6998	0	2	1	**-22.5**	**-151.3**	218.2	39.5	6349.66	67.38	**22.4**	**-54.82**	**#####**
7149	0	2	1	**-40.0**	**175.3**	188.2	53.4	6349.66	55.86	**34.0**	**-81.22**	**405.97**
7229	0	2	1	**34.4**	**-118.6**	205.1	-54.3	6349.66	-54.99	**-34.8**	**69.41**	**-37.50**
7230	0	2	1	**34.3**	**-118.5**	179.9	-47.5	6349.66	-61.18	**-28.6**	**84.52**	**62.42**
7258	0	2	1	**41.0**	**71.4**	2.0	54.0	6349.66	55.28	**34.5**	**83.52**	**236.66**
7463	0	2	1	**34.0**	**80.4**	10.9	48.5	6349.66	60.33	**29.5**	**79.79**	**192.49**
7577	0	2	1	**-17.7**	**-149.6**	181.1	32.0	6349.66	72.41	**17.4**	**-88.95**	**114.67**
7646	0	2	1	**29.1**	**-13.5**	359.3	41.6	6349.66	65.84	**23.9**	**85.02**	**173.87**
7663	0	2	1	**48.8**	**-113.5**	349.6	61.4	6349.66	47.32	**42.5**	**80.52**	**120.19**
7745	0	2	1	**-38.5**	**176.0**	6.7	-60.4	6349.66	-48.49	**-41.4**	**-84.05**	**118.55**
7774	0	2	1	**48.8**	**-113.5**	349.6	61.4	6349.66	47.32	**42.5**	**80.52**	**120.19**
7787	0	2	1	**-37.0**	**174.9**	1.3	-51.8	6349.66	-57.38	**-32.4**	**-85.49**	**368.98**
7797	0	2	1	**35.0**	**139.0**	355.3	54.8	6349.66	54.49	**35.3**	**86.13**	**57.93**
7815	0	2	1	**66.0**	**-17.2**	6.4	76.0	6349.66	26.42	**63.5**	**86.36**	**111.42**
8159	0	2	1	**39.0**	**37.0**	152.1	-49.2	6349.66	-59.72	**-30.1**	**65.57**	**294.66**
8171	0	2	1	**62.8**	**-137.3**	172.0	-71.0	6349.66	-34.44	**-55.4**	**81.70**	**75.72**

Table A4.1 Recent sample site details, structure corrected data and derived actual palaeomagnetic data. (Data after McElhinny & Lock, 1996)

Table A4.2 Pliocene Palaeomagnetic Data

Site Details						Structure Corrected		Derived Actual Paleomagnetic Data				
Number	Age	Age	Age	Site	Site	Correct	Correct	Paleo	Paleo	Palaeo	Pole	Pole
Result	Low Mag	High Mag	Mean	Lat	Long	Dec	Inc	Radius	Colatitude	Latitude	Latitude	Longitude
1367	0	1	0.5	**18.5**	**-72.5**	358.0	11.0	6360.22	84.31	**5.6**	**77.04**	**116.41**
2159	0	1	0.5	**52.5**	**-2.8**	290.0	2.0	6360.22	88.85	**1.0**	**12.95**	**251.78**
2969	0	1	0.5	**8.5**	**-71.2**	358.0	10.0	6360.22	84.82	**5.0**	**86.13**	**139.81**
3315	0	1	0.5	**-29.5**	**30.8**	343.0	-56.0	6360.22	-53.36	**-36.5**	**-74.10**	**89.70**
6061	0	1	0.5	**35.2**	**139.2**	4.9	47.7	6360.22	61.11	**28.8**	**82.45**	**284.51**
6062	0	1	0.5	**35.2**	**139.2**	51.8	46.7	6360.22	61.95	**27.9**	**45.81**	**223.46**
6983	0	1	0.5	**37.2**	**128.8**	8.3	61.7	6360.22	47.04	**42.9**	**81.44**	**173.99**
7516	0	1	0.5	**40.3**	**15.6**	351.3	56.1	6360.22	53.26	**36.7**	**82.32**	**260.76**
7593	0	1	0.5	**45.8**	**85.5**	2.3	68.1	6360.22	38.73	**51.2**	**84.33**	**100.22**
8073	0	1	0.5	**26.6**	**106.7**	22.6	17.6	6360.22	80.85	**9.0**	**62.40**	**231.73**
8198	0	1	0.5	**-6.5**	**146.8**	117.6	5.9	6360.22	86.90	**3.0**	**-27.76**	**236.71**
8199	0	1	0.5	**-6.5**	**146.8**	85.8	6.3	6360.22	86.70	**3.2**	**3.79**	**233.03**
8200	0	1	0.5	**-6.5**	**146.8**	338.4	-31.3	6360.22	-72.97	**-16.9**	**-66.41**	**208.39**
8201	0	1	0.5	**-6.5**	**146.8**	191.5	-0.7	6360.22	-89.50	**-0.4**	**76.56**	**205.84**
3077	0	2	1	**9.0**	**-72.0**	39.8	3.9	6349.66	87.76	**2.0**	**49.85**	**25.25**
6345	0	2	1	**23.5**	**121.3**	184.4	-23.5	6349.66	-77.48	**-12.3**	**78.26**	**279.71**
6347	0	2	1	**23.0**	**121.2**	190.0	-31.2	6349.66	-72.91	**-16.8**	**78.91**	**241.58**
7463	0	2	1	**34.0**	**80.4**	18.8	31.7	6349.66	72.60	**17.2**	**66.37**	**210.31**
6237	1	3	2	**40.5**	**16.5**	157.8	-56.1	6328.61	-52.99	**-36.7**	**72.39**	**282.23**
369	0	5	2.5	**37.4**	**-121.3**	181.1	52.0	6318.13	56.91	**32.6**	**-19.50**	**-122.28**
370	0	5	2.5	**39.0**	**-122.5**	68.0	61.0	6318.13	47.55	**42.1**	**39.76**	**-59.63**
373	0	5	2.5	**42.3**	**-124.2**	327.0	66.6	6318.13	40.54	**49.1**	**66.15**	**-185.32**
2539	0	5	2.5	**53.6**	**-9.6**	355.0	58.0	6318.13	50.91	**38.7**	**75.09**	**185.65**
2709	0	5	2.5	**-24.0**	**-65.0**	168.0	52.0	6318.13	56.91	**32.6**	**-76.10**	**-18.53**
8072	0	5	2.5	**26.6**	**106.7**	3.4	15.6	6318.13	81.37	**7.9**	**71.74**	**275.91**

8156	0	5	2.5	**37.3**	**128.5**	202.7	-24.6	6318.13	-76.47	**-12.9**	**58.79**	**262.11**
6348	1	4	2.5	**23.0**	**121.2**	214.4	-26.6	6318.13	-75.32	**-14.1**	**56.49**	**219.38**
7510	1	4	2.5	**42.0**	**12.5**	357.8	52.0	6318.13	56.91	**32.6**	**80.92**	**204.26**
6343	2	3	2.5	**24.0**	**121.2**	184.4	-31.0	6318.13	-72.67	**-16.7**	**82.16**	**268.72**
1135	1	5	3	**33.0**	**73.0**	353.6	38.9	6307.66	67.35	**22.0**	**78.21**	**283.22**
6346	2	4	3	**23.5**	**121.2**	203.0	-26.9	6307.66	-75.02	**-14.2**	**66.72**	**228.49**
3391	2	5	3.5	**35.0**	**36.0**	170.1	-36.2	6297.22	-69.09	**-20.1**	**73.44**	**250.29**
6249	2	5	3.5	**31.5**	**35.3**	25.1	46.9	6297.22	61.17	**28.1**	**68.18**	**125.82**
7583	2	5	3.5	**41.5**	**19.6**	205.0	-48.0	6297.22	-60.25	**-29.0**	**66.65**	**131.81**
7710	2	6	4	**24.8**	**125.4**	178.5	-27.0	6286.81	-74.71	**-14.3**	**80.39**	**314.10**
720	3	5	4	**37.1**	**14.5**	353.5	54.0	6286.81	54.73	**34.5**	**84.44**	**267.18**
6344	3	5	4	**24.0**	**121.2**	218.2	-30.0	6286.81	-72.92	**-16.1**	**53.68**	**214.81**
750	4	5	4.5	**43.1**	**10.5**	179.0	-58.0	6276.41	-50.57	**-38.7**	**86.25**	**202.40**
1024	0	10	5	**39.9**	**139.8**	10.1	54.9	6266.04	53.67	**35.4**	**81.29**	**250.83**
6565	0	10	5	**1.3**	**110.3**	358.4	-3.7	6266.04	-86.70	**-1.9**	**-85.13**	**129.46**
7819	3	7	5	**43.2**	**11.0**	177.3	-56.9	6266.04	-51.65	**-37.5**	**84.74**	**214.76**
1141	3	8	5.5	**-27.0**	**-66.5**	26.6	46.9	6255.70	60.77	**28.1**	**28.26**	**-40.17**
6225	3	8	5.5	**38.4**	**-122.4**	178.0	-46.5	6255.70	-61.09	**-27.8**	**80.36**	**68.12**

Table A4.2 Pliocene sample site details, structure corrected data and derived actual palaeomagnetic data. (Data after McElhinny & Lock, 1996)

Table A4.3 Miocene Palaeomagnetic Data

Site Details						Structure Corrected		Derived Actual Paleomagnetic Data				
Number	Age	Age	Age	Site	Site	Correct	Correct	Paleo	Paleo	Palaeo	Pole	Pole
Result	Low Mag	High Mag	Mean	Lat	Long	Dec	Inc	Radius	Colatitude	Latitude	Latitude	Longitude
6578	2	10	6	**-9.5**	**161.4**	6.6	-15.5	6245.38	-80.49	**-7.9**	**-83.49**	**72.04**
7157	5	7	6	**40.0**	**141.0**	2.0	58.9	6245.38	49.35	**39.7**	**88.34**	**207.42**
7503	5	7	6	**-41.8**	**174.1**	208.3	59.9	6245.38	48.25	**40.8**	**-68.99**	**93.50**
7734	5	7	6	**42.0**	**13.2**	332.0	42.0	6245.38	64.47	**24.2**	**61.70**	**256.53**
7735	5	7	6	**41.8**	**14.0**	184.0	-48.0	6245.38	-59.76	**-29.0**	**78.00**	**177.15**
8236	5	7	6	**42.7**	**13.6**	180.1	-41.4	6245.38	-64.91	**-23.8**	**72.39**	**193.30**
8237	5	7	6	**43.5**	**13.0**	169.7	-48.4	6245.38	-59.42	**-29.4**	**74.71**	**228.72**
7727	3	10	6.5	**43.5**	**17.8**	184.0	-51.0	6235.08	-57.06	**-31.7**	**78.98**	**179.96**
428	5	10	7.5	**47.3**	**7.2**	215.3	83.0	6214.55	13.46	**76.2**	**35.87**	**-2.35**
408	7	8	7.5	**36.2**	**-106.2**	320.2	53.1	6214.55	54.96	**33.7**	**57.86**	**-186.26**
1241	2	14	8	**38.5**	**24.0**	228.7	-45.8	6204.32	-61.15	**-27.2**	**48.83**	**112.45**
358	5	11	8	**15.9**	**120.5**	16.7	28.3	6204.32	72.97	**15.1**	**73.95**	**204.12**
359	5	11	8	**12.2**	**123.4**	355.0	17.2	6204.32	79.08	**8.8**	**84.94**	**379.27**
7245	6	11	8.5	**31.7**	**131.4**	152.0	-48.6	6194.12	-58.76	**-29.6**	**66.18**	**47.72**
7120	7	10	8.5	**37.9**	**-1.6**	332.0	15.0	6194.12	80.08	**7.6**	**52.38**	**227.66**
7582	5	14	9.5	**41.5**	**19.6**	35.0	44.0	6173.78	62.24	**25.8**	**58.38**	**124.12**
1788	8	11	9.5	**37.0**	**14.5**	173.0	-49.0	6173.78	-58.23	**-29.9**	**82.21**	**244.34**
8067	9	11	10	**41.5**	**2.0**	2.0	46.0	6163.64	60.59	**27.4**	**77.80**	**173.73**
8197	5	16	10.5	**36.8**	**139.3**	7.2	50.3	6153.53	56.93	**31.1**	**83.02**	**259.50**
390	9	14	11.5	**36.5**	**137.0**	357.5	55.6	6133.37	51.85	**36.1**	**87.42**	**87.37**
1023	10	14	12	**39.9**	**139.8**	4.5	63.2	6123.32	43.53	**44.7**	**82.66**	**164.83**
6963	10	14	12	**14.3**	**-87.4**	1.7	38.8	6123.32	65.45	**21.9**	**79.63**	**-78.78**
7156	10	14	12	**40.0**	**141.0**	175.1	-56.9	6123.32	-50.47	**-37.5**	**86.20**	**405.43**
6883	11	13	12	**37.0**	**-116.3**	166.6	-53.1	6123.32	-54.15	**-33.7**	**79.17**	**151.63**
7556	11	13	12	**36.2**	**138.6**	214.7	-51.2	6123.32	-55.87	**-31.9**	**61.71**	**222.43**

1246	7	18	12.5	**39.0**	**27.0**	327.0	52.0	6113.30	55.06	**32.6**	**63.47**	**-61.41**
1069	11	14	12.5	**36.3**	**136.9**	1.8	47.4	6113.30	58.98	**28.5**	**84.51**	**300.55**
3386	10	16	13	**23.5**	**121.4**	181.3	-25.2	6103.30	-73.54	**-13.2**	**82.86**	**291.32**
6995	10	16	13	**31.3**	**131.0**	154.7	-40.8	6103.30	-63.86	**-23.3**	**67.28**	**394.29**
7257	11	15	13	**35.2**	**-120.8**	218.2	-40.9	6103.30	-63.79	**-23.4**	**56.17**	**-26.12**
7497	12	15	13.5	**42.8**	**141.9**	22.0	51.0	6093.32	55.77	**31.7**	**70.85**	**251.14**
1806	5	23	14	**30.5**	**111.5**	357.8	62.8	6083.37	43.72	**44.2**	**74.13**	**105.93**
6184	5	23	14	**15.2**	**147.8**	208.1	-30.7	6083.37	-70.15	**-16.5**	**62.84**	**223.84**
6265	5	23	14	**39.4**	**21.8**	15.0	37.0	6083.37	66.23	**20.6**	**69.88**	**158.30**
7601	5	23	14	**23.5**	**100.8**	23.9	51.6	6083.37	55.15	**32.2**	**66.34**	**156.73**
332	12	16	14	**34.0**	**-118.8**	305.9	-27.3	6083.37	-72.12	**-14.5**	**-16.92**	**-65.11**
5719	4	26	15	**41.0**	**114.7**	8.2	61.5	6063.53	45.07	**42.6**	**82.83**	**168.76**
1200	5	25	15	**30.0**	**91.0**	357.1	21.8	6063.53	74.90	**11.3**	**74.87**	**281.78**
1244	10	20	15	**40.0**	**26.5**	186.0	-54.0	6063.53	-52.79	**-34.5**	**84.55**	**145.35**
1022	13	17	15	**39.9**	**139.8**	359.8	58.4	6063.53	48.44	**39.1**	**88.34**	**134.64**
5973	13	17	15	**35.0**	**-117.0**	347.1	47.5	6063.53	58.42	**28.6**	**78.70**	**139.03**
7081	8	23	15.5	**24.9**	**121.4**	185.9	-43.8	6053.64	-61.18	**-25.6**	**83.44**	**173.40**
1070	13	18	15.5	**35.1**	**135.5**	2.8	47.3	6053.64	58.49	**28.5**	**85.72**	**281.59**
5964	14	17	15.5	**40.8**	**-116.5**	339.0	62.0	6053.64	44.43	**43.2**	**74.02**	**-182.16**
6966	14	17	15.5	**38.0**	**-117.0**	353.4	61.3	6053.64	45.23	**42.4**	**81.62**	**-151.03**
6967	14	17	15.5	**38.0**	**-117.0**	346.3	47.8	6053.64	58.08	**28.9**	**77.25**	**128.62**
6990	12	20	16	**32.9**	**128.9**	357.7	45.4	6043.78	59.87	**26.9**	**86.60**	**344.76**
263	10	23	16.5	**35.2**	**-118.3**	353.7	63.7	6033.94	42.31	**45.3**	**76.65**	**-136.96**
360	10	23	16.5	**13.4**	**122.0**	302.6	9.3	6033.94	80.81	**4.7**	**33.67**	**34.21**
361	10	23	16.5	**10.2**	**123.8**	23.9	17.6	6033.94	76.71	**9.0**	**66.41**	**203.91**
6664	10	23	16.5	**37.5**	**139.0**	335.9	47.0	6033.94	58.53	**28.2**	**69.31**	**399.25**
1007	15	19	17	**38.3**	**27.0**	151.0	-49.0	6024.12	-56.82	**-29.9**	**66.01**	**293.58**
1008	16	18	17	**39.1**	**26.2**	6.0	49.5	6024.12	56.41	**30.3**	**82.68**	**163.12**
7155	16	18	17	**40.0**	**141.0**	145.6	-60.0	6024.12	-46.43	**-40.9**	**64.29**	**70.34**
7789	16	18	17	**34.8**	**138.0**	4.4	59.6	6024.12	46.86	**40.4**	**80.99**	**158.95**
1071	15	20	17.5	**35.9**	**136.0**	34.4	49.8	6014.32	56.07	**30.6**	**61.87**	**219.82**

7733	14	23	18.5	**41.9**	**12.9**	196.0	-43.0	5994.79	-61.17	**-25.0**	**71.60**	**143.01**
6272	15	22	18.5	**42.6**	**9.0**	153.0	-49.5	5994.79	-56.13	**-30.3**	**67.19**	**265.49**
389	15	23	19	**36.5**	**137.0**	193.0	-52.7	5985.06	-53.29	**-33.3**	**79.57**	**221.95**
1063	16	22	19	**36.0**	**139.0**	273.7	-52.0	5985.06	-53.91	**-32.6**	**17.70**	**196.83**
5960	16	23	19.5	**34.8**	**-116.5**	41.7	56.8	5975.35	49.35	**37.4**	**56.82**	**-49.25**
6178	16	23	19.5	**7.5**	**134.6**	234.5	-3.5	5975.35	-82.77	**-1.8**	**35.99**	**221.09**
6663	16	23	19.5	**36.2**	**136.3**	220.9	-49.4	5975.35	-56.03	**-30.3**	**56.70**	**217.86**
6988	16	23	19.5	**32.9**	**128.9**	152.8	-45.5	5975.35	-59.12	**-27.0**	**66.88**	**41.28**
7158	16	23	19.5	**41.1**	**140.3**	115.1	-55.6	5975.35	-50.52	**-36.1**	**41.66**	**70.99**
7271	16	23	19.5	**42.2**	**76.7**	357.0	59.0	5975.35	47.12	**39.8**	**87.69**	**4.89**
7488	16	23	19.5	**38.0**	**69.0**	310.0	33.0	5975.35	67.54	**18.0**	**44.69**	**333.78**
7489	16	23	19.5	**38.0**	**68.6**	167.0	-33.0	5975.35	-67.54	**-18.0**	**70.87**	**287.97**
7490	16	23	19.5	**37.7**	**68.2**	336.0	30.0	5975.35	69.31	**16.1**	**63.16**	**305.63**
7491	16	23	19.5	**38.1**	**67.4**	349.0	35.0	5975.35	66.32	**19.3**	**72.80**	**283.62**
8110	16	23	19.5	**30.0**	**31.0**	198.0	-24.0	5975.35	-72.64	**-12.6**	**69.28**	**154.54**
8111	16	23	19.5	**30.0**	**31.0**	197.0	-51.0	5975.35	-54.69	**-31.7**	**74.76**	**96.17**
7513	10	30	20	**42.1**	**1.8**	245.8	62.9	5965.67	42.76	**44.3**	**16.60**	**-38.46**
6486	14	26	20	**41.5**	**116.0**	358.5	59.0	5965.67	47.04	**39.8**	**88.17**	**79.24**
7228	14	26	20	**41.0**	**116.2**	358.5	59.0	5965.67	47.04	**39.8**	**87.75**	**87.06**
532	15	25	20	**7.5**	**134.5**	234.5	-3.5	5965.67	-82.64	**-1.8**	**36.00**	**220.82**
582	12	29	20.5	**35.0**	**33.0**	350.0	42.0	5956.00	61.48	**24.2**	**79.32**	**268.41**
7248	18	24	21	**35.0**	**-117.0**	0.0	55.2	5946.36	50.65	**35.7**	**85.65**	**-117.00**
7249	18	24	21	**35.0**	**-117.0**	18.8	45.3	5946.36	58.98	**26.8**	**73.77**	**-18.10**
7154	20	23	21.5	**40.0**	**141.0**	123.0	-54.8	5936.74	-50.95	**-35.3**	**46.80**	**68.93**
1021	18	26	22	**39.9**	**139.8**	307.4	51.0	5927.14	54.25	**31.7**	**48.85**	**61.38**
739	5	40	22.5	**29.2**	**89.5**	220.7	-31.3	5917.56	-67.89	**-16.9**	**52.82**	**180.84**
6579	10	35	22.5	**-9.5**	**161.4**	7.6	-30.5	5917.56	-68.35	**-16.4**	**-75.83**	**131.26**
7496	15	30	22.5	**42.8**	**141.9**	209.0	-64.0	5917.56	-41.14	**-45.7**	**69.05**	**205.02**
7487	16	29	22.5	**38.8**	**69.6**	317.0	33.5	5917.56	66.59	**18.3**	**50.54**	**329.55**
7603	16	29	22.5	**23.5**	**100.7**	21.1	35.5	5917.56	65.36	**19.6**	**70.72**	**183.02**
7691	20	25	22.5	**11.1**	**-69.5**	3.0	8.0	5917.56	79.86	**4.0**	**86.90**	**38.31**

331	14	32	23	**34.0**	**-119.6**	72.6	36.1	5908.00	64.89	**20.0**	**27.50**	**-42.66**
344	18	28	23	**41.9**	**-122.4**	4.9	57.6	5908.00	48.01	**38.2**	**86.35**	**-35.52**
6922	21	25	23	**57.1**	**-133.6**	202.0	-58.0	5908.00	-47.61	**-38.7**	**69.72**	**-6.57**
356	22	24	23	**38.0**	**-107.3**	166.2	-65.3	5908.00	-39.52	**-47.4**	**74.13**	**-141.01**

Table A4.3 Miocene sample site details, structure corrected data and derived actual palaeomagnetic data. (Data after McElhinny & Lock, 1996)

Table A4.4 Oligocene Palaeomagnetic Data

Site Details						Structure Corrected		Derived Actual Paleomagnetic Data				
Number	Age	Age	Age	Site	Site	Correct	Correct	Paleo	Paleo	Palaeo	Pole	Pole
Result	Low Mag	High Mag	Mean	Lat	Long	Dec	Inc	Radius	Colatitude	Latitude	Latitude	Longitude
325	21	27	24	**34.8**	**-118.4**	33.5	53.2	5888.96	51.99	**33.8**	**62.99**	**-45.13**
6552	15	34	24.5	**-22.6**	**-68.3**	20.0	-27.0	5879.47	-69.87	**-14.3**	**-71.23**	**197.90**
1072	21	28	24.5	**36.0**	**136.3**	55.3	51.6	5879.47	53.30	**32.2**	**46.10**	**208.22**
8230	20	30	25	**32.5**	**130.4**	200.1	-44.5	5870.00	-58.82	**-26.2**	**72.90**	**219.42**
7121	21	29	25	**37.9**	**-1.6**	322.0	-44.0	5870.00	-59.18	**-25.8**	**-12.66**	**31.21**
8091	16	35	25.5	**38.2**	**66.3**	3.0	30.0	5860.55	67.98	**16.1**	**73.62**	**236.40**
8228	16	35	25.5	**33.3**	**129.8**	353.0	52.9	5860.55	52.00	**33.5**	**82.63**	**81.35**
7153	25	27	26	**40.0**	**141.0**	134.9	-57.3	5851.12	-47.84	**-37.9**	**56.33**	**69.71**
7276	16	38	27	**41.3**	**71.3**	342.0	34.0	5832.33	65.33	**18.6**	**67.63**	**298.85**
354	26	28	27	**36.8**	**-105.4**	350.0	50.8	5832.33	53.55	**31.5**	**81.97**	**-194.87**
5725	10	45	27.5	**28.4**	**84.0**	277.4	46.3	5822.97	57.02	**27.6**	**20.73**	**21.20**
5726	10	45	27.5	**28.4**	**84.0**	182.8	-60.2	5822.97	-44.67	**-41.1**	**72.93**	**90.72**
7492	16	39	27.5	**37.7**	**68.1**	312.0	32.0	5822.97	66.40	**17.4**	**46.88**	**333.21**
537	23	35	29	**39.8**	**20.9**	58.0	38.8	5795.01	61.94	**21.9**	**41.33**	**106.16**
6181	23	35	29	**13.3**	**144.7**	66.1	15.1	5795.01	74.88	**7.7**	**26.14**	**224.18**
6239	23	35	29	**40.0**	**20.2**	222.4	-27.8	5795.01	-68.43	**-14.8**	**49.67**	**124.50**
6370	23	35	29	**34.5**	**-120.0**	80.1	38.9	5795.01	61.88	**22.0**	**23.07**	**-49.20**
6541	23	35	29	**56.2**	**162.2**	130.0	-59.0	5795.01	-45.69	**-39.8**	**56.75**	**72.86**
7122	23	35	29	**37.9**	**-1.6**	39.0	-28.0	5795.01	-68.32	**-14.9**	**-20.06**	**-40.10**
7272	23	35	29	**42.4**	**78.2**	0.0	44.0	5795.01	58.42	**25.8**	**79.18**	**258.20**
7581	23	35	29	**41.5**	**19.6**	225.0	-41.0	5795.01	-60.50	**-23.5**	**51.93**	**113.22**
7643	23	35	29	**33.9**	**76.5**	182.4	12.2	5795.01	76.25	**6.2**	**-42.30**	**73.35**
8229	23	35	29	**34.9**	**130.7**	35.9	45.3	5795.01	57.48	**26.8**	**60.20**	**214.92**
6179	26	32	29	**7.5**	**134.6**	68.4	5.3	5795.01	79.45	**2.7**	**22.50**	**216.24**
7804	15	45	30	**-42.5**	**-72.5**	344.6	-62.8	5776.47	-41.52	**-44.2**	**-77.69**	**-16.86**

588	20	40	30	**39.8**	**142.0**	0.0	63.5	5776.47	40.73	**45.1**	**80.53**	**142.00**
8209	20	40	30	**20.4**	**58.8**	282.0	75.2	5776.47	25.25	**62.1**	**23.48**	**31.74**
391	24	36	30	**33.3**	**-107.9**	171.0	-47.3	5776.47	-55.81	**-28.5**	**82.47**	**-188.61**
533	25	35	30	**7.5**	**134.5**	66.7	5.2	5776.47	79.24	**2.6**	**24.18**	**216.03**
3226	5	56	30.5	**36.8**	**30.3**	329.0	37.0	5767.24	62.78	**20.6**	**62.17**	**289.13**
6569	5	56	30.5	**1.1**	**110.9**	193.3	-30.6	5767.24	-66.56	**-16.5**	**64.20**	**139.91**
6570	5	56	30.5	**1.1**	**110.9**	318.7	24.3	5767.24	69.96	**12.7**	**45.42**	**48.86**
615	15	46	30.5	**34.6**	**76.1**	8.1	40.8	5767.24	60.34	**23.3**	**81.55**	**199.65**
616	15	46	30.5	**34.6**	**76.1**	15.2	49.1	5767.24	54.32	**30.0**	**77.54**	**156.78**
7512	29	35	32	**42.1**	**1.8**	340.4	50.5	5739.65	52.94	**31.2**	**74.12**	**259.81**
1013	29	39	34	**52.9**	**-168.2**	32.2	72.1	5703.17	29.42	**57.1**	**70.99**	**-114.74**
469	31	37	34	**46.2**	**-121.8**	27.0	63.5	5703.17	40.21	**45.1**	**71.68**	**-52.95**
1020	29	40	34.5	**39.9**	**139.8**	141.7	-53.8	5694.10	-49.75	**-34.3**	**60.92**	**63.06**
2970	5	65	35	**8.1**	**-71.3**	216.0	10.0	5685.05	75.82	**5.0**	**-47.90**	**-129.52**
6588	12	58	35	**-35.5**	**174.2**	61.6	-47.6	5685.05	-54.70	**-28.7**	**-40.66**	**103.05**
6215	20	50	35	**16.5**	**102.0**	38.2	28.4	5685.05	66.81	**15.1**	**53.56**	**175.13**
534	30	40	35	**7.5**	**134.5**	101.5	-15.4	5685.05	-73.31	**-7.8**	**13.11**	**59.97**
1088	32	38	35	**68.2**	**-31.0**	27.0	-81.0	5685.05	-15.68	**-72.4**	**53.56**	**-42.92**
8196	32	38	35	**43.5**	**13.5**	13.0	45.0	5685.05	56.61	**26.6**	**75.69**	**144.06**
5988	34	36	35	**39.6**	**-114.6**	324.4	58.9	5685.05	44.93	**39.7**	**63.35**	**-181.01**
5989	34	36	35	**39.7**	**-114.6**	354.5	49.1	5685.05	53.55	**30.0**	**84.59**	**120.26**
5990	34	36	35	**39.6**	**-114.3**	295.3	63.2	5685.05	40.42	**44.7**	**44.33**	**-169.33**
7247	32	39	35.5	**43.4**	**12.6**	13.0	45.0	5676.02	56.52	**26.6**	**75.82**	**142.62**
7160	30	42	36	**46.0**	**10.5**	13.0	49.8	5667.01	52.83	**30.6**	**76.90**	**138.25**
306	35	39	37	**46.3**	**-123.0**	194.1	-56.0	5649.05	-47.40	**-36.5**	**79.30**	**-17.89**
6182	35	39	37	**13.3**	**144.7**	55.3	-7.8	5649.05	-76.33	**-3.9**	**-28.94**	**78.79**
7097	35	39	37	**-38.8**	**143.4**	23.8	-72.4	5649.05	-28.72	**-57.6**	**-63.15**	**117.97**
7514	35	39	37	**42.1**	**1.8**	25.9	11.8	5649.05	74.52	**6.0**	**55.31**	**134.11**
7580	35	39	37	**41.5**	**19.6**	229.0	-40.0	5649.05	-59.62	**-22.8**	**49.38**	**109.27**
6566	10	65	37.5	**1.3**	**110.3**	120.0	-6.1	5640.11	-76.97	**-3.1**	**29.48**	**34.55**
343	15	60	37.5	**64.5**	**-128.5**	244.0	88.0	5640.11	3.54	**86.0**	**62.78**	**-135.46**

1745	15	60	37.5	**64.6**	**-127.9**	9.0	79.0	5640.11	18.81	**68.8**	**82.61**	**-104.83**
8036	25	50	37.5	**22.5**	**-83.9**	332.0	28.0	5640.11	66.50	**14.9**	**64.25**	**-166.15**
8037	25	50	37.5	**22.5**	**-83.9**	293.0	74.0	5640.11	26.41	**60.2**	**30.22**	**-112.19**

Table A4.4 Oligocene sample site details, structure corrected data and derived actual palaeomagnetic data. (Data after McElhinny & Lock, 1996)

Table A4.5 Eocene
Palaeomagnetic Data

Site Details						Structure Corrected		Derived Actual Paleomagnetic Data				
Number	Age	Age	Age	Site	Site	Correct	Correct	Paleo	Paleo	Palaeo	Pole	Pole
Result	Low Mag	High Mag	Mean	Lat	Long	Dec	Inc	Radius	Colatitude	Latitude	Latitude	Longitude
7274	16	60	38	**42.4**	**77.1**	182.2	-48.7	5631.18	-53.35	**-29.6**	**84.01**	**239.94**
535	33	43	38	**7.5**	**134.5**	68.8	21.4	5631.18	69.75	**11.1**	**22.43**	**205.64**
1012	34	42	38	**52.1**	**-173.9**	58.7	78.6	5631.18	19.41	**68.0**	**58.24**	**-141.24**
459	32	45	38.5	**46.0**	**-122.5**	18.5	57.5	5622.27	45.78	**38.1**	**76.85**	**-31.39**
476	23	56	39.5	**40.6**	**-122.6**	355.2	42.8	5604.52	57.32	**24.8**	**81.20**	**84.80**
1550	23	56	39.5	**40.0**	**18.5**	25.7	50.6	5604.52	51.61	**31.3**	**70.09**	**104.85**
6269	23	56	39.5	**38.7**	**21.7**	23.0	32.0	5604.52	63.91	**17.4**	**66.95**	**138.03**
6996	23	56	39.5	**31.3**	**131.0**	148.6	21.1	5604.52	69.57	**10.9**	**-30.14**	**165.37**
7602	23	56	39.5	**23.5**	**100.7**	84.7	38.9	5604.52	59.85	**22.0**	**15.88**	**164.22**
7731	23	56	39.5	**42.7**	**13.6**	345.0	39.0	5604.52	59.78	**22.0**	**72.69**	**242.34**
6478	20	60	40	**40.2**	**16.0**	132.0	-61.4	5595.67	-41.70	**-42.5**	**55.28**	**-44.21**
353	35	49	42	**44.6**	**-120.4**	5.5	64.4	5560.49	38.21	**46.2**	**81.93**	**-95.40**
5729	36	48	42	**61.6**	**-148.3**	216.2	-75.5	5560.49	-23.87	**-62.7**	**73.68**	**-90.01**
8038	25	60	42.5	**22.8**	**-83.2**	329.0	28.0	5551.74	65.46	**14.9**	**61.61**	**-163.42**
8039	25	60	42.5	**22.8**	**-83.2**	333.0	61.0	5551.74	41.78	**42.1**	**56.75**	**-116.68**
1017	35	50	42.5	**19.5**	**-72.5**	203.7	-23.6	5551.74	-67.69	**-12.3**	**67.71**	**6.09**
7724	35	50	42.5	**43.5**	**16.7**	352.0	46.0	5551.74	54.57	**27.4**	**79.84**	**236.73**
8158	36	49	42.5	**56.5**	**163.3**	18.8	64.5	5551.74	38.04	**46.4**	**78.16**	**267.90**
7433	23	65	44	**41.7**	**71.5**	352.0	42.0	5525.62	57.04	**24.2**	**79.20**	**290.06**
7434	23	65	44	**42.5**	**71.5**	163.0	-54.0	5525.62	-48.11	**-34.5**	**77.41**	**-15.50**
7664	23	65	44	**40.0**	**20.3**	42.0	37.0	5525.62	60.15	**20.6**	**54.46**	**113.56**
7730	23	65	44	**42.0**	**12.8**	149.0	-44.0	5525.62	-55.71	**-25.8**	**64.59**	**275.42**
1138	38	50	44	**43.0**	**-109.5**	352.2	60.1	5525.62	42.49	**41.0**	**82.90**	**-157.39**
6540	38	50	44	**54.8**	**162.1**	310.0	59.0	5525.62	43.57	**39.8**	**57.93**	**78.11**
7226	38	50	44	**22.8**	**108.4**	185.0	-34.0	5525.62	-61.90	**-18.6**	**83.04**	**147.75**

7709	40	48	44	**24.4**	**124.3**	24.1	23.8	5525.62	67.27	**12.4**	**67.87**	**213.69**
1871	25	65	45	**-41.1**	**146.1**	95.0	-77.0	5508.30	-21.43	**-65.2**	**-36.01**	**119.36**
1874	25	65	45	**-35.6**	**137.5**	289.0	-73.0	5508.30	-27.19	**-58.6**	**-39.70**	**171.66**
6365	30	60	45	**32.6**	**71.8**	339.3	0.9	5508.30	77.43	**0.5**	**62.43**	**300.00**
7465	35	55	45	**60.9**	**-147.1**	321.3	57.3	5508.30	45.04	**37.9**	**62.38**	**105.48**
291	35	56	45.5	**10.0**	**-84.6**	182.9	8.7	5499.67	73.92	**4.4**	**-63.76**	**-90.91**
884	35	56	45.5	**41.7**	**2.5**	18.3	42.1	5499.67	56.71	**24.3**	**73.27**	**116.72**
1523	35	56	45.5	**43.5**	**-5.5**	4.0	33.5	5499.67	61.89	**18.3**	**74.28**	**161.37**
1815	35	56	45.5	**43.0**	**-3.8**	358.0	31.0	5499.67	63.26	**16.7**	**73.66**	**182.56**
3330	35	56	45.5	**39.0**	**39.5**	152.5	-48.0	5499.67	-52.62	**-29.0**	**68.41**	**-46.10**
5711	35	56	45.5	**41.5**	**36.4**	166.4	-34.4	5499.67	-61.38	**-18.9**	**73.02**	**261.38**
6113	35	56	45.5	**40.8**	**30.9**	32.3	-55.8	5499.67	-46.32	**-36.3**	**-0.66**	**8.16**
6268	35	56	45.5	**38.7**	**21.7**	90.0	43.0	5499.67	56.11	**25.0**	**20.40**	**84.04**
6542	35	56	45.5	**56.5**	**163.3**	18.0	66.0	5499.67	35.98	**48.3**	**79.48**	**259.39**
6581	35	56	45.5	**-9.5**	**161.4**	10.1	-32.2	5499.67	-62.61	**-17.5**	**-69.73**	**134.70**
7275	35	56	45.5	**41.2**	**74.7**	5.0	37.0	5499.67	59.87	**20.6**	**78.21**	**233.05**
7672	35	56	45.5	**40.6**	**37.1**	152.4	-42.5	5499.67	-56.44	**-24.6**	**66.99**	**298.13**
7673	35	56	45.5	**40.4**	**37.0**	144.1	-47.5	5499.67	-52.99	**-28.6**	**61.97**	**-48.21**
7725	35	56	45.5	**42.5**	**18.5**	188.0	-41.0	5499.67	-57.41	**-23.5**	**78.24**	**163.36**
7726	35	56	45.5	**41.8**	**19.5**	31.0	46.0	5499.67	54.06	**27.4**	**65.31**	**112.94**
305	42	50	46	**46.5**	**-123.5**	24.6	61.0	5491.06	41.33	**42.1**	**73.34**	**-49.99**
6273	42	50	46	**42.6**	**9.0**	166.0	-57.7	5491.06	-44.53	**-38.3**	**79.55**	**-60.26**
6331	29	65	47	**-7.0**	**-79.2**	333.4	-20.6	5473.90	-68.18	**-10.6**	**-60.37**	**-21.98**
256	38	56	47	**47.8**	**-122.8**	176.5	-66.5	5473.90	-35.24	**-49.0**	**82.70**	**-138.90**
1442	38	56	47	**27.0**	**142.0**	113.7	14.2	5473.90	71.13	**7.2**	**-11.08**	**204.00**
7113	35	60	47.5	**23.6**	**107.0**	325.5	33.2	5465.35	61.67	**18.1**	**58.73**	**33.16**
1816	45	50	47.5	**28.7**	**87.0**	20.7	-8.0	5465.35	-73.76	**-4.0**	**-40.81**	**60.36**
6369	44	52	48	**29.8**	**90.8**	194.6	-23.7	5456.82	-66.49	**-12.4**	**75.53**	**203.09**
6584	45	51	48	**44.2**	**-113.6**	161.6	-57.5	5456.82	-44.43	**-38.1**	**76.92**	**-191.14**
613	46	50	48	**34.6**	**76.1**	1.7	16.2	5456.82	70.01	**8.3**	**75.31**	**249.79**
614	46	50	48	**34.6**	**76.1**	353.9	23.0	5456.82	66.82	**12.0**	**77.40**	**282.69**

454	42	55	48.5	**65.0**	**-156.0**	13.0	83.0	5448.31	11.80	**76.2**	**76.25**	**-144.84**
455	42	55	48.5	**64.0**	**-158.0**	190.0	-83.0	5448.31	-11.80	**-76.2**	**75.48**	**-149.86**
7013	42	56	49	**34.2**	**73.6**	202.5	-17.2	5439.82	-69.34	**-8.8**	**65.97**	**192.05**
6016	43	56	49.5	**62.0**	**-148.0**	302.0	84.0	5431.34	10.12	**78.1**	**65.91**	**-169.42**
5949	47	52	49.5	**50.6**	**-120.3**	355.0	73.4	5431.34	26.26	**59.2**	**76.60**	**-129.88**
457	35	65	50	**78.7**	**-82.4**	265.8	80.9	5422.89	15.12	**72.2**	**70.55**	**-133.77**
1448	35	65	50	**39.5**	**20.8**	35.1	42.5	5422.89	55.66	**24.6**	**61.65**	**110.12**
6266	35	65	50	**39.3**	**21.8**	335.0	34.5	5422.89	60.47	**19.0**	**67.28**	**274.01**
6435	35	65	50	**26.4**	**102.3**	178.7	-13.7	5422.89	-70.69	**-6.9**	**82.81**	**292.14**
6054	40	60	50	**67.1**	**-142.1**	21.8	76.5	5422.89	21.83	**64.4**	**81.68**	**-69.45**
6055	40	60	50	**67.1**	**-142.1**	2.4	79.8	5422.89	16.85	**70.2**	**83.89**	**-135.55**
6399	49	51	50	**53.7**	**-126.8**	2.5	64.5	5422.89	37.16	**46.4**	**88.28**	**-8.03**
7442	45	56	50.5	**48.0**	**-123.5**	168.8	-70.1	5414.46	-30.51	**-54.1**	**76.78**	**-149.05**
458	48	53	50.5	**46.2**	**-111.5**	197.0	67.0	5414.46	34.28	**49.7**	**12.92**	**-121.23**
6400	50	51	50.5	**49.0**	**-125.5**	349.8	69.6	5414.46	31.14	**53.4**	**78.48**	**-152.81**
288	42	60	51	**11.2**	**-85.8**	176.3	-16.0	5406.04	-69.45	**-8.2**	**79.99**	**-106.15**
990	47	55	51	**48.0**	**-118.5**	15.6	68.9	5406.04	31.96	**52.3**	**76.32**	**-81.50**
1019	47	57	52	**39.9**	**139.8**	343.6	50.9	5389.26	49.40	**31.6**	**77.48**	**58.29**
5959	50	54	52	**49.9**	**-119.5**	20.0	72.0	5389.26	27.93	**57.0**	**73.60**	**-84.92**
7729	23	83	53	**42.0**	**12.9**	50.0	29.0	5372.57	62.83	**15.5**	**46.93**	**106.54**
339	50	56	53	**63.1**	**-149.0**	135.2	-82.4	5372.57	-12.60	**-75.1**	**70.11**	**-175.86**
420	51	55	53	**47.0**	**-123.1**	16.3	67.3	5372.57	33.66	**50.1**	**76.30**	**-82.03**
6676	30	80	55	**64.5**	**-129.6**	279.0	71.0	5339.39	28.96	**55.4**	**55.32**	**-186.79**
8086	45	65	55	**71.5**	**-22.7**	339.8	69.3	5339.39	31.08	**52.9**	**75.00**	**200.83**
8088	45	65	55	**71.8**	**-23.5**	355.3	72.6	5339.39	26.88	**57.9**	**81.14**	**170.42**
3404	50	60	55	**70.0**	**-25.0**	168.0	-62.0	5339.39	-39.19	**-43.2**	**70.00**	**177.59**
6081	50	60	55	**57.5**	**-7.0**	170.5	-64.4	5339.39	-36.69	**-46.2**	**83.18**	**229.14**
7273	50	60	55	**42.6**	**76.4**	190.0	-49.0	5339.39	-50.36	**-29.9**	**81.91**	**184.53**
8207	50	60	55	**20.4**	**58.8**	337.1	-10.5	5339.39	-70.99	**-5.3**	**-44.65**	**89.94**
2684	38	74	56	**43.5**	**12.7**	171.0	-52.5	5322.92	-47.55	**-33.1**	**83.34**	**276.73**
544	51	61	56	**39.0**	**139.7**	334.3	49.2	5322.92	50.06	**30.1**	**70.21**	**60.61**

612	55	58	56.5	**68.2**	**-31.7**	158.0	-75.0	5314.71	-23.51	**-61.8**	**81.40**	**237.17**
1301	56	58	57	**28.7**	**87.0**	335.5	-5.9	5306.52	-72.50	**-3.0**	**-38.09**	**117.16**
6910	56	58	57	**60.0**	**-149.3**	78.0	-69.0	5306.52	-31.25	**-52.5**	**43.35**	**-193.55**
7466	56	58	57	**60.9**	**-147.1**	123.7	-54.2	5306.52	-46.03	**-34.7**	**53.21**	**121.82**
2437	50	65	57.5	**34.6**	**92.4**	9.0	14.0	5298.35	68.94	**7.1**	**74.31**	**239.72**
2438	50	65	57.5	**34.6**	**92.8**	215.0	-34.0	5298.35	-59.35	**-18.6**	**60.41**	**180.54**
2506	50	65	57.5	**57.4**	**-6.3**	179.5	-55.9	5298.35	-44.54	**-36.4**	**78.06**	**175.39**
1584	56	60	58	**68.9**	**-32.0**	158.5	-62.8	5290.20	-38.02	**-44.2**	**70.27**	**189.96**
6580	35	83	59	**-9.5**	**161.4**	17.6	-39.1	5273.95	-56.20	**-22.1**	**-60.81**	**130.39**
6056	53	65	59	**61.5**	**-148.2**	248.2	-69.6	5273.95	-30.33	**-53.4**	**58.00**	**-85.98**
6057	53	65	59	**61.5**	**-148.2**	314.0	63.2	5273.95	37.49	**44.7**	**64.03**	#####

Table A4.5 Eocene sample site details, structure corrected data and derived actual palaeomagnetic data. (Data after McElhinny & Lock, 1996)

Table A4.6 Paleocene Palaeomagnetic Data

Site Details						Structure Corrected		Derived Actual Paleomagnetic Data				
Number	Age	Age	Age	Site	Site	Correct	Correct	Paleo	Paleo	Palaeo	Pole	Pole
Result	Low Mag	High Mag	Mean	Lat	Long	Dec	Inc	Radius	Colatitude	Latitude	Latitude	Longitude
8046	56	63	59.5	**28.3**	**88.5**	176.2	-7.9	5265.85	-71.11	**-4.0**	**79.97**	**289.60**
298	56	65	60.5	**37.2**	**-122.4**	281.3	-46.5	5249.71	-51.27	**-27.8**	**14.86**	**-70.08**
482	56	65	60.5	**63.6**	**-149.6**	142.6	-85.1	5249.71	-8.02	**-80.3**	**69.43**	**-163.55**
1299	56	65	60.5	**33.7**	**-117.7**	334.0	43.2	5249.71	53.44	**25.2**	**68.61**	**-192.59**
6543	56	65	60.5	**54.8**	**167.6**	76.0	62.0	5249.71	38.53	**43.2**	**46.56**	**229.13**
7800	56	65	60.5	**-10.0**	**121.0**	95.6	-14.6	5249.71	-68.05	**-7.4**	**1.39**	**53.58**
596	58	63	60.5	**35.0**	**134.0**	74.1	52.1	5249.71	47.21	**32.7**	**33.67**	**191.99**
7751	54	68	61	**43.5**	**-1.5**	187.0	-39.0	5241.67	-55.91	**-22.0**	**79.13**	**146.14**
1551	56	67	61.5	**44.0**	**-73.0**	311.0	17.0	5233.64	66.80	**8.7**	**45.03**	**185.95**
8175	60	63	61.5	**56.0**	**162.0**	230.0	-69.0	5233.64	-30.82	**-52.5**	**63.65**	**224.17**
6492	60	65	62.5	**40.3**	**30.7**	187.3	-30.1	5217.65	-60.47	**-16.2**	**77.69**	**179.47**
8157	61	65	63	**56.3**	**163.2**	28.0	60.2	5209.68	39.97	**41.1**	**72.23**	**261.99**
581	39	88	63.5	**35.0**	**33.0**	326.0	32.0	5201.73	59.32	**17.4**	**61.25**	**-55.92**
1172	62	65	63.5	**32.4**	**-112.9**	197.3	7.7	5201.73	70.33	**3.9**	**-35.36**	**-132.98**
475	40	90	65	**41.0**	**-123.0**	28.2	63.1	5177.98	36.91	**44.6**	**67.52**	**-75.07**
6405	45	85	65	**34.5**	**-107.0**	156.8	-49.1	5177.98	-48.77	**-30.0**	**70.56**	**-169.90**
101	50	80	65	**29.9**	**91.0**	0.0	18.0	5177.98	65.65	**9.2**	**84.45**	**271.00**
7728	50	80	65	**39.6**	**-107.7**	335.7	63.2	5177.98	36.81	**44.7**	**68.61**	**-150.23**
523	59	71	65	**60.3**	**-154.7**	296.1	75.2	5177.98	22.64	**62.1**	**62.33**	#####
2049	60	70	65	**34.1**	**74.8**	156.5	32.5	5177.98	58.79	**17.7**	**-21.04**	**96.23**
8044	60	70	65	**28.3**	**88.5**	177.1	-12.9	5177.98	-67.84	**-6.5**	**83.32**	**292.27**
6461	56	75	65.5	**50.0**	**-115.3**	283.0	20.0	5170.10	64.67	**10.3**	**27.29**	**-197.59**
3326	35	97	66	**40.8**	**38.9**	346.0	40.0	5162.24	54.48	**22.8**	**77.81**	**287.72**

Table A4.6 Paleocene sample site details, structure corrected data and derived actual palaeomagnetic data. (Data after McElhinny & Lock, 1996)

Table A4.7 Late Cretaceous Palaeomagnetic Data

Site Details						Structure Corrected		Derived Actual Paleomagnetic Data				
Number	Age	Age	Age	Site	Site	Correct	Correct	Paleo	Paleo	Palaeo	Pole	Pole
Result	Low Mag	High Mag	Mean	Lat	Long	Dec	Inc	Radius	Colatitude	Latitude	Latitude	Longitude
6222	56	77	66.5	**45.5**	**-109.9**	291.3	75.4	5154.39	22.26	**62.5**	**49.16**	**-142.57**
8215	62	71	66.5	**39.6**	**142.0**	283.5	9.4	5154.39	68.99	**4.7**	**23.36**	**60.61**
8174	66	68	67	**56.0**	**162.0**	251.0	-66.0	5146.57	-33.67	**-48.3**	**52.27**	**220.94**
1157	35	100	67.5	**-30.3**	**139.5**	358.0	68.0	5138.76	31.41	**51.1**	**1.09**	**138.46**
1161	35	100	67.5	**-30.4**	**139.4**	205.0	74.0	5138.76	24.06	**60.2**	**-51.33**	**123.39**
1165	35	100	67.5	**-30.5**	**139.3**	157.0	75.0	5138.76	22.74	**61.8**	**-50.77**	**153.11**
1166	35	100	67.5	**-30.2**	**139.0**	184.0	33.0	5138.76	58.09	**18.0**	**-86.17**	**76.61**
7768	50	85	67.5	**38.2**	**26.0**	329.0	49.9	5138.76	47.83	**30.7**	**66.12**	**-44.57**
6551	56	80	68	**-22.8**	**-68.4**	221.0	36.0	5130.97	56.41	**20.0**	**-52.56**	**-132.41**
1016	63	73	68	**18.4**	**-72.6**	314.3	8.8	5130.97	68.92	**4.4**	**47.05**	**-151.12**
6224	42	97	69.5	**18.1**	**-66.8**	126.9	29.8	5107.70	59.35	**16.0**	**-19.42**	**-19.96**
7892	56	83	69.5	**56.7**	**162.1**	241.6	-65.1	5107.70	-34.37	**-47.1**	**56.85**	**227.37**
520	65	74	69.5	**61.2**	**-142.4**	225.5	51.2	5107.70	46.60	**31.9**	**20.90**	**-176.09**
1195	65	74	69.5	**21.8**	**39.7**	174.6	8.7	5107.70	68.65	**4.4**	**-46.53**	**47.02**
6159	65	74	69.5	**32.3**	**-111.5**	23.2	58.2	5107.70	40.98	**38.9**	**65.91**	**-72.23**
7161	65	74	69.5	**43.5**	**146.8**	335.0	56.0	5107.70	42.85	**36.5**	**72.13**	**77.30**
7861	65	74	69.5	**45.2**	**25.6**	89.0	48.0	5107.70	48.87	**29.0**	**28.42**	**84.51**
8043	65	74	69.5	**28.3**	**88.5**	4.0	-11.2	5107.70	-67.62	**-5.7**	**-39.18**	**83.73**
6007	50	90	70	**42.6**	**-111.0**	344.0	66.0	5099.98	33.37	**48.3**	**72.65**	**-141.55**
8057	55	85	70	**52.0**	**9.5**	11.8	61.6	5099.98	37.82	**42.8**	**82.76**	**93.39**
6204	60	80	70	**38.8**	**-9.4**	296.0	80.0	5099.98	15.55	**70.6**	**44.05**	**-28.99**
6207	60	80	70	**38.8**	**-9.4**	358.0	53.0	5099.98	45.18	**33.6**	**83.80**	**-22.64**
2197	65	75	70	**-37.2**	**-70.6**	167.4	42.8	5099.98	52.16	**24.8**	**-79.99**	**11.90**
7481	65	75	70	**31.7**	**-110.8**	176.7	-38.1	5099.98	-54.91	**-21.4**	**85.63**	**-149.00**
7482	65	75	70	**31.7**	**-110.8**	56.1	60.8	5099.98	38.57	**41.8**	**44.97**	**-63.79**

1764	68	73	70.5	**61.1**	**-135.5**	166.7	-71.4	5092.27	-27.13	**-56.1**	**83.52**	#####
5943	68	73	70.5	**61.0**	**-135.0**	166.7	-71.4	5092.27	-27.13	**-56.1**	**83.48**	**-202.57**
8173	69	72	70.5	**56.0**	**162.0**	218.0	-56.0	5092.27	-42.72	**-36.5**	**65.23**	**256.44**
289	60	83	71.5	**10.4**	**-85.4**	359.6	-7.8	5076.92	-68.60	**-3.9**	**-58.20**	**-84.69**
6218	60	83	71.5	**43.5**	**5.5**	9.5	46.8	5076.92	49.38	**28.0**	**82.39**	**114.49**
242	68	76	72	**32.1**	**-111.5**	160.5	-54.7	5069.27	-43.58	**-35.2**	**69.30**	**-152.12**
456	56	89	72.5	**78.7**	**-82.5**	261.0	56.0	5061.63	42.47	**36.5**	**44.64**	**-152.09**
53	60	88	74	**-29.8**	**-70.9**	356.0	-41.5	5038.84	-52.31	**-23.9**	**-81.44**	**-49.13**
297	65	83	74	**37.6**	**-122.5**	351.2	41.5	5038.84	52.31	**23.9**	**83.03**	#####
388	65	83	74	**35.9**	**137.2**	197.0	-49.8	5038.84	-46.97	**-30.6**	**75.10**	**193.45**
1297	65	83	74	**30.0**	**-115.7**	3.5	44.5	5038.84	50.49	**26.2**	**80.06**	**-99.86**
6058	65	83	74	**61.5**	**-148.2**	112.6	-64.1	5038.84	-34.93	**-45.8**	**55.64**	**-217.68**
6059	65	83	74	**61.5**	**-148.2**	94.2	78.5	5038.84	17.51	**67.9**	**55.85**	**-115.88**
7255	65	83	74	**37.8**	**-1.9**	6.3	38.6	5038.84	53.97	**21.8**	**84.66**	**105.58**
7793	65	83	74	**37.8**	**-2.0**	6.3	38.6	5038.84	53.97	**21.8**	**84.66**	**105.48**
7860	65	83	74	**45.7**	**25.9**	65.0	26.0	5038.84	60.34	**13.7**	**37.63**	**109.90**
7891	65	83	74	**56.7**	**162.1**	215.0	-53.2	5038.84	-44.48	**-33.8**	**65.70**	**264.46**
7897	65	83	74	**56.0**	**161.5**	158.5	-62.1	5038.84	-36.89	**-43.4**	**77.26**	**427.40**
8035	65	83	74	**56.6**	**-126.2**	158.0	-69.0	5038.84	-29.67	**-52.5**	**77.97**	**-189.04**
8227	65	83	74	**56.0**	**161.0**	157.5	-67.4	5038.84	-31.46	**-50.2**	**77.63**	**92.14**
7005	65	84	74.5	**47.8**	**14.7**	298.5	35.3	5031.27	55.68	**19.5**	**43.03**	**-68.48**
7006	65	84	74.5	**47.8**	**14.7**	155.8	-48.3	5031.27	-47.94	**-29.3**	**72.02**	**275.07**
7007	65	84	74.5	**47.2**	**15.2**	295.6	47.8	5031.27	48.27	**28.9**	**45.03**	**-57.04**
7008	65	84	74.5	**47.2**	**15.2**	137.2	-56.8	5031.27	-41.55	**-37.4**	**61.61**	**-56.24**
6373	50	100	75	**48.6**	**20.7**	34.5	47.5	5023.72	48.40	**28.6**	**64.90**	**113.84**
481	60	90	75	**41.2**	**-118.4**	241.3	74.0	5023.72	23.53	**60.2**	**27.37**	**-141.62**
2933	70	80	75	**38.5**	**-9.2**	352.0	40.0	5023.72	53.02	**22.8**	**83.50**	**249.75**
3273	70	80	75	**39.0**	**-9.0**	351.7	40.7	5023.72	52.62	**23.3**	**83.28**	**249.65**
6165	71	81	76	**47.5**	**-111.9**	354.4	64.6	5008.68	34.22	**46.5**	**81.02**	**-132.49**
8172	73	79	76	**56.0**	**162.0**	32.0	49.0	5008.68	47.24	**29.9**	**65.65**	**271.35**
1292	55	98	76.5	**61.6**	**-162.0**	23.6	71.0	5001.18	27.13	**55.4**	**79.00**	**-89.00**

426	56	97	76.5	**43.6**	**12.7**	319.0	39.0	5001.18	53.35	**22.0**	**58.23**	**-75.70**
552	56	97	76.5	**26.5**	**102.3**	357.6	31.6	5001.18	57.23	**17.1**	**83.39**	**84.48**
300	65	88	76.5	**43.0**	**-111.0**	333.0	70.5	5001.18	27.72	**54.7**	**65.07**	**-141.06**
1458	65	89	77	**47.5**	**18.1**	318.0	53.0	4993.70	44.24	**33.6**	**61.46**	**-59.60**
6972	65	89	77	**46.0**	**12.0**	346.6	38.5	4993.70	53.55	**21.7**	**76.15**	**243.16**
7200	65	89	77	**62.5**	**174.4**	5.5	84.4	4993.70	8.70	**78.9**	**71.14**	**176.97**
7732	65	89	77	**41.8**	**13.9**	357.0	43.0	4993.70	50.95	**25.0**	**86.42**	**234.57**
1296	65	90	77.5	**34.1**	**-118.6**	72.8	48.3	4986.24	47.51	**29.3**	**34.00**	**-60.42**
1350	65	90	77.5	**-43.5**	**146.8**	353.3	-82.9	4986.24	-10.95	**-76.0**	**-54.36**	**148.98**
347	65	91	78	**34.0**	**-120.4**	24.1	43.9	4978.79	50.25	**25.7**	**69.95**	**-54.06**
7857	65	91	78	**45.4**	**25.4**	112.0	43.0	4978.79	50.80	**25.0**	**14.25**	**73.24**
6322	74	83	78.5	**47.1**	**-112.1**	326.3	68.4	4971.36	29.94	**51.6**	**66.56**	**-156.22**
7184	74	83	78.5	**22.2**	**-79.9**	300.0	17.0	4971.36	63.45	**8.7**	**35.66**	**-152.36**
6223	74	85	79.5	**46.1**	**-111.1**	154.6	-72.5	4956.56	-25.08	**-57.8**	**66.65**	**-138.41**
2164	65	95	80	**40.0**	**-122.5**	46.0	52.0	4949.18	44.58	**32.6**	**56.24**	**-57.20**
96	70	90	80	**15.2**	**-23.1**	321.0	2.0	4949.18	69.14	**1.0**	**52.58**	**-98.50**
6203	70	90	80	**44.2**	**86.0**	12.5	51.3	4949.18	45.08	**32.0**	**81.07**	**167.02**
287	65	97	81	**11.4**	**-85.8**	357.4	27.1	4934.47	58.59	**14.4**	**69.85**	**-92.25**
371	65	97	81	**39.3**	**-122.5**	47.6	47.8	4934.47	47.35	**28.9**	**54.38**	**-53.66**
372	65	97	81	**38.9**	**-122.6**	55.6	30.2	4934.47	57.14	**16.2**	**45.24**	**-42.76**
551	65	97	81	**32.0**	**119.0**	13.7	58.0	4934.47	39.76	**38.7**	**69.12**	**144.15**
1144	65	97	81	**41.0**	**-87.5**	336.0	6.0	4934.47	67.38	**3.0**	**62.72**	**147.49**
1268	65	97	81	**41.6**	**83.5**	16.0	39.0	4934.47	52.64	**22.0**	**76.97**	**187.20**
1814	65	97	81	**43.0**	**-3.8**	351.0	47.0	4934.47	47.87	**28.2**	**83.32**	**261.81**
2432	65	97	81	**29.9**	**91.2**	357.0	15.0	4934.47	63.80	**7.6**	**85.45**	**307.51**
3140	65	97	81	**6.0**	**-74.0**	179.0	12.0	4934.47	65.01	**6.1**	**-58.99**	**-72.24**
5710	65	97	81	**41.5**	**34.0**	170.6	-40.0	4934.47	-52.08	**-22.8**	**81.94**	**280.72**
5720	65	97	81	**40.1**	**112.9**	12.4	63.4	4934.47	34.89	**45.0**	**72.88**	**137.55**
6271	65	97	81	**42.5**	**25.0**	342.0	59.0	4934.47	38.91	**39.8**	**75.04**	**-23.76**
6384	65	97	81	**36.9**	**-5.2**	58.1	39.0	4934.47	52.64	**22.0**	**44.45**	**65.74**
6433	65	97	81	**26.5**	**102.4**	8.1	38.8	4934.47	52.75	**21.9**	**77.25**	**132.93**

6651	65	97	81	**25.0**	**101.5**	45.6	46.6	4934.47	48.12	**27.9**	**48.96**	**155.62**
6913	65	97	81	**-15.8**	**-74.3**	309.7	-47.2	4934.47	-47.74	**-28.4**	**-39.64**	**-26.62**
6917	65	97	81	**-17.5**	**-71.4**	259.7	-44.1	4934.47	-49.69	**-25.9**	**-3.70**	**-22.65**
6952	65	97	81	**38.5**	**76.4**	7.6	37.1	4934.47	53.67	**20.7**	**83.59**	**183.79**
6954	65	97	81	**39.5**	**75.0**	11.0	40.0	4934.47	52.08	**22.8**	**81.28**	**171.95**
7105	65	97	81	**-9.2**	**34.1**	346.5	-46.5	4934.47	-48.19	**-27.8**	**-55.29**	**51.89**
7112	65	97	81	**22.2**	**108.7**	349.3	35.3	4934.47	54.61	**19.5**	**73.84**	**75.75**
7114	65	97	81	**26.0**	**117.4**	27.1	40.2	4934.47	51.97	**22.9**	**64.20**	**172.93**
7115	65	97	81	**23.1**	**113.3**	36.6	27.1	4934.47	58.59	**14.4**	**56.59**	**180.83**
7665	65	97	81	**39.9**	**20.2**	35.0	33.0	4934.47	55.78	**18.0**	**61.69**	**110.56**
7799	74	88	81	**-9.7**	**119.6**	46.8	-33.5	4934.47	-55.53	**-18.3**	**-40.66**	**67.20**
1188	78	84	81	**-41.8**	**171.5**	3.0	-80.0	4934.47	-15.05	**-70.6**	**-56.82**	**170.08**
519	74	89	81.5	**33.9**	**-117.6**	323.6	45.1	4927.14	49.00	**26.6**	**60.47**	**-182.92**
6645	74	90	82	**33.7**	**-117.7**	323.6	45.1	4919.83	48.93	**26.6**	**60.38**	**-182.56**
448	65	100	82.5	**27.3**	**-114.5**	38.6	62.9	4912.54	35.21	**44.3**	**50.82**	**-79.79**
1801	65	100	82.5	**47.0**	**17.8**	316.7	25.8	4912.54	58.92	**13.6**	**53.38**	**277.78**
8041	79	89	84	**22.8**	**-83.2**	228.0	22.0	4890.75	60.32	**11.4**	**-20.13**	**-126.65**
262	80	88	84	**35.2**	**-118.5**	22.3	55.7	4890.75	41.27	**36.2**	**68.74**	**-74.85**

Table A4.7 Late Cretaceous sample site details, structure corrected data and derived actual palaeomagnetic data. (Data after McElhinny & Lock, 1996)

Table A4.8 Mid Cretaceous Palaeomagnetic Data

Site Details						Structure Corrected		Derived Actual Paleomagnetic Data				
Number	Age	Age	Age	Site	Site	Correct	Correct	Paleo	Paleo	Palaeo	Pole	Pole
Result	Low Mag	High Mag	Mean	Lat	Long	Dec	Inc	Radius	Colatitude	Latitude	Latitude	Longitude
5998	80	90	85	**48.6**	**-122.8**	36.7	74.6	4876.31	22.08	**61.1**	**63.43**	**-92.64**
7700	79	92	85.5	**51.3**	**-123.8**	285.2	52.8	4869.11	43.28	**33.4**	**42.89**	**-188.34**
595	80	92	86	**35.0**	**134.0**	73.4	43.0	4861.93	49.61	**25.0**	**33.36**	**194.91**
6931	83	89	86	**43.6**	**12.5**	315.3	43.5	4861.93	49.31	**25.4**	**57.13**	**-66.84**
6337	65	112	88.5	**-4.7**	**-80.1**	58.9	-16.7	4826.27	-61.72	**-8.5**	**-29.48**	**-140.12**
399	88	90	89	**37.4**	**-118.9**	351.0	69.1	4819.19	28.27	**52.6**	**65.03**	**-129.01**
449	88	91	89.5	**30.0**	**-115.3**	12.0	52.1	4812.12	43.27	**32.7**	**70.86**	**-89.54**
7450	20	160	90	**-63.4**	**-57.0**	34.1	-64.4	4805.07	-33.02	**-46.2**	**-72.13**	**207.76**
270	40	140	90	**36.4**	**-114.7**	35.9	54.1	4805.07	41.76	**34.6**	**61.27**	**-60.37**
6209	40	140	90	**31.0**	**82.5**	296.1	9.0	4805.07	64.47	**4.5**	**34.21**	**4.01**
531	80	100	90	**34.8**	**33.1**	283.0	48.0	4805.07	45.98	**29.0**	**31.97**	**-22.58**
5723	80	100	90	**-36.4**	**149.9**	30.8	-65.4	4805.07	-32.04	**-47.5**	**-60.44**	**116.50**
6640	83	97	90	**35.0**	**-120.0**	23.0	12.0	4805.07	63.31	**6.1**	**68.64**	**-13.45**
279	85	95	90	**36.8**	**-115.3**	354.6	60.6	4805.07	36.52	**41.6**	**72.90**	**-126.28**
538	85	95	90	**-11.9**	**-77.1**	349.0	-27.1	4805.07	-57.06	**-14.4**	**-66.67**	**-53.25**
2434	85	95	90	**31.7**	**91.0**	347.0	36.0	4805.07	52.82	**20.0**	**77.98**	**31.64**
400	87	93	90	**37.3**	**-119.0**	337.6	68.1	4805.07	29.26	**51.2**	**62.64**	**-142.91**
6374	85	97	91	**48.5**	**20.4**	325.8	32.3	4791.02	54.49	**17.5**	**61.78**	**275.78**
443	65	120	92.5	**27.0**	**-114.0**	269.8	55.5	4770.05	40.40	**36.0**	**20.10**	**-157.65**
1290	65	120	92.5	**30.2**	**91.5**	338.0	36.0	4770.05	52.44	**20.0**	**70.37**	**29.39**
6111	88	97	92.5	**48.5**	**-120.4**	62.7	31.7	4770.05	54.54	**17.2**	**43.00**	**-38.63**
6112	88	97	92.5	**48.5**	**-120.4**	0.3	58.8	4770.05	37.78	**39.5**	**86.27**	**-117.57**
7507	88	97	92.5	**41.0**	**16.5**	327.0	40.0	4770.05	50.34	**22.8**	**64.96**	**-65.62**
7172	91	95	93	**-0.7**	**123.4**	60.5	-32.1	4763.10	-54.27	**-17.4**	**-24.01**	**72.74**
7174	91	95	93	**-1.7**	**121.8**	285.9	-38.9	4763.10	-50.86	**-22.0**	**-13.36**	**171.86**

7699	92	97	94.5	**51.3**	**-123.8**	322.7	56.6	4742.32	39.32	**37.2**	**66.77**	**-200.57**
1051	65	125	95	**34.0**	**134.0**	100.2	46.9	4735.43	46.00	**28.1**	**16.43**	**181.57**
1052	65	125	95	**34.0**	**134.0**	23.5	51.5	4735.43	43.00	**32.2**	**68.04**	**180.66**
7459	65	125	95	**-62.6**	**-61.1**	210.5	-85.1	4735.43	-7.23	**-80.3**	**-56.18**	**-54.51**
7756	80	110	95	**40.7**	**-1.2**	343.0	56.0	4735.43	39.73	**36.5**	**74.78**	**-46.57**
7758	80	110	95	**41.2**	**-0.8**	27.0	34.0	4735.43	53.04	**18.6**	**68.71**	**91.83**
7764	80	110	95	**41.3**	**-1.1**	340.9	44.9	4735.43	47.21	**26.5**	**75.77**	**-78.73**
6923	90	100	95	**57.1**	**-133.6**	9.5	69.5	4735.43	27.34	**53.2**	**82.69**	**-97.00**
6924	90	100	95	**56.9**	**-134.0**	68.7	62.0	4735.43	34.76	**43.2**	**53.26**	**-71.39**
1982	77	114	95.5	**-25.8**	**-65.8**	5.0	-46.0	4728.55	-46.48	**-27.4**	**-71.82**	**-77.49**
275	93	98	95.5	**22.8**	**58.6**	355.7	18.3	4728.55	59.83	**9.4**	**81.69**	**31.96**
276	93	98	95.5	**22.8**	**58.6**	339.0	6.0	4728.55	64.57	**3.0**	**70.67**	**-19.33**
100	80	112	96	**29.9**	**91.0**	333.0	38.0	4721.69	50.89	**21.3**	**66.03**	**30.86**
2433	92	100	96	**31.5**	**92.0**	358.0	35.0	4721.69	52.40	**19.3**	**83.68**	**77.44**
447	83	112	97.5	**27.7**	**-114.8**	10.1	41.1	4701.20	49.02	**23.6**	**74.35**	**-85.41**
6545	83	112	97.5	**41.9**	**14.0**	10.1	40.8	4701.20	49.19	**23.3**	**82.35**	**108.80**
6550	83	112	97.5	**43.6**	**12.5**	302.3	40.6	4701.20	49.30	**23.2**	**48.00**	**-60.74**
7238	83	112	97.5	**40.4**	**73.2**	357.8	56.0	4701.20	39.44	**36.5**	**79.73**	**65.34**
1516	65	132	98.5	**45.6**	**14.1**	336.0	41.0	4687.61	48.94	**23.5**	**72.04**	**278.05**
6553	73	124	98.5	**-11.5**	**-76.5**	335.0	-27.8	4687.61	-55.36	**-14.8**	**-57.56**	**-36.09**
594	85	112	98.5	**35.0**	**134.0**	64.6	63.7	4687.61	32.87	**45.3**	**42.26**	**175.48**
738	93	105	99	**29.2**	**89.5**	262.6	26.0	4680.85	56.06	**13.7**	**10.32**	**32.76**
52	94	104	99	**-29.8**	**-70.9**	6.5	-55.5	4680.85	-39.65	**-36.0**	**-68.88**	**-82.46**
451	97	102	99.5	**36.7**	**-118.8**	332.3	61.5	4674.09	34.75	**42.6**	**63.59**	**-155.36**
12	50	150	100	**49.0**	**-1.0**	204.7	-11.6	4667.35	-61.64	**-5.9**	**62.00**	**127.43**
6208	50	150	100	**33.5**	**80.0**	356.7	17.3	4667.35	59.45	**8.9**	**85.93**	**304.36**
6642	50	150	100	**64.8**	**-140.0**	98.0	-80.0	4667.35	-14.23	**-70.6**	**63.08**	**-172.53**
7594	50	150	100	**45.6**	**84.9**	19.4	58.9	4667.35	36.88	**39.7**	**75.37**	**137.01**
8146	50	150	100	**50.0**	**-115.0**	340.4	68.5	4667.35	28.01	**51.8**	**73.88**	**-149.57**
7180	80	120	100	**27.6**	**-114.8**	358.9	31.3	4667.35	53.55	**16.9**	**81.10**	**-120.53**
7181	80	120	100	**27.0**	**-114.0**	284.1	52.5	4667.35	41.69	**33.1**	**28.91**	**-161.47**

7464	80	120	100	**33.8**	**80.4**	6.2	22.1	4667.35	57.53	**11.5**	**84.64**	**183.03**
6436	88	112	100	**7.0**	**-78.5**	346.0	-24.0	4667.35	-56.74	**-12.6**	**-47.60**	**-61.04**
6437	88	112	100	**7.0**	**-78.5**	324.7	-26.4	4667.35	-55.72	**-13.9**	**-36.92**	**-41.82**
7232	88	112	100	**28.2**	**-115.2**	356.0	38.0	4667.35	50.30	**21.3**	**78.04**	**-130.21**
444	90	110	100	**31.6**	**-116.8**	348.0	60.4	4667.35	35.64	**41.4**	**65.68**	**-133.91**
7702	95	105	100	**-75.7**	**-140.0**	352.6	-48.6	4667.35	-44.28	**-29.6**	**-59.86**	**29.68**
6412	83	118	100.5	**-55.5**	**-68.2**	286.5	-70.6	4660.63	-25.72	**-54.8**	**-54.32**	**-22.69**
453	90	112	101	**64.7**	**-158.0**	349.0	77.0	4653.92	18.11	**65.2**	**81.76**	**-182.45**
1353	90	112	101	**16.6**	**-97.0**	348.7	23.0	4653.92	56.99	**12.0**	**70.68**	**-126.78**
1530	90	112	101	**17.8**	**-99.5**	332.7	46.8	4653.92	45.27	**28.0**	**54.71**	**-133.83**
6014	97	107	102	**49.1**	**-117.0**	318.0	74.0	4640.55	21.73	**60.2**	**61.92**	**-148.76**
8042	97	107	102	**28.3**	**88.5**	352.0	-40.0	4640.55	-48.98	**-22.8**	**-20.28**	**94.93**
7592	50	157	103.5	**43.0**	**90.0**	17.9	40.3	4620.61	48.61	**23.0**	**76.67**	**180.82**
7163	83	125	104	**38.1**	**68.7**	356.0	49.0	4613.99	43.52	**29.9**	**81.12**	**50.57**
7166	83	125	104	**38.8**	**69.0**	2.0	52.0	4613.99	41.56	**32.6**	**80.25**	**76.86**
7167	83	125	104	**37.9**	**70.2**	321.0	41.0	4613.99	48.17	**23.5**	**60.07**	**0.19**
1457	97	112	104.5	**47.5**	**18.1**	300.0	38.0	4607.39	49.66	**21.3**	**47.29**	**-58.57**
1746	97	112	104.5	**48.6**	**-114.6**	349.0	59.0	4607.39	36.33	**39.8**	**81.45**	**-164.10**
6026	104	105	104.5	**50.0**	**-121.0**	38.7	63.9	4607.39	32.12	**45.6**	**66.28**	**-65.27**
1761	100	110	105	**59.4**	**-129.9**	286.2	54.8	4600.80	39.48	**35.3**	**48.99**	**-198.43**
477	65	146	105.5	**40.0**	**-122.5**	337.7	64.9	4594.23	31.10	**46.9**	**66.42**	**-151.85**
1068	65	146	105.5	**36.0**	**128.5**	33.0	60.9	4594.23	34.66	**41.9**	**60.38**	**167.31**
3312	65	146	105.5	**-25.0**	**-50.0**	29.3	-24.2	4594.23	-55.77	**-12.7**	**-63.02**	**-113.12**
6119	65	146	105.5	**30.1**	**103.0**	2.1	30.7	4594.23	52.98	**16.5**	**82.86**	**116.62**
8234	65	146	105.5	**31.6**	**116.0**	18.0	50.6	4594.23	42.31	**31.3**	**68.87**	**151.24**
6248	88	124	106	**29.7**	**98.7**	39.7	51.6	4587.67	41.59	**32.2**	**54.51**	**145.61**
6233	90	124	107	**22.2**	**-79.9**	295.7	26.4	4574.60	54.62	**13.9**	**33.10**	**-141.18**
7458	103	111	107	**-62.7**	**-61.1**	298.1	-79.4	4574.60	-14.73	**-69.5**	**-66.11**	**-27.45**
8102	105	111	108	**11.3**	**-61.0**	65.7	18.1	4561.59	57.80	**9.3**	**26.48**	**-1.51**
3548	80	140	110	**38.0**	**-122.5**	78.0	47.0	4535.74	44.00	**28.2**	**33.83**	**-67.62**
1515	88	132	110	**44.8**	**14.5**	330.0	48.0	4535.74	43.40	**29.0**	**69.10**	**-59.84**

6950	100	120	110	**-43.6**	**-71.8**	7.4	-58.0	4535.74	-36.55	**-38.7**	**-79.01**	**-95.52**
6270	89	132	110.5	**45.0**	**14.5**	339.0	48.0	4529.32	43.34	**29.0**	**75.32**	**-61.51**
7138	89	132	110.5	**25.6**	**100.2**	186.9	-47.7	4529.32	-43.52	**-28.8**	**68.41**	**113.19**
7139	89	132	110.5	**23.4**	**100.9**	79.4	43.3	4529.32	46.05	**25.2**	**23.40**	**151.35**
7140	89	132	110.5	**21.6**	**101.4**	60.8	37.8	4529.32	48.91	**21.2**	**35.72**	**155.53**
7144	89	132	110.5	**24.3**	**98.4**	60.9	32.0	4529.32	51.65	**17.4**	**37.08**	**157.60**
1199	97	124	110.5	**31.0**	**91.0**	347.7	24.0	4529.32	55.06	**12.6**	**78.96**	**25.16**
6962	97	124	110.5	**14.3**	**-87.0**	252.9	35.7	4529.32	49.94	**19.8**	**-3.39**	**-134.12**
7110	97	124	110.5	**16.2**	**102.6**	28.1	40.5	4529.32	47.55	**23.1**	**54.42**	**139.28**
7759	97	124	110.5	**19.0**	**109.4**	4.3	41.8	4529.32	46.86	**24.1**	**65.59**	**117.01**
8191	97	124	110.5	**37.0**	**-8.0**	345.7	47.8	4529.32	43.46	**28.9**	**75.73**	**-51.57**
6177	65	157	111	**30.0**	**103.0**	2.0	34.2	4522.91	50.57	**18.8**	**80.43**	**112.33**
6568	65	157	111	**1.4**	**110.0**	89.7	16.0	4522.91	58.10	**8.2**	**0.99**	**168.12**
6585	65	157	111	**29.4**	**104.4**	16.5	34.2	4522.91	50.57	**18.8**	**73.14**	**153.54**
6121	97	125	111	**30.1**	**96.9**	3.3	29.0	4522.91	52.90	**15.5**	**82.48**	**117.43**
8040	97	125	111	**22.8**	**-83.2**	247.0	23.0	4522.91	55.39	**12.0**	**-4.38**	**-132.65**
3586	109	113	111	**-16.7**	**34.2**	335.8	-54.4	4522.91	-39.10	**-34.9**	**-50.71**	**58.29**
6064	65	160	112.5	**38.6**	**112.1**	10.4	47.5	4503.76	43.39	**28.6**	**78.94**	**152.38**
7777	106	119	112.5	**54.9**	**-131.3**	343.9	55.7	4503.76	38.00	**36.2**	**80.01**	**128.44**
6120	97	132	114.5	**29.7**	**98.6**	48.2	49.0	4478.44	42.24	**29.9**	**49.11**	**148.57**
5974	90	140	115	**28.0**	**-115.5**	31.4	23.4	4472.14	54.61	**12.2**	**62.41**	**-49.00**
8216	114	119	116.5	**39.5**	**142.0**	94.2	20.4	4453.34	55.55	**10.5**	**18.25**	**201.99**
8217	114	119	116.5	**39.5**	**142.0**	283.4	-14.3	4453.34	-57.84	**-7.3**	**10.79**	**198.96**
7701	115	120	117.5	**-75.5**	**-139.4**	125.2	-78.0	4440.88	-16.05	**-67.0**	**-62.93**	**-169.18**
1456	112	124	118	**47.5**	**18.1**	284.0	46.0	4434.67	43.59	**27.4**	**40.29**	**-43.20**
5712	112	124	118	**41.5**	**36.4**	186.3	3.2	4434.67	61.53	**1.6**	**-19.79**	**30.52**
6206	112	124	118	**38.8**	**-9.4**	342.5	53.6	4434.67	38.88	**34.1**	**72.62**	**-48.58**
7498	112	125	118.5	**-43.5**	**-69.0**	6.5	-60.6	4428.48	-33.65	**-41.6**	**-76.50**	**-84.59**

Table A4.8 Mid Cretaceous sample site details, structure corrected data and derived actual palaeomagnetic data. (Data after McElhinny & Lock, 1996)

Table A4.9 Early Cretaceous Palaeomagnetic Data

Site Details						Structure Corrected		Derived Actual Paleomagnetic Data				
Number	Age	Age	Age	Site	Site	Correct	Correct	Paleo	Paleo	Palaeo	Pole	Pole
Result	Low Mag	High Mag	Mean	Lat	Long	Dec	Inc	Radius	Colatitude	Latitude	Latitude	Longitude
7162	97	141	119	**38.1**	**68.7**	176.0	-23.0	4422.29	-54.16	**-12.0**	**86.09**	**304.70**
7164	97	141	119	**38.1**	**66.9**	6.0	37.0	4422.29	48.14	**20.6**	**84.06**	**115.74**
7165	97	141	119	**38.1**	**66.9**	6.0	49.0	4422.29	41.71	**29.9**	**78.92**	**88.12**
6169	83	157	120	**8.8**	**-68.0**	357.7	11.9	4409.97	58.14	**6.0**	**66.84**	**-72.97**
760	100	140	120	**42.8**	**10.3**	199.3	-38.0	4409.97	-47.53	**-21.3**	**75.83**	**95.05**
1621	110	130	120	**32.5**	**-6.0**	295.0	71.0	4409.97	23.92	**55.4**	**39.47**	**-34.42**
6202	110	130	120	**44.2**	**86.0**	12.7	48.6	4409.97	41.84	**29.6**	**80.37**	**147.24**
363	97	146	121.5	**10.2**	**123.8**	297.1	-15.8	4391.59	-56.49	**-8.1**	**-16.02**	**174.36**
1210	97	146	121.5	**-9.3**	**125.6**	12.1	51.1	4391.59	40.13	**31.8**	**29.89**	**134.57**
1522	97	146	121.5	**43.5**	**-5.5**	318.0	21.5	4391.59	54.36	**11.1**	**57.05**	**-94.77**
1525	97	146	121.5	**43.5**	**-4.2**	309.0	31.5	4391.59	50.30	**17.0**	**52.27**	**-81.93**
6434	97	146	121.5	**26.8**	**102.5**	22.1	37.1	4391.59	47.76	**20.7**	**66.26**	**146.27**
6485	97	146	121.5	**44.5**	**118.5**	6.8	58.5	4391.59	35.01	**39.2**	**78.64**	**138.67**
6652	97	146	121.5	**25.0**	**101.5**	43.7	36.2	4391.59	48.18	**20.1**	**50.36**	**155.32**
6661	97	146	121.5	**26.0**	**117.2**	23.5	33.5	4391.59	49.42	**18.3**	**65.67**	**164.51**
6662	97	146	121.5	**26.0**	**117.4**	18.0	-4.8	4391.59	-60.38	**-2.4**	**-31.77**	**98.98**
6953	97	146	121.5	**38.5**	**76.4**	14.8	41.0	4391.59	45.85	**23.5**	**77.56**	**134.67**
6955	97	146	121.5	**39.5**	**75.0**	191.6	-33.0	4391.59	-49.64	**-18.0**	**81.07**	**155.76**
7085	97	146	121.5	**35.1**	**107.6**	16.4	50.5	4391.59	40.51	**31.2**	**71.26**	**142.41**
7111	97	146	121.5	**22.7**	**108.7**	355.9	39.1	4391.59	46.80	**22.1**	**69.22**	**100.25**
7133	97	146	121.5	**25.5**	**99.5**	42.0	51.1	4391.59	40.13	**31.8**	**49.59**	**141.21**
7239	97	146	121.5	**40.4**	**73.2**	353.1	44.1	4391.59	44.22	**25.9**	**82.63**	**32.39**
7584	97	146	121.5	**37.5**	**101.5**	225.0	-39.6	4391.59	-46.55	**-22.5**	**55.68**	**167.08**

7599	97	146	121.5	**23.4**	**100.4**	84.4	39.6	4391.59	46.55	**22.5**	**19.76**	**150.55**
7600	97	146	121.5	**23.4**	**100.6**	295.8	-36.0	4391.59	-48.28	**-20.0**	**-1.94**	**142.85**
7669	97	146	121.5	**39.8**	**20.0**	3.0	36.0	4391.59	48.28	**20.0**	**87.02**	**68.80**
374	112	132	122	**36.1**	**128.7**	28.0	56.7	4385.50	36.29	**37.3**	**63.79**	**167.69**
2685	89	157	123	**43.5**	**12.7**	290.5	51.5	4373.34	39.71	**32.2**	**43.78**	**-43.28**
2750	100	146	123	**5.0**	**-1.8**	330.0	38.5	4373.34	46.89	**21.7**	**43.58**	**-32.06**
1092	118	128	123	**50.6**	**-1.2**	354.9	38.8	4373.34	46.75	**21.9**	**81.87**	**206.06**
6900	100	150	125	**35.1**	**-120.3**	10.6	20.9	4349.19	54.06	**10.8**	**81.34**	**-38.92**
6901	100	150	125	**35.1**	**-120.3**	46.1	20.4	4349.19	54.25	**10.5**	**52.78**	**-45.09**
1789	120	130	125	**56.2**	**-126.1**	25.0	69.0	4349.19	25.61	**52.5**	**75.30**	**-80.05**
6419	120	130	125	**-72.5**	**-98.1**	231.2	-48.3	4349.19	-41.44	**-29.3**	**-36.18**	**-58.39**
6342	112	141	126.5	**38.6**	**68.8**	350.5	55.4	4331.23	36.76	**35.9**	**73.97**	**47.85**
1267	97	157	127	**41.8**	**82.0**	22.0	42.0	4325.27	44.65	**24.2**	**73.73**	**151.95**
7202	97	157	127	**63.2**	**175.3**	201.2	50.7	4325.27	39.77	**31.4**	**24.65**	**160.55**
6336	112	146	129	**-4.7**	**-80.0**	90.3	-12.3	4301.55	-56.57	**-6.2**	**-2.34**	**-136.64**
6544	112	146	129	**41.9**	**14.0**	334.0	36.1	4301.55	47.24	**20.0**	**70.84**	**-64.65**
6960	112	146	129	**15.5**	**-91.5**	156.1	-14.1	4301.55	-55.93	**-7.2**	**61.58**	**-136.35**
6961	112	146	129	**15.2**	**-90.2**	324.5	7.1	4301.55	58.36	**3.6**	**53.75**	**-146.92**
7598	118	140	129	**45.0**	**11.0**	306.2	41.2	4301.55	44.81	**23.6**	**52.75**	**-58.96**
50	124	135	129.5	**-29.8**	**-70.9**	8.0	-41.5	4295.66	-44.59	**-23.9**	**-73.18**	**-90.63**
6205	124	135	129.5	**38.8**	**-9.4**	317.0	58.0	4295.66	34.61	**38.7**	**57.08**	**-54.87**
6973	124	135	129.5	**46.0**	**12.0**	322.2	39.5	4295.66	45.58	**22.4**	**63.57**	**-67.62**
875	100	160	130	**45.8**	**-62.3**	0.0	-63.0	4289.78	-30.66	**-44.5**	**15.14**	**-62.30**
7100	100	160	130	**37.2**	**128.8**	18.6	33.2	4289.78	48.40	**18.1**	**75.00**	**195.99**
7103	100	160	130	**37.2**	**128.8**	20.3	28.2	4289.78	50.50	**15.0**	**73.95**	**204.31**
1109	65	200	132.5	**-25.6**	**-70.6**	40.3	-53.8	4260.57	-37.22	**-34.3**	**-49.48**	**-107.62**
7116	124	141	132.5	**46.0**	**12.0**	329.7	40.1	4260.57	44.92	**22.8**	**68.89**	**-69.48**
620	131	135	133	**-23.9**	**-70.1**	19.6	-31.5	4254.77	-48.73	**-17.0**	**-66.15**	**-108.67**
402	124	146	135	**65.8**	**-154.6**	229.1	86.1	4231.70	5.16	**82.2**	**62.17**	**-162.97**
6247	124	146	135	**29.7**	**98.5**	57.7	50.2	4231.70	39.21	**31.0**	**42.63**	**145.08**
51	132	138	135	**-29.8**	**-70.9**	14.5	-46.0	4231.70	-41.60	**-27.4**	**-68.34**	**-97.67**

1624	65	208	136.5	**49.7**	**-125.0**	20.5	28.7	4214.53	49.41	**15.3**	**73.00**	**-10.42**
1813	132	141	136.5	**43.0**	**-3.8**	319.0	18.0	4214.53	53.43	**9.2**	**58.17**	**-91.38**
3030	132	141	136.5	**46.1**	**18.3**	333.7	46.7	4214.53	41.05	**27.9**	**72.11**	**-52.96**
6508	122	152	137	**39.3**	**-123.0**	0.4	45.7	4208.83	41.54	**27.1**	**80.83**	**-121.34**
1127	135	141	138	**38.0**	**-122.7**	78.0	47.0	4197.47	40.72	**28.2**	**34.99**	**-71.54**
1049	132	146	139	**-18.6**	**-70.3**	345.1	-25.6	4186.17	-50.29	**-13.5**	**-65.28**	**-42.07**
1455	132	146	139	**47.5**	**18.1**	277.0	38.0	4186.17	45.12	**21.3**	**35.35**	**-41.47**
7456	132	146	139	**-62.7**	**-61.1**	24.5	-66.9	4186.17	-26.59	**-49.5**	**-78.94**	**-136.54**
6932	124	155	139.5	**43.6**	**12.5**	293.7	34.0	4180.54	46.83	**18.6**	**43.17**	**-53.79**
8075	120	160	140	**31.0**	**110.4**	57.5	30.1	4174.92	48.39	**16.2**	**43.34**	**170.52**
8078	120	160	140	**29.7**	**113.9**	42.8	-50.1	4174.92	-38.74	**-30.9**	**-0.71**	**88.73**
197	130	150	140	**44.5**	**-117.0**	29.6	62.1	4174.92	30.56	**43.4**	**66.76**	**-77.46**
7455	135	146	140.5	**-62.7**	**-61.1**	320.1	-62.2	4169.31	-30.44	**-43.5**	**-70.80**	**20.16**
730	132	152	142	**43.5**	**12.6**	280.5	31.3	4152.56	47.64	**16.9**	**34.16**	**-48.81**
7201	132	152	142	**62.4**	**174.8**	47.9	38.7	4152.56	44.43	**21.8**	**58.24**	**274.11**
261	126	160	143	**45.3**	**-116.7**	0.1	54.5	4141.46	35.73	**35.0**	**81.03**	**-116.33**
6477	140	146	143	**42.1**	**14.2**	326.0	42.1	4141.46	42.70	**24.3**	**65.49**	**-51.86**
6646	135	152	143.5	**42.5**	**-124.5**	262.0	43.0	4135.93	42.20	**25.0**	**25.57**	**-172.01**
6647	135	152	143.5	**42.5**	**-123.7**	124.0	37.0	4135.93	45.03	**20.6**	**10.71**	**-87.05**
8190	135	152	143.5	**37.0**	**-8.0**	323.8	46.5	4135.93	40.39	**27.8**	**61.16**	**-60.51**

Table A4.9 Early Cretaceous sample site details, structure corrected data and derived actual palaeomagnetic data. (Data after McElhinny & Lock, 1996)

Table A4.10 Late Jurassic Palaeomagnetic Data

Site Details						Structure Corrected		Derived Actual Paleomagnetic Data				
Number	Age	Age	Age	Site	Site	Correct	Correct	Paleo	Paleo	Palaeo	Pole	Pole
Result	Low Mag	High Mag	Mean	Lat	Long	Dec	Inc	Radius	Colatitude	Latitude	Latitude	Longitude
6567	132	157	144.5	**1.3**	**110.3**	272.4	-8.8	4124.90	-55.41	**-4.4**	**-1.24**	**165.65**
1110	125	165	145	**-31.2**	**-71.5**	341.5	-40.9	4119.41	-43.05	**-23.4**	**-68.79**	**-34.71**
8136	135	155	145	**37.4**	**23.5**	225.2	19.6	4119.41	51.67	**10.1**	**-3.58**	**-10.40**
8138	135	155	145	**37.3**	**23.4**	202.1	16.3	4119.41	52.82	**8.3**	**-12.76**	**5.50**
619	134	159	146.5	**-23.9**	**-70.1**	211.9	28.4	4103.00	48.22	**15.1**	**-58.07**	**-118.27**
5997	146	149	147.5	**48.5**	**-122.8**	343.6	-1.5	4092.12	-57.33	**-0.8**	**-7.51**	**-108.93**
8208	145	152	148.5	**20.4**	**58.8**	300.1	-66.5	4081.30	-26.27	**-49.0**	**6.00**	**81.45**
1454	146	152	149	**47.5**	**18.1**	265.0	41.0	4075.90	42.55	**23.5**	**30.22**	**-33.13**
7667	146	152	149	**39.9**	**20.2**	29.0	29.0	4075.90	47.67	**15.5**	**68.12**	**94.33**
7761	145	155	150	**36.7**	**-5.0**	15.6	41.6	4065.15	42.15	**23.9**	**74.01**	**35.94**
6548	146	155	150.5	**43.6**	**12.5**	268.8	33.6	4059.79	45.64	**18.4**	**28.12**	**-41.64**
6974	146	155	150.5	**46.0**	**12.0**	309.7	30.6	4059.79	46.86	**16.5**	**54.65**	**-64.02**
462	146	157	151.5	**40.0**	**-120.9**	13.1	10.7	4049.11	53.77	**5.4**	**79.04**	**-14.94**
463	146	157	151.5	**40.2**	**-121.0**	290.9	1.5	4049.11	56.72	**0.8**	**35.59**	**-194.82**
6383	146	157	151.5	**36.8**	**-5.0**	42.6	47.5	4049.11	39.01	**28.6**	**56.77**	**46.03**
6388	146	157	151.5	**25.8**	**117.3**	22.9	27.6	4049.11	47.89	**14.6**	**65.11**	**160.61**
6510	146	157	151.5	**26.7**	**102.4**	17.9	45.6	4049.11	40.01	**27.0**	**62.96**	**128.17**
6564	146	157	151.5	**1.1**	**110.4**	311.1	-2.1	4049.11	-56.53	**-1.1**	**-32.53**	**158.61**
7109	146	157	151.5	**16.6**	**103.0**	26.6	37.3	4049.11	43.95	**20.9**	**53.17**	**134.22**
7123	146	157	151.5	**37.9**	**-1.6**	178.0	50.0	4049.11	37.63	**30.8**	**0.28**	**-0.38**
7141	146	157	151.5	**25.4**	**100.2**	7.3	25.3	4049.11	48.75	**13.3**	**73.03**	**119.31**
7499	146	157	151.5	**38.0**	**-1.8**	31.0	56.0	4049.11	33.97	**36.5**	**62.62**	**36.95**
7500	146	157	151.5	**38.0**	**-1.8**	323.0	35.0	4049.11	44.94	**19.3**	**61.68**	**-65.45**
8170	146	157	151.5	**42.0**	**17.5**	228.1	26.2	4049.11	48.42	**13.8**	**4.18**	**-16.43**
8233	146	157	151.5	**31.6**	**116.0**	16.7	43.7	4049.11	40.97	**25.5**	**68.52**	**146.96**

314	150	153	151.5	**38.5**	**-120.8**	61.9	6.9	4049.11	55.00	**3.5**	**41.22**	**-46.91**
316	150	156	153	**37.9**	**-120.4**	101.7	-3.5	4033.18	-55.87	**-1.8**	**28.50**	**-187.66**
427	152	157	154.5	**47.3**	**7.2**	10.0	56.0	4017.35	33.71	**36.5**	**79.11**	**37.86**
7686	140	170	155	**10.4**	**-72.5**	319.0	9.0	4012.10	53.83	**4.5**	**44.89**	**-120.88**
7687	140	170	155	**10.4**	**-72.5**	309.0	3.0	4012.10	55.73	**1.5**	**37.82**	**-126.89**
546	154	156	155	**41.3**	**-1.0**	316.3	43.0	4012.10	40.94	**25.0**	**58.70**	**-61.62**
3119	154	156	155	**52.9**	**18.0**	19.7	57.7	4012.10	32.53	**38.3**	**77.91**	**77.98**
299	154	157	155.5	**43.1**	**-111.0**	324.0	61.0	4006.86	30.16	**42.1**	**62.57**	**-150.86**
7454	154	157	155.5	**-63.2**	**-62.2**	183.3	58.0	4006.86	32.29	**38.7**	**-84.28**	**135.77**
7755	155	157	156	**40.7**	**-1.2**	330.0	48.0	4001.64	38.29	**29.0**	**66.73**	**-52.85**
7757	155	157	156	**41.2**	**-0.8**	343.0	56.0	4001.64	33.57	**36.5**	**71.21**	**-30.93**
7763	155	157	156	**41.3**	**-1.1**	324.1	40.6	4001.64	41.96	**23.2**	**63.85**	**-63.93**
763	152	161	156.5	**40.3**	**9.7**	296.5	50.5	3996.42	36.86	**31.2**	**46.19**	**-41.15**
1108	65	250	157.5	**-31.1**	**-70.1**	344.7	-29.8	3986.03	-46.31	**-16.0**	**-72.56**	**-30.56**
6888	140	175	157.5	**16.2**	**-93.5**	177.2	0.9	3986.03	56.03	**0.5**	**-39.76**	**-90.48**
6666	154	161	157.5	**45.8**	**11.0**	309.8	40.8	3986.03	41.70	**23.3**	**56.32**	**-56.17**
315	154	162	158	**38.5**	**-120.8**	153.9	-29.0	3980.85	-46.56	**-15.5**	**69.77**	**-188.31**
2436	152	166	159	**33.6**	**92.1**	339.0	58.0	3970.52	31.99	**38.7**	**61.80**	**68.41**
6501	157	161	159	**46.5**	**6.0**	11.5	55.5	3970.52	33.63	**36.0**	**77.84**	**37.61**
7218	140	180	160	**51.9**	**-3.5**	177.3	-57.3	3960.25	-32.38	**-37.9**	**84.07**	**-17.64**
885	142	178	160	**37.4**	**-3.8**	37.5	32.4	3960.25	45.00	**17.6**	**61.06**	**59.03**
6639	155	165	160	**35.0**	**-120.0**	41.0	-27.0	3960.25	-47.06	**-14.3**	**-3.55**	**-148.76**

Table A4.10 Late Jurassic sample site details, structure corrected data and derived actual palaeomagnetic data. (Data after McElhinny & Lock, 1996)

Table A4.11 Early Jurassic Palaeomagnetic Data

Site Details						Structure Corrected		Derived Actual Paleomagnetic Data				
Number	Age	Age	Age	Site	Site	Correct	Correct	Paleo	Paleo	Palaeo	Pole	Pole
Result	Low Mag	High Mag	Mean	Lat	Long	Dec	Inc	Radius	Colatitude	Latitude	Latitude	Longitude
623	146	176	161	**17.5**	**-97.2**	154.3	22.2	3950.02	48.65	**11.5**	**-26.52**	**-75.86**
6559	146	178	162	**39.5**	**3.0**	41.4	48.1	3939.83	37.64	**29.1**	**59.00**	**54.65**
6011	154	170	162	**43.2**	**-110.8**	329.0	59.0	3939.83	31.07	**39.8**	**65.34**	**-150.37**
6297	150	175	162.5	**59.0**	**15.0**	24.0	65.0	3934.76	26.56	**47.0**	**77.71**	**73.70**
700	159	170	164.5	**43.4**	**-110.5**	334.8	53.7	3914.57	34.26	**34.2**	**69.71**	**-154.24**
1094	100	230	165	**62.0**	**5.0**	77.0	40.0	3909.56	41.26	**22.8**	**47.17**	**75.95**
49	157	174	165.5	**-18.6**	**-70.3**	339.6	-35.7	3904.55	-43.05	**-19.8**	**-57.08**	**-44.33**
6918	157	174	165.5	**-18.1**	**-70.7**	330.9	-42.3	3904.55	-40.17	**-24.5**	**-50.63**	**-41.06**
6912	157	177	167	**-15.8**	**-74.3**	110.5	31.3	3889.60	44.62	**16.9**	**-25.50**	**-27.50**
618	157	178	167.5	**-23.9**	**-70.1**	29.3	-39.9	3884.64	-41.04	**-22.7**	**-56.01**	**-105.18**
6010	157	178	167.5	**43.2**	**-110.5**	18.0	68.0	3884.64	23.74	**51.1**	**64.93**	**-93.43**
6240	157	178	167.5	**36.7**	**109.2**	14.4	45.9	3884.64	38.24	**27.3**	**71.81**	**138.75**
6555	157	178	167.5	**49.2**	**20.1**	2.0	56.0	3884.64	32.59	**36.5**	**81.71**	**27.59**
6556	157	178	167.5	**49.2**	**20.1**	40.0	59.0	3884.64	30.63	**39.8**	**65.01**	**70.93**
6557	157	178	167.5	**49.2**	**20.1**	75.0	46.0	3884.64	38.19	**27.4**	**44.39**	**76.79**
7142	157	178	167.5	**23.6**	**100.5**	83.3	36.8	3884.64	42.37	**20.5**	**21.58**	**146.54**
7143	157	178	167.5	**24.3**	**98.4**	99.7	35.2	3884.64	43.03	**19.4**	**11.30**	**141.71**
7666	157	178	167.5	**39.9**	**20.2**	6.0	46.0	3884.64	38.19	**27.4**	**77.39**	**37.41**
8232	157	178	167.5	**31.6**	**116.0**	12.4	33.5	3884.64	43.71	**18.3**	**72.48**	**145.53**
792	166	170	168	**48.7**	**7.5**	30.1	53.2	3879.69	34.25	**33.8**	**70.45**	**65.01**
6019	166	172	169	**44.0**	**-71.1**	187.0	24.0	3869.82	47.05	**12.6**	**-2.82**	**-76.22**
8063	166	174	170	**39.3**	**45.4**	55.2	47.3	3860.00	37.29	**28.5**	**50.49**	**96.84**
346	166	178	172	**31.4**	**-110.7**	339.4	19.9	3840.49	48.07	**10.3**	**70.49**	**-162.29**
2489	168	176	172	**-82.6**	**-50.0**	53.0	-69.0	3840.49	-22.61	**-52.5**	**-70.95**	**200.19**
6423	164	182	173	**-72.5**	**-98.1**	16.3	-67.6	3830.80	-23.75	**-50.5**	**-81.57**	**132.32**

1620	170	177	173.5	**32.5**	**-6.0**	315.0	26.0	3825.97	45.82	**13.7**	**53.33**	**-64.13**
2801	170	177	173.5	**32.2**	**-6.0**	134.1	-26.8	3825.97	-45.54	**-14.2**	**52.52**	**-63.38**
1453	161	187	174	**47.5**	**18.1**	304.0	43.0	3821.16	38.99	**25.0**	**54.17**	**-44.90**
8152	100	250	175	**27.0**	**106.7**	2.8	6.2	3811.56	51.99	**3.1**	**78.74**	**118.06**
7253	150	200	175	**-43.5**	**-70.4**	353.4	-29.8	3811.56	-44.29	**-16.0**	**-84.81**	**-7.93**
6021	170	180	175	**40.5**	**-74.3**	358.7	26.4	3811.56	45.51	**13.9**	**85.89**	**-87.36**
6426	170	180	175	**40.5**	**-75.0**	354.7	30.4	3811.56	44.06	**16.3**	**83.34**	**-108.61**
6547	166	187	176.5	**43.6**	**12.5**	310.1	50.8	3797.24	34.86	**31.5**	**56.35**	**-39.61**
364	146	208	177	**13.4**	**121.2**	75.7	27.7	3792.48	44.82	**14.7**	**19.50**	**167.63**
1067	146	208	177	**36.7**	**127.3**	313.4	43.1	3792.48	38.65	**25.1**	**54.17**	**76.47**
1298	146	208	177	**33.7**	**-117.7**	25.7	11.0	3792.48	50.27	**5.6**	**68.62**	**-51.52**
2825	146	208	177	**38.5**	**-109.5**	18.9	64.2	3792.48	26.21	**46.0**	**62.32**	**-91.56**
3329	146	208	177	**40.4**	**39.9**	146.5	3.5	3792.48	52.53	**1.8**	**-6.30**	**66.05**
6386	146	208	177	**27.2**	**111.5**	22.5	42.8	3792.48	38.79	**24.8**	**60.58**	**140.71**
6387	146	208	177	**29.7**	**120.2**	28.2	38.0	3792.48	40.87	**21.3**	**61.12**	**160.01**
863	65	290	177.5	**47.7**	**-59.3**	85.8	-48.3	3787.74	-36.09	**-29.3**	**34.66**	**-104.88**
7826	152	204	178	**-26.0**	**-70.5**	42.0	-35.5	3783.01	-41.79	**-19.6**	**-50.53**	**-115.04**
102	166	195	180.5	**45.9**	**9.0**	14.1	52.7	3759.52	33.47	**33.3**	**76.24**	**43.38**
6005	157	208	182.5	**41.0**	**-122.0**	27.0	63.3	3740.92	26.52	**44.8**	**62.54**	**-95.92**
6073	157	208	182.5	**40.3**	**-75.3**	359.3	32.4	3740.92	42.51	**17.6**	**82.79**	**-79.07**
7668	157	208	182.5	**39.9**	**20.2**	18.0	37.0	3740.92	40.72	**20.6**	**74.18**	**67.91**
7684	175	190	182.5	**10.4**	**-73.4**	351.2	41.3	3740.92	38.92	**23.7**	**48.69**	**-81.77**
7685	175	190	182.5	**10.1**	**-73.7**	7.6	47.2	3740.92	36.19	**28.4**	**45.87**	**-67.26**
6933	173	195	184	**43.6**	**12.5**	312.7	49.5	3727.08	34.90	**30.3**	**57.84**	**-39.68**
7743	182	190	186	**34.7**	**-119.8**	154.4	-2.1	3708.77	-51.78	**-1.1**	**69.18**	**-192.57**
103	178	195	186.5	**45.8**	**9.2**	337.3	43.2	3704.22	37.71	**25.2**	**73.85**	**-48.87**
7753	166	208	187	**16.8**	**98.7**	359.8	31.4	3699.68	42.41	**17.0**	**59.21**	**98.44**
6889	146	235	190.5	**16.9**	**-95.0**	293.7	2.7	3668.18	51.04	**1.4**	**28.81**	**-149.35**
6890	146	235	190.5	**15.6**	**-92.2**	187.7	-4.8	3668.18	-50.44	**-2.4**	**65.11**	**-77.99**
3380	186	196	191	**45.0**	**-64.0**	1.1	38.0	3663.72	39.49	**21.3**	**84.44**	**-56.77**
2391	178	208	193	**38.5**	**-109.5**	173.0	-17.5	3645.98	-46.38	**-9.0**	**82.65**	**-153.11**

5968	178	208	193	**47.7**	**11.5**	50.5	59.7	3645.98	28.30	**40.6**	**58.67**	**56.21**
5969	178	208	193	**47.8**	**12.5**	15.1	55.0	3645.98	31.17	**35.5**	**75.82**	**45.90**
5970	178	208	193	**47.8**	**13.0**	80.8	57.1	3645.98	29.93	**37.7**	**44.07**	**56.28**
6004	178	208	193	**40.9**	**-122.0**	343.3	43.8	3645.98	36.85	**25.6**	**73.36**	**-158.98**
6241	178	208	193	**36.2**	**109.3**	0.5	47.4	3645.98	35.18	**28.5**	**71.37**	**110.20**
6511	178	208	193	**26.8**	**102.3**	30.3	44.6	3645.98	36.49	**26.2**	**55.16**	**133.98**
6558	178	208	193	**49.1**	**19.2**	39.0	63.0	3645.98	26.06	**44.5**	**64.50**	**59.15**
6968	178	208	193	**47.6**	**12.2**	59.8	58.5	3645.98	29.07	**39.2**	**54.12**	**57.96**
6969	178	208	193	**47.7**	**13.5**	61.5	61.3	3645.98	27.24	**42.4**	**53.57**	**56.14**
6970	178	208	193	**48.0**	**15.6**	47.8	60.2	3645.98	27.97	**41.1**	**60.13**	**59.84**
6971	178	208	193	**46.3**	**14.4**	56.4	51.6	3645.98	33.05	**32.2**	**54.54**	**65.94**
7670	178	208	193	**39.9**	**20.1**	26.0	42.0	3645.98	37.64	**24.2**	**68.28**	**66.44**
7108	178	210	194	**16.7**	**101.8**	37.2	40.1	3637.17	38.35	**22.8**	**44.32**	**133.42**
6124	190	200	195	**54.8**	**-128.1**	265.0	56.0	3628.41	30.44	**36.5**	**42.77**	**-171.54**
6125	190	200	195	**54.4**	**-128.2**	227.0	50.0	3628.41	33.72	**30.8**	**27.12**	**-155.34**
6126	190	200	195	**54.5**	**-127.1**	326.0	47.0	3628.41	35.20	**28.2**	**70.52**	#####
7435	146	245	195.5	**32.0**	**119.0**	350.0	-3.0	3624.04	-50.34	**-1.5**	**-17.75**	**127.07**
7436	146	245	195.5	**32.0**	**119.0**	350.0	75.0	3624.04	16.03	**61.8**	**47.73**	**114.91**
6546	187	204	195.5	**43.6**	**12.5**	289.3	54.0	3624.04	31.55	**34.5**	**45.47**	**-32.27**
6464	157	235	196	**60.1**	**-134.1**	338.0	9.0	3619.68	48.56	**4.5**	**66.96**	**91.75**
6465	157	235	196	**59.4**	**-133.5**	337.0	-7.0	3619.68	-49.14	**-3.5**	**12.05**	**-115.91**
6916	190	208	199	**-17.5**	**-71.4**	179.9	44.1	3593.73	36.19	**25.9**	**-53.69**	**-71.30**
7003	150	250	200	**24.7**	**102.5**	4.2	7.1	3585.16	48.64	**3.6**	**72.98**	**113.32**
559	190	210	200	**-32.6**	**22.5**	340.0	-59.0	3585.16	-28.27	**-39.8**	**-58.15**	**40.38**
7125	180	230	205	**25.3**	**105.4**	355.0	13.0	3542.88	46.39	**6.6**	**71.24**	**94.08**
7126	180	230	205	**25.3**	**105.4**	346.0	-18.0	3542.88	-44.92	**-9.2**	**-18.47**	**115.78**
7127	180	230	205	**25.3**	**105.3**	1.0	-4.0	3542.88	-48.94	**-2.0**	**-23.63**	**104.48**
1452	187	223	205	**47.5**	**18.1**	305.0	53.0	3542.88	31.38	**33.6**	**56.22**	**-32.01**

Table A4.11 Early Jurassic sample site details, structure corrected data and derived actual palaeomagnetic data. (Data after McElhinny & Lock, 1996)

Table A4.12 Triassic Palaeomagnetic Data

Site Details						Structure Corrected		Derived Actual Paleomagnetic Data				
Number	Age	Age	Age	Site	Site	Correct	Correct	Paleo	Paleo	Palaeo	Pole	Pole
Result	Low Mag	High Mag	Mean	Lat	Long	Dec	Inc	Radius	Colatitude	Latitude	Latitude	Longitude
6020	203	208	205.5	**40.5**	**-74.3**	6.3	12.9	3538.70	46.36	**6.5**	**84.37**	**-20.24**
5821	178	235	206.5	**61.8**	**5.3**	77.0	40.0	3530.38	37.26	**22.8**	**49.98**	**71.84**
7634	178	235	206.5	**27.9**	**9.3**	346.0	26.3	3530.38	42.18	**13.9**	**67.30**	**-15.60**
8089	208	210	209	**47.8**	**18.5**	313.0	52.0	3509.74	31.61	**32.6**	**60.58**	**-32.79**
8090	208	210	209	**47.6**	**18.5**	307.0	52.0	3509.74	31.61	**32.6**	**57.31**	**-32.31**
1177	190	230	210	**-46.4**	**169.0**	343.0	78.0	3501.54	12.66	**67.0**	**-34.20**	**164.56**
881	209	212	210.5	**48.5**	**20.6**	289.0	59.0	3497.46	27.58	**39.8**	**49.79**	**-22.10**
540	209	220	214.5	**16.6**	**101.8**	43.2	42.9	3465.14	35.40	**24.9**	**39.61**	**132.78**
35	200	230	215	**-73.3**	**-15.0**	50.9	-52.0	3461.14	-31.17	**-32.6**	**-65.97**	**245.55**
2435	209	223	216	**34.3**	**93.5**	215.0	-48.0	3453.17	-33.04	**-29.0**	**57.28**	**128.85**
7107	209	223	216	**16.7**	**101.8**	39.5	44.4	3453.17	34.64	**26.1**	**41.04**	**130.44**
7135	209	223	216	**38.0**	**30.8**	220.2	32.1	3453.17	39.34	**17.4**	**5.43**	**6.53**
6921	210	229	219.5	**57.1**	**-133.1**	298.1	-31.0	3425.55	-39.40	**-16.7**	**29.10**	**-93.25**
442	208	235	221.5	**27.0**	**-114.0**	220.0	35.0	3409.97	37.84	**19.3**	**-3.45**	**-137.27**
517	208	235	221.5	**40.9**	**-122.2**	70.1	23.6	3409.97	41.58	**12.3**	**41.34**	**-65.99**
1975	208	235	221.5	**-32.5**	**138.5**	98.4	75.3	3409.97	14.82	**62.3**	**-33.43**	**156.15**
6351	208	235	221.5	**35.2**	**109.2**	329.6	43.7	3409.97	34.50	**25.5**	**60.96**	**73.01**
7203	208	235	221.5	**62.5**	**174.5**	6.5	-41.5	3409.97	-35.40	**-23.9**	**27.21**	**170.27**
7671	208	235	221.5	**40.0**	**20.1**	20.0	23.0	3409.97	41.76	**12.0**	**73.52**	**73.50**
8085	208	235	221.5	**71.5**	**-22.7**	46.9	44.7	3409.97	34.08	**26.3**	**65.08**	**81.07**
8087	208	235	221.5	**71.8**	**-23.5**	45.1	33.6	3409.97	38.34	**18.4**	**61.87**	**87.76**
6074	216	229	222.5	**40.3**	**-75.3**	1.8	7.5	3402.23	46.05	**3.8**	**86.12**	**-55.80**
1429	157	290	223.5	**35.6**	**136.5**	10.8	-7.0	3394.52	-46.08	**-3.5**	**-9.88**	**128.63**
259	209	240	224.5	**45.2**	**-116.7**	83.2	-31.1	3386.85	-38.92	**-16.8**	**29.97**	**-162.77**

260	209	240	224.5	**44.8**	**-117.0**	318.6	33.8	3386.85	38.01	**18.5**	**62.00**	**-177.16**
6213	150	300	225	**18.3**	**-97.7**	47.7	-59.6	3383.03	-26.32	**-40.4**	**-0.11**	**-116.84**
6214	150	300	225	**18.3**	**-97.7**	323.5	-3.0	3383.03	-46.99	**-1.5**	**-20.12**	**-70.10**
8066	209	241	225	**38.7**	**71.0**	226.8	-63.8	3383.03	-23.65	**-45.5**	**51.91**	**99.30**
7748	216	235	225.5	**35.6**	**-105.3**	347.5	2.1	3379.22	47.18	**1.1**	**77.94**	**-154.76**
7171	223	229	226	**36.7**	**30.6**	223.7	-25.2	3375.41	-40.67	**-13.2**	**56.21**	**84.65**
8240	223	229	226	**36.5**	**-79.7**	180.3	-3.6	3375.41	-46.73	**-1.8**	**83.23**	**-77.85**
764	208	245	226.5	**39.8**	**9.0**	293.0	41.7	3371.62	34.92	**24.0**	**44.16**	**-38.27**
1086	208	245	226.5	**37.1**	**129.0**	282.0	-52.6	3371.62	-30.07	**-33.2**	**26.04**	**162.06**
1375	208	245	226.5	**44.8**	**-65.1**	36.2	-9.1	3371.62	-45.21	**-4.6**	**5.17**	**-89.99**
2760	208	245	226.5	**61.0**	**11.0**	217.2	-45.4	3371.62	-33.40	**-26.9**	**70.52**	**97.35**
3123	208	245	226.5	**-17.5**	**-65.0**	359.0	-20.0	3371.62	-42.17	**-10.3**	**-59.66**	**-63.67**
3136	208	245	226.5	**9.0**	**-71.0**	189.0	-56.0	3371.62	-28.29	**-36.5**	**36.87**	**-65.68**
3137	208	245	226.5	**9.0**	**-71.0**	343.0	27.0	3371.62	40.07	**14.3**	**46.69**	**-86.92**
6003	208	245	226.5	**41.1**	**-122.0**	95.1	33.3	3371.62	38.01	**18.2**	**28.47**	**-77.76**
7508	208	245	226.5	**37.1**	**-8.4**	345.9	23.0	3371.62	41.29	**12.0**	**74.51**	**-45.41**
1111	215	239	227	**-31.2**	**-71.5**	191.7	74.6	3367.83	15.25	**61.1**	**-46.06**	**-75.91**
181	223	235	229	**56.9**	**-133.9**	234.6	63.1	3352.76	23.90	**44.6**	**39.62**	**-159.29**
1622	223	235	229	**49.7**	**-125.0**	327.2	-25.3	3352.76	-40.37	**-13.3**	**13.24**	**-103.87**
1623	223	235	229	**49.7**	**-125.0**	359.6	-32.3	3352.76	-38.13	**-17.5**	**11.57**	**-124.75**
6406	223	235	229	**34.8**	**-106.6**	352.6	12.7	3352.76	43.98	**6.4**	**77.46**	**-130.92**
295	223	239	231	**63.1**	**-145.9**	98.5	-26.7	3337.84	-39.76	**-14.1**	**46.75**	**-213.28**
8059	227	235	231	**45.8**	**10.0**	346.1	27.6	3337.84	39.48	**14.6**	**79.62**	**-47.94**
3051	223	240	231.5	**46.4**	**11.7**	329.0	25.0	3334.12	40.23	**13.1**	**69.17**	**-57.62**
7119	223	240	231.5	**40.0**	**70.2**	355.0	70.0	3334.12	18.87	**53.9**	**58.76**	**67.08**
5724	229	235	232	**28.4**	**84.0**	334.3	-54.1	3330.42	-28.94	**-34.6**	**1.87**	**96.12**
7170	229	235	232	**36.7**	**30.6**	20.7	21.1	3330.42	41.34	**10.9**	**70.75**	**75.69**
7169	232	235	233.5	**48.0**	**15.5**	100.0	43.6	3319.37	33.63	**25.5**	**33.67**	**56.44**
1451	223	245	234	**47.5**	**18.1**	305.0	37.0	3315.70	36.10	**20.6**	**55.49**	**-40.31**
882	228	241	234.5	**48.5**	**20.6**	298.0	43.0	3312.04	33.79	**25.0**	**52.70**	**-33.53**
883	235	241	238	**41.6**	**2.2**	1.1	6.3	3286.64	44.80	**3.2**	**86.31**	**14.34**

6242	235	241	238	**48.7**	**7.0**	27.1	35.1	3286.64	36.44	**19.4**	**72.43**	**70.71**
6350	235	241	238	**35.4**	**109.6**	329.5	37.5	3286.64	35.60	**21.0**	**61.63**	**71.16**
6404	235	241	238	**34.5**	**-107.0**	165.6	-9.4	3286.64	-43.99	**-4.7**	**74.13**	**-146.18**
7590	235	241	238	**23.6**	**107.2**	56.1	6.9	3286.64	44.64	**3.5**	**40.09**	**156.87**
8076	235	241	238	**31.0**	**110.4**	77.6	23.0	3286.64	40.25	**12.0**	**30.80**	**157.68**
8077	235	241	238	**29.4**	**110.2**	63.6	26.8	3286.64	39.12	**14.2**	**38.70**	**156.60**
8079	235	241	238	**29.7**	**113.9**	55.1	14.2	3286.64	42.71	**7.2**	**44.52**	**165.18**
3175	237	239	238	**45.8**	**10.2**	161.5	-21.5	3286.64	-40.68	**-11.1**	**77.07**	**-57.34**
8135	237	240	238.5	**37.4**	**23.5**	156.1	26.9	3283.05	39.04	**14.2**	**0.81**	**38.29**
8137	237	240	238.5	**37.3**	**23.4**	307.6	-19.2	3283.05	-41.29	**-9.9**	**7.76**	**55.25**
8169	238	241	239.5	**42.0**	**17.5**	166.0	25.7	3275.88	39.32	**13.5**	**3.48**	**26.33**
6230	235	245	240	**25.5**	**103.0**	216.3	-30.7	3272.31	-37.73	**-16.5**	**51.78**	**138.85**
7000	235	245	240	**37.2**	**128.7**	76.8	37.2	3272.31	35.55	**20.8**	**36.70**	**173.62**
7099	235	245	240	**37.2**	**128.8**	1.1	19.4	3272.31	41.10	**10.0**	**78.27**	**132.36**
7106	235	245	240	**16.7**	**101.8**	51.4	31.8	3272.31	37.38	**17.2**	**36.24**	**137.83**
8058	238	242	240	**42.0**	**20.0**	37.8	26.0	3272.31	39.19	**13.7**	**62.83**	**78.01**
880	239	241	240	**48.5**	**20.6**	272.0	40.0	3272.31	34.54	**22.8**	**39.06**	**-26.26**
5715	239	241	240	**40.8**	**29.5**	34.5	47.4	3272.31	31.57	**28.5**	**62.05**	**68.74**
7159	239	241	240	**46.0**	**10.5**	341.8	41.1	3272.31	34.12	**23.6**	**74.95**	**-31.93**
7746	239	241	240	**35.7**	**-105.3**	154.0	-1.3	3272.31	-45.89	**-0.7**	**68.47**	**-164.37**
7767	239	242	240.5	**38.2**	**26.0**	271.2	33.2	3268.75	36.88	**18.1**	**30.30**	**-18.02**
180	241	245	243	**35.8**	**-111.5**	289.6	29.8	3251.06	37.77	**16.0**	**38.98**	**-159.43**
879	241	245	243	**48.5**	**20.6**	294.0	24.0	3251.06	39.52	**12.6**	**48.52**	**-40.78**
1065	241	245	243	**37.0**	**128.0**	331.5	25.1	3251.06	39.20	**13.2**	**65.50**	**81.34**
1124	241	245	243	**28.6**	**106.9**	40.0	13.1	3251.06	42.54	**6.6**	**53.85**	**154.35**
5713	241	245	243	**41.2**	**29.0**	292.1	47.1	3251.06	31.49	**28.3**	**45.20**	**-14.39**
5714	241	245	243	**40.8**	**29.5**	228.9	-55.2	3251.06	-27.69	**-35.7**	**54.08**	**66.15**
5982	241	245	243	**45.2**	**-108.9**	117.1	-23.4	3251.06	-39.70	**-12.2**	**48.68**	**-168.34**
6114	241	245	243	**29.7**	**106.6**	46.1	11.9	3251.06	42.86	**6.0**	**50.61**	**157.17**
6349	241	245	243	**35.5**	**110.2**	335.2	32.5	3251.06	36.91	**17.7**	**65.25**	**73.20**
7176	241	245	243	**29.5**	**110.0**	52.5	28.5	3251.06	38.18	**15.2**	**45.61**	**154.51**

7177	241	245	243	**29.5**	**110.0**	62.8	40.6	3251.06	34.09	**23.2**	**39.11**	**149.97**
7179	241	245	243	**31.0**	**120.0**	215.7	-22.6	3251.06	-39.93	**-11.8**	**57.32**	**163.92**
7233	241	245	243	**46.5**	**11.8**	330.8	13.0	3251.06	42.57	**6.6**	**70.17**	**-64.80**
7589	241	245	243	**26.0**	**117.2**	299.0	-23.6	3251.06	-39.64	**-12.3**	**3.42**	**151.18**
8098	241	245	243	**43.6**	**-5.8**	184.0	-15.0	3251.06	-42.03	**-7.6**	**84.82**	**25.35**
6163	242	245	243.5	**29.9**	**106.3**	50.4	17.1	3247.54	41.42	**8.7**	**47.68**	**155.51**
6164	242	245	243.5	**29.9**	**106.3**	49.4	14.9	3247.54	42.01	**7.6**	**48.41**	**156.27**
7015	242	245	243.5	**29.6**	**103.4**	27.7	15.6	3247.54	41.83	**7.9**	**61.82**	**144.43**
8054	243	245	244	**67.5**	**104.0**	124.5	82.0	3244.04	7.99	**74.3**	**62.22**	**118.24**
607	241	248	244.5	**32.0**	**105.5**	35.9	12.8	3240.54	42.48	**6.5**	**58.73**	**155.23**
8056	241	248	244.5	**37.0**	**128.0**	271.9	-33.4	3240.54	-36.50	**-18.2**	**27.91**	**170.28**

Table A4.12 Triassic sample site details, structure corrected data and derived actual palaeomagnetic data. (Data after McElhinny & Lock, 1996)

Table A4.13 Permian Palaeomagnetic Data

Site Details						Structure Corrected		Derived Actual Paleomagnetic Data				
Number	Age	Age	Age	Site	Site	Correct	Correct	Paleo	Paleo	Palaeo	Pole	Pole
Result	Low Mag	High Mag	Mean	Lat	Long	Dec	Inc	Radius	Colatitude	Latitude	Latitude	Longitude
1440	235	256	245.5	**46.0**	**15.0**	151.4	-11.4	3233.56	-42.76	**-5.8**	**70.43**	**-60.96**
1441	235	256	245.5	**46.0**	**15.0**	225.9	-15.0	3233.56	-41.81	**-7.6**	**59.14**	**83.97**
1066	243	248	245.5	**37.0**	**128.0**	325.9	46.1	3233.56	31.75	**27.5**	**59.29**	**92.72**
7016	245	248	246.5	**29.6**	**103.4**	12.0	-2.6	3226.62	-44.92	**-1.3**	**-14.53**	**94.68**
7178	245	248	246.5	**31.0**	**120.0**	27.6	40.9	3226.62	33.72	**23.4**	**58.22**	**149.24**
7326	244	250	247	**72.9**	**84.0**	264.0	-75.0	3223.16	-14.26	**-61.8**	**69.05**	**127.26**
1521	241	256	248.5	**43.5**	**-5.5**	163.5	-14.0	3212.83	-41.80	**-7.1**	**77.62**	**-67.48**
1524	241	256	248.5	**43.3**	**-4.5**	334.5	12.5	3212.83	42.20	**6.3**	**71.68**	**-71.39**
1560	241	256	248.5	**43.2**	**-1.5**	21.0	14.0	3212.83	41.80	**7.1**	**74.56**	**62.33**
1561	241	256	248.5	**43.2**	**-1.5**	70.1	10.5	3212.83	42.72	**5.3**	**42.16**	**57.88**
1562	241	256	248.5	**43.2**	**-1.5**	298.5	-17.2	3212.83	-40.95	**-8.8**	**16.80**	**35.49**
2166	241	256	248.5	**58.2**	**-6.3**	24.2	39.0	3212.83	34.27	**22.0**	**76.65**	**83.96**
6098	241	256	248.5	**-9.5**	**124.5**	274.4	-57.1	3212.83	-26.38	**-37.7**	**-10.46**	**151.27**
6099	241	256	248.5	**-9.6**	**124.4**	253.8	-62.0	3212.83	-23.58	**-43.2**	**-2.45**	**147.01**
6221	241	256	248.5	**40.1**	**-117.5**	170.3	-39.0	3212.83	-34.27	**-22.0**	**73.11**	**-136.56**
6919	241	256	248.5	**-16.0**	**-69.0**	282.2	-30.1	3212.83	-37.24	**-16.2**	**-20.02**	**-29.99**
7124	241	256	248.5	**37.9**	**-1.6**	184.0	6.0	3212.83	43.87	**3.0**	**-5.89**	**-4.39**
8099	241	256	248.5	**43.0**	**-4.3**	340.0	17.0	3212.83	41.00	**8.7**	**74.93**	**-63.94**
1198	247	250	248.5	**29.5**	**103.4**	16.4	-4.5	3212.83	-44.25	**-2.3**	**-13.29**	**91.72**
1293	247	250	248.5	**29.6**	**103.4**	17.8	-6.9	3212.83	-43.64	**-3.5**	**-12.35**	**90.93**
1302	247	250	248.5	**29.6**	**103.4**	19.6	-11.6	3212.83	-42.43	**-5.9**	**-10.84**	**90.08**
6385	247	250	248.5	**29.7**	**98.7**	25.2	6.7	3212.83	43.69	**3.4**	**64.31**	**141.43**
7204	247	250	248.5	**25.0**	**102.7**	25.5	-11.9	3212.83	-42.35	**-6.0**	**-13.82**	**85.32**
7754	247	250	248.5	**26.7**	**104.0**	359.3	-5.9	3212.83	-43.90	**-3.0**	**-17.19**	**104.51**
3554	208	290	249	**-39.1**	**-70.5**	277.2	54.5	3209.41	27.69	**35.0**	**-30.88**	**-102.99**

3590	208	290	249	**43.0**	**-1.0**	152.0	-22.5	3209.41	-39.44	**-11.7**	**69.54**	**-59.58**
7208	245	253	249	**42.9**	**2.8**	192.4	-8.4	3209.41	-43.21	**-4.2**	**80.40**	**64.65**
1167	240	260	250	**-30.2**	**139.0**	10.0	-63.0	3202.58	-22.89	**-44.5**	**-52.61**	**132.61**
278	245	256	250.5	**36.8**	**-115.3**	134.8	-17.2	3199.17	-40.78	**-8.8**	**55.30**	**-169.79**
530	245	256	250.5	**40.0**	**79.0**	28.2	50.5	3199.17	29.51	**31.2**	**63.12**	**109.98**
562	245	256	250.5	**43.4**	**6.3**	195.9	-13.8	3199.17	-41.68	**-7.0**	**77.91**	**66.75**
593	245	256	250.5	**42.8**	**-0.5**	157.5	1.5	3199.17	44.82	**0.8**	**0.24**	**15.15**
1303	245	256	250.5	**37.5**	**114.4**	326.3	34.3	3199.17	35.74	**18.8**	**61.60**	**71.45**
1965	245	256	250.5	**26.7**	**102.9**	23.5	-4.5	3199.17	-44.06	**-2.3**	**-14.29**	**86.27**
1966	245	256	250.5	**26.1**	**103.1**	30.1	5.9	3199.17	43.71	**3.0**	**58.75**	**145.01**
2091	245	256	250.5	**-9.0**	**126.0**	158.6	53.3	3199.17	28.19	**33.9**	**-34.91**	**138.14**
3207	245	256	250.5	**44.0**	**6.8**	206.2	-13.4	3199.17	-41.78	**-6.8**	**71.45**	**74.43**
3214	245	256	250.5	**43.5**	**6.8**	203.5	-12.0	3199.17	-42.15	**-6.1**	**73.09**	**73.69**
3215	245	256	250.5	**43.5**	**6.8**	207.0	-23.5	3199.17	-39.04	**-12.3**	**70.34**	**65.02**
3352	245	256	250.5	**19.0**	**79.6**	306.0	-50.0	3199.17	-29.73	**-30.8**	**0.41**	**103.26**
3379	245	256	250.5	**46.5**	**-63.8**	183.2	-12.8	3199.17	-41.94	**-6.5**	**87.33**	**-10.67**
6001	245	256	250.5	**41.1**	**-122.1**	245.1	-33.0	3199.17	-36.16	**-18.0**	**45.89**	**-71.85**
6008	245	256	250.5	**34.8**	**-101.4**	332.4	11.1	3199.17	42.38	**5.6**	**65.80**	**-151.01**
6065	245	256	250.5	**40.1**	**113.2**	336.8	23.0	3199.17	39.18	**12.0**	**70.64**	**64.54**
6244	245	256	250.5	**43.8**	**87.6**	159.3	-64.2	3199.17	-22.11	**-46.0**	**63.56**	**70.21**
6364	245	256	250.5	**32.6**	**71.8**	289.3	-50.3	3199.17	-29.60	**-31.1**	**19.33**	**101.40**
6377	245	256	250.5	**-32.0**	**-69.5**	188.2	61.4	3199.17	23.84	**42.5**	**-55.49**	**-75.34**
6403	245	256	250.5	**34.2**	**-106.7**	157.5	-6.2	3199.17	-43.63	**-3.1**	**69.08**	**-154.40**
6488	245	256	250.5	**42.8**	**118.9**	154.8	-22.0	3199.17	-39.46	**-11.4**	**71.17**	**61.91**
6561	245	256	250.5	**-46.0**	**168.0**	173.3	64.6	3199.17	21.85	**46.5**	**-67.59**	**174.54**
7001	245	256	250.5	**37.2**	**128.7**	258.0	12.2	3199.17	42.10	**6.2**	**19.73**	**84.54**
7101	245	256	250.5	**37.2**	**128.8**	178.3	-11.5	3199.17	-42.28	**-5.8**	**79.40**	**122.57**
7118	245	256	250.5	**38.8**	**68.6**	188.0	-48.0	3199.17	-30.61	**-29.0**	**68.79**	**79.90**
7130	245	256	250.5	**44.0**	**2.8**	190.2	-10.8	3199.17	-42.46	**-5.4**	**82.06**	**62.74**
7243	245	256	250.5	**44.0**	**88.1**	198.0	-59.0	3199.17	-25.23	**-39.8**	**66.92**	**107.73**
7739	245	256	250.5	**-31.0**	**150.5**	158.0	74.4	3199.17	14.65	**60.8**	**-44.37**	**158.12**

7747	250	255	252.5	**35.6**	**-105.3**	140.3	-13.0	3185.63	-41.71	**-6.6**	**58.30**	**-159.28**
7104	248	260	254	**-8.5**	**35.4**	117.8	58.6	3175.55	25.26	**39.3**	**-19.30**	**58.98**
386	253	256	254.5	**40.9**	**-122.2**	156.4	-29.7	3172.21	-36.89	**-15.9**	**69.96**	**-166.72**
6616	230	280	255	**56.6**	**-2.8**	192.0	-25.4	3168.88	-38.12	**-13.4**	**81.56**	**116.18**
779	240	270	255	**50.3**	**11.7**	203.7	-25.4	3168.88	-38.12	**-13.4**	**75.10**	**86.47**
7207	255	256	255.5	**42.9**	**2.8**	182.6	-4.4	3165.55	-43.62	**-2.2**	**86.06**	**29.92**
8064	255	256	255.5	**38.2**	**72.3**	179.8	-37.6	3165.55	-34.26	**-21.1**	**72.46**	**71.93**
8065	255	256	255.5	**38.8**	**71.2**	137.4	-42.0	3165.55	-32.68	**-24.2**	**56.84**	**29.28**
6887	246	266	256	**16.2**	**-93.5**	263.0	2.5	3162.23	44.05	**1.3**	**6.84**	**-137.53**
3053	245	268	256.5	**46.3**	**11.8**	148.0	-13.0	3158.91	-41.36	**-6.6**	**68.40**	**-60.25**
7715	253	260	256.5	**45.0**	**-116.8**	78.6	-45.1	3158.91	-31.41	**-26.6**	**32.05**	**-153.87**
1382	250	270	260	**39.3**	**17.5**	57.0	-7.0	3135.93	-42.57	**-3.5**	**10.45**	**-17.74**
6903	250	270	260	**-41.6**	**-65.4**	139.2	47.1	3135.93	30.38	**28.3**	**-59.21**	**-25.19**
8188	250	270	260	**45.1**	**1.5**	192.4	-10.6	3135.93	-41.67	**-5.3**	**80.92**	**66.25**
1527	256	269	262.5	**43.7**	**3.3**	199.2	-11.8	3119.74	-41.15	**-6.0**	**75.81**	**65.31**
7206	256	269	262.5	**42.9**	**2.8**	182.5	0.4	3119.74	43.97	**0.2**	**-1.05**	**1.06**
5967	260	269	264.5	**46.5**	**-63.0**	173.1	2.0	3106.92	43.40	**1.0**	**3.29**	**-58.26**
6560	260	269	264.5	**-46.0**	**168.0**	257.2	46.1	3106.92	30.50	**27.5**	**-44.26**	**124.28**
2920	208	323	265.5	**37.3**	**31.7**	41.0	13.5	3100.55	40.47	**6.8**	**58.28**	**85.79**
147	256	275	265.5	**47.3**	**5.6**	189.9	1.3	3100.55	43.48	**0.7**	**4.21**	**-1.21**
6152	256	275	265.5	**43.7**	**3.4**	203.9	-20.4	3100.55	-38.67	**-10.5**	**72.25**	**59.56**
43	245	290	267.5	**29.2**	**79.9**	277.2	-52.1	3087.90	-27.77	**-32.7**	**22.38**	**109.89**
516	245	290	267.5	**40.9**	**-122.2**	149.4	62.2	3087.90	22.55	**43.5**	**20.81**	**-110.15**
529	245	290	267.5	**40.8**	**-75.8**	170.4	-19.1	3087.90	-38.86	**-9.8**	**77.72**	**-105.27**
536	245	290	267.5	**44.0**	**7.0**	204.9	-7.2	3087.90	-41.87	**-3.6**	**72.32**	**74.73**
887	245	290	267.5	**33.7**	**-6.2**	144.0	-4.0	3087.90	-42.65	**-2.0**	**59.78**	**-58.50**
888	245	290	267.5	**31.3**	**-4.0**	138.0	-2.7	3087.90	-42.97	**-1.4**	**54.39**	**-55.55**
1085	245	290	267.5	**37.1**	**129.0**	230.3	-26.6	3087.90	-36.81	**-14.1**	**52.02**	**177.51**
1646	245	290	267.5	**51.7**	**-117.0**	129.8	-44.3	3087.90	-31.02	**-26.0**	**61.28**	**-172.48**
1799	245	290	267.5	**46.1**	**18.0**	177.4	-5.0	3087.90	-42.41	**-2.5**	**87.68**	**-31.07**
1800	245	290	267.5	**46.8**	**17.5**	79.0	-11.0	3087.90	-40.93	**-5.6**	**27.72**	**-29.09**

2466	245	290	267.5	**43.2**	**-1.5**	217.5	-11.3	3087.90	-40.86	**-5.7**	**63.65**	**62.29**
3048	245	290	267.5	**41.0**	**9.0**	110.0	-15.5	3087.90	-39.80	**-7.9**	**42.01**	**-45.05**
3049	245	290	267.5	**41.0**	**9.0**	142.5	-2.0	3087.90	-43.14	**-1.0**	**62.64**	**-55.92**
3254	245	290	267.5	**53.2**	**-6.9**	194.0	-33.0	3087.90	-34.90	**-18.0**	**81.60**	**64.46**
3255	245	290	267.5	**53.5**	**-6.1**	226.0	-19.0	3087.90	-38.89	**-9.8**	**62.26**	**69.92**
3539	245	290	267.5	**45.9**	**8.8**	143.4	-16.8	3087.90	-39.46	**-8.6**	**65.44**	**-56.93**
6462	245	290	267.5	**51.7**	**-117.0**	135.0	-46.0	3087.90	-30.35	**-27.4**	**63.98**	**-171.55**
6479	245	290	267.5	**29.7**	**-2.2**	151.6	1.4	3087.90	43.28	**0.7**	**-9.39**	**17.10**
6975	245	290	267.5	**42.5**	**75.5**	163.0	-48.0	3087.90	-29.55	**-29.0**	**69.30**	**51.43**
6976	245	290	267.5	**42.5**	**75.5**	210.0	-50.0	3087.90	-28.70	**-30.8**	**64.05**	**108.78**
7009	245	290	267.5	**46.7**	**14.9**	109.7	-17.3	3087.90	-39.33	**-8.9**	**45.19**	**-42.95**
7010	245	290	267.5	**46.7**	**14.9**	80.1	-10.9	3087.90	-40.96	**-5.5**	**28.19**	**-32.20**
7011	245	290	267.5	**46.7**	**14.5**	132.1	-18.8	3087.90	-38.94	**-9.7**	**58.76**	**-49.57**
7088	245	290	267.5	**30.0**	**-2.0**	164.0	-5.5	3087.90	-42.29	**-2.8**	**68.44**	**-32.31**
7244	245	290	267.5	**43.0**	**84.0**	174.0	-14.0	3087.90	-40.18	**-7.1**	**82.03**	**54.91**
7927	245	290	267.5	**47.2**	**85.2**	235.0	-63.5	3087.90	-21.77	**-45.1**	**55.68**	**117.81**
6376	256	280	268	**-32.2**	**-69.5**	176.2	60.2	3084.75	23.67	**41.1**	**-55.79**	**-66.79**
7129	256	280	268	**44.0**	**2.8**	172.5	9.5	3084.75	41.26	**4.8**	**2.97**	**7.74**
1381	250	290	270	**35.7**	**136.2**	4.9	4.8	3072.25	42.24	**2.4**	**77.41**	**151.47**
7652	262	282	272	**48.5**	**7.3**	185.0	-12.0	3059.85	-40.31	**-6.1**	**86.52**	**75.49**
7655	262	282	272	**48.3**	**7.3**	191.5	-13.0	3059.85	-40.06	**-6.6**	**82.31**	**80.72**
149	256	290	273	**43.7**	**3.5**	199.2	-19.9	3053.70	-38.22	**-10.3**	**74.84**	**54.58**
274	256	290	273	**47.7**	**-54.7**	184.9	-5.8	3053.70	-41.75	**-2.9**	**86.67**	**23.90**
439	256	290	273	**38.2**	**-109.2**	145.3	-8.0	3053.70	-41.21	**-4.0**	**62.99**	**-164.86**
515	256	290	273	**40.9**	**-122.2**	228.9	-29.3	3053.70	-35.63	**-15.7**	**55.25**	**-71.84**
757	256	290	273	**45.8**	**9.3**	139.2	-16.1	3053.70	-39.20	**-8.2**	**62.76**	**-55.18**
1005	256	290	273	**43.7**	**3.3**	188.4	-6.6	3053.70	-41.55	**-3.3**	**82.49**	**51.16**
1243	256	290	273	**42.3**	**-71.2**	180.1	16.4	3053.70	39.13	**8.4**	**3.17**	**-71.26**
1286	256	290	273	**61.7**	**-142.3**	218.0	14.5	3053.70	39.61	**7.4**	**26.11**	**-168.22**
1379	256	290	273	**40.7**	**-75.2**	308.9	-34.4	3053.70	-34.08	**-18.9**	**15.86**	**-48.24**
1380	256	290	273	**40.7**	**-75.3**	209.8	30.1	3053.70	35.39	**16.2**	**8.66**	**-92.23**

1528	256	290	273	**43.7**	**3.3**	190.3	6.4	3053.70	41.60	**3.2**	**2.54**	**-3.52**
1798	256	290	273	**50.5**	**20.3**	197.0	-6.0	3053.70	-41.70	**-3.0**	**78.75**	**114.98**
2996	256	290	273	**46.2**	**11.0**	149.8	-19.1	3053.70	-38.43	**-9.8**	**69.59**	**-52.71**
6210	256	290	273	**40.5**	**78.8**	212.2	-57.7	3053.70	-24.76	**-38.3**	**59.23**	**104.67**
6211	256	290	273	**40.7**	**79.6**	222.7	-49.3	3053.70	-28.68	**-30.2**	**57.09**	**116.39**
6332	256	290	273	**43.8**	**3.3**	172.0	6.0	3053.70	41.70	**3.0**	**2.37**	**8.62**
6333	256	290	273	**43.8**	**3.3**	194.0	-10.0	3053.70	-40.72	**-5.0**	**78.95**	**58.71**
6334	256	290	273	**43.8**	**3.3**	195.0	-13.0	3053.70	-39.98	**-6.6**	**78.05**	**56.71**
6532	256	290	273	**60.0**	**10.3**	198.9	-36.5	3053.70	-33.41	**-20.3**	**79.54**	**111.01**
6534	256	290	273	**60.8**	**10.5**	317.0	-61.0	3053.70	-22.98	**-42.1**	**41.63**	**31.37**
6682	256	290	273	**-31.3**	**150.7**	112.0	76.7	3053.70	12.13	**64.7**	**-35.11**	**164.48**
7117	256	290	273	**38.8**	**68.7**	145.0	-39.0	3053.70	-32.57	**-22.0**	**60.66**	**29.63**
8100	256	290	273	**43.4**	**-5.4**	170.0	-19.0	3053.70	-38.46	**-9.8**	**79.44**	**-41.49**
602	250	300	275	**45.0**	**-67.0**	169.0	16.0	3041.47	39.07	**8.2**	**6.40**	**-60.05**
860	250	300	275	**48.0**	**-58.9**	171.7	-22.6	3041.47	-37.35	**-11.8**	**82.96**	**-104.51**
1058	250	300	275	**48.1**	**-66.3**	171.0	-32.0	3041.47	-34.68	**-17.4**	**80.89**	**-100.53**
6194	250	300	275	**45.7**	**-64.5**	177.8	30.4	3041.47	35.16	**16.3**	**10.56**	**-63.21**
6196	250	300	275	**45.7**	**-64.5**	176.9	18.6	3041.47	38.41	**9.6**	**7.33**	**-62.56**
6198	250	300	275	**45.7**	**-64.5**	180.4	12.9	3041.47	39.85	**6.5**	**5.85**	**-64.76**
6199	250	300	275	**45.7**	**-64.5**	174.8	14.4	3041.47	39.47	**7.3**	**6.33**	**-61.18**
6201	250	300	275	**45.7**	**-64.5**	169.8	11.8	3041.47	40.12	**6.0**	**5.99**	**-57.91**
6587	250	300	275	**40.7**	**-76.4**	176.0	2.0	3041.47	42.49	**1.0**	**-1.72**	**-73.70**
6143	260	290	275	**53.6**	**-9.9**	184.9	-57.2	3041.47	-24.92	**-37.8**	**78.26**	**0.29**
6045	265	285	275	**-32.1**	**-69.5**	248.7	40.0	3041.47	32.10	**22.8**	**-37.86**	**-108.33**
1549	270	280	275	**34.5**	**-97.0**	152.8	-8.6	3041.47	-40.90	**-4.3**	**65.24**	**-142.60**
1984	266	290	278	**-30.3**	**-67.7**	189.0	59.0	3023.34	23.84	**39.8**	**-53.72**	**-73.83**
1590	256	303	279.5	**34.4**	**-97.2**	138.0	8.0	3014.36	40.68	**4.0**	**1.65**	**-71.33**
7933	256	303	279.5	**47.2**	**85.2**	77.6	-72.2	3014.36	-15.47	**-57.3**	**41.93**	**64.70**
7935	256	303	279.5	**47.5**	**70.7**	208.0	-65.0	3014.36	-20.35	**-47.0**	**63.99**	**92.55**
7980	256	303	279.5	**43.7**	**103.0**	212.1	-46.2	3014.36	-29.55	**-27.5**	**64.57**	**140.61**
7986	256	303	279.5	**66.0**	**64.0**	213.0	-21.0	3014.36	-37.44	**-10.9**	**68.86**	**177.34**

674	270	290	280	**41.7**	**-105.4**	146.9	-20.0	3011.38	-37.67	**-10.3**	**65.34**	**-158.51**
7194	256	311	283.5	**59.0**	**-128.7**	180.6	-19.2	2990.73	-37.61	**-9.9**	**83.38**	**48.12**
7196	256	311	283.5	**53.2**	**-121.5**	247.1	-3.8	2990.73	-41.36	**-1.9**	**49.03**	**-53.32**
1508	245	323	284	**43.5**	**3.0**	306.7	18.6	2987.80	37.73	**9.6**	**54.07**	**-53.73**
7473	245	323	284	**54.0**	**-2.2**	192.8	-7.6	2987.80	-40.42	**-3.8**	**80.95**	**111.82**
5977	250	320	285	**34.4**	**-97.2**	147.3	13.8	2981.97	38.85	**7.0**	**0.26**	**-77.39**
6432	250	320	285	**52.1**	**-3.3**	174.9	-19.5	2981.97	-37.43	**-10.0**	**86.85**	**-82.65**
6491	250	320	285	**48.5**	**-59.1**	173.0	-5.0	2981.97	-40.95	**-2.5**	**85.36**	**-139.72**
7186	250	320	285	**48.7**	**-59.0**	248.9	64.8	2981.97	20.25	**46.7**	**38.51**	**-83.37**
7219	250	320	285	**51.9**	**-3.5**	192.5	-16.7	2981.97	-38.13	**-8.5**	**82.29**	**81.82**
7242	250	320	285	**50.0**	**7.0**	212.6	-3.8	2981.97	-41.24	**-1.9**	**68.91**	**87.73**
7520	250	320	285	**35.0**	**-96.0**	139.8	25.4	2981.97	35.87	**13.4**	**5.63**	**-73.66**
8195	250	320	285	**38.4**	**-79.6**	158.2	-9.2	2981.97	-39.96	**-4.6**	**70.64**	**-125.60**
321	270	300	285	**40.6**	**-77.0**	170.6	-5.3	2981.97	-40.88	**-2.7**	**79.20**	**-111.80**
732	270	300	285	**49.1**	**-57.3**	171.0	-18.0	2981.97	-37.81	**-9.2**	**83.52**	**-115.41**
8105	269	303	286	**55.5**	**-4.6**	191.6	-24.1	2976.17	-36.15	**-12.6**	**83.10**	**94.47**
3344	282	290	286	**51.0**	**-4.0**	188.0	-19.0	2976.17	-37.48	**-9.8**	**84.82**	**65.83**
3394	282	290	286	**51.0**	**-4.0**	198.0	-25.0	2976.17	-35.91	**-13.1**	**78.66**	**63.21**

Table A4.13 Permian sample site details, structure corrected data and derived actual palaeomagnetic data. (Data after McElhinny & Lock, 1996)

Table A4.14 Carboniferous Palaeomagnetic Data

Site Details						Structure Corrected		Derived Actual Paleomagnetic Data				
Number	Age	Age	Age	Site	Site	Correct	Correct	Paleo	Paleo	Palaeo	Pole	Pole
Result	Low Mag	High Mag	Mean	Lat	Long	Dec	Inc	Radius	Colatitude	Latitude	Latitude	Longitude
352	256	323	289.5	**41.0**	**-76.0**	166.6	-3.6	2956.07	-40.92	**-1.8**	**77.59**	**-120.93**
414	256	323	289.5	**47.2**	**-55.1**	171.0	-4.0	2956.07	-40.83	**-2.0**	**83.69**	**-123.61**
734	256	323	289.5	**52.2**	**-3.3**	173.3	-12.3	2956.07	-38.87	**-6.2**	**85.71**	**254.86**
1002	256	323	289.5	**46.1**	**-60.4**	196.0	-28.0	2956.07	-34.85	**-14.9**	**76.46**	**-18.12**
1026	256	323	289.5	**39.5**	**-78.2**	170.1	12.5	2956.07	38.83	**6.3**	**1.09**	**-72.01**
1028	256	323	289.5	**41.0**	**-76.8**	180.6	-6.6	2956.07	-40.22	**-3.3**	**81.21**	**-74.26**
1287	256	323	289.5	**61.7**	**-142.3**	225.9	10.9	2956.07	39.21	**5.5**	**28.27**	**-173.33**
1369	256	323	289.5	**38.0**	**-80.5**	173.7	17.2	2956.07	37.68	**8.8**	**0.49**	**-76.65**
1548	256	323	289.5	**34.9**	**-98.6**	128.0	20.0	2956.07	36.97	**10.3**	**8.82**	**-69.94**
1553	256	323	289.5	**44.0**	**-73.0**	184.0	-18.0	2956.07	-37.48	**-9.2**	**81.08**	**-57.12**
1580	256	323	289.5	**58.9**	**-2.8**	190.1	-17.1	2956.07	-37.70	**-8.7**	**81.29**	**132.10**
1869	256	323	289.5	**-31.5**	**150.9**	24.0	84.0	2956.07	5.51	**78.1**	**-26.44**	**153.40**
2772	256	323	289.5	**53.4**	**-6.2**	223.0	-7.0	2956.07	-40.13	**-3.5**	**63.49**	**73.81**
3252	256	323	289.5	**52.9**	**-8.0**	196.0	-10.0	2956.07	-39.42	**-5.0**	**79.85**	**88.81**
3504	256	323	289.5	**50.0**	**20.0**	212.0	8.0	2956.07	39.90	**4.0**	**13.77**	**-0.48**
6116	256	323	289.5	**61.5**	**5.4**	201.2	-10.2	2956.07	-39.37	**-5.1**	**74.06**	**128.74**
6117	256	323	289.5	**61.7**	**4.8**	207.6	-30.8	2956.07	-34.06	**-16.6**	**74.74**	**104.47**
6158	256	323	289.5	**52.0**	**-5.0**	187.0	21.0	2956.07	36.72	**10.9**	**15.44**	**-9.34**
6168	256	323	289.5	**38.8**	**-4.8**	114.0	19.0	2956.07	37.23	**9.8**	**17.89**	**30.70**
6300	256	323	289.5	**53.2**	**-1.8**	211.6	-17.2	2956.07	-37.68	**-8.8**	**71.01**	**78.07**
6302	256	323	289.5	**53.2**	**-1.8**	220.9	-23.2	2956.07	-36.15	**-12.1**	**66.02**	**70.04**
6318	256	323	289.5	**54.8**	**-5.0**	188.0	12.0	2956.07	38.95	**6.1**	**16.06**	**-10.22**
6320	256	323	289.5	**54.8**	**-5.0**	171.0	-27.0	2956.07	-35.13	**-14.3**	**84.82**	**-90.53**
6408	256	323	289.5	**43.8**	**87.8**	185.0	-74.0	2956.07	-13.84	**-60.2**	**57.57**	**90.03**
6409	256	323	289.5	**43.8**	**87.8**	226.0	-56.0	2956.07	-24.80	**-36.5**	**56.99**	**121.44**

6410	256	323	289.5	**46.7**	**86.1**	168.0	-48.0	2956.07	-28.28	**-29.0**	**73.49**	**65.82**
6411	256	323	289.5	**47.2**	**86.6**	151.0	-58.0	2956.07	-23.82	**-38.7**	**65.68**	**58.22**
7021	256	323	289.5	**-30.2**	**139.3**	137.9	77.6	2956.07	11.01	**66.3**	**-38.04**	**148.66**
7022	256	323	289.5	**-30.2**	**139.3**	110.0	81.5	2956.07	7.72	**73.4**	**-32.56**	**147.92**
7807	270	310	290	**28.5**	**-9.8**	96.0	-2.0	2953.22	-41.26	**-1.0**	**24.79**	**-56.05**
8109	280	300	290	**32.8**	**-6.1**	144.7	31.9	2953.22	33.71	**17.3**	**4.01**	**12.65**
1373	290	303	296.5	**46.1**	**-59.9**	171.0	6.0	2916.80	39.83	**3.0**	**6.59**	**-54.11**
6468	290	303	296.5	**46.5**	**13.2**	141.8	-8.1	2916.80	-39.34	**-4.1**	**64.68**	**-53.24**
7939	290	303	296.5	**47.2**	**85.2**	287.0	-54.0	2916.80	-25.39	**-34.5**	**35.29**	**115.36**
673	290	305	297.5	**41.7**	**-105.4**	146.9	-20.0	2911.30	-36.41	**-10.3**	**65.04**	**-155.61**
160	250	350	300	**42.0**	**-74.0**	175.6	16.8	2897.64	37.03	**8.6**	**5.05**	**-71.34**
7211	250	350	300	**41.0**	**-76.5**	177.8	9.2	2897.64	38.83	**4.6**	**2.19**	**-75.12**
7213	250	350	300	**40.0**	**-78.4**	175.9	-3.1	2897.64	-40.23	**-1.6**	**79.81**	**-93.53**
7215	250	350	300	**40.8**	**-75.8**	178.0	-28.7	2897.64	-33.97	**-15.3**	**74.72**	**-80.04**
7216	250	350	300	**40.8**	**-77.7**	170.0	-7.3	2897.64	-39.27	**-3.7**	**77.89**	**-109.28**
6296	280	320	300	**59.0**	**15.0**	202.0	-10.0	2897.64	-38.64	**-5.0**	**75.40**	**126.90**
7438	290	310	300	**34.5**	**-97.2**	145.0	16.0	2897.64	37.22	**8.2**	**2.44**	**-76.88**
9	290	323	306.5	**49.0**	**-1.3**	213.4	27.7	2862.84	33.83	**14.7**	**18.78**	**-20.19**
31	290	323	306.5	**49.0**	**-2.0**	350.0	-1.0	2862.84	-40.22	**-0.5**	**9.15**	**4.52**
129	290	323	306.5	**49.0**	**-1.3**	213.0	8.0	2862.84	38.64	**4.0**	**14.24**	**-21.84**
157	290	323	306.5	**36.4**	**-83.2**	158.0	16.0	2862.84	36.78	**8.2**	**1.63**	**-70.23**
206	290	323	306.5	**55.5**	**-133.5**	107.3	-23.4	2862.84	-34.96	**-12.2**	**50.53**	**-192.88**
368	290	323	306.5	**36.0**	**-83.7**	157.0	18.0	2862.84	36.30	**9.2**	**1.89**	**-70.32**
460	290	323	306.5	**39.5**	**-78.5**	162.9	-5.1	2862.84	-39.29	**-2.6**	**73.60**	**-119.78**
484	290	323	306.5	**46.7**	**-1.5**	221.0	21.0	2862.84	35.56	**10.9**	**16.92**	**-25.00**
724	290	323	306.5	**33.8**	**-86.2**	150.0	20.0	2862.84	35.81	**10.3**	**1.72**	**-69.18**
1205	290	323	306.5	**-31.7**	**-69.5**	102.7	47.2	2862.84	27.70	**28.4**	**-33.52**	**-36.55**
1557	290	323	306.5	**60.0**	**11.0**	196.0	-27.0	2862.84	-34.02	**-14.3**	**80.65**	**119.41**
1749	290	323	306.5	**45.9**	**-60.0**	160.9	17.1	2862.84	36.51	**8.7**	**10.71**	**-48.57**
3336	290	323	306.5	**21.4**	**79.0**	66.1	59.2	2862.84	22.47	**40.0**	**28.77**	**102.50**
6335	290	323	306.5	**-4.0**	**-80.5**	257.3	50.3	2862.84	26.49	**31.1**	**-9.22**	**-106.65**

6378	290	323	306.5	**-31.7**	**-69.5**	102.7	47.2	2862.84	27.70	**28.4**	**-33.52**	**-36.55**
6407	290	323	306.5	**43.8**	**87.6**	155.0	-62.0	2862.84	-21.01	**-43.2**	**61.72**	**68.94**
6489	290	323	306.5	**43.9**	**120.1**	148.6	11.5	2862.84	37.83	**5.8**	**9.81**	**139.02**
6502	290	323	306.5	**45.3**	**-70.6**	203.0	-84.0	2862.84	-5.33	**-78.1**	**50.17**	**-67.35**
6506	290	323	306.5	**25.2**	**99.2**	209.2	61.0	2862.84	21.55	**42.1**	**6.08**	**88.82**
6507	290	323	306.5	**23.9**	**99.2**	294.5	63.9	2862.84	19.96	**45.6**	**30.68**	**78.03**
6576	290	323	306.5	**46.0**	**-68.6**	171.0	-1.0	2862.84	-40.22	**-0.5**	**82.89**	**-123.24**
6965	290	323	306.5	**51.9**	**-3.8**	204.8	-25.2	2862.84	-34.49	**-13.2**	**74.97**	**62.56**
7094	290	323	306.5	**49.8**	**13.7**	198.0	12.0	2862.84	37.72	**6.1**	**13.22**	**2.50**
7823	290	323	306.5	**49.2**	**16.7**	196.0	12.0	2862.84	37.72	**6.1**	**12.39**	**6.76**
8055	303	311	307	**37.0**	**128.0**	255.5	-2.4	2860.20	-39.87	**-1.2**	**36.16**	**178.24**
6200	307	309	308	**45.7**	**-64.5**	176.2	13.8	2854.95	37.19	**7.0**	**8.56**	**-62.18**
789	307	311	309	**50.8**	**16.3**	192.0	-2.0	2849.72	-39.81	**-1.0**	**82.35**	**106.22**
547	300	320	310	**48.8**	**-64.4**	323.1	-47.3	2844.52	-27.48	**-28.5**	**25.12**	**-46.58**
6044	303	318	310.5	**-31.8**	**-69.4**	233.0	33.0	2841.93	32.12	**18.0**	**-45.91**	**-107.01**
1228	303	323	313	**46.0**	**-66.4**	158.0	38.0	2829.05	30.49	**21.3**	**17.04**	**-54.93**
6195	309	317	313	**45.7**	**-64.5**	353.8	-9.0	2829.05	-37.96	**-4.5**	**7.89**	**-60.65**
7102	307	320	313.5	**37.2**	**128.8**	341.1	-9.2	2826.49	-37.88	**-4.6**	**0.84**	**140.27**
6197	311	317	314	**45.7**	**-64.5**	176.1	9.1	2823.94	37.86	**4.6**	**7.89**	**-62.08**
7472	300	330	315	**-22.6**	**132.0**	266.1	82.3	2818.85	6.70	**74.9**	**-22.89**	**124.75**
265	281	350	315.5	**33.5**	**-82.5**	167.5	-19.7	2816.31	-35.30	**-10.1**	**67.06**	**-101.21**
6190	311	323	317	**31.2**	**-110.1**	310.9	8.3	2808.74	37.84	**4.2**	**48.82**	**-154.87**
7252	303	333	318	**-43.5**	**-70.4**	69.6	77.5	2803.73	10.52	**66.1**	**-39.09**	**-57.66**
5709	300	340	320	**-22.3**	**131.3**	215.5	82.6	2793.76	6.39	**75.4**	**-27.44**	**127.13**
7090	300	340	320	**-23.9**	**133.7**	211.4	66.7	2793.76	17.87	**49.3**	**-38.68**	**121.88**
6193	317	323	320	**45.7**	**-64.5**	357.9	-18.7	2793.76	-35.25	**-9.6**	**10.46**	**-63.27**
6397	317	323	320	**45.9**	**-64.5**	172.8	15.6	2793.76	35.98	**7.9**	**10.11**	**-60.21**
862	309	333	321	**47.7**	**-59.3**	161.7	11.7	2788.81	36.81	**5.9**	**12.08**	**-48.21**
6095	310	333	321.5	**56.0**	**-2.5**	194.0	19.0	2786.34	35.09	**9.8**	**21.50**	**-11.10**
6681	311	333	322	**-31.3**	**150.7**	186.3	68.4	2783.88	16.77	**51.6**	**-47.94**	**147.99**
7002	311	333	322	**37.2**	**128.7**	100.5	-22.5	2783.88	-34.21	**-11.7**	**35.56**	**85.88**

3205	318	333	325.5	**26.2**	**0.2**	136.0	40.0	2766.80	29.20	**22.8**	**4.04**	**20.06**
514	290	363	326.5	**41.2**	**-122.2**	52.3	35.1	2761.98	30.62	**19.4**	**53.25**	**-79.86**
1084	290	363	326.5	**36.8**	**128.5**	270.0	-5.2	2761.98	-37.89	**-2.6**	**28.21**	**172.68**
2942	290	363	326.5	**51.8**	**-5.2**	202.0	-9.0	2761.98	-37.06	**-4.5**	**76.57**	**71.24**
7017	290	363	326.5	**-30.2**	**139.3**	163.1	66.2	2761.98	17.96	**48.6**	**-47.18**	**146.88**
7018	290	363	326.5	**-30.2**	**139.3**	162.2	75.1	2761.98	12.15	**62.0**	**-41.68**	**144.24**
7073	290	363	326.5	**51.2**	**-2.5**	253.0	63.0	2761.98	19.74	**44.5**	**42.19**	**-28.35**
7832	320	335	327.5	**50.5**	**4.4**	205.9	77.7	2757.17	10.20	**66.4**	**41.16**	**-1.49**
320	323	333	328	**40.6**	**-77.0**	161.0	27.8	2754.77	32.53	**14.8**	**9.36**	**-66.78**
1029	323	333	328	**40.1**	**-78.2**	323.1	-30.4	2754.77	-31.85	**-16.3**	**12.97**	**-59.23**
6395	323	333	328	**45.9**	**-64.5**	175.0	22.1	2754.77	33.95	**11.5**	**12.03**	**-61.65**
6586	323	333	328	**40.7**	**-76.4**	183.3	24.0	2754.77	33.49	**12.6**	**7.25**	**-78.23**
2439	323	340	331.5	**36.0**	**95.0**	125.0	39.0	2738.16	29.21	**22.0**	**16.66**	**119.66**
2440	323	340	331.5	**36.0**	**95.0**	243.0	41.0	2738.16	28.59	**23.5**	**19.90**	**68.04**
10	290	377	333.5	**48.7**	**-3.0**	210.5	6.6	2728.78	37.13	**3.3**	**14.81**	**-21.48**
11	290	377	333.5	**48.6**	**-2.4**	196.1	29.2	2728.78	31.86	**15.6**	**17.56**	**-11.23**
1368	323	345	334	**38.0**	**-80.4**	157.9	8.4	2726.45	36.71	**4.2**	**3.28**	**-67.38**
682	333	343	338	**46.2**	**4.2**	77.6	-1.6	2707.99	-37.92	**-0.8**	**28.56**	**-38.90**
861	333	343	338	**48.3**	**-58.8**	351.2	-27.3	2707.99	-32.10	**-14.5**	**16.44**	**-53.94**
5706	323	356	339.5	**46.6**	**-61.0**	161.0	47.0	2701.16	26.20	**28.2**	**21.41**	**-52.12**
5707	323	356	339.5	**46.6**	**-61.0**	347.0	-44.0	2701.16	-27.23	**-25.8**	**19.86**	**-54.72**
731	330	350	340	**49.1**	**-57.3**	0.7	-35.2	2698.89	-29.90	**-19.4**	**19.20**	**-57.67**
6301	333	349	341	**53.2**	**-1.8**	220.9	-23.2	2694.37	-32.95	**-12.1**	**66.66**	**62.22**
236	333	350	341.5	**43.0**	**-6.0**	101.3	18.5	2692.11	34.02	**9.5**	**29.02**	**32.86**
1867	333	350	341.5	**-32.7**	**151.5**	154.0	45.0	2692.11	26.81	**26.6**	**-55.41**	**171.88**
6299	333	350	341.5	**53.2**	**-1.8**	203.0	35.8	2692.11	29.65	**19.8**	**25.03**	**-14.12**
1374	323	363	343	**44.8**	**-65.1**	148.4	31.2	2685.38	30.84	**16.8**	**17.17**	**-48.77**
1438	323	363	343	**50.0**	**10.0**	19.5	5.1	2685.38	36.86	**2.6**	**77.52**	**77.94**
1439	323	363	343	**51.5**	**10.5**	173.1	-9.0	2685.38	-36.03	**-4.5**	**85.15**	**-46.17**
1506	323	363	343	**46.0**	**-66.4**	160.0	11.0	2685.38	35.60	**5.6**	**11.83**	**-54.66**
3124	323	363	343	**-17.5**	**-65.0**	2.0	-23.0	2685.38	-32.89	**-12.0**	**-50.36**	**-66.70**

6231	323	363	343	**25.5**	**103.0**	52.7	-19.9	2685.38	-33.61	**-10.3**	**3.20**	**76.83**
6317	323	363	343	**54.8**	**-5.0**	217.0	47.0	2685.38	26.05	**28.2**	**32.14**	**-23.19**
6319	323	363	343	**54.8**	**-5.0**	223.0	29.0	2685.38	31.41	**15.5**	**28.54**	**-28.86**
6930	323	363	343	**43.0**	**-5.8**	142.0	25.1	2685.38	32.38	**13.2**	**15.51**	**14.21**
7942	323	363	343	**43.5**	**102.9**	279.5	-7.8	2685.38	-36.28	**-3.9**	**28.95**	**144.74**
8238	323	363	343	**73.7**	**-23.7**	358.1	7.6	2685.38	36.33	**3.8**	**69.96**	**159.59**
7471	339	350	344.5	**-22.6**	**132.0**	237.3	37.7	2678.70	28.96	**21.1**	**-35.29**	**102.06**
207	333	363	348	**55.5**	**-133.5**	95.2	-24.6	2663.28	-32.23	**-12.9**	**46.43**	**-183.91**
6680	333	363	348	**-31.3**	**150.7**	354.0	-15.9	2663.28	-34.24	**-8.1**	**-65.17**	**158.75**
6592	50	650	350	**63.4**	**-127.0**	324.0	70.0	2654.58	15.02	**53.9**	**73.23**	**-158.88**
6593	50	650	350	**63.4**	**-127.0**	59.0	60.0	2654.58	20.46	**40.9**	**66.69**	**-77.79**
6596	50	650	350	**63.0**	**-126.8**	28.0	69.0	2654.58	15.63	**52.5**	**75.03**	**-97.48**
509	323	377	350	**53.8**	**-9.9**	216.3	67.0	2654.58	16.80	**49.7**	**39.41**	**-22.70**
511	323	377	350	**53.8**	**-10.0**	201.8	-23.5	2654.58	-32.39	**-12.3**	**77.20**	**53.92**
1087	323	377	350	**78.0**	**16.0**	227.4	29.8	2654.58	30.84	**16.0**	**50.14**	**-20.08**
1093	323	377	350	**62.0**	**5.0**	210.0	25.0	2654.58	32.03	**13.1**	**32.20**	**-13.26**
1409	323	377	350	**-24.1**	**132.3**	217.5	72.0	2654.58	13.76	**57.0**	**-34.67**	**122.16**
1412	323	377	350	**-23.6**	**134.5**	206.5	76.5	2654.58	10.69	**64.4**	**-33.06**	**128.83**
2533	323	377	350	**51.4**	**-2.5**	196.0	9.0	2654.58	35.61	**4.5**	**16.63**	**-12.14**
5818	333	377	355	**61.4**	**5.5**	218.0	2.0	2633.17	36.79	**1.0**	**28.51**	**-19.31**
6481	350	360	355	**31.9**	**-1.8**	161.7	56.0	2633.17	22.09	**36.5**	**10.75**	**5.10**
1376	349	363	356	**44.8**	**-65.1**	146.0	25.0	2628.95	31.72	**13.1**	**16.86**	**-47.21**
859	350	363	356.5	**48.0**	**-58.9**	343.5	-22.7	2626.85	-32.24	**-11.8**	**16.64**	**-49.80**
1370	350	363	356.5	**45.1**	**-63.9**	163.0	22.0	2626.85	32.40	**11.4**	**13.67**	**-54.62**

Table A4.14 Carboniferous sample site details, structure corrected data and derived actual palaeomagnetic data. (Data after McElhinny & Lock, 1996)

Table A4.15 Devonian
Palaeomagnetic Data

Site Details						Structure Corrected		Derived Actual Paleomagnetic Data				
Number	Age	Age	Age	Site	Site	Correct	Correct	Paleo	Paleo	Palaeo	Pole	Pole
Result	Low Mag	High Mag	Mean	Lat	Long	Dec	Inc	Radius	Colatitude	Latitude	Latitude	Longitude
7567	333	391	362	**-24.0**	**-68.5**	197.9	55.1	2604.01	22.22	**35.6**	**-44.85**	**-77.94**
5820	350	377	363.5	**61.8**	**5.3**	210.0	25.0	2597.88	31.35	**13.1**	**32.67**	**-12.70**
1057	360	367	363.5	**48.1**	**-66.3**	154.0	19.0	2597.88	32.72	**9.8**	**17.57**	**-51.91**
1031	363	367	365	**-33.2**	**148.5**	29.2	-19.3	2591.79	-32.57	**-9.9**	**-58.72**	**118.11**
5722	363	367	365	**-36.9**	**149.9**	21.1	-39.6	2591.79	-27.47	**-22.5**	**-61.27**	**129.69**
6480	363	367	365	**31.9**	**-1.8**	154.3	55.6	2591.79	21.91	**36.1**	**11.82**	**7.72**
7086	363	367	365	**30.0**	**-2.0**	154.9	54.3	2591.79	22.44	**34.8**	**9.36**	**7.45**
7089	363	367	365	**-23.9**	**133.7**	224.9	29.1	2591.79	30.29	**15.6**	**-42.57**	**104.79**
7659	364	373	368.5	**-18.0**	**125.5**	27.5	-19.9	2577.74	-32.26	**-10.3**	**-45.37**	**104.96**
205	363	377	370	**55.5**	**-133.5**	98.9	-32.3	2571.79	-29.25	**-17.5**	**49.63**	**-181.68**
273	363	377	370	**47.7**	**-54.7**	181.6	28.0	2571.79	30.32	**14.9**	**17.39**	**-55.55**
351	363	377	370	**41.0**	**-76.0**	191.8	26.7	2571.79	30.63	**14.1**	**10.84**	**-82.09**
461	363	377	370	**39.7**	**-78.4**	163.8	8.5	2571.79	34.61	**4.3**	**6.09**	**-69.23**
609	363	377	370	**36.2**	**72.5**	318.0	-6.5	2571.79	-35.02	**-3.3**	**8.03**	**95.31**
1237	363	377	370	**40.0**	**-78.2**	160.0	36.0	2571.79	28.27	**20.0**	**13.01**	**-68.63**
1563	363	377	370	**46.0**	**-63.0**	213.0	2.0	2571.79	35.93	**1.0**	**13.92**	**-82.22**
1564	363	377	370	**45.8**	**-62.1**	7.0	-23.0	2571.79	-31.49	**-12.0**	**14.47**	**-65.87**
1952	363	377	370	**-36.9**	**149.8**	310.4	10.0	2571.79	34.30	**5.0**	**-11.77**	**123.80**
6459	363	377	370	**75.5**	**-96.5**	145.8	-31.1	2571.79	-29.56	**-16.8**	**70.79**	**140.92**
7806	363	377	370	**28.5**	**-9.8**	64.0	21.0	2571.79	31.95	**10.9**	**37.50**	**27.03**
6108	363	380	371.5	**57.4**	**-4.2**	193.1	28.2	2565.87	30.20	**15.0**	**27.65**	**-11.60**
1056	367	380	373.5	**48.1**	**-66.3**	225.0	18.0	2558.05	32.43	**9.2**	**22.02**	**-90.45**
6649	367	381	374	**-24.0**	**133.0**	21.0	-6.9	2556.11	-34.72	**-3.5**	**-55.09**	**112.10**
7949	367	381	374	**47.2**	**85.2**	310.0	-47.0	2556.11	-24.80	**-28.2**	**28.88**	**106.72**
1003	370	379	374.5	**-35.5**	**150.0**	0.4	-38.7	2554.17	-27.33	**-21.8**	**-62.83**	**149.60**

204	363	391	377	**55.5**	**-133.5**	111.9	-21.0	2544.54	-31.61	**-10.9**	**54.35**	**-190.05**
855	363	391	377	**60.5**	**-1.5**	220.4	3.1	2544.54	35.33	**1.6**	**29.55**	**-27.02**
876	363	391	377	**45.8**	**-62.3**	148.0	-38.0	2544.54	-27.42	**-21.3**	**65.32**	**-98.07**
1437	363	391	377	**50.0**	**10.0**	177.6	24.8	2544.54	30.75	**13.0**	**19.27**	**11.30**
7824	363	391	377	**49.2**	**16.7**	89.0	-37.0	2544.54	-27.70	**-20.6**	**41.68**	**-21.78**
7951	363	391	377	**43.5**	**102.8**	208.5	-0.7	2544.54	-35.81	**-0.4**	**68.62**	**152.79**
7952	363	391	377	**43.7**	**103.0**	180.2	-10.7	2544.54	-33.79	**-5.4**	**77.49**	**103.51**
7981	363	391	377	**43.7**	**103.0**	189.3	-18.2	2544.54	-32.22	**-9.3**	**74.77**	**122.15**
7982	363	391	377	**43.7**	**103.0**	21.8	-11.2	2544.54	-33.69	**-5.7**	**11.68**	**90.86**
1579	377	381	379	**59.0**	**-2.8**	193.8	40.8	2536.91	26.54	**23.3**	**32.91**	**-10.09**
7506	377	381	379	**24.9**	**2.1**	118.9	34.2	2536.91	28.37	**18.8**	**9.34**	**27.03**
8239	377	381	379	**73.7**	**-23.7**	195.2	13.0	2536.91	33.22	**6.6**	**40.89**	**-34.65**
867	377	386	381.5	**56.5**	**-3.0**	220.0	3.0	2527.47	35.11	**1.5**	**26.04**	**-27.30**
1055	367	400	383.5	**48.1**	**-66.3**	26.0	-28.0	2520.00	-29.71	**-14.9**	**20.42**	**-79.71**
513	377	391	384	**41.1**	**-122.3**	77.1	29.0	2518.14	29.45	**15.5**	**40.93**	**-82.93**
1462	377	391	384	**58.2**	**-3.4**	205.0	3.1	2518.14	34.96	**1.6**	**25.02**	**-18.90**
6115	377	391	384	**61.5**	**5.4**	185.4	3.8	2518.14	34.82	**1.9**	**26.76**	**1.95**
6650	377	391	384	**-23.6**	**132.1**	2.9	10.6	2518.14	33.46	**5.3**	**9.82**	**133.72**
7948	377	391	384	**50.0**	**86.0**	225.0	3.0	2518.14	34.98	**1.5**	**21.54**	**60.16**
7950	377	391	384	**51.0**	**86.0**	83.0	45.0	2518.14	25.07	**26.6**	**47.43**	**124.44**
7945	380	391	385.5	**48.5**	**58.7**	94.0	28.0	2512.59	29.62	**14.9**	**38.92**	**98.03**
873	363	409	386	**60.5**	**5.0**	16.0	-29.0	2510.75	-29.36	**-15.5**	**31.76**	**-4.15**
1091	363	417	390	**50.0**	**-5.0**	213.0	60.0	2496.17	19.24	**40.9**	**33.07**	**-17.37**
2411	363	417	390	**53.6**	**-9.9**	192.0	28.0	2496.17	29.43	**14.9**	**24.57**	**-16.35**
6022	363	417	390	**40.5**	**78.6**	79.9	24.6	2496.17	30.21	**12.9**	**38.93**	**118.15**
6562	363	417	390	**24.5**	**103.0**	279.2	2.7	2496.17	34.73	**1.4**	**25.07**	**64.62**
6563	363	417	390	**25.0**	**99.3**	199.5	-62.1	2496.17	-18.27	**-43.4**	**42.00**	**107.40**
7983	363	417	390	**43.7**	**103.0**	119.4	17.3	2496.17	31.80	**8.9**	**23.59**	**133.06**
271	381	400	390.5	**45.7**	**-70.9**	208.9	18.3	2494.37	31.56	**9.4**	**16.85**	**-86.23**
6141	363	423	393	**53.6**	**-9.9**	207.5	72.1	2485.41	12.82	**57.1**	**41.92**	**-17.81**
6144	363	423	393	**53.6**	**-9.4**	213.4	61.7	2485.41	18.38	**42.9**	**37.42**	**-22.03**

6147	363	423	393	**53.5**	**-9.5**	322.1	37.3	2485.41	26.98	**20.9**	**68.33**	**-58.48**
6150	363	423	393	**53.5**	**-9.5**	318.4	34.2	2485.41	27.79	**18.8**	**66.71**	**-61.03**
1344	245	545	395	**52.1**	**-2.4**	199.0	-11.3	2478.31	-32.79	**-5.7**	**77.93**	**55.10**
2759	377	417	397	**58.0**	**-3.5**	28.0	-14.0	2471.28	-32.16	**-7.1**	**27.97**	**-19.93**
6503	377	417	397	**45.3**	**-70.6**	18.0	37.0	2471.28	26.90	**20.6**	**69.48**	**-47.09**
7947	377	417	397	**49.5**	**76.5**	168.0	48.0	2471.28	23.65	**29.0**	**26.22**	**81.83**
591	380	417	398.5	**-33.5**	**19.0**	354.0	64.0	2466.05	17.14	**45.7**	**-16.44**	**17.16**
150	391	412	401.5	**78.7**	**15.0**	58.2	11.9	2455.70	32.37	**6.0**	**62.07**	**118.73**
866	394	411	402.5	**56.5**	**-3.0**	224.9	46.2	2452.28	24.04	**27.5**	**37.03**	**-24.12**
44	363	443	403	**30.3**	**79.0**	64.1	29.0	2450.57	28.66	**15.5**	**38.58**	**112.50**
7987	363	443	403	**65.9**	**88.5**	297.0	-63.0	2450.57	-17.52	**-44.5**	**54.56**	**116.05**
7988	363	443	403	**65.9**	**88.5**	280.9	-57.0	2450.57	-20.16	**-37.6**	**56.13**	**125.89**
28	391	417	404	**63.1**	**11.6**	238.0	-11.0	2447.17	-32.44	**-5.6**	**61.79**	**85.84**
126	391	417	404	**43.0**	**-6.0**	113.0	34.0	2447.17	27.41	**18.6**	**28.29**	**22.77**
424	391	417	404	**46.1**	**-68.9**	25.2	-20.2	2447.17	-30.57	**-10.4**	**17.54**	**-82.03**
486	391	417	404	**-37.4**	**148.3**	340.1	-59.2	2447.17	-19.21	**-40.0**	**-55.02**	**159.57**
548	391	417	404	**48.8**	**-64.4**	174.6	76.9	2447.17	9.59	**65.0**	**39.25**	**-63.24**
857	391	417	404	**48.1**	**-66.3**	213.0	58.0	2447.17	19.72	**38.7**	**30.78**	**-78.65**
1725	391	417	404	**42.4**	**-71.2**	146.2	-1.4	2447.17	-34.30	**-0.7**	**64.54**	**-118.02**
3210	391	417	404	**56.9**	**-3.5**	38.0	-47.4	2447.17	-23.61	**-28.5**	**36.53**	**-21.37**
7185	391	417	404	**48.7**	**-59.0**	330.7	-54.3	2447.17	-21.19	**-34.8**	**29.50**	**-47.27**
7217	391	417	404	**51.9**	**-3.5**	246.3	38.4	2447.17	26.27	**21.6**	**36.58**	**-33.81**
8084	390	420	405	**-22.6**	**140.3**	333.5	-17.7	2443.79	-31.05	**-9.1**	**-49.06**	**160.86**
1526	400	412	406	**51.7**	**-4.9**	196.0	-5.0	2440.43	-33.52	**-2.5**	**79.50**	**51.75**
7692	400	412	406	**55.8**	**-123.3**	52.7	-25.6	2440.43	-29.32	**-13.5**	**33.67**	**-151.20**
7821	400	412	406	**55.9**	**-133.3**	52.7	-25.6	2440.43	-29.32	**-13.5**	**33.76**	**-161.23**
528	391	423	407	**40.8**	**-75.8**	358.3	-54.2	2437.07	-21.14	**-34.7**	**19.67**	**-75.15**
1556	391	423	407	**60.0**	**10.0**	26.0	-16.0	2437.07	-31.31	**-8.2**	**30.42**	**-5.32**
1838	391	423	407	**-35.2**	**149.0**	12.3	-36.5	2437.07	-26.66	**-20.3**	**-60.86**	**137.68**
2777	391	423	407	**43.0**	**-6.0**	109.0	34.0	2437.07	27.30	**18.6**	**29.79**	**23.98**
6904	391	423	407	**-41.6**	**-65.4**	263.8	85.9	2437.07	3.12	**81.8**	**-41.86**	**-69.57**

6964	391	423	407	**51.9**	**-3.8**	232.2	31.9	2437.07	27.82	**17.3**	**31.30**	**-29.36**
7214	391	423	407	**40.8**	**-75.8**	358.0	-52.5	2437.07	-21.77	**-33.1**	**19.04**	**-75.02**
7642	391	423	407	**49.9**	**14.2**	355.0	21.0	2437.07	30.27	**10.9**	**79.77**	**-0.12**

Table A4.15 Devonian sample site details, structure corrected data and derived actual palaeomagnetic data. (Data after McElhinny & Lock, 1996)

Table A4.16 Silurian Palaeomagnetic Data

Site Details						Structure Corrected		Derived Actual Paleomagnetic Data				
Number	Age	Age	Age	Site	Site	Correct	Correct	Paleo	Paleo	Palaeo	Pole	Pole
Result	Low Mag	High Mag	Mean	Lat	Long	Dec	Inc	Radius	Colatitude	Latitude	Latitude	Longitude
7984	391	428	409.5	43.7	103.0	161.9	1.8	2428.76	33.97	**0.9**	**10.90**	**113.18**
7985	391	428	409.5	43.7	103.0	190.6	-1.7	2428.76	-33.99	**-0.9**	**75.95**	**128.07**
1260	406	415	410.5	46.7	-68.1	206.0	28.7	2425.46	28.44	**15.3**	**20.27**	**-80.96**
1636	412	417	414.5	45.0	-67.1	179.3	38.0	2412.42	26.00	**21.3**	**19.00**	**-66.78**
2582	410	420	415	56.5	-5.5	40.0	-49.0	2410.80	-22.74	**-29.9**	**37.27**	**-23.69**
6615	410	421	415.5	56.6	-2.8	30.4	-43.2	2409.19	-24.52	**-25.2**	**34.23**	**-17.52**
6617	410	421	415.5	56.6	-2.8	24.0	-10.9	2409.19	-31.95	**-5.5**	**26.24**	**-16.69**
1635	412	419	415.5	45.0	-67.1	163.6	41.3	2409.19	25.07	**23.7**	**20.68**	**-59.75**
253	417	421	419	45.2	-67.0	216.0	62.0	2398.02	17.60	**43.2**	**30.26**	**-78.88**
7565	400	440	420	-24.0	-68.5	261.0	75.0	2394.86	10.60	**61.8**	**-25.22**	**-80.08**
27	417	423	420	63.1	11.6	329.0	-7.0	2394.86	-32.51	**-3.5**	**32.93**	**30.86**
254	417	423	420	45.1	-67.2	25.0	-24.0	2394.86	-29.11	**-12.6**	**17.91**	**-79.68**
649	417	423	420	6.5	99.9	300.0	78.0	2394.86	8.66	**67.0**	**10.76**	**92.27**
1025	417	423	420	39.5	-78.2	345.1	-31.6	2394.86	-27.40	**-17.1**	**12.80**	**-71.23**
1027	417	423	420	41.0	-76.8	359.3	-29.7	2394.86	-27.85	**-15.9**	**13.15**	**-76.46**
2404	417	423	420	53.6	-9.9	306.0	45.0	2394.86	23.85	**26.6**	**61.31**	**-52.84**
2537	417	423	420	53.6	-9.9	291.0	50.0	2394.86	22.26	**30.8**	**55.64**	**-48.69**
6146	417	423	420	53.5	-9.5	282.2	0.3	2394.86	33.78	**0.2**	**47.57**	**-63.14**
6149	417	423	420	53.5	-9.5	282.3	14.4	2394.86	31.08	**7.3**	**48.93**	**-59.65**
7210	417	423	420	41.0	-76.5	4.0	-40.2	2394.86	-25.22	**-22.9**	**15.83**	**-78.27**
7212	417	423	420	40.0	-78.4	337.9	-38.8	2394.86	-25.60	**-21.9**	**15.84**	**-68.67**
8081	417	423	420	24.8	99.1	49.6	-3.2	2394.86	-33.23	**-1.6**	**1.63**	**74.42**
7469	417	426	421.5	49.9	14.1	208.0	-40.0	2390.15	-25.23	**-22.8**	**69.13**	**48.26**
307	417	428	422.5	40.6	-85.8	146.5	43.9	2387.03	24.09	**25.7**	**19.61**	**-71.96**
7096	417	428	422.5	49.5	-56.2	23.6	-14.2	2387.03	-31.02	**-7.2**	**20.18**	**-68.90**

7137	417	428	422.5	37.4	105.6	49.4	-13.1	2387.03	-31.23	**-6.6**	**14.55**	**81.60**
7384	391	458	424.5	50.6	58.3	184.0	64.0	2380.82	16.55	**45.7**	**34.08**	**56.93**
166	423	428	425.5	39.5	-79.5	330.6	-44.2	2377.74	-23.91	**-25.9**	**18.00**	**-67.42**
508	423	428	425.5	53.8	-9.9	66.3	-27.3	2377.74	-28.19	**-14.5**	**36.81**	**-42.60**
510	423	428	425.5	53.8	-10.0	14.0	-14.2	2377.74	-30.90	**-7.2**	**23.46**	**-17.78**
2535	423	428	425.5	53.9	-9.8	34.0	-54.0	2377.74	-20.70	**-34.5**	**35.67**	**-23.88**
2536	423	428	425.5	53.6	-9.9	49.0	1.0	2377.74	33.40	**0.5**	**62.41**	**53.87**
6902	423	428	425.5	-41.6	-65.4	116.1	-38.6	2377.74	-25.47	**-21.8**	**-27.25**	**-91.15**
7072	425	428	426.5	51.2	-2.5	95.0	-24.0	2374.67	-28.87	**-12.6**	**45.14**	**-45.49**
7147	425	434	429.5	49.3	-56.3	28.0	-49.0	2365.55	-22.31	**-29.9**	**28.87**	**-68.04**
7148	425	434	429.5	49.3	-56.3	24.0	-26.0	2365.55	-28.33	**-13.7**	**22.62**	**-68.37**
1444	417	443	430	46.7	-1.0	214.0	11.0	2364.04	31.34	**5.6**	**19.02**	**-18.92**
1804	417	443	430	28.5	109.0	87.4	12.1	2364.04	31.13	**6.1**	**25.41**	**143.87**
6648	417	443	430	-24.0	132.0	292.0	20.0	2364.04	29.57	**10.3**	**-10.65**	**104.25**
7091	428	433	430.5	54.4	-2.5	43.4	-24.1	2362.54	-28.70	**-12.6**	**30.67**	**-25.06**
5931	426	436	431	48.2	-57.8	29.6	1.0	2361.04	33.17	**0.5**	**70.23**	**-4.75**
6140	428	436	432	53.6	-9.9	107.4	11.7	2358.05	31.12	**5.9**	**36.68**	**28.05**
6142	428	436	432	53.6	-9.9	87.3	-31.9	2358.05	-26.91	**-17.3**	**44.83**	**-49.51**
1601	423	443	433	49.1	-55.7	194.0	28.0	2355.07	27.77	**14.9**	**21.89**	**-62.68**
6167	423	443	433	38.8	-4.8	62.0	-36.0	2355.07	-25.89	**-20.0**	**23.83**	**-29.73**
7591	423	443	433	49.5	-55.0	32.9	41.1	2355.07	24.56	**23.6**	**66.67**	**-20.24**
7960	423	443	433	50.0	88.6	25.0	3.0	2355.07	32.72	**1.5**	**73.61**	**142.66**
8083	420	450	435	-22.6	140.3	199.9	-7.5	2349.15	-31.80	**-3.8**	**7.52**	**150.72**
1600	428	443	435.5	49.1	-55.7	180.0	47.0	2347.68	22.77	**28.2**	**26.33**	**-55.70**
1787	428	443	435.5	49.1	-55.4	356.0	-16.8	2347.68	-30.00	**-8.6**	**19.15**	**-53.28**
7957	428	443	435.5	49.5	74.5	124.0	4.0	2347.68	32.43	**2.0**	**26.56**	**104.30**

Table A4.16 Silurian sample site details, structure corrected data and derived actual palaeomagnetic data. (Data after McElhinny & Lock, 1996)

Table A4.17 Ordovician Palaeomagnetic Data

Site Details						Structure Corrected		Derived Actual Paleomagnetic Data				
Number	Age	Age	Age	Site	Site	Correct	Correct	Paleo	Paleo	Palaeo	Pole	Pole
Result	Low Mag	High Mag	Mean	Lat	Long	Dec	Inc	Radius	Colatitude	Latitude	Latitude	Longitude
1230	428	449	438.5	**45.8**	**-62.1**	335.0	-61.0	2338.92	-17.60	**-42.1**	**29.49**	**-53.66**
6476	430	449	439.5	**45.8**	**-62.1**	344.0	-60.0	2336.03	-18.01	**-40.9**	**28.34**	**-56.54**
5991	439	443	441	**40.5**	**-77.2**	357.4	-47.8	2331.72	-22.37	**-28.9**	**18.15**	**-76.16**
5992	439	443	441	**40.1**	**-78.5**	333.0	-43.0	2331.72	-23.79	**-25.0**	**18.33**	**-67.38**
5993	439	443	441	**41.0**	**-77.5**	351.6	-44.0	2331.72	-23.51	**-25.8**	**17.69**	**-73.99**
7566	430	455	442.5	**-24.0**	**-68.5**	320.6	74.0	2327.44	10.90	**60.2**	**-15.42**	**-75.65**
703	428	458	443	**36.6**	**-81.6**	121.7	53.4	2326.01	20.46	**34.0**	**24.27**	**-62.56**
8053	438	449	443.5	**67.5**	**104.0**	160.4	14.3	2324.60	30.19	**7.3**	**38.12**	**116.38**
7794	443	446	444.5	**60.5**	**116.4**	358.0	-52.0	2321.77	-20.91	**-32.6**	**39.60**	**117.33**
7250	440	450	445	**54.4**	**-3.2**	338.6	-42.8	2320.36	-23.73	**-24.8**	**31.75**	**6.74**
590	435	458	446.5	**-33.0**	**19.5**	145.0	-37.0	2316.15	-25.21	**-20.6**	**-11.54**	**5.06**
203	436	458	447	**55.5**	**-133.5**	115.0	-13.9	2314.76	-30.14	**-7.1**	**56.40**	**-188.81**
7795	446	449	447.5	**60.5**	**116.4**	187.0	16.0	2313.36	29.72	**8.2**	**30.90**	**112.36**
1233	428	470	449	**34.2**	**-85.3**	138.5	26.1	2309.20	27.63	**13.8**	**12.16**	**-66.98**
7476	440	460	450	**38.5**	**-78.2**	143.0	24.0	2306.45	28.04	**12.6**	**14.81**	**-61.18**
88	443	458	450.5	**48.2**	**-4.5**	355.0	-58.0	2305.07	-18.57	**-38.7**	**29.68**	**-2.67**
2018	443	458	450.5	**40.0**	**-78.0**	168.6	31.8	2305.07	26.33	**17.2**	**14.06**	**-72.81**
7320	443	458	450.5	**40.8**	**-75.6**	346.0	-47.0	2305.07	-22.36	**-28.2**	**18.96**	**-70.02**
7641	443	458	450.5	**49.9**	**14.2**	183.0	-59.0	2305.07	-18.18	**-39.8**	**68.03**	**16.70**
8006	443	458	450.5	**66.0**	**64.0**	259.0	-17.0	2305.07	-29.42	**-8.7**	**56.50**	**124.87**
8007	443	458	450.5	**66.0**	**64.0**	240.0	-12.0	2305.07	-30.37	**-6.1**	**63.00**	**138.67**
6533	449	453	451	**60.8**	**10.5**	53.0	-40.0	2303.70	-24.31	**-22.8**	**42.42**	**-15.95**
202	449	458	453.5	**55.8**	**-133.4**	76.4	-2.7	2296.89	-31.96	**-1.4**	**39.18**	**-174.98**
2009	449	458	453.5	**-31.3**	**-69.4**	147.3	35.9	2296.89	25.27	**19.9**	**-50.97**	**-47.91**
3253	449	458	453.5	**53.5**	**-6.1**	145.0	-25.0	2296.89	-27.72	**-13.1**	**69.76**	**-56.55**

7441	449	458	453.5	**46.5**	**-69.0**	339.0	-28.0	2296.89	-27.08	**-14.9**	**20.69**	**-58.96**
872	430	480	455	**60.7**	**5.6**	322.0	21.0	2292.84	28.48	**10.9**	**71.88**	**-65.16**
526	450	460	455	**35.5**	**-80.0**	220.5	23.5	2292.84	27.98	**12.3**	**12.85**	**-98.21**
1011	450	460	455	**35.0**	**-80.2**	162.2	41.0	2292.84	23.94	**23.5**	**11.99**	**-72.92**
6028	452	458	455	**54.5**	**-3.0**	0.3	-81.5	2292.84	-5.99	**-73.4**	**48.51**	**-3.05**
2405	443	475	459	**53.6**	**-9.9**	197.0	48.0	2282.18	21.84	**29.0**	**32.42**	**-17.30**
2406	443	475	459	**53.6**	**-9.9**	335.0	20.0	2282.18	28.55	**10.3**	**74.59**	**-59.37**
7714	449	470	459.5	**46.8**	**-68.7**	327.0	-21.0	2280.86	-28.33	**-10.9**	**21.67**	**-52.55**
8052	458	464	461	**67.5**	**104.0**	311.4	16.6	2276.93	29.14	**8.5**	**68.47**	**19.75**
1977	458	467	462.5	**54.5**	**-2.8**	284.0	73.0	2273.01	11.22	**58.6**	**55.68**	**-22.36**
1978	458	467	462.5	**54.5**	**-2.8**	329.0	-49.0	2273.01	-21.44	**-29.9**	**35.16**	**10.51**
7796	462	464	463	**59.8**	**118.1**	342.0	7.0	2271.71	30.84	**3.5**	**80.86**	**31.90**
156	458	470	464	**36.1**	**-83.5**	319.7	-12.7	2269.13	-29.77	**-6.4**	**11.86**	**-64.35**
1098	458	470	464	**52.1**	**-7.4**	324.3	-62.6	2269.13	-16.40	**-44.0**	**38.04**	**4.67**
1552	458	470	464	**44.0**	**-73.0**	311.0	-9.0	2269.13	-30.44	**-4.5**	**21.09**	**-48.81**
1554	458	470	464	**44.0**	**-73.0**	10.0	-29.0	2269.13	-26.54	**-15.5**	**17.76**	**-77.67**
1993	458	470	464	**52.5**	**-3.0**	304.0	-52.0	2269.13	-20.44	**-32.6**	**38.65**	**18.76**
1997	458	470	464	**52.5**	**-3.0**	112.0	51.0	2269.13	20.77	**31.7**	**41.37**	**22.98**
3399	458	470	464	**55.2**	**-4.9**	202.0	21.0	2269.13	28.19	**10.9**	**28.28**	**-16.49**
5981	458	470	464	**49.5**	**-54.8**	172.0	49.0	2269.13	21.40	**29.9**	**28.25**	**-51.49**
6430	458	470	464	**52.1**	**-3.3**	153.8	69.8	2269.13	12.95	**53.7**	**40.21**	**4.14**
6431	458	470	464	**52.1**	**-3.3**	173.3	43.0	2269.13	23.15	**25.0**	**29.06**	**-0.29**
6577	458	470	464	**46.0**	**-68.6**	92.0	40.0	2269.13	23.95	**22.8**	**40.36**	**-36.43**
7237	457	472	464.5	**47.0**	**-66.0**	60.0	69.0	2267.84	13.35	**52.5**	**52.22**	**-46.94**
7199	464	467	465.5	**54.7**	**-3.1**	0.0	-41.0	2265.27	-23.65	**-23.5**	**31.05**	**-3.10**
158	464	470	467	**35.9**	**-84.0**	346.0	-44.0	2261.43	-22.80	**-25.8**	**13.65**	**-78.46**
733	464	470	467	**52.2**	**-3.3**	181.7	54.5	2261.43	19.51	**35.0**	**32.69**	**-3.97**
1762	464	470	467	**48.5**	**-59.1**	143.8	35.0	2261.43	25.10	**19.3**	**26.84**	**-42.79**
1999	464	470	467	**52.5**	**-3.0**	167.3	30.9	2261.43	26.03	**16.7**	**26.89**	**3.21**
2410	464	470	467	**53.7**	**-6.4**	193.0	26.0	2261.43	27.08	**13.7**	**27.06**	**-13.00**
2529	464	470	467	**54.7**	**-3.1**	312.0	-63.0	2261.43	-16.17	**-44.5**	**42.55**	**13.21**

5980	464	470	467	**49.5**	**-54.7**	162.0	50.0	2261.43	21.02	**30.8**	**29.23**	**-47.40**
6138	464	470	467	**52.2**	**-3.3**	171.0	54.0	2261.43	19.69	**34.5**	**32.68**	**0.29**
6327	464	470	467	**52.6**	**-3.0**	116.4	67.9	2261.43	13.87	**50.9**	**44.95**	**14.66**
8051	464	470	467	**67.5**	**104.0**	314.5	28.1	2261.43	26.64	**14.9**	**71.10**	**23.18**
1759	467	470	468.5	**48.5**	**-58.9**	150.0	40.7	2257.63	23.65	**23.3**	**27.12**	**-45.88**
2530	467	470	468.5	**54.7**	**-3.1**	14.0	-51.0	2257.63	-20.66	**-31.7**	**34.46**	**-9.04**
104	443	495	469	**43.7**	**-5.8**	202.0	78.0	2256.36	8.16	**67.0**	**36.07**	**-9.57**
648	443	495	469	**6.4**	**99.9**	338.0	62.0	2256.36	16.56	**43.2**	**21.68**	**93.30**
2407	443	495	469	**53.2**	**-6.9**	177.0	28.0	2256.36	26.60	**14.9**	**26.62**	**-5.40**
2408	443	495	469	**53.6**	**-6.2**	233.0	-18.0	2256.36	-28.61	**-9.2**	**61.36**	**46.71**
2409	443	495	469	**53.5**	**-6.2**	203.0	2.0	2256.36	31.52	**1.0**	**23.51**	**-19.07**
3127	443	495	469	**-18.0**	**-67.0**	42.0	84.0	2256.36	4.20	**78.1**	**-14.85**	**-64.09**
3142	443	495	469	**-24.0**	**-65.0**	52.0	53.0	2256.36	19.99	**33.6**	**-10.95**	**-49.08**
5930	443	495	469	**46.7**	**-68.1**	94.1	17.3	2256.36	28.74	**8.9**	**37.92**	**-30.66**
2827	440	500	470	**56.2**	**-5.8**	59.0	-57.0	2253.84	-18.54	**-37.6**	**44.17**	**-28.13**
1253	445	497	471	**-23.9**	**16.5**	342.0	9.0	2251.34	30.20	**4.5**	**5.01**	**7.52**
8125	464	478	471	**49.5**	**-54.5**	88.0	33.0	2251.34	25.45	**18.0**	**44.14**	**-17.75**
7093	467	475	471	**49.8**	**13.7**	312.0	83.0	2251.34	4.88	**76.2**	**52.91**	**7.69**
5979	471	475	473	**49.5**	**-56.0**	165.0	55.0	2246.36	19.21	**35.5**	**30.78**	**-50.31**
622	464	485	474.5	**55.2**	**-5.0**	248.3	47.7	2242.65	21.55	**28.8**	**43.33**	**-32.98**
6294	464	485	474.5	**59.0**	**15.0**	138.0	62.0	2242.65	16.46	**43.2**	**45.53**	**30.70**
6535	464	485	474.5	**59.0**	**15.5**	119.0	68.1	2242.65	13.66	**51.2**	**50.71**	**34.53**
7961	458	495	476.5	**50.8**	**74.6**	109.0	2.0	2237.75	31.26	**1.0**	**33.76**	**110.77**
397	470	485	477.5	**48.0**	**-2.5**	235.0	75.0	2235.32	9.89	**61.8**	**41.77**	**-13.37**
483	470	485	477.5	**46.7**	**-1.5**	261.0	72.0	2235.32	11.58	**57.0**	**43.74**	**-17.43**
492	470	485	477.5	**53.6**	**-9.5**	192.0	28.0	2235.32	26.35	**14.9**	**27.62**	**-15.48**
6229	470	485	477.5	**25.5**	**103.0**	300.7	66.1	2235.32	14.58	**48.5**	**32.18**	**88.18**
8050	470	485	477.5	**67.5**	**104.0**	319.9	32.4	2235.32	25.40	**17.6**	**73.77**	**22.75**
6304	460	500	480	**48.2**	**-4.5**	252.0	50.5	2229.28	20.56	**31.2**	**38.73**	**-29.85**
687	458	505	481.5	**51.7**	**-117.0**	114.4	-22.7	2225.69	-27.32	**-11.8**	**54.56**	**-163.12**
6246	458	505	481.5	**36.0**	**118.0**	342.9	-37.7	2225.69	-24.06	**-21.1**	**12.79**	**125.06**

589	470	495	482.5	**-34.1**	**18.4**	174.0	-47.0	2223.31	-21.57	**-28.2**	**-12.63**	**16.14**
1445	470	495	482.5	**46.7**	**-1.0**	244.0	5.0	2223.31	30.53	**2.5**	**28.30**	**-32.24**
1757	470	495	482.5	**48.5**	**-58.9**	148.5	33.6	2223.31	25.00	**18.4**	**26.11**	**-44.67**
2542	470	495	482.5	**52.0**	**-5.2**	61.0	-34.0	2223.31	-24.90	**-18.6**	**36.09**	**-32.31**
6402	470	495	482.5	**49.5**	**-55.0**	171.0	22.0	2223.31	27.42	**11.4**	**22.30**	**-50.53**
6490	470	495	482.5	**48.5**	**-59.1**	163.0	34.0	2223.31	24.90	**18.6**	**24.36**	**-51.33**
7825	470	495	482.5	**-26.0**	**-66.5**	101.7	49.2	2223.31	20.91	**30.1**	**-28.33**	**-43.11**
6157	477	490	483.5	**52.0**	**-5.0**	298.0	75.0	2220.94	9.83	**61.8**	**55.67**	**-20.50**
1158	450	520	485	**-30.3**	**139.5**	333.0	-12.0	2217.41	-29.21	**-6.1**	**-54.67**	**162.03**
1162	450	520	485	**-30.4**	**139.4**	273.0	11.0	2217.41	29.39	**5.6**	**-24.75**	**106.74**
6303	477	495	486	**48.2**	**-4.5**	261.0	71.0	2215.07	12.01	**55.4**	**45.03**	**-21.41**
13	470	505	487.5	**48.7**	**-3.0**	325.0	37.0	2211.57	24.08	**20.6**	**65.02**	**-36.65**
1447	470	505	487.5	**46.7**	**-1.0**	267.0	1.0	2211.57	31.07	**0.5**	**37.22**	**-41.33**
6006	470	505	487.5	**82.5**	**-43.4**	16.0	-16.0	2211.57	-28.41	**-8.2**	**54.33**	**-56.40**
8049	485	495	490	**67.5**	**104.0**	333.3	37.2	2205.81	23.97	**20.8**	**79.45**	**18.52**
8082	485	500	492.5	**-22.6**	**140.3**	274.5	4.3	2200.10	30.34	**2.2**	**-17.16**	**108.50**
500	480	510	495	**53.5**	**-9.9**	237.5	47.8	2194.46	21.06	**28.9**	**39.45**	**-33.00**
1345	480	510	495	**52.3**	**-3.1**	127.9	39.2	2194.46	23.36	**22.2**	**35.27**	**19.43**
450	481	513	497	**38.5**	**-108.5**	156.3	18.8	2190.00	27.62	**9.7**	**12.67**	**-97.49**
214	495	500	497.5	**30.7**	**-99.3**	97.0	3.0	2188.88	30.41	**1.5**	**22.79**	**-66.28**
213	495	503	499	**30.9**	**-98.4**	121.0	7.0	2185.57	29.67	**3.5**	**13.15**	**-72.57**
2245	495	503	499	**31.0**	**-99.2**	101.7	13.3	2185.57	28.56	**6.7**	**21.67**	**-68.95**
1255	450	550	500	**-26.5**	**17.5**	120.0	-68.0	2183.37	-13.35	**-51.1**	**-19.32**	**5.27**
269	495	505	500	**36.4**	**-114.7**	122.1	-14.4	2183.37	-28.34	**-7.3**	**46.50**	**-150.44**
1289	495	505	500	**-79.2**	**-86.0**	22.0	13.0	2183.37	28.59	**6.6**	**-51.21**	**-69.38**
1446	495	505	500	**46.7**	**-1.0**	329.0	9.0	2183.37	29.29	**4.5**	**67.27**	**-41.71**
5976	495	505	500	**34.4**	**-97.2**	109.2	10.5	2183.37	29.03	**5.3**	**21.24**	**-67.75**
8048	495	505	500	**67.5**	**104.0**	331.7	32.5	2183.37	24.79	**17.7**	**78.53**	**15.83**
8202	500	505	502.5	**-40.7**	**145.0**	58.3	11.1	2177.92	28.85	**5.6**	**-22.27**	**171.34**
6172	494	514	504	**32.1**	**-107.7**	262.0	5.0	2174.68	29.87	**2.5**	**23.71**	**-140.29**
210	503	505	504	**30.8**	**-99.0**	135.0	9.0	2174.68	29.18	**4.5**	**8.68**	**-78.59**

211	503	505	504	**30.6**	**-98.9**	134.0	11.0	2174.68	28.83	**5.6**	**9.07**	**-78.34**
212	503	505	504	**30.8**	**-98.4**	132.0	10.0	2174.68	29.00	**5.0**	**9.74**	**-76.96**
697	503	505	504	**36.1**	**-83.9**	170.0	24.0	2174.68	26.44	**12.6**	**9.98**	**-79.40**
698	503	505	504	**36.1**	**-83.9**	153.0	17.0	2174.68	27.75	**8.7**	**10.73**	**-71.47**

Table A4.17 Ordovician sample site details, structure corrected data and derived actual palaeomagnetic data. (Data after McElhinny & Lock, 1996)

Table A4.18 Cambrian Palaeomagnetic Data

Site Details						Structure Corrected		Derived Actual Paleomagnetic Data				
Number	Age	Age	Age	Site	Site	Correct	Correct	Paleo	Paleo	Palaeo	Pole	Pole
Result	Low Mag	High Mag	Mean	Lat	Long	Dec	Inc	Radius	Colatitude	Latitude	Latitude	Longitude
8010	495	518	506.5	**53.0**	**90.0**	331.0	14.0	2169.33	28.23	**7.1**	**72.29**	**41.08**
8011	495	518	506.5	**52.0**	**93.0**	331.0	12.0	2169.33	28.58	**6.1**	**71.73**	**45.29**
2543	500	520	510	**53.6**	**-9.9**	227.0	23.0	2161.93	26.48	**12.0**	**32.69**	**-32.69**
7475	505	515	510	**38.5**	**-78.2**	92.0	17.0	2161.93	27.59	**8.7**	**32.62**	**-44.86**
162	505	518	511.5	**36.8**	**-115.3**	130.0	-18.0	2158.80	-27.37	**-9.2**	**50.23**	**-148.70**
7626	505	518	511.5	**33.2**	**-8.2**	300.0	-31.0	2158.80	-24.83	**-16.7**	**18.74**	**14.38**
7627	505	518	511.5	**33.2**	**-8.2**	121.0	20.0	2158.80	27.00	**10.3**	**16.99**	**15.81**
1000	512	518	515	**46.1**	**-60.4**	293.0	-66.0	2151.57	-14.08	**-48.3**	**39.27**	**-43.59**
6467	512	525	518.5	**39.8**	**-77.5**	137.7	36.0	2144.46	23.57	**20.0**	**21.06**	**-60.74**
65	495	545	520	**49.7**	**-1.7**	281.0	80.0	2141.45	6.53	**70.6**	**50.51**	**-11.81**
1159	495	545	520	**-30.5**	**138.6**	40.0	15.0	2141.45	27.69	**7.6**	**-8.21**	**156.16**
1163	495	545	520	**-30.6**	**138.6**	47.0	-9.0	2141.45	-28.73	**-4.5**	**-46.76**	**107.72**
1169	495	545	520	**-31.5**	**138.6**	246.0	-40.0	2141.45	-22.60	**-22.8**	**-20.43**	**160.60**
2704	495	545	520	**-24.0**	**-66.0**	41.0	-34.0	2141.45	-23.99	**-18.6**	**-40.69**	**-86.59**
2705	495	545	520	**-24.0**	**-66.0**	44.0	-25.0	2141.45	-25.84	**-13.1**	**-40.73**	**-89.55**
2706	495	545	520	**-22.0**	**-65.0**	87.0	-4.0	2141.45	-29.58	**-2.0**	**-20.47**	**-96.75**
2710	495	545	520	**-23.5**	**-66.0**	53.2	-19.3	2141.45	-26.91	**-9.9**	**-37.17**	**-93.06**
161	518	525	521.5	**36.8**	**-115.3**	130.0	-14.0	2138.45	-27.82	**-7.1**	**50.35**	**-149.38**
2562	500	550	525	**-23.7**	**17.2**	212.3	-24.7	2131.54	-25.78	**-13.0**	**-1.45**	**30.64**
215	505	545	525	**39.6**	**-77.7**	128.0	2.0	2131.54	29.78	**1.0**	**18.52**	**-53.32**
216	505	545	525	**36.1**	**-84.0**	146.0	8.0	2131.54	28.77	**4.0**	**11.19**	**-68.08**
6039	505	545	525	**52.6**	**-1.5**	232.0	1.0	2131.54	29.94	**0.5**	**30.11**	**-28.55**
6245	505	545	525	**36.0**	**118.0**	321.0	-34.7	2131.54	-23.72	**-19.1**	**16.57**	**133.32**
6929	505	545	525	**43.0**	**-5.8**	142.0	30.4	2131.54	24.64	**16.3**	**22.31**	**10.31**
7970	505	545	525	**50.1**	**95.1**	41.0	-14.0	2131.54	-27.73	**-7.1**	**26.98**	**75.06**

7971	505	545	525	**50.1**	**95.1**	318.0	13.0	2131.54	27.91	**6.6**	**64.30**	**48.87**
8012	505	545	525	**51.0**	**86.0**	96.0	-26.0	2131.54	-25.53	**-13.7**	**46.86**	**47.19**
8013	505	545	525	**51.0**	**86.0**	134.0	-22.0	2131.54	-26.29	**-11.4**	**62.92**	**41.58**
8014	505	545	525	**51.0**	**86.0**	0.0	-4.0	2131.54	-29.44	**-2.0**	**21.56**	**86.00**
64	518	545	531.5	**49.7**	**-1.7**	208.0	29.0	2119.00	24.78	**15.5**	**26.94**	**-14.45**
163	518	545	531.5	**36.8**	**-115.3**	124.0	-3.0	2119.00	-29.44	**-1.5**	**47.88**	**-152.71**
624	518	545	531.5	**49.7**	**-1.7**	316.0	82.0	2119.00	5.22	**74.3**	**53.31**	**-7.77**
1747	518	545	531.5	**46.0**	**-60.1**	281.0	32.0	2119.00	24.16	**17.4**	**45.28**	**-94.93**
1748	518	545	531.5	**45.9**	**-60.0**	323.8	49.5	2119.00	19.84	**30.3**	**60.01**	**-83.64**
1753	518	545	531.5	**47.5**	**-53.2**	279.3	47.6	2119.00	20.39	**28.7**	**46.81**	**-83.36**
2943	518	545	531.5	**51.8**	**-5.0**	185.0	23.0	2119.00	25.95	**12.0**	**25.92**	**-7.43**
7968	518	545	531.5	**52.0**	**86.8**	171.0	3.0	2119.00	29.44	**1.5**	**22.80**	**91.58**
7972	518	545	531.5	**46.3**	**96.1**	227.8	29.1	2119.00	24.76	**15.6**	**27.52**	**75.62**
1131	525	545	535	**61.0**	**126.8**	58.1	3.9	2112.40	29.19	**2.0**	**62.68**	**191.27**
6675	525	545	535	**64.3**	**-131.8**	265.0	-79.0	2112.40	-7.04	**-68.8**	**64.02**	**-115.61**
122	530	540	535	**52.5**	**-2.8**	321.8	14.5	2112.40	27.40	**7.4**	**67.59**	**-51.10**
2158	530	540	535	**52.5**	**-2.8**	307.0	30.0	2112.40	24.50	**16.1**	**60.91**	**-45.74**
61	538	554	546	**48.8**	**-3.0**	191.8	38.2	2092.33	22.50	**21.5**	**26.64**	**-8.02**
62	535	559	547	**48.8**	**-3.0**	88.8	-37.1	2090.55	-22.74	**-20.7**	**43.52**	**-35.20**
8150	500	600	550	**25.3**	**103.0**	296.7	-18.8	2085.27	-26.30	**-9.7**	**11.72**	**126.84**
252	550	560	555	**-18.3**	**13.5**	278.0	-34.0	2076.63	-23.26	**-18.6**	**-19.92**	**38.08**
702	525	600	562.5	**36.6**	**-81.6**	275.8	-16.6	2064.03	-26.41	**-8.5**	**29.86**	**-50.92**
7979	548	590	569	**46.5**	**95.5**	224.0	-14.0	2053.46	-26.72	**-7.1**	**60.52**	**134.90**

Table A4.18 Cambrian sample site details, structure corrected data and derived actual palaeomagnetic data. (Data after McElhinny & Lock, 1996)

Table A4.19
Neoproterozoic
Palaeomagnetic Data

Site Details						Structure Corrected		Derived Actual Paleomagnetic Data				
Number	Age	Age	Age	Site	Site	Correct	Correct	Paleo	Paleo	Palaeo	Pole	Pole
Result	Low Mag	High Mag	Mean	Lat	Long	Dec	Inc	Radius	Colatitude	Latitude	Latitude	Longitude
1645	541	605	573	**45.6**	**-75.4**	288.7	-49.3	2047.10	-19.23	**-30.2**	**36.92**	**-52.44**
1256	550	600	575	**-26.5**	**17.5**	87.0	31.0	2043.97	23.51	**16.7**	**-22.98**	**43.14**
7772	550	600	575	**64.6**	**-132.9**	64.0	56.0	2043.97	17.15	**36.5**	**66.72**	**-90.78**
7773	550	600	575	**63.4**	**-128.5**	62.0	77.0	2043.97	7.95	**65.2**	**66.15**	**-110.91**
1754	560	590	575	**50.2**	**-66.5**	105.4	82.1	2043.97	4.98	**74.5**	**48.65**	**-59.23**
7975	518	650	584	**52.8**	**93.5**	328.0	-9.0	2030.20	-27.24	**-4.5**	**28.26**	**109.48**
7976	518	650	584	**51.3**	**90.7**	144.0	-21.0	2030.20	-25.22	**-10.9**	**67.16**	**50.53**
7978	518	650	584	**46.4**	**96.0**	221.0	8.0	2030.20	27.40	**4.0**	**23.79**	**76.73**
1242	545	630	587.5	**42.3**	**-71.2**	218.7	70.8	2025.00	11.08	**55.1**	**33.34**	**-79.47**
8114	580	600	590	**-31.6**	**138.6**	56.6	29.3	2021.34	23.58	**15.7**	**-17.02**	**159.04**
7474	579	615	597	**38.5**	**-78.2**	68.0	84.0	2011.29	3.75	**78.1**	**39.82**	**-73.67**
6038	545	650	597.5	**52.6**	**-1.5**	145.0	-66.0	2010.59	-13.16	**-48.3**	**62.47**	**-17.91**
7649	545	650	597.5	**69.5**	**29.5**	125.0	67.0	2010.59	12.73	**49.7**	**60.39**	**50.92**
2156	400	800	600	**52.5**	**-2.8**	63.3	85.7	2007.09	2.69	**81.4**	**53.64**	**1.26**
249	550	650	600	**-18.3**	**13.5**	102.0	-13.0	2007.09	-26.28	**-6.6**	**-11.19**	**-12.70**
251	550	650	600	**-18.3**	**13.5**	291.0	-48.0	2007.09	-19.20	**-29.0**	**-24.11**	**33.16**
6938	550	650	600	**54.0**	**-59.5**	110.8	50.1	2007.09	18.63	**30.9**	**44.43**	**-34.79**
1168	590	610	600	**-30.5**	**139.0**	189.0	-44.0	2007.09	-20.23	**-25.8**	**-10.48**	**142.15**
1196	590	620	605	**21.3**	**43.7**	348.3	27.6	2000.20	23.66	**14.6**	**44.33**	**37.17**
164	545	670	607.5	**36.8**	**-115.3**	77.5	0.5	1996.81	28.13	**0.3**	**37.59**	**-79.79**
560	600	620	610	**-32.4**	**138.0**	191.9	-9.6	1993.47	-26.65	**-4.8**	**-6.22**	**143.34**
6354	600	620	610	**-32.4**	**138.0**	185.2	-3.6	1993.47	-27.60	**-1.8**	**-4.89**	**140.42**
7597	600	620	610	**-31.2**	**138.7**	17.4	7.1	1993.47	27.05	**3.6**	**-5.18**	**146.55**

1164	600	650	625	**-30.5**	**139.3**	22.0	39.0	1974.16	21.06	**22.0**	**-10.75**	**147.17**
1337	600	650	625	**56.2**	**-5.8**	163.5	-6.7	1974.16	-26.85	**-3.4**	**79.20**	**-49.02**
2826	600	650	625	**56.2**	**-5.8**	166.0	-12.0	1974.16	-26.01	**-6.1**	**79.58**	**-41.73**
800	600	664	632	**52.7**	**-2.7**	78.3	16.8	1965.59	25.12	**8.6**	**50.57**	**38.18**
6040	600	664	632	**52.5**	**-3.0**	94.1	19.0	1965.59	24.75	**9.8**	**44.61**	**32.92**
6041	600	664	632	**52.5**	**-3.0**	94.1	19.0	1965.59	24.75	**9.8**	**44.61**	**32.92**
801	557	719	638	**52.7**	**-2.7**	71.9	54.2	1958.46	16.99	**34.7**	**54.66**	**26.00**
54	628	652	640	**48.8**	**-3.0**	226.4	-15.7	1956.12	-25.18	**-8.0**	**60.95**	**36.38**
1254	600	700	650	**-27.0**	**17.5**	20.0	-11.0	1944.76	-25.78	**-5.6**	**-50.62**	**3.94**
250	617	685	651	**-18.3**	**13.5**	354.0	34.0	1943.66	21.77	**18.6**	**3.36**	**11.27**
7740	646	660	653	**70.1**	**28.7**	110.3	52.3	1941.46	17.40	**32.9**	**59.54**	**62.29**
2762	546	786	666	**31.6**	**55.8**	24.6	-31.9	1927.63	-22.00	**-17.3**	**11.29**	**46.65**
248	660	680	670	**-18.3**	**13.5**	12.0	36.0	1923.53	21.15	**20.0**	**2.42**	**17.81**
2077	600	750	675	**48.2**	**-113.8**	267.9	15.5	1918.52	24.73	**7.9**	**41.83**	**-147.92**
799	605	749	677	**52.5**	**-3.1**	135.8	-24.5	1916.55	-23.21	**-12.8**	**64.31**	**-42.44**
7771	650	720	685	**64.6**	**-132.9**	59.0	-62.0	1908.83	-14.01	**-43.2**	**55.38**	**-154.33**
1160	650	750	700	**-30.4**	**139.4**	199.0	-21.1	1895.09	-23.52	**-10.9**	**-7.96**	**146.94**
8149	670	730	700	**25.3**	**103.0**	290.7	-56.6	1895.09	-15.71	**-37.2**	**18.96**	**118.54**
1660	720	726	723	**68.3**	**-121.5**	74.0	-7.0	1875.76	-25.46	**-3.5**	**52.66**	**-164.45**
2080	720	726	723	**73.6**	**-95.9**	95.0	36.5	1875.76	20.52	**20.3**	**62.85**	**-45.97**
6599	700	750	725	**63.2**	**-127.0**	303.0	45.0	1874.17	18.66	**26.6**	**67.55**	**-171.65**
6600	700	750	725	**63.2**	**-127.0**	323.0	37.0	1874.17	20.40	**20.6**	**74.18**	**-177.32**
6602	700	750	725	**62.7**	**-126.6**	275.0	42.0	1874.17	19.35	**24.2**	**58.40**	**-165.63**
6644	700	750	725	**64.8**	**-140.0**	228.0	-13.0	1874.17	-24.54	**-6.6**	**70.29**	**-73.76**
1213	680	780	730	**34.7**	**-98.8**	236.8	20.7	1870.27	23.28	**10.7**	**20.18**	**-119.43**
2765	720	740	730	**26.0**	**73.0**	354.5	53.5	1870.27	16.43	**34.0**	**42.34**	**70.90**
342	700	780	740	**64.5**	**-128.0**	262.9	47.9	1862.72	17.85	**29.0**	**57.44**	**-162.41**
1713	700	780	740	**64.7**	**-127.0**	262.0	49.0	1862.72	17.57	**29.9**	**57.56**	**-160.87**
1744	700	780	740	**64.6**	**-127.9**	258.0	42.0	1862.72	19.23	**24.2**	**55.44**	**-162.51**
6595	700	780	740	**63.0**	**-126.8**	269.0	49.0	1862.72	17.57	**29.9**	**57.89**	**-161.40**
6598	700	780	740	**63.2**	**-127.0**	277.0	52.0	1862.72	16.78	**32.6**	**60.51**	**-162.59**

6601	700	780	740	**62.7**	**-126.6**	295.0	46.0	1862.72	18.31	**27.4**	**64.76**	**-168.49**
6594	730	780	755	**63.0**	**-126.8**	264.0	6.0	1852.01	25.29	**3.0**	**51.75**	**-170.14**
6597	730	780	755	**63.2**	**-127.0**	273.0	40.0	1852.01	19.55	**22.8**	**58.11**	**-166.23**
6643	733	777	755	**64.8**	**-140.0**	180.0	-6.0	1852.01	-25.29	**-3.0**	**89.91**	**40.00**
1674	776	780	778	**63.8**	**-128.5**	304.0	19.5	1836.95	23.06	**10.0**	**67.26**	**-185.64**
1675	776	780	778	**63.8**	**-128.5**	266.0	48.0	1836.95	17.58	**29.0**	**57.79**	**-162.91**
6603	776	780	778	**62.9**	**-126.6**	68.0	78.0	1836.95	6.64	**67.0**	**64.69**	**-112.08**
6080	771	805	788	**57.5**	**-7.0**	140.8	64.5	1830.88	12.54	**46.4**	**47.12**	**4.64**
6093	771	805	788	**58.1**	**-5.3**	118.0	59.0	1830.88	14.44	**39.8**	**49.49**	**14.51**
2052	600	1000	800	**47.0**	**-88.5**	280.6	-9.5	1823.94	-24.40	**-4.8**	**37.90**	**-57.54**
892	750	850	800	**-28.4**	**21.6**	91.0	-6.0	1823.94	-24.91	**-3.0**	**-25.15**	**-6.12**
1700	780	850	815	**72.8**	**-110.1**	101.0	18.0	1815.79	23.02	**9.2**	**59.00**	**-61.92**
1712	780	850	815	**64.7**	**-127.0**	266.0	-17.0	1815.79	-23.17	**-8.7**	**57.44**	**-80.15**
6591	780	850	815	**63.4**	**-127.0**	97.0	-21.0	1815.79	-22.55	**-10.9**	**57.85**	**-172.68**
2155	650	1000	825	**52.5**	**-2.8**	156.0	-34.0	1810.65	-20.28	**-18.6**	**69.54**	**-26.59**
341	780	880	830	**64.5**	**-128.0**	271.0	24.0	1808.17	21.98	**12.6**	**57.12**	**-171.58**
1743	780	880	830	**64.6**	**-127.9**	267.0	21.0	1808.17	22.46	**10.9**	**55.71**	**-170.53**
1156	800	880	840	**-30.3**	**139.5**	178.0	73.0	1803.37	8.90	**58.6**	**-39.19**	**139.90**
1693	800	900	850	**50.5**	**-116.0**	274.0	19.0	1798.79	22.65	**9.8**	**46.82**	**-150.16**

Table A4.19 Neoproterozoic sample site details, structure corrected data and derived actual palaeomagnetic data. (Data after McElhinny & Lock, 1996)

Table A4.20

Mesoproterozoic
Palaeomagnetic Data

Site Details						Structure Corrected		Derived Actual Paleomagnetic Data				
Number	Age	Age	Age	Site	Site	Correct	Correct	Paleo	Paleo	Palaeo	Pole	Pole
Result	Low Mag	High Mag	Mean	Lat	Long	Dec	Inc	Radius	Colatitude	Latitude	Latitude	Longitude
891	800	1050	925	**-28.4**	**21.6**	170.0	-7.0	1770.30	-24.03	-3.5	**-4.68**	**17.53**
247	900	1000	950	**-18.3**	**13.5**	312.0	40.0	1762.76	18.60	22.8	**-5.45**	**-0.28**
1641	900	1000	950	**46.9**	**-92.3**	292.0	-42.0	1762.76	-18.20	-24.2	**37.86**	**-70.79**
6091	946	994	970	**58.2**	**-5.2**	318.0	16.0	1757.32	22.57	8.2	**69.25**	**-51.66**
6092	946	994	970	**58.2**	**-5.2**	315.0	17.0	1757.32	22.43	8.7	**68.09**	**-51.50**
8242	938	1016	977	**58.6**	**-5.1**	122.3	50.5	1755.52	16.19	31.2	**47.91**	**15.49**
2656	900	1100	1000	**54.5**	**-62.0**	136.0	52.0	1750.02	15.76	32.6	**42.07**	**-47.27**
1642	950	1050	1000	**46.9**	**-91.8**	308.0	-1.0	1750.02	-24.59	-0.5	**29.27**	**-69.72**
1898	900	1180	1040	**-26.2**	**128.7**	322.0	-35.0	1741.72	-19.33	-19.3	**-40.59**	**144.27**
7989	980	1100	1040	**66.2**	**88.5**	20.4	-61.4	1741.72	-12.98	-42.5	**53.77**	**80.89**
7990	980	1100	1040	**66.0**	**88.5**	41.5	-17.4	1741.72	-22.17	-8.9	**46.97**	**67.00**
7991	980	1100	1040	**66.2**	**88.5**	39.3	-55.9	1741.72	-14.64	-36.4	**53.74**	**72.80**
7992	980	1100	1040	**66.0**	**88.5**	16.6	-56.8	1741.72	-14.39	-37.4	**52.01**	**81.88**
2053	1000	1092	1046	**47.0**	**-88.5**	276.8	8.1	1740.60	23.48	4.1	**44.67**	**-122.29**
1694	900	1200	1050	**50.5**	**-116.0**	331.0	47.0	1739.87	16.88	28.2	**64.15**	**-134.83**
2051	1050	1060	1055	**47.0**	**-88.5**	272.4	1.5	1738.98	24.36	0.8	**42.69**	**-122.60**
945	1070	1088	1079	**47.7**	**-85.7**	293.8	23.8	1734.96	21.12	12.4	**51.98**	**-118.07**
946	1070	1088	1079	**47.7**	**-85.7**	298.2	13.4	1734.96	22.66	6.8	**53.62**	**-120.62**
8163	1050	1115	1082.5	**45.4**	**-92.7**	275.2	35.7	1734.41	19.12	19.8	**43.91**	**-119.63**
944	1084	1100	1092	**47.7**	**-85.7**	297.3	45.5	1732.95	17.15	27.0	**52.92**	**-111.45**
3057	1050	1150	1100	**48.6**	**-88.1**	117.5	-64.5	1731.78	-11.87	-46.4	**52.83**	**-105.67**
3060	1050	1150	1100	**47.6**	**-85.0**	297.6	37.7	1731.78	18.72	21.1	**53.10**	**-113.28**
3061	1050	1150	1100	**47.6**	**-85.0**	154.3	-71.5	1731.78	-9.19	-56.2	**55.69**	**-92.05**
3062	1050	1150	1100	**47.7**	**-85.8**	293.6	32.3	1731.78	19.70	17.5	**51.92**	**-115.85**
3065	1050	1150	1100	**47.6**	**-84.7**	106.3	-74.8	1731.78	-7.75	-61.5	**49.22**	**-96.13**

2612	1090	1110	1100	**48.7**	**-88.1**	115.0	-75.5	1731.78	-7.43	-62.7	**51.36**	**-98.92**
2613	1090	1110	1100	**48.7**	**-88.1**	296.5	39.5	1731.78	18.38	22.4	**53.69**	**-116.55**
3063	1089	1139	1114	**47.0**	**-84.7**	299.9	40.4	1729.82	18.18	23.1	**53.22**	**-111.55**
3064	1089	1139	1114	**47.0**	**-84.7**	124.8	-67.9	1729.82	-10.61	-50.9	**52.23**	**-98.99**
3058	1100	1130	1115	**47.5**	**-91.0**	287.7	47.3	1729.69	16.71	28.5	**49.92**	**-116.18**
539	1100	1180	1140	**33.5**	**-110.4**	351.1	-77.6	1726.51	-6.43	-66.3	**27.14**	**-109.28**
2505	1000	1300	1150	**-0.6**	**34.8**	99.0	-59.0	1725.33	-13.60	-39.8	**1.53**	**21.36**
8104	1100	1200	1150	**24.6**	**79.9**	50.2	87.3	1725.33	1.46	84.6	**25.53**	**81.14**
6605	1152	1168	1160	**61.2**	**-45.5**	267.0	48.0	1724.21	16.50	29.0	**56.42**	**-76.34**
2566	1152	1228	1190	**-25.8**	**16.5**	4.4	-7.4	1721.13	-23.31	-3.7	**-49.02**	**13.85**
893	1178	1300	1239	**-28.4**	**21.6**	29.0	-11.0	1716.92	-22.76	-5.6	**-47.41**	**5.51**
2081	1190	1290	1240	**72.6**	**-97.0**	260.4	-0.4	1716.84	-24.20	-0.2	**62.98**	**-34.18**
173	760	1740	1250	**47.4**	**-113.1**	34.7	-25.0	1716.09	-20.71	-13.1	**29.46**	**-126.47**
2639	1100	1400	1250	**49.4**	**-114.5**	28.3	-34.7	1716.09	-19.10	-19.1	**32.00**	**-125.04**
2076	1200	1400	1300	**48.2**	**-113.8**	201.7	40.2	1712.83	18.04	22.9	**31.14**	**-121.49**
8103	1200	1400	1300	**24.6**	**79.9**	161.4	63.2	1712.83	12.18	44.7	**13.01**	**83.86**
1604	1231	1411	1321	**54.5**	**-61.6**	291.0	12.0	1711.66	22.55	6.1	**56.27**	**-101.75**
1738	1300	1400	1350	**57.0**	**-69.0**	178.9	-4.7	1710.22	-23.53	-2.4	**80.51**	**-71.67**
3435	1300	1400	1350	**37.6**	**-90.7**	243.3	41.0	1710.22	17.85	23.5	**28.14**	**-108.80**
3318	1320	1400	1360	**34.3**	**-96.7**	264.0	59.0	1709.77	13.48	39.8	**31.86**	**-112.54**
8246	1000	1800	1400	**47.3**	**-79.8**	339.1	60.7	1708.15	12.95	41.7	**59.12**	**-88.76**
8247	1000	1800	1400	**47.3**	**-79.8**	283.3	-68.6	1708.15	-10.21	-51.9	**44.08**	**-65.90**
2978	1350	1500	1425	**57.8**	**-62.0**	297.0	63.0	1707.27	12.20	44.5	**61.43**	**-85.19**
8243	900	1959	1429.5	**58.6**	**-5.1**	149.1	57.2	1707.13	13.99	37.8	**46.07**	**5.21**
6604	1300	1600	1450	**61.2**	**-45.5**	290.0	1.0	1706.49	23.97	0.5	**60.19**	**-95.67**
7623	1500	1560	1530	**-16.8**	**135.7**	279.6	78.8	1704.52	5.78	68.4	**-15.75**	**129.78**
7616	1500	1600	1550	**-17.1**	**135.9**	247.3	65.4	1704.13	11.36	47.5	**-21.16**	**124.66**
7620	1500	1600	1550	**-16.9**	**135.8**	246.2	71.1	1704.13	9.20	55.6	**-20.41**	**126.82**
7622	1500	1600	1550	**-16.8**	**135.7**	336.1	-55.6	1704.13	-14.41	-36.1	**-29.85**	**142.37**
7624	1550	1600	1575	**-16.8**	**135.7**	324.7	5.3	1703.68	23.36	2.7	**2.55**	**122.44**
7625	1550	1600	1575	**-16.8**	**135.7**	316.7	6.3	1703.68	23.22	3.2	**0.52**	**120.01**

1628	1500	1700	1600	**56.4**	**-79.0**	162.0	69.0	1703.29	10.03	52.5	**46.76**	**-74.49**
2060	1500	1700	1600	**56.8**	**-69.3**	193.0	58.0	1703.29	13.72	38.7	**43.34**	**-73.51**
2065	1500	1700	1600	**56.3**	**-68.5**	225.0	39.0	1703.29	18.17	22.0	**41.92**	**-85.74**

Table A4.20 Mesoproterozoic sample site details, structure corrected data and derived actual palaeomagnetic data. (Data after McElhinny & Lock, 1996)

Table A4.21
Palaeoproterozoic
Palaeomagnetic Data

Site Details						Structure Corrected		Derived Actual Paleomagnetic Data				
Number	Age	Age	Age	Site	Site	Correct	Correct	Paleo	Paleo	Paleo	Pole	Pole
Result	Low Mag	High Mag	Mean	Lat	Long	Dec	Inc	Radius	Colatitude	Latitude	Latitude	Longitude
1629	1540	1670	1605	**56.5**	**-79.0**	42.0	-44.0	1703.22	-17.17	**-25.8**	**42.50**	**-94.54**
1630	1540	1670	1605	**56.4**	**-79.0**	40.0	-46.0	1703.22	-16.74	**-27.4**	**42.49**	**-93.54**
1895	1450	1800	1625	**60.8**	**-78.2**	305.0	8.0	1702.94	22.98	**4.0**	**65.91**	**-129.79**
7606	1600	1700	1650	**-17.1**	**135.9**	342.7	-23.6	1702.62	-20.76	**-12.3**	**-36.76**	**143.46**
7611	1600	1700	1650	**-17.1**	**135.9**	0.7	-25.3	1702.62	-20.50	**-13.3**	**-37.60**	**135.59**
7613	1600	1700	1650	**-17.1**	**135.9**	351.3	-38.2	1702.62	-18.31	**-21.5**	**-35.17**	**139.23**
7615	1600	1700	1650	**-17.1**	**135.9**	350.2	-40.9	1702.62	-17.79	**-23.4**	**-34.60**	**139.52**
7619	1640	1680	1660	**-16.9**	**135.8**	349.1	-36.4	1702.51	-18.64	**-20.2**	**-35.16**	**140.04**
7621	1640	1680	1660	**-17.0**	**135.9**	346.5	-38.6	1702.51	-18.24	**-21.8**	**-34.66**	**141.00**
7614	1650	1700	1675	**-17.1**	**135.9**	318.0	-55.1	1702.34	-14.53	**-35.6**	**-27.57**	**146.82**
7617	1650	1700	1675	**-17.1**	**135.9**	326.5	-56.4	1702.34	-14.17	**-37.0**	**-28.70**	**144.76**
7618	1650	1700	1675	**-17.1**	**135.9**	334.3	-50.1	1702.34	-15.80	**-30.9**	**-31.16**	**143.83**
7610	1660	1710	1685	**-17.1**	**135.9**	288.2	-5.3	1702.24	-23.34	**-2.7**	**-22.85**	**160.00**
7612	1660	1710	1685	**-17.1**	**135.9**	122.0	33.0	1702.24	19.24	**18.0**	**-26.39**	**154.08**
7607	1680	1715	1697.5	**-17.1**	**138.0**	103.1	37.1	1702.11	18.51	**20.7**	**-20.34**	**157.26**
7608	1680	1715	1697.5	**-17.1**	**138.0**	100.0	47.2	1702.11	16.47	**28.4**	**-19.21**	**155.19**
7609	1680	1715	1697.5	**-17.1**	**137.9**	96.1	50.8	1702.11	15.63	**31.5**	**-18.09**	**154.27**
2270	1600	1800	1700	**62.4**	**-110.7**	30.0	-11.0	1702.09	-22.56	**-5.6**	**41.64**	**-125.57**
1638	1650	1750	1700	**62.0**	**-111.9**	132.0	59.0	1702.09	13.42	**39.8**	**51.81**	**-95.70**
1627	1688	1738	1713	**56.4**	**-79.0**	119.0	-46.0	1701.97	-16.73	**-27.4**	**61.03**	**-110.32**
7604	1700	1750	1725	**-17.1**	**135.9**	191.1	-25.6	1701.87	-20.44	**-13.5**	**2.98**	**139.76**
2272	1650	1850	1750	**62.4**	**-110.7**	33.6	-15.2	1701.67	-21.97	**-7.7**	**42.64**	**-127.05**
7605	1715	1800	1757.5	**-17.1**	**135.9**	284.8	-22.8	1701.61	-20.87	**-11.9**	**-21.21**	**157.58**

1940	1737	1787	1762	**-17.5**	**127.0**	121.0	2.0	1701.58	23.77	**1.0**	**-28.24**	**150.09**
2737	1781	1789	1785	**64.1**	**-94.4**	347.0	-50.0	1701.42	-15.81	**-30.8**	**48.55**	**-89.09**
127	1700	1900	1800	**21.0**	**85.8**	213.7	21.2	1701.33	21.10	**11.0**	**3.13**	**74.26**
1728	1700	1900	1800	**59.8**	**-80.1**	257.2	53.0	1701.33	15.07	**33.6**	**53.67**	**-105.44**
1735	1700	1900	1800	**57.0**	**-69.0**	158.8	13.6	1701.33	22.19	**6.9**	**35.78**	**-59.31**
1736	1700	1900	1800	**57.0**	**-69.0**	73.8	12.3	1701.33	22.37	**6.2**	**56.45**	**-27.60**
1737	1700	1900	1800	**57.0**	**-69.0**	312.1	-11.6	1701.33	-22.47	**-5.9**	**39.45**	**-47.45**
1637	1770	1830	1800	**62.0**	**-111.9**	129.0	21.0	1701.33	21.13	**10.9**	**45.81**	**-88.20**
6622	1750	1900	1825	**66.2**	**28.1**	343.0	34.0	1701.19	19.06	**18.6**	**82.23**	**-16.81**
6623	1750	1900	1825	**66.2**	**28.1**	312.0	45.0	1701.19	16.94	**26.6**	**72.54**	**-18.10**
6624	1750	1900	1825	**66.2**	**28.1**	19.0	46.0	1701.19	16.72	**27.4**	**80.42**	**62.36**
14	1820	1840	1830	**62.0**	**-112.1**	159.0	46.0	1701.16	16.72	**27.4**	**46.01**	**-103.56**
2422	1800	1900	1850	**55.1**	**-67.0**	42.0	56.0	1701.06	14.27	**36.5**	**64.11**	**-44.80**
1678	1800	2000	1900	**46.1**	**-82.7**	349.0	12.0	1700.84	22.41	**6.1**	**67.76**	**-93.78**
7547	1800	2000	1900	**-24.0**	**29.0**	345.1	76.3	1700.84	6.94	**64.0**	**-17.28**	**27.14**
7548	1800	2000	1900	**-24.0**	**29.0**	229.8	50.6	1700.84	15.66	**31.3**	**-33.42**	**14.70**
382	1905	1985	1945	**-27.0**	**27.5**	12.1	82.9	1700.69	3.73	**76.0**	**-23.35**	**28.35**
310	1800	2200	2000	**-22.8**	**117.3**	304.0	-18.7	1700.54	-21.46	**-9.6**	**-33.32**	**138.58**
7540	1900	2100	2000	**-23.3**	**117.5**	316.0	-6.9	1700.54	-23.10	**-3.5**	**-38.54**	**137.89**
7542	1900	2100	2000	**-22.8**	**117.7**	300.2	-16.0	1700.54	-21.85	**-8.2**	**-32.16**	**140.03**
1701	1600	2500	2050	**53.9**	**-73.5**	44.0	-49.0	1700.43	-16.04	**-29.9**	**41.26**	**-88.29**
1702	1600	2500	2050	**56.5**	**-71.5**	108.0	28.0	1700.43	20.05	**14.9**	**46.46**	**-43.25**
1703	1600	2500	2050	**56.0**	**-70.8**	78.0	-27.0	1700.43	-20.21	**-14.3**	**47.55**	**-100.84**
1704	1600	2500	2050	**57.9**	**-70.0**	2.0	-30.0	1700.43	-19.72	**-16.1**	**38.18**	**-70.86**
1705	1600	2500	2050	**56.3**	**-68.5**	211.8	38.3	1700.43	18.27	**21.5**	**39.95**	**-80.95**
561	2038	2062	2050	**-25.6**	**27.5**	357.8	70.9	1700.43	9.26	**55.3**	**-16.34**	**27.13**
1122	2038	2062	2050	**-25.5**	**27.5**	195.6	-40.0	1700.43	-17.95	**-22.8**	**-8.15**	**32.30**
1507	2038	2062	2050	**-25.0**	**30.0**	10.0	64.7	1700.43	11.58	**46.6**	**-13.58**	**32.06**
6466	2038	2062	2050	**-25.0**	**29.5**	175.1	-60.9	1700.43	-12.83	**-41.9**	**-12.21**	**28.39**
8245	1850	2300	2075	**46.3**	**-83.9**	18.6	59.6	1700.38	13.23	**40.4**	**58.61**	**-75.85**
2523	2000	2200	2100	**5.3**	**-2.0**	156.0	40.0	1700.34	17.95	**22.8**	**-11.09**	**5.34**

7648	2100	2200	2150	**69.5**	**29.5**	278.0	41.0	1700.27	17.75	**23.5**	**65.09**	**-16.28**
8249	2100	2200	2150	**47.0**	**-81.0**	271.9	69.6	1700.27	9.78	**53.4**	**46.43**	**-95.26**
1639	2135	2195	2165	**46.5**	**-81.1**	195.6	33.1	1700.25	19.20	**18.1**	**27.84**	**-86.84**
6626	2100	2300	2200	**66.2**	**28.1**	265.0	39.0	1700.22	18.14	**22.0**	**59.15**	**-9.11**
7539	2100	2300	2200	**-23.3**	**117.5**	314.0	-4.7	1700.22	-23.39	**-2.4**	**-38.05**	**138.76**
1677	2175	2250	2212.5	**46.1**	**-82.7**	237.0	48.0	1700.20	16.27	**29.0**	**35.87**	**-99.55**
1666	2215	2223	2219	**46.9**	**-80.2**	192.0	55.0	1700.20	14.54	**35.5**	**32.62**	**-83.75**
8250	2209	2235	2222	**-28.0**	**23.0**	264.8	-21.1	1700.20	-21.10	**-10.9**	**-24.15**	**46.14**
1664	2150	2300	2225	**46.8**	**-80.3**	319.0	69.0	1700.19	10.01	**52.5**	**53.87**	**-91.45**
3204	2150	2300	2225	**46.5**	**-82.8**	302.0	77.0	1700.19	6.61	**65.2**	**49.69**	**-91.48**
7647	2292	2368	2330	**69.5**	**29.5**	69.0	73.4	1700.12	8.22	**59.2**	**70.91**	**53.59**
1175	2200	2500	2350	**61.7**	**-112.8**	288.0	46.0	1700.11	16.71	**27.4**	**62.30**	**-148.84**
8244	2300	2400	2350	**46.3**	**-83.9**	5.4	5.5	1700.11	23.28	**2.8**	**69.38**	**-77.84**
8248	2300	2400	2350	**47.0**	**-81.0**	216.3	5.5	1700.11	23.28	**2.8**	**27.04**	**-96.23**
2078	2300	2450	2375	**46.3**	**-83.5**	304.1	51.7	1700.10	15.39	**32.3**	**53.11**	**-104.97**
6625	2390	2490	2440	**66.2**	**28.1**	115.0	54.0	1700.07	14.80	**34.5**	**57.25**	**53.44**
1360	2400	2600	2500	**-4.3**	**35.1**	59.7	-53.1	1700.06	-15.03	**-33.7**	**-11.71**	**21.88**

Table A4.21 Palaeoproterozoic sample site details, structure corrected data and derived actual palaeomagnetic data. (Data after McElhinny & Lock, 1996)

Table A4.22 Archaean Palaeomagnetic Data

Site Details						Structure Corrected		Derived Actual Paleomagnetic Data				
Number	Age	Age	Age	Site	Site	Correct	Correct	Paleo	Paleo	Palaeo	Pole	Pole
Result	Low Mag	High Mag	Mean	Lat	Long	Dec	Inc	Radius	Colatitude	Latitude	Latitude	Longitude
183	2400	2800	2600	**-21.4**	**119.6**	263.7	54.6	1700.04	14.64	**35.1**	**-22.26**	**103.85**
394	2500	2700	2600	**48.0**	**-83.3**	6.0	48.0	1700.04	16.27	**29.0**	**64.13**	**-79.45**
1692	2550	2650	2600	**53.7**	**-75.0**	17.5	-28.0	1700.04	-20.04	**-14.9**	**34.31**	**-82.17**
393	2550	2750	2650	**48.3**	**-82.8**	359.0	56.0	1700.03	14.26	**36.5**	**62.56**	**-83.33**
7538	2670	2690	2680	**-0.9**	**34.7**	74.2	-43.3	1700.02	-17.28	**-25.2**	**-5.50**	**18.01**
3046	2701	2709	2705	**45.4**	**-110.0**	160.0	-40.0	1700.02	-17.94	**-22.8**	**61.72**	**-122.85**
1676	2701	2712	2706.5	**48.6**	**-79.8**	287.0	2.0	1700.02	23.75	**1.0**	**49.86**	**-116.48**
309	2700	2900	2800	**-22.8**	**117.3**	154.1	79.6	1700.01	5.38	**69.8**	**-27.62**	**119.95**
311	2700	2900	2800	**-21.0**	**117.8**	320.0	-53.8	1700.01	-14.85	**-34.3**	**-31.99**	**129.00**
308	2850	2870	2860	**-20.9**	**117.5**	265.0	-65.1	1700.01	-11.44	**-47.1**	**-19.48**	**129.60**
1691	2800	3000	2900	**53.7**	**-75.0**	149.0	-36.0	1700.01	-18.69	**-20.0**	**67.83**	**-100.93**
184	2800	3200	3000	**-21.2**	**119.7**	266.2	-37.7	1700.01	-18.38	**-21.1**	**-18.89**	**139.12**
8143	2900	3150	3025	**22.0**	**85.4**	282.7	60.2	1700.01	13.04	**41.1**	**24.26**	**71.43**
182	3436	3468	3452	**-21.3**	**119.6**	335.5	31.8	1700.00	19.42	**17.2**	**-3.48**	**111.66**

Table A4.22 Archaean sample site details, structure corrected data and derived actual palaeomagnetic data. (Data after McElhinny & Lock, 1996)

A5. PUBLICATIONS

MAXLOW J. 1998. Global expansion tectonics: Empirical small Earth modelling of an exponentially expanding Earth. *Proceedings of International Symposium on New Concepts in Global Tectonics, 1998, Tsukuba, Japan,* 159-164.

MAXLOW J. 2000a. Earth expansion: Quantification using Oceanic magnetic isochron mapping. *Himalayan Geology* **23**, 1-14.

MAXLOW J. 2000b. Global Expansion Tectonics. *Nexus New Times Magazine* **7/6**, 41-46.

A6. CD-ROM DISC

This CD-ROM disc contains video animations of selected figures from Volume 1 of 2 of this thesis. These animations were created from a series of 72 GIF images per globe and assembled as video clips in Adobe Premier version 5.0 at 640 x 480 pixel frame size, 24 fps frame rate and saved as either MPG files or AVI files. The Video animations use the same numbering system as figures shown in the text volume, except the word Figure is replaced by Video and the number is prefaced by the letter A, eg. Figure 3.15 becomes Video A3.15. To run these video animations a computer with a Pentium II, 330 Mhz processor or better, 32 Mb RAM and 8 Mb graphics card is required. At less than these specifications the animations may show erratic motion. To get better resolution the video animations can also be opened separately from a standard media player or via Windows Explorer.

LIST OF VIDEOS

Video A1.1a Recent to Permian spherical models of an expanding Earth.

Video A1.1b Permian to Archaean spherical models of an expanding Earth.

Video A2.10 Archaean to Future spherical models of an expanding Earth.

Video A2.13 Archaean-Mesoproterozoic expanding Earth model.

Video A2.14 Four phases of expanding Earth developmental history.

Video A2.31 The expanding Earth projected to 5 million years into the future.

Video A3.5 Recent VLBI, SLR, GPS and DORIS horizontal plate motion.

Video A3.13 Expanding Earth Archaean to Future palaeomagnetic north poles.

Video A3.14 Expanding Earth Archaean to Future palaeomagnetic south poles.

Video A3.15 Palaeogeography on an Archaean to Future expanding Earth.

Video A3.15a Palaeozoic palaeogeography.

Video A3.15b Mesozoic palaeogeography.

Video A3.15c Cenozoic palaeogeography.

Video A3.18 Rodinia on a Late Neoproterozoic expanding Earth.

Video A3.20 Gondwana on an Ordovician expanding Earth.

Video A3.22 Pangaea on an Early Permian expanding Earth.

Video A3.23 Triassic to Eocene Alpine-Himalayan orogenesis.

Video A3.26 Mid- to Late-Cambrian agnostid trilobite and Early Ordovician platform trilobite faunas on an Ordovician expanding Earth.

Video A3.27 Permian reptile and Mesozoic Dinosaurian locations on a Triassic expanding Earth.

Video A3.28 New Zealand Middle and Late Jurassic marine taxa on a Late Jurassic expanding Earth.

Video A3.29 *Glossopteris* flora on an Early Carboniferous expanding Earth.

Video A3.30 Precambrian glacial deposits on a Neoproterozoic expanding Earth.

Video A3.32 Early Palaeozoic glacial deposits on an Ordovician expanding Earth.

Video A3.34 Late Palaeozoic glacial, carbonate and coal deposits on a Permian expanding Earth.

Video A3.35 Late Palaeozoic to Triassic coal and Permo-Carboniferous carbonate reefs on a Permian expanding Earth.

Video A3.36 Permo-Carboniferous to Triassic carbonate reefs plotted on an Early Jurassic expanding Earth.

Video A3.37 Palaeozoic, Mesozoic, and Cenozoic oil and gas on a Mid Cretaceous expanding Earth.

Video A3.38 Early to Late Cretaceous coal on a Late Cretaceous expanding Earth.

Video A3.40 Precambrian metals on a Neoproterozoic expanding Earth.

Video A3.41 Mid- to Late-Phanerozoic metals on an Early Jurassic expanding Earth.